THE DESIGN OF A DEEP WATER CATENARY RISER

VOLUME II

James R. Dingwall, B.Eng(Hons), Diploma

Thesis submitted for the Degree of Doctor of Philosophy

Department of Naval Architecture and Ocean Engineering

University of Glasgow

August 1997

Contents

VOLUME II

List of Figures

Chapter 1

Chapter 2

Chapter 3

Chapter 4

Chapter 5

Chapter 6

Chapter 7

Chapter 8

Chapter 9

Chapter 10

List of Tables

Chapter 1

Chapter 2

Chapter 3

Chapter 4

Chapter 5

Chapter 6

Chapter 7

Chapter 8

Acknowledgements

The author is grateful for all the advice, help and support obtained from both the Department of Naval Architecture and Ocean Engineering at the University of Glasgow and BAeSEMA in Glasgow during the research study presented in this thesis.

The author is particularly indebted to:

Professor A. Incecik	for supervising this research and for his assistance, encouragement and support.
Mr N.S. Miller	for all his work and ideas which helped to initiate this research project.
Dr D. Barrie	for all his advice and for being my industrial supervisor at BAeSEMA.
Mr I.C. Smith	for securing BAeSEMA sponsorship for this research.
Mr A. Watters	for all the information and assistance that was provided during the dynamic analysis phase of the research.

Finally, the financial support from the EPSRC (Engineering and Physical Science Research Council) and BAeSEMA is gratefully acknowledged.

Dedicated to my Parents

Declaration

Except where reference is made to the work of others,
this thesis is believed to be original.

m_s	Structural Unit Mass
m_{am}	Added Unit Mass
$\dot{m}$	Fluid Mass Flow Rate
Nu	Nusselt Number
P	Pressure
Pr	Prandtl Number
Q	Rate of Heat Loss
q	Applied Force per Unit Length
q	Rate of Heat Loss per Unit Length
R	Specific Gas Constant
Re	Reynolds Number
r	Profile Radius
r	Position Vector
r	Pipe Surface Radius
1/R	Profile Curvature
s	Distance Along Riser From Origin (usually seabed end)
SF	Shear Force
T	Axial Tension
T	Temperature
Tp	Natural Period of Vibration
Tp	Wave Period
T_T	Total Mooring Tether Load
t	Time
t	Wall Thickness
U	Overall Heat Transfer Coefficient
U	Fluid Velocity
$\dot{U}$	Fluid Acceleration
U_C	Constant Current Velocity (with respect to depth)
U_S	Surface Current Velocity
u_m	Mean Fluid Velocity
V	Vertical Load Component
W_B	Weight (in air) of the Buoy
w	Submerged Unit Length
X_{max}	Maximum Allowable Displacement
x	Horizontal Distance
$\dot{x}$	Horizontal Velocity
$\ddot{x}$	Horizontal Acceleration
y	Vertical Distance

$\dot{y}$	Vertical Velocity
$\ddot{y}$	Vertical Acceleration
y_c	Vertical Distance Up the Buoyancy Compartment
α	Coefficient of Thermal Expansion (solid)
α	Cable Sag Parameter
α	Change in Riser Profile Angle at the Surface (from the horizontal)
β	Coefficient of Thermal Expansion (fluid)
β	Non-Dimensional Natural Frequency Parameter
ε	Axial Strain
φ	Profile Slope (measured from the vertical)
η	Permissible Usage Factor
λ	Eigenvalue
λ	Wave Length
μ	Dynamic Viscosity
θ	Profile Slope (measured from the horizontal)
ρ	Density
ρ_{sw}	Sea Water Density
σ	Stress
υ	Kinematic Viscosity
ω	Natural Frequency (circular)
∇	Volume of Fluid Displaced

Summary

Deep water production more than anything else will sustain the petroleum industry turnaround well into the 21st Century. However the challenges presented by deep water are considerable both commercially and technically especially if the fields are marginal. Engineering solutions must aim to minimise the operator's capital risk and maximise his ability to avoid large capital commitments prior to verification of acceptable reservoir performance.

Among the more daunting technical issues to be addressed is hydrate and paraffin subsea pipeline blockage. Generally considered little more than a nuisance in most shallow water areas, the high flow rates, remoteness and the miles of very low temperature water through which deep water production must pass, make it quite a serious problem for producers. Another physical reality of deep water production are the considerable lengths of riser involved. These generate large riser weights which result in high loads being exerted upon both the riser and surface connection system.

The overall aim of this study is to propose and develop a cost effective production design concept suitable for oil reservoirs situated in deep (1500 m) water which can be quickly and safely installed in areas with limited weather windows. The proposed design is based upon a *steel catenary riser* which will connect an FPSO directly into either a wellhead or seabed pipeline system thereby eliminating both the connection complexities and high cost associated with a central manifold. The catenary geometry will ensure that the structure is inherently compliant whilst a carrier pipe arrangement will provide structural protection and buoyancy to a flowline bundle contained within. The interface between the riser and the surface production vessel is a critical part of any riser system and so for the purposes of this study two design arrangements are considered. The first is based upon a direct connection between an FPSO turret and riser where as the second is a hybrid design in which the riser is supported by a sub-surface buoy which is hydraulically connected to an FPSO using flexible flowlines. This hybrid connection has the advantage of decoupling FPSO and riser motions. Design development is carried out by examining a range of critical areas. Each investigation forms the basis of a chapter as described below.

In Chapter 2, the loading and geometric characteristics of a selection of conceivable riser profiles are examined and compared with one another. The analysis carried out establishes that for all three mathematical curves considered i.e. elliptic, parabolic and catenary, maximum bending moments due to self-weight occur at the seabed, except in the case of an elliptic curve when the profiles horizontal offset exceeds water depth. The

elliptic and parabolic curves, although convenient mathematically would be very difficult to attain on a practical basis, a catenary however describes the form assumed by a perfect flexible inextensible chain of uniform density suspended from two supports.

Chapter 3 is devoted to the design of a buoyancy system which is required in order to support the riser's submerged weight. Two different systems suitable for deep water are investigated. The syntactic foam design provides the riser with a buoyancy system that is simple to use during both riser installation and operation. Its characteristics are not influenced by external factors and it doesn't impose any additional stresses on the riser, however it is very expensive. Nitrogen gas however is relatively cheap, although this is somewhat compromised by a considerably more complex arrangement, involving internal gas tight compartments, high pressure lines and a high pressure gas source.

Chapter 4 examines the problems associated with production oil temperature. A heat loss analysis is carried out using EXCEL spreadsheets. This analysis identifies a requirement for good pipeline and flowline insulation in order for oil transportation problems such as hydration to be avoided within a deep water environment. A structural thermal stress assessment is also undertaken.

In Chapter 5 an installation loading analysis investigates the effects of riser geometry and submerged unit weight on bending stress, axial stress and lifting load. Bending and axial stresses resulting from surface and sub-surface vessel displacements are also calculated along with the corresponding deflection profiles. This chapter also examines the static structural response of the riser to in-plane current loads. The response (in terms of deflection and stress) is characterised by the riser's submerged unit weight, geometry (horizontal surface offset) and the side of the riser on which the current acts i.e. *Concave* or *Convex*. One important characteristic which becomes apparent when a catenary riser is subjected to external forces are the large angular rotations which are generated at the top end. These have to be accommodated in order to avoid creating seriously high bending moments both in the riser as well as in the surface or sub-surface connection assembly. This can be achieved through the use of flexible joints. A design for a surface (or sub-surface) connection system using flexible joints is proposed in this chapter.

In Chapter 6 a resonant period analysis is undertaken using a numerical procedure based upon a finite difference technique and validated by an analytical method developed by Blevin for vibrating stretched strings. From this analysis it is shown that the resonant periods rapidly converge as the mode number is increased. Overall the results suggest that the riser's high natural periods are substantially influenced by carrier pipe diameter and

can therefore be positioned so as to avoid external excitation periods by selecting appropriate diameters.

As an alternative to the direct connection of the riser to the surface production vessel a study to investigate the advantages of a hybrid connection is carried out in Chapter 7. In this study a vertically tethered sub-surface buoy from which a catenary riser is suspended is designed and evaluated. The loads imposed upon the buoy and its tethers along with the lateral stiffness that this arrangement provides are evaluated using spreadsheets.

In Chapter 8 a detailed capital cost analysis for the catenary riser is undertaken. It is found that the economics compare favourably with known production systems designed for the same operational environment.

CHAPTER 5

Static Installation and Environmental Loading Analysis

5.1 General Description

The objective of this chapter is to establish and analyse the response of the catenary riser in terms of it's deflection and structural stressing to the following external loading conditions:

- Functional loads acting alone during installation
- Functional and environmental loads both acting during operation

The term *during installation* in this instance refers only to the lifting phase of the whole installation process as previously described in Section 3.3.4. The term *during operation* refers to the period after the riser has been completely installed.

These two conditions are considered to be the main sources of loading (and structural failure) exerted upon the riser and so it is important that both the resulting axial and bending stresses are established so that the technical feasibility of the design can be assessed.

5.1.1 Functional Loads During Installation

Functional loads are loads which are a necessary consequence of the systems existence, use and treatment in the various situations under ideal conditions. Ideal conditions mean no current, waves, etc., i.e. no environmental loads acting. In the case of the installation of the riser, functional loads include the risers self-weight as well as the applied loads required in order to pull one end of the riser to the surface for connection to either an FPSO or sub-surface buoy. For the purposes of this investigation the functional loads are considered to be static.

5.1.2 Functional and Environmental Loads Acting Together During Operation

Environmental loads are loads due to wind, waves, current and other environmental phenomena and in this study are assumed to be static. In this analysis two principle environmental conditions are examined:

- Surface end displacement in the surge direction generated by either FPSO or sub-surface buoy movement under the action of wind, waves or current.
- Current forces acting directly upon the catenary riser.

5.2 Strength Criteria

In this study the riser is to be designed against the following possible forms of failure:

- Excessive yielding
- Local buckling

5.2.1 Yielding of the Riser

The riser is fabricated using high strength steel with a yield stress of 450 N/mm². This material parameter therefore establishes a maximum permissible longitudinal stress according to the following expression as laid down in DNV's *'Rules for the design construction and inspection of submarine pipelines and pipeline risers'* :

$$\sigma_{xp} = \eta_{xp}\,\sigma_y \qquad (5.1)$$

where: σ_{xp} = maximum permissible longitudinal stress
η_{xp} = permissible usage factor
σ_y = material yield stress

DNV rules recommends the following usage factors:

0.86	Riser installation -	Functional loads acting alone
0.80	Riser operation -	Functional and environmental loads acting together

Inputting these values along with the yield stress stated above into Eqn (5.1) leads to the following maximum permissible longitudinal stresses:

$\sigma_{xp} = 387\ \mathrm{N/mm^2}$	Riser installation
$\sigma_{xp} = 360\ \mathrm{N/mm^2}$	Riser operation

5.2.2 Local Buckling of the Riser

Buckling of moderately thick tubes *D/t < 150* will occur in modes similar to that illustrated in Figure 5.1. The formation of a number of localised axisymmetric bulges at the region of maximum curvature have been observed in experiments. These bulges correlate well to those obtained for an axial compression condition and when localised buckling is analysed theoretically, as an axial compression problem buckling stresses are found to be similar to those obtained for a simply-supported shell. As a consequence of this the following axial compression equation can be used to *conservatively* estimate the local buckling strength of a tube or pipe in bending:

$$\sigma_{xcr} = \sigma_y \left[1 - 0.0024\left(\frac{D}{t}\right) + 0.000003\left(\frac{D}{t}\right)^2 \right] \qquad (5.2)$$

and as before the maximum permissible bending stress can be attained by using a permissible usage factor (as described previously) i.e.

$$\sigma_{xpb} = \eta_{xp}\, \sigma_{xcr} \qquad (5.3)$$

Equation (5.2) clearly demonstrates the dependence of the local buckling stress on the pipes *D/t* ratio and its non-dependence on the materials elasticity modulus *E*. However it should be noted that buckling strengths to a certain extent are also determined by the level of imperfection within the pipe as well as it's boundary conditions. The proceeding table presents buckling strength data obtained from Eqn (5.2) for a selection of pipe diameters in both installation and operational modes. The pipe wall thickness is 10 mm.

Riser Condition	**Buckling Strength** (N/mm^2)	**Max Permissible Bending Stress** (N/mm^2)
Installation		
Diameter = 1.0 m	355.5	305.7
Diameter = 1.1 m	347.5	298.9
Diameter = 1.2 m	339.8	292.2
Operation		
Diameter = 1.0 m	355.5	284.4
Diameter = 1.1 m	347.5	278.0
Diameter = 1.2 m	339.8	271.8

Table 5.1

Buckling Strengths for Various Riser Conditions

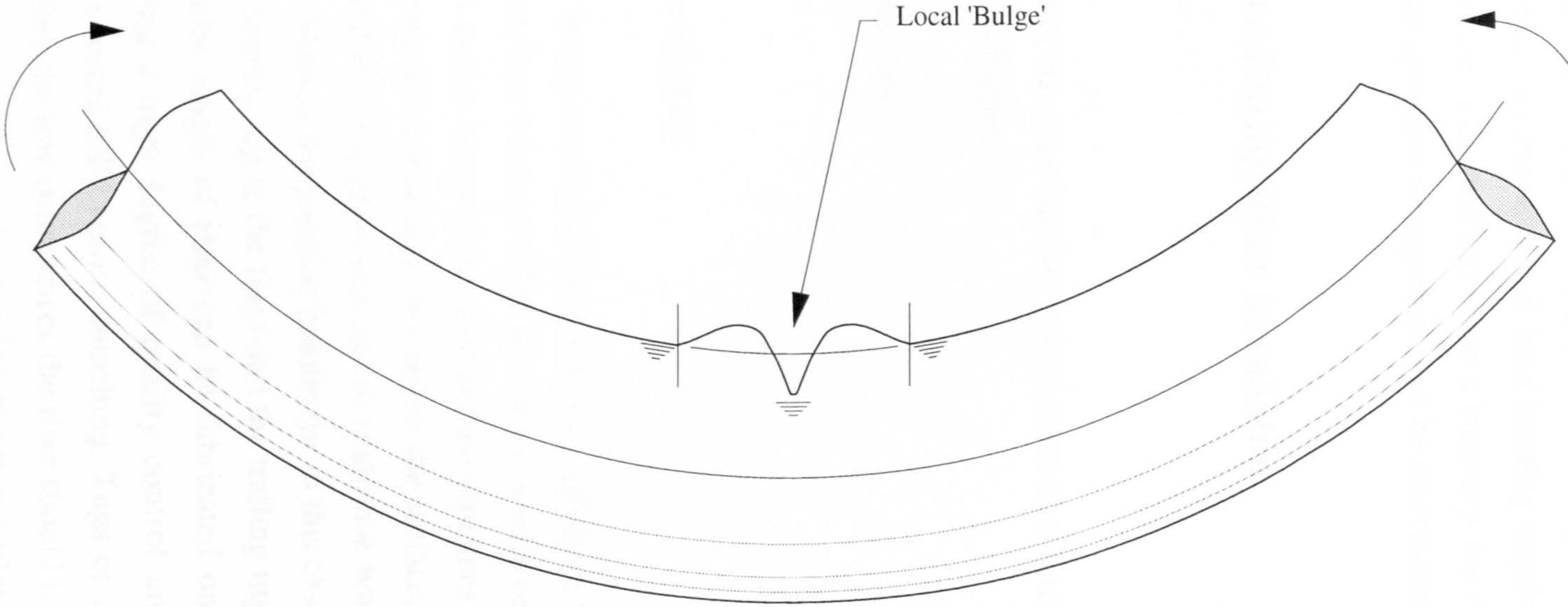

Figure 5.1

Collapse Form of a Tube Under Pure Bending Conditions

As the diameter is increased from 1.0 to 1.2 m it is apparent from the tabulated results that the resistance of the pipe to local buckling decreases with a reduction of just over 4% in load bearing capacity.

The maximum working stress values determined for both yielding and buckling cases enable the limiting deflection and external load bearing capability of the riser to be established. If this exercise is carried out upon a catenary riser of varying weight and geometric profile then an optimum arrangement can be determined.

5.3 Loads Exerted During Riser Installation

5.3.1 Introduction

The installation of the riser can be broken down into three separate stages which are depicted pictorially in Figure 5.2.

(a) Controlled Depth Tow
(b) Sinkage
(c) Lift

Controlled Depth Tow Method

It is proposed that the transportation of the riser to the offshore field will be carried out using a Controlled Depth Tow Method (CDTM). This is a relatively new method which is currently being utilised to tow out prefabricated seabed pipelines or bundles whereby the bundle is towed free from the seabed and well below the surface, in order to allow a safe passage of obstacles and existing pipelines and to minimise wave influences. With the Controlled Depth Tow Method the pipeline bundle (or in this case the riser) is suspended between two tugs, the leading tug at the front and the trailing tug at the end as shown in Figure 5.2(a). The entire length of riser can be fabricated onshore under controlled circumstances, allowing a high degree of quality control and ultimately increased reliability, as it can be tested fully before launching. Tugs or a pull barge are used to launch the bundle. Before the tow commences the riser should have a limited submerged weight which can be accurately set by leaving a pre-calculated number of flowlines empty (i.e. full of air) whilst flooding the riser's compartments with seawater. During the tow a lift force is generated upon the riser which effectively reduces it's submerged unit weight and hence it's deflection.

(a) Controlled Depth Tow Method - CDTM

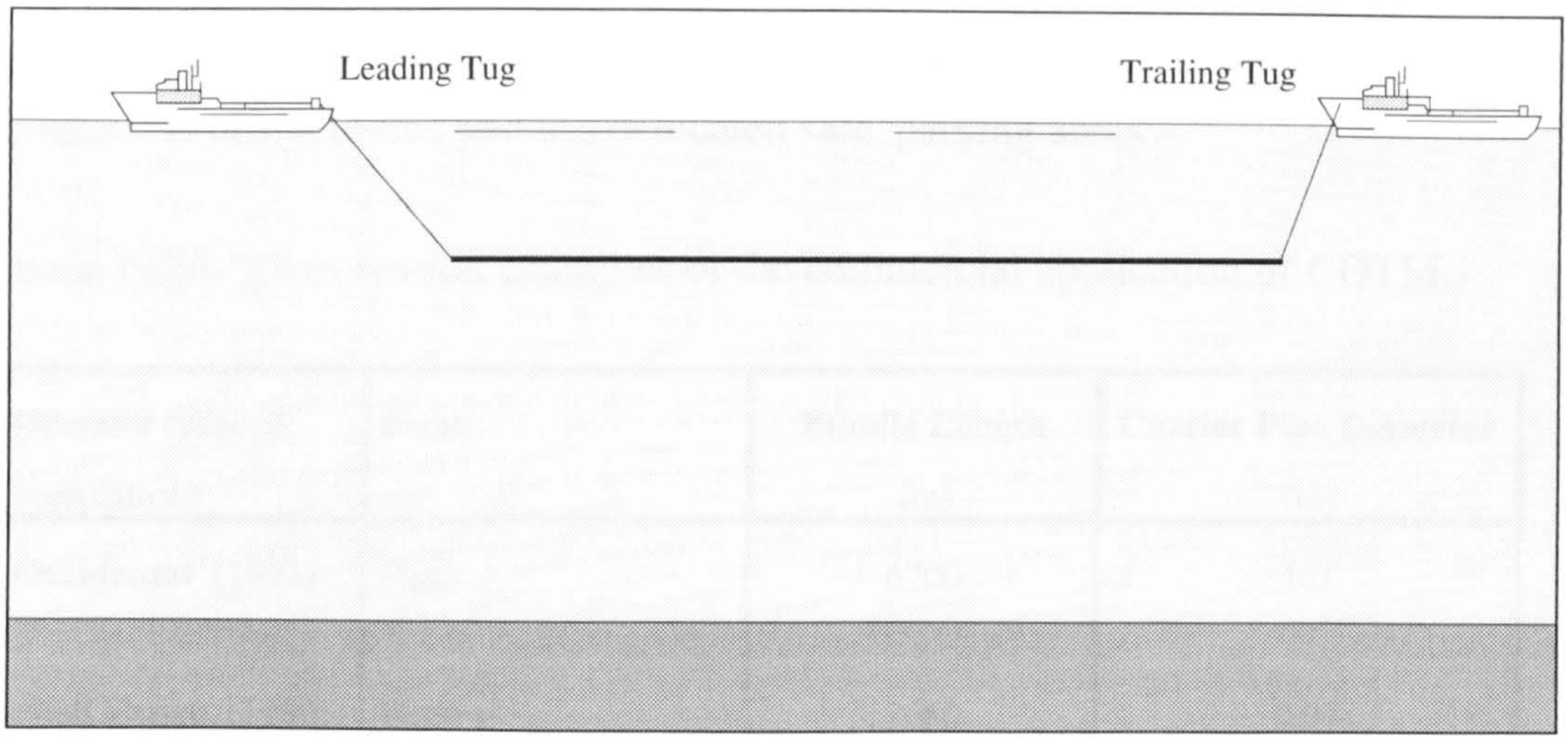

(b) Sinkage

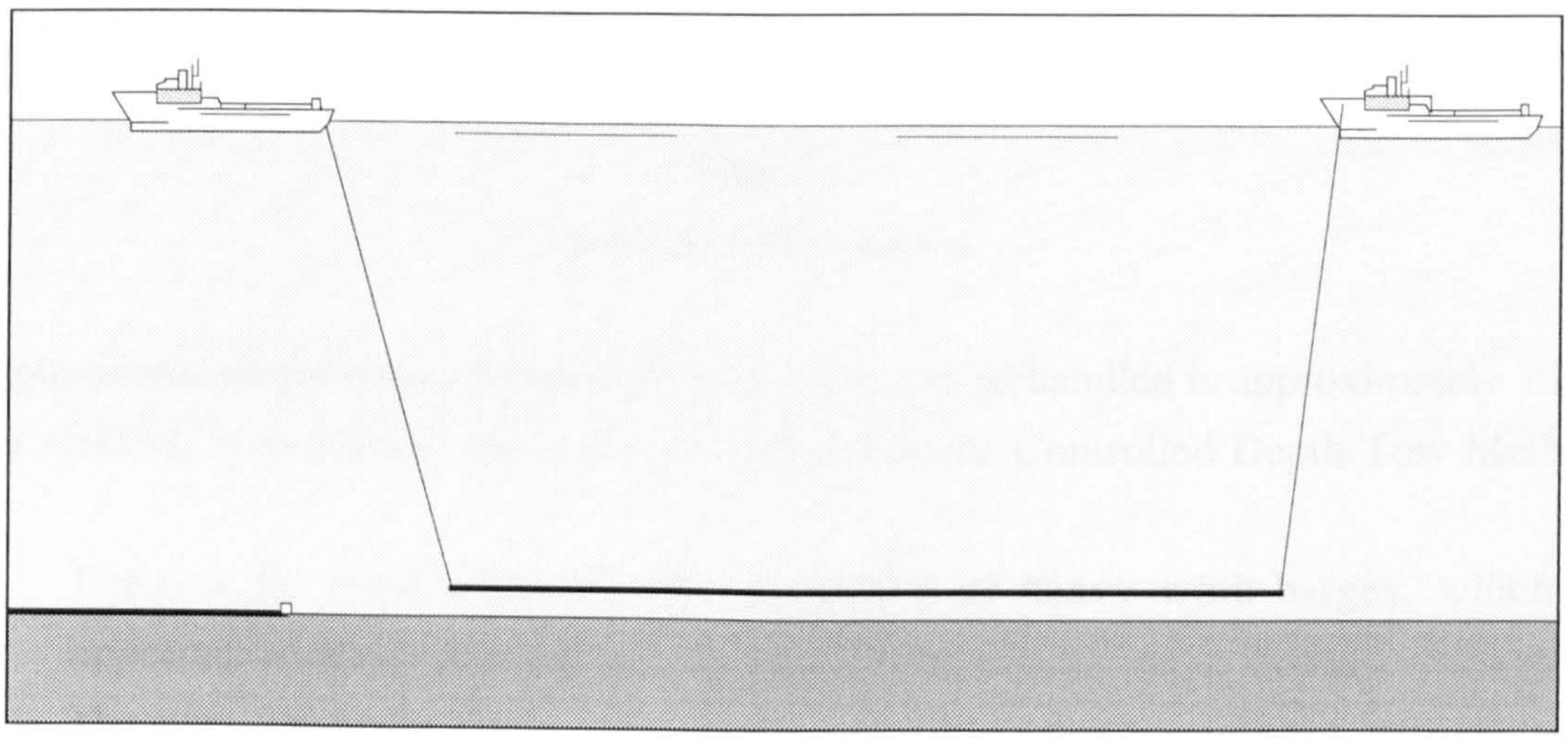

(c) Lift

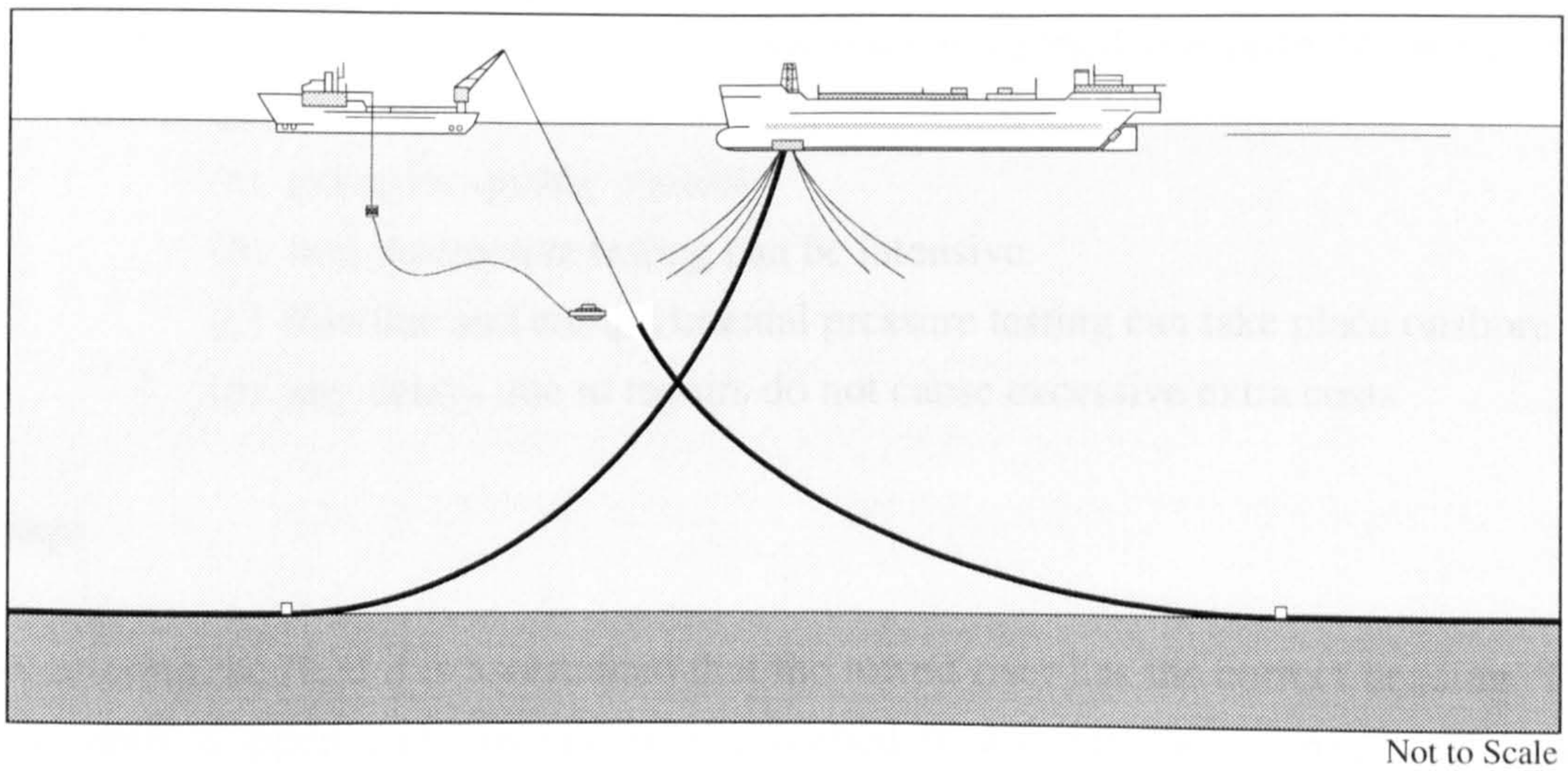

Not to Scale

Figure 5.2

Catenary Riser Installation (FPSO)

By controlling the towing speed in combination with the tension maintained by the trailing tug at the rear, the riser configuration and it's deflections are kept under control during transport to it's offshore field location. The tow takes place along a pre-surveyed route which is obstacle free and has dedicated safe 'parking areas'.

The table below gives several examples of the commercial application of CDTM.

Operator (year of installation)	Field	**Bundle Length** (m)	**Carrier Pipe Diameter** (m)
Occidental (1992)	Piper	6700	1.0
Shell Expro (1990)	Osprey	2680	0.97
Shell Expro (1984)	Central Cormorant	1250	0.66

Table 5.2

Completed CDTM Projects

The maximum single length pipelines/risers which can be handled is approximately 7 km using CDTM. In summary, the major advantages of the Controlled Depth Tow Method are:

- There is no requirement for the anchoring of heavy work-barges, which is important in deep water fields.
- The stress levels are low
- Less expensive offshore spread
- The construction of the riser (or pipeline) is carried out onshore, which has advantages such as:
  - (a) extensive quality control
  - (b) non-destructive testing can be intensive
  - (c) flowline and compartmental pressure testing can take place onshore
  - (d) any delays due to repairs do not cause excessive extra costs

Sinkage

Upon entering the field it is ascertained that the towed riser has the correct heading. The riser is then stopped and lowered to the seabed in a controlled manner and if the submerged weight needs to be increased an additional flowline can be flooded. Lowering the riser on to the seabed requires an increase in pullforce of the trailing tug and a

decrease of the pullforce of the leading tug, while simultaneously paying out sufficient tow wire. All these actions are performed in a pre-planned and controlled manner.

Lift

In terms of the structural loading imposed upon the riser the latter stage 'lift' is the most critical and for this reason the following study aims to identify both the resulting axial and bending stresses during this phase for risers of differing geometric profile and weight. As well as the stressing within the riser the analysis also calculates the lifting loads required to pull one end of the riser off the seabed and up to the surface. These are obviously important when considering the requirement capabilities of both lifting barge and cable.

5.3.2 Computer Modelling

The risers lift profile sequence as shown in Figure 5.3 is modelled using a FORTRAN computer program as depicted in block diagram form in Figure 5.4. The output from this is fed into an EXCEL spreadsheet which is then used to both calculate the loads generated during lift. This computational lift model has already been used before in Section 3.3.4 to analyse the compartmental buoyancy and weight characteristics during lift. The FORTRAN computer program is listed in Appendix B.

5.3.3 Analysis Output

This analysis establishes the following load characteristics at five riser upper end elevations (1 - 5) equally separated (by 250 m) using equations formulated in Chapter 2:

(a) Lift Cable Horizontal Load (H) - H

(b) Lift Cable Vertical Load (V) - *Equation (2.58) when* $x = a$

(c) Lift Cable Axial Load - *Eqn (2.57) when* $x = a$

(e) Axial Stress at the Top End of the Riser - *Equation (2.57) when* $x = a$

(d) Axial Stress at the Seabed - *Equation (2.57) when* $x = 0$

(f) Bending Stress Distribution along the Riser - *Equation (2.62) in conjunction with Equation (2.52)*

Results are presented for catenary risers with horizontal surface offsets of 1000, 1500 and 2000 m with submerged unit weights of 100, 500, 1000, 1500 and 2000 N/m. All the results are presented graphically using EXCEL.

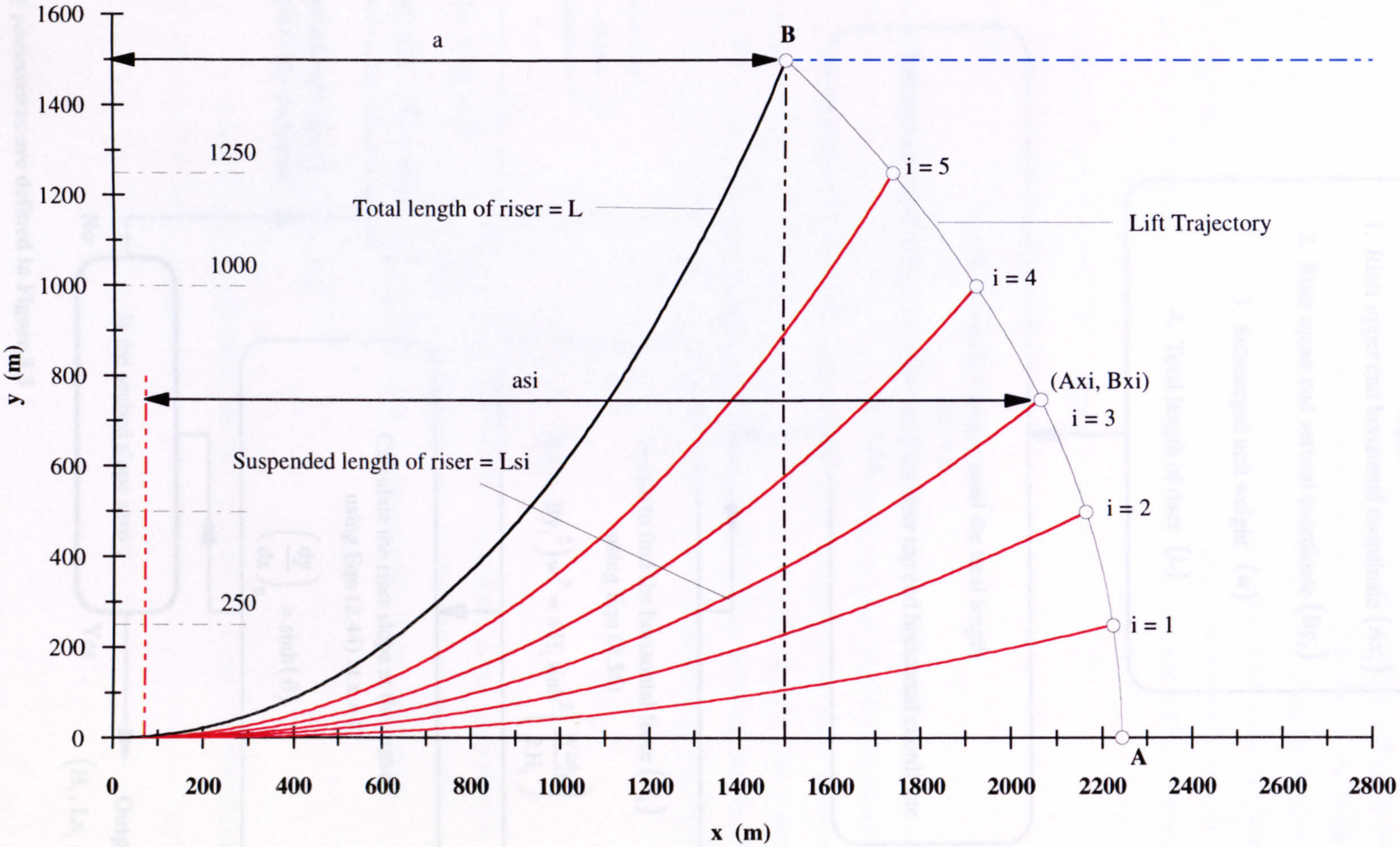

Figure 5.3
Riser Lift Parameter Definitions

Riser upper end elevation (i) :
where i = 1 to 5

Input

1. Riser upper end horizontal coordinate $\left(Ax_i\right)$
2. Riser upper end vertical coordinate $\left(By_i\right)$
3. Submerged unit weight $\left(w\right)$
4. Total length of riser $\left(L\right)$

Let the suspended length equal the total length

$$Ls_i = L$$

Let the suspended horizontal offset equal the riser top end horizontal coordinate

$$as_i = Ax_i$$

Iterate to find the horizontal force $\left(H_i\right)$
using Eqn (2.56)

$$\left(Ls_i - By_i^{\,2}\right) w^2 = 4\,H_i \sinh^2\left(\frac{w\,as_i}{2\,H_i}\right)$$

Calculate the riser slope at the seabed
using Eqn (2.44) at x = 0

$$\left(\frac{dy}{dx}\right)_0 = \sinh\left(\vartheta\right)$$

Is the seabed slope zero ?

No

$n = -0.001$

$Ls_i = Ls_i + n$

$as_i = as_i - \left(L - Ls_i\right)$

Suspended length $\left(Ls_i\right)$
is progressively decreased

Yes

Output

$\left(H_i, Ls_i \text{ and } as_i\right)$

Catenary parameters are defined in Figure 5.3

Figure 5.4
Block Calculation Diagram for the Catenary Riser Lift Sequence

5.3.4 Lift Trajectory

Loads exerted upon the riser during the lift are not only determined by the risers operational geometry and submerged unit weight but by the trajectory the top end of the riser describes as it is pulled towards the surface. The type of lift trajectory is dictated by the horizontal and vertical loads exerted upon the top end of the riser through the lifting cable. Both the bending and axial stresses that result during this lifting process are severely influenced by the type of trajectory and so in order to demonstrate this three lift trajectories have been analysed for a riser with a 1500 m horizontal surface offset:

- Catenary curve (denoted *AB* in Figure 5.3)
- Parabolic curve
- Straight line

These examples have been used because of their practicality and mathematical simplicity. A lift trajectory obviously has to be such that all the points that lie on must not be a distance from the seabed connection greater than the length of the riser. From a simple trial and error analysis it is found that the catenary curve and straight line represent the best and worst lift trajectories respectively in terms of the bending loads they both generate. The results presented in this section are therefore evaluated using these two lift trajectories only .

5.3.5 Seabed Conditions

Lift calculations are based upon a zero slope condition at the seabed with the riser being securely connected axially to either the rest of the subsea production system or other assembly anchored to the seabed i.e. it is a structurally fixed connection.

5.3.6 Environmental Loading

Lift calculations are based upon the non-existence of any environmental loads such as current or waves.

5.3.7 The Loading Characteristics of Catenary and Straight Line Lifting Trajectories

Lift Cable Horizontal Loading

A catenary lift trajectory (see Figure 5.34) is dependent upon the riser being pulled outwards and therefore kept very taut as it is lifted off the seabed. During the lift there is a progressive slackening and increase in sag as the upper end of the riser is pulled inwards as well as upwards towards its operational surface position . This necessitates the applied horizontal force on top end of the riser to be initially high and then to subsequently reduce during the lift as shown in Figure 5.35(a). However if a straight line trajectory is adopted (see Figure 5.37) the opposite occurs with the upper end of the riser effectively being pulled outwards during its ascent resulting in the system becoming more taut and less slack. This requires a linear increase in horizontal load throughout the lift as demonstrated in Figure 5.38(a). The difference in loading throughout the lift for both profiles is demonstrated below in tabular format for a riser with a submerged unit weight of 1000 N/m and horizontal surface offset of 1500 m.

Top End Elevation Above the Seabed (m)	**Lift Cable Horizontal Load (kN)**	
	Catenary Curve Lift Trajectory	Straight Line Lift Trajectory
250	8827	155
500	4446	309
750	2778	464
1000	1907	619
1250	1334	773
1500	928	928

Table 5.3

Horizontal Cable Loads for a Catenary Curve and Straight Line Lift Trajectory

Figures 5.35(a) and 5.38(a) also illustrate the effect that the risers submerged unit weight has on horizontal loading during lift. A greater suspended weight requires a greater horizontal supporting load.

Lift Cable Vertical Loading

Vertical lifting load is a direct function of the weight of suspended riser and so in both lift cases the vertical load is shown to increase in response to both an increase in riser submerged unit weight and amount of riser suspended during the ascent (see Figures 5.35(b) and 5.38(b)). The straight line lift trajectory ensures that the riser is systematically pulled off the seabed as opposed to the catenary lift case in which 90% of the riser is already suspended by the time the upper end is 250 m above the seabed. These lift characteristics result in the following:

- A vertical load that increase linearly throughout the lift for the straight line case
- A vertical load that increases rapidly up to an elevation of 250 m whereby it levels off as the upper end approaches the surface

The observations are demonstrated below in tabular format for a riser with a submerged unit weight of 1000 N/m and horizontal surface offset of 1500 m.

Top End Elevation Above the Seabed (m)	**Lift Cable Vertical Load (kN)**	
	Catenary Curve Lift Trajectory	Straight Line Lift Trajectory
250	2116	374
500	2167	748
750	2175	1122
1000	2194	1496
1250	2213	1870
1500	2244	2244

Table 5.4

Vertical Cable Loads for a Catenary Curve and Straight Line Lift Trajectory

Axial Stress

During ascent axial stressing at both ends of the riser is graphically shown by Figures 5.35(d) to (e). and 5.38(d) to (e) to decrease in the case of the catenary lift trajectory and increase when a straight line trajectory is taken up. These characterising features are a direct outcome of the horizontal and vertical loadings applied at the risers top end from the lift cable that are required in order for either of the two trajectories to be attained during lift. The differences in axial stress at the top end of the riser throughout the lift for

both trajectories are demonstrated below in tabular format for a riser with a submerged unit weight of 1000 N/m and horizontal surface offset of 1500 m.

Top End Elevation Above the Seabed (m)	**Axial Stress at the Top End of the Riser (N/mm2)** Catenary Curve Lift Trajectory	Straight Line Lift Trajectory
250	86.2	3.8
500	47.0	7.7
750	33.5	11.5
1000	27.6	15.4
1250	24.6	19.2
1500	23.1	23.1

Table 5.5

Top End Axial Stresses for a Catenary Curve and Straight Line Lift Trajectory

The table above shows that when a catenary lift trajectory is adopted a considerably greater axial load is exerted upon the riser, however this is seen as being advantageous in terms of resisting the effects of a simultaneous current load which would inevitably occur. The more taut the riser is held the less it will deflect under a current force.

Bending Stress

Bending stress can be considered to be the most critical load imposed upon the riser. If local buckling and ultimate failure is to be avoided riser curvature must be minimised and this is an area where the type of riser lift profile chosen becomes very important. Tables 5.36 and 5.39 tabulate the maximum bending stress for catenary and straight line lift trajectories respectively which in both cases occurs at the seabed end. Two distinguishing features should be noted:

- During ascent the bending stress at the seabed increases for the catenary lift trajectory and decreases in the case of the straight line trajectory. Therefore the maximum bending stress imposed during the catenary lift trajectory doesn't occur until the riser attains its operational condition.

- At the start of the ascent the bending stress values at the seabed are found to be considerably higher for the straight line case than those resulting from a catenary lift profile, this difference however depreciates to zero as the top end of the riser

ascends towards the surface. At an upper end elevation of 250 m the calculated maximum bending stress for the straight line profile is over five times that experienced during the catenary lift.

The catenary lift trajectory holds the riser very taut thereby minimising the sag and hence curvature within the system. As the riser is pulled towards the surface and hence closer to its operational geometry more sag is introduced with the result that the bending stress at the seabed is increased. The straight line trajectory generates considerable curvature at the seabed as lift commences, however this is shown to progressively reduce as more riser is pulled off the seabed, resulting in a decrease in maximum bending stress throughout the ascent.

The graphs in Figure 5.40 illustrates how the bending stress at the seabed (maximum) changes between the two lift trajectories at a specified riser upper end elevation. As the upper end of the riser is moved horizontally from point (a) to point (b) (straight line to catenary respectively, see Figures 5.34 and 5.37) at any one of the five levels, the bending stress is shown to decrease. These graphs present data consistent with results already expressed above and are useful in establishing a lift trajectory tolerance. In a practical situation an exact lift trajectory such as the catenary curve could not possibly be adhered to exactly especially when non-ideal environmental conditions may exist. Figure 5.40 is therefore a valuable tool in terms of providing an operator with data on how far he can allow the upper end of the riser to stray from the ideal line without risk of damage to the to the system. It should be noted that the consequences of pulling the upper end of the riser to the right of the catenary lift trajectory include excessive axial loading of both the riser and lifting cable with the risk of exceeding their tensile strengths. The capability of the lifting barge is also a determinate factor on high far to the right the upper end of the riser can be pulled.

5.3.8 Failure Analysis

The results presented so far indicate that the highest axial stressing is generated as a result of the catenary lift trajectory where as the highest bending stresses are found to be a feature of a straight line lift profile. Since the axial stressing is tensile it therefore presents less of a problem than bending which is the predominate cause of buckling.

If the maximum strength criteria established in Section 5.2 is applied it can be confidently ascertained that the straight line lift trajectory would result in failure of the riser through buckling at the seabed (point of maximum bending stress). Calculated maximum bending

stresses exceed those determined using the buckling strength formula (Eqn (5.2)) by just over 100%.

5.3.9 The Effects of Riser Geometry on Lifting Loads

As previously mentioned, the catenary trajectory, through a simple trial and error analysis was found to be the most ideal in terms of minimising the bending loads and as a consequence of this a lift analysis using this trajectory has been conducted upon catenary risers with horizontal surface offsets of 1000 and 2000 m. The purposes of this is to establish the effects that riser geometry has on the loads exerted during lift. As the horizontal surface offset is increased the following trends can be observed for a given lift elevation and submerged unit weight (see Figures 5.41 to 5.46) :

- Horizontal load increases
- Vertical load increases
- Axial stress increases
- Bending stress reduces

The first three characteristics can be explained by simply noting that increasing the risers horizontal surface offset necessitates a greater length of riser and hence there is more suspended weight to be supported. Increasing the horizontal surface offset also reduces the risers curvature during lift resulting in smaller bending stress throughout the length of the riser.

5.4 Surface Connection Assembly

When the catenary riser is exposed to externally applied forces such as those generated by either a sea current acting upon it or the displacement of the surface or sub-surface vessel the upper end of the riser is forced to pivot. If however rotation or angular deflection is resisted by the connection assembly at the vessel interface bending stresses are induced which can be considerable and because both current loading and surface disturbance are constantly varying fatigue loading also becomes a serious issue. Therefore in order to ensure production feasibility under severe operating conditions these loads have to be minimised. This can be achieved through the use of a flex-joint which limits the bending stresses transmitted to connecting members by accommodating all combinations of angular, tension and radial forces. The flex-joint was developed and is currently manufactured by an American company called Oil States Industries (OSI) based in Arlington, Texas.

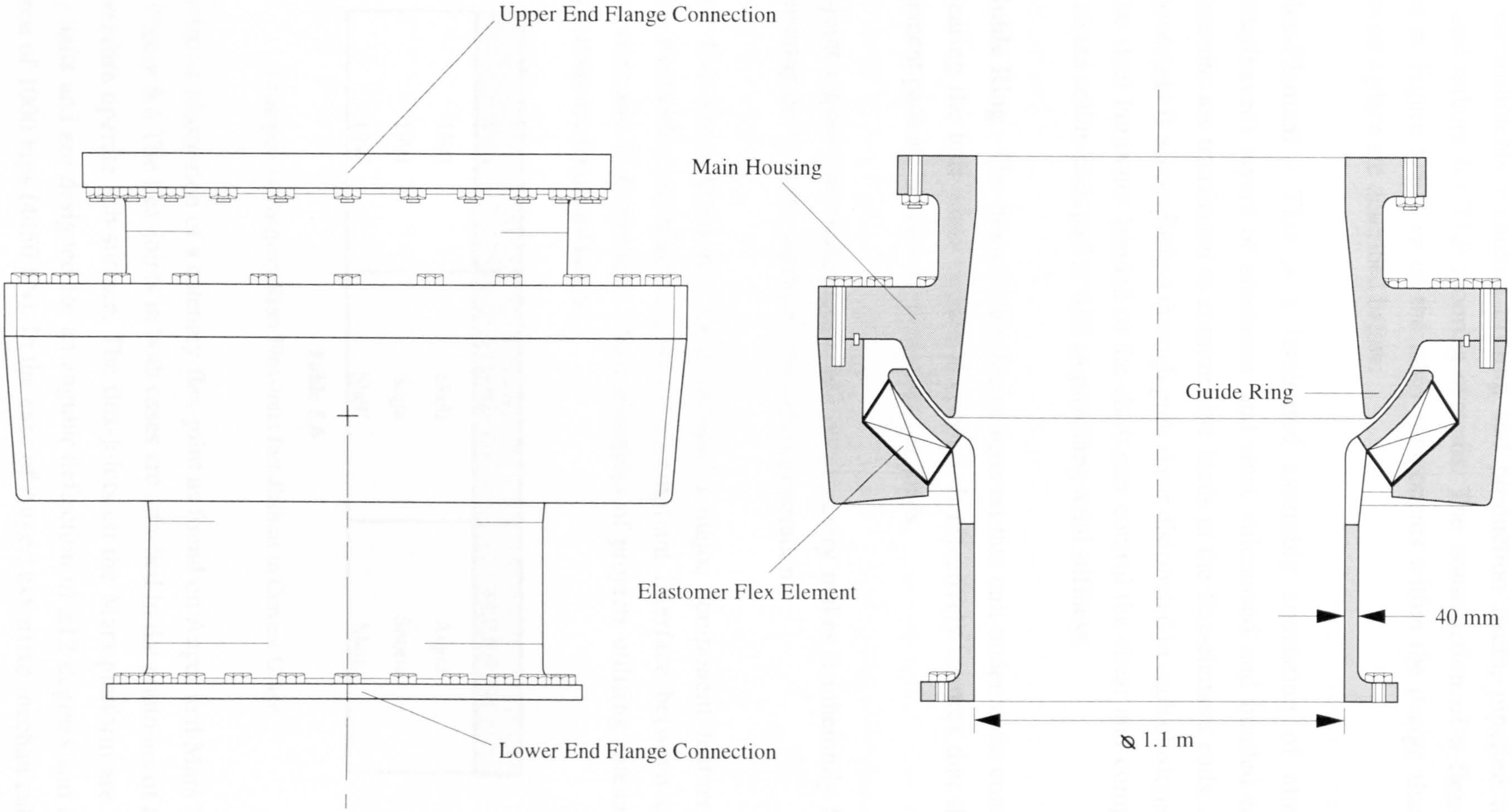

Figure 5.5

Flex-Joint

Scale 1:20

Flex-joints are utilised as load and motion compensation components in all types of offshore environments including drilling and production risers, pipeline transport systems, and tethers for TLP mooring systems. The construction of a flex-joint is illustrated in Figure 5.5. Two of the main components within the design that enable rotation to take place are described below:

Flex-Element - This is a laminated assembly consisting of alternating (interleaved) layers of elastomer and steel vulcanised and bonded together. Tensions are transferred to compressive loads in the flex-element pads. Angular movement is accomplished through pure shear distributed in each elastomer layer. The steel laminates bonded to the elastomer control the shear and compression stresses within each pad as well as providing axial stiffness.

Guide Ring - The flex-element flange rests on this unit under static conditions , clearing the unit when tension is applied. It effectively ensures that the flex-element pads are never subjected to tensile loads.

The flex-joint requires no maintenance and its geometry makes it inherently fail-safe thereby ensuring the systems suitability for sub-sea operation.

In the last five years flex-joints have become a major component feature within connection assemblies seeking to provide a compliant interface between catenary production riser and TLP platform. Three examples of projects utilising catenary flex-joint installations are tabulated below:

Year	User	TLP Project
1991	Shell	Auger
1991	Saga	Snorre
1995	Shell	Mars

Table 5.6

Examples of Catenary Riser Flex-Joint Installations in Current Usage

A representative illustration of a catenary flex-joint as found on Auger and Mars TLP's is shown in Figure 5.6 The flex-joints in both cases are attached to the pontoons of the TLP and so therefore operate sub-surface. The flex-joints on the Mars platform are 18 inch (457 mm) units and are designed for an angular deflection of ±12 degrees and an axial tensile force of 1000 kips (4450 kN). In the case of Auger, extensive mechanical testing was carried out on a prototype unit before final production units were put into operation.

The objectives of these tests were to (1) demonstrate the structural integrity of the flexible joint, (2) demonstrate that the flexible joint has sufficient fatigue life and (3) experimentally determine the failure mode of the flexible joint. The following conclusions were drawn from the results:

(1) Elastomer fatigue performance, although not precisely predictable is adequate.
(2) The failure mode of the flex-joint is not catastrophic
(3) The flex-joint would most likely function without leaking even if cracks were present. This is due to the presence of high axial loads that close any cracks that develop.

As Figure 5.7 illustrates both Auger and Mars projects utilise single flowline steel catenary risers which are hung off from one of the TLP pontoons. Riser articulation with the pontoon is achieved using a flex-joint assembly thereby necessitating a flex-joint for each riser. This study however proposes to connect a carrier pipe to a flex-joint and allow multiple flowlines bundled together to pass through it. In order to achieve this, the flex-joint must have an internal diameter large enough to accommodate a flowline bundle which for the proposed riser design (specified in Chapter 2) consists of:

- Two 12" production oil flowlines
- Two 8" wellhead injection flowlines
- One electrical umbilical
- (Several small diameter buoyancy gas injection lines)

An approximate minimum diameter based upon both flowline dimensions and the required expansion clearances would be 1.0 m, which is more than twice the diameter of the unit currently employed on the Mars platform. The maximum axial design load would also have to be significantly uprated to take into account the operating depth specification of 1500 m. The flex-joints on Auger are designed to accommodate axial loads generated by a single flowline for 872 metres of water.

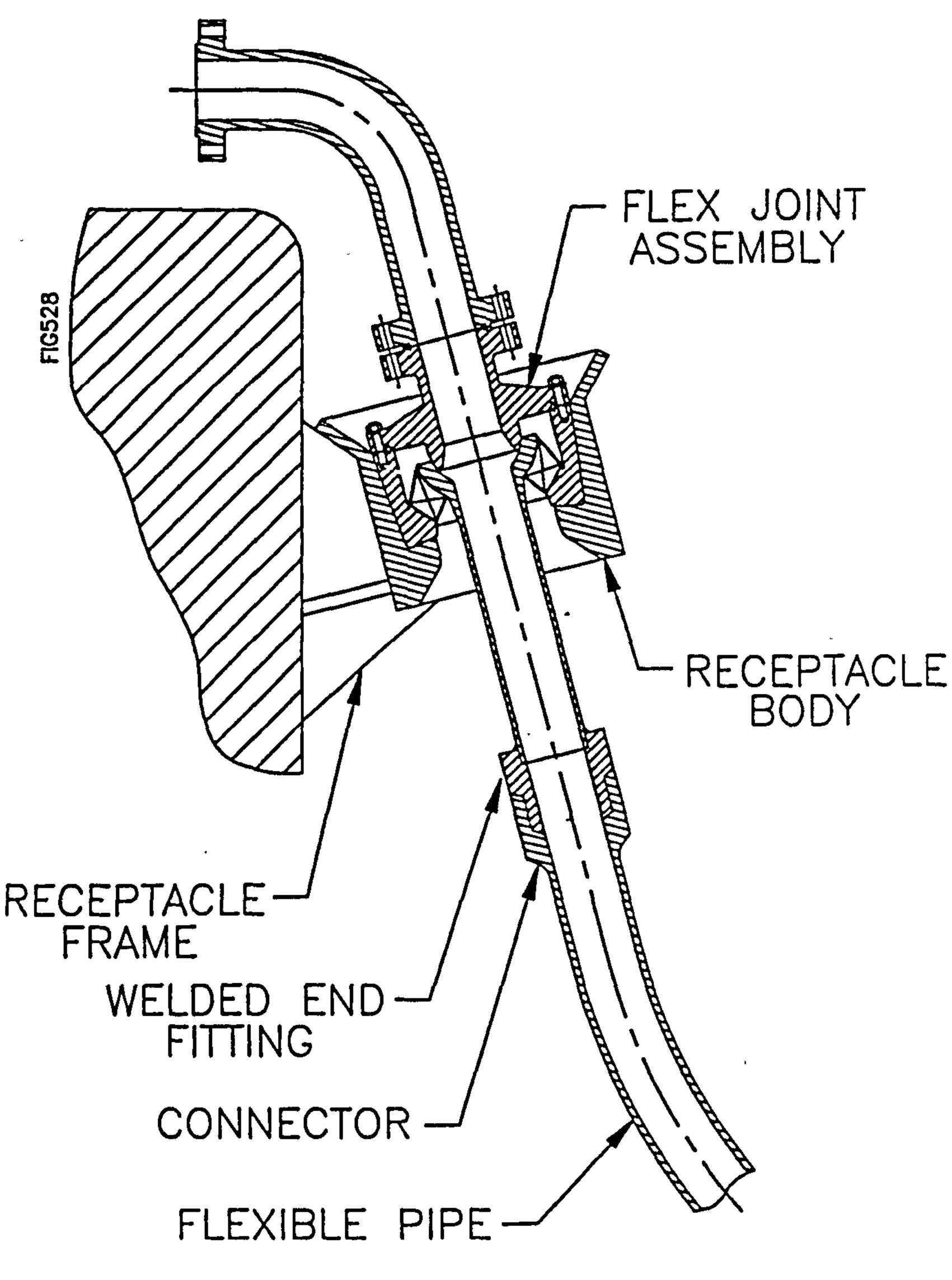

Figure 5.6
Auger TLP Catenary Riser Flex-Joint Unit

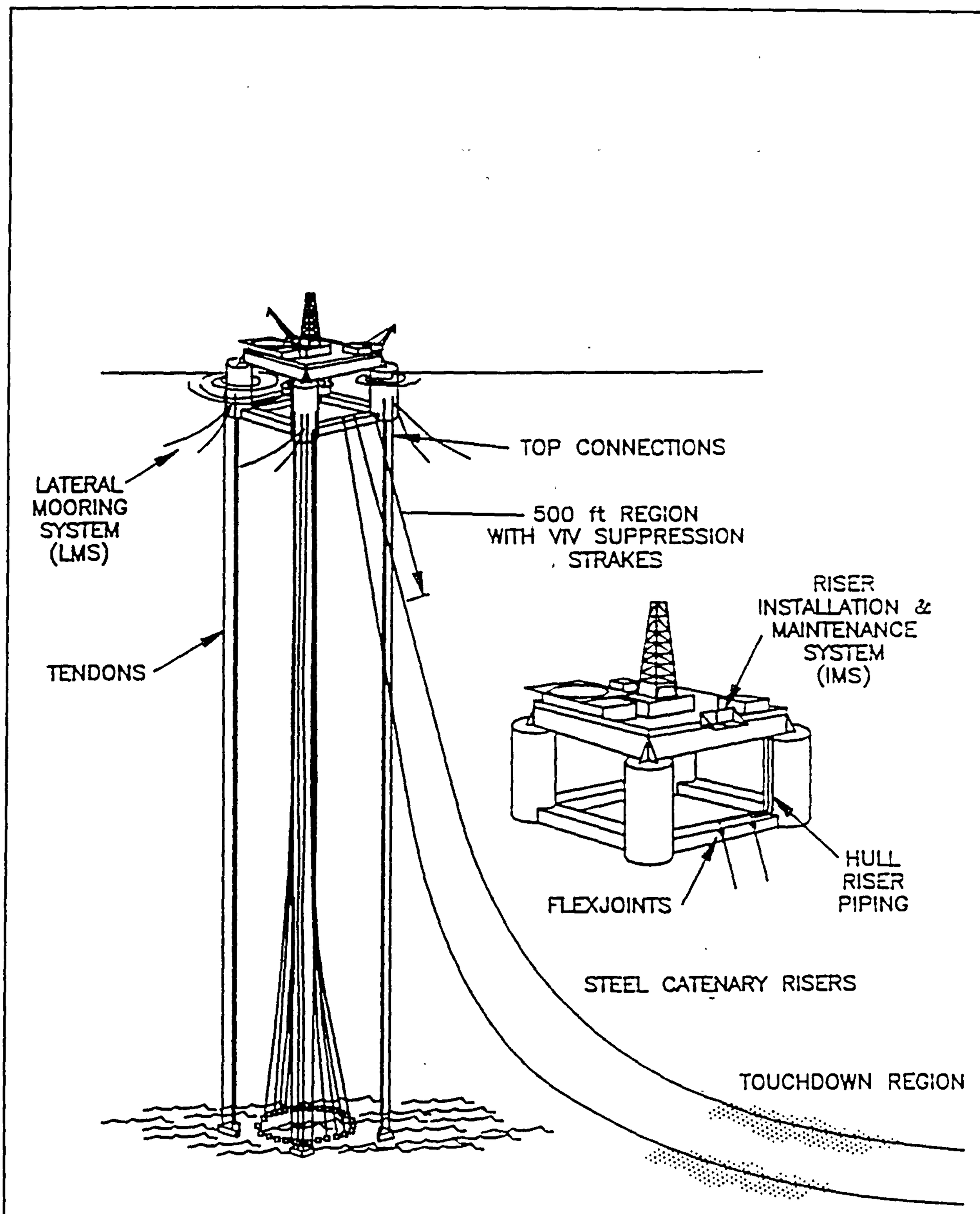

Figure 5.7
Auger TLP Production System

After consultation with OSI the following design criteria was drawn up. The data below represents an preliminary estimation of what could be reasonably manufactured currently if required.

1. Maximum Axial Design Load	8000 kN
2. Maximum Design Deflection Angle	±15 degs
3. Rotational Stiffness	10 kNm/deg
4. Internal Diameter	1.0 m

Table 5.7

Flex-Joint Design Criteria

It is proposed to attach the carrier pipe to the flex-joint using a flange connection. The flowlines which are steel (and load supporting) throughout the length of the riser would then connect into flexible composite flowlines below the flex-joint so as to ensure that they bend without generating both excessive loads and bending stiffness when the carrier pipe and flex-joint rotate. The intention is not to subject the flexible flowlines to any axial load, and so above the flowline connection point all the axial load will be transmitted within the carrier pipe to the flex-joint. To accommodate the extra axial load the wall thickness of the carrier pipe is increased. This arrangement is illustrated in Figure 5.8.

For both FPSO and sub-surface buoy concepts it is essential that the flowlines end up vertically oriented. This forms one of the main objectives behind a proposed connection assembly design which incorporates two flex-joints for an in-plane two riser arrangement. The assembly consists of a central load bearing component whose geometry can compared to that of an upside down 'Y'. The arms are set at an angle corresponding to the catenary risers design geometry (i.e. zero external load) with flex-joints attached at the ends to provide the necessary rotational capacity in order for external load conditions to be accommodated. The entire surface connection assembly design is illustrated in Figures 5.9 to 5.12.

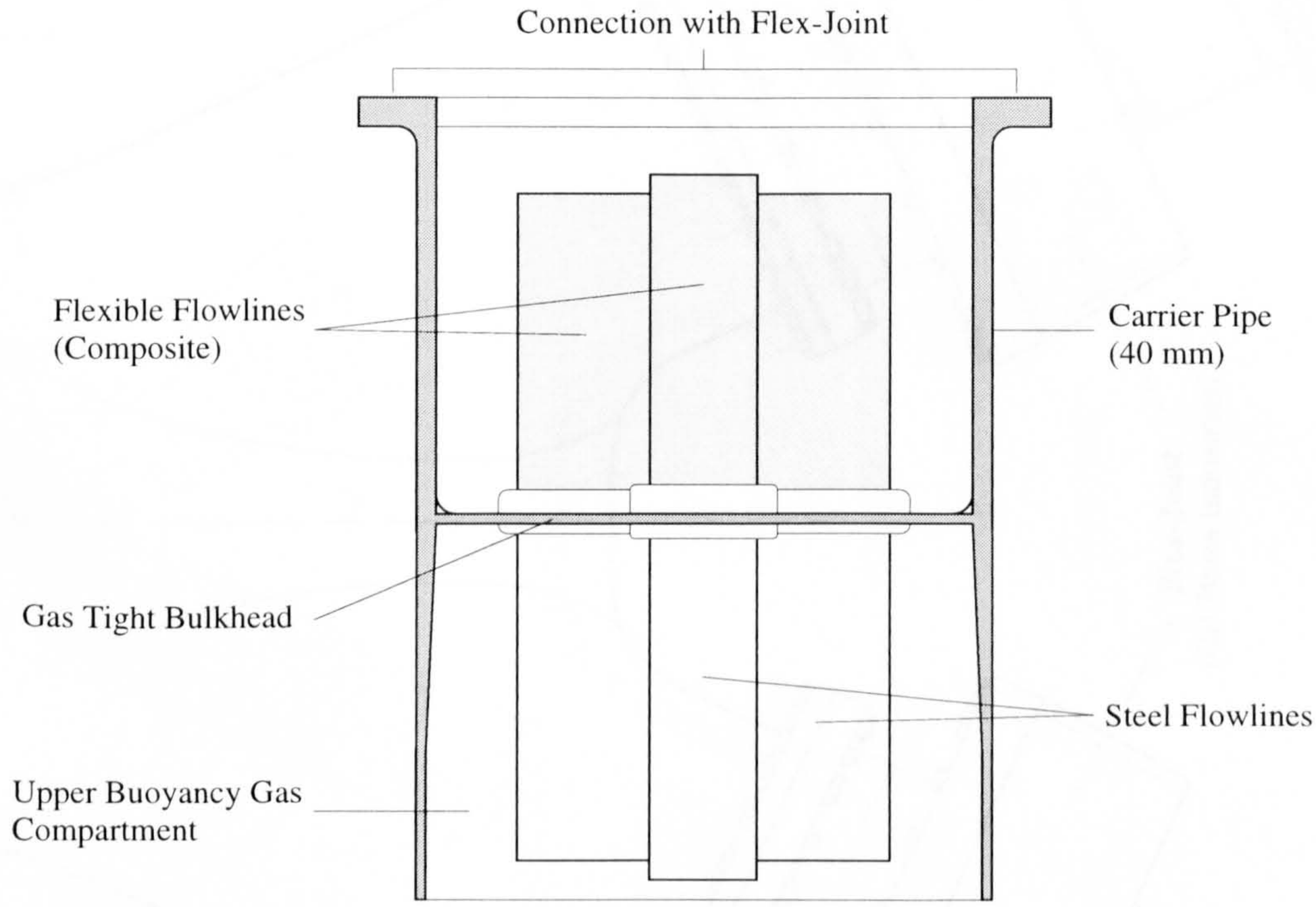

Scale 1:20

Figure 5.8

Upper End of the Riser (Cut-Away View)

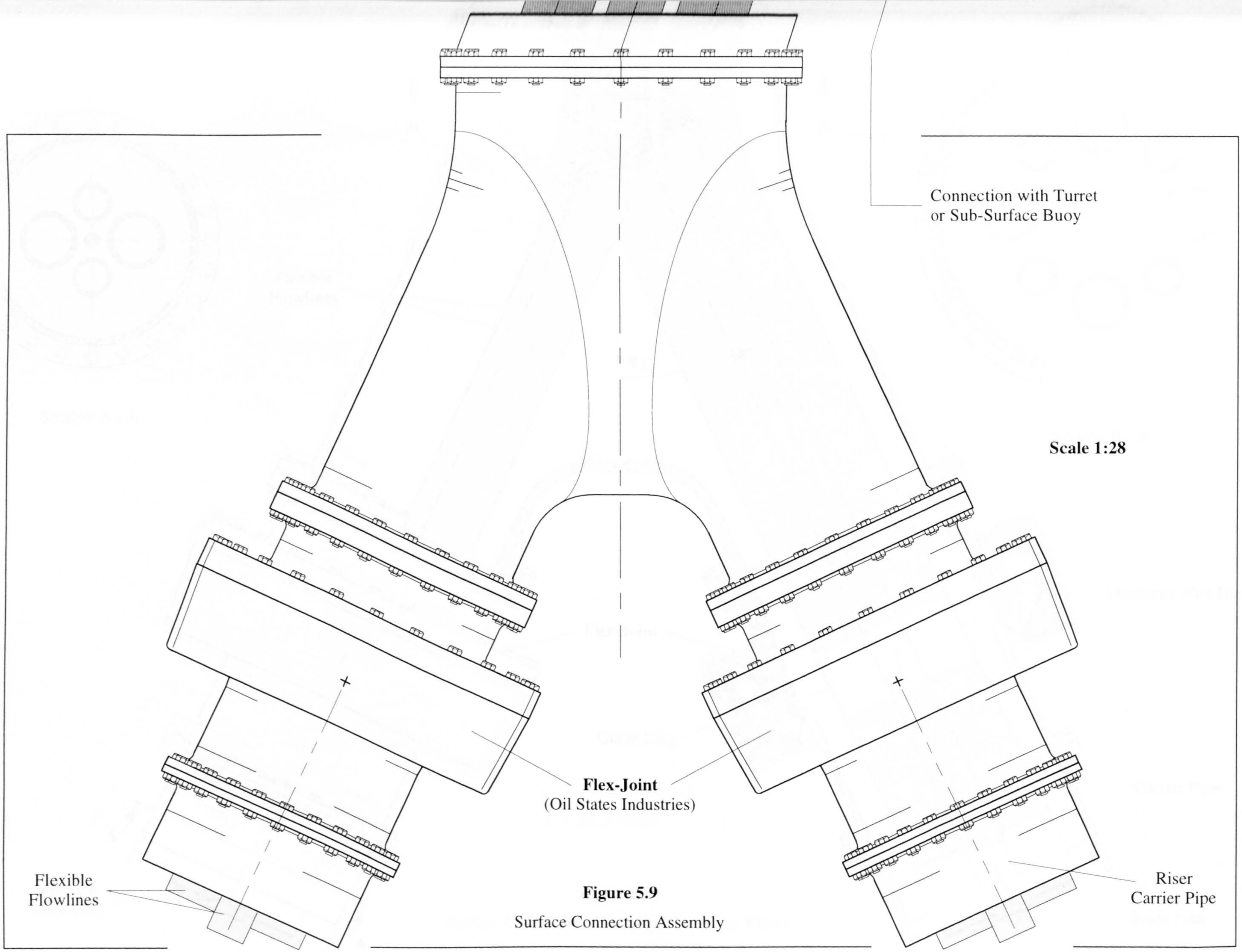

Figure 5.9

Surface Connection Assembly

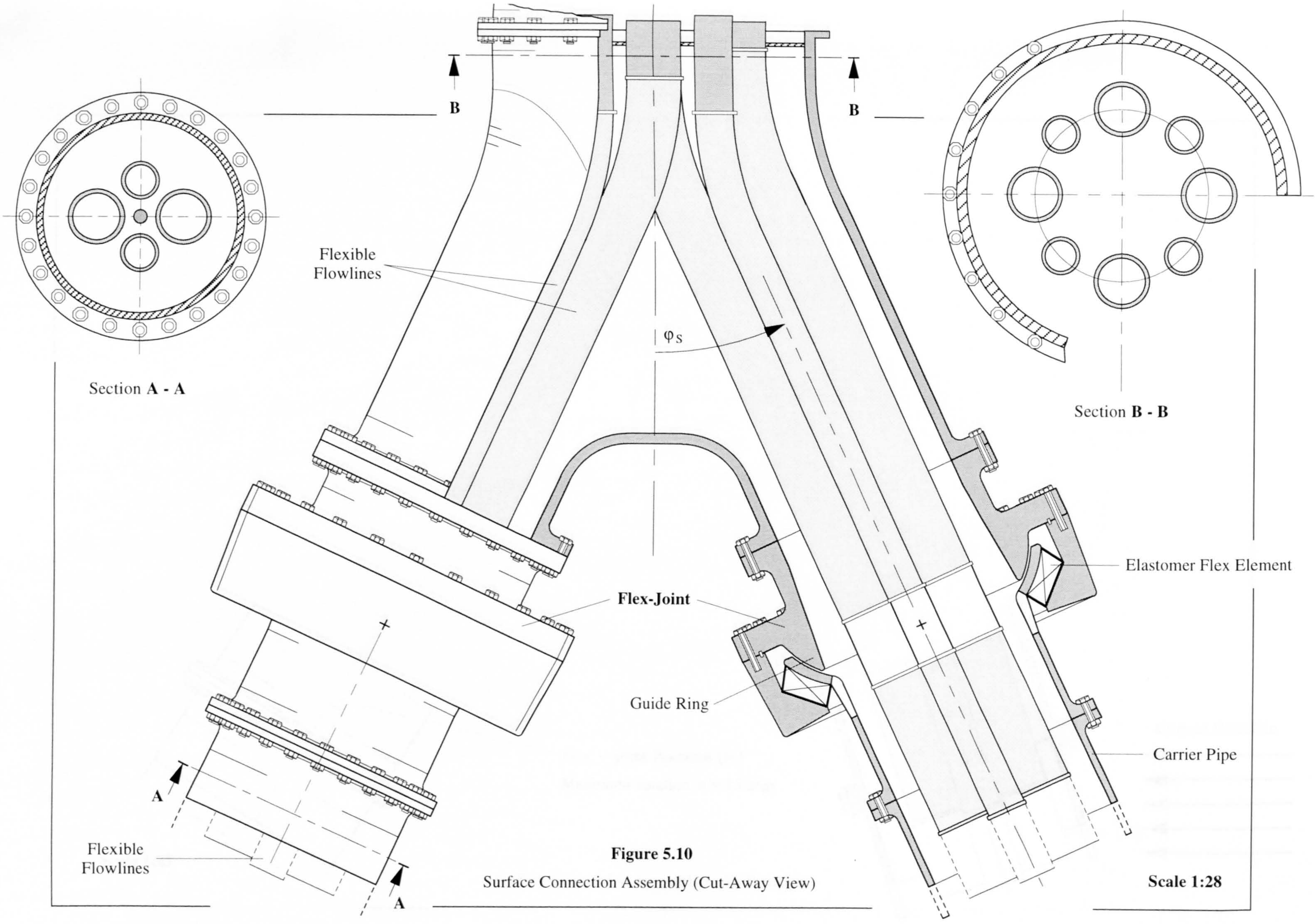

Figure 5.10

Surface Connection Assembly (Cut-Away View)

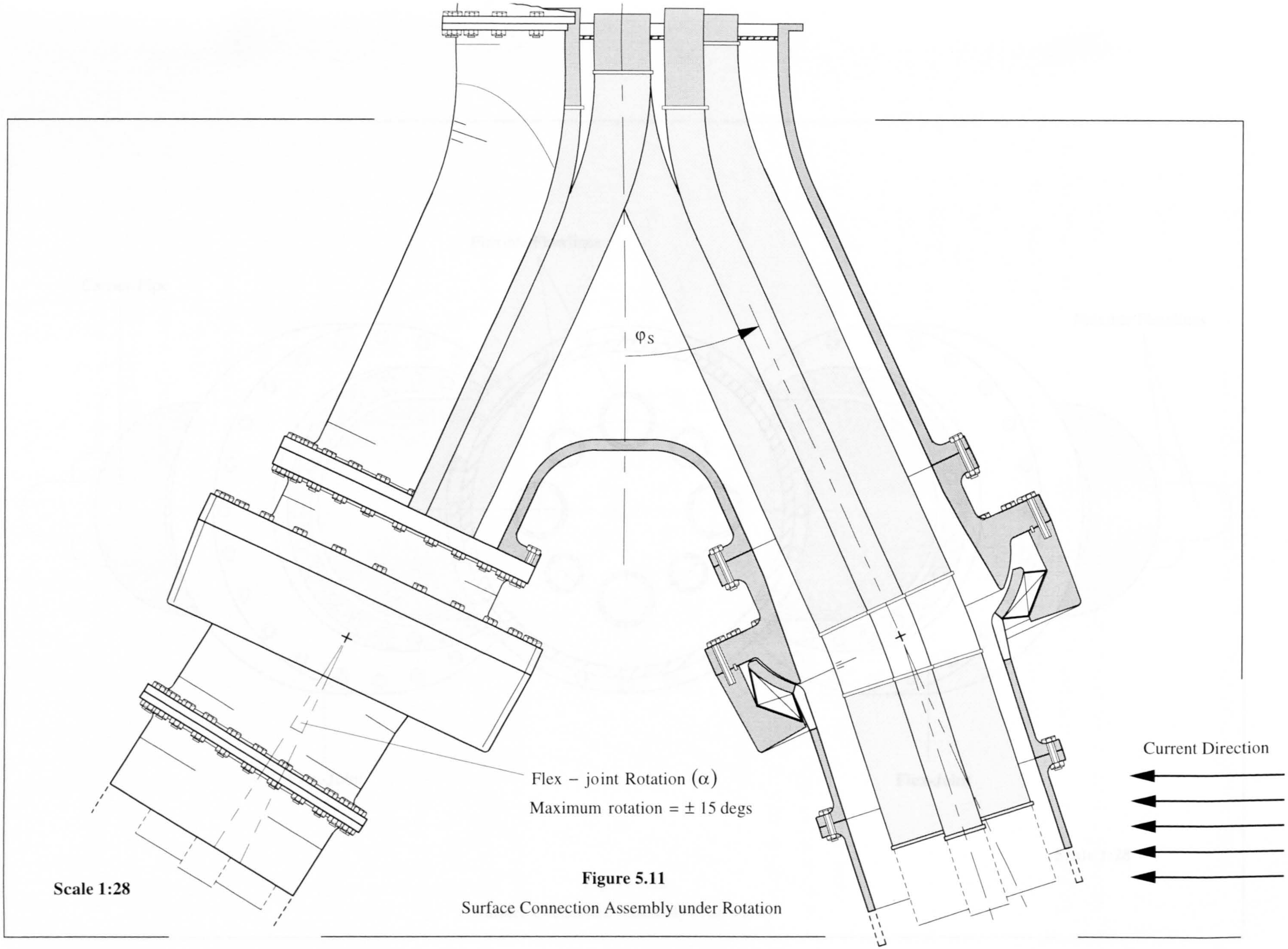

Figure 5.11

Surface Connection Assembly under Rotation

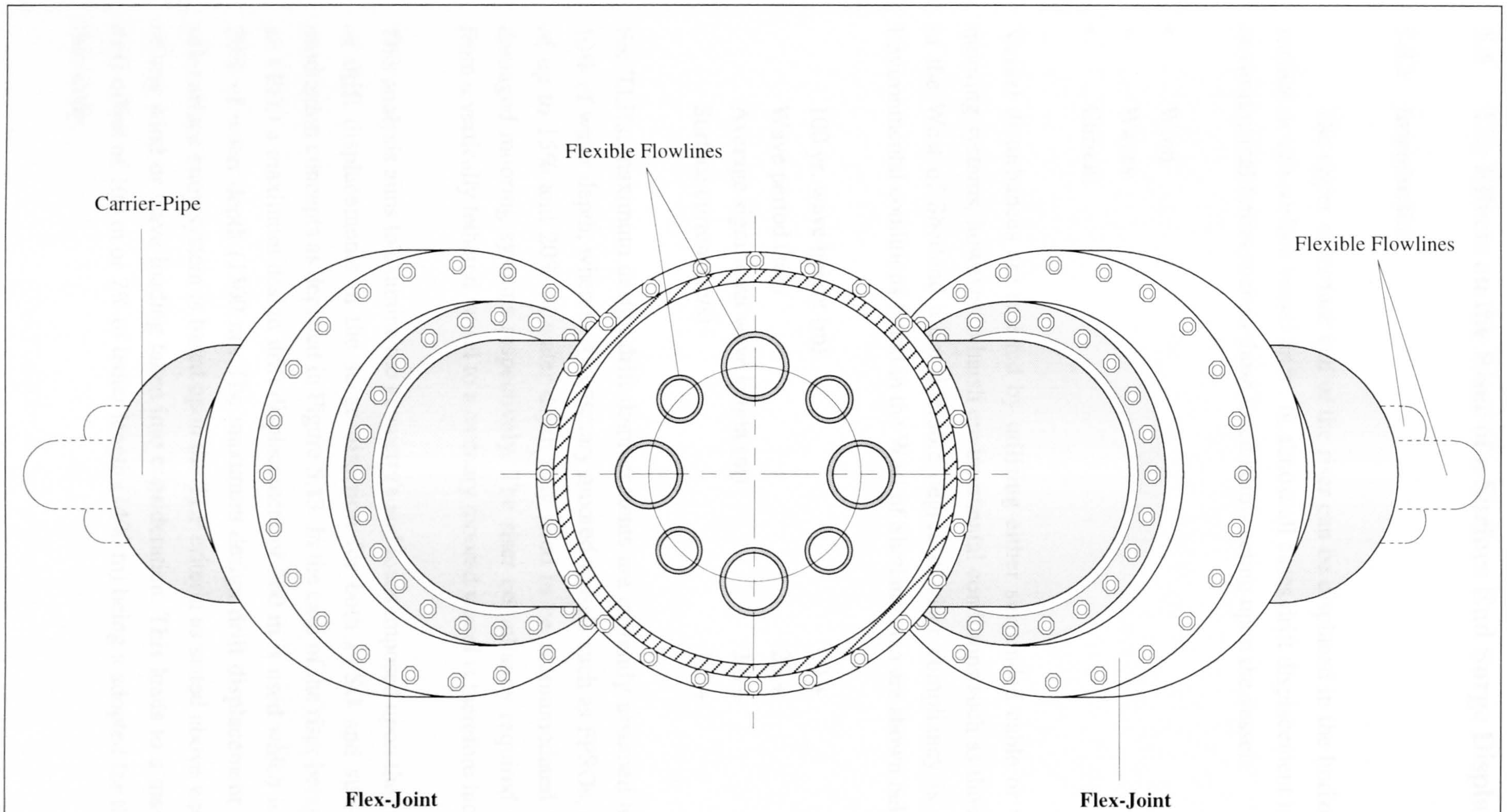

Figure 5.12

Surface Connection Assembly (Top View)

5.5 The Effects on the Riser of a Surface End Surge Displacement

5.5.1 Introduction

The upper or surface end of the riser can be displaced in the horizontal plane by surface or sub-surface vessel drift . In almost all cases drift displacement is generated by environmental forces such as those listed below acting upon the vessel.

- Wind
- Waves
- Current

Vessel disturbances are resisted by utilising either suspended cable or vertical tether mooring systems, however in harsh environmental conditions such as those experienced in the West of Shetland a considerable degree of riser compliancy is still required. Environmental conditions found in the West of Shetland area are shown below:

100 yr. wave height (m)	30 +
Wave period (sec)	20 +
Average significant wave height (m)	3.0 +
Surface current (m/s)	1.0 +

For TLP's, maximum design drift displacements are currently assumed to be less than 10% of water depth, whereas for catenary moored vessels such as FPSOs, displacements of up to 15% and 20% of water depth may need to be accommodated for intact and damaged mooring systems respectively. The riser compliancy required when moving from a vertically tethered vessel to a catenary moored vessel is therefore increased.

This analysis aims to examine the geometry's and loads imposed upon the riser as a result of drift displacements in the surge direction for both FPSO and sub-surface buoy production concepts as depicted in Figure 5.13. In the case of the riser being connected to an FPSO a maximum design drift displacement of 300 m is used which is equivalent to 20% of water depth (1500 m). The maximum design drift displacement for a tethered sub-surface buoy system is based upon the TLP criteria as stated above with the absence of any wind or wave loading taken into consideration. This leads to a maximum design drift offset of 100 m or 7% of tether length (1400 m) being a adopted for the purposes of this study.

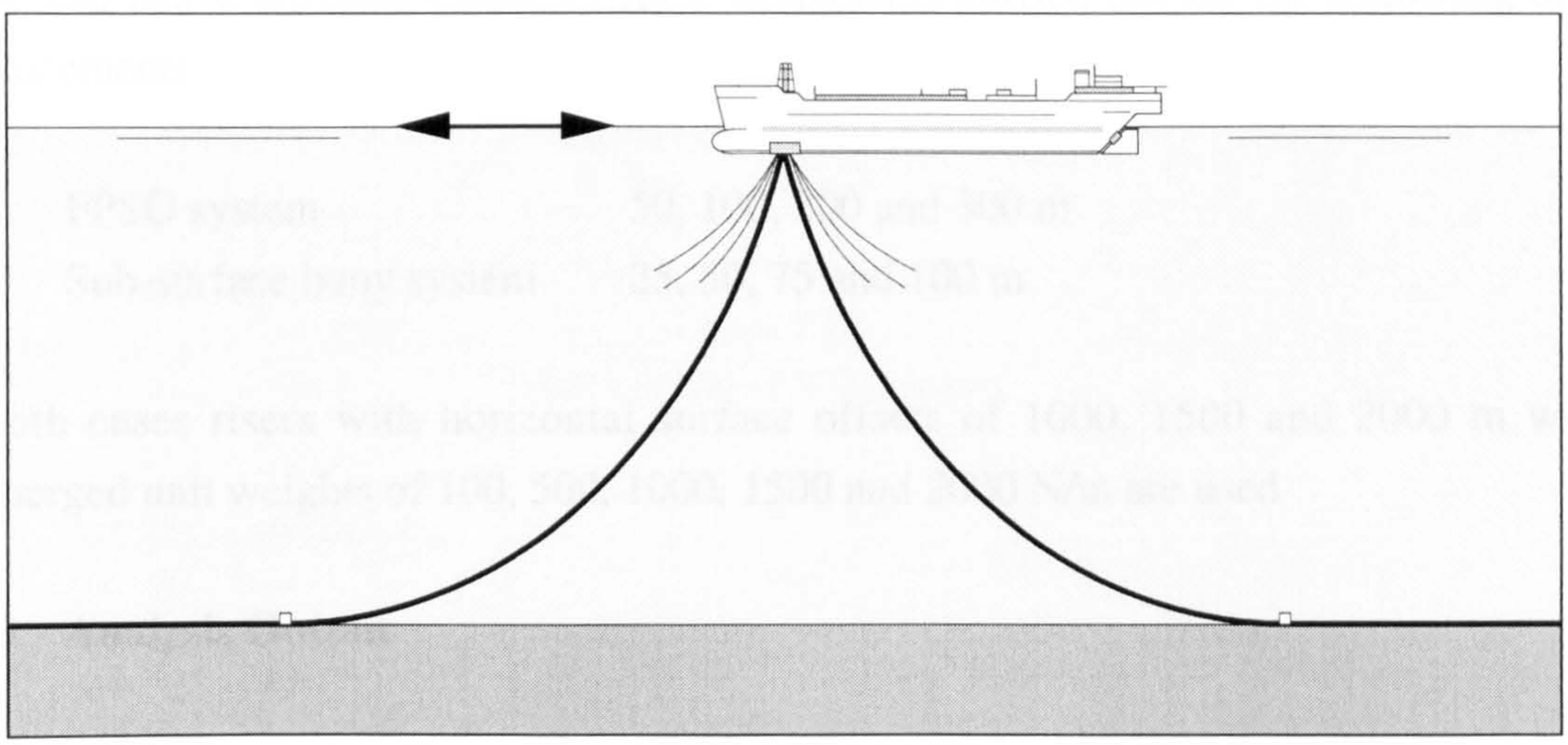

(a) FPSO Based Production System

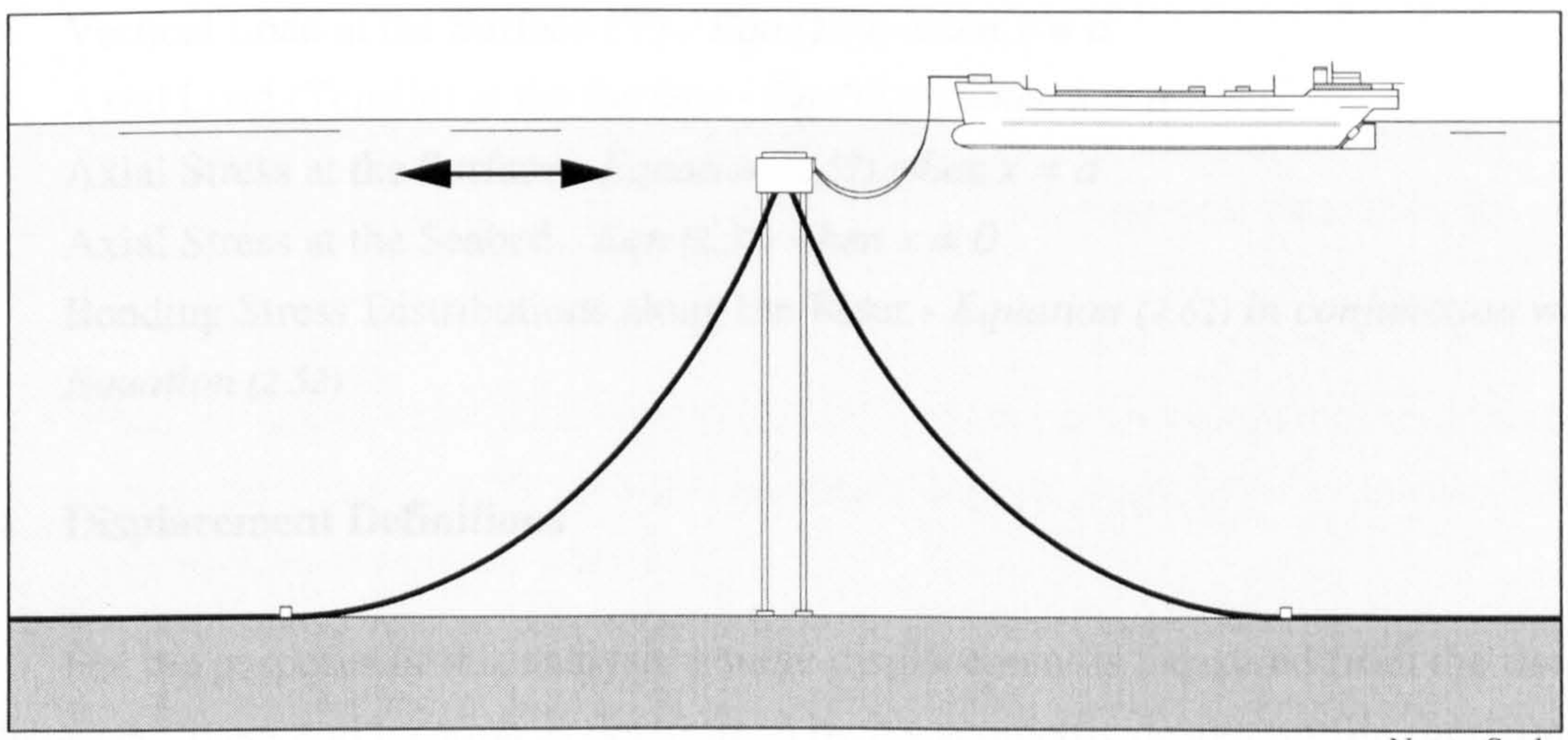

Not to Scale

(b) Sub-Surface Buoy Based Production System

Figure 5.13

Surge Displacements for Two Production Concepts

5.5.2 Computer Modelling

Surface displacement riser profiles and generated loads are attained using the same FORTRAN program and EXCEL spreadsheet as used in Section 2.4 to establish surge and heave stiffness characteristics. Analysis is carried out for the following drift displacements:

FPSO system	50, 100, 200 and 300 m
Sub-surface buoy system	25, 50, 75 and 100 m

In both cases risers with horizontal surface offsets of 1000, 1500 and 2000 m with submerged unit weights of 100, 500, 1000, 1500 and 2000 N/m are used

5.5.3 Analysis Output

This analysis ascertains the following geometric and loading characteristics generated as a result of an upper end in-plane surge displacement:

(a) Surge Displacement Profiles
(b) Riser Inclination at the Surface - *Eqn (2.44) when $x = a$*
(c) Horizontal Load at the Surface (H) - *H*
(d) Vertical Load at the Surface (V) - *Eqn (2.58) when $x = a$*
(e) Axial Load (Tensile) at the Surface - *Eqn (2.57) when $x = a$*
(f) Axial Stress at the Surface - *Equation (2.57) when $x = a$*
(g) Axial Stress at the Seabed - *Eqn (2.57) when $x = 0$*
(h) Bending Stress Distributions along the Riser - *Equation (2.62) in conjunction with Equation (2.52)*

5.5.4 Displacement Definitions

For the purposes of this analysis a surge displacement is measured from the riser's un-displaced upper end location as determined by it's geometric design profile (horizontal surface offset). Its direction from this position is defined as follows:

Positive Displacements -	upper end of the riser is shifted in a direction away from its designed seabed touch down point
Negative Displacements -	upper end is moved towards its designed seabed touch down point

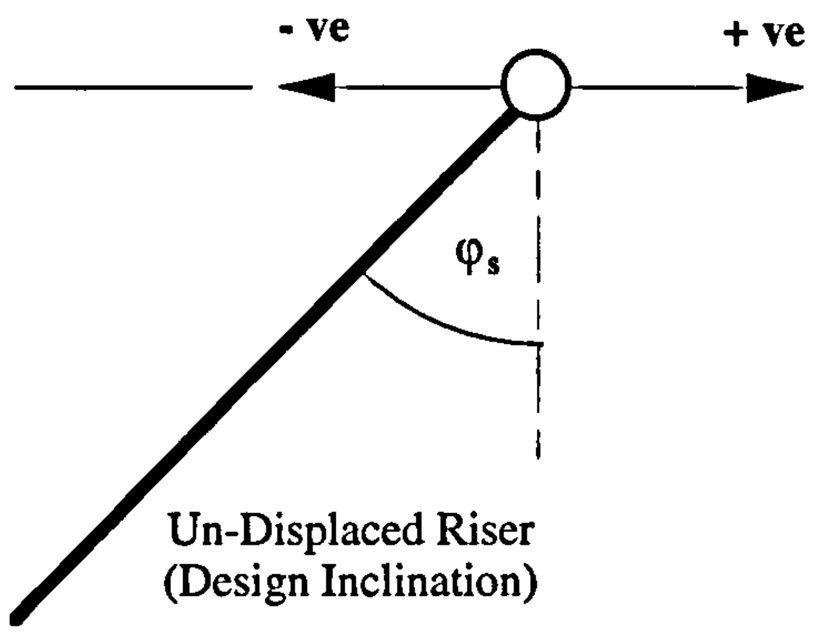

Figure 5.14
Drift Displacement Definitions

5.5.5 Seabed Conditions

This analysis is based upon the same zero slope condition as previously utilised in the installation case i.e. the riser attains a level attitude as it reaches the seabed. The analysis also allows the connected seabed pipeline to be pulled off the seabed when the risers upper end is positively displaced This should have the effect of reducing bending stresses at the seabed, however its practicality is still to be determined.

5.5.6 Geometric and Loading Characteristics

Riser Profile

The riser profiles resulting from in-plane drift displacements demonstrate two characteristics:

- When the upper end of the riser is shifted in a direction away from its designed seabed touch down point (positive displacement) the seabed end plus connecting pipeline is pulled off the seabed.
- When the upper end is moved in the opposite direction i.e. towards its designed seabed touch down point (negative displacement) the riser is deposited on the seabed.

The length of riser and pipeline which is either pulled off on deposited on the seabed is termed the *touch-down length*. Both un-displaced and displaced riser geometry's are illustrated in black and red respectively in graph (a) of Figures 5.47 to 5.57.

The touch down length is a direct function of both the magnitude of the drift and the original design geometry of the riser which in this study is dictated by the risers horizontal surface offset *(a)*. The effect of increasing the horizontal surface offset from 1000 to 2000 m is to increase the touch down length for a given surface displacement. The objective for the designer is to limit this length so as to reduce the amount of abrasion inflicted upon the riser and pipeline surface.

Maximum drift offsets corresponding to the FPSO production system create large touch down lengths and for horizontal surface offsets of 1500 and 2000 m the length would clearly be unacceptable. Results obtained for the sub-surface buoy system are significantly more favourable since the maximum drift is only a third of that used for the FPSO system. A horizontal surface offset of 1000 m offers the optimum riser geometry out of all those considered, however the other two geometry's (a = 1500 and 2000 m) would all be considered acceptable.

Surface Inclination

Angular deflection of the risers surface end from its design inclination (dictated by its design geometry) which is generated as a result of a surface drift displacement is tabulated in table (b) within Figures 5.47 to 5.57. The effects of the risers design geometry as determined by it's horizontal surface offset on deflection angles is also demonstrated. A summary of the rotational data comprehensively presented in Figures 5.47 to 5.57 for both FPSO and sub-surface buoy systems is tabulated below in Tables 5.8 and 5.9.

Horizontal Surface Offset (m)	**Angular Deflection (degs)** -300 m	-100 m	+100 m	+300 m
1000	-9.6	-3.8	+4.6	+16.4
1500	-13.3	-5.2	+6.1	+21.3
2000	-16.5	-6.4	+7.3	+25.0

Table 5.8

Calculated Rotations for the FPSO System

Positive and negative angles of deflection are defined diagramatically in Figure 5.15.

Horizontal Surface Offset (m)	Angular Deflection (degs) -100 m	-50 m	+50 m	+100 m
1000	-4.4	-2.3	+2.5	-5.2
1500	-5.8	-3.0	+3.3	-6.9
2000	-7.1	-3.6	+4.0	-8.3

Table 5.9

Calculated Rotations for the Sub-Surface Buoy System

The following conclusions can be drawn from Tables 5.8 and 5.9:

- Increasing the drift displacement increases the deflection angle
- A negative displacement generates a smaller deflection angle than a positive displacement of equal magnitude
- Increasing the risers horizontal surface offset has the effect of increasing the angular deflection for a given displacement

The results above reveal problems in terms of the upper end rotating beyond the flex-joints maximum rotational capability of ±15° for maximum FPSO displacements for all three riser geometry's. This is however not the case for the sub-surface buoy system where the maximum rotational capability of the flex-joint is not exceeded for any of the conditions and parameters imposed. The results in fact illustrate the existence of considerable spare deflection capacity which is extremely valuable in terms of accommodating other loads such as current.

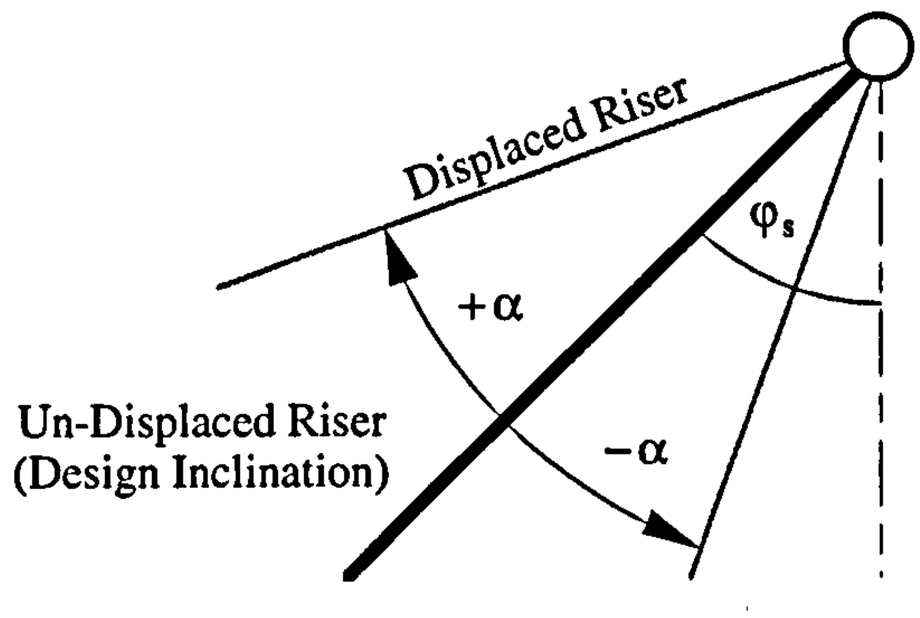

Figure 5.15

Rotational Definitions

Axial Load at the Surface

The change in axial force exerted upon the flex-joint unit as a result of a surface drift displacement is illustrated in graph (e) within Figures 5.47 to 5.57 The sensitivity of this load change to riser parameters such as submerged unit weight and catenary geometry is also demonstrated.

The direction and magnitude of the displacement determines the extent to which the suspended structural length changes as previously established. If the system is subjected to a positive surface drift the amount of suspended structure increases with a resulting increase in surface load. However if the drift is negative more riser/pipeline is deposited on the seabed consequently reducing the suspended length and hence the axial load on the surface connection.

The influence of the risers design geometry on the change in axial load as a result of displacement is demonstrated in the tables below. Surface axial load data presented in Figures 5.47 to 5.57 is summarised below for both FPSO and sub-surface buoy systems using a riser with a submerged unit weight of 2000 N/m (the heaviest examined in this study).

Horizontal Surface Offset (m)	Axial Load (kN)				
	-300 m	-100 m	0	+100 m	+300 m
1000	3244	3636	3951	4399	6063
1500	3569	4265	4856	5753	9733
2000	3952	5057	6067	7727	17008

Table 5.10

Calculated Axial Loads for the FPSO System

The effect of altering the risers design geometry by increasing its horizontal surface offset is to increase the change in load for a given displacement. Utilising the data above, if a = 1000 m a drift displacement of +300 m increases the axial surface load by 53% compared to 100% for a = 1500 m and 180% for a = 2000 m. Increasing *a* has the effect of increasing the length of riser being pulled off the seabed for a given displacement.

In the case of the FPSO system the results show that the flex-joints maximum axial design load of 8000 kN is exceeded when the following parameters and conditions are imposed:

a = 1500 m	w = 2000 N/m	Displacement > +200 m
a = 2000 m	w = 1500 N/m	Displacement > +200 m
	w = 2000 N/m	Displacement > +100 m

The flex-joints maximum design load is not exceeded in the case of the sub-surface buoy system as verified by the table below (w = 2000 N/m).

Horizontal Surface Offset (m)	Axial Load (kN)				
	-100 m	-50 m	0	+50 m	+100 m
1000	3448	3604	3792	4018	4296
1500	4091	4385	4750	5210	5798
2000	4896	5395	6039	6889	8000

Table 5.11

Calculated Axial Loads for the Sub-Surface Buoy System

This is partially due to the slightly shorter riser lengths involved (vertical offset = 1400 m) but primarily due to the smaller maximum design drift displacements.

Axial Stress

Axial stress is a direct function of axial load and therefore follows the same characteristics when drift displacement takes place. The maximum axial stress (exerted at the risers upper end) is found to remain below maximum permissible levels as established in Section 5.2 for both FPSO and sub-surface buoy maximum design displacements using all the varied parameters. It should be noted that under all conditions the riser is subjected to a tensile axial stress.

Bending Stress

The maximum bending load that is exerted upon the catenary productions riser always occurs at the seabed touch-down point irrespective of the surface ends position. This is

demonstrated clearly in graph (h) within Figures 5.47 to 5.57 The effects of surface displacement on the maximum bending load can be characterised as follows:

- If the surface end of the riser is subjected to a positive displacement then riser/pipeline is pulled off the seabed thereby reducing structural curvature at the seabed ultimately resulting in a decrease in bending stress.
- If the surface end of the riser is subjected to a negative displacement then riser is deposited on the seabed consequently increasing structural curvature and hence bending stress at the seabed.
- The extent to which bending stress either increases or decreases is a non-linear function of displacement magnitude.
- A negative displacement generates a greater change in bending load than a positive displacement of equal magnitude.

Actual bending stress values are tabulated in Tables 5.48 to 5.58 for both FPSO and sub-surface buoy systems using catenary risers of varying diameter and horizontal surface offset. The effect of changing the risers geometry by increasing the horizontal surface offset parameter is to reduce the seabed curvature and hence maximum bending stress for any given displacement. This means that a = 2000 m provides the optimum catenary geometry out of all those considered in terms of limiting bending stress and ultimately minimising the risk of local buckling.

The maximum permissible bending stress (as established in Section 5.2) is shown to have been exceeded in the following cases:

<u>FPSO System</u>

a = 1000 m	Displacement > -50 m
a = 1500 m	Displacement > -200 m

<u>Sub-Surface Buoy System</u>

a = 1000 m	Displacement > -50 m

This again illustrates the advantages of a sub-surface buoy system

5.6 The Effects of Subjecting the Riser to a Current Load.

5.6.1 Introduction

The aim of this analysis is to establish both the loading and deflection behaviour of a catenary riser when exposed to an in-plane current load. The analysis is undertaken using a finite element software package to model the riser system in order that the following characteristics can be attained :

- Deflection profile
- Surface deflection angle
- Surface loads (horizontal, vertical and axial)
- Axial stress distribution
- Maximum bending stress and its location along the riser

If the sensitivity of these characteristics to current velocity are determined and subsequently analysed in conjunction with the maximum permissible riser loads as set out in Section 5.2 and maximum flex-joint design capabilities as stated in Section 5.3 limiting current velocities can then be established. Such an evaluation forms the main part of the study presented within this section and is conducted upon catenary risers of varying submerged weight and profile geometry.

5.6.2 Current Profiles

Oceanic sea currents can be broken down into several constituent components:

(a) Storm Surge Currents

(b) Tidal currents

These are generated as a result of tidal actions. They are regular and predictable and the maximum tidal current is associated with the lowest and highest astronomical tide.

(c) Residual currents

Huge volumes of water are transported and circulated as a result of density differences. These contrasts are created by variations in water temperature which are set up as a consequence of atmospheric conditions and by the mixing of cold and warm waters . An example of this is found in the NE Atlantic where the current system is predominantly governed by the mixing of warm water from the Mediterranean outflow and cold water

spreading down from the subarctic. It should be noted that residual currents are conditioned to a large extent by the local seabed topography.

(d) Sea-Surface Drift Currents

These are induced through the action of both wind and waves (Stokes drift) acting upon the sea surface and therefore only effect the transport of water within the upper layers.

Sea current profiles are therefore determined from a complex array of variables which has had the effect of limiting the development of prediction methods. The collection of suitable field data is very difficult and expensive. As a consequence, if any measurements are available through the water column for the site concerned these are generally used to define the shape of the current profile. Otherwise some combination of power law or logarithmic law variation near the seabed or surface are used as a starting point for the development of a plausible profile associated with the specific depth-averaged current magnitude.

In order to demonstrate the type of current profiles that risers are being designed for, so as to enable them meet the challenges of deep water, several examples are presented below:

1. Kvaerner Engineering Riser Project [Ref 5.9]

100 year return period current

Surface	1.5 m/s
25 m	1.35 m/s
50 m	1.25 m/s
100 m	0.8 m/s
250 m	0.4 m/s
Seabed	0.2 m/s

10 year return period current

Surface	1.2 m/s
25 m	1.05 m/s
50 m	0.95 m/s
100 m	0.6 m/s
250 m	0.3 m/s
Seabed	0.1 m/s

This data corresponds to Blocks 6303, 6305 and 6406 off the west coast of Norway for 1000 m of water.

2. Continental Slope Experiment [Ref 5.10]

The Continental Slope Experiment (CONSLEX) provided one of the most comprehensive collections of current data obtained from the NE Atlantic. The experiment was conducted from Autumn 1982 to Winter 1983 and covered the continental slope from West of Scotland to the North of Shetland. Figure 5.16 shows sketches of mean and maximal current speeds at the location of moorings which survived the experiment as illustrated in Figure 5.17.

3. Drilling Offshore Brazil [Ref 5.12]

Figure 5.18 shows two typical subsea current profiles taken at different times during deep water drilling operations off the Suriname coast. The two profiles illustrate the variability of the South Equatorial Current, also known as the Guiana Current which flows through the region from east to west parallel to the coastline.

4. Analysis of a 6,000 ft Drilling Riser During Installation and Storm Hangoff [Ref 5.13]

The current profile depicted in Figure 5.19 was used to asses the behavioural sensitivity of a deep water drilling riser to current velocities during operations. The current profile was increased linearly until the riser displacement attained its maximum design state which was determined from the maximum permissible bending stress and allowable rotation at the surface.

From all the research carried out into current characteristics the profile illustrated in Figure 5.19 appears provide a good general representation of them all. Although it is a simple profile it takes into account the influence of storm surge and surface drift in that the maximum current speed occurs at the surface. As the effects of storm surge and surface drift diminish with depth the velocity is tapered down to a value which is kept constant down towards the seabed.

This profile is adopted within the current sensitivity analysis conducted upon the proposed catenary riser design and presented within this section. From the research carried out a surface current velocity (U_s) of 1.3 m/s is selected which is then tapered down to a depth of 50 m from where it remains constant (U_c) down to a depth of 1400 m.

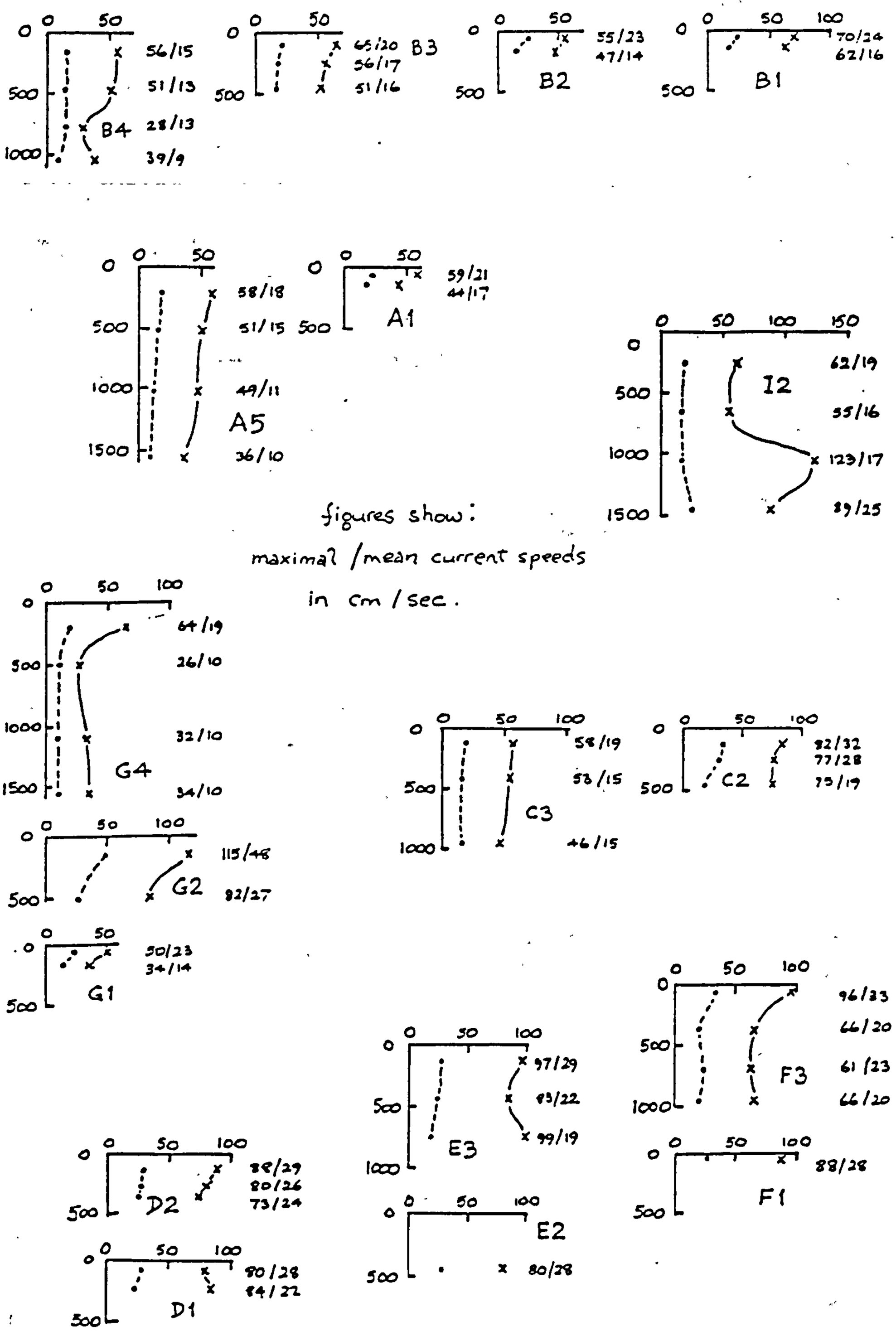

Figure 5.16

Current Profiles obtained from the Continental Slope Experiment (CONSLEX)

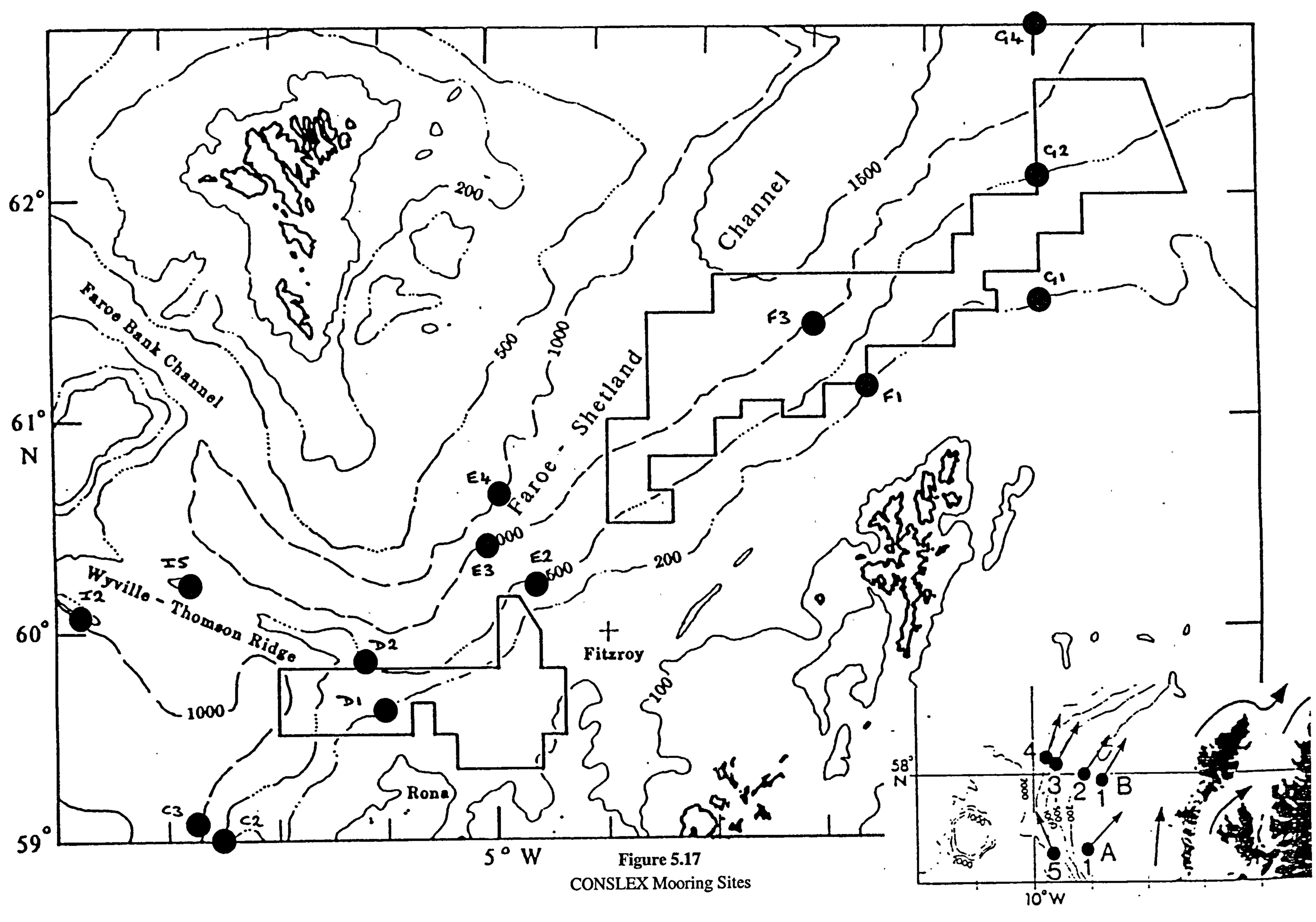

Figure 5.17
CONSLEX Mooring Sites

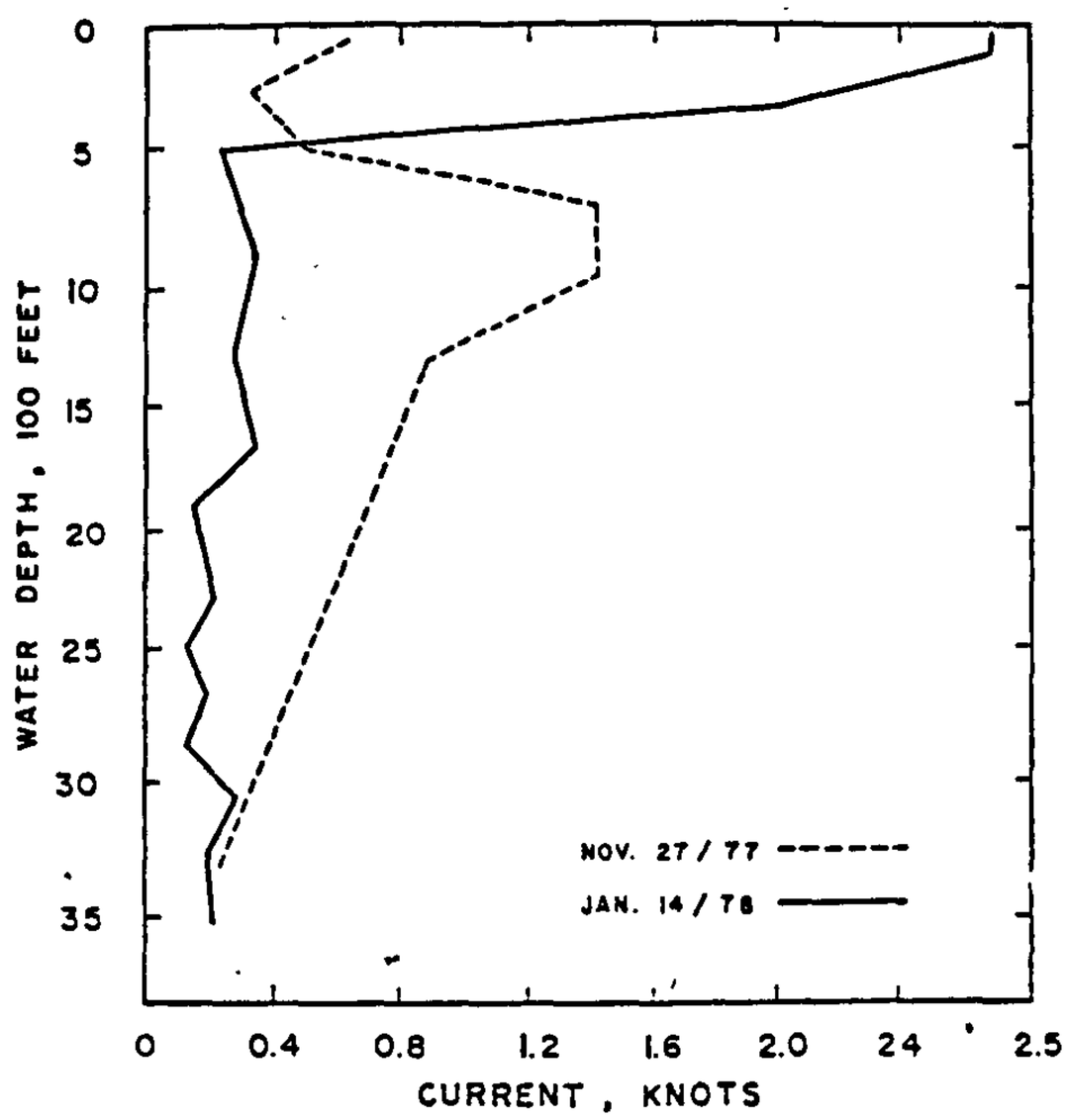

Figure 5.18
Deep Water Current Profiles - Offshore Brazil

(1 Knot = 0.514 m/s, 1 ft = 0.305 m)

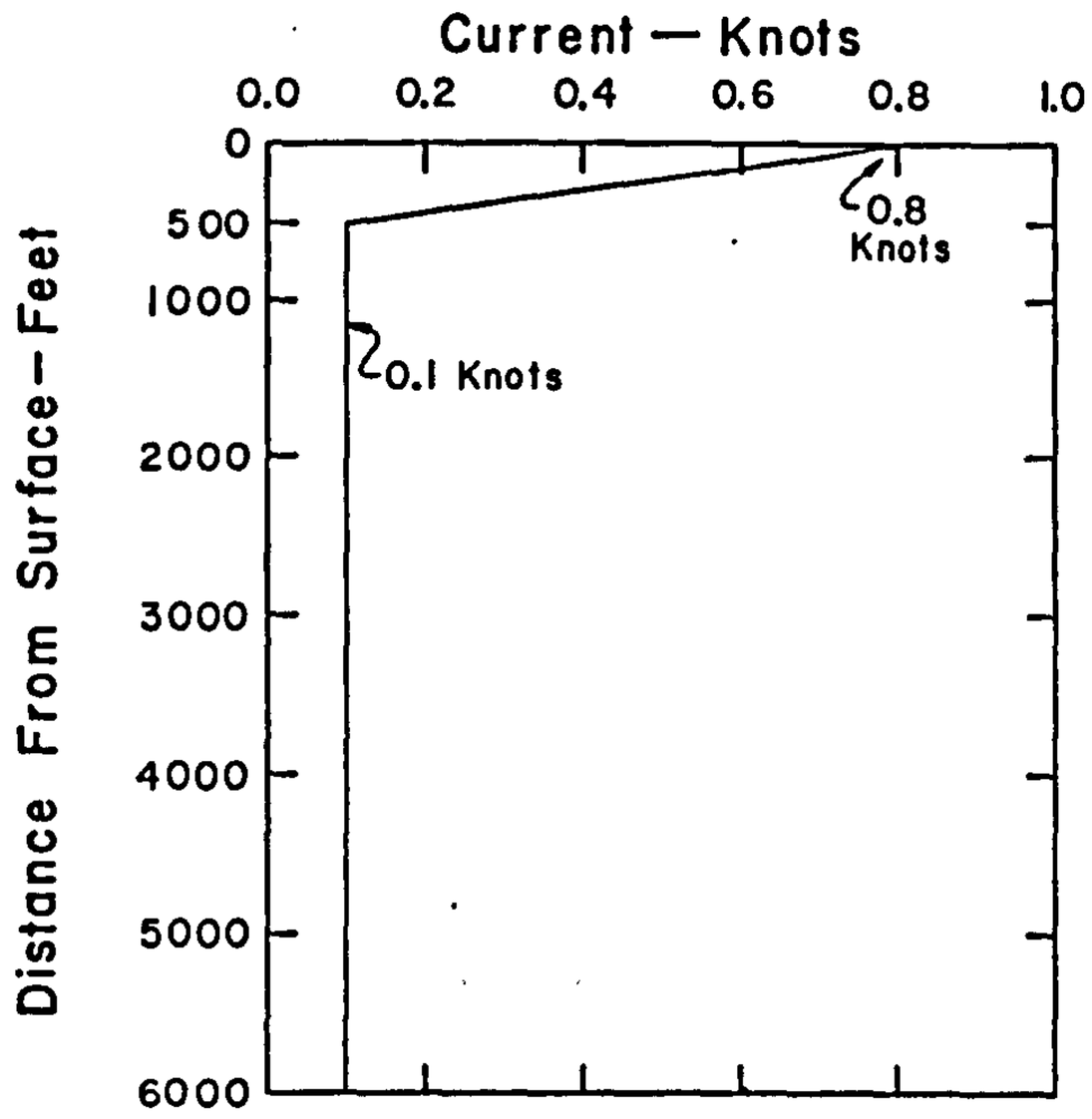

Figure 5.19
Assumed Profile for a Deep Water Drilling Riser Analysis

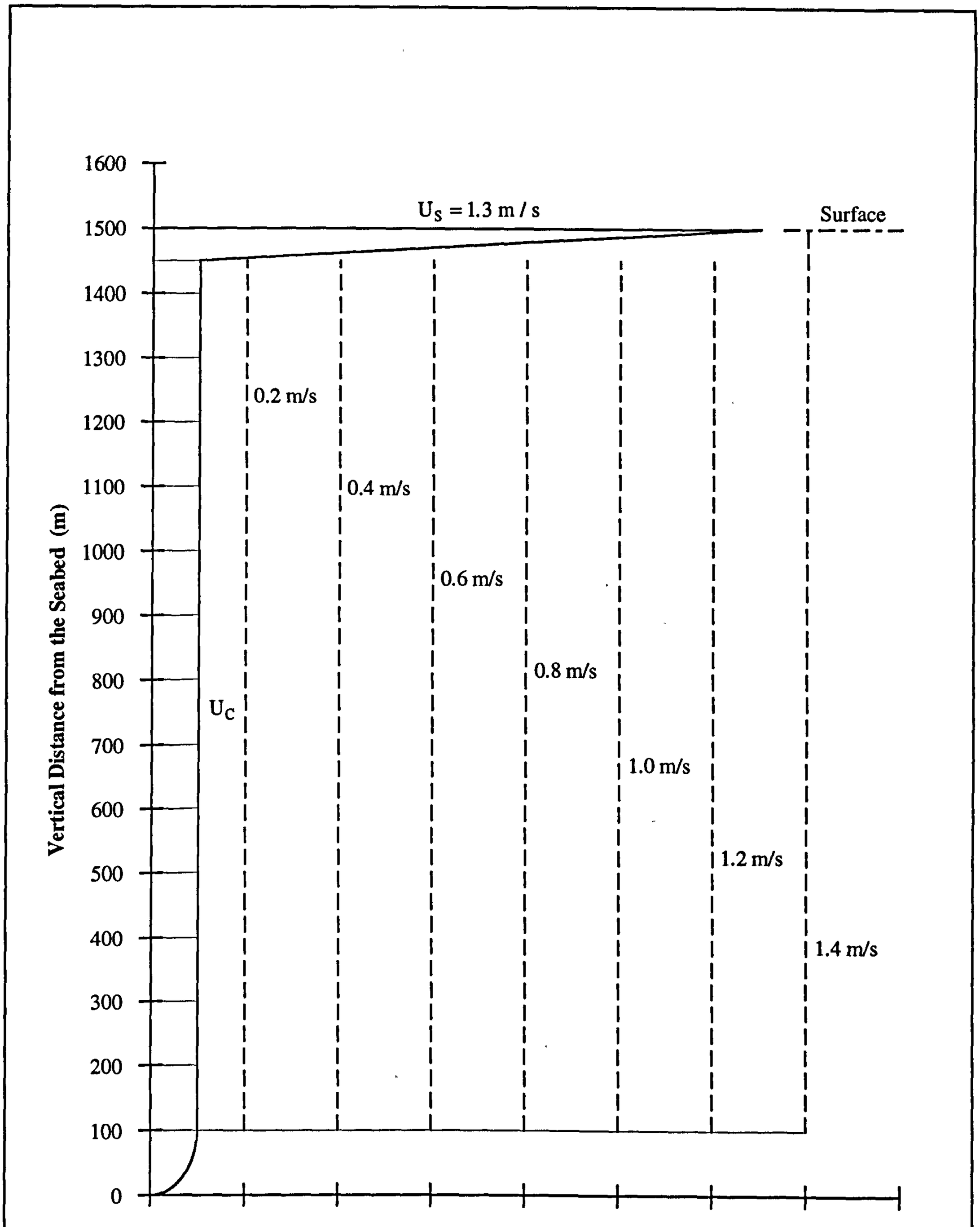

Figure 5.20
Assumed Current Profile

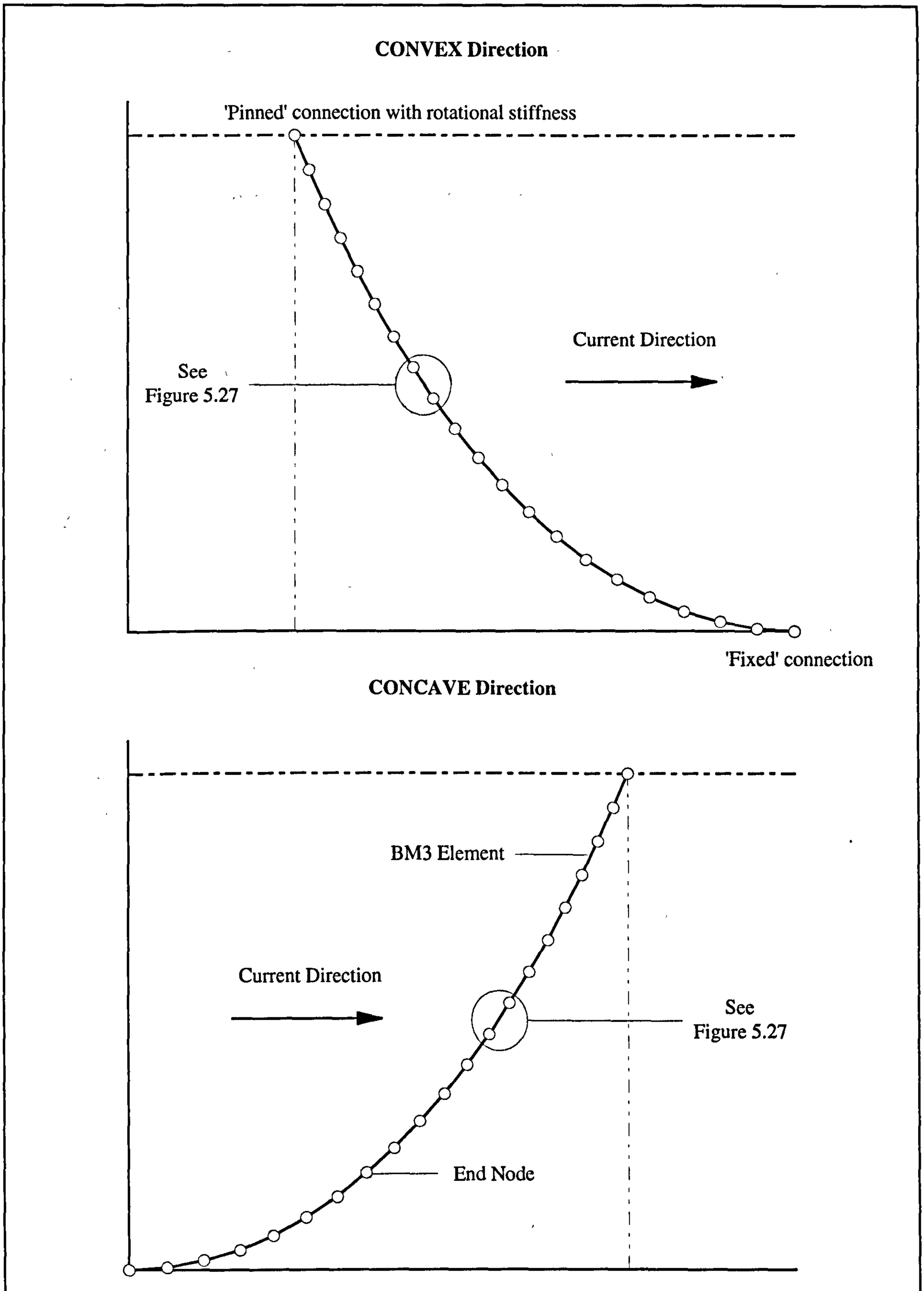

Figure 5.21
Current Directional Definitions

Between 1400 m and 1500 m (depth of seabed) the current velocity is reduced zero through an elliptic profile to take into account seabed ground effects. A sensitivity analysis is carried out by increasing the uniform velocity U_c from 0.1 m/s to 1.4 m/s in 0.1 m/s increments, this is illustrated in Figure 5.20.

5.6.3 Riser Orientation within the Current Flow

The catenary riser's orientation within a current flow obviously has an effect on its deflection behaviour. In this analysis current flow is directed upon the riser within the same plane and so this means that for a production system as set out in Figure 5.13 current loading will be exerted on both the *Convex* and *Concave* sides of the riser. These two in-plane loading conditions are defined pictorially in Figure 5.21. These two defining terms are used extensively throughout the subsequent analysis.

5.6.4 Finite Element Model

The current loading analysis is conducted using LUSAS which is a general purpose finite element system capable of analysing a comprehensive range of engineering problems, both dynamic and static, linear and non-linear. The system is based upon the finite element displacement method of analysis and contains a comprehensive range of element types.

In this study the catenary riser is modelled using a series of Kirchhoff Thin Beam Elements (BM3) linked together by nodes. The BM3 element allows a geometrically non-linear analysis to be carried out. Geometric non-linearities arise from significant changes in the structural configuration during loading. The element in question is shown below:

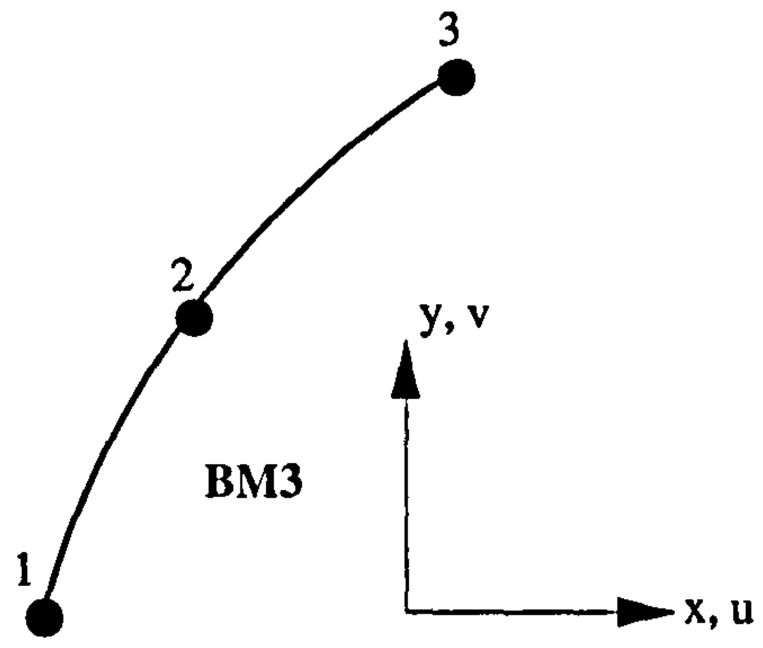

Figure 5.22
Kirchhoff Thin Beam Element in 2-Dimensions

Element Description	Parabolically curved thin beam elements in which shear deformations are excluded. The elements can accommodate varying geometric properties along the length.
Number of Nodes	3
Freedoms	U, V, θ_z : at the end nodes (1 and 3) dU : relative displacement at the mid node (2)
Node Co-ordinates	x, y : at each node
Geometric Properties	A, Izz, Iz : at each node where A = Cross sectional area Izz = 2nd moment of area about the local z-axis Iz = 1st moment of area about the local z-axis
Loading	Concentrated loads Px, Py : at end nodes
Output	Fx, Mz, Fy : forces and moment in local directions u, v : nodal deflections
Non-linear Solutions	Total Lagrangian : For large displacements, small rotations and small strains. Updated Lagrangian : For large displacements, large rotations and small strains

For a non-linear analysis, since it is no longer possible to directly obtain a stress distribution which equilibrates a given set of external loads, a solution procedure is usually adopted in which the total required load is applied in a number of increments. Within each increment a linear prediction of the non-linear response is made, and subsequent iterative corrections are performed in order to restore equilibrium by the elimination of the residual or *out of balance* forces. The iterative corrections are referred to some form of *convergence* criteria which indicates to what extent an equilibrate state has been achieved. Such a solution procedure is therefore commonly referred to as an *incremental-iterative* method as shown in Figure 5.23. In LUSAS the incremental iterative solution is based on Newton-Raphson iterations. In the Newton-Raphson procedure an initial prediction of the incremental solution is based on the *tangent stiffness* from which incremental displacements, and their iterative corrections may be derived.

The catenary riser is modelled using 100 BM3 elements linked together in series by nodes as shown in Figure 5.21 for just 20 elements. Geometric characteristics are uniform along the entire riser length and material behaviour is assumed to be linear. **It should be noted that these elements neglect tension stiffness and therefore the results obtained from this analysis should be taken with caution.**

An example of an input data file is given in Figure 5.24. These data files are generated by using an EXCEL spreadsheet, the output of which is then converted to an MS-DOS WORD file using a simple *cut and paste* operation. The functions within the spreadsheet are illustrated in block format in Figure 5.25.

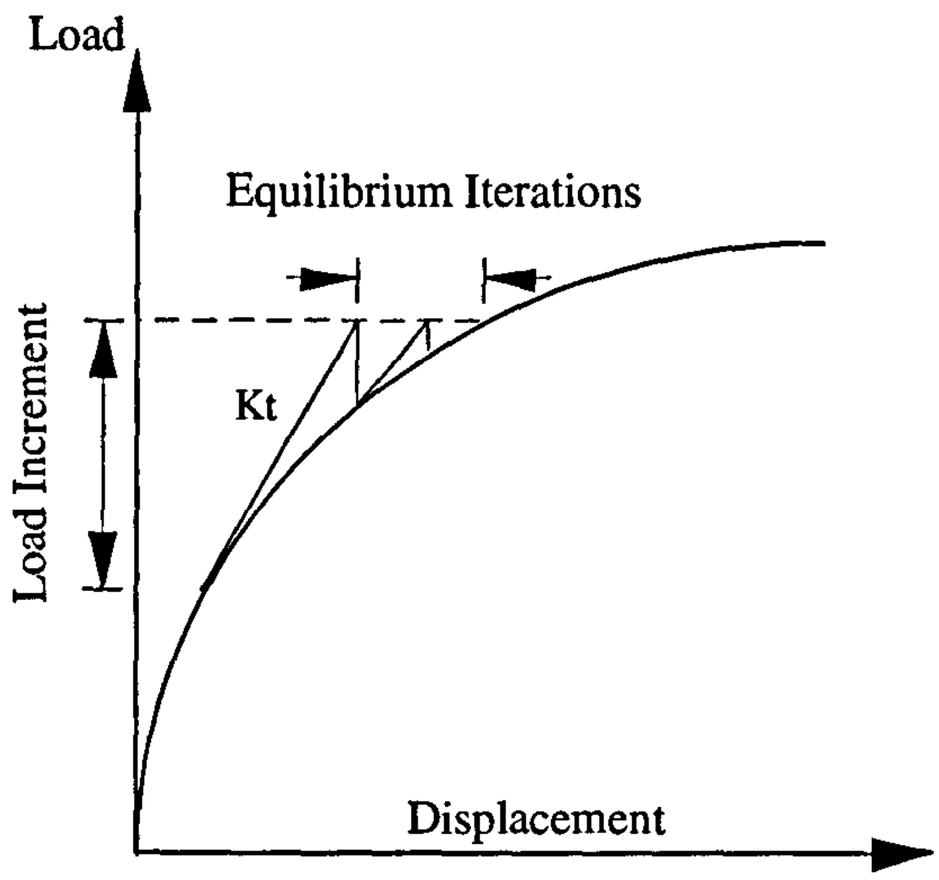

Figure 5.23

Incremental/Iterative Nonlinear Solution Procedure

5.6.5 Current Load Calculation

The forces imposed upon a slender tubular subsea pipeline or riser as a consequence of fluid motion can be determined using the Morrison equation. This expression is based upon the assumption that the fluid motion is not affected by the presence of the structure and that the total fluid force can be expressed as the sum of inertia forces (due to fluid acceleration) and drag forces (due to fluid velocity). The Morrison equation can be written as follows:

$$dF = C_M \rho_{sw} a_s \dot{U} + \frac{1}{2} C_D \rho_{sw} D|U|U \qquad \text{[force/unit length]} \qquad (5.4)$$

inertia force *drag force*

where:
C_M = inertia coefficient
C_D = drag coefficient
ρ_{sw} = sea water density
a_s = cross-sectional area
$\dot{U}$ = fluid acceleration
U = fluid velocity normal to the cylinder
D = pipe diameter

```
PROBLEM     Riser Deflection under a Current Load (CONVEX)

OPTIONS     -117   -118 ———————————— Invokes material assignment input
              └———————— Invokes geometric assignment input
UNITS       N   M

OPTION      40 ———————— Suppresses the stress output of nodal
                        displacement increments
C           Updated Lagrangian Geometric Nonlinearity

OPTION      54 ———————— Updated Lagrangian geometric nonlinearity

BM3 Element Topology

FIRST       1   1   2   3
INC         1   2   2   2   100
                  ┌———— Inputs the node numbers of the elements
                  │     (describes the 'connectivity' of the finite element
                  │     discetiastion)

NODE COORDINATES
 1    0.0    0.0
 2    11.2    0.1
 3    22.4    0.3
 4    33.6    0.6
 5    44.9    1.1
 6    56.1    1.7
 7    67.3    2.4
 8    78.4    3.3
 9    89.6    4.3
10     100.8     5.5
11     111.9     6.8
12     123.0     8.2
13     134.2     9.7
14     145.3     11.4
15     156.3     13.2 ——— y - coordinate
16     167.4     15.1
17     178.4     17.2
18     189.4     19.4
  │       └———————— x - coordinate
  └———————————————— Node number (seabed to surface)
196    1478.3    1448.3
197    1482.7    1458.6
198    1487.1    1468.9
199    1491.4    1479.3
200    1495.7    1489.6
201    1500.0    1500.0
                  ┌———— Odd no. - End node
                  │     Even no. - Mid node
```

Figure 5.24 (a)
An Example of a LUSAS Input Data File

```
BM3 Geometric Properties
 1    100    1    0.0342    0.0051    0.0    ...
                  0.0342    0.0051    0.0    ...
                  0.0342    0.0051    0.0    ...
BM3 Material Properties
 1    100    1    2.07E+11    0.3
Support Nodes
 1    1    0    R    R    R
 201    201    0    R    R    S    10000
LOAD CASE
CL
 3    3    0    -0.5    -33982.3    0.0
 5    5    0    -2.3    -33957.7    0.0
 7    7    0    -6.4    -33921.2    0.0
 9    9    0    -13.4    -33873.0    0.0
 11    11    0    -24.3    -33813.7    0.0
 13    13    0    -39.6    -33744.0    0.0
 15    15    0    -60.2    -33664.4    0.0
 17    17    0    -86.4    -33575.7    0.0
 19    19    0    -118.8    -33478.8    0.0
 21    21    0    -157.8    -33374.5    0.0

 189    189    0    -8147.2    -30429.9    0.0
 191    191    0    -8188.3    -30449.4    0.0
 193    193    0    -8228.5    -30469.0    0.0
 195    195    0    -8650.5    -30326.1    0.0
 197    197    0    -12750.4    -28641.6    0.0
 199    199    0    -18707.5    -26218.8    0.0

NONL CONT
INCR          0.1    0.2
ITER          12
FIRST         NR
INC           (12)
CONV          D    D    D    D    D    D
OUTPUT        0    10    2
TERM          1.0

C             Plot File
END
```

2nd moment of area

Cross - sectional area

Poisson's ratio

Young's elasticity modulus

Defines the boundary conditions
R = restrained
S = spring freedom

x, y, theta

(F_x)

Total horizontal force acting upon element (11) situated between nodes 19 and 21

(F_y)

Total vertical force acting upon element (100) situated between nodes 197 and 199

Controls how the nonlinear analysis is carried out in terms of the number of increments and iterations used as well as defining the iteration convergence crteria.

Figure 5.24 (b)
An Example of a LUSAS Input Data File

Spreadsheet Input

1. Horizontal Surface Offset (a)
2. Sea Depth/Vertical Offset (b)
3. Riser Diameter and Wall Thickness (D & t)
4. Young's Elasticity Modulus (E)
5. Submerged Unit Weight (w)
6. Normal Drag Coefficient (C_{DN})
7. Tangential Drag Coefficient (C_{DT})
8. Uniform Current Velocity (U_C)

↓

The catenary riser is divided up into a 100 straight elements of equal length. The slope angle of each element is obtained

↓

The components of current load in both the horizontal and vertical directions which are exerted upon each element are obtained. The self-weight of each element which is calculated by simply multiplying the submerged unit weight by the element length is then added to the vertical current load component (Section 5.5.9 provides a detailed analysis on how this is achieved)

↓

The riser is broken up into 100 BM3 elements of equal length. The x-y coordinates of all end and mid-nodes are calculated

↓

LUSAS input data files are created for both CONVEX and and CONCAVE conditions (an example is shown in Figure 5.24)

Figure 5.25

Block Diagram for the LUSAS Input Data File Spreadsheet

The inertia coefficient is conventionally taken as the added mass coefficient plus one to account for the Froude Krylov or undisturbed pressure force due to fluid acceleration. The drag force term includes a modulus sign to ensure that the drag force remains in the same direction as the velocity of the fluid. Although the Morrison equation was originally developed for vertical piles in shallow water, for engineering purposes it is assumed to be valid for cylinders and pipes of arbitrary orientation in deep and shallow water with the proviso that the coefficients C_M and C_D are determined empirically for the appropriate condition. Both coefficients are dependent upon many parameters such as Reynolds number, Keulegan-Carpenter number, a relative current number and surface roughness ratio.

As previously stated the aim of this analysis is to only evaluate the effects of a steady current acting upon the catenary riser and therefore any loads imposed as a result of wave motion are neglected. As a consequence of this the Morrison equation can be reduced down to include just the drag force term because a steady current condition by its very nature is based upon zero fluid acceleration thereby eliminating the inertia force term.

The Morrison equation therefore becomes:

$$dF = \frac{1}{2} C_D \rho_{sw} D|U|U \qquad \text{[force/unit length]} \qquad (5.5)$$

The extension of the Morrison equation to inclined cylinders can be defined ambiguously depending upon whether:

(1) The current velocity is combined with the cylinders projected area normal to the current direction to compute force components in the three orthogonal directions (called the projected area method).

$$F = \frac{1}{2} \rho_{sw} C_D D(L \sin\theta) U^2 \qquad \text{(see Figure 5.26)} \qquad (5.6)$$

where: L = the length of the inclined pipe or cylinder

(2) The current velocity incident on the cylinder is first resolved into a normal velocity component before computing component forces in the three orthogonal directions (called the normal velocity approach).

$$F = \frac{1}{2} \rho_{sw} C_D D(U \sin\theta)^2 L \qquad (5.7)$$

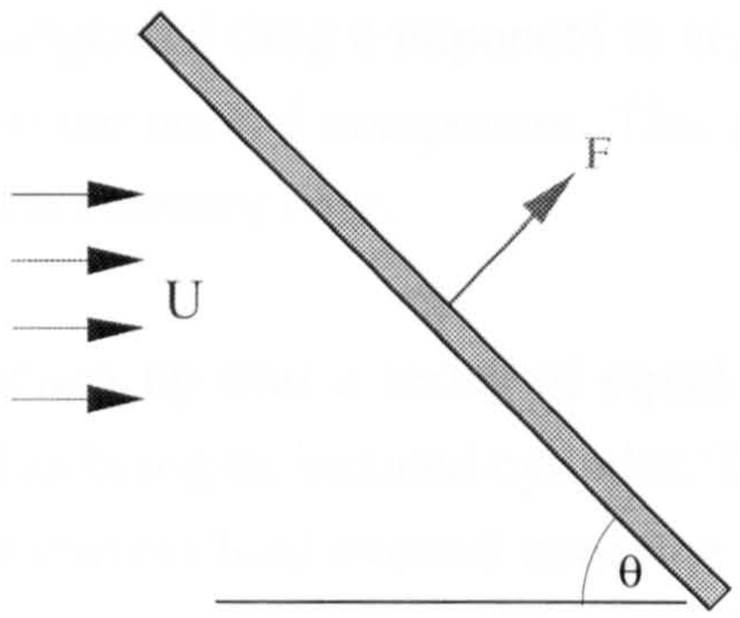

Figure 5.26

An Inclined Cylinder Within a Fluid Flow

The first method of solution is more conservative than the second method since it gives a greater estimate of current force, however the normal velocity approach appears to provide a better correlation with the results obtained from a limited number experiments carried out with inclined cylinders. As a result of this the normal velocity method is widely recommended for use in design calculations and is therefore the method used in this analysis, however fundamental questions on the mechanics of fluid loading on inclined cylinders still remain open and are the subject of continuing research.

On closer examination the drag on a pipe or cylinder making an angle θ with the direction of current flow is found to be composed of two parts: one normal as depicted in Figure 5.26 and one tangential.

$$F_N = \frac{1}{2}\rho_{sw} C_{DN} D\left(U \sin\theta\right)^2 L \tag{5.8}$$

$$F_T = \frac{1}{2}\rho_{sw} C_{DT} \pi D\left(U \cos\theta\right)^2 L \tag{5.9}$$

where C_{DN} = the coefficient of normal drag

C_{DT} = the coefficient of tangential drag

The dominant constituent of normal drag is pressure or form drag which is created as a result of pressure differences over the surface of the pipe and is therefore dependent upon the diameter of the pipe. However when flow occurs past a plane surface parallel to it, the fluid exerts a drag force on the surface as a direct result of viscous action. The resultant frictional force in the downstream direction is usually known as the skin friction or tangential drag and is therefore a function surface area.

In most subsea cases the tangential drag component is neglected on the basis of it being negligible in comparison to the normal component. This assertion is justified later on in this section in the case of the catenary riser.

If the catenary riser is broken up into a series of equal length straight elements each element can be considered as being an inclined cylinder. This allows Eqns (5.8) and (5.9) to be used to calculate the current load exerted upon the catenary riser on an elemental basis for a given diameter, current velocity and drag coefficient. This is diagramatically shown in Figure 5.27 for both *Convex* and *Concave* current directions. The *total* load exerted upon each element in both the horizontal and vertical directions can be easily attained using the following expressions:

$$F_x = F_N \sin\theta + F_T \cos\theta \tag{5.10}$$

$$F_y = F_N \cos\theta - (F_T \sin\theta + w\,ds) \qquad \textbf{Convex} \tag{5.11}$$

$$F_y = F_T \sin\theta - (F_N \cos\theta + w\,ds) \qquad \textbf{Concave} \tag{5.12}$$

where: w = the risers submerged unit weight
ds = the length of an element

The catenary riser is divided up in to the same number of straight elements as there are BM3 curved elements (100) with the load equations above being solved simultaneously for each one using an EXCEL spreadsheet as defined in Section 5.6.4. A LUSAS F.E model utilising BM3 elements requires any external loads to be applied to the end-nodes and so the spreadsheet generates an input data file with the elemental loads being applied to the bottom node of the corresponding element.

One inherent problem facing the user of Morrison's equation is the large scatter of drag coefficient values. However, there is a useful degree of correlation between the coefficients and the Reynolds number flow parameter. Nevertheless, the scatter, and hence uncertainty remains. Figure 5.28 presents plots of C_{DN} and C_{DT} against Reynolds number for both smooth and rough cylinders. For an inclined cylinder research suggests that for the majority of engineering design calculations it is widely considered to be acceptable for the Reynolds number to be based upon the velocity component normal to the cylinder in the case C_{DN} and the velocity component tangential to the cylinder in the case of C_{DT}.

Catenary Riser Straight Element

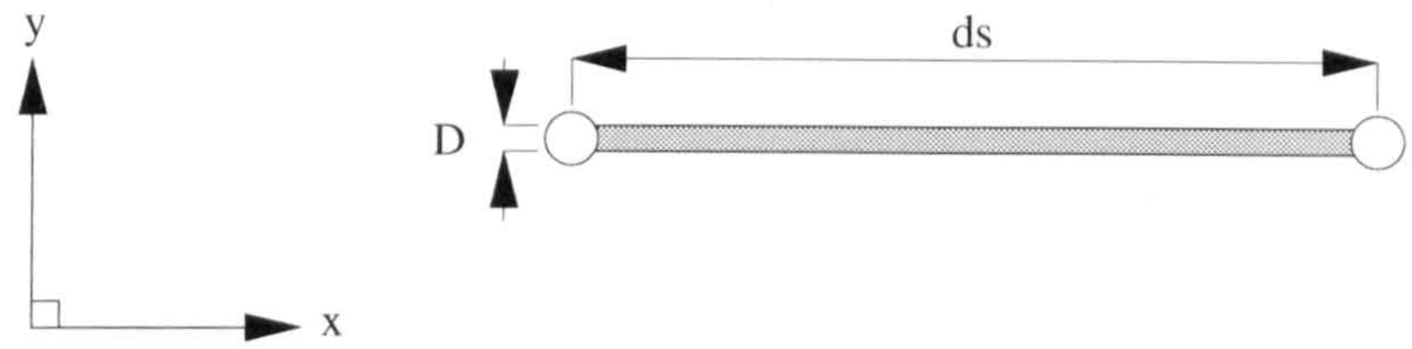

CONVEX Current Direction

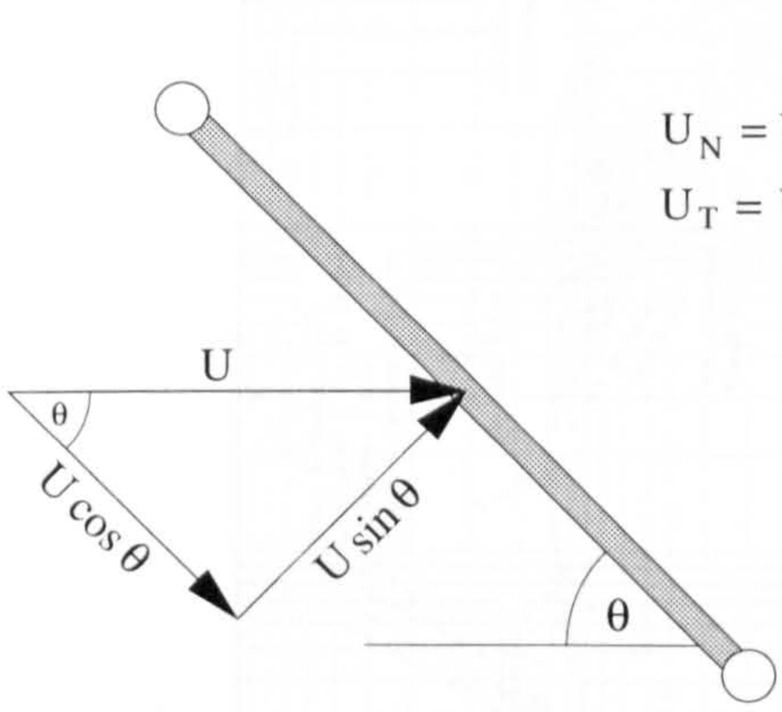

$$U_N = U \sin\theta$$
$$U_T = U \cos\theta$$

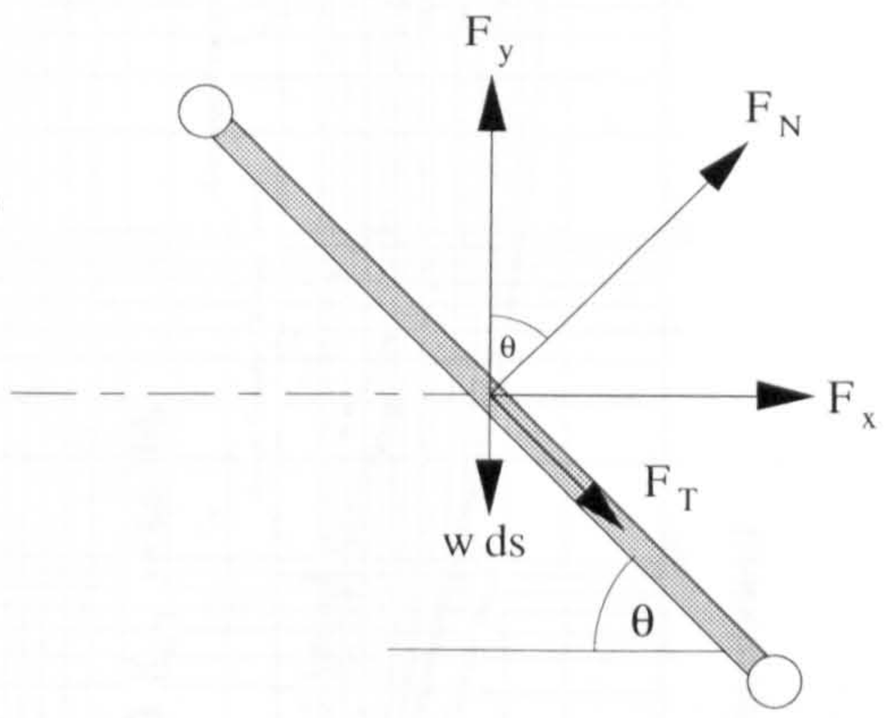

(a)

$$F_T = \frac{1}{2}\rho_{sw} C_{DT} \pi D U_T^{\,2} ds$$

$$F_T = \frac{1}{2}\rho_{sw} C_{DT} \pi D (U\cos\theta)^2 ds$$

$$F_N = \frac{1}{2}\rho_{sw} C_{DN} D U_N^{\,2} ds$$

$$F_N = \frac{1}{2}\rho_{sw} C_{DN} D (U\sin\theta)^2 ds$$

CONCAVE Current Direction

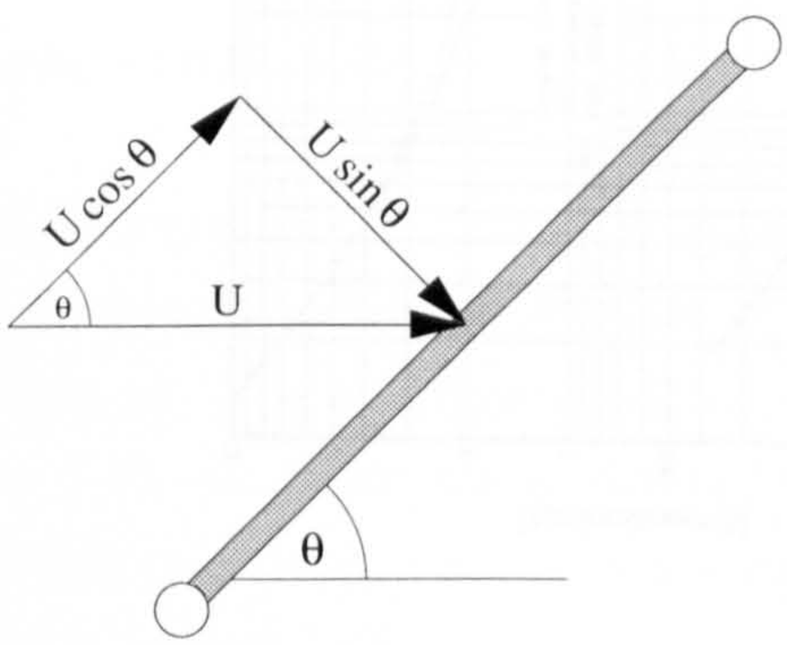

$$U_N = U \sin\theta$$
$$U_T = U \cos\theta$$

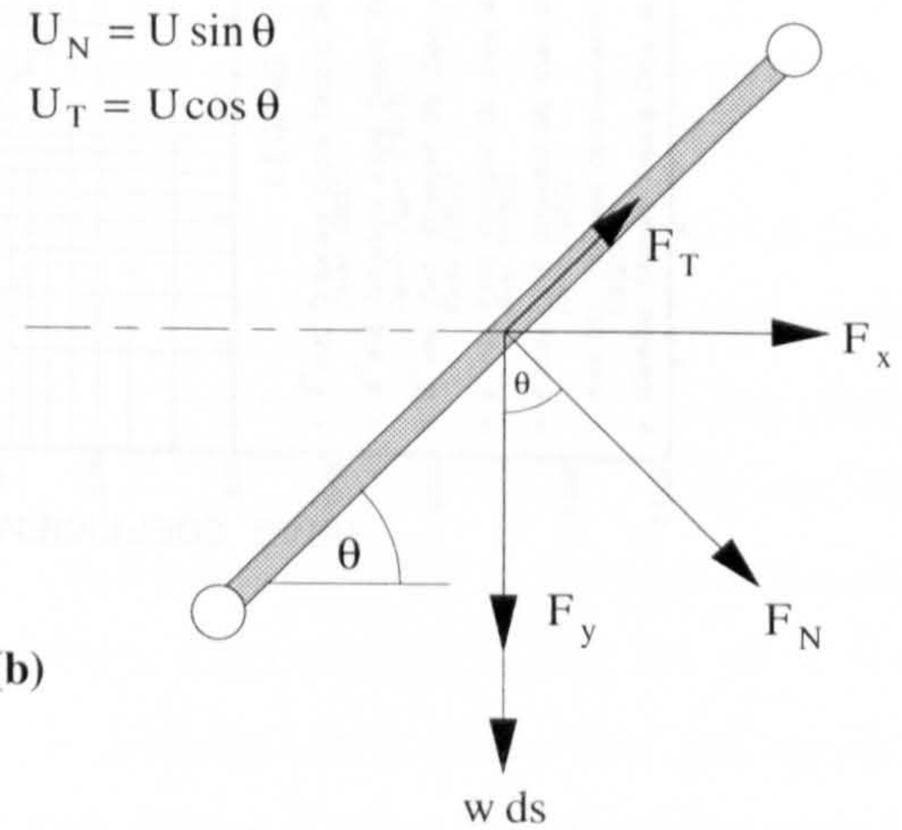

(b)

Figure 5.27

Current Forces Acting upon a Riser Element

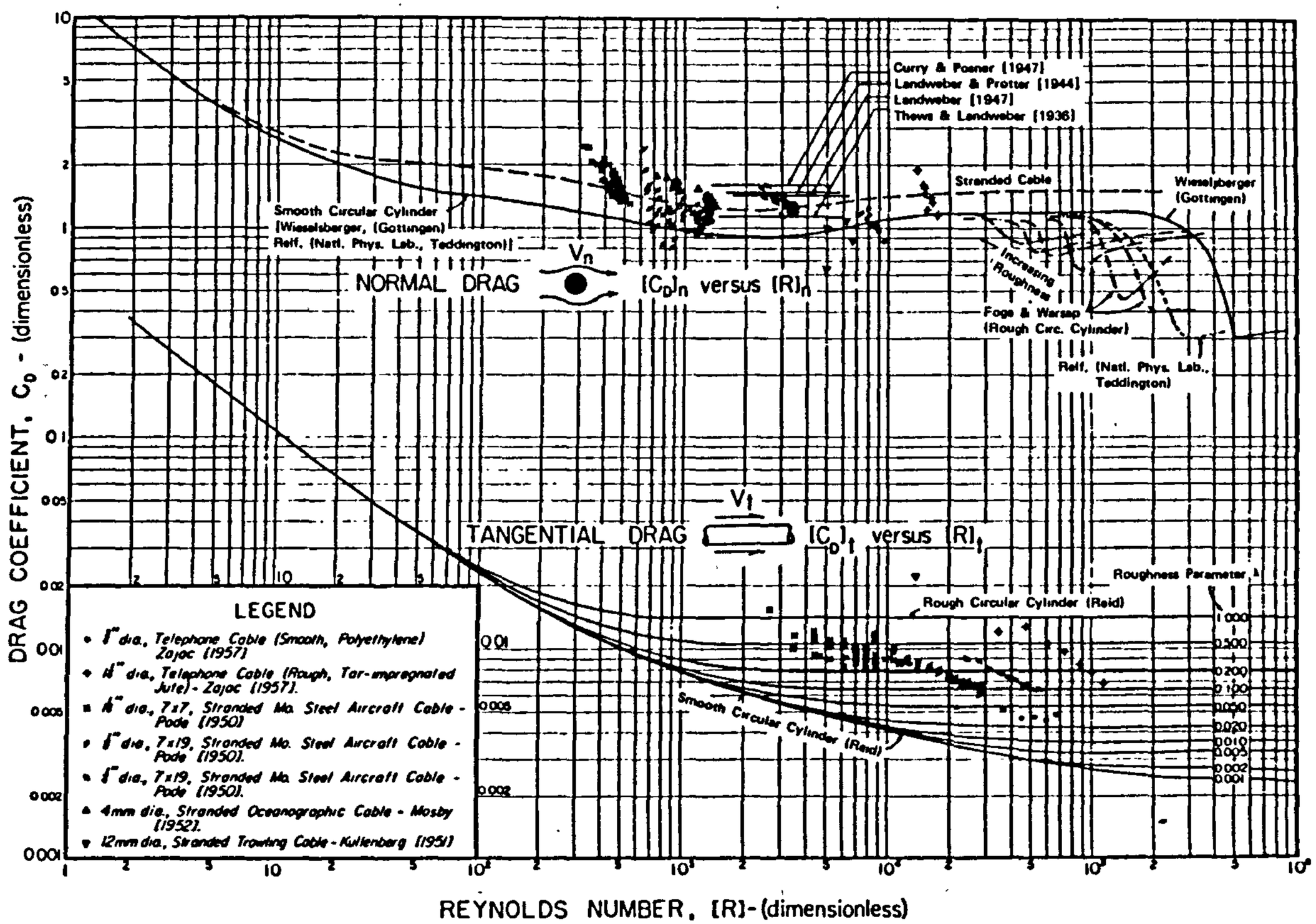

Figure 5.28

Drag Coefficient versus Reynolds Number for Normal and Tangential Flow

Normal Drag $$Re_N = \frac{U_N D}{\upsilon} = \frac{U \sin\theta}{\upsilon} \quad (5.13)$$

Tangential Drag $$Re_T = \frac{U_T D}{\upsilon} = \frac{U \cos\theta}{\upsilon} \quad (5.14)$$

The assertion on normal drag can be partially substantiated using empirical results obtained by the National Advisory Committee for Aeronautics (NACA) during experimental investigations into the pressure distribution about a yawed circular cylinder in the critical Reynolds number range. A graphical plot of these results showing the variation of the normal drag coefficient with Reynolds number for several angles of yaw is given in Figure 5.29. If NACA's empirical results are applied (using Eqn (5.13)) to a 1.1 m diameter cylinder at several angles of inclination to an incident flow with a velocity of 0.4 m/s then the following table can be formulated.

Inclination Angle of the Cylinder [θ] (degs)	Normal Velocity Component [U_N] (m/s)	Normal Reynolds Number [Re_N]	Normal Drag Coefficient [C_{DN}] (taken from Figure 5.29)
30	0.20	1.29 E05	0.7
45	0.28	1.81 E05	1.1
60	0.35	2.26 E05	1.1
75	0.39	2.52 E05	1.1
90	0.40	2.59 E05	1.15

Table 5.12

NACA Empirical Results Applied to an Inclined Cylinder Exposed to a 0.4 m/s Incident Flow

The table demonstrates how in-sensitive the normal drag coefficient (C_{DN}) is to the angle of inclination for angles greater than 45° with a variation of less than 5% between 45 and 90° (vertical). The coefficient values of 1.1 to 1.15 correspond well to those plotted in Figure 5.28 for Reynolds numbers between 0.2×10^5 and 2.6×10^5. For inclination angles less than 45° however, the normal drag coefficient appears to decrease, the reasons for which are not fully understood. The conclusion from all this is that for $45° < \theta < 90°$ where θ is the angle between the cylinder axis and the flow direction, the method of resolving the flow normal to the cylinder and using a normal Reynolds number to determine the normal drag coefficient is correct as proved experimentally. However extending this method to all angles is deemed acceptable for the purposes of design calculations.

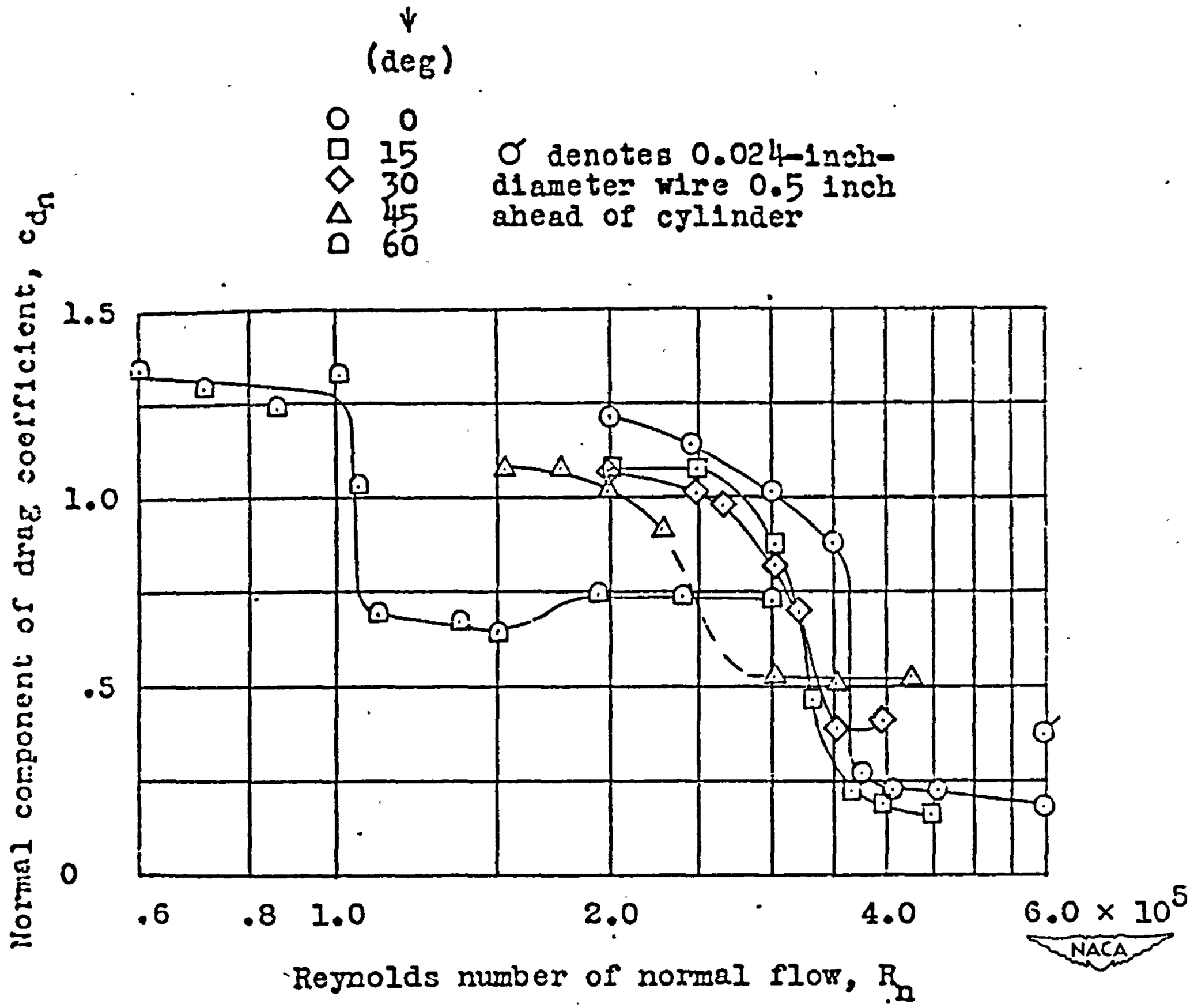

Figure 5.29

Variation of Drag Coefficient with Reynolds Number for a Circular Cylinder at Several Angles of Inclination (NACA Technical Note 2463)

The overall effect of these characteristics is to make the current load calculations concerning the catenary riser complex, since both normal and tangential drag coefficients are function of:

- Incident current velocity which is increased from 0.1 m/s to 1.4 m/s during the analysis

- Riser slope which changes from seabed to surface (0 to 67.5° respectively for a horizontal surface offset of 1500 m)

Therefore in order to reduce this complexity the analysis presented in this section is based upon average values. The assumption behind this being that the riser's behaviour under a current load is in-sensitive to drag coefficients lying within a practical range. This is substantiated in a sensitivity analysis carried out later on in this section.

Drag coefficients are also a function of the surface roughness of the cylinder. This roughness is created as a result of marine fouling which is a term used to describe the attachment of marine organisms (plant and animal) to a subsea structure, once the structure has been in service. Marine fouling is dependent on many factors including, water temperature, salinity, pressure, pollution and sunlight. The most varied and abundant fouling growth therefore occurs in both the splash-zone and upper layer (or euphotic zone) of the ocean (0 to approx. 50 m depth) . This region is characterised by penetrating sunlight, the highest temperatures, lowest pressure and potentially the highest pollution levels, however approximately 98% of the riser's structure is situated below this level, in water that is dark and cold. As a result of this, the analysis is conducted using a drag coefficient based upon the assumption that the build up of marine growth over the operational life span of the riser is negligible and hence the riser surface can be considered as being smooth. This assertion is backed up by Figure 5.30 which illustrates typical marine growth distributions against depth. The riser or carrier pipe surface would in any case be coated in an attempt to impede both growth attachment and corrosion which is another source of surface roughness.

As previously stated the current load analysis is carried out using incident current velocities from 0.1 to 1.4 m/s. This generates Reynolds numbers in the range 1.3×10^5 to 1.0×10^6 for a riser diameter of 1.1 m and a kinematic viscosity of 1.7×10^{-6} m^2/s (obtained from Figure 5.31 using an average seawater temperature of 2.0°C). It is shown from Figure 5.28 that over this range the tangential drag coefficient (C_{DT}) is virtually constant at 0.0025 for a smooth cylinder.

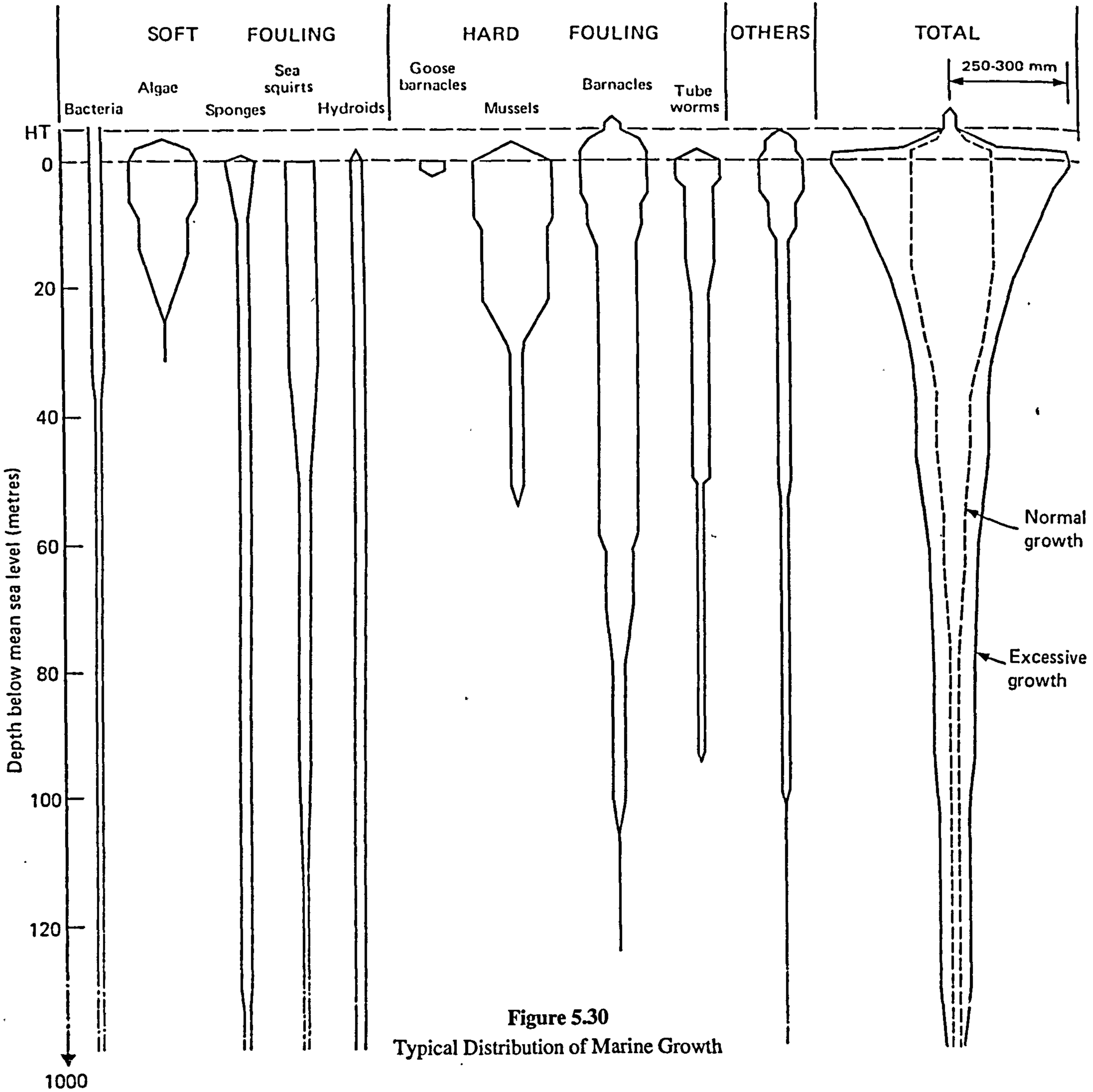

Figure 5.30
Typical Distribution of Marine Growth

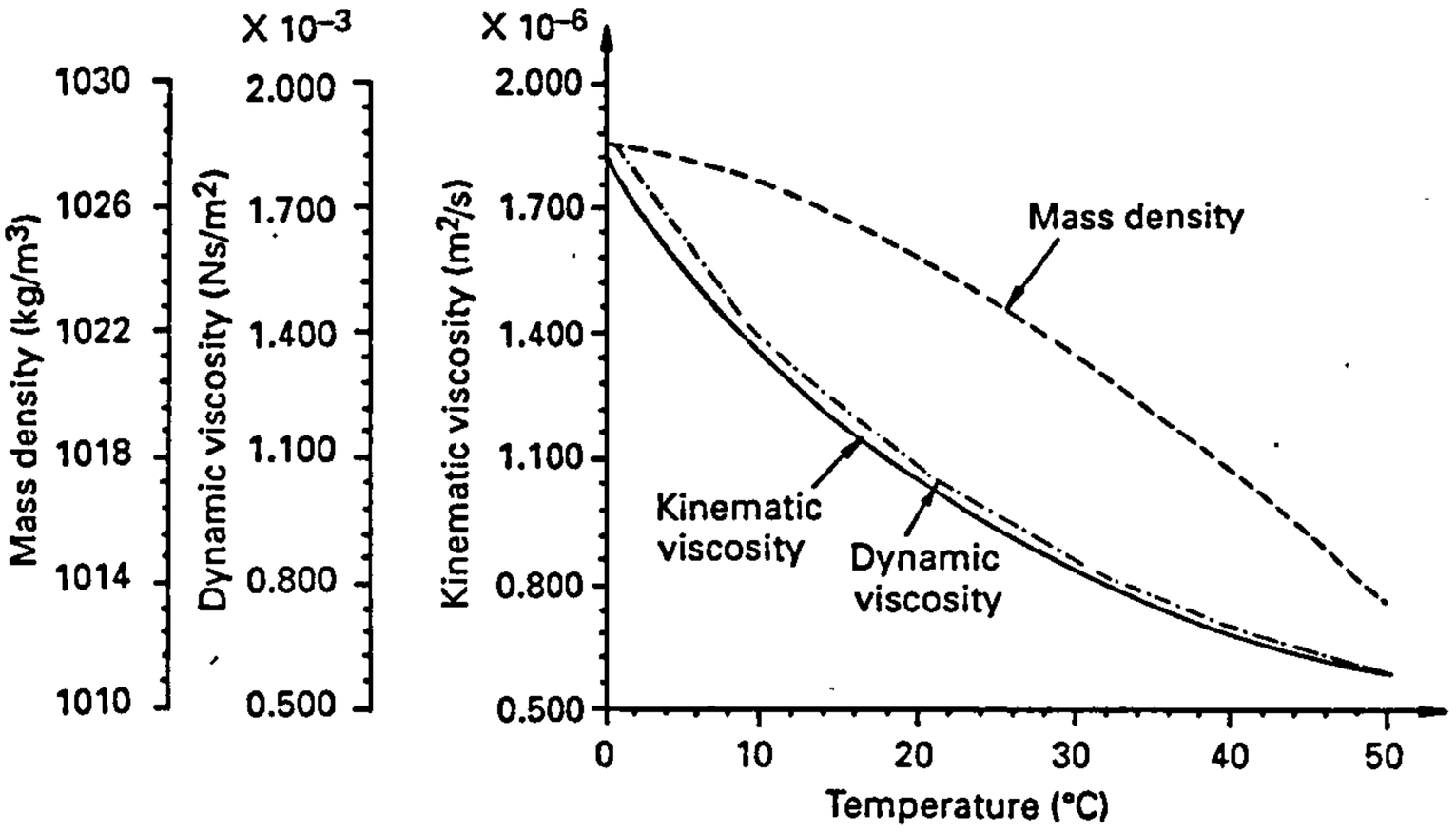

Figure 5.31

Variation of the Physical Properties of Seawater with Temperature

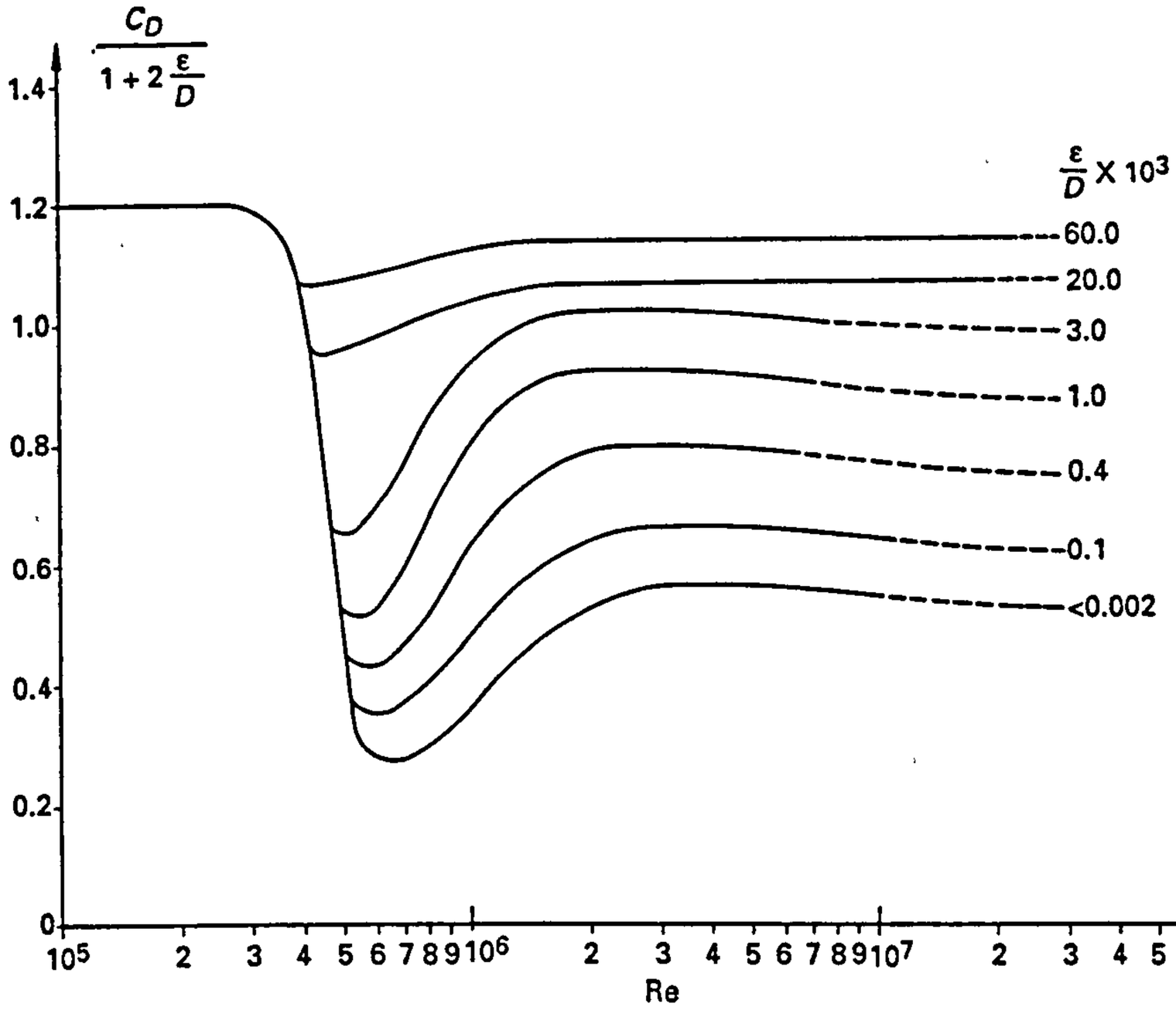

ε is the roughness height

D is the pipe diameter

Figure 5.32

Drag Coefficient versus Reynolds Number for Normal Flow

However this feature does not occur in the case of the normal drag coefficient where there is a sharp drop in coefficient value within the Reynolds number range $2.0\times10^5 - 1.0\times10^6$, see Figure 5.32. This flow range is characterised by a laminar separation over the cylinder, followed by a re-attachment and turbulent separation. The turbulent boundary layer, because of fuller velocity profile and higher turbulence, has a higher kinetic energy which can sustain a larger pressure rise as the flow decelerates over the downstream half of the cylinder. The boundary layer, therefore remains attached for longer distances around the cylinder before separating. This causes the width of the wake to decrease and thus the pressure drag decreases giving the net effect of a sharp drop in the drag coefficient from a value of 1.2 to approximately 0.4.

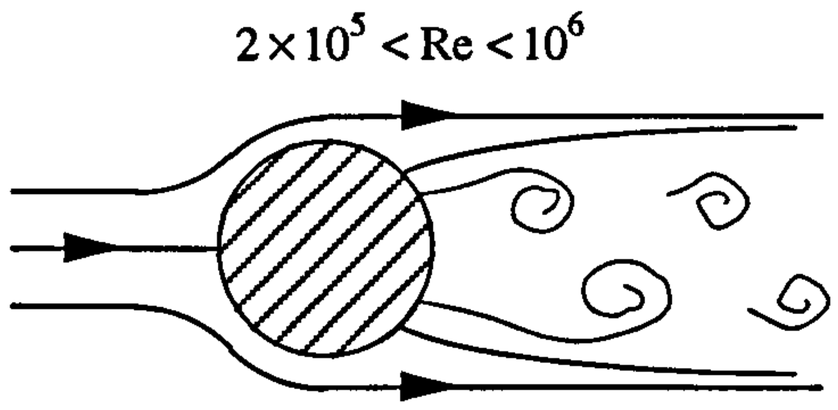

Figure 5.33
Flow Around a Cylinder

As a result of this feature the analysis is carried out using a normal drag coefficient of 0.8 for $1.3\times10^5 < Re_N < 1.0\times10^6$. This means that the tangential drag coefficient is only 0.3% of the normal drag coefficient, thereby justifying the claim that the tangential force component can be neglected. However in this analysis it is left in for the sake of completeness.

5.6.6 Surface and Seabed Boundary Conditions

The riser's surface connection is modelled so as to represent as closely as possible a flex-joint assembly as defined in Section 5.4. The surface boundary condition in the F.E data input file (see Figure 5.21) is therefore *pinned* with a rotational stiffness of 10 kNm/deg. This stiffness is the actual value estimated by OSI and is a function of the elastomers performance.

The boundary connection at the seabed is considerably more difficult to model due to the complex nature of the interaction between riser and seabed surface. After several attempts it was found that LUSAS was unable to model a catenary riser whose lower end was attached to a flat surface in such a way that it would either lift off or drop down on to depending upon the orientation of the external load as in the case of the lift and surface

displacement studies. In order for satisfactory results to be obtained from the F.E analysis the riser is simply fixed at it's seabed end thereby eliminating any vertical, horizontal or rotational movement. This condition is not too far removed from reality and does represent a worse case condition in terms of bending load at the seabed.

5.6.7 Analysis Output

For each riser model, the average computing time for the F.E analysis was approximately 90 minutes. It was noted that the running time was roughly a function of the current load size and with the result that it took LUSAS considerably more time to evaluate a heavy riser in a large current than a near buoyant riser in a small current. The data generated by LUSAS from the F.E analysis is down loaded into data output files in MS-DOS . The raw load and deflection data is then removed and transported into WORD text files by using *cut and paste* commands since most of the output file contains data and information of no concern. This load and deflection data is further transferred into EXCEL spreadsheets where it is transformed into meaningful presentation using either a graphical or tabulated format.

The results presented in the Figures and Tables 5.59 to 5.121 consist of the following:

(a) A complete deflection diagram (to scale) for the proposed in-plane two riser arrangement. The deflections for both *Convex* and *Concave* conditions correspond to a specified current velocity. The riser's design profile (zero current) is shown in black as opposed to the deflected profiles which are plotted in red.

(b) Enlarged deflection diagrams (to scale) at both the riser's surface and seabed ends. Deflections corresponding to a range of current velocities are shown for both *Convex* and *Concave* conditions.

(c) Tabulated data giving the maximum bending stress along the riser together with it's location (measured from the seabed end) for a range of current velocities. The axial stress at this position is also shown.

(d) A graph illustrating the axial stress distribution along the riser for a range of current velocities. The black line gives the axial stress distribution for an un-deflected riser where as the red lines correspond to a riser subjected to a current load.

(e) Tabulated data giving the horizontal and vertical reaction forces at the surface for a range of current velocities.

(d) Tabulated data showing the angular deflection of the riser at the surface connection for a range of current velocities.

The results given above are calculated for risers with horizontal surface offsets of 1000, 1500 and 2000 m with submerged unit weights of 100, 1000 and 2000 N/m.

5.6.8 Discussion of the Results

Deflections

The effect of imposing a current on the *Concave* side of the catenary riser is to pull the lower end away from the seabed and in doing so increase the riser's curvature at the seabed connection point. A current acting on the *Convex* side has the opposite effect in that it pushes the lower end towards the seabed, thereby reducing the curvature at the seabed whilst increasing it slightly further up. The linear increase in current velocity towards the surface appears to have a negligible impact on the deflection profile of the riser at its upper end which retains a straight profile throughout the range of velocities. However the angular deflection at the surface illustrates clearly the influence of the *velocity squared term* within the Morrison Equation, (see Eqn (5.5)). The response of the riser system in terms of it's deflection behaviour to parameters such as submerged unit weight and horizontal surface offset is demonstrated comprehensively by the vast array of results from which the following characteristics can be identified:

- For a given current velocity the extent to which the riser deflects reduces as the submerged weight is increased.
- For a given current velocity the extent to which the riser deflects reduces as the horizontal surface offset is increased.

The effect of increasing the submerged weight of the riser is to increase the load components that oppose or counteract the drag loads exerted as a result of the current acting upon the riser. A good analogy is a horizontal force acting upon a pendulum, the heavier the pendulum weight is, the harder it is to displace from it equilibrium position. Increasing the horizontal surface offset also has the same effect in that it reduces deflection, although to a lesser extent. As this surface offset is increased the overall slope of the riser is reduced thereby decreasing the normal current load component through the $sin\,\theta$ term in Eqn (5.8).

Bending Stress

Bending stress is a function of curvature and therefore their values reflect the extent to which the riser deflects when subjected to a current load. For the *Concave* case, the maximum bending stress is always generated at the point of contact with the seabed (as in

the case of zero current) as opposed to the *Convex* condition in which the current load effectively moves the maximum bending stress from the seabed end to a location slightly further along the riser. This location appears to be predominantly influenced by the submerged unit weight. For a given horizontal offset the distance from the seabed to the position of maximum bending stress diminishes as the submerged unit weight is increased. However if the deflection of the riser from it's design profile is negligible as a consequence of a low current velocity and a high submerged unit weight the bending stress distribution along the riser remains unchanged with the maximum bending stress occurring at the seabed. If stress values are compared between both *Convex* and *Concave* cases it is clear that for a given current velocity the maximum bending stress is always greater for the *Concave* riser condition. The consequence of this is that for the two proposed riser arrangements, the maximum bending loads generated within the *Concave* facing riser will dictate the limiting current conditions for the whole system. The following tables attempt to summarise the bending stress data tabulated in Tables 5.59. to 5.121 by presenting the limiting current velocities in terms of the maximum permissible bending stress as determined in Section 5.2.

Horizontal Surface Offset = 1000 m

Submerged Unit Weight (N/m)	Limiting Current Velocity (m/s)	
	Convex Condition	**Concave Condition**
100	0.2	0.1
1000	0.4	0.2
2000	0.6	0.3

Table 5.13

Limiting Current Velocities for a = 1000 m

The results shown in these tables also confirm the statements made earlier that deflections can be reduced by either increasing the submerged weight or increasing the horizontal surface offset thereby increasing the limiting current velocity. Increasing the horizontal surface offset also the added effect of reducing the bending stress created from its design profile (see Section 2.3), thus leaving the riser with a greater strength capacity to cope with the effects of current loading.

Horizontal Surface Offset = 1500 m

Submerged Unit Weight (N/m)	Limiting Current Velocity (m/s)	
	Convex Condition	**Concave Condition**
100	0.3	0.3
1000	0.9	0.5
2000	1.3	0.6

Table 5.14

Limiting Current Velocities for a = 1500 m

Horizontal Surface Offset = 2000 m

Submerged Unit Weight (N/m)	Limiting Current Velocity (m/s)	
	Convex Condition	**Concave Condition**
100	0.4	0.4
1000	1.2	0.7
2000	1.4	0.8

Table 5.15

Limiting Current Velocities for a = 2000 m

Axial Stress

The change in axial stress along the riser as a result of imposing a current load is demonstrated in Figures 5.59 to 5.121. The most noticeable feature is found when comparing axial stress distributions between *Convex* and *Concave* conditions. When a current is exerted upon the convex side of the riser the effect is to reduce the axial stress (tensile) along the entire length of the riser, the greater the current velocity the larger the reduction is. However when concave side of the riser is subjected to a current load the opposite occurs and the axial stress is increased. The reasons behind these characteristics are linked to how the riser deflects in both cases:

- CONVEX case - The riser is pushed upwards by the current thereby reducing its vertical load which ultimately results in a decrease in axial tensile stress. If the submerged weight is relatively low and the current relatively high the riser is shown to go into compression (negative stress in the graphs) at the seabed. From a buckling point of view this is not advantageous.

- CONCAVE case - The riser is pushed downwards by the current thereby increasing it's vertical load which ultimately results in an increase in axial tensile stress. A higher axial tensile stress at the seabed partially counteracts the compressive stress resulting from bending and so is beneficial in terms of local buckling.

Surface Loads

As discussed earlier in this chapter, loads imposed upon the surface connection are as important as the loads exerted upon the riser. Tables 5.59 to 5.121 tabulate the axial loads along with their horizontal and vertical components that would be exerted upon the surface flex-joint assembly as a result of current loads acting upon the riser. The results can be summarised as follow:

<u>CONVEX case</u>

- Vertical loads reduce as the current velocity increases
- Horizontal loads increase as the current velocity increases
- The resultant axial load (tensile) reduces as the current velocity increases

The main danger in this particular case is that the axial load exerted upon the flex-joint becomes compressive which is a condition that detrimental to the operational performance of the system. For all the scenario's evaluated this does not happen.

<u>CONCAVE case</u>

- Vertical loads increase as the current velocity increases
- Horizontal loads are reduced as the current velocity increases
- The resultant axial load (tensile) increases as the current velocity increases

In this case the main concern can be identified as being a condition in which the axial load exceeds the flex-joints maximum design load of approximately 8000 kN. The highest load found in this study is 7009 kN which corresponds to a horizontal offset of 2000 m, a submerged unit weight of 2000 N/m and a current velocity of 1.2 m/s.

Angular Deflection

Another limiting constraint at the surface end of the riser is the maximum allowable rotation which for the purposes of this study is taken as $\pm 15^{\circ}$ from the design inclination. Deflection angles are tabulated in Tables 5.59 to 5.121 in which the sign convention used corresponds to that used in earlier work (see Figure 5.14) For the *Convex* condition the effect of a current is to push the riser further away from the vertical as opposed to the *Concave* case in which the riser is moved closer to the vertical. There are several

scenario's characterised by a low submerged unit weight and a high current velocity where the angular deflection exceeds the maximum design rotation.

5.5.9 The Drag Coefficient Effect

As a consequence of the doubt that surrounds the selection of a drag coefficient value it was thought necessary to carry out a sensitivity analysis. The normal drag coefficient was varied between 0.3 and 1.2 in increments of 0.1 and the following features were calculated using exactly the same methods as outlined in this section:

- Enlarged deflection profiles (surface and seabed)
- Maximum bending stress
- Axial load at the surface

A catenary riser with a horizontal offset of 1500 m and a submerged unit weight of 1000 N/m was used in a *Convex* condition subjected to a 0.4 m/s current velocity. The results of this analysis are illustrated graphically in Figures 5.122 and 5.123 The variation in deflection profile is virtually indistinguishable. The variation in bending stress and axial stress over the coefficient range is approximately 10% and 3% respectively.

References

1. DET NORSKE VERITAS. (1976) *Rules for the Design, Construction and Inspection of Submarine Pipelines and Pipeline Risers.*

2. J.P. Kenny & Partners Ltd. (1984) *Buckling of Offshore Structures*, Prepared for the U.K. Dept of Energy.

3. Oil States Industries. (1995) *History and Usage of Flex-Joint and Bearing Products Fabricated by Oil States Industries*, OSI, Arlington, Texas.

4. Phifer, E.H., Kopp, F., Swanson, R.C., Allen, D.W. and Langner, C.G. (1994) *Design and Installation of Auger Steel Catenary Risers*, Shell Development Co, In Proc Offshore Technology Conference, OTC 7620.

5. Kopp, F. and Barry, D.W. (1994) *Design and Installation of Auger Pipeline*, Shell Development Co, In Proc Offshore Technology Conference, OTC 7619.

6. Howells, H. (1996) *Steel Catenary Risers West of Shetland*, 2H Offshore Engineering Ltd, Technological Feature, In The Journal of Offshore Engineering, May 1996.

7. Rooduyn, E.J. (1991) *Towed Production Systems: Further Developments in Design and Installation*, In Proc Subsea International 91, U.K.

8. Rooduyn, E.J. (1985) *Submarine Flowlines: Transportation of Pre-Fabricated Pipelines with the Controlled Depth Tow Method*, In Proc Subsea International 85, London.

9. Kvaerner Engineering (1991) *Mobil Riser Study: Riser System Design Basis*, Project No. 2429.

10. Ellett, D.J. (1989) *Ocean Circulation West of Shetland and North of Britain: A General Synopsis*, Dunstaffnage Marine Lab, Oban, Pres Metocean/NWAG Seminar, October 1989.

11. Ellett, D.J. (1992) *West of Shetlands Frontier Tranches: Physical Oceanography*, Pres Mobil EIA Seminar, February 1992.

12. Shanks, F.E., Hammett, D.S. and Zinkgraf, H.L. (1979) *Experience Drilling in Deepwater High Current Areas*, SEDCO Inc, In Proc Offshore Technology Conference, OTC 3582.

13. Long, R. and Young, R.D (1983) *Analysis of a 6000 ft Riser During Installation and Storm Hangoff*, Harry J. Sweet & Assocs Inc, In Proc Offshore Technology Conference, OTC 4596.

14. Berteaux, H.O. (1976) *Buoy Engineering*, John Wiley & Sons.

15. Patel, M.H. (1989) *Dynamics of Offshore Structures*, Butterworth & Co.

16. Burnsall, W.J. and Loftin, L.K. (1951) *Experimental Investigation of the Pressure Distribution About a Yawed Circular Cylinder in the Critical Reynolds Range*, National Advisory Committee for Aeronautics (NACA), Technical Note 2463, Langley Aeronautical Lab.

CHAPTER 5

Results

Figures 5.34 - 5.123

Tables 5.36 - 5.121

Lift Cable Horizontal Load (H)

(a)

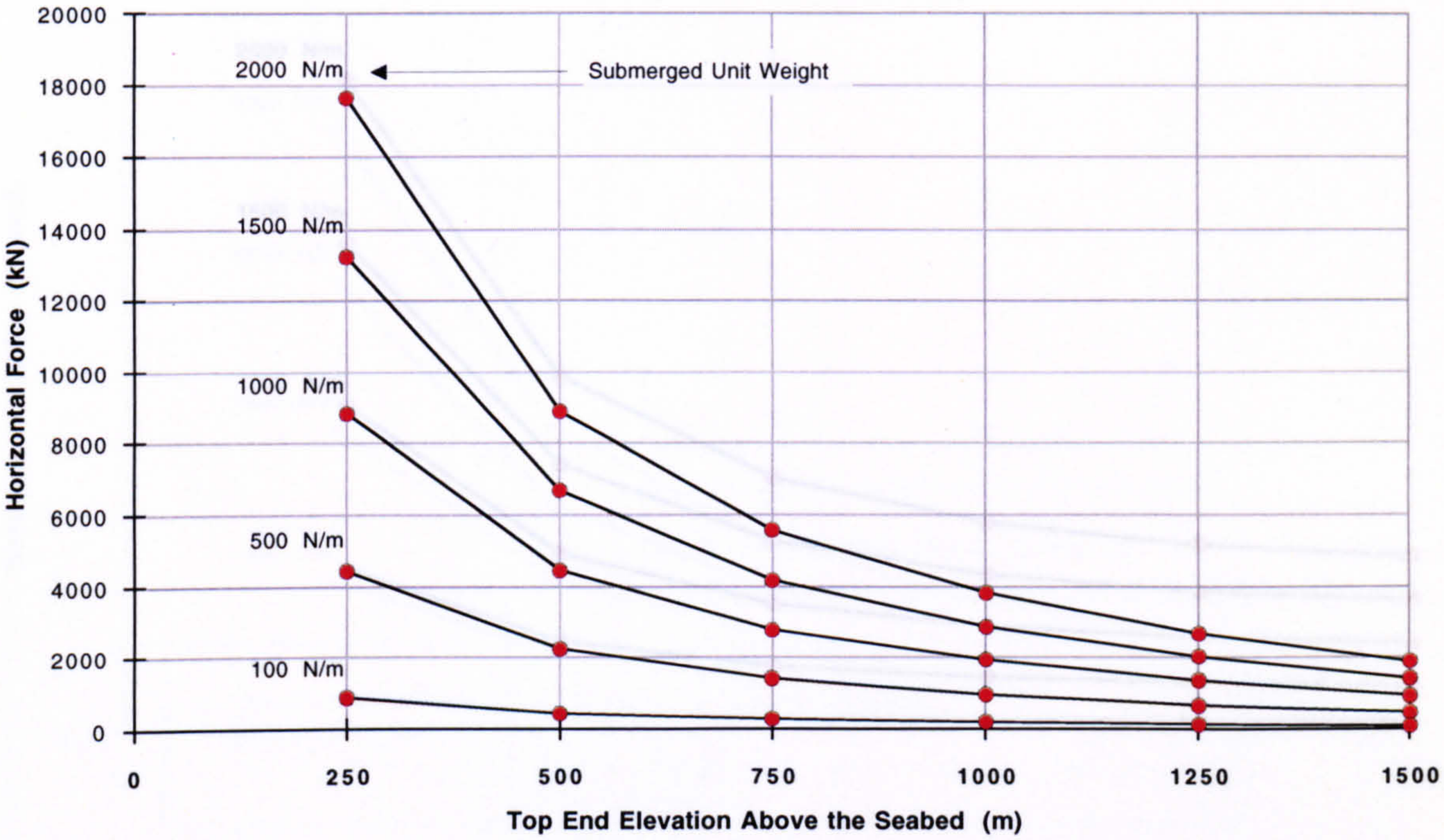

Lift Cable Vertical Load (V)

(b)

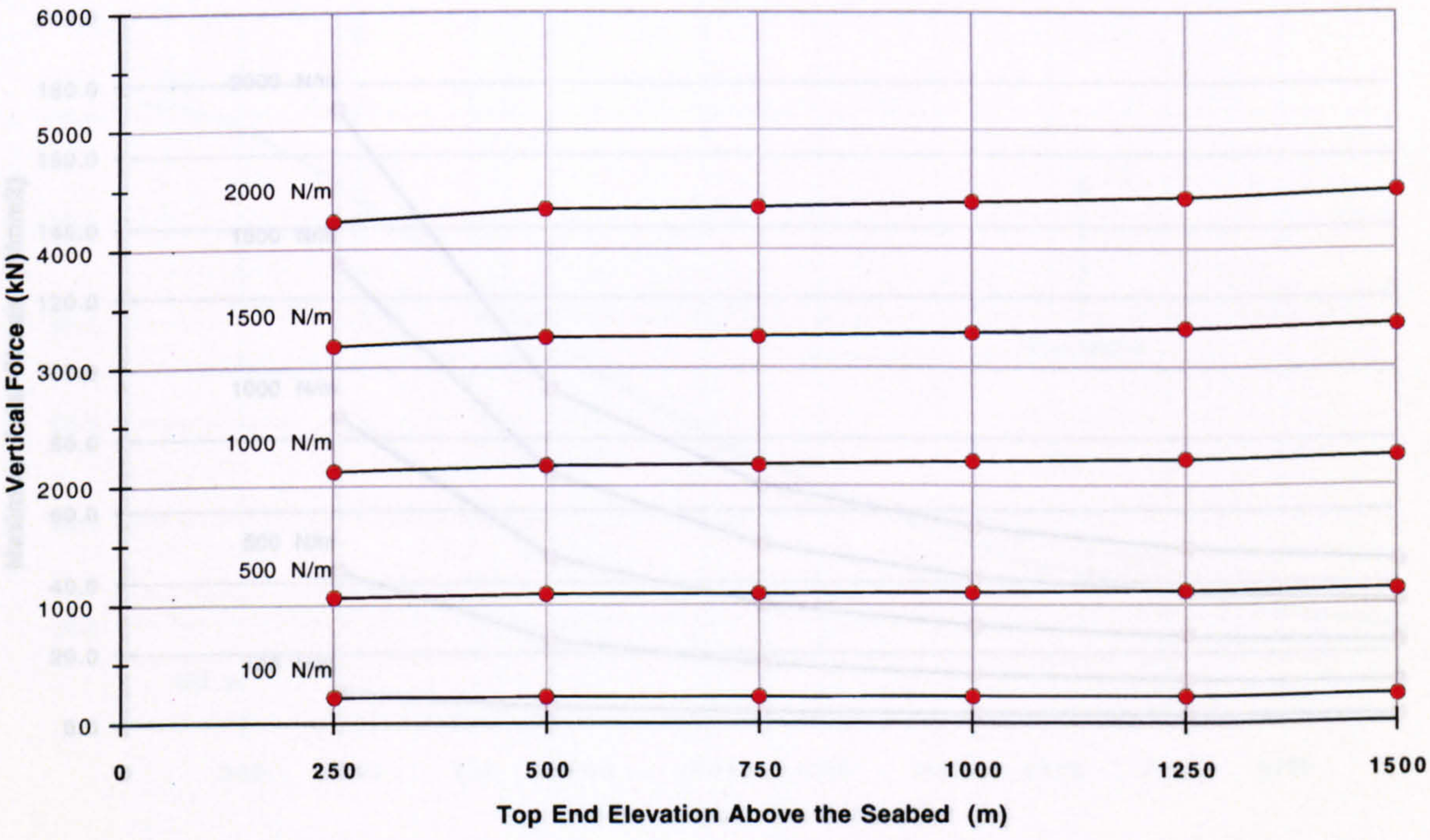

Horizontal Surface Offset = 1500 m

Sea Depth = 1500 m

Figure 5.35

Lift Cable Axial Load

(c)

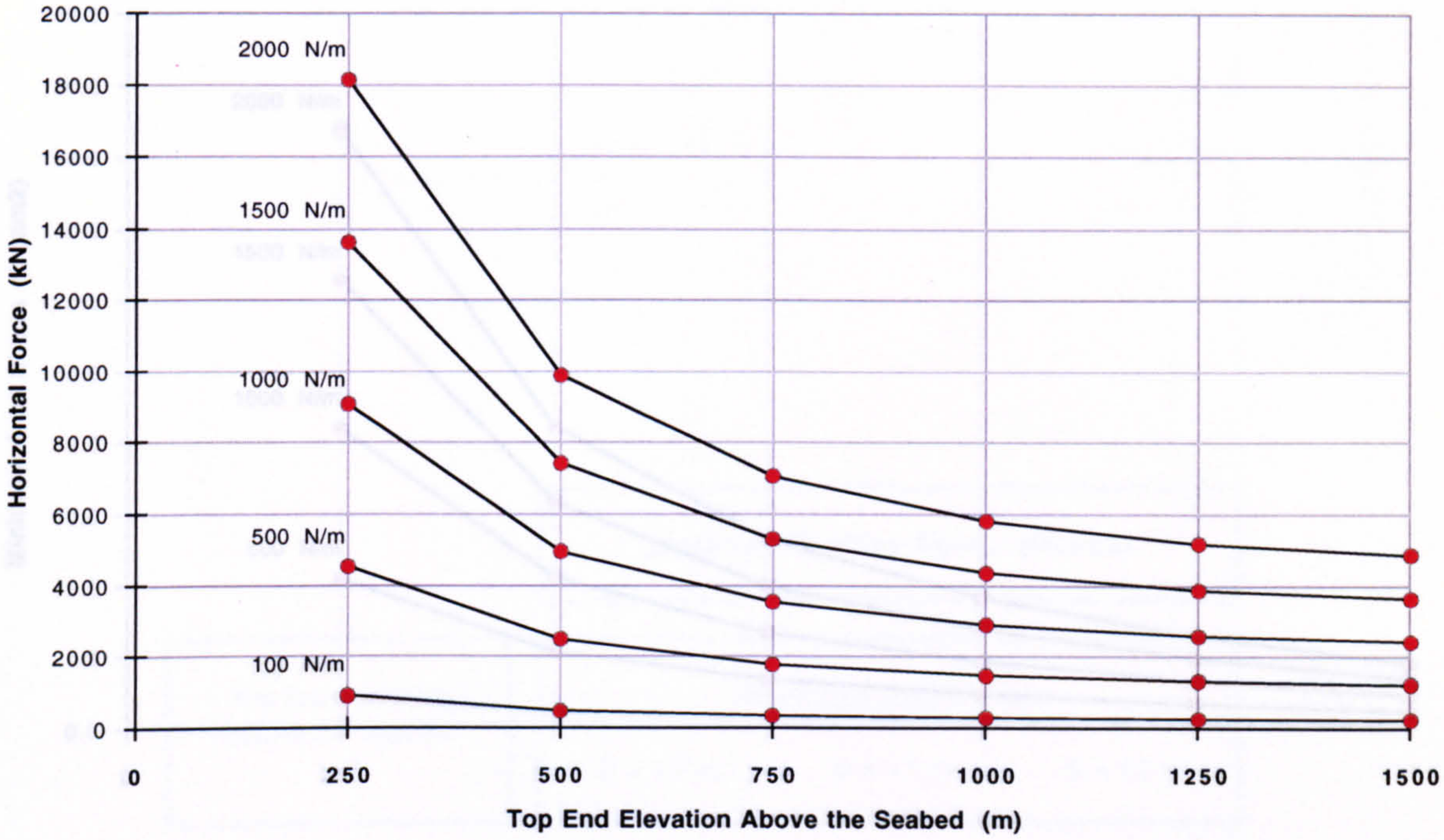

Axial Stress at the Top End of the Riser

(d)

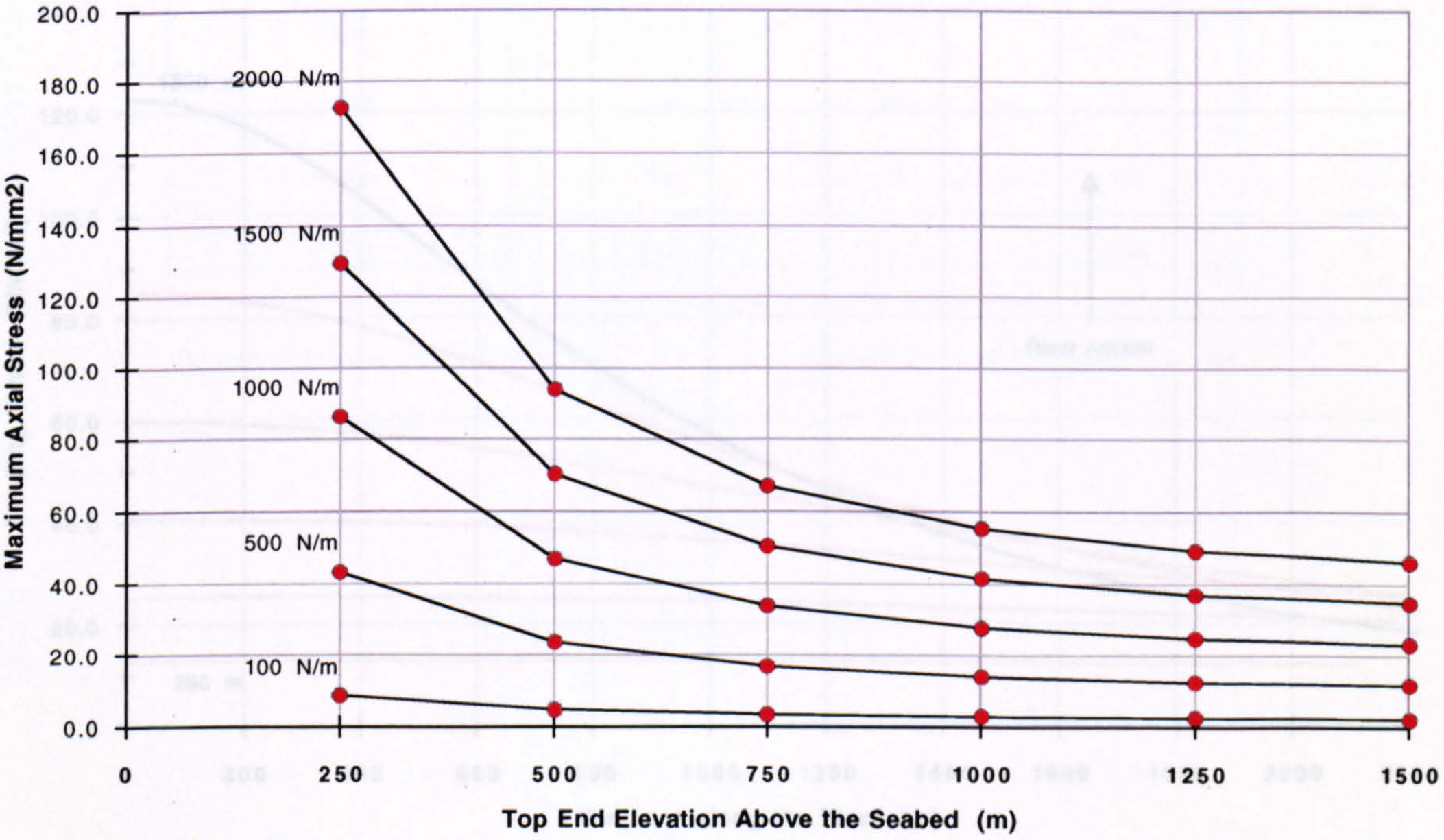

Horizontal Surface Offset = 1500 m

Sea Depth = 1500 m

Carrier Pipe Outer Diameter = 1.1 m

Carrier Pipe Wall Thickness = 10 mm

Figure 5.35

Axial Stress at the Seabed

(e)

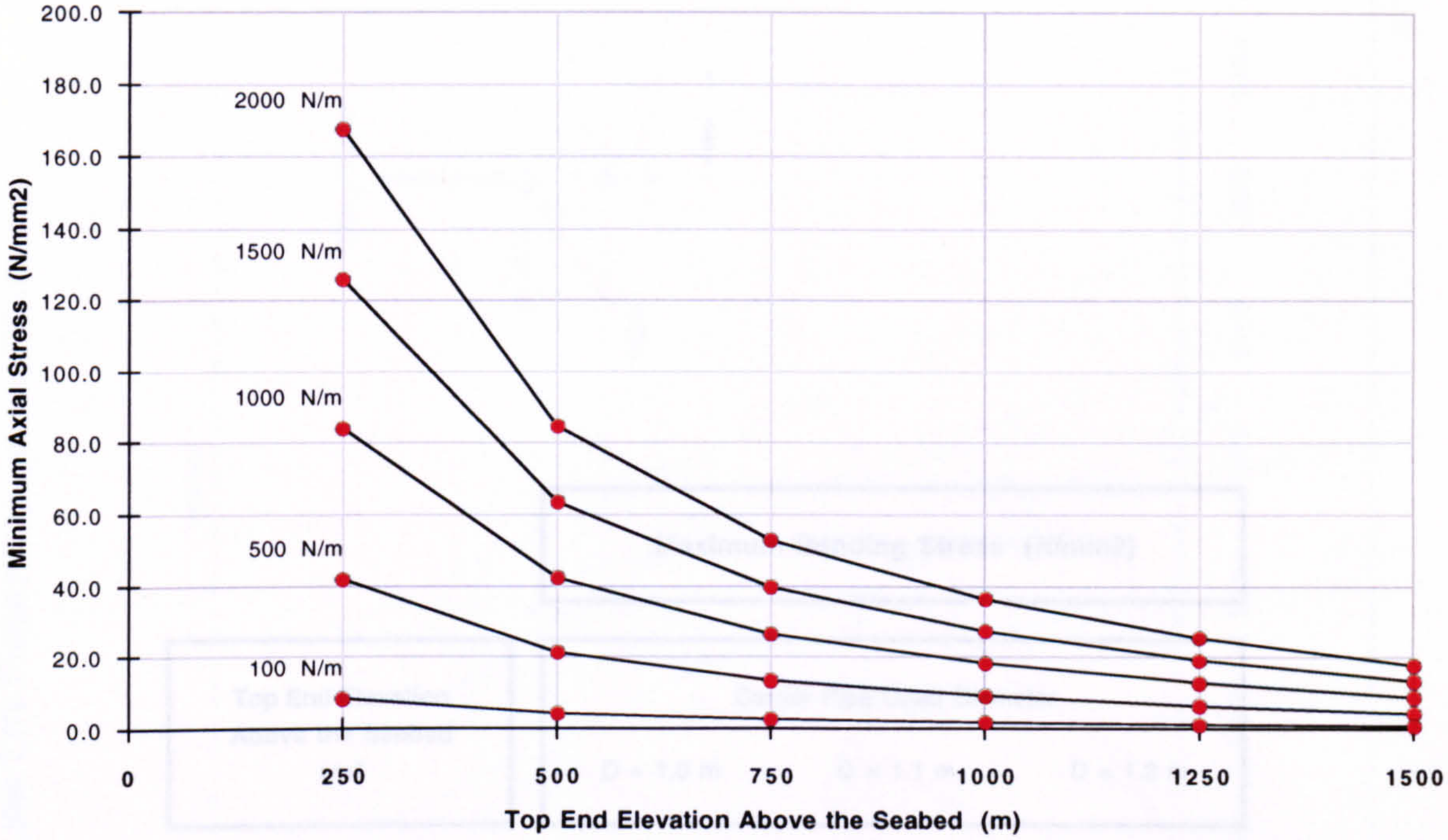

Bending Stress Distributions along the Riser

(f)

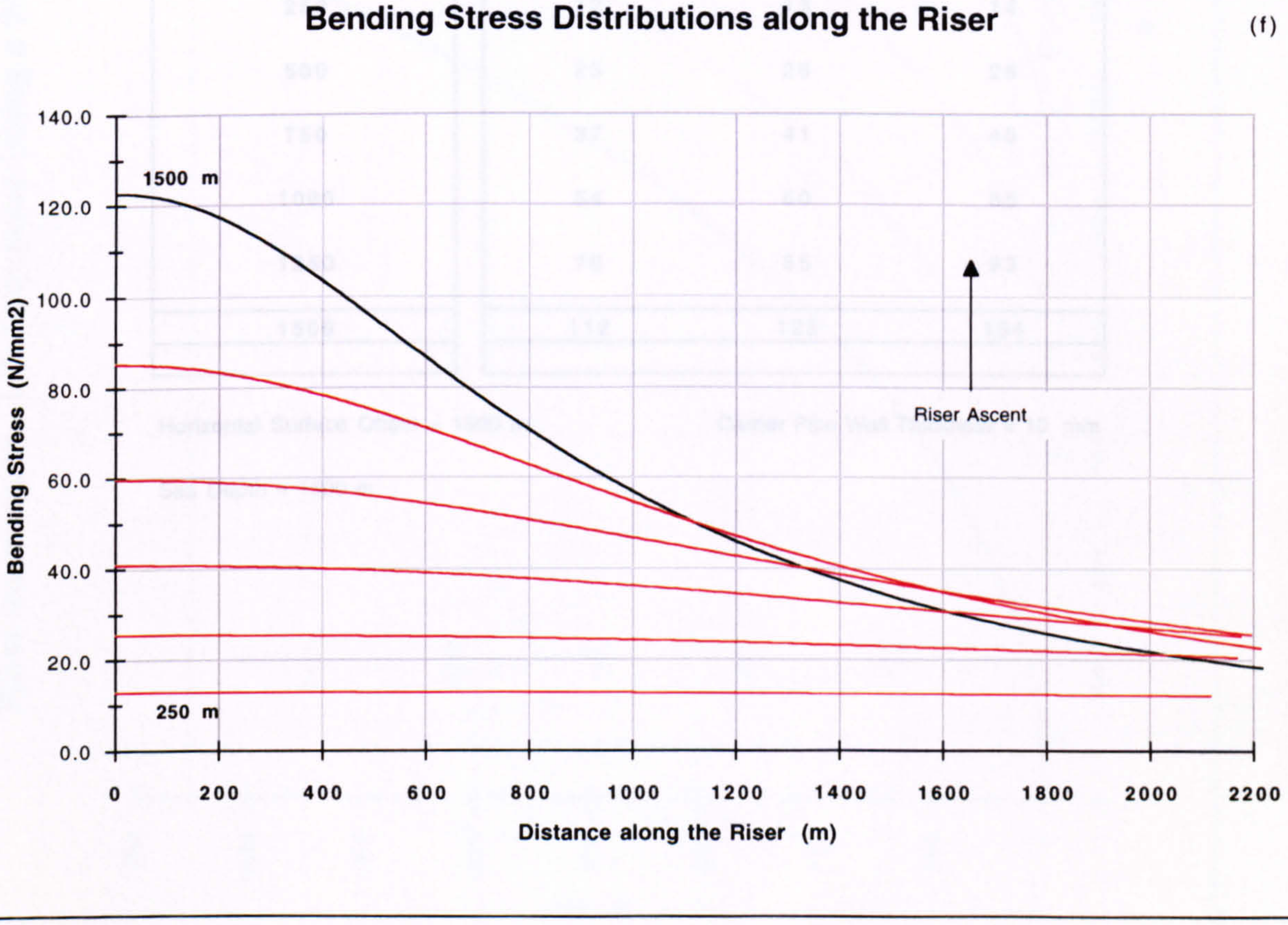

Horizontal Surface Offset = 1500 m

Sea Depth = 1500 m

Carrier Pipe Outer Diameter = 1.1 m

Carrier Pipe Wall Thickness = 10 mm

Figure 5.35

Bending Stress at the Seabed - Catenary Curve Lift Trajectory (a = 1500 m)

Top End Elevation Above the Seabed (m)	Maximum Bending Stress (N/mm2)		
	Carrier Pipe Outer Diameter		
	D = 1.0 m	D = 1.1 m	D = 1.2 m
0	0	0	0
250	12	13	14
500	23	26	28
750	37	41	45
1000	54	60	65
1250	78	85	93
1500	112	123	134

Horizontal Surface Offset = 1500 m

Carrier Pipe Wall Thickness = 10 mm

Sea Depth = 1500 m

Table 5.36

Riser Installation - Lift Sequence Using a Straight Line Lift Trajectory (a = 1500 m)

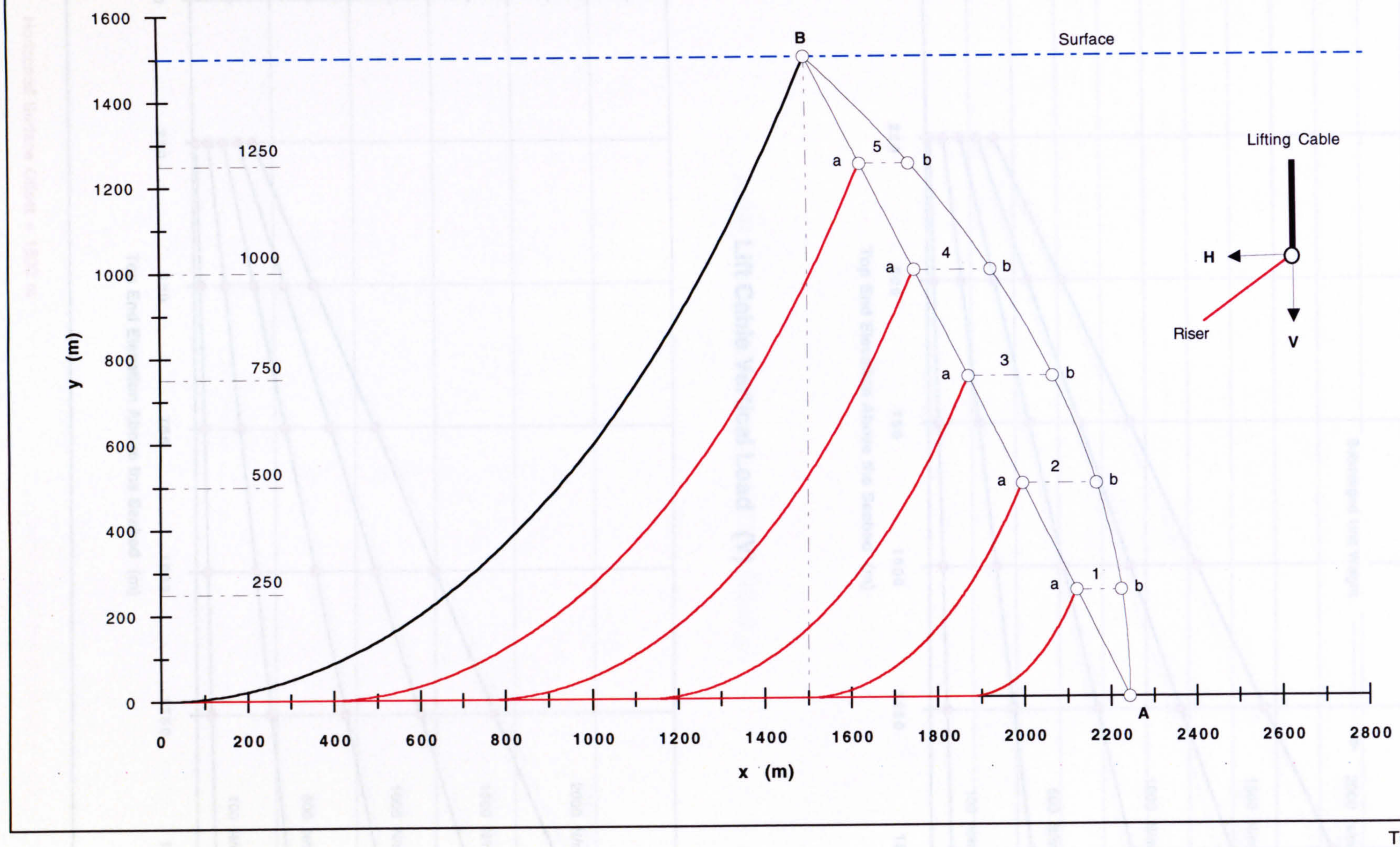

To Scale

Horizontal Surface Offset = 1500 m

Sea Depth = 1500 m

Figure 5.37

Lift Cable Horizontal Load (H)

(a)

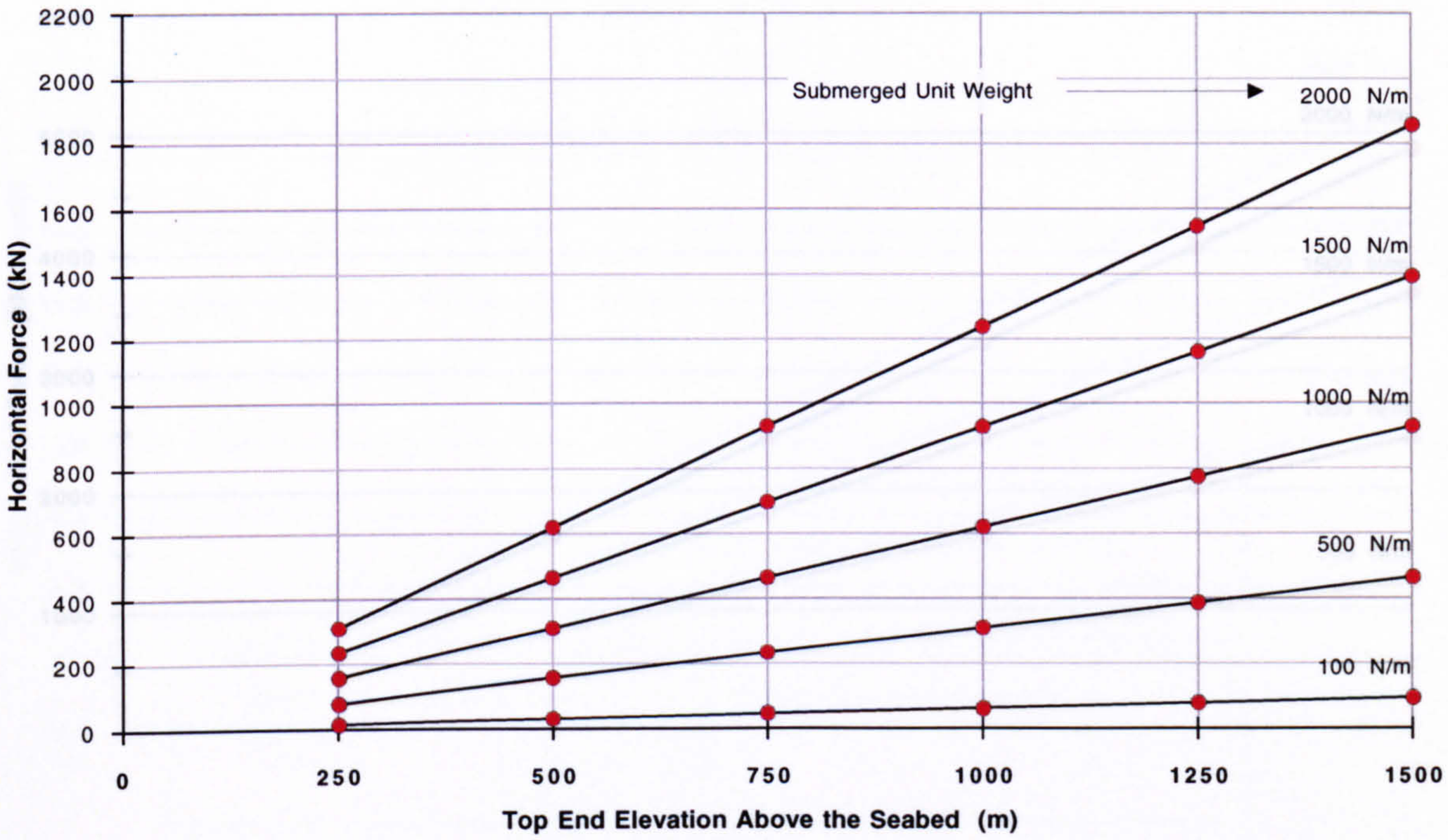

Lift Cable Vertical Load (V)

(b)

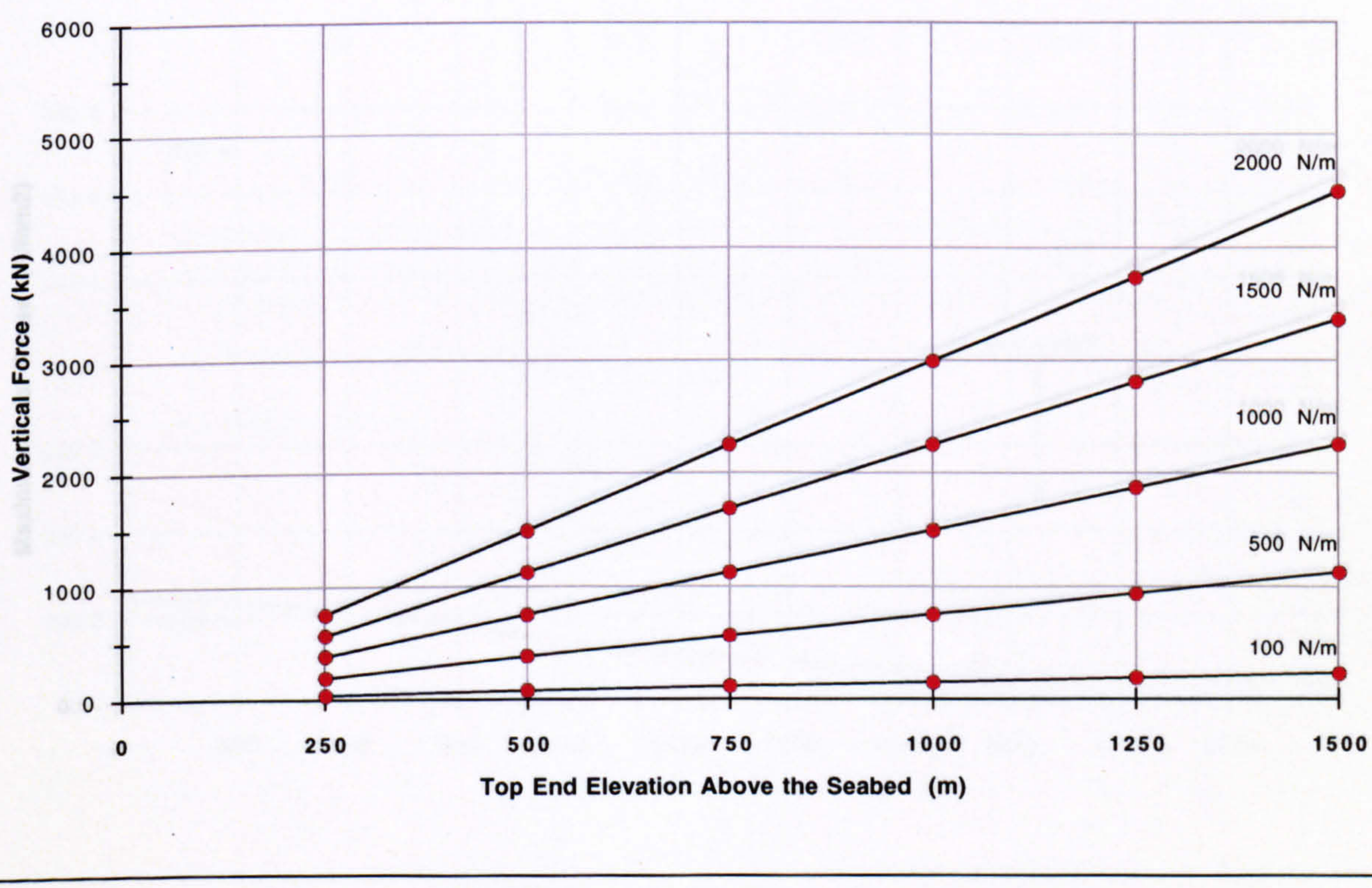

Horizontal Surface Offset = 1500 m

Sea Depth = 1500 m

Figure 5.38

Lift Cable Axial Loading

(c)

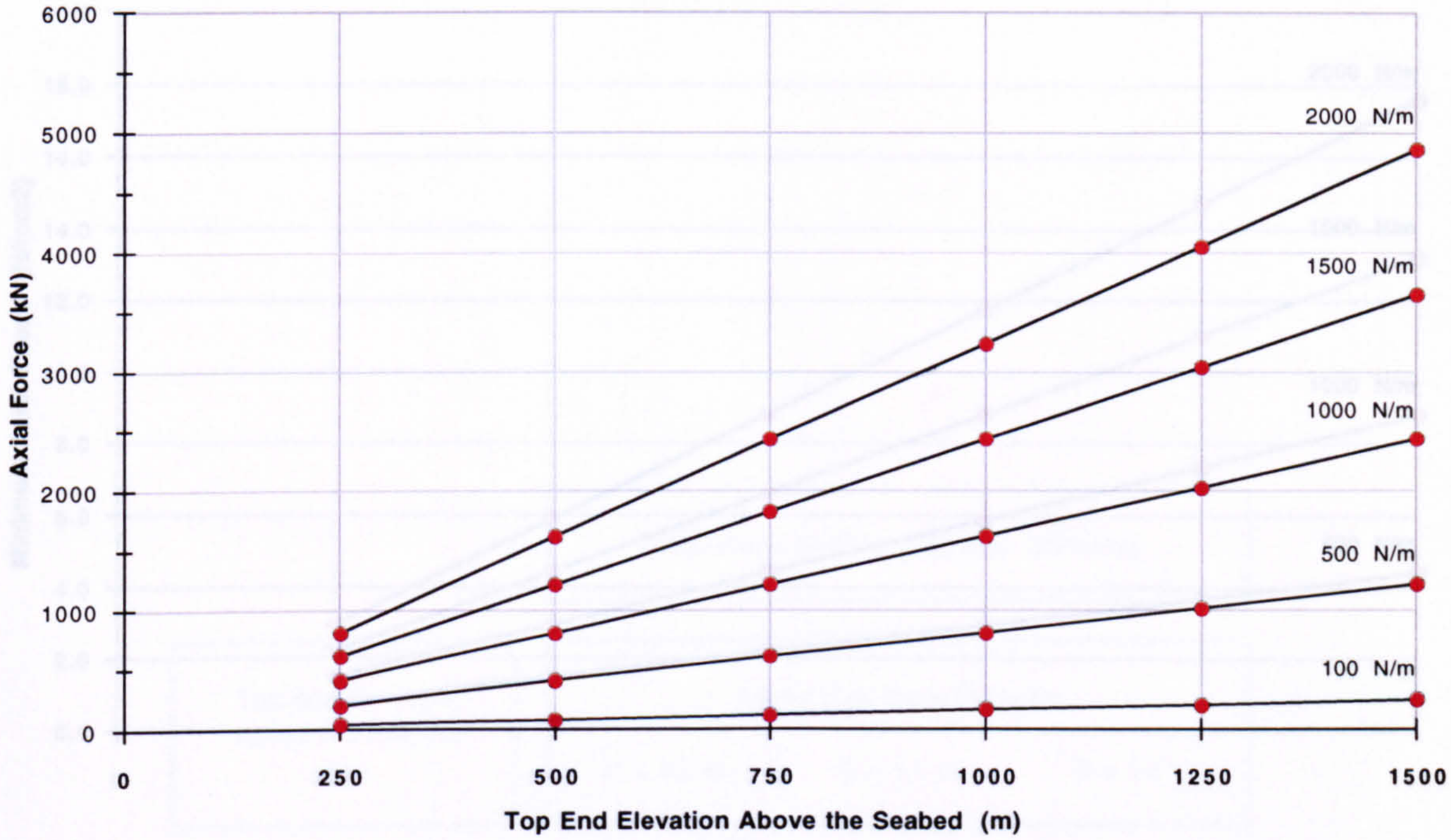

Axial Stress at the Top End of the Riser

(d)

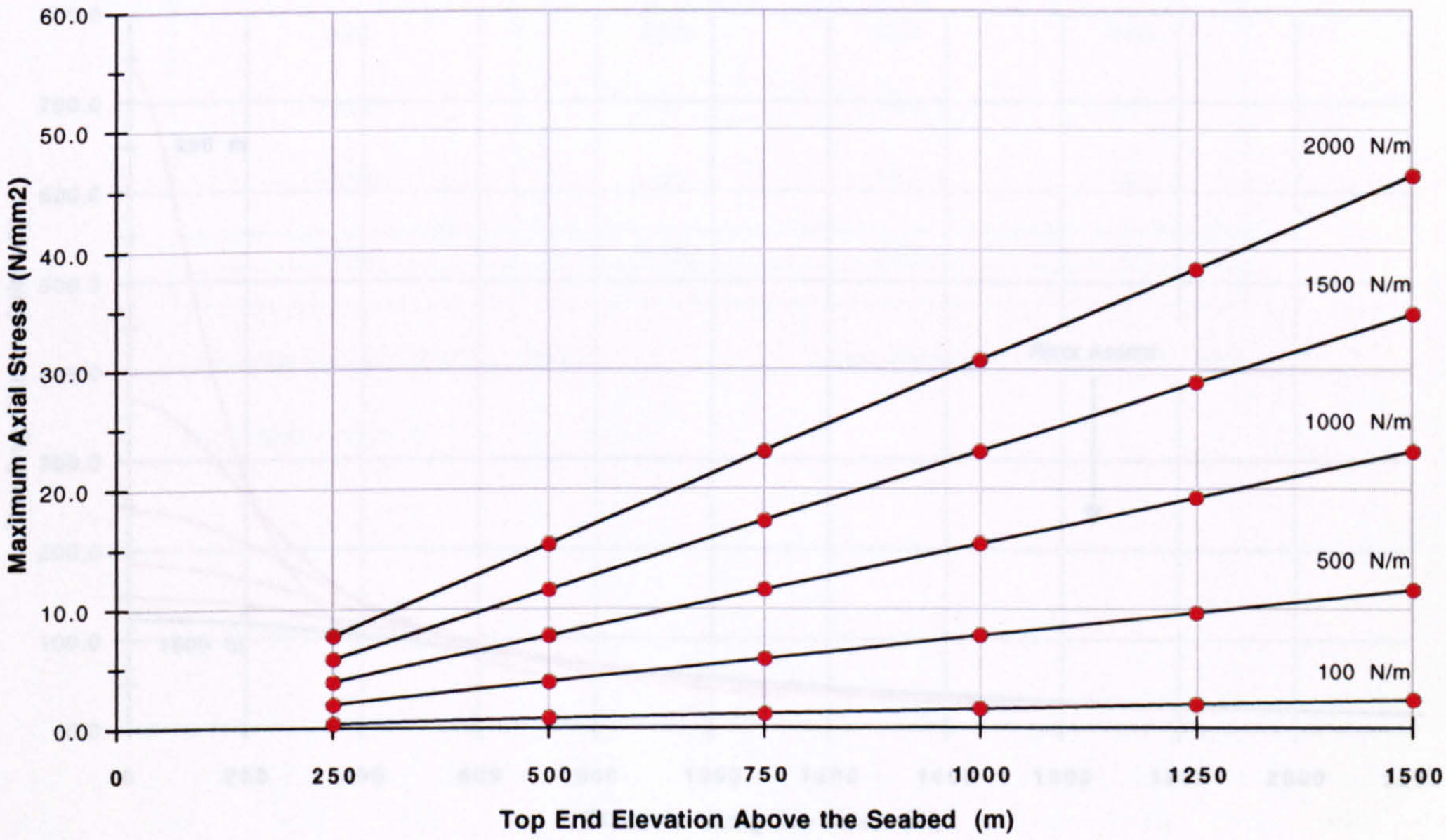

Horizontal Surface Offset = 1500 m

Sea Depth = 1500 m

Carrier Pipe Outer Diameter = 1.1 m

Carrier Pipe Wall Thickness = 10 mm

Figure 5.38

Axial Stress at the Seabed

(e)

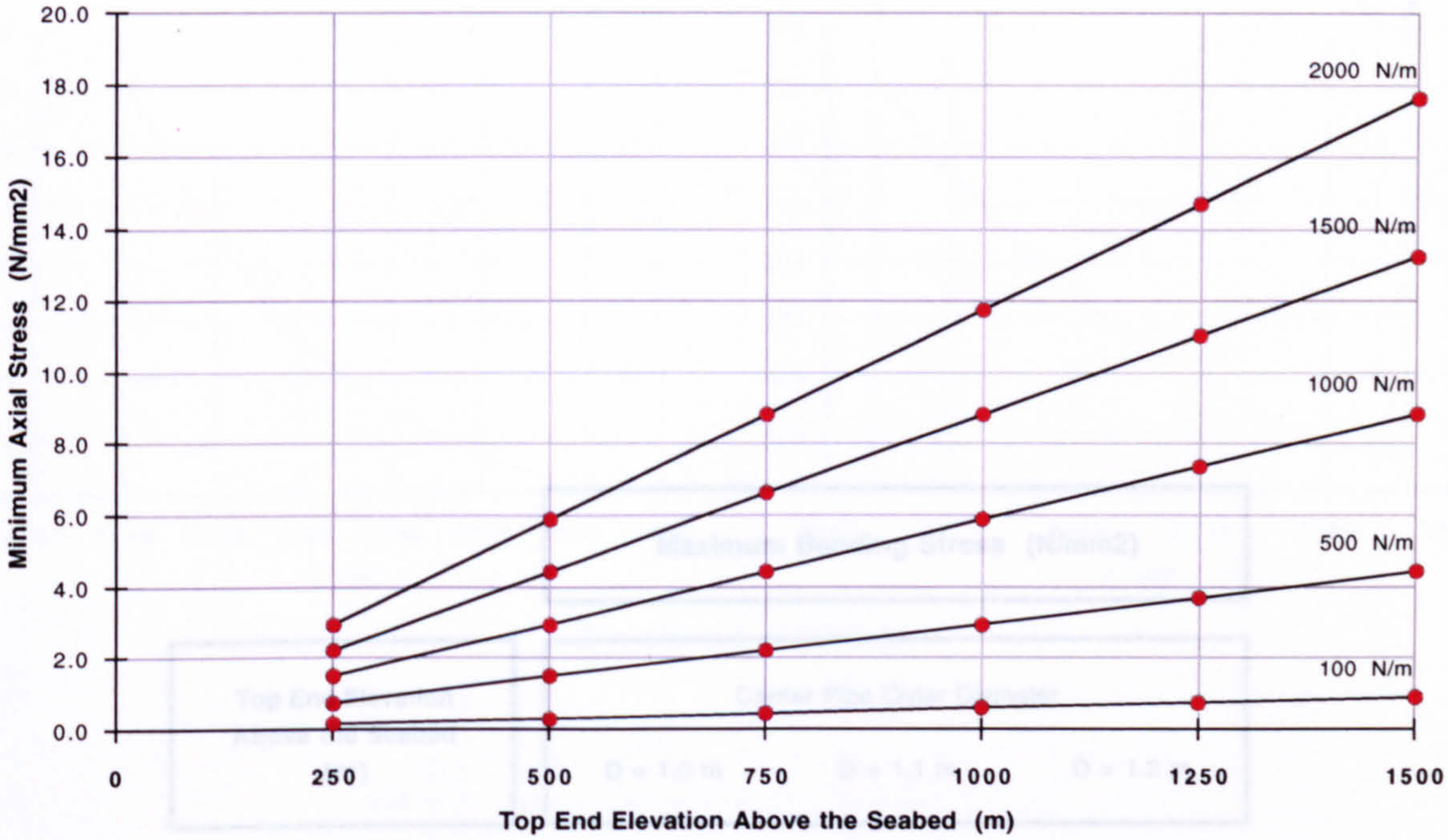

Bending Stress Distributions along the Riser

(f)

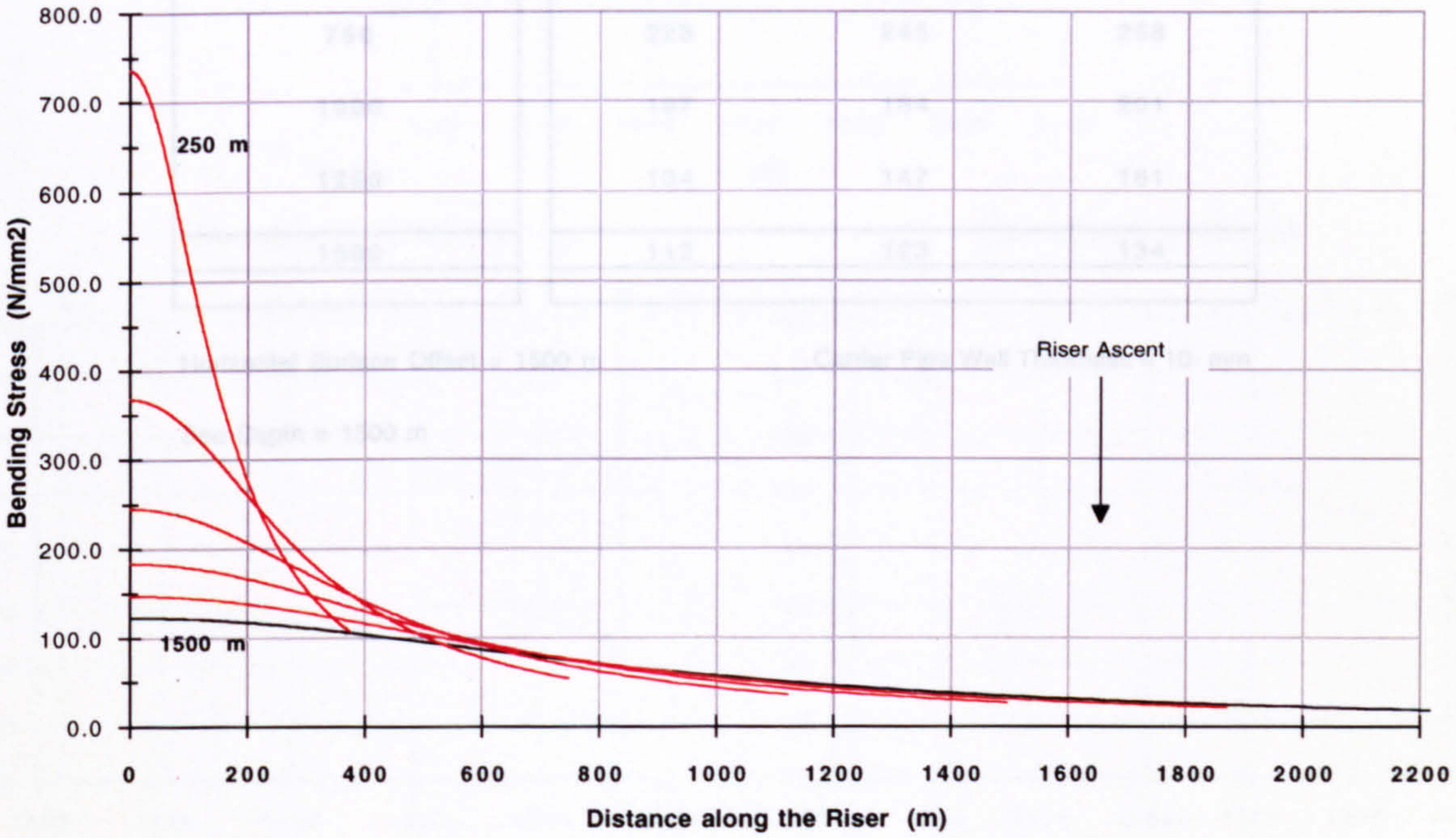

Horizontal Surface Offset = 1500 m

Sea Depth = 1500 m

Carrier Pipe Outer Diameter = 1.1 m

Carrier Pipe Wall Thickness = 10 mm

Figure 5.38

Bending Stress at the Seabed - Straight Line Lift Trajectory (a = 1500 m)

Top End Elevation Above the Seabed (m)	Maximum Bending Stress (N/mm2)		
	Carrier Pipe Outer Diameter		
	D = 1.0 m	D = 1.1 m	D = 1.2 m
0	0	0	0
250	669	736	802
500	335	368	402
750	223	245	268
1000	167	184	201
1250	134	147	161
1500	112	123	134

Horizontal Surface Offset = 1500 m

Carrier Pipe Wall Thickness = 10 mm

Sea Depth = 1500 m

Table 5.39

Maximum Bending Stress (Seabed)

Elevation 1 (250 m)

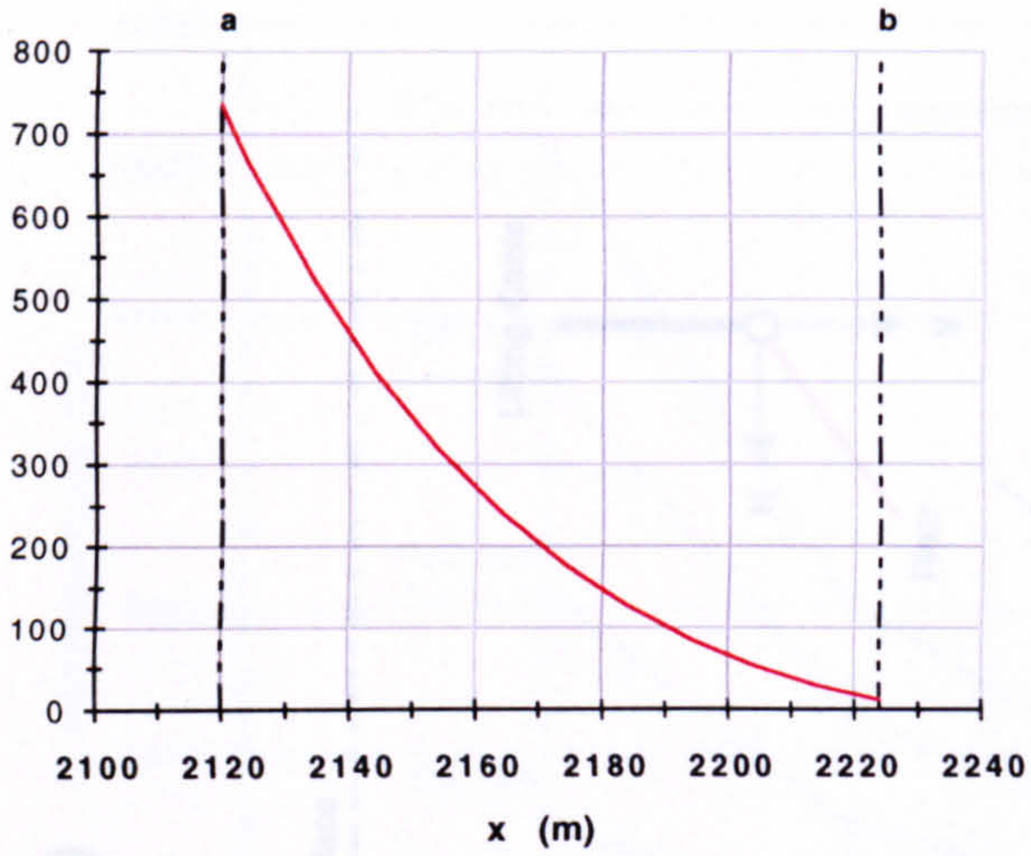

Elevation 2 (750 m)

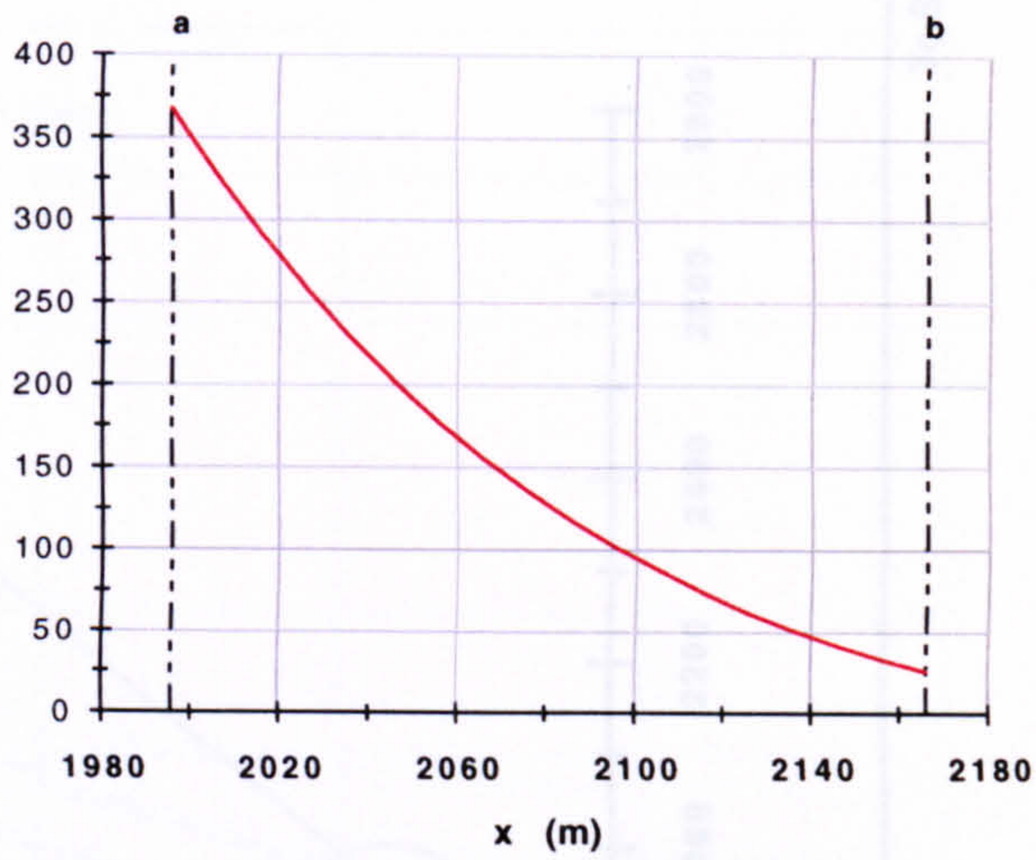

Elevation 3 (1000 m)

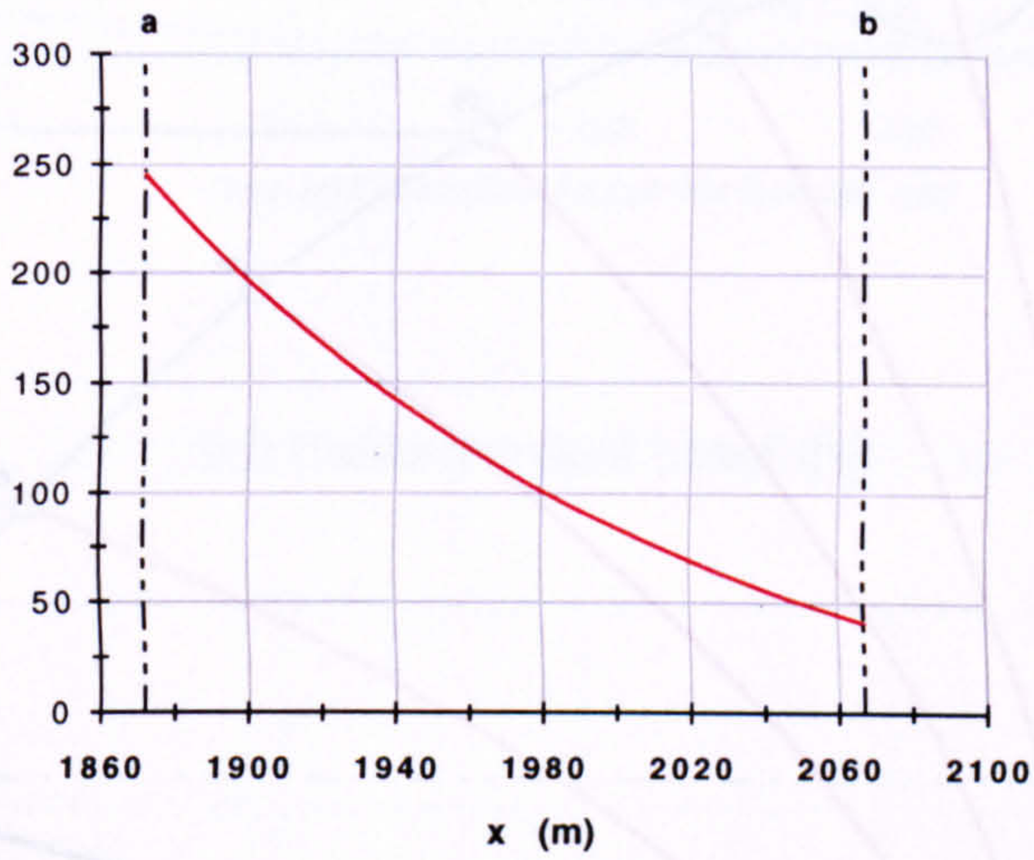

Elevation 4 (1000 m)

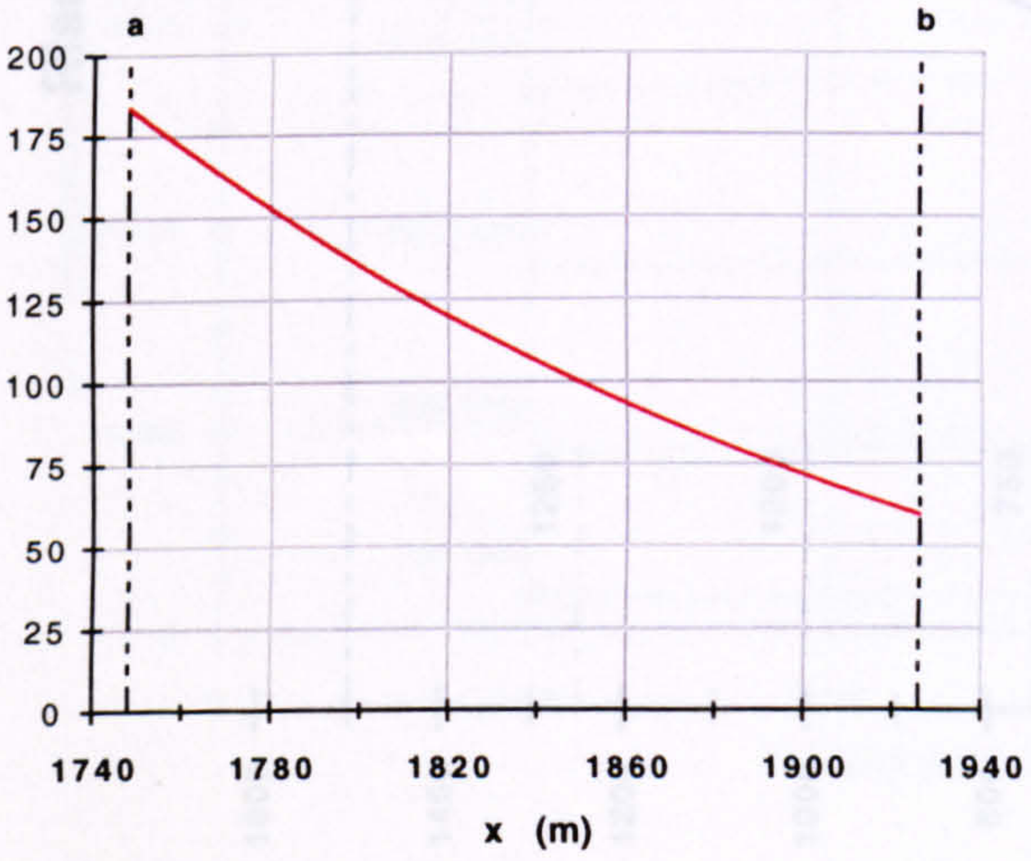

Elevation 5 (1250 m)

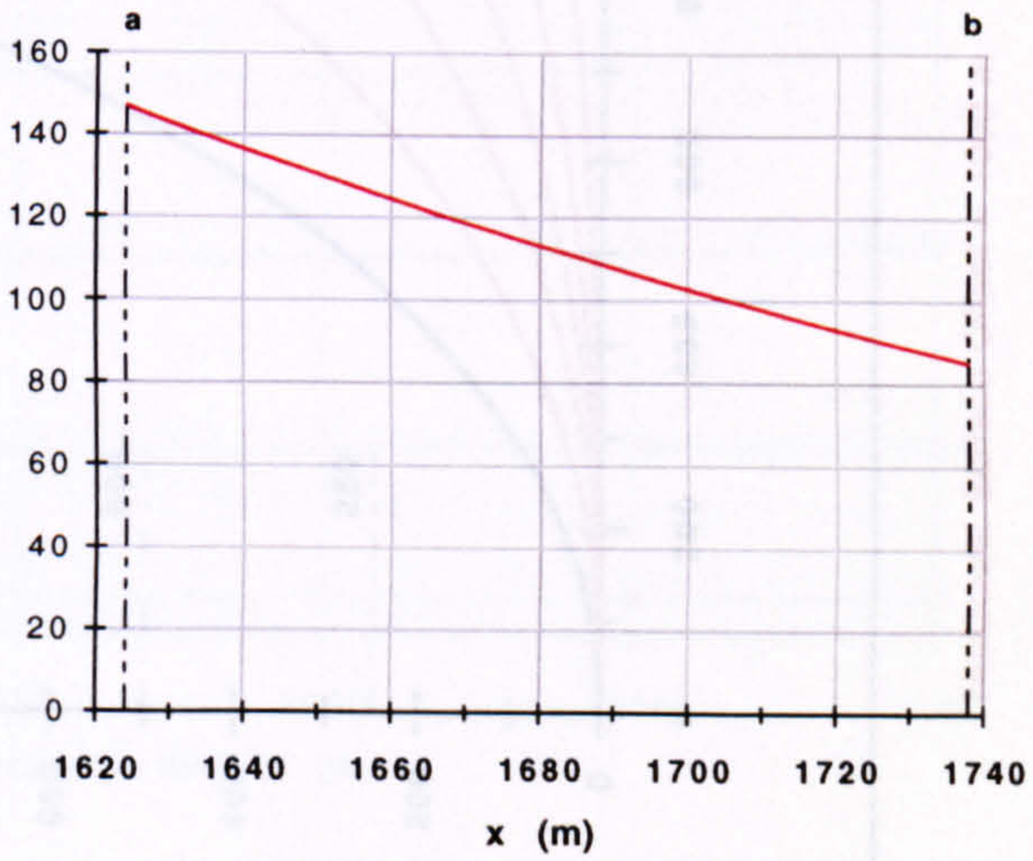

Horizontal Surface Offset = 1500 m

Carrier Pipe Outer Diameter = 1.1 m

Sea Depth = 1500 m

Figure 5.40

Riser Installation - Lift Sequence (a = 1000 m)

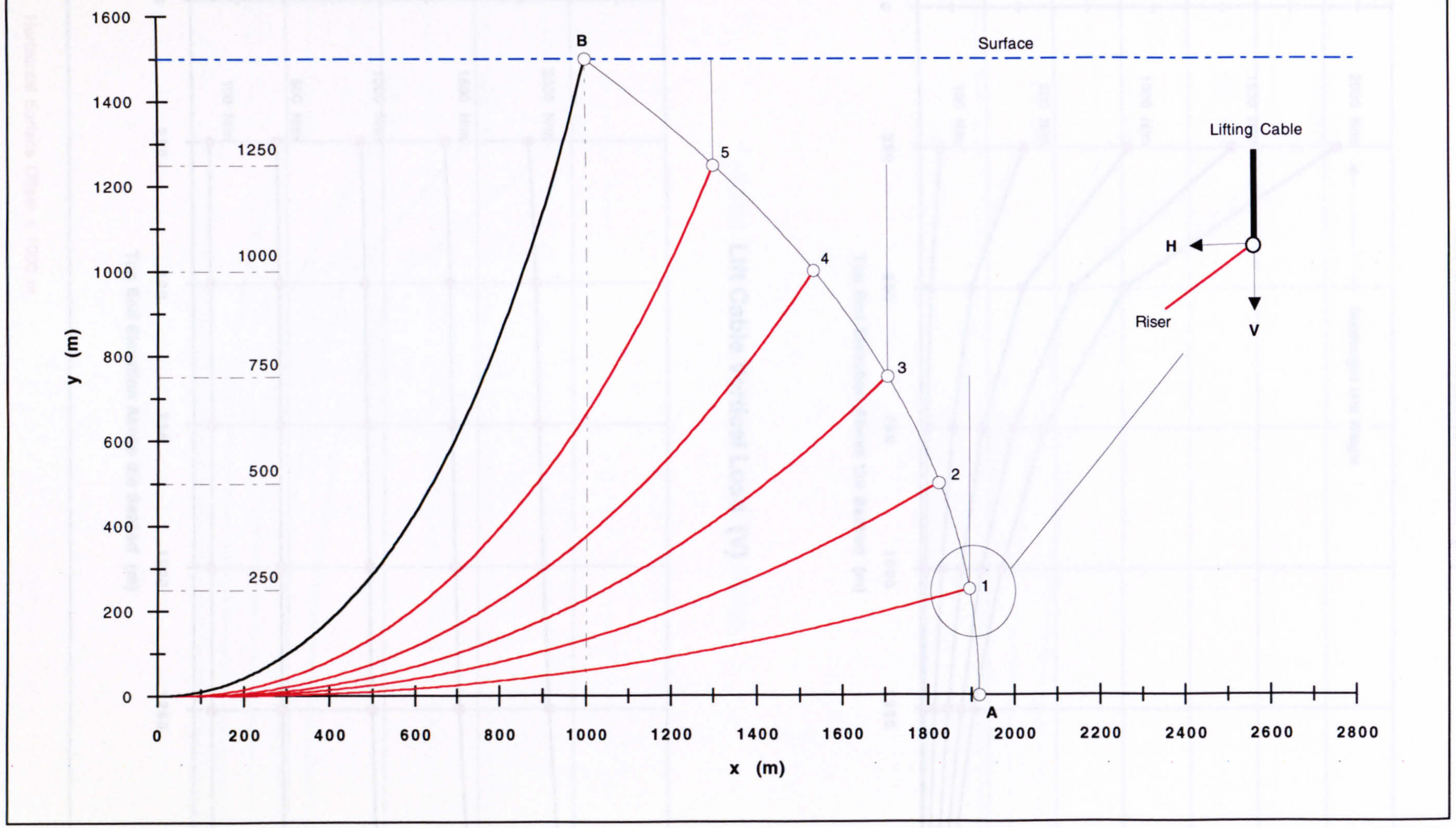

To Scale

Horizontal Surface Offset = 1000 m

Sea Depth = 1500 m

Figure 5.41

Lift Cable Horizontal Load (H)

(a)

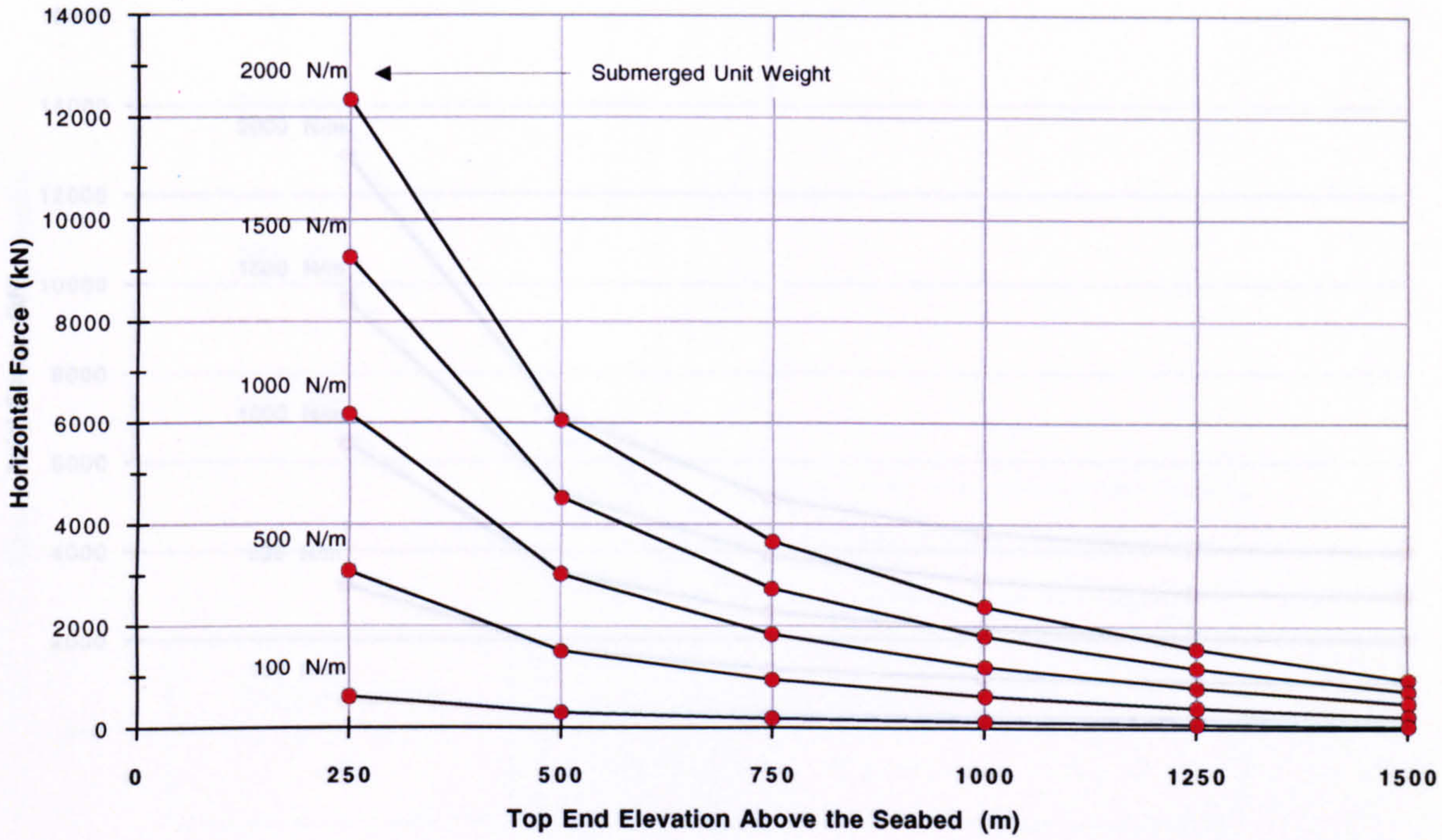

Lift Cable Vertical Load (V)

(b)

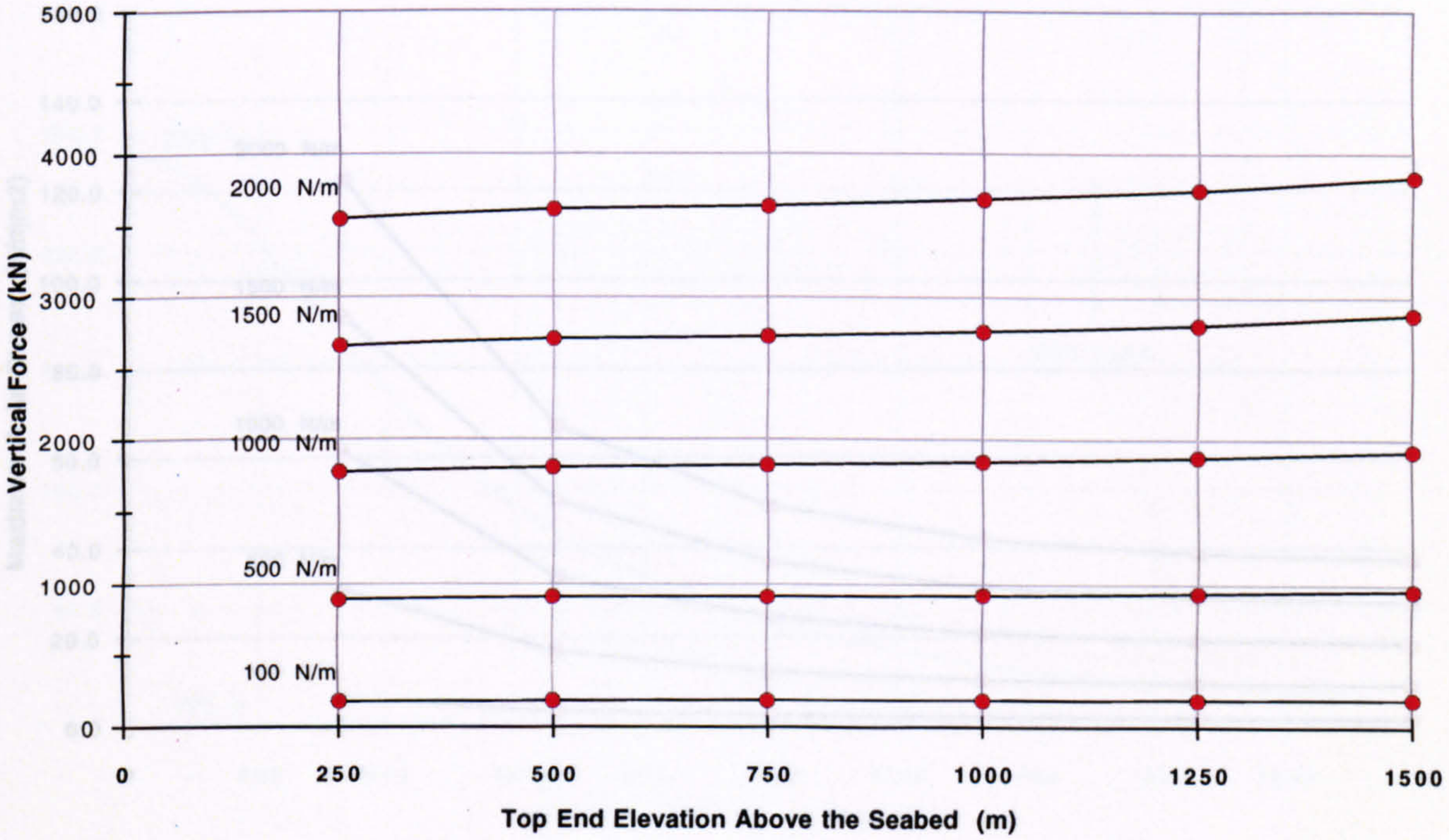

Horizontal Surface Offset = 1000 m

Sea Depth = 1500 m

Figure 5.42

Lift Cable Axial Load

(c)

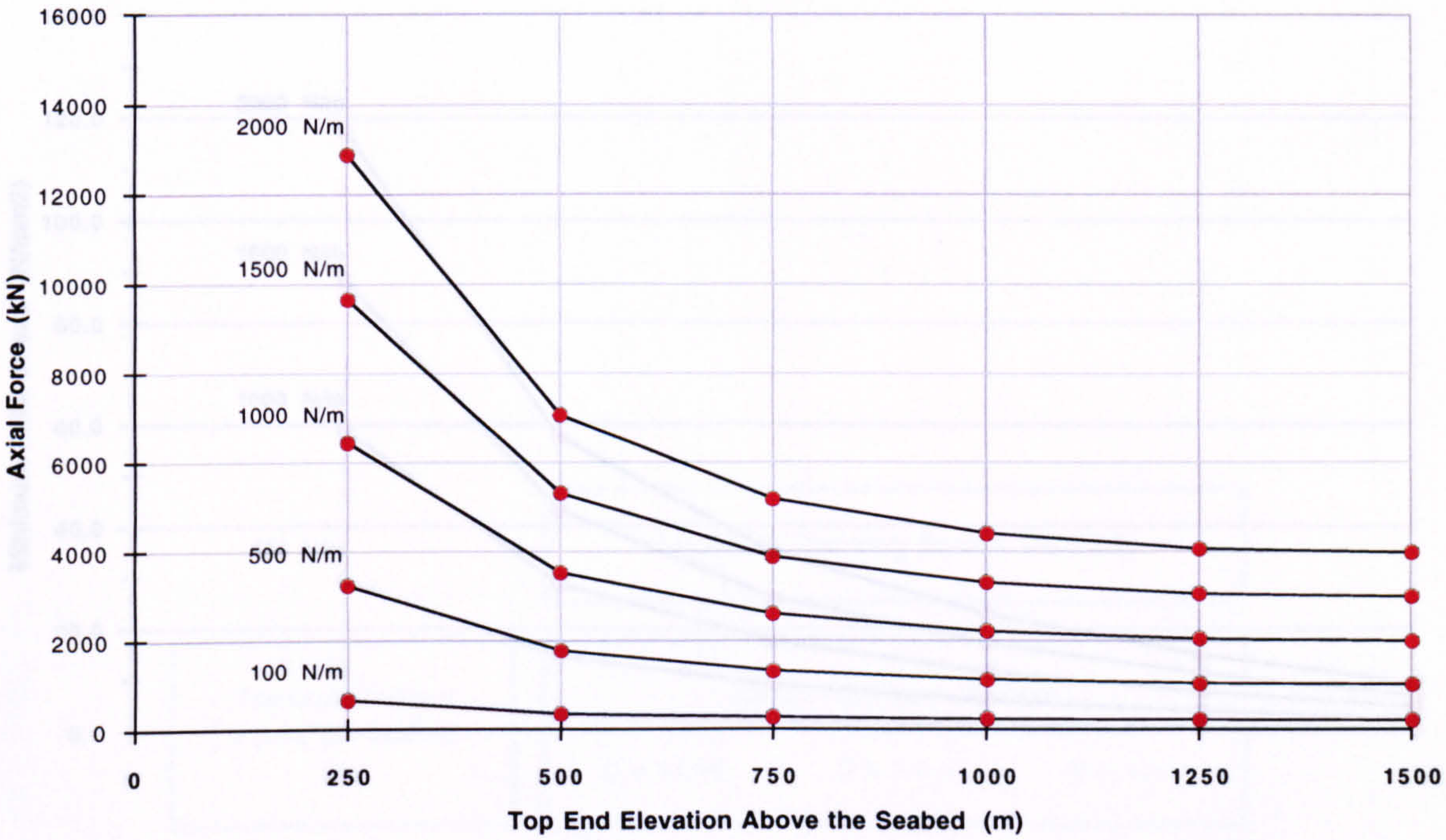

Axial Stress at the Top End of the Riser

(d)

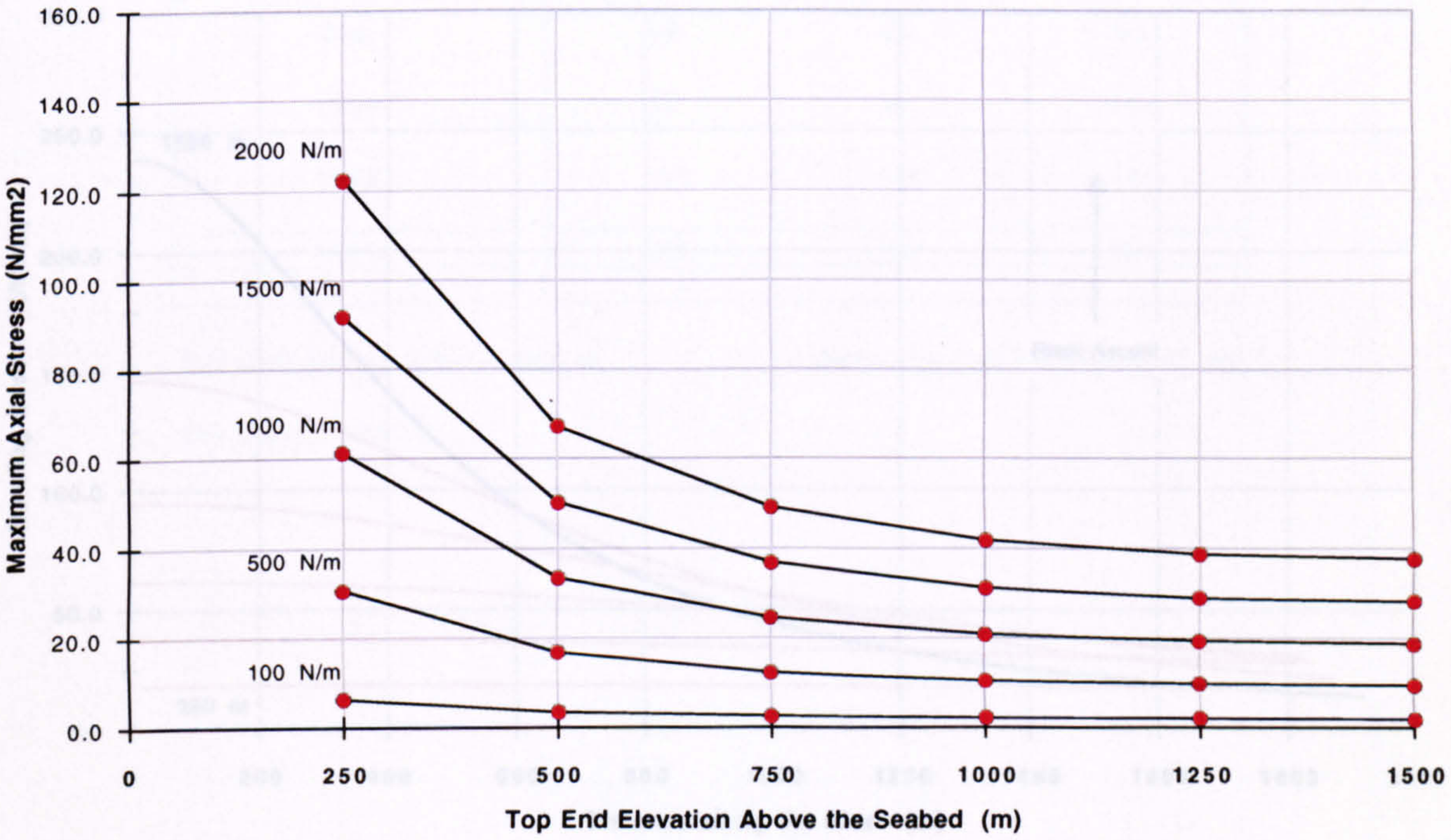

Horizontal Surface Offset = 1000 m

Sea Depth = 1500 m

Carrier Pipe Outer Diameter = 1.1 m

Carrier Pipe Wall Thickness = 10 mm

Figure 5.42

Axial Stress at the Seabed

(e)

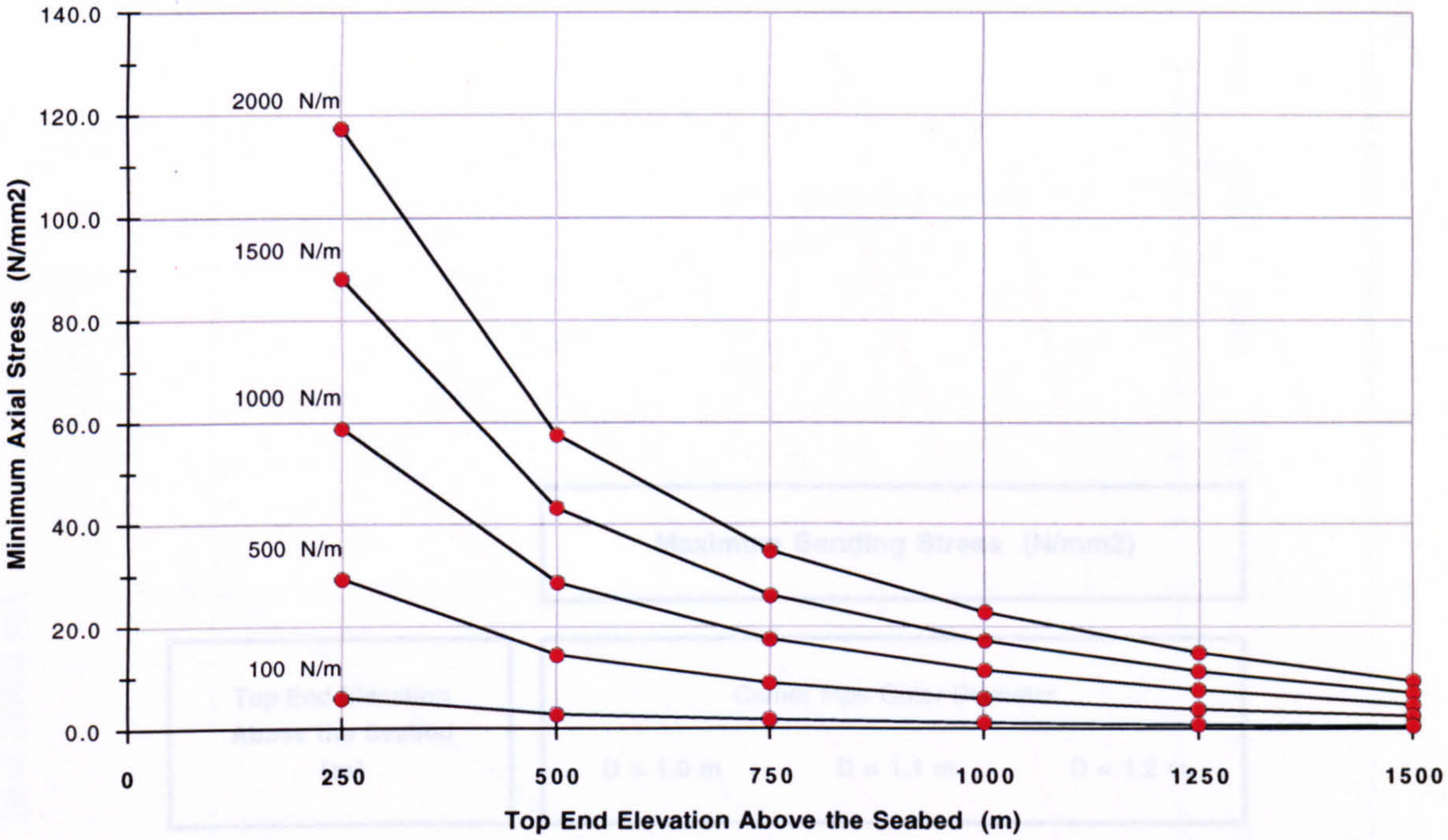

Bending Stress Distributions along the Riser

(f)

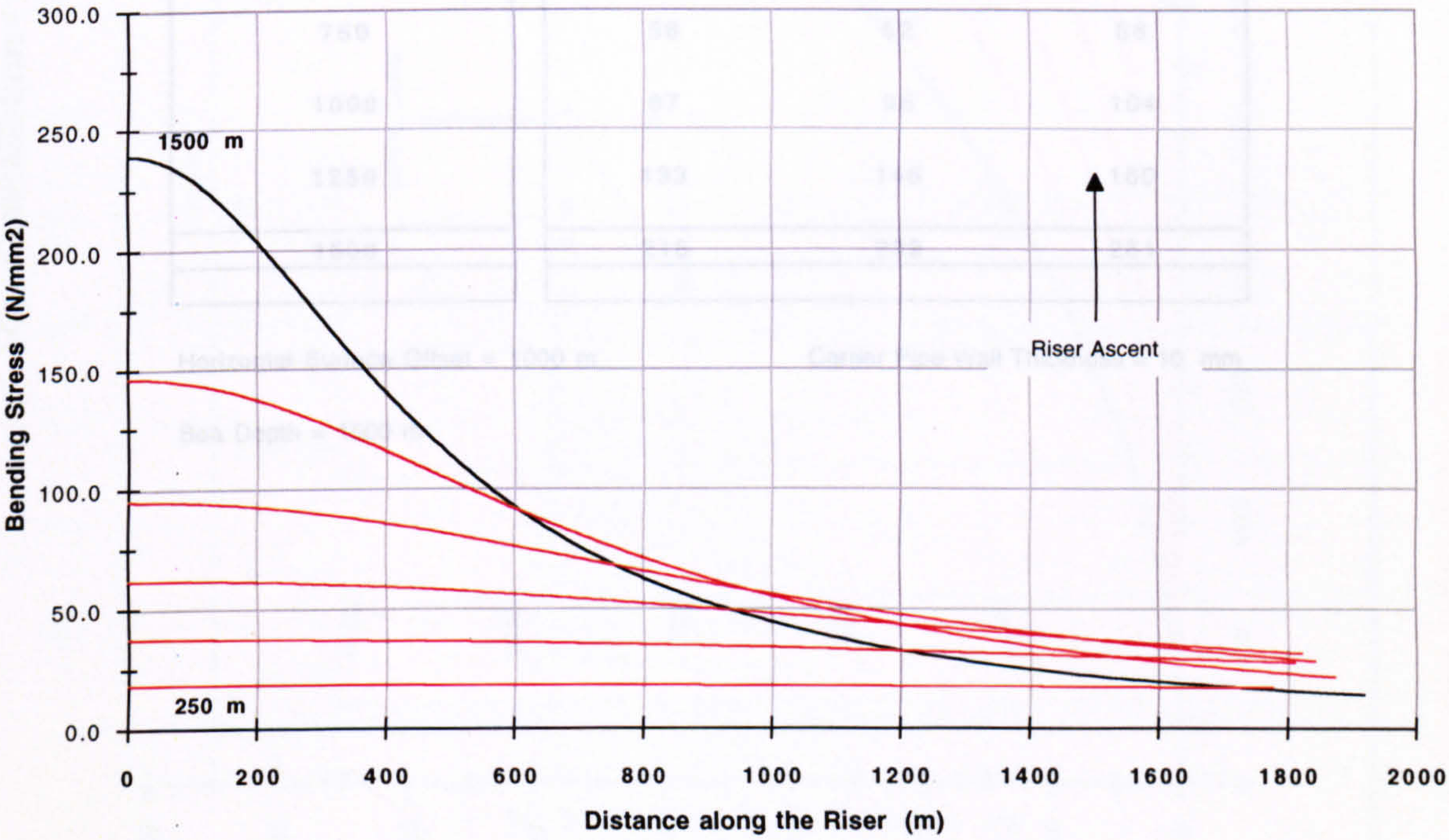

Horizontal Surface Offset = 1000 m

Sea Depth = 1500 m

Carrier Pipe Outer Diameter = 1.1 m

Carrier Pipe Wall Thickness = 10 mm

Figure 5.42

Bending Stress at the Seabed - Catenary Curve Lift Trajectory (a = 1000 m)

Top End Elevation Above the Seabed (m)	Maximum Bending Stress (N/mm2)		
	Carrier Pipe Outer Diameter		
	D = 1.0 m	D = 1.1 m	D = 1.2 m
0	0	0	0
250	17	18	20
500	34	38	41
750	56	62	68
1000	87	95	104
1250	133	146	160
1500	218	239	261

Horizontal Surface Offset = 1000 m

Carrier Pipe Wall Thickness = 10 mm

Sea Depth = 1500 m

Table 5.43

Riser Installation - Lift Sequence (a = 2000 m)

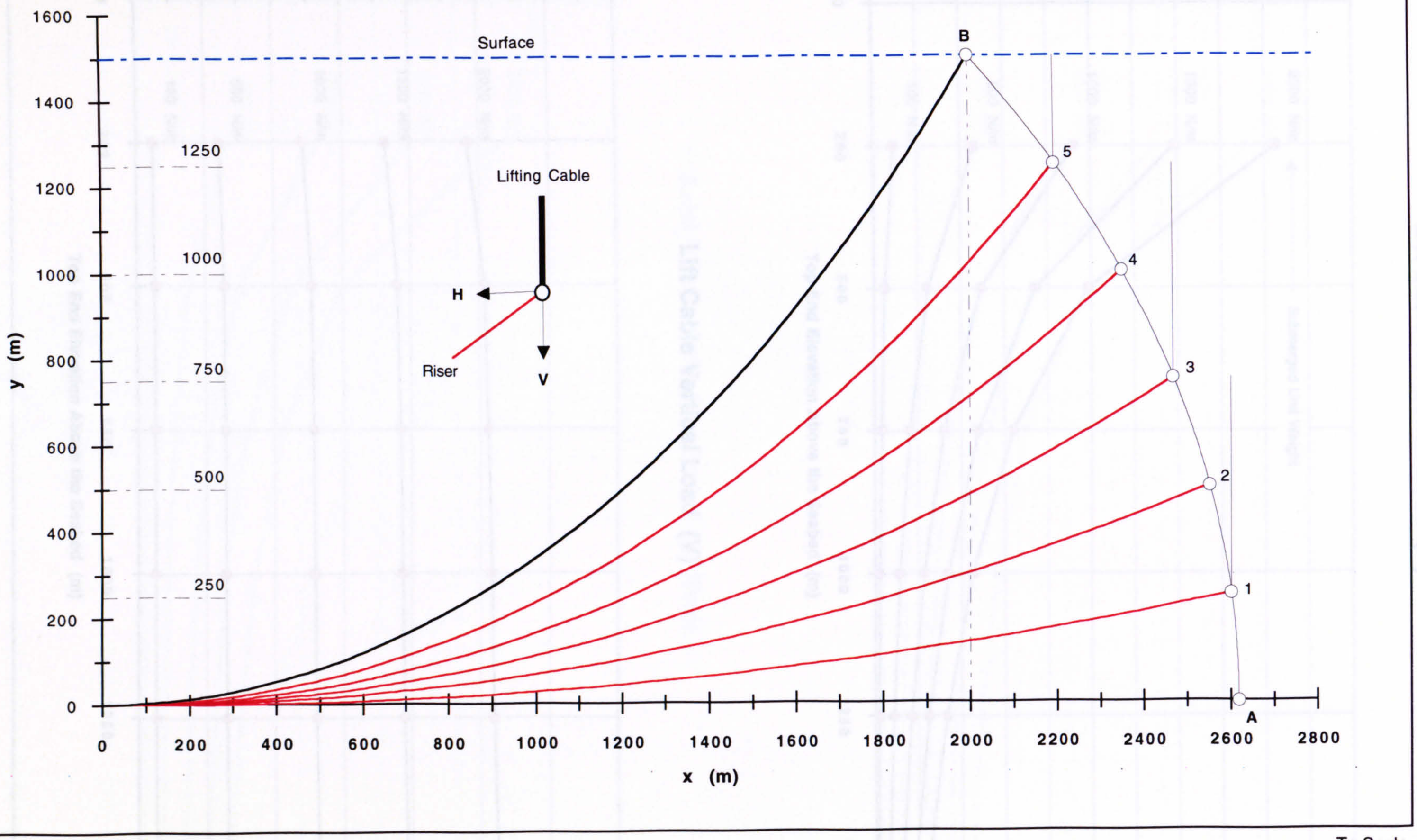

To Scale

Horizontal Surface Offset = 2000 m

Sea Depth = 1500 m

Figure 5.44

Lift Cable Horizontal Load (H)

(a)

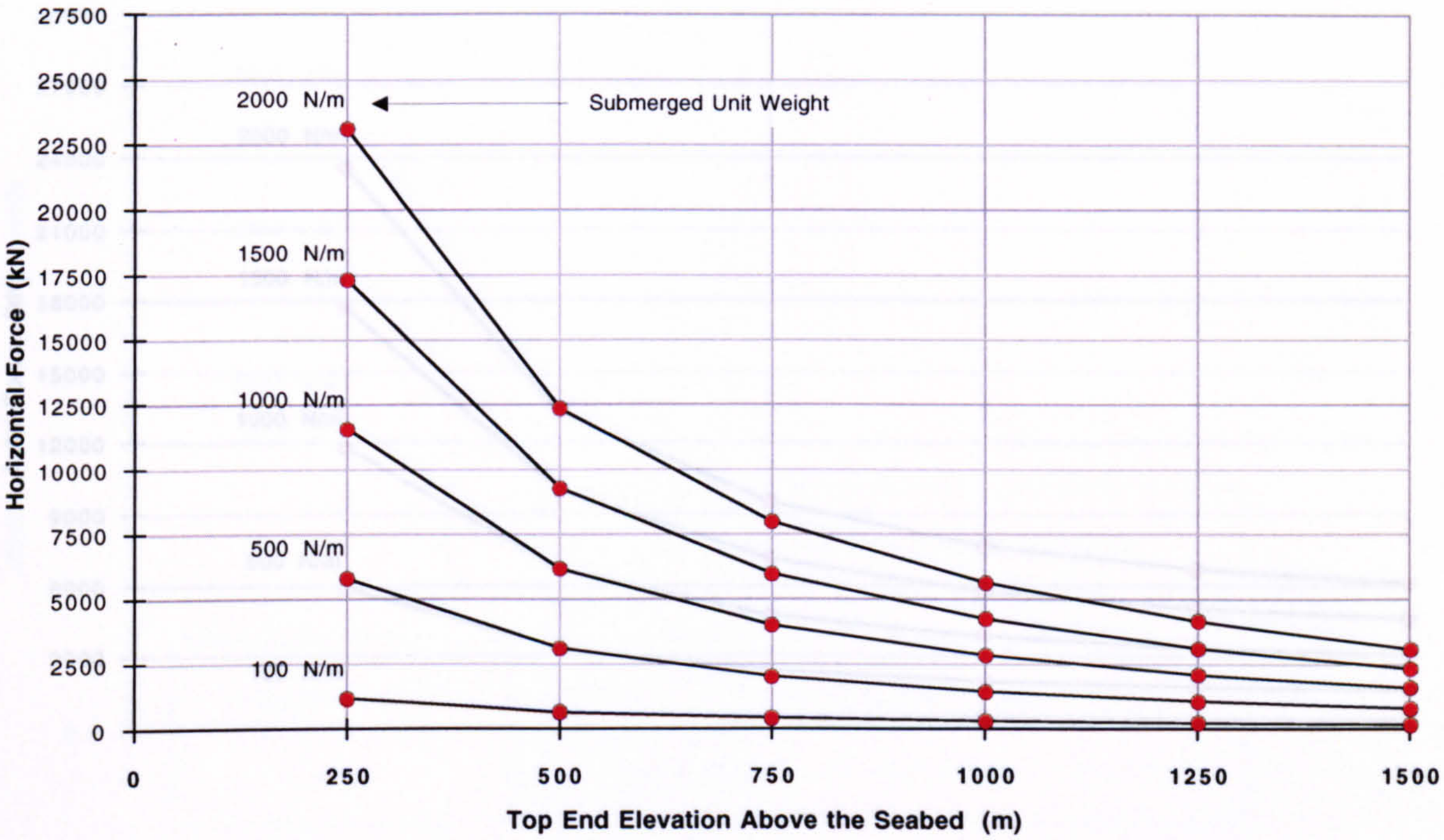

Lift Cable Vertical Load (V)

(b)

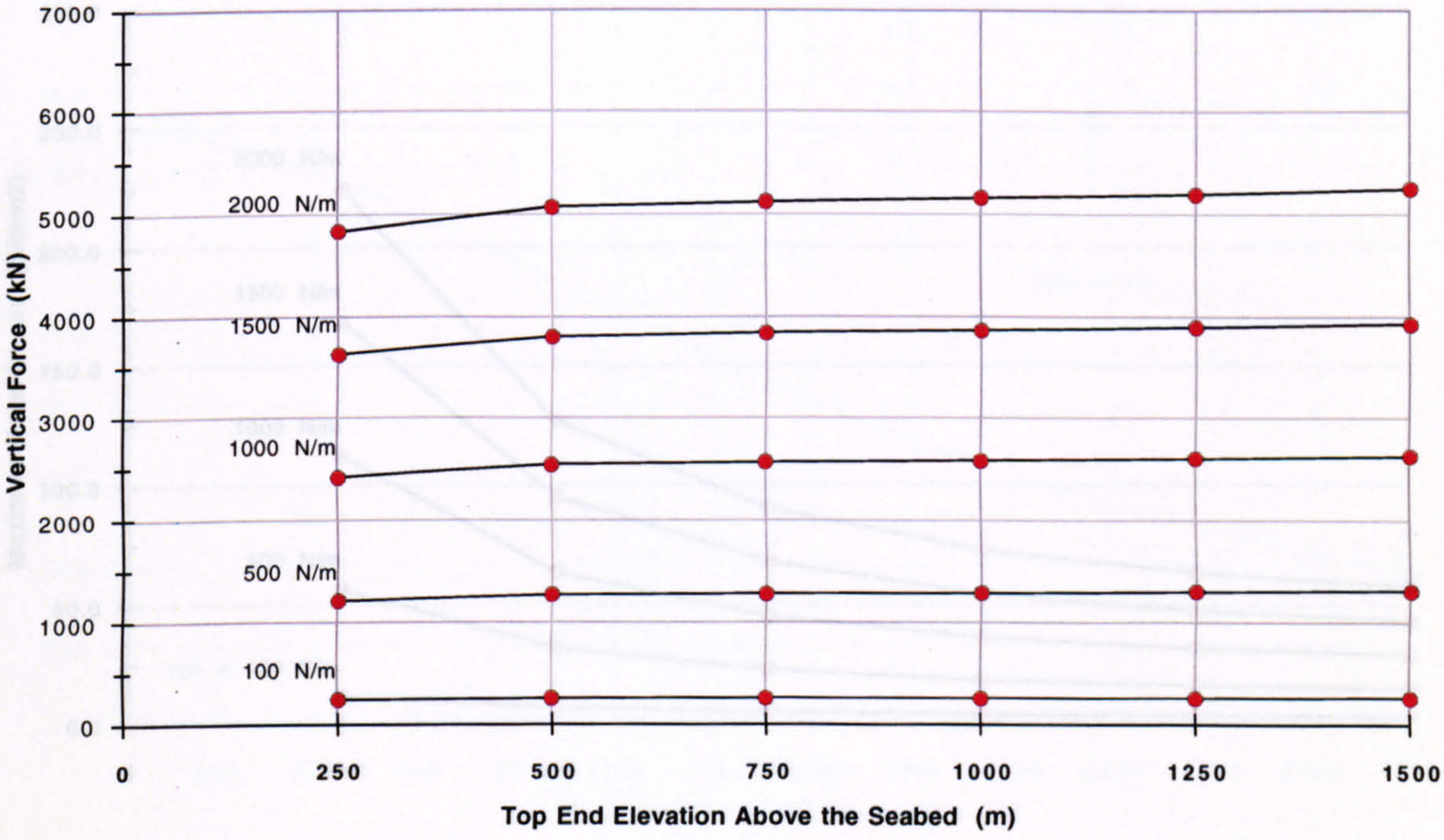

Horizontal Surface Offset = 2000 m

Sea Depth = 1500 m

Figure 5.45

Lift Cable Axial Load

(c)

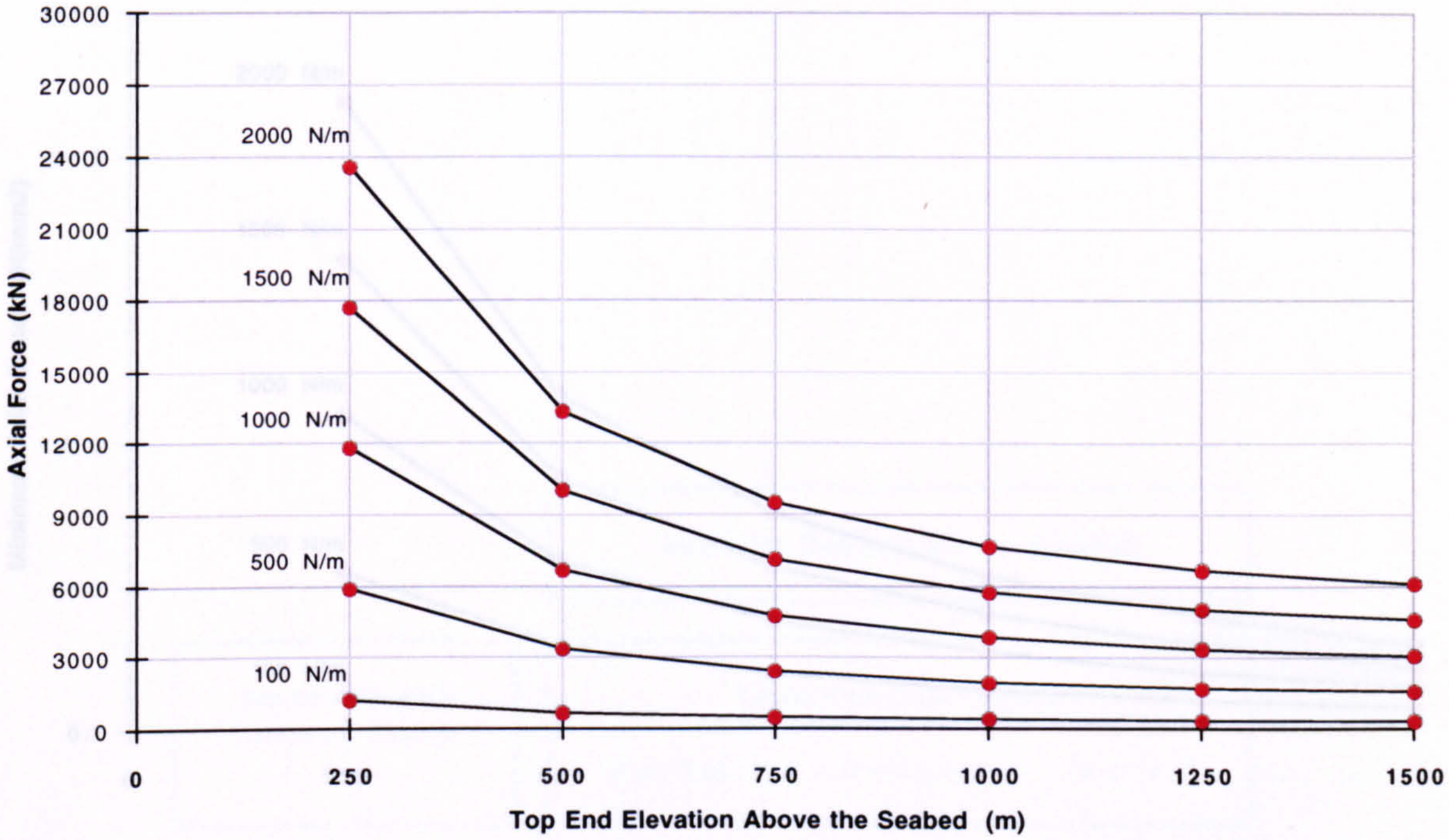

Axial Stress at the Top End of the Riser

(d)

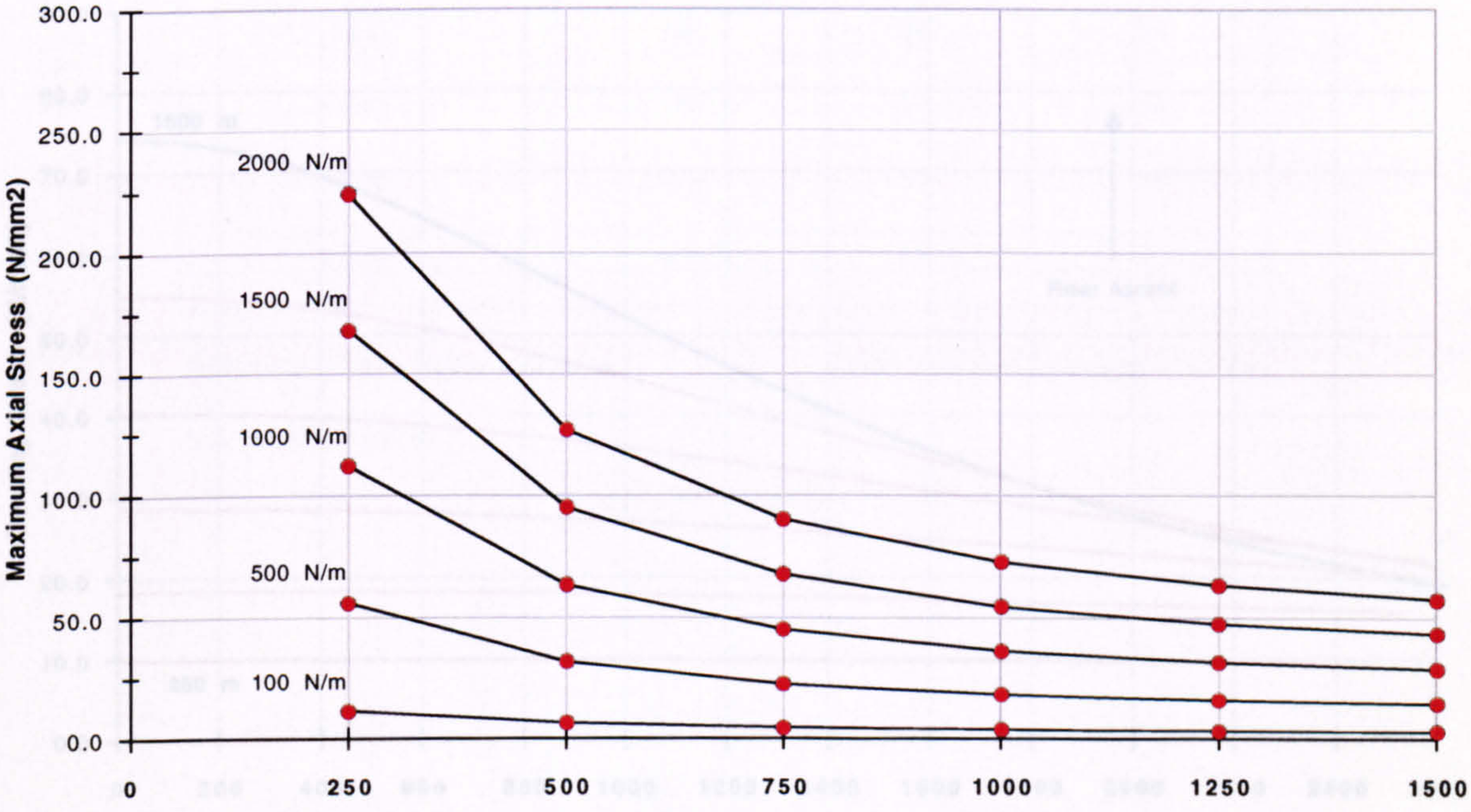

Horizontal Surface Offset = 2000 m

Sea Depth = 1500 m

Carrier Pipe Outer Diameter = 1.1 m

Carrier Pipe Wall Thickness = 10 mm

Figure 5.45

Axial Stress at the Seabed

(e)

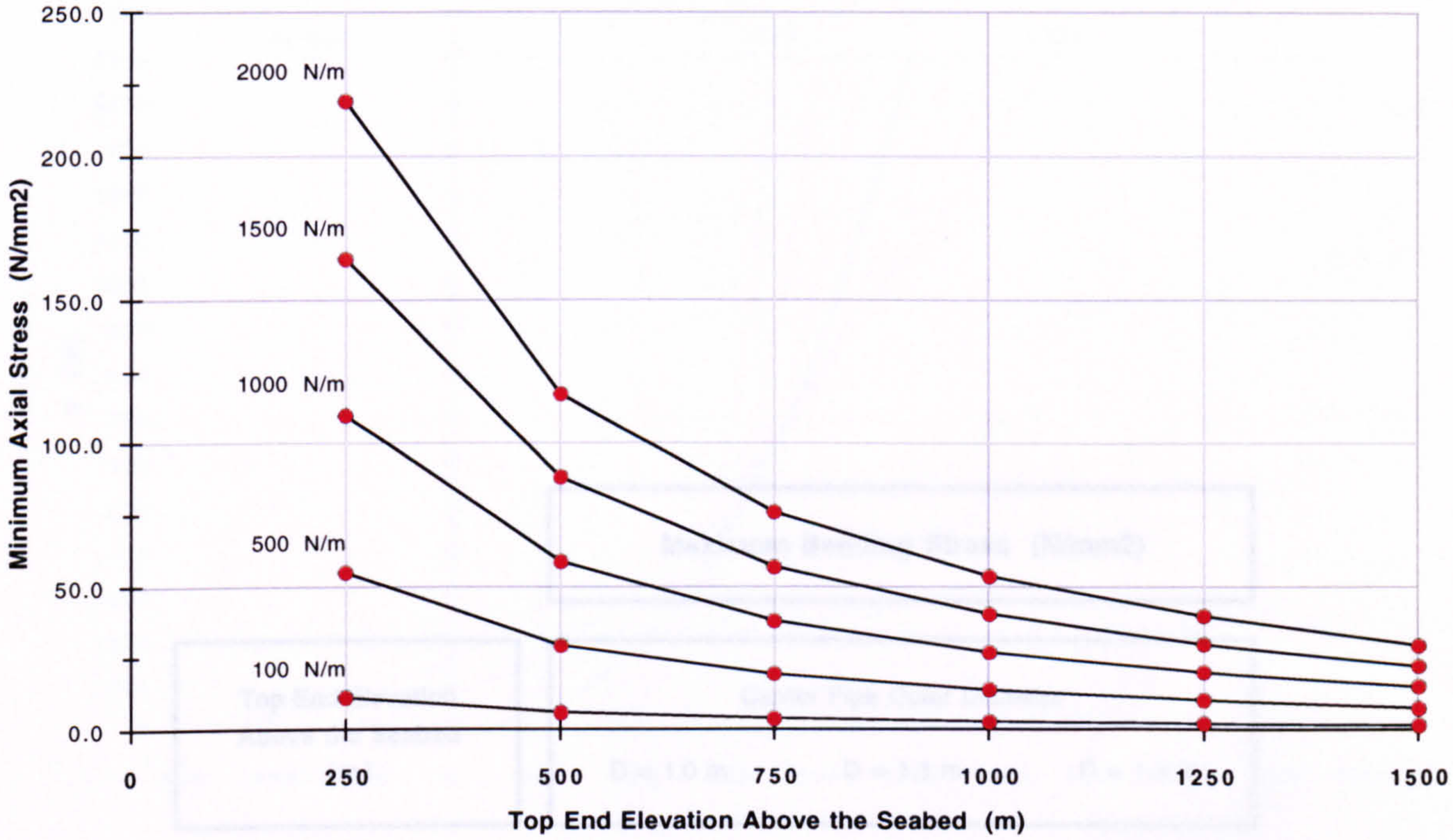

Bending Stress Distributions along the Riser

(f)

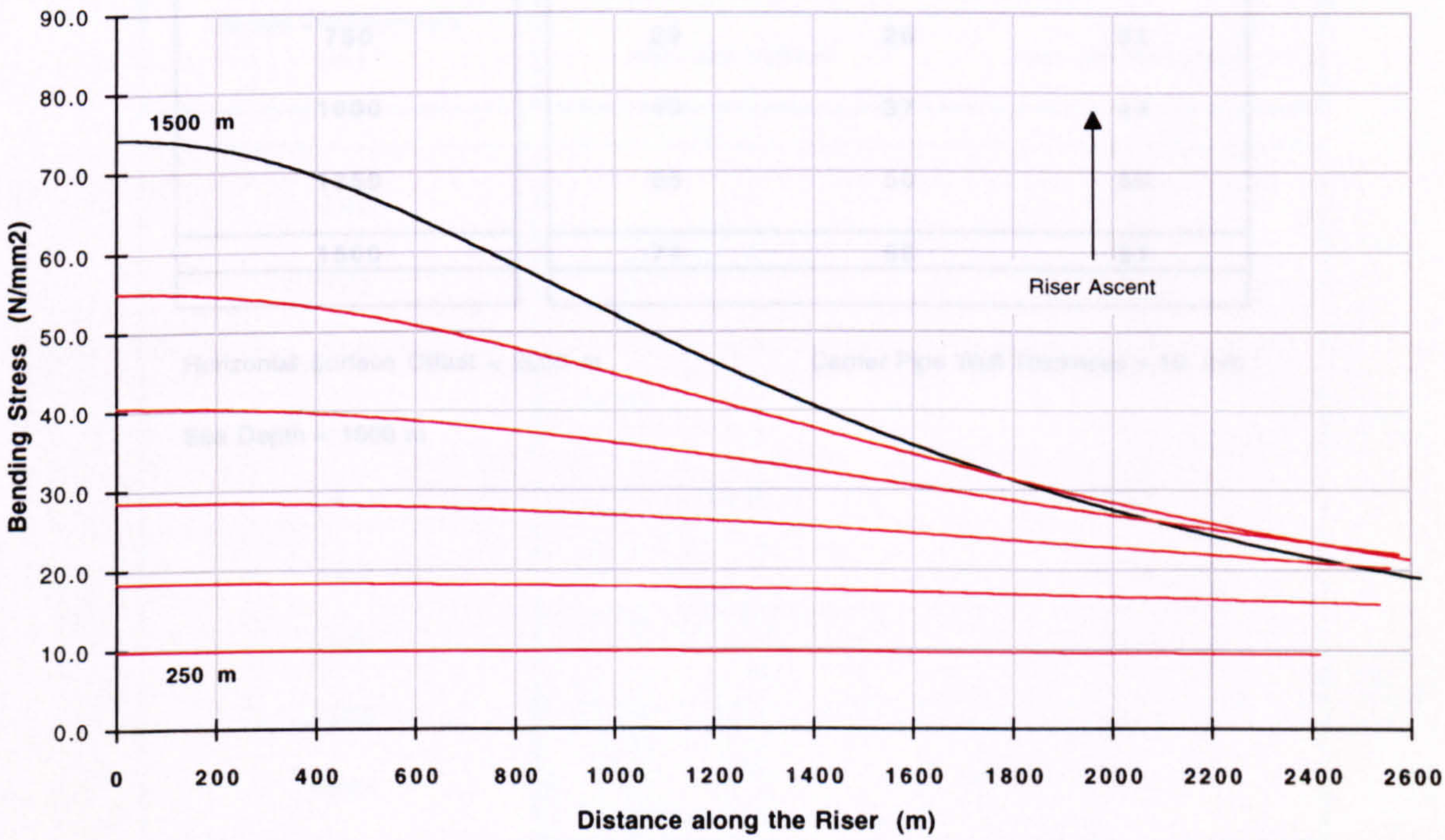

Horizontal Surface Offset = 2000 m

Sea Depth = 1500 m

Carrier Pipe Outer Diameter = 1.1 m

Carrier Pipe Wall Thickness = 10 mm

Figure 5.45

Bending Stress at the Seabed - Catenary Curve Lift Trajectory (a = 2000 m)

Top End Elevation Above the Seabed (m)	Maximum Bending Stress (N/mm2)		
	Carrier Pipe Outer Diameter		
	D = 1.0 m	D = 1.1 m	D = 1.2 m
0	0	0	0
250	10	9	11
500	18	17	20
750	29	26	31
1000	40	37	44
1250	55	50	60
1500	74	68	81

Horizontal Surface Offset = 2000 m

Carrier Pipe Wall Thickness = 10 mm

Sea Depth = 1500 m

Table 5.46

Surge Displacement Profiles (a = 1000 m)

(a)

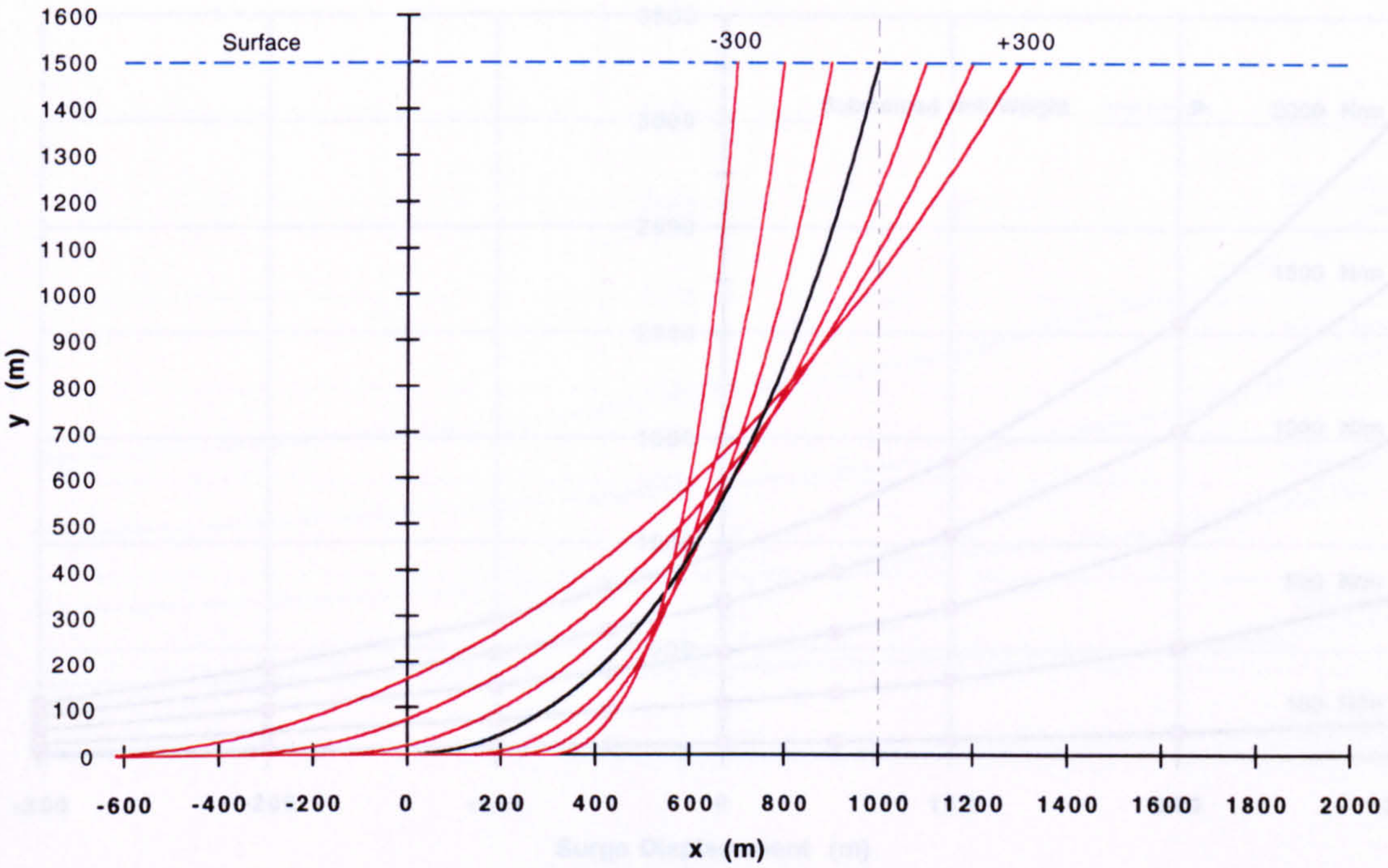

Riser Inclination at the Surface

(b)

Surge Displacement (m)	Surface Inclination (degs) from the Vertical	from the Horizontal
-300	4.3	85.7
-200	6.9	83.1
-100	10.1	79.9
-50	11.9	78.1
0	13.9	76.1
+50	16.1	73.9
+100	18.5	71.5
+200	24.0	66.0
+300	30.3	59.7

Mean Horizontal Surface Offset = 1000 m

Sea Depth = 1500 m

Figure 5.47

Horizontal Load at the Surface (H)

(c)

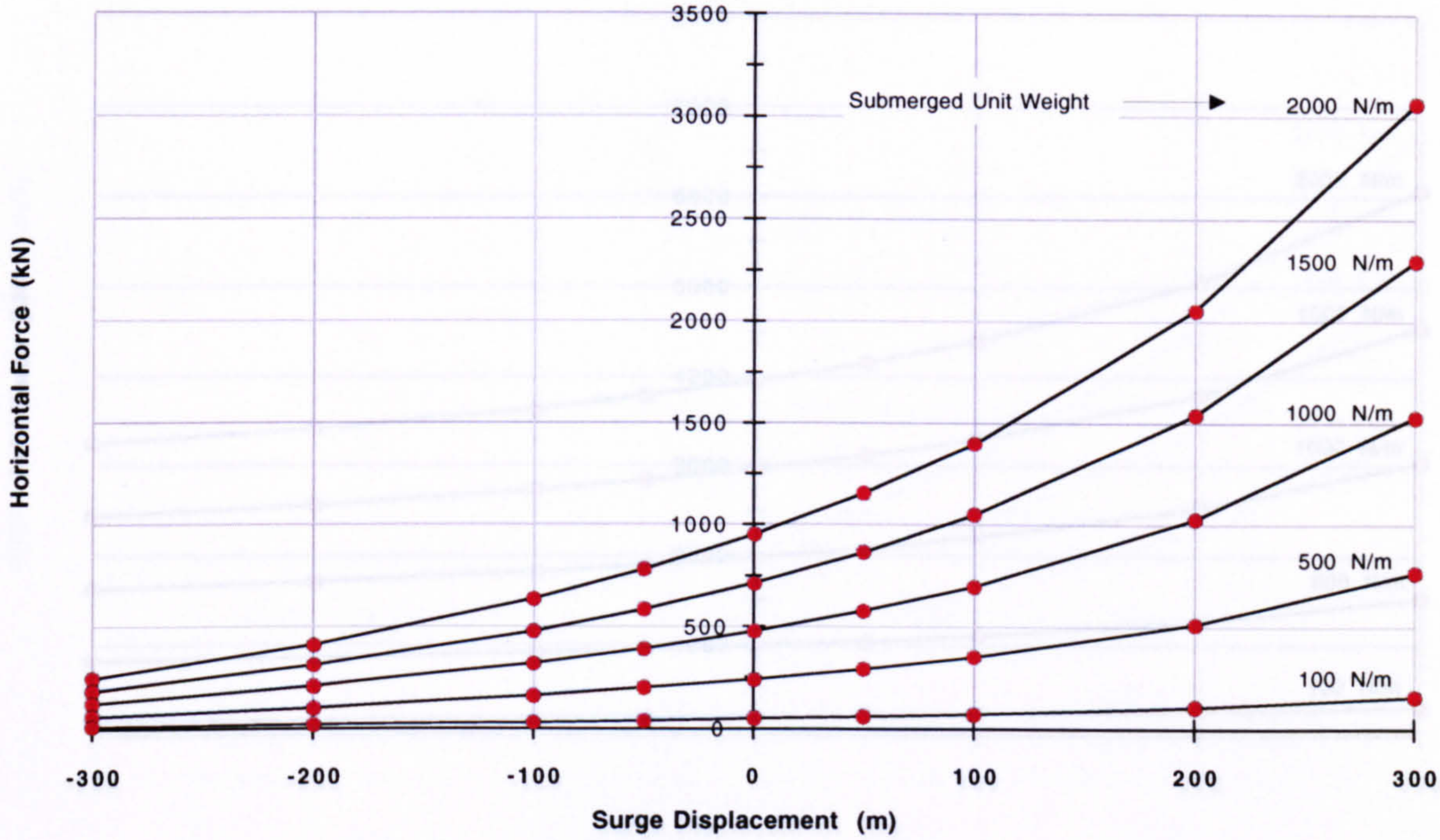

Vertical Load at the Surface (V)

(d)

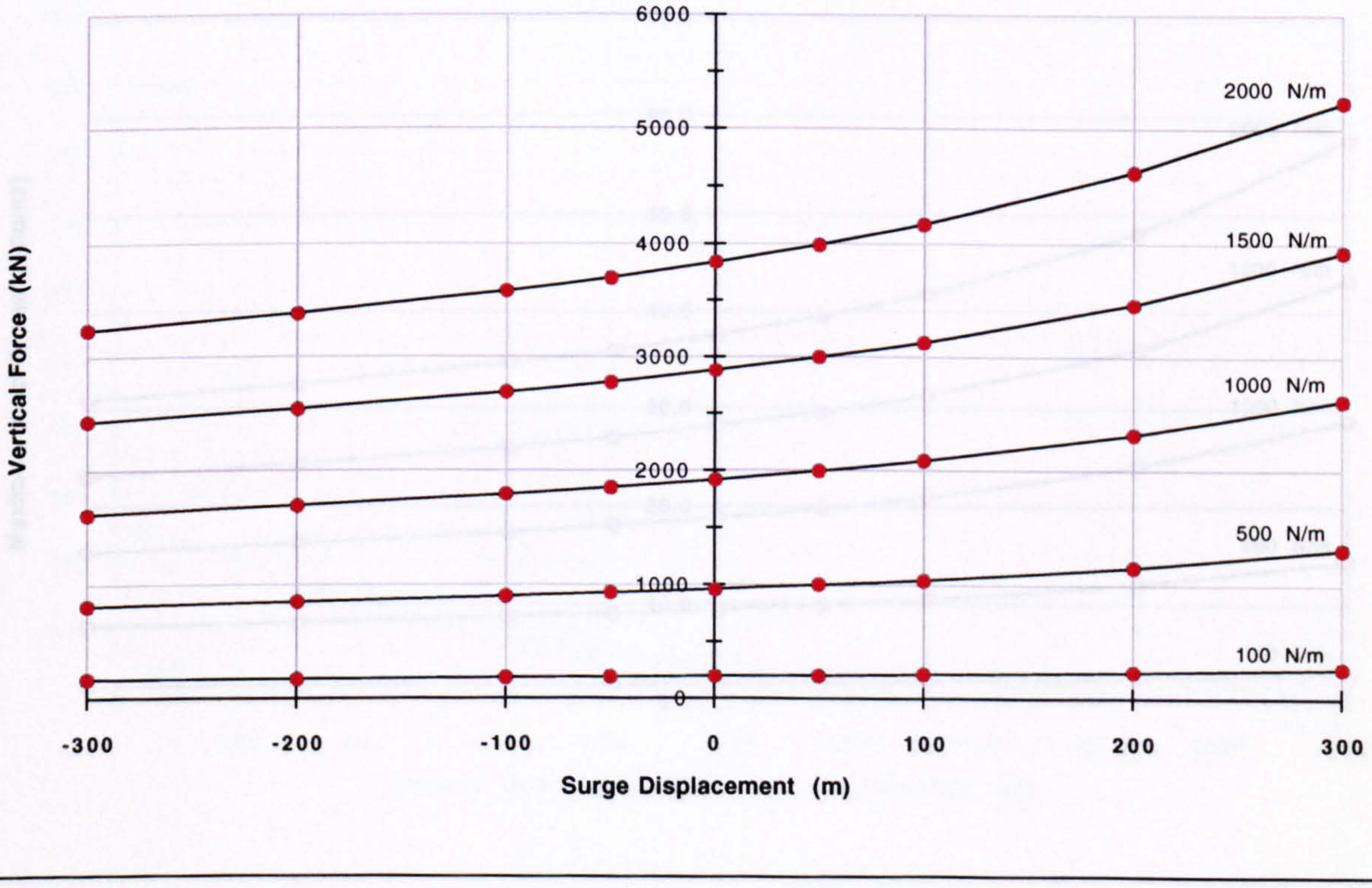

Horizontal Surface Offset = 1000 m

Sea Depth = 1500 m

Figure 5.47

Axial Load (Tensile) at the Surface (e)

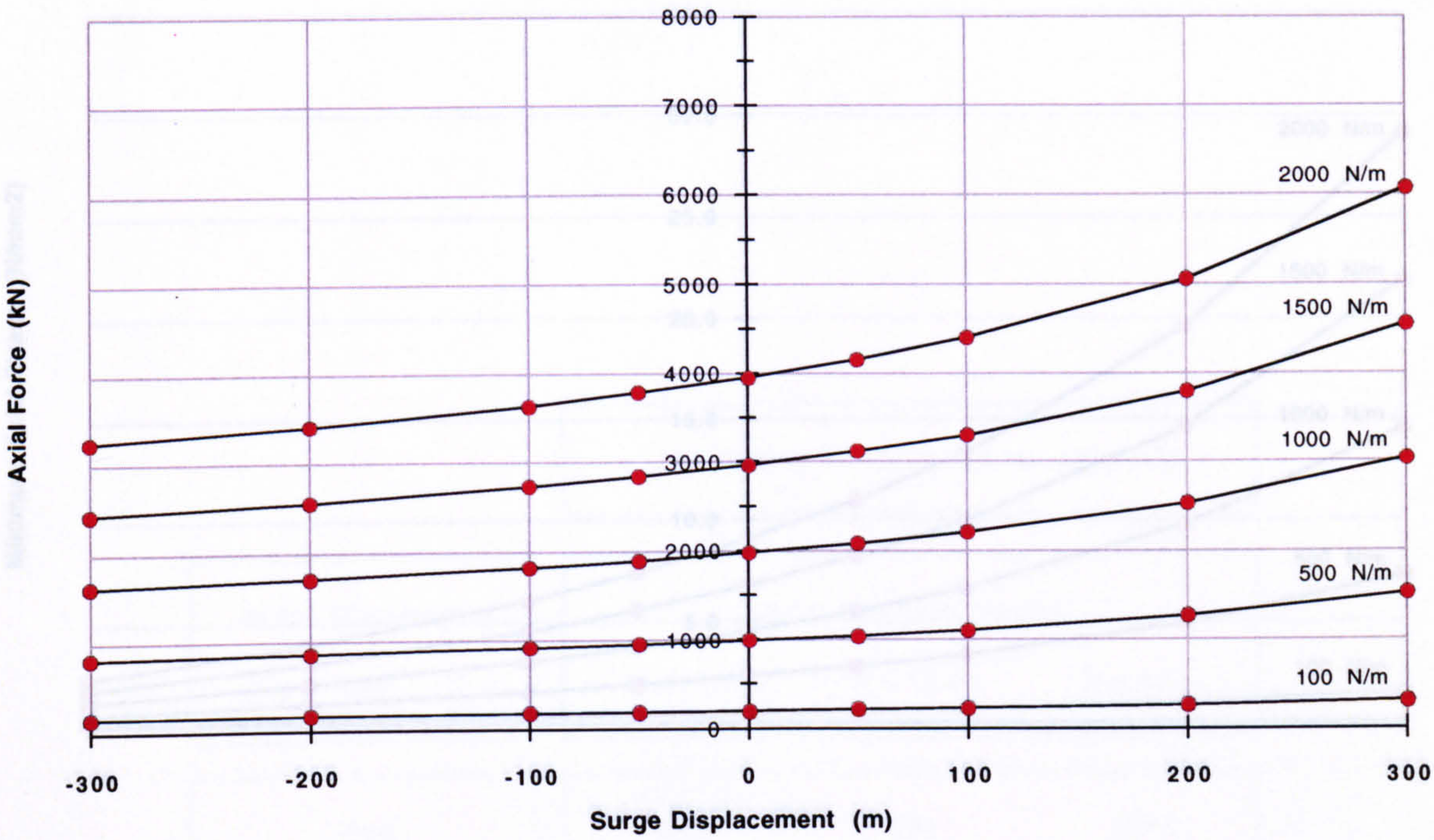

Axial Stress at the Surface (f)

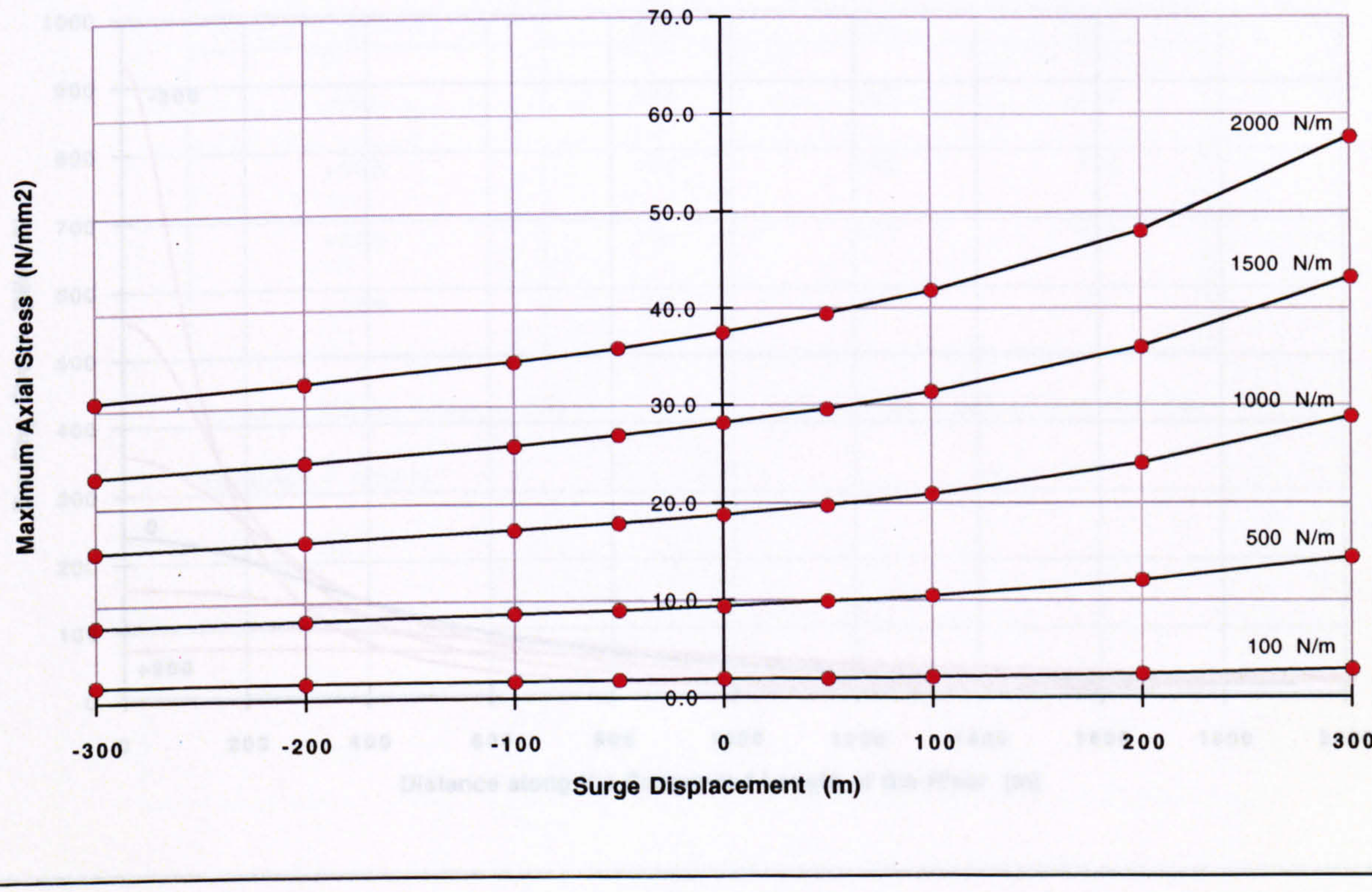

Horizontal Surface Offset = 1000 m

Sea Depth = 1500 m

Carrier Pipe Outer Diameter = 1.1 m

Carrier Pipe Wall Thickness = 10 mm

Figure 5.47

Axial Stress at the Seabed

(g)

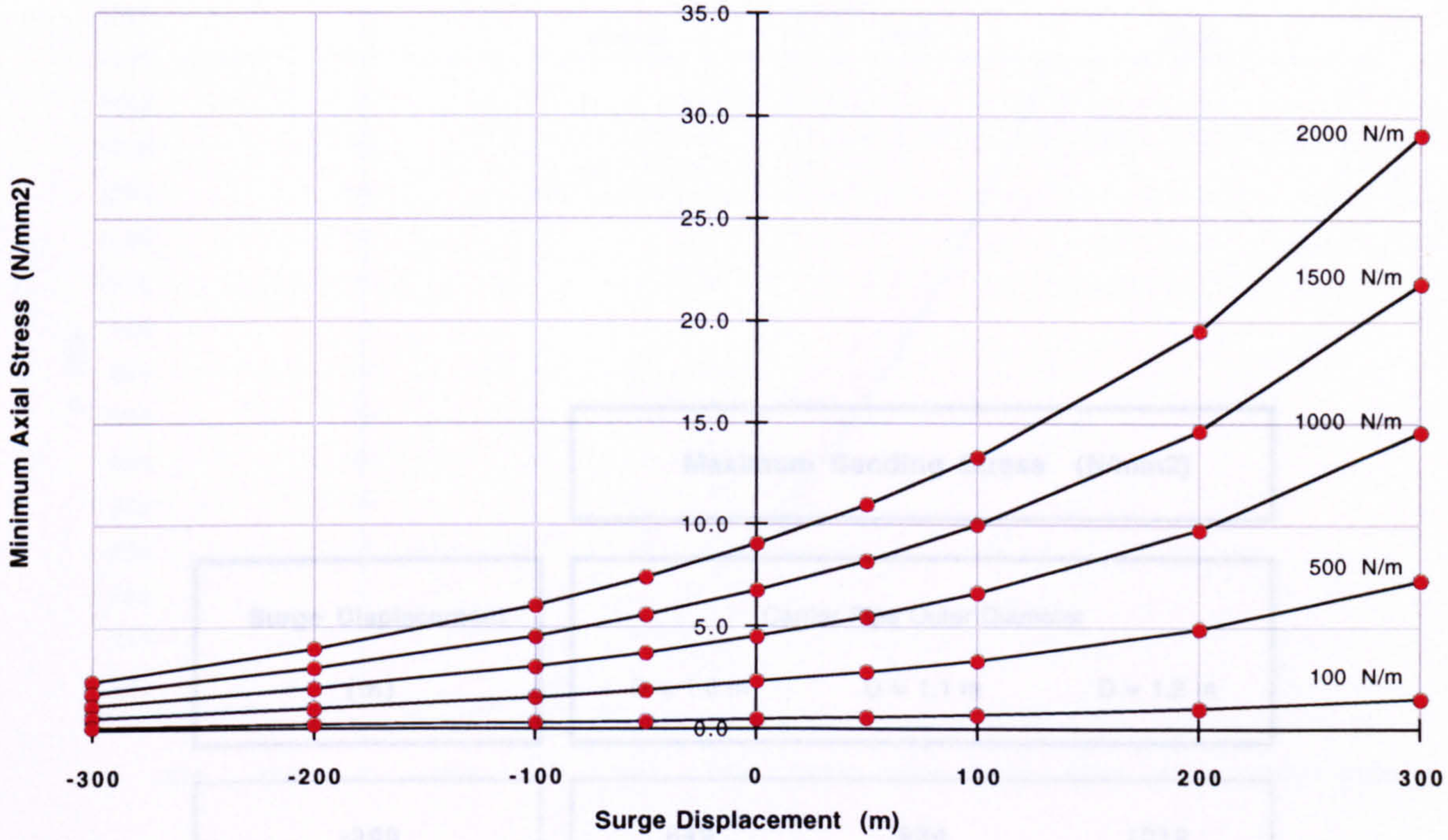

Bending Stress Distributions along the Riser

(h)

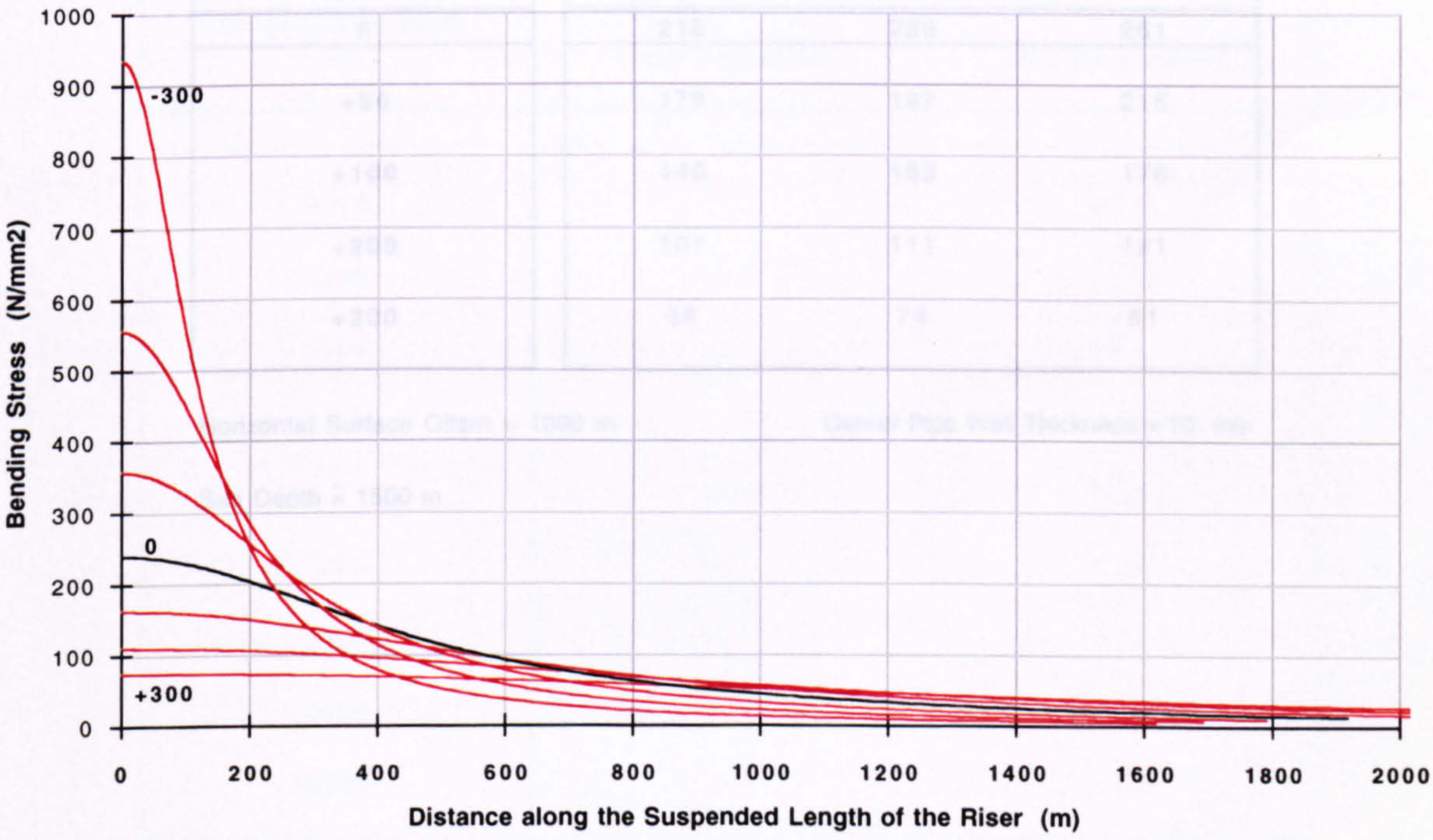

Horizontal Surface Offset = 1000 m

Sea Depth = 1500 m

Carrier Pipe Outer Diameter = 1.1 m

Carrier Pipe Wall Thickness = 10 mm

Figure 5.47

Bending Stress at the Seabed - Surge Displacement (a = 1000 m, b = 1500 m)

Surge Displacement (m)	Maximum Bending Stress (N/mm2)		
	Carrier Pipe Outer Diameter		
	D = 1.0 m	D = 1.1 m	D = 1.2 m
-300	849	934	1019
-200	506	557	607
-100	325	358	391
-50	265	292	318
0	218	239	261
+50	179	197	215
+100	148	163	178
+200	101	111	121
+300	68	74	81

Horizontal Surface Offset = 1000 m

Carrier Pipe Wall Thickness = 10 mm

Sea Depth = 1500 m

Table 5.48

Surge Displacement Profiles (a = 1500 m)

(a)

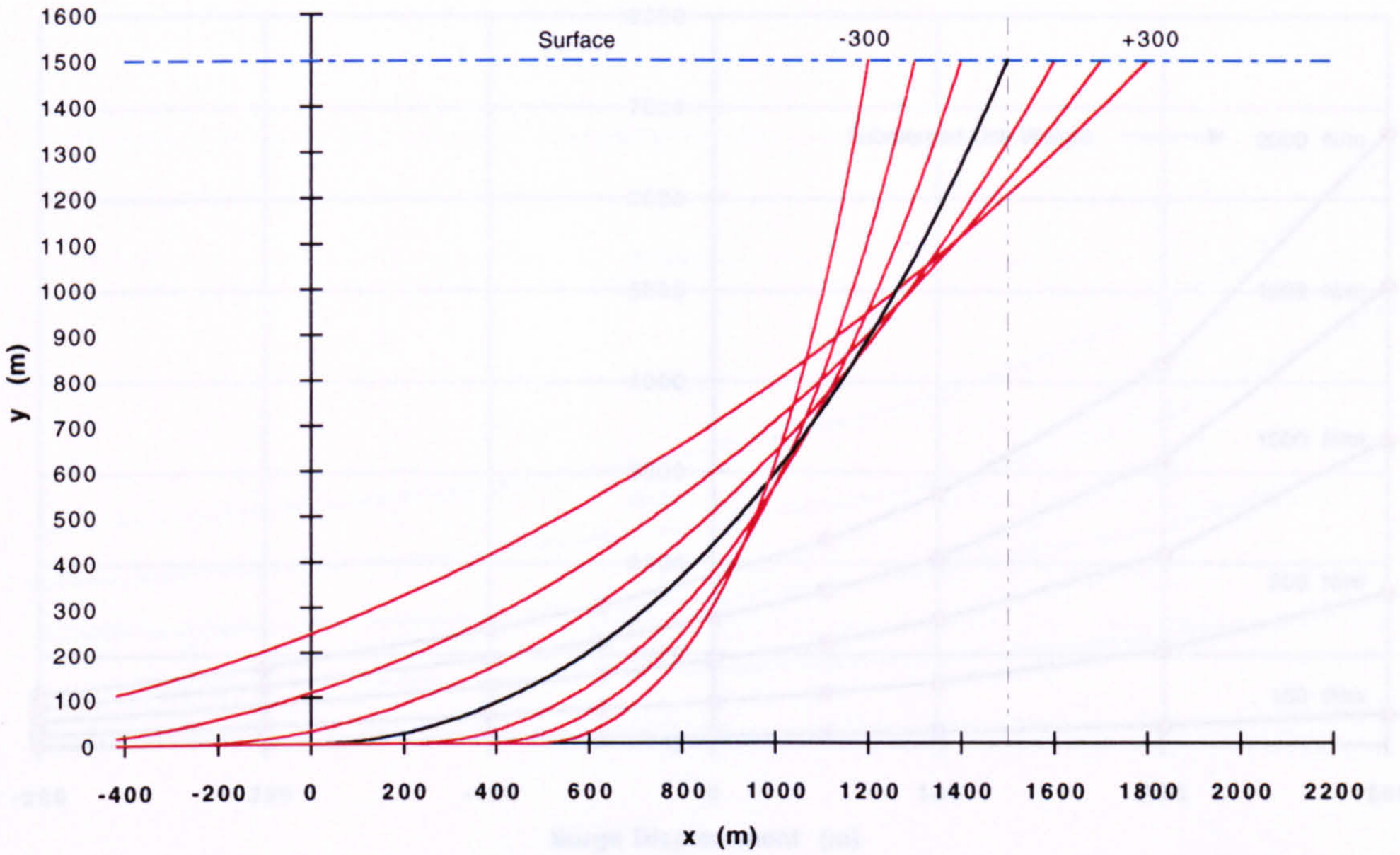

Riser Inclination at the Surface

(b)

Surge Displacement (m)	Surface Inclination (degs) from the Vertical	from the Horizontal
-300	9.2	80.8
-200	12.9	77.1
-100	17.3	72.7
-50	19.8	70.2
0	22.5	67.5
+50	25.4	64.6
+100	28.6	61.4
+200	35.7	54.3
+300	43.8	46.2

Mean Horizontal Surface Offset = 1500 m

Sea Depth = 1500 m

Figure 5.49

Horizontal Load at the Surface (H)

(c)

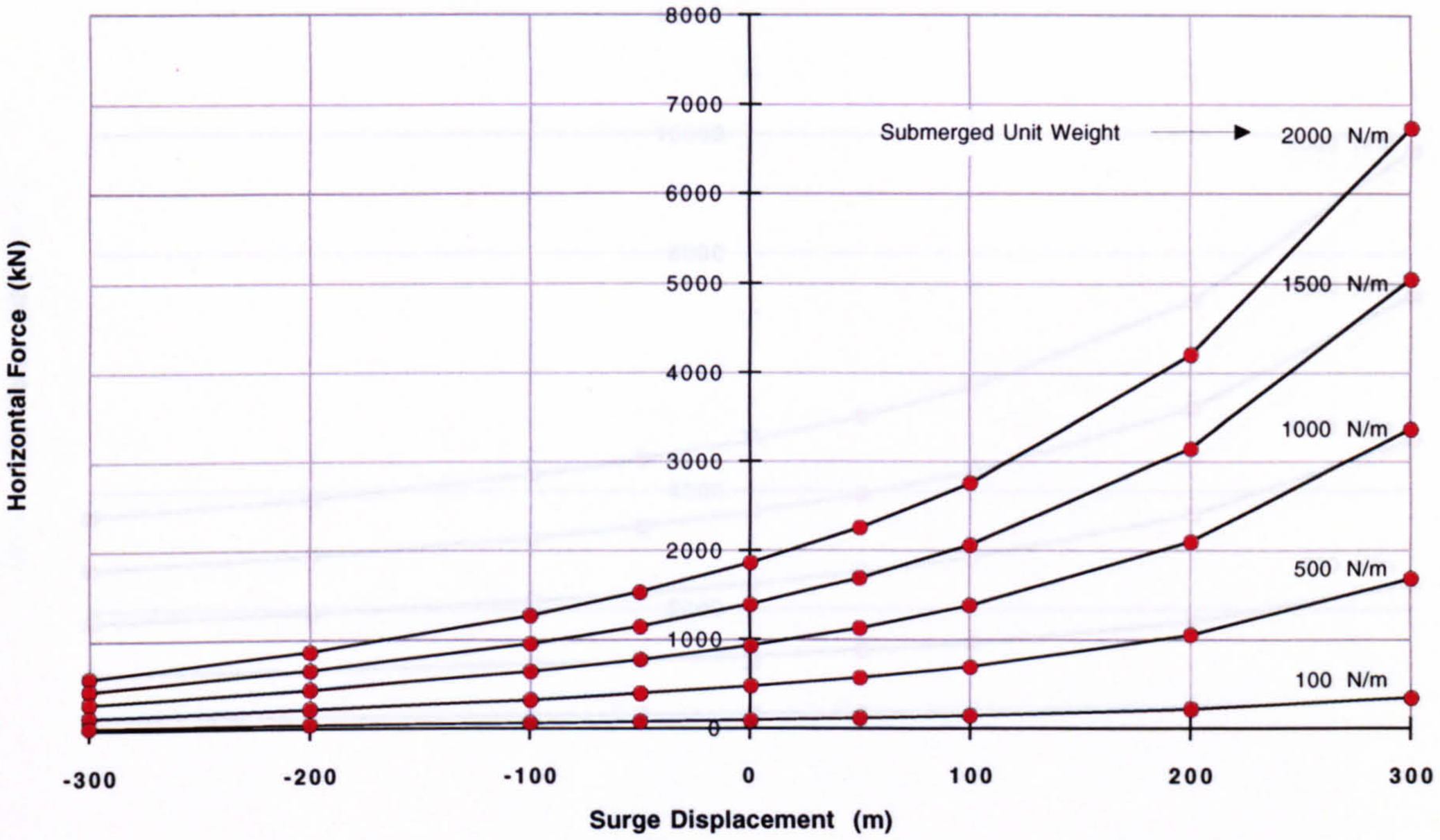

Vertical Load at the Surface (V)

(d)

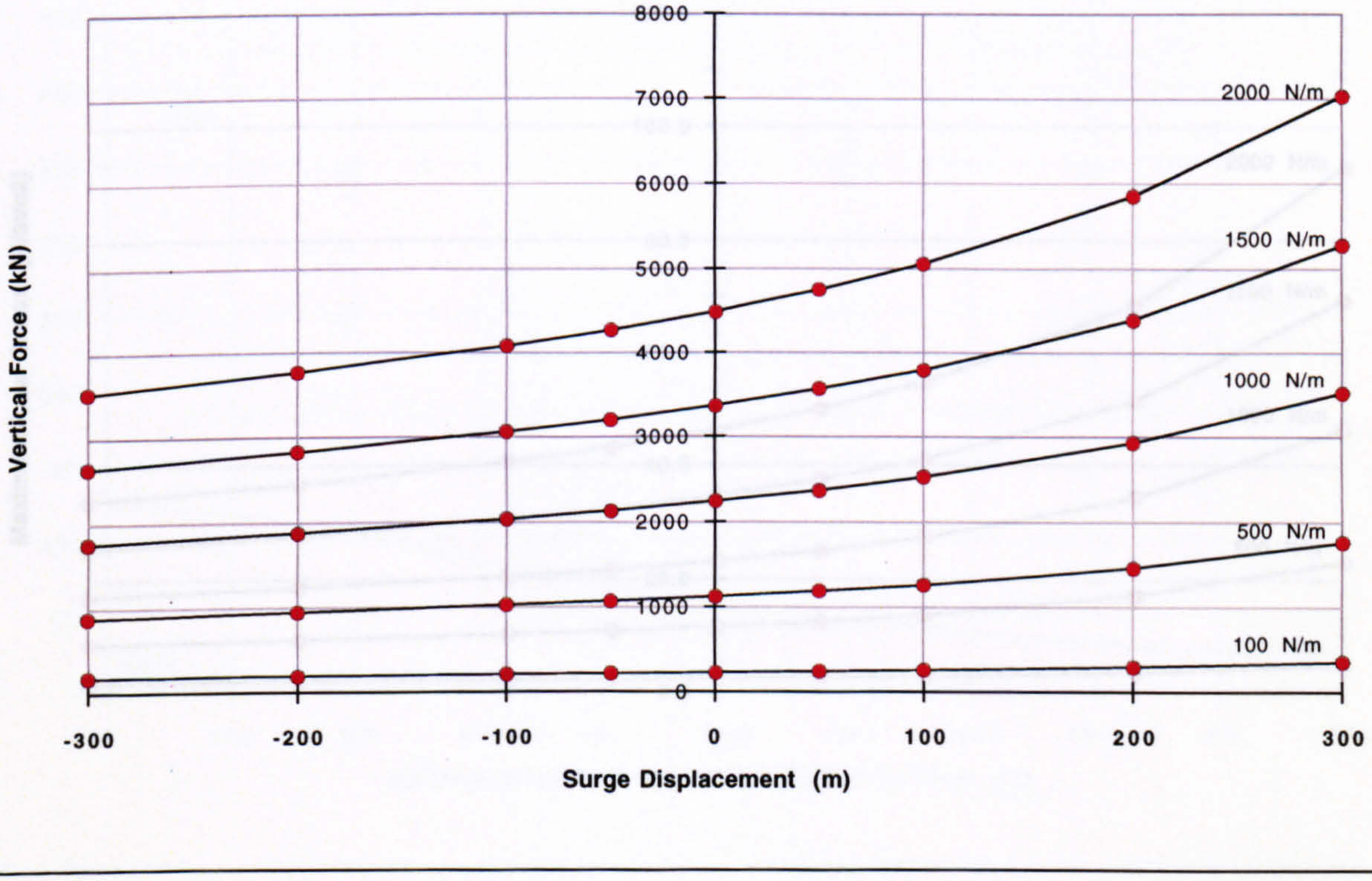

Horizontal Surface Offset = 1500 m

Sea Depth = 1500 m

Figure 5.49

Axial Load (Tensile) at the Surface

(e)

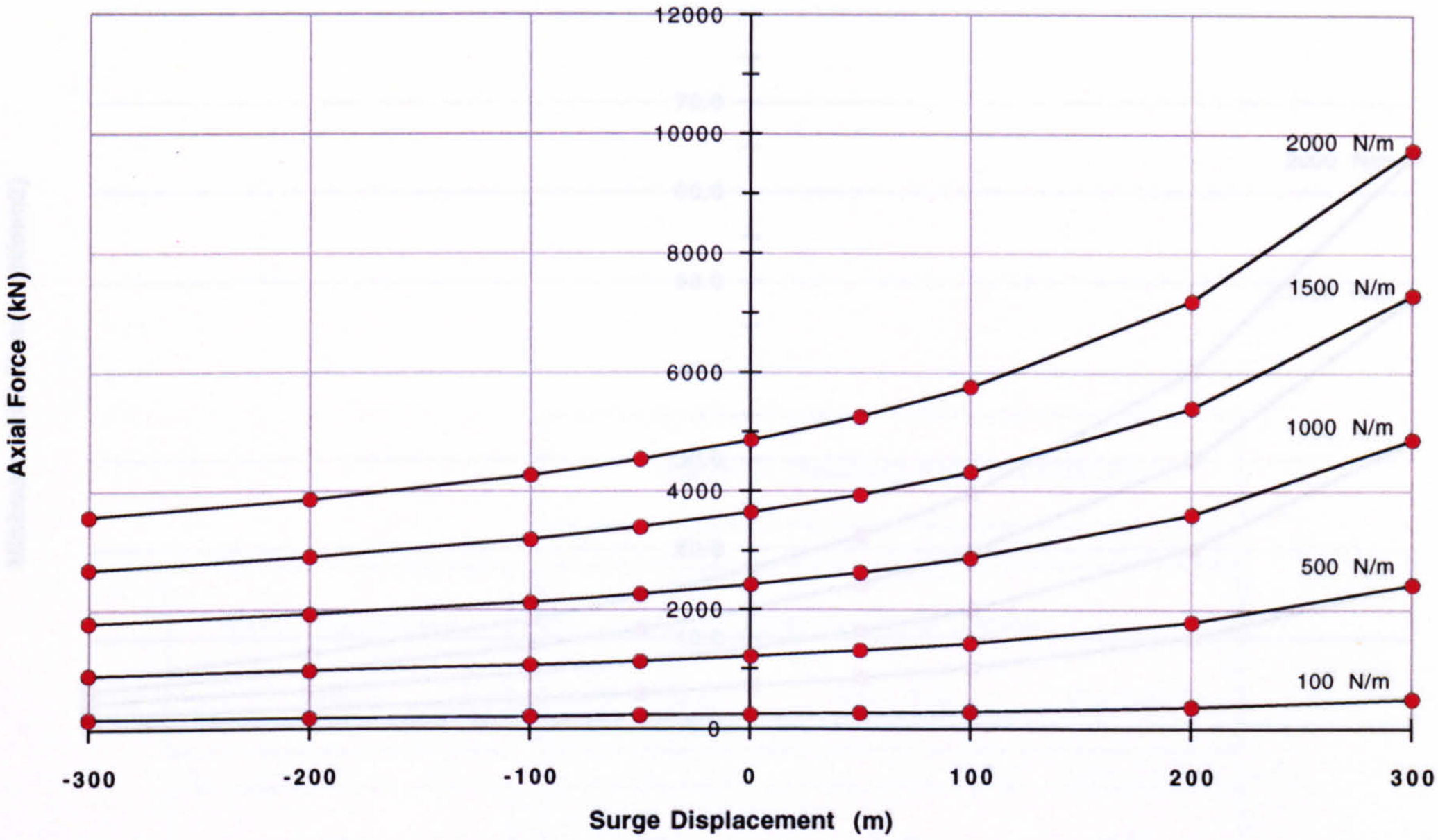

Axial Stress at the Surface

(f)

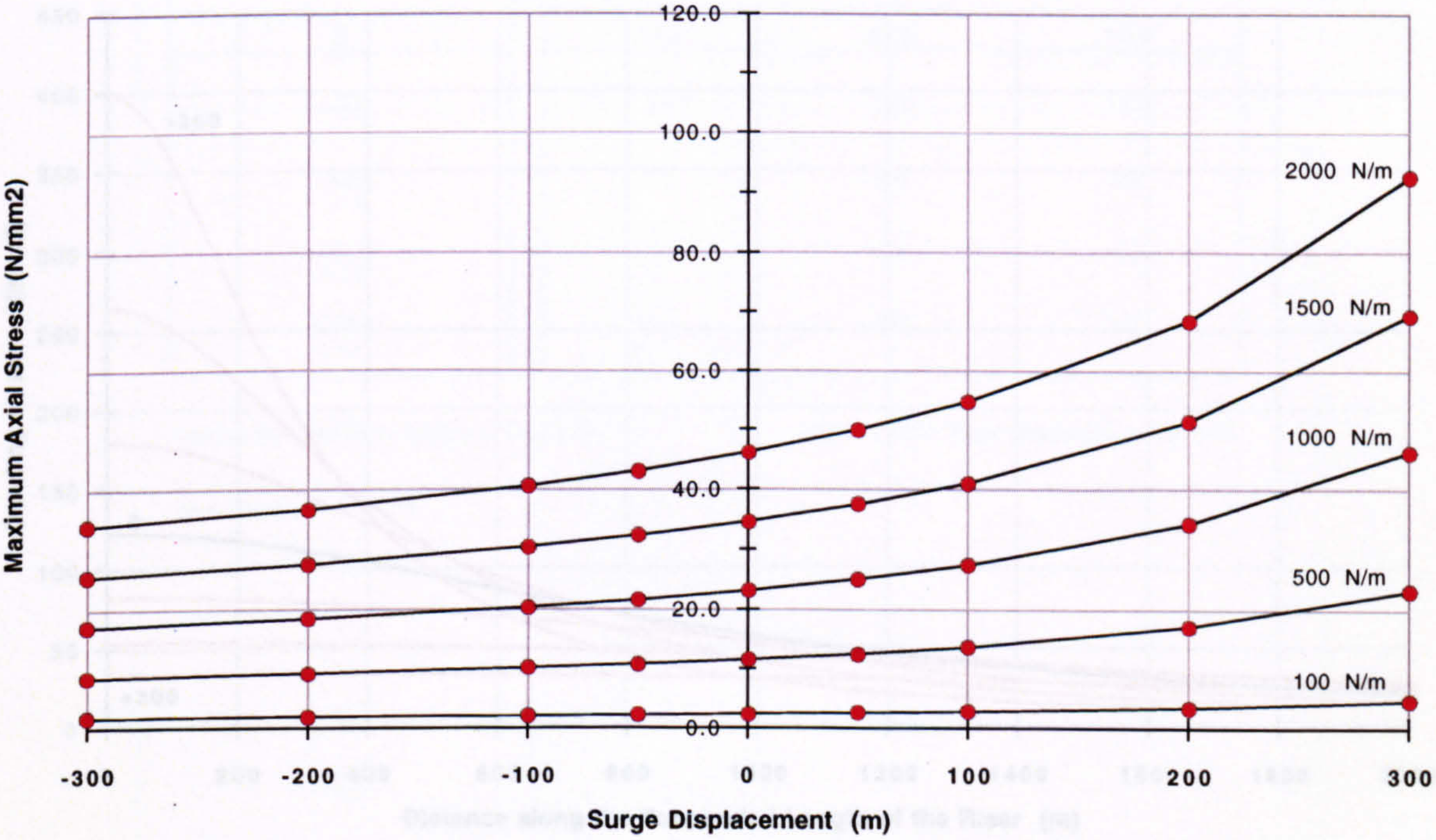

Horizontal Surface Offset = 1500 m

Sea Depth = 1500 m

Carrier Pipe Outer Diameter = 1.1 m

Carrier Pipe Wall Thickness = 10 mm

Figure 5.49

Axial Stress at the Seabed

(g)

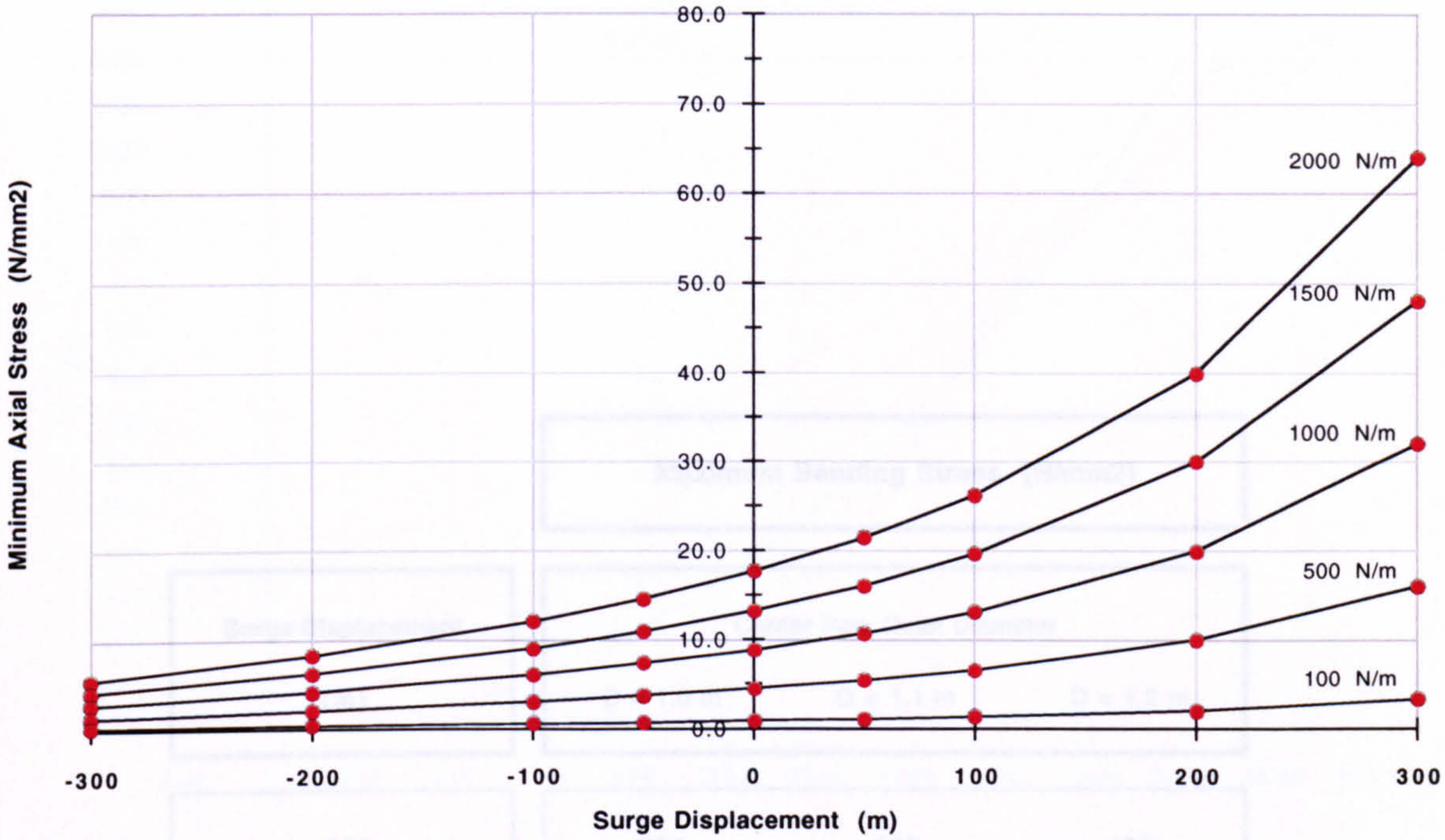

Bending Stress Distributions along the Riser

(h)

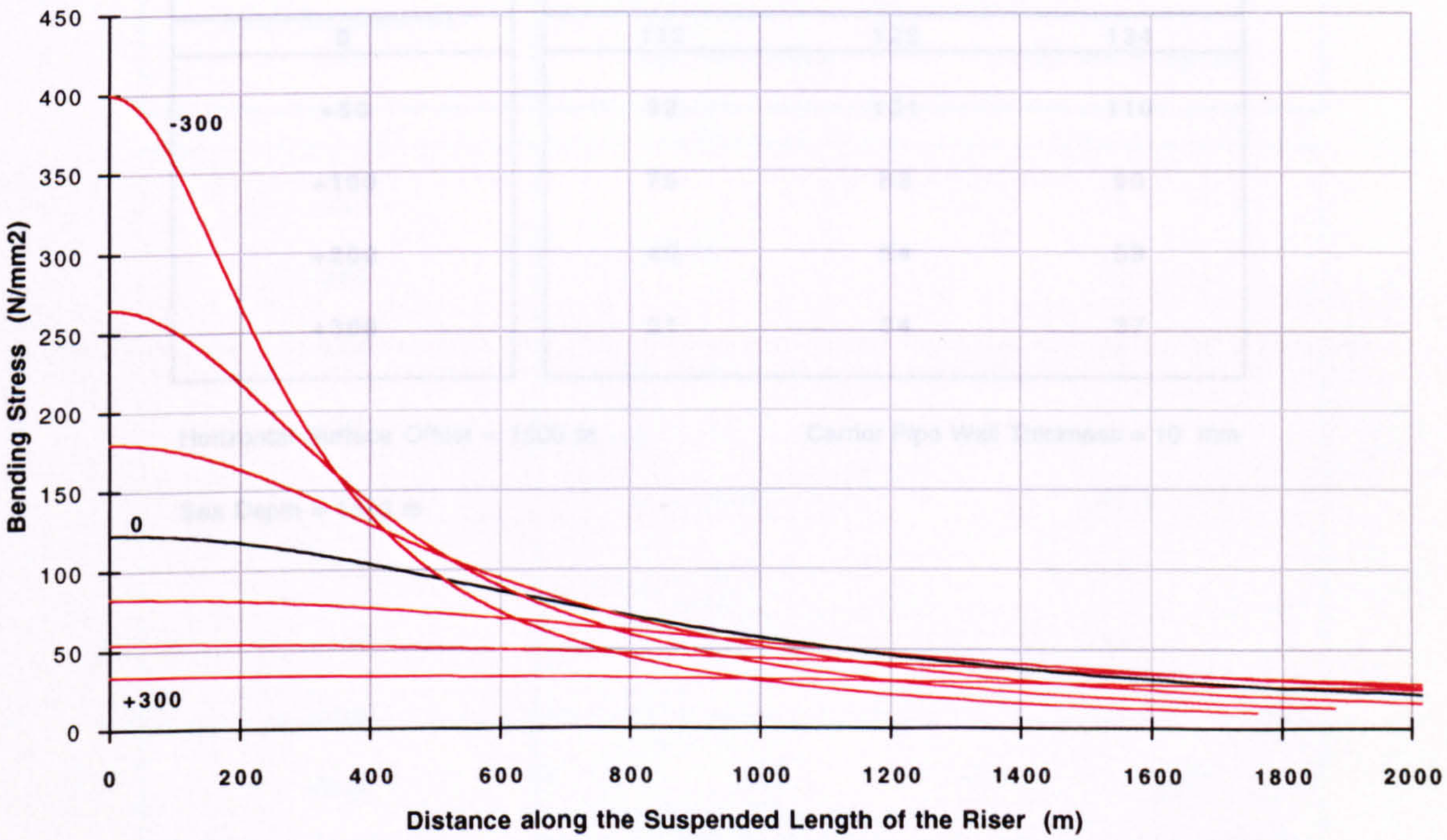

Horizontal Surface Offset = 1500 m

Sea Depth = 1500 m

Carrier Pipe Outer Diameter = 1.1 m

Carrier Pipe Wall Thickness = 10 mm

Figure 5.49

Bending Stress at the Seabed - Surge Displacement (a = 1500 m, b = 1500 m)

Surge Displacement (m)	Maximum Bending Stress (N/mm2)		
	Carrier Pipe Outer Diameter		
	D = 1.0 m	D = 1.1 m	D = 1.2 m
-300	364	400	436
-200	241	265	289
-100	164	180	196
-50	135	149	162
0	112	123	134
+50	92	101	110
+100	75	83	90
+200	49	54	59
+300	31	34	37

Horizontal Surface Offset = 1500 m

Carrier Pipe Wall Thickness = 10 mm

Sea Depth = 1500 m

Table 5.50

Surge Displacement Profiles (a = 2000 m)

(a)

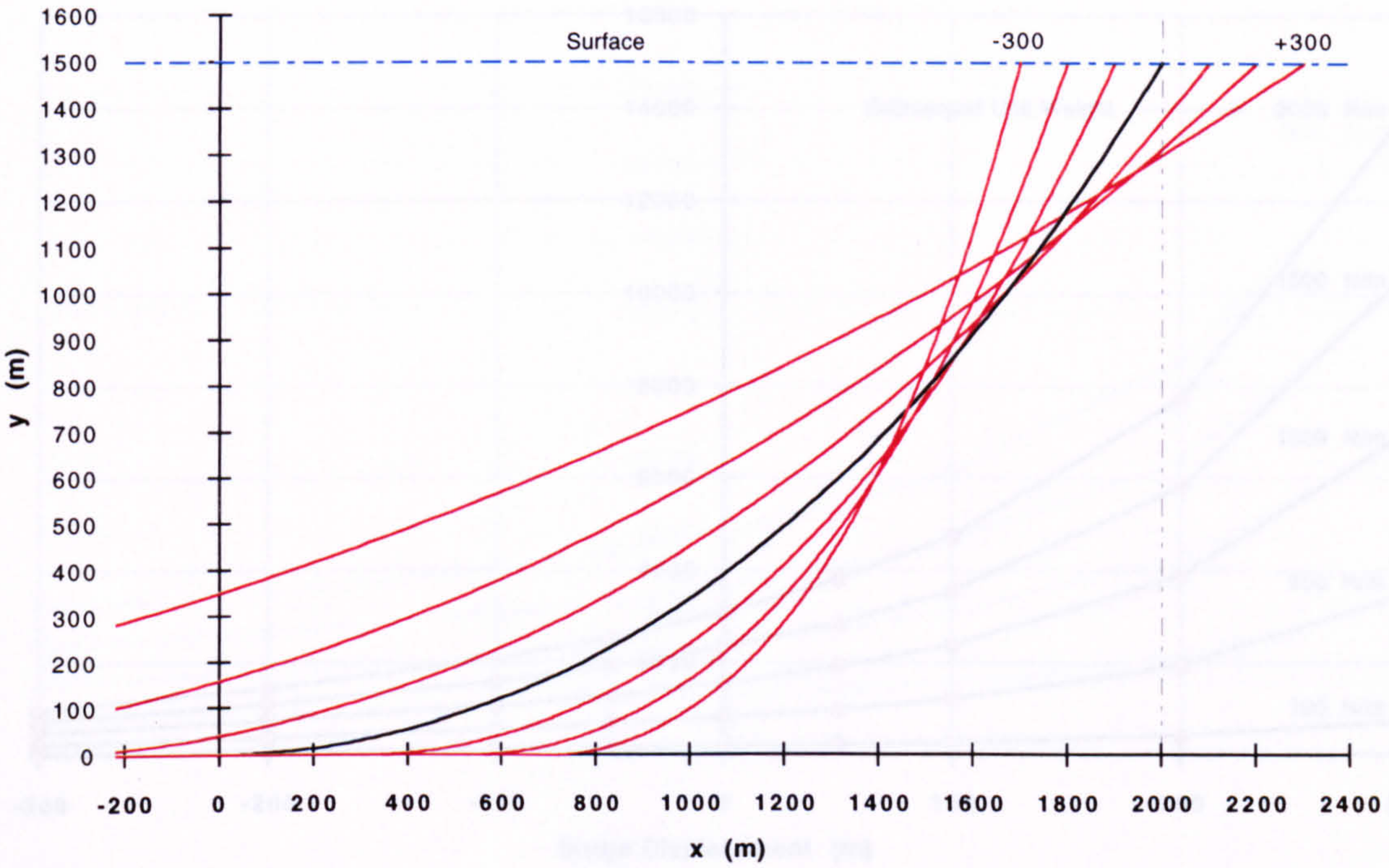

Riser Inclination at the Surface

(b)

Surge Displacement (m)	Surface Inclination (degs) from the Vertical	from the Horizontal
-300	13.9	76.1
-200	18.6	71.4
-100	24.0	66.0
-50	27.1	62.9
0	30.4	59.6
+50	33.9	56.1
+100	37.7	52.3
+200	46.1	43.9
+300	55.4	34.6

Mean Horizontal Surface Offset = 2000 m

Sea Depth = 1500 m

Figure 5.51

Horizontal Load at the Surface (H)

(c)

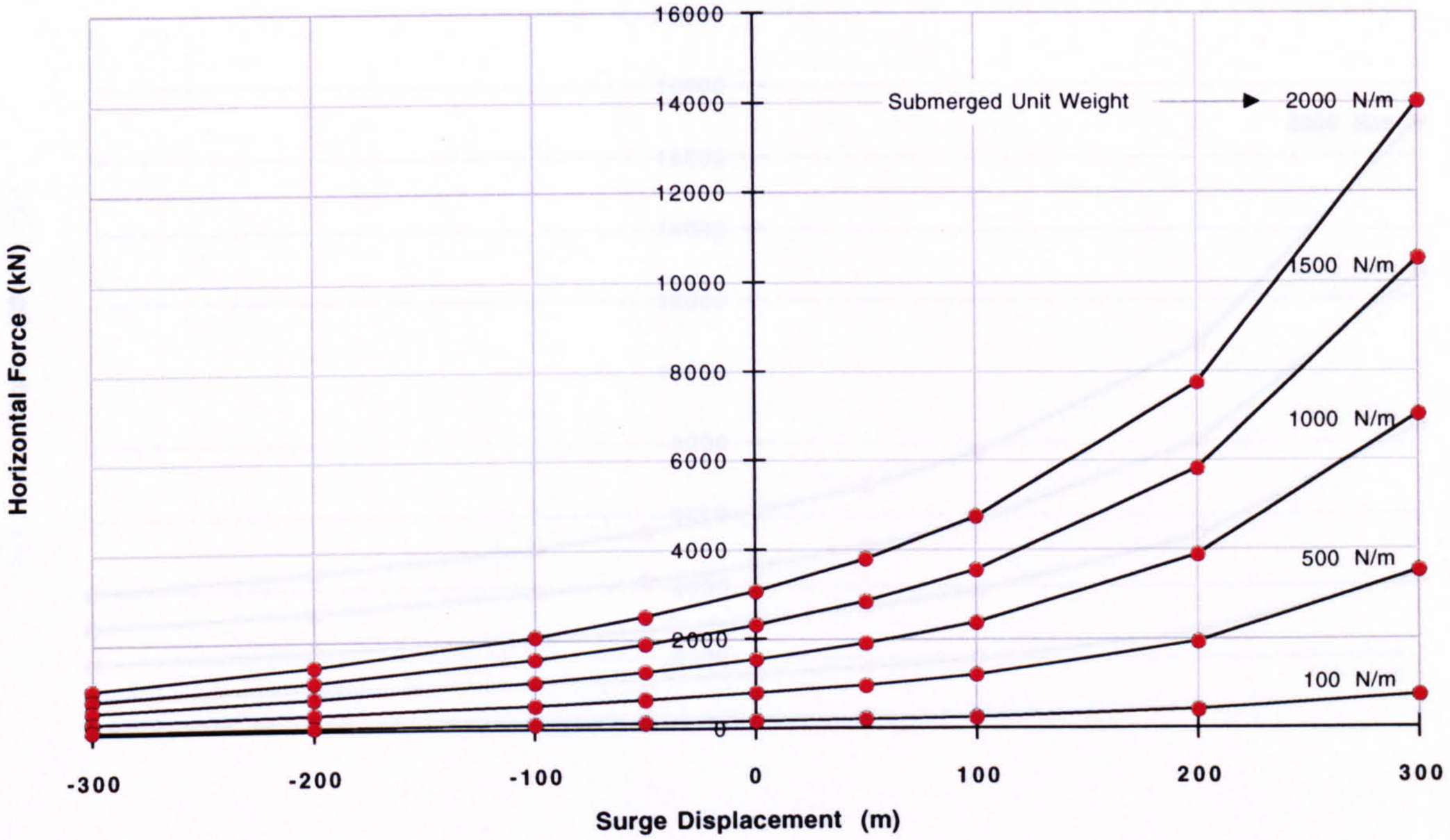

Vertical Load at the Surface (V)

(d)

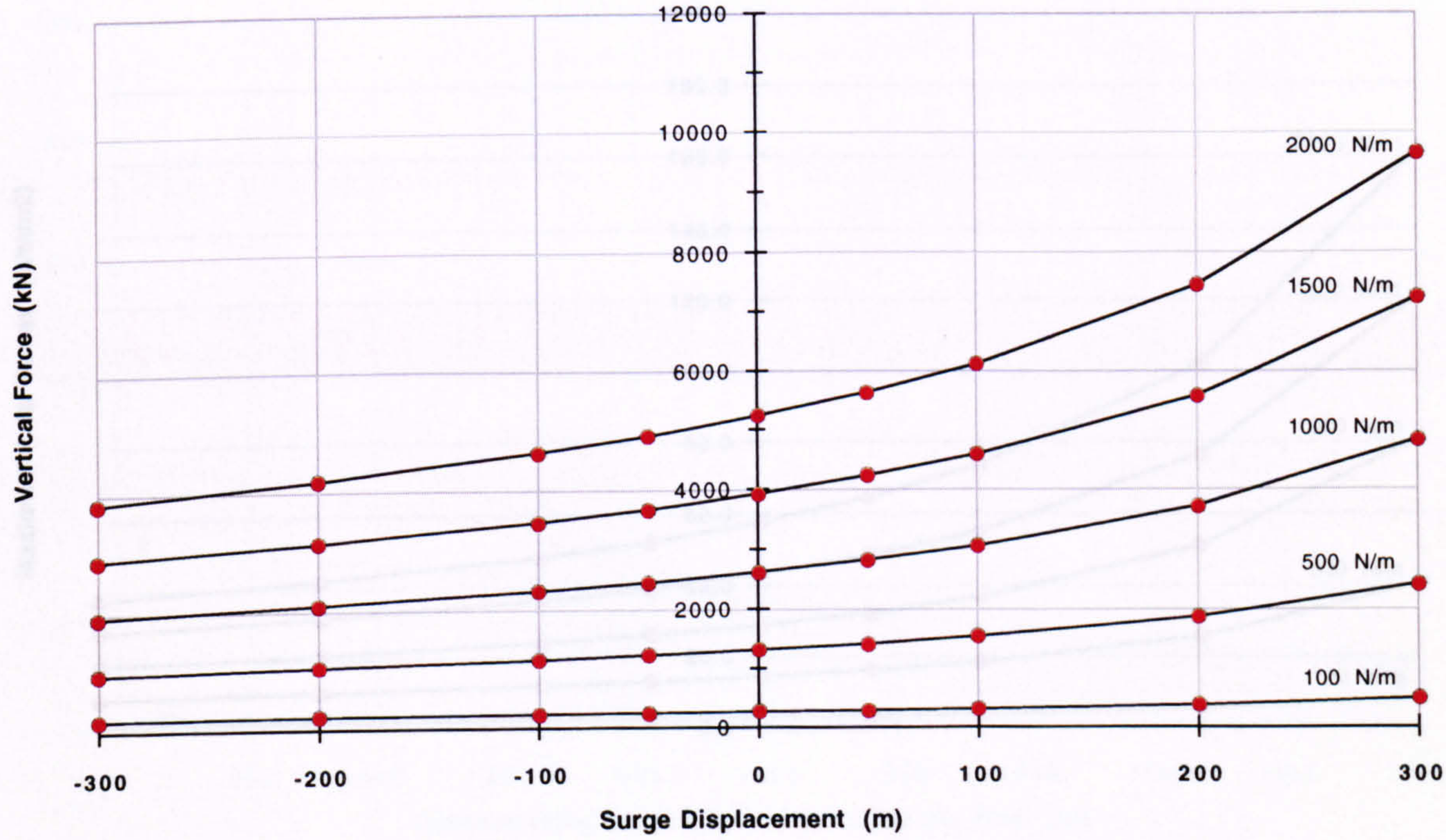

Horizontal Surface Offset = 2000 m

Sea Depth = 1500 m

Figure 5.51

Axial Load (Tensile) at the Surface

(e)

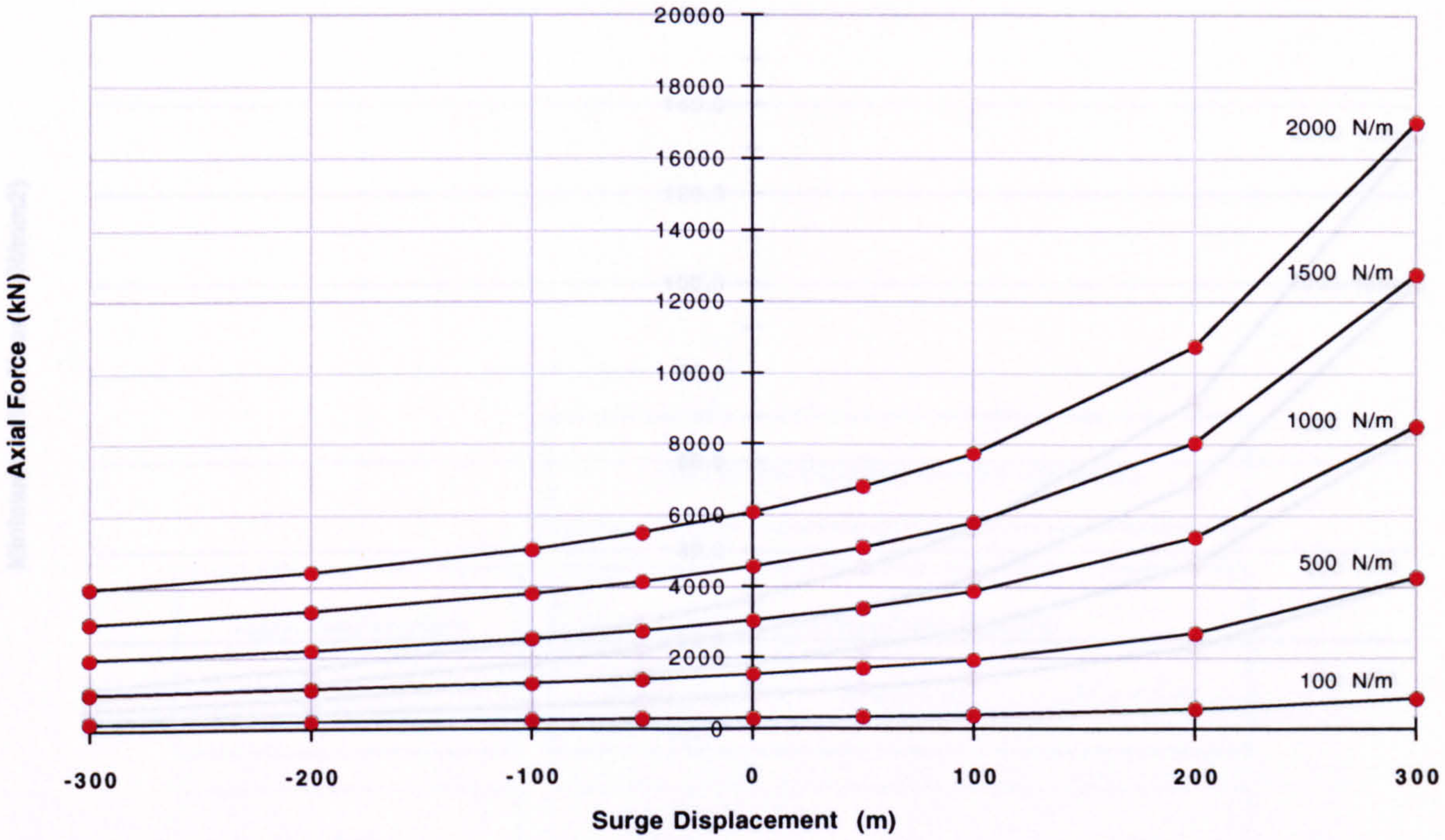

Axial Stress at the Surface

(f)

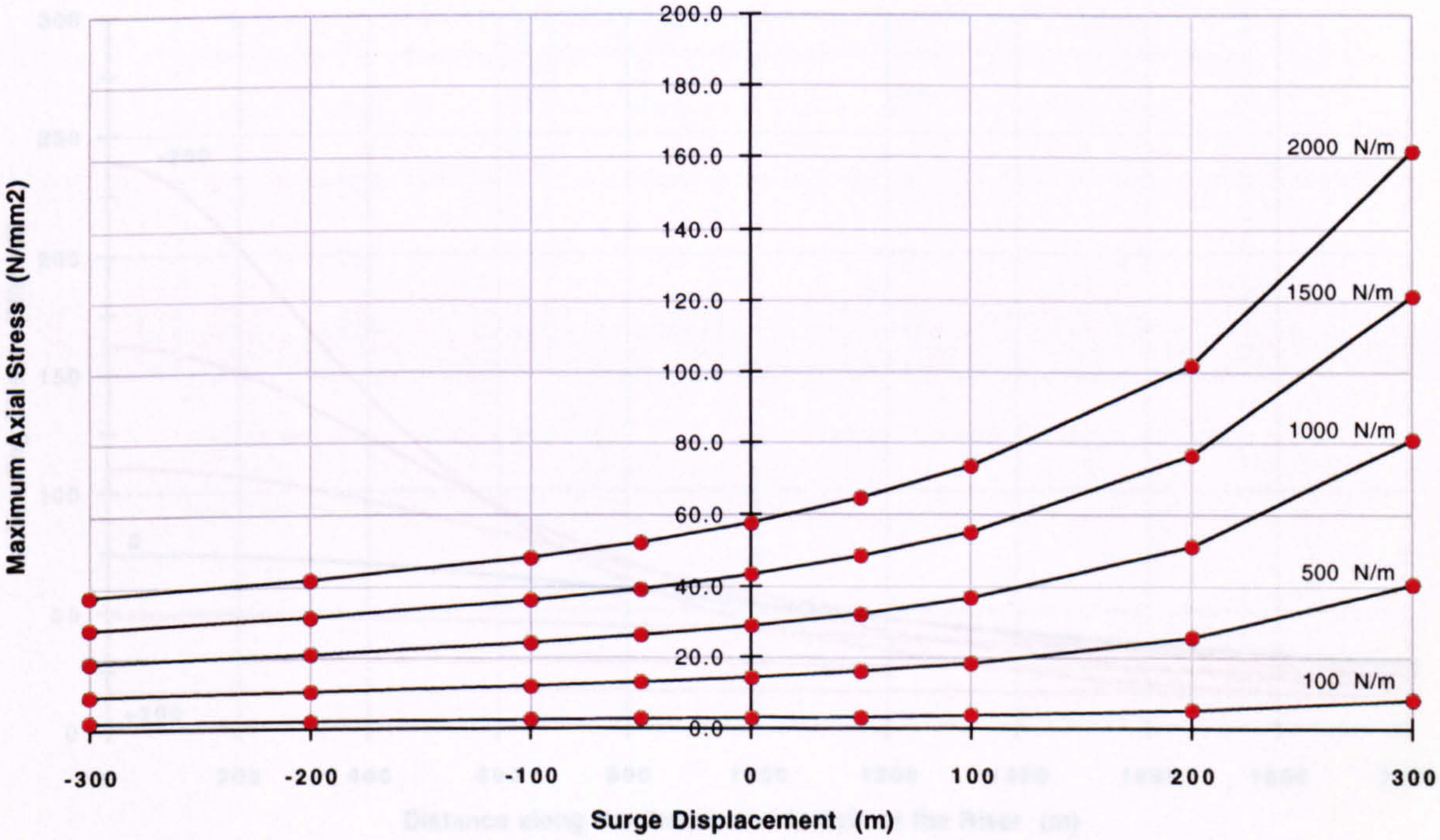

Horizontal Surface Offset = 2000 m

Sea Depth = 1500 m

Carrier Pipe Outer Diameter = 1.1 m

Carrier Pipe Wall Thickness = 10 mm

Figure 5.51

Axial Stress at the Seabed

(g)

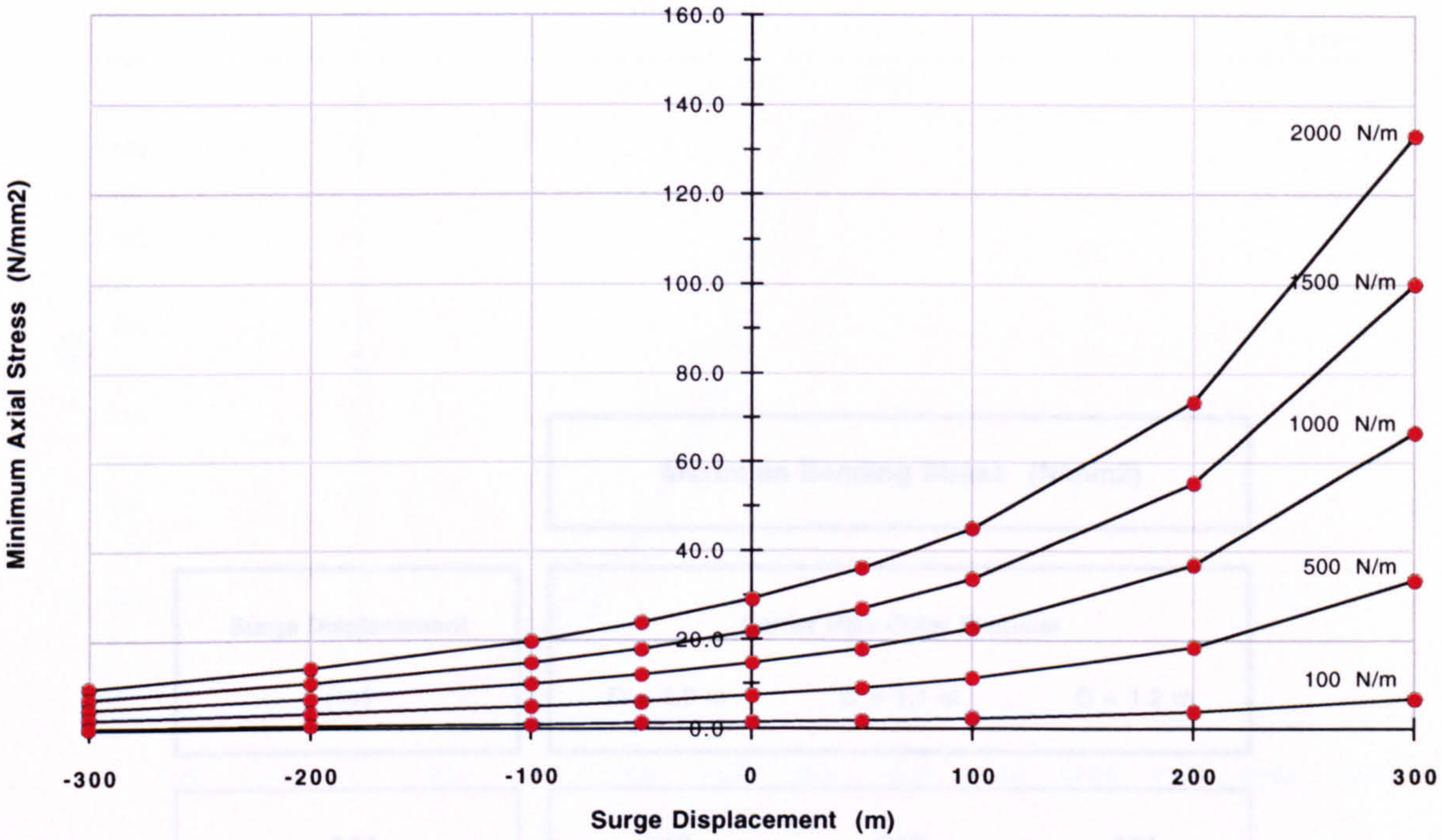

Bending Stress Distributions along the Riser

(h)

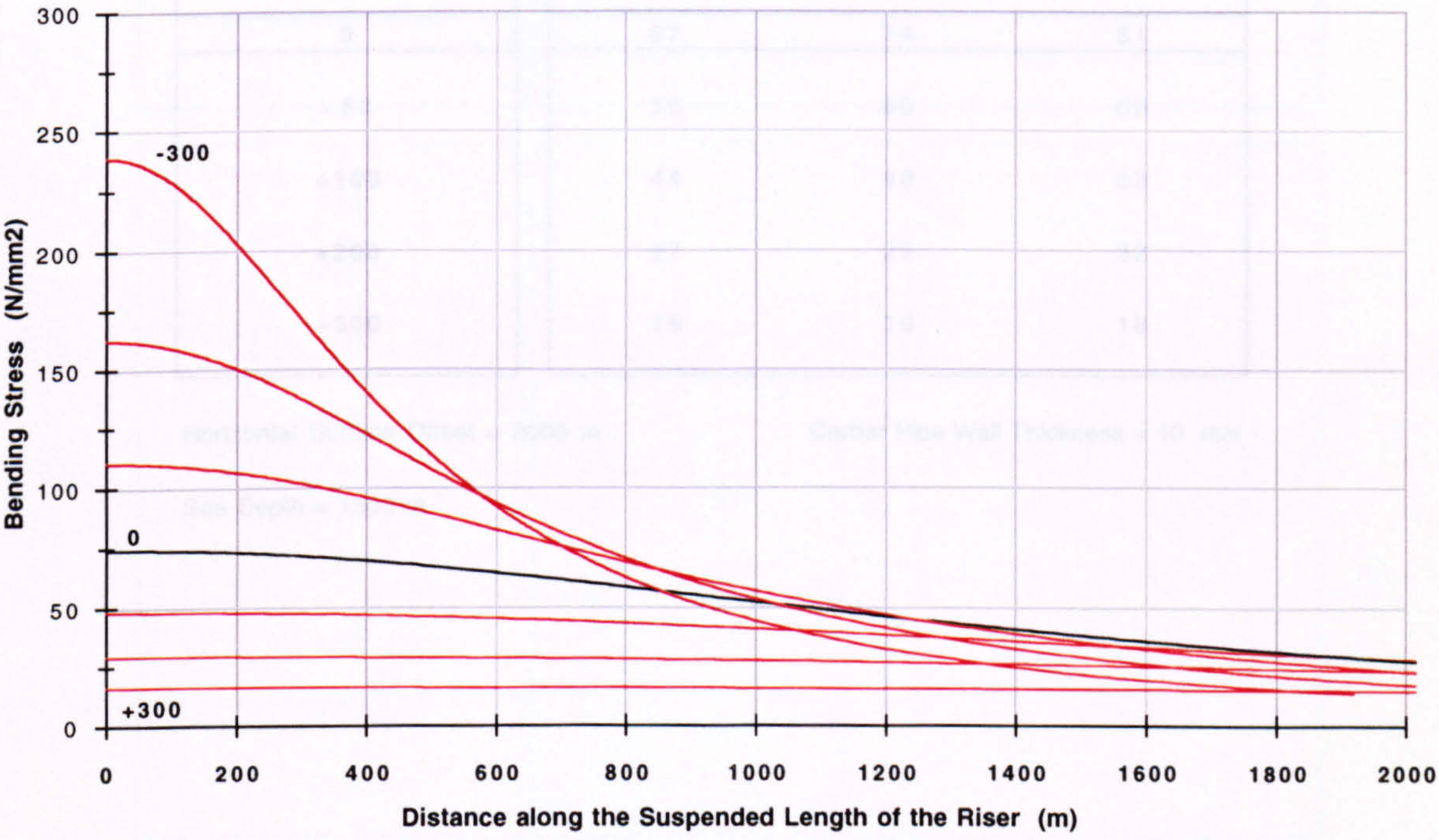

Horizontal Surface Offset = 2000 m

Sea Depth = 1500 m

Carrier Pipe Outer Diameter = 1.1 m

Carrier Pipe Wall Thickness = 10 mm

Figure 5.51

Bending Stress at the Seabed - Surge Displacement (a = 2000 m, b = 1500 m)

Surge Displacement (m)	Maximum Bending Stress (N/mm2)		
	Carrier Pipe Outer Diameter		
	D = 1.0 m	D = 1.1 m	D = 1.2 m
-300	217	239	261
-200	148	163	177
-100	101	111	121
-50	83	91	99
0	67	74	81
+50	55	60	66
+100	44	48	53
+200	27	29	32
+300	15	16	18

Horizontal Surface Offset = 2000 m

Carrier Pipe Wall Thickness = 10 mm

Sea Depth = 1500 m

Table 5.52

Surge Displacement Profiles (a = 1000 m)

(a)

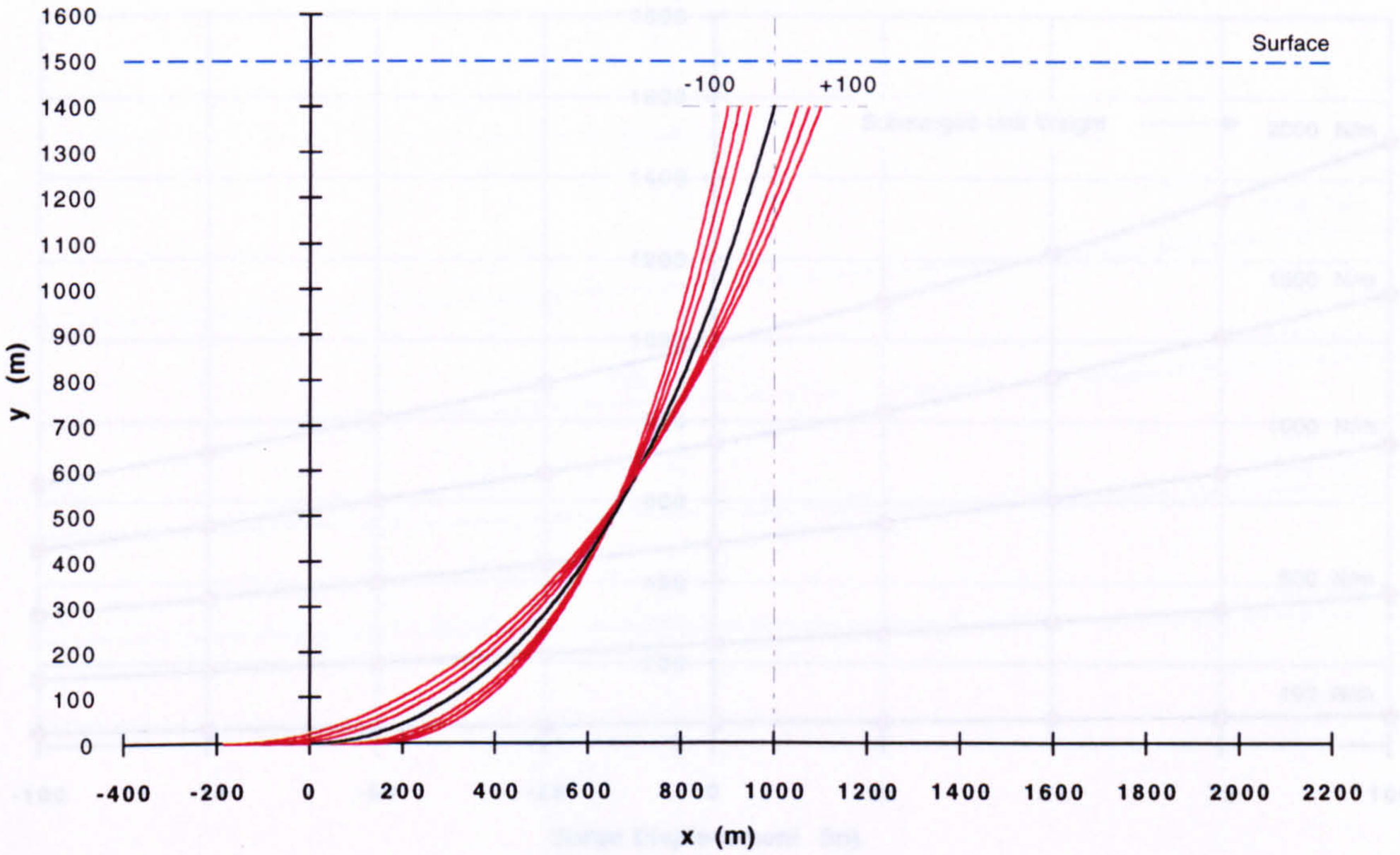

Riser Inclination at the Surface

(b)

Surge Displacement (m)	Surface Inclination (degs) from the Vertical	from the Horizontal
-100	10.8	79.2
-75	11.8	78.2
-50	12.9	77.1
-25	14.0	76.0
0	15.2	74.8
+25	16.4	73.6
+50	17.7	72.3
+75	19.0	71.0
+100	20.4	69.6

Horizontal Surface Offset = 1000 m

Sea Depth = 1500 m

Vertical Offset = 1400 m

Figure 5.53

Horizontal Load at the Surafce (H)

(c)

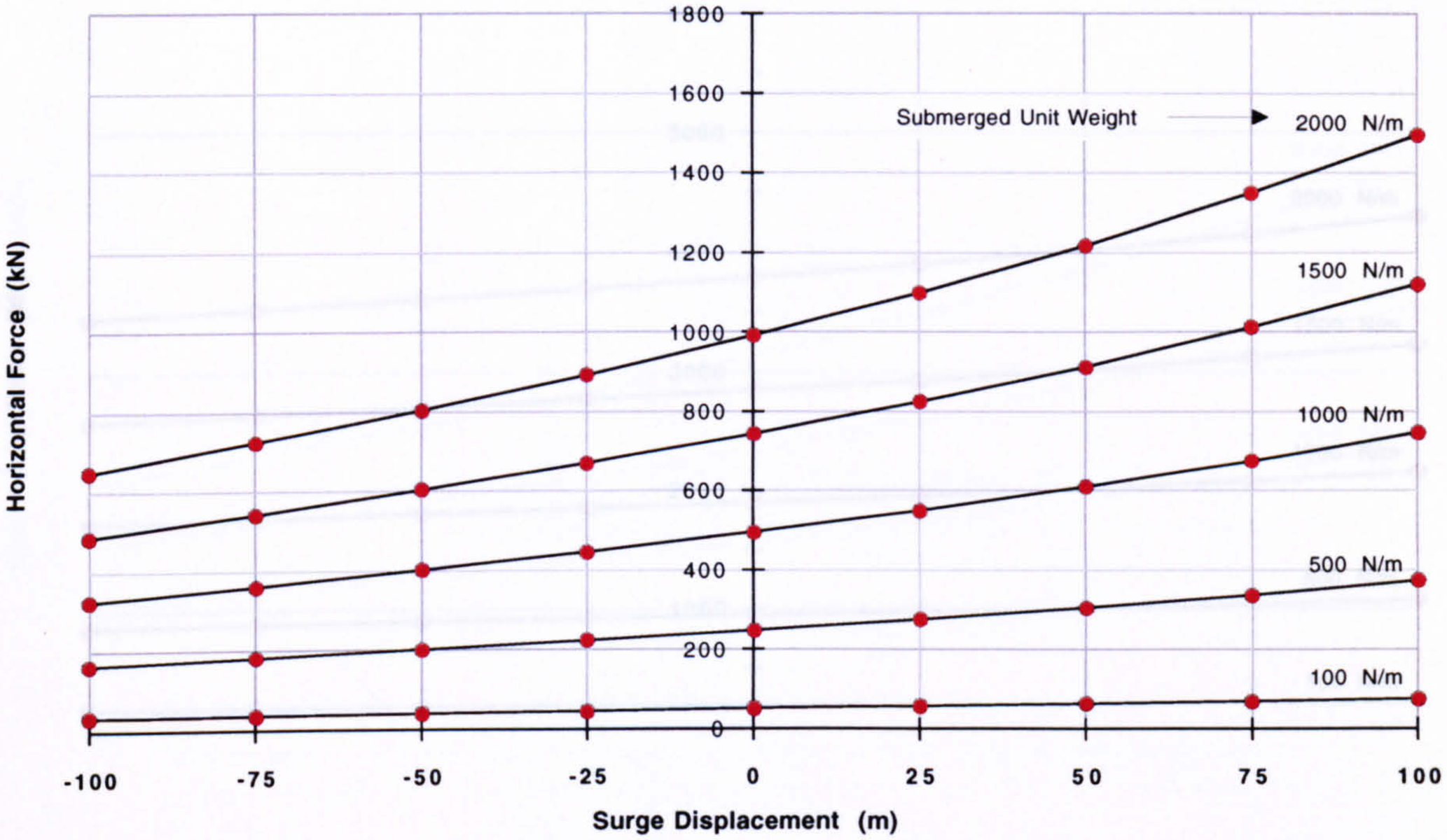

Vertical Load at the Surface (V)

(d)

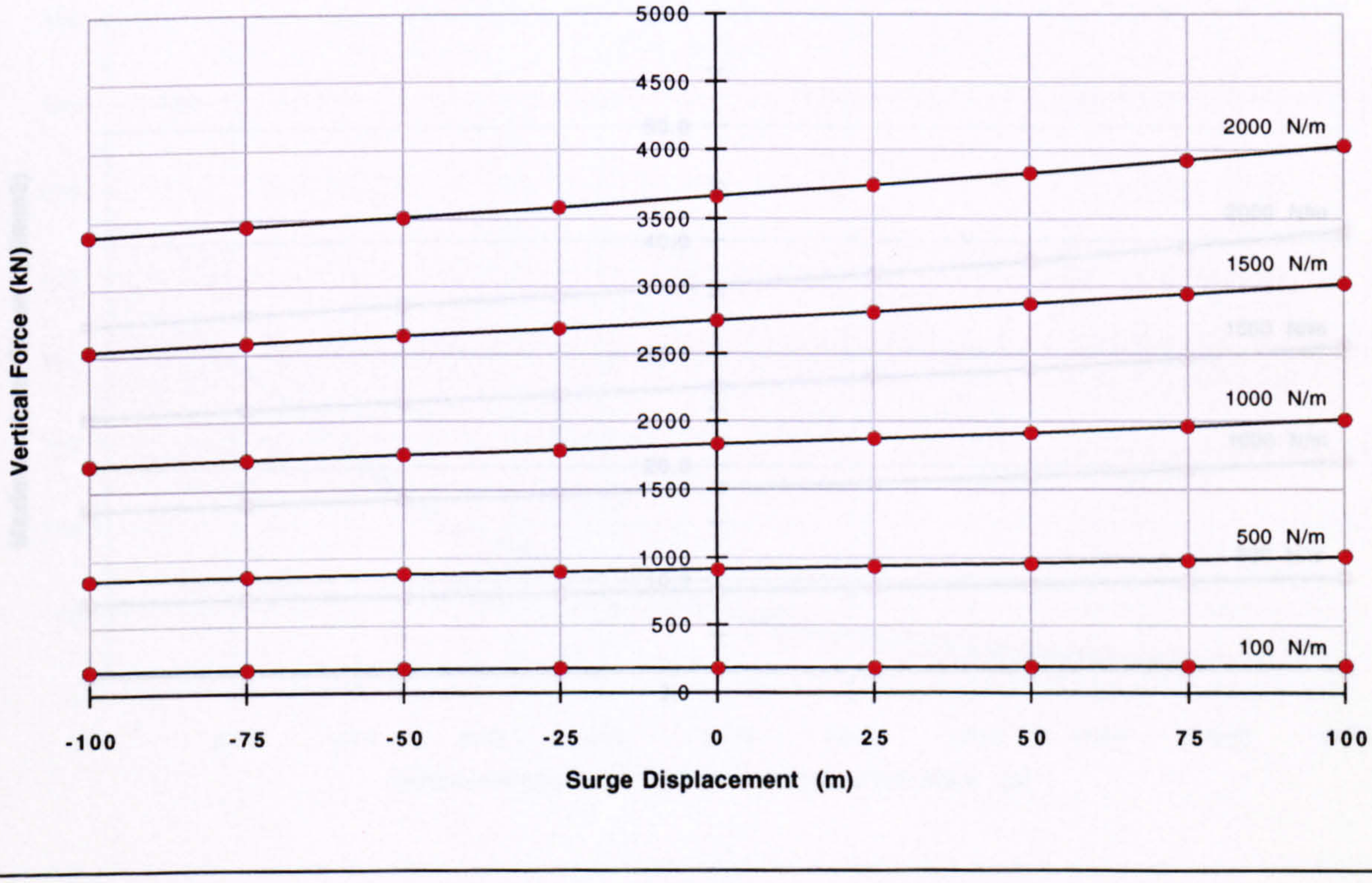

Horizontal Surface Offset = 1000 m

Sea Depth = 1500 m

Vertical Offset = 1400 m

Sea Depth = 1500 m

Figure 5.53

Axial Load (Tensile) at the Surface (e)

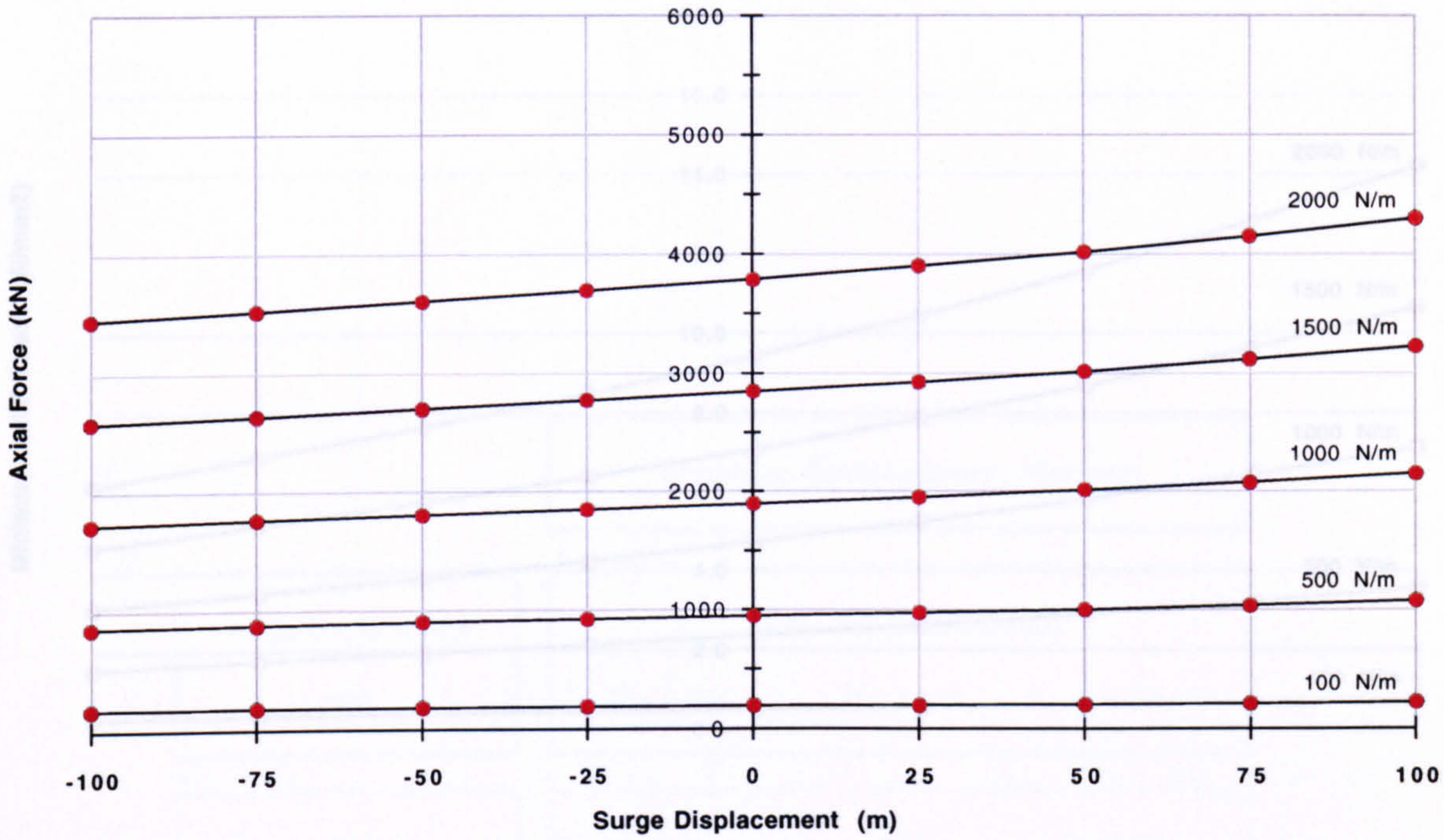

Axial Stress at the Surface (f)

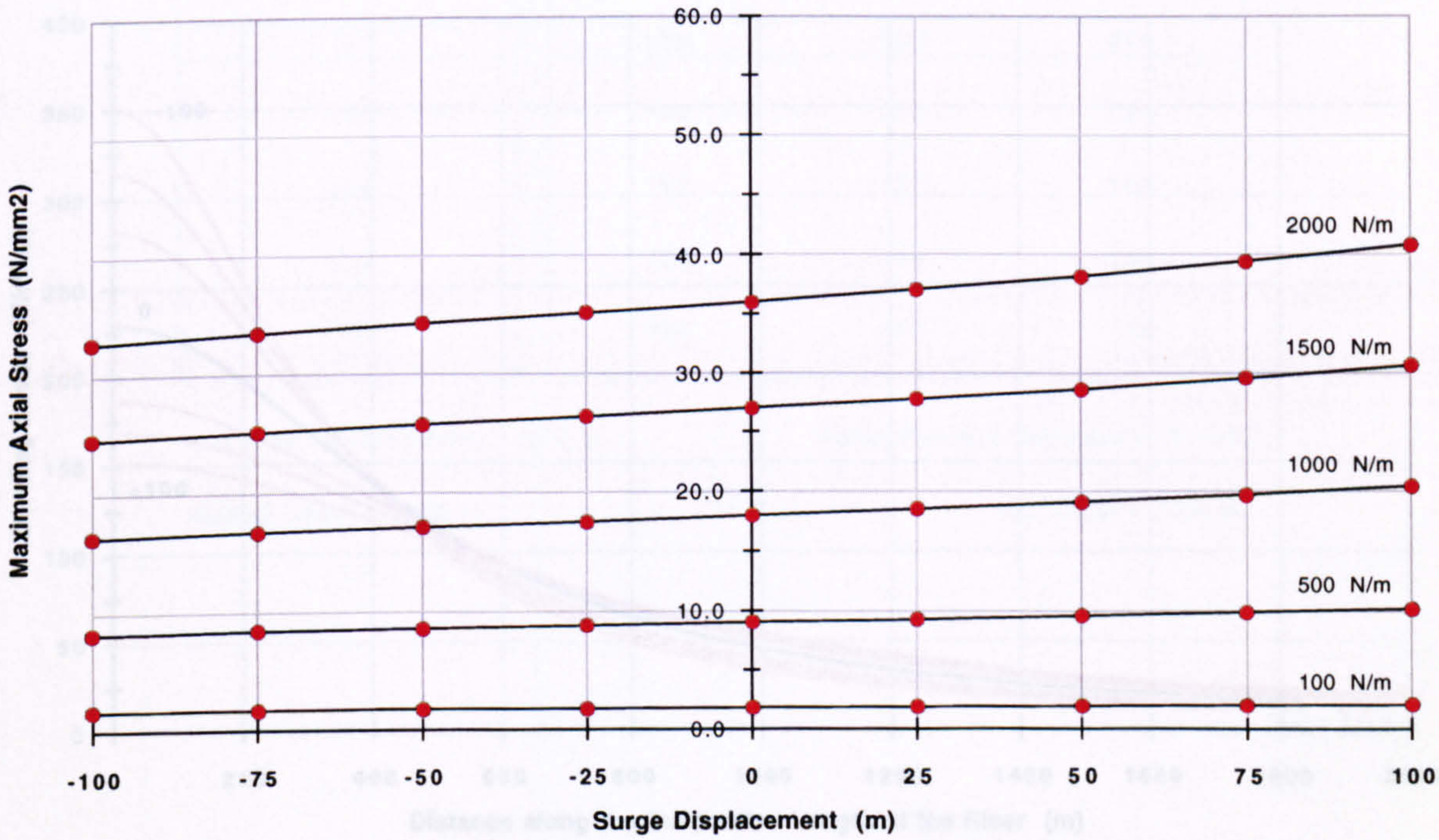

Horizontal Surface Offset = 1000 m

Vertical Offset = 1400 m

Sea Depth = 1500 m

Carrier Pipe Outer Diameter = 1.1 m

Carrier Pipe Wall Thickness = 10 mm

Figure 5.53

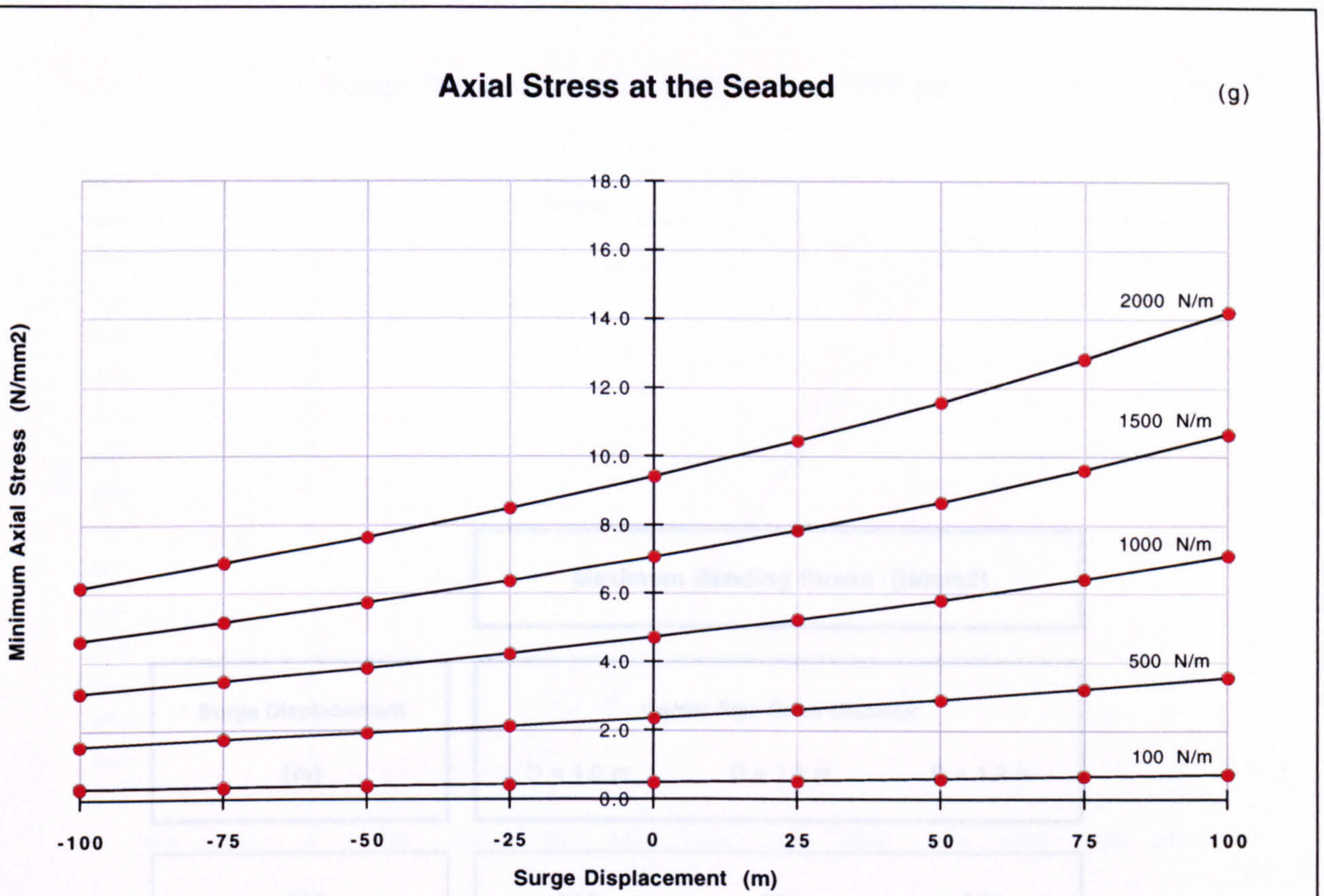

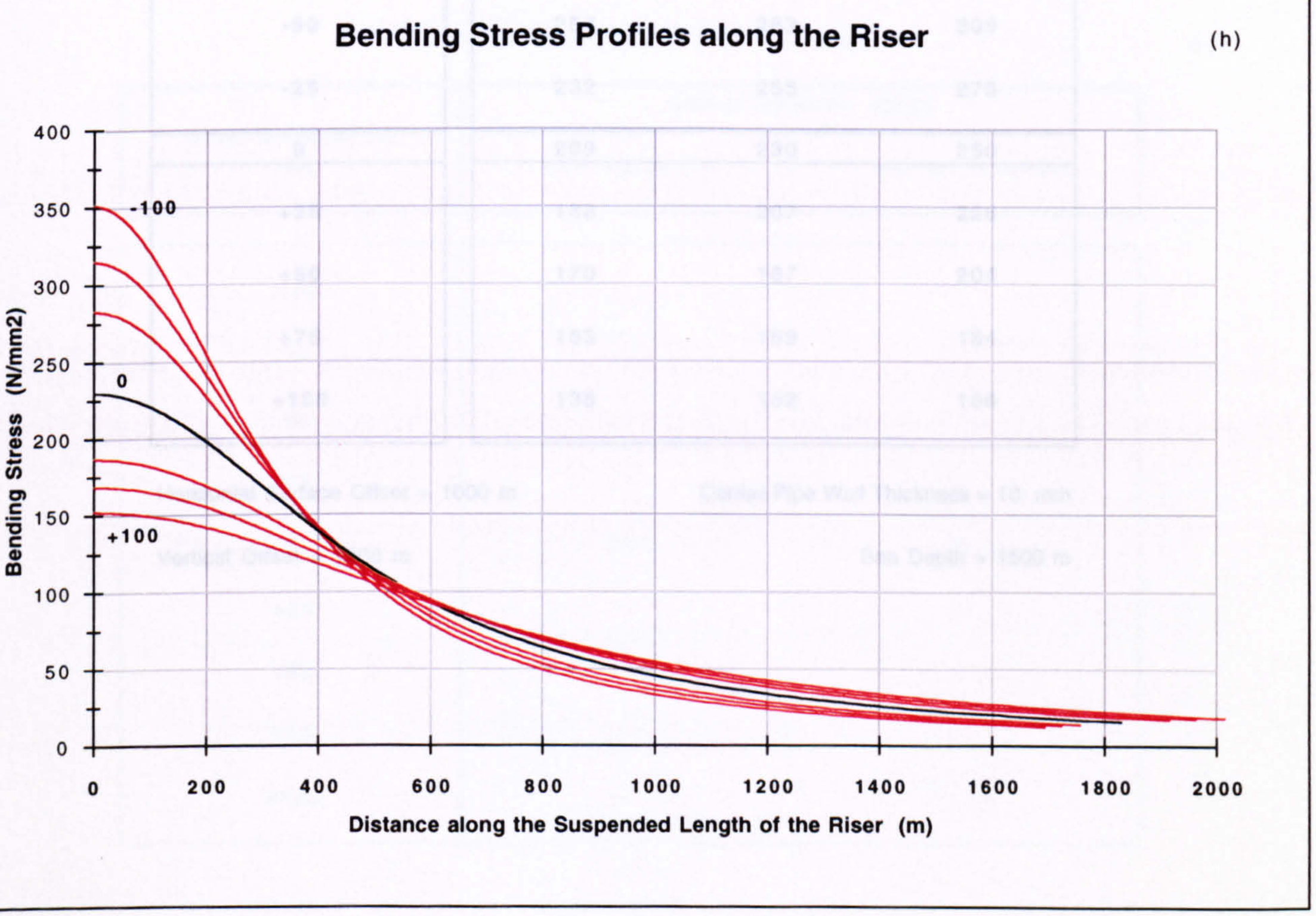

Horizontal Surface Offset = 1000 m

Vertical Offset = 1400 m

Sea Depth = 1500 m

Carrier Pipe Outer Diameter = 1.1 m

Carrier Pipe Wall Thickness = 10 mm

Figure 5.53

Bending Stress at the Seabed - Surge Displacement (a = 1000 m, b = 1400 m)

Surge Displacement (m)	Maximum Bending Stress (N/mm2)		
	Carrier Pipe Outer Diameter		
	D = 1.0 m	D = 1.1 m	D = 1.2 m
-100	319	351	383
-75	286	315	344
-50	257	283	309
-25	232	255	278
0	209	230	250
+25	188	207	226
+50	170	187	204
+75	153	169	184
+100	138	152	166

Horizontal Surface Offset = 1000 m

Carrier Pipe Wall Thickness = 10 mm

Vertical Offset = 1400 m

Sea Depth = 1500 m

Table 5.54

Surge Displacement Profiles (a = 1500 m)

(a)

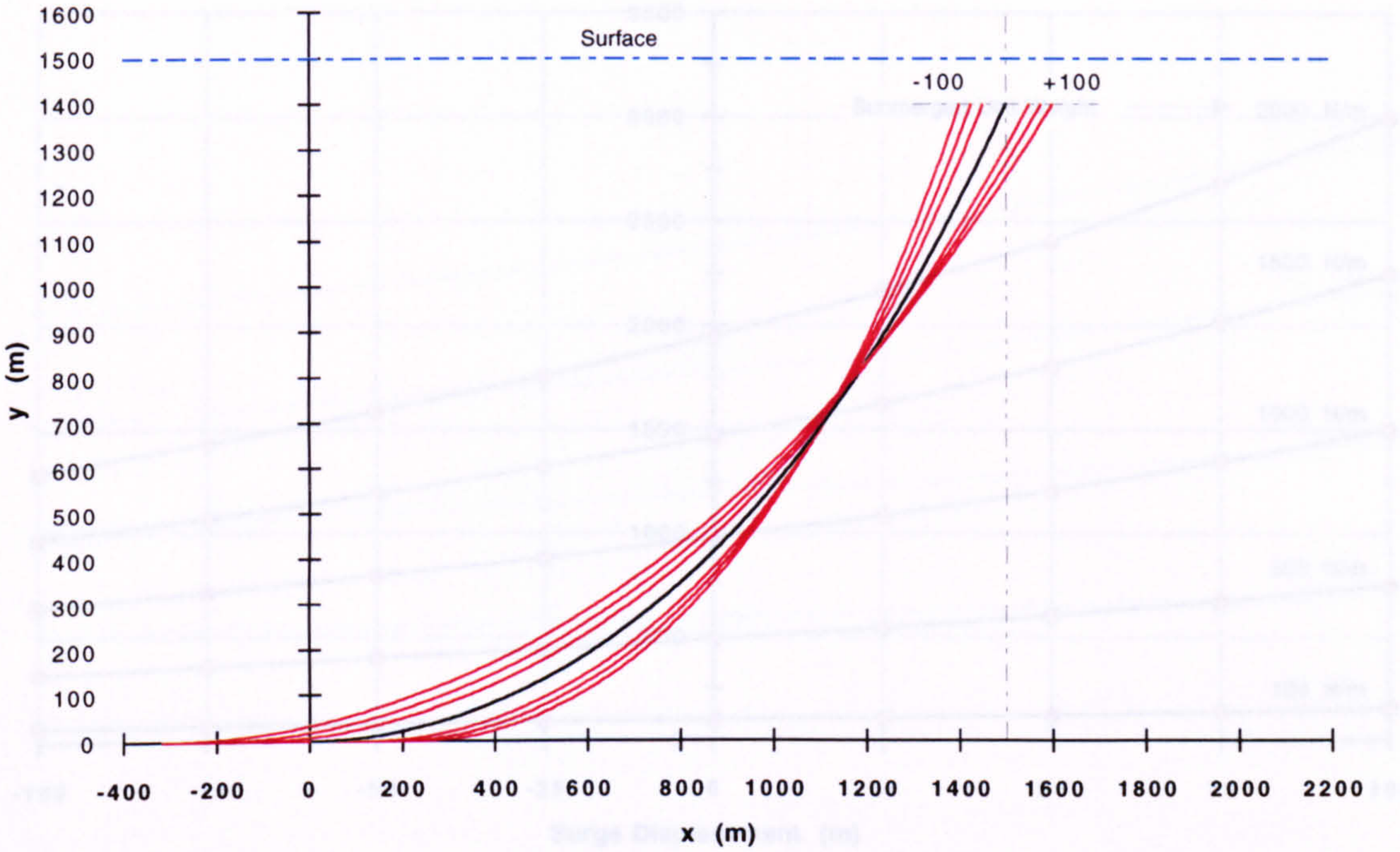

Riser Inclination at the Surface

(b)

Surge Displacement (m)	Surface Inclination (degs) from the Vertical	from the Horizontal
-100	18.4	71.6
-75	19.8	70.2
-50	21.2	68.8
-25	22.7	67.3
0	24.2	65.8
+25	25.9	64.1
+50	27.5	62.5
+75	29.3	60.7
+100	31.1	58.9

Horizontal Surface Offset = 1500 m

Sea Depth = 1500 m

Vertical Offset = 1400 m

Figure 5.55

Horizontal Load at the Surface (H)

(c)

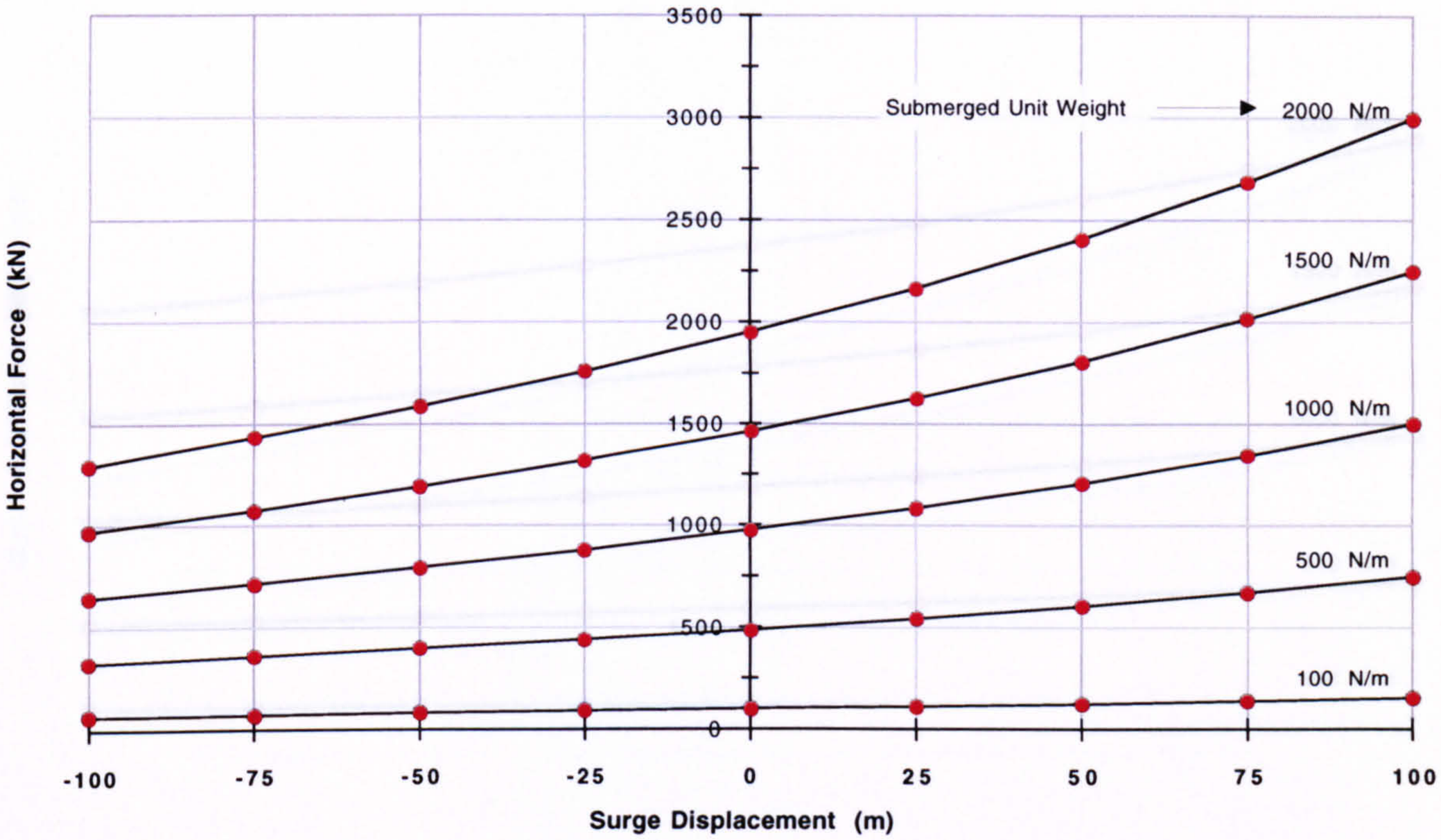

Vertical Load at the Surface (V)

(d)

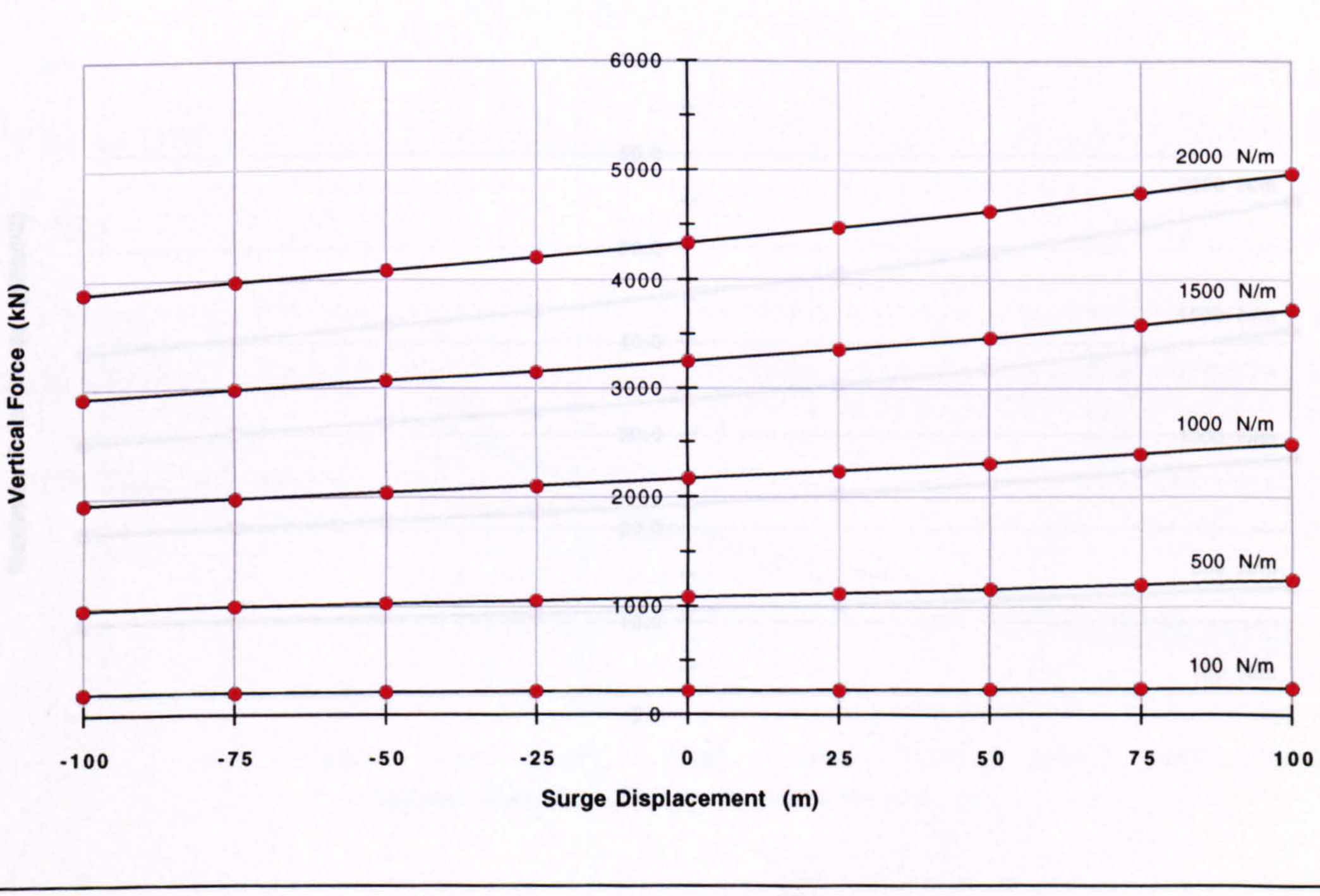

Horizontal Surface Offset = 1500 m

Vertical Offset = 1400 m

Sea Depth = 1500 m

Sea Depth = 1500 m

Figure 5.55

Axial Load (Tensile) at the Surface

(e)

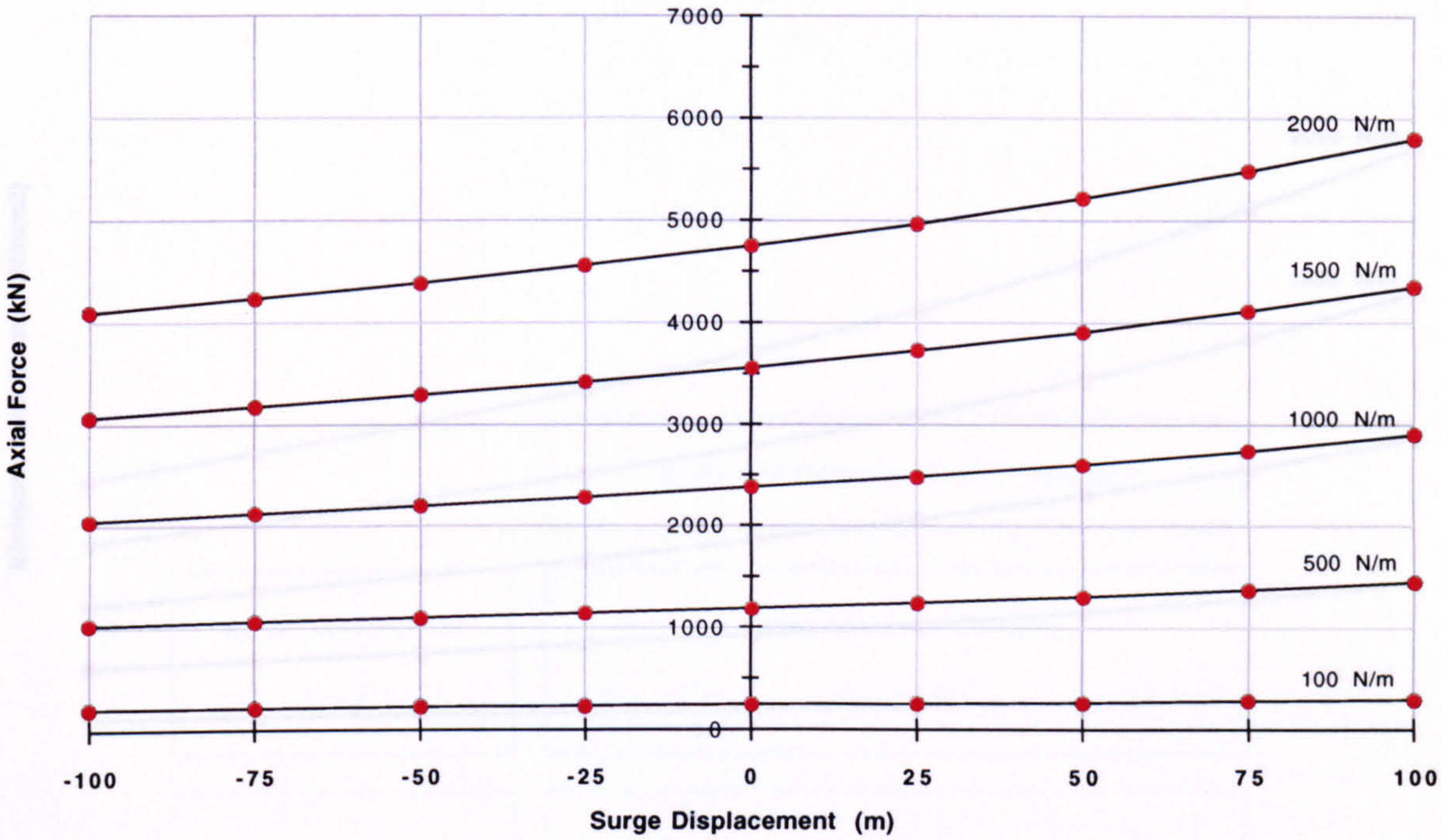

Axial Stress at the Surface

(f)

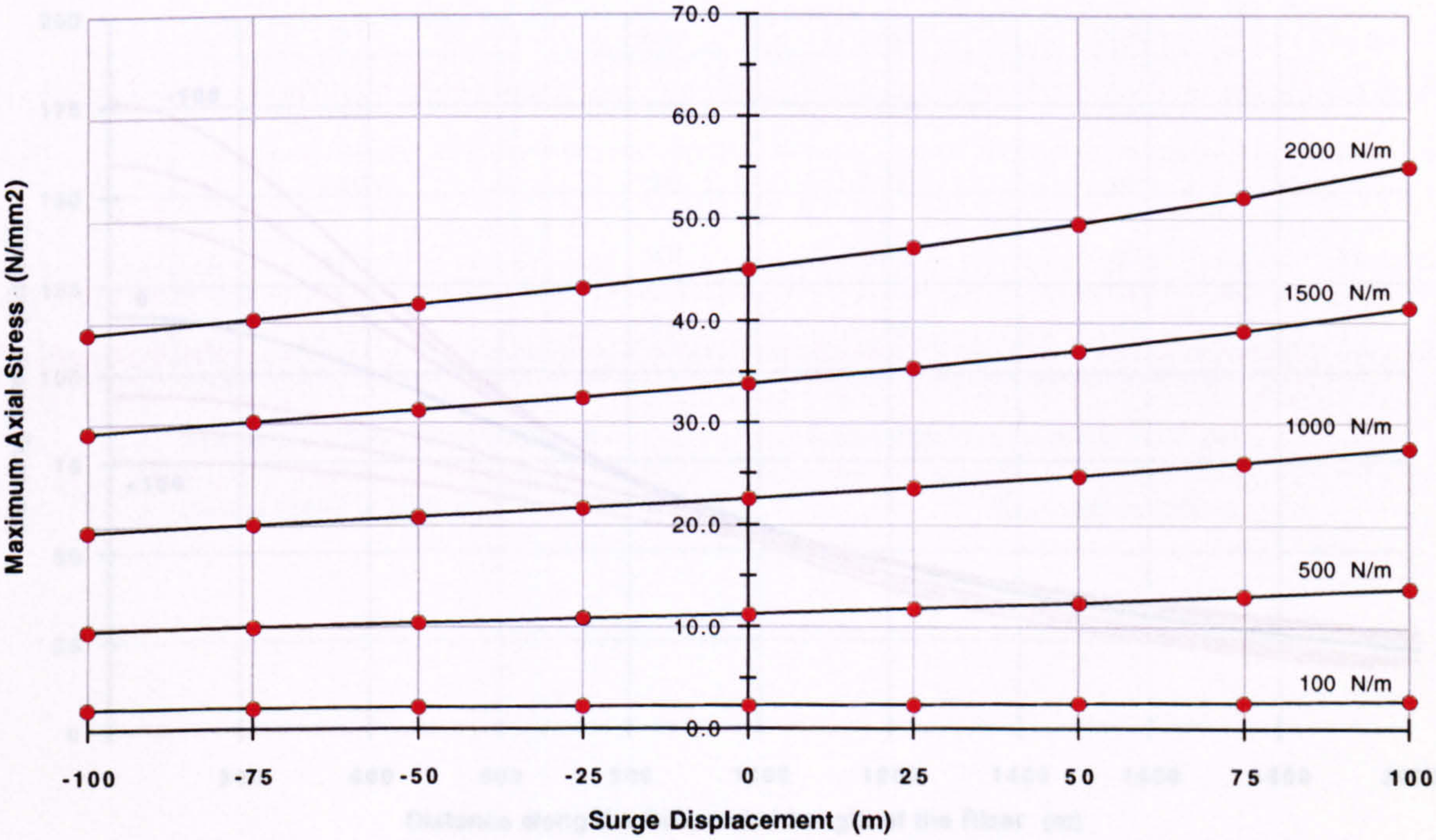

Horizontal Surface Offset = 1500 m

Vertical Offset = 1400 m

Sea Depth = 1500 m

Carrier Pipe Outer Diameter = 1.1 m

Carrier Pipe Wall Thickness = 10 mm

Figure 5.55

Axial Stress at the Seabed

(g)

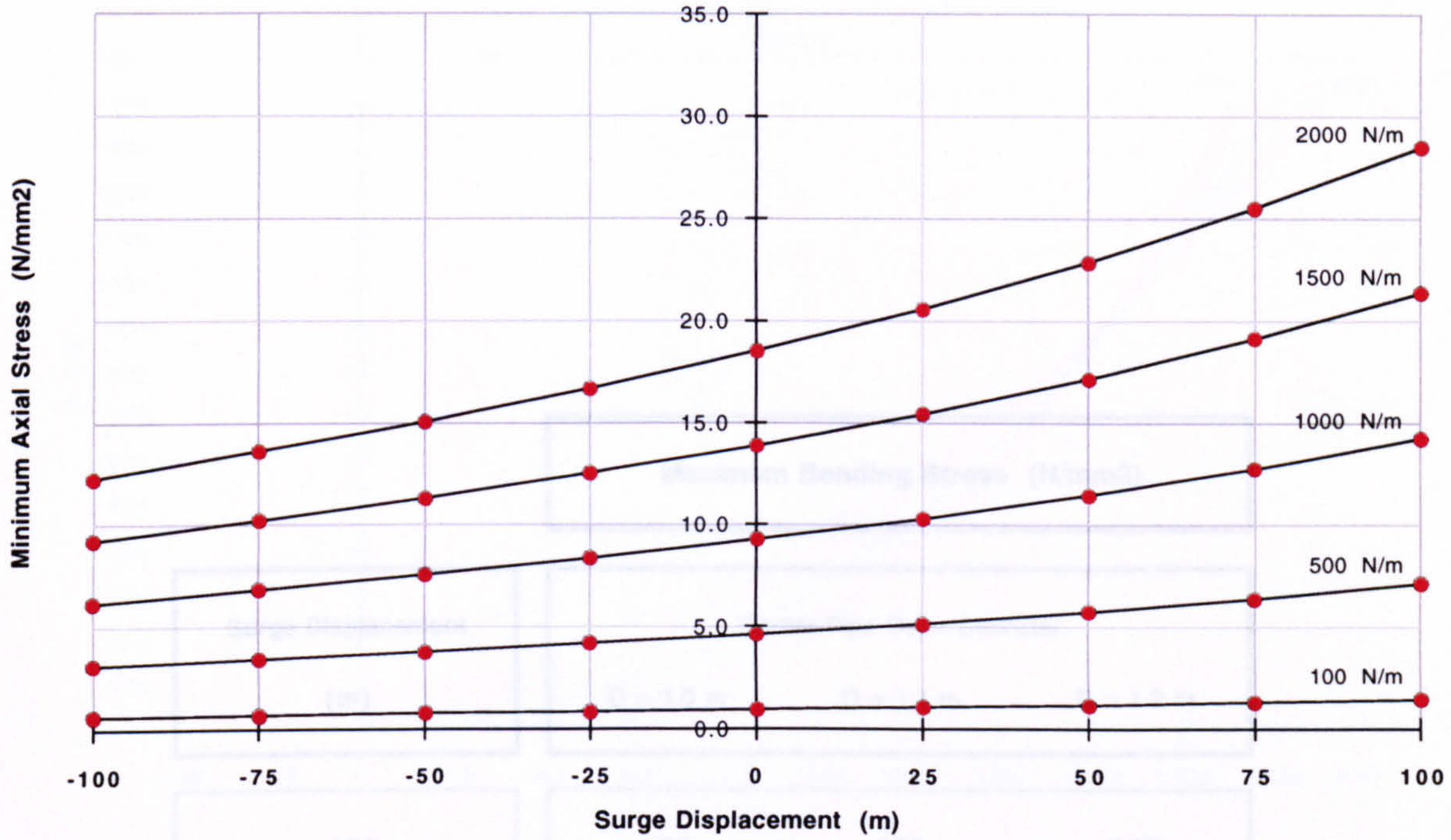

Bending Stress Profiles along the Riser

(h)

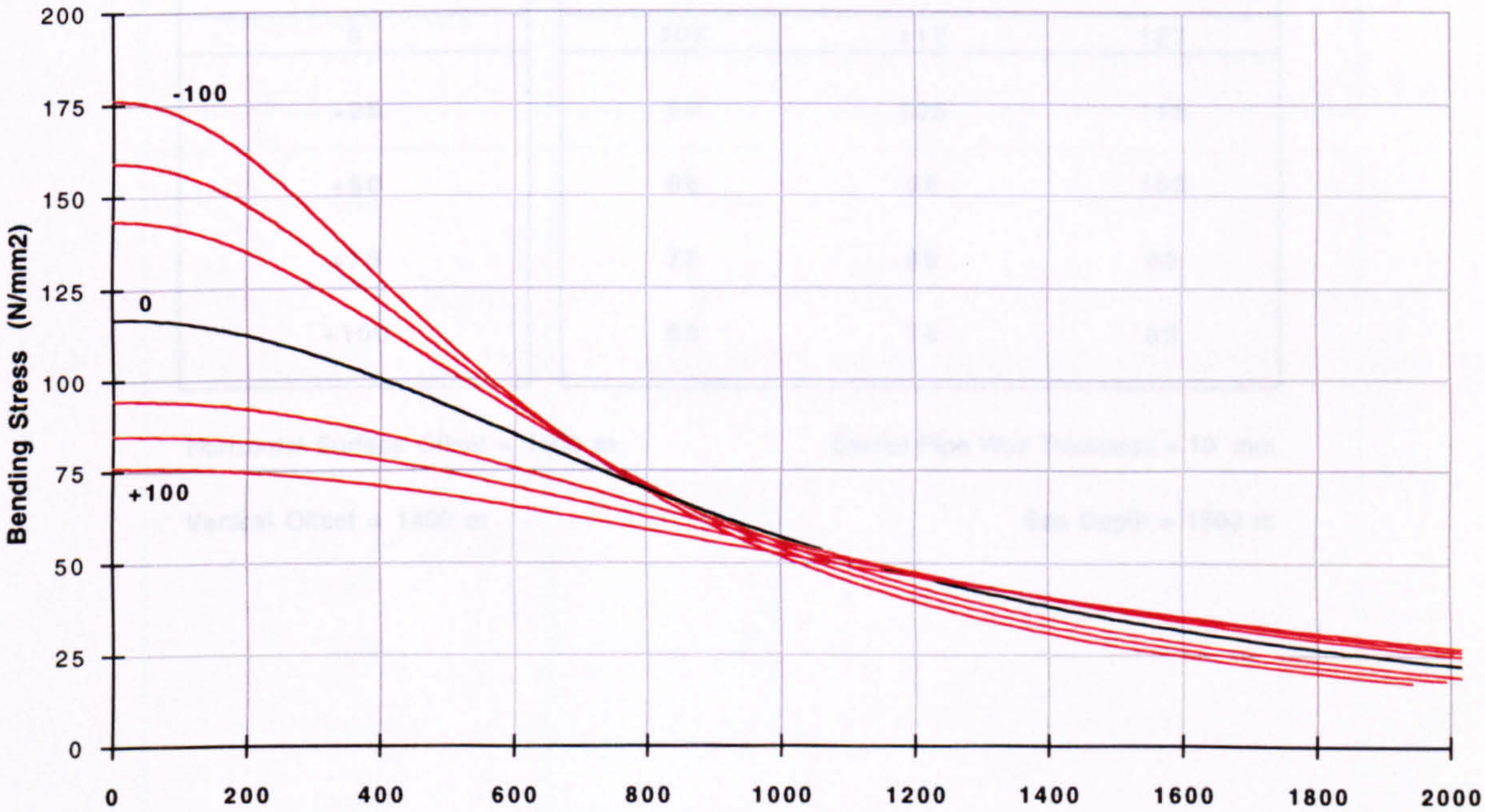

Horizontal Surface Offset = 1500 m

Vertical Offset = 1400 m

Sea Depth = 1500 m

Carrier Pipe Outer Diameter = 1.1 m

Carrier Pipe Wall Thickness = 10 mm

Figure 5.55

Bending Stress at the Seabed - Surge Displacement (a = 1500 m, b = 1400 m)

Surge Displacement (m)	Maximum Bending Stress (N/mm2)		
	Carrier Pipe Outer Diameter		
	D = 1.0 m	D = 1.1 m	D = 1.2 m
-100	160	176	192
-75	145	159	174
-50	131	144	157
-25	118	130	141
0	106	117	127
+25	96	105	115
+50	86	95	103
+75	77	85	93
+100	69	76	83

Horizontal Surface Offset = 1500 m

Carrier Pipe Wall Thickness = 10 mm

Vertical Offset = 1400 m

Sea Depth = 1500 m

Table 5.56

Surge Displacement Profiles (a = 2000 m)

(a)

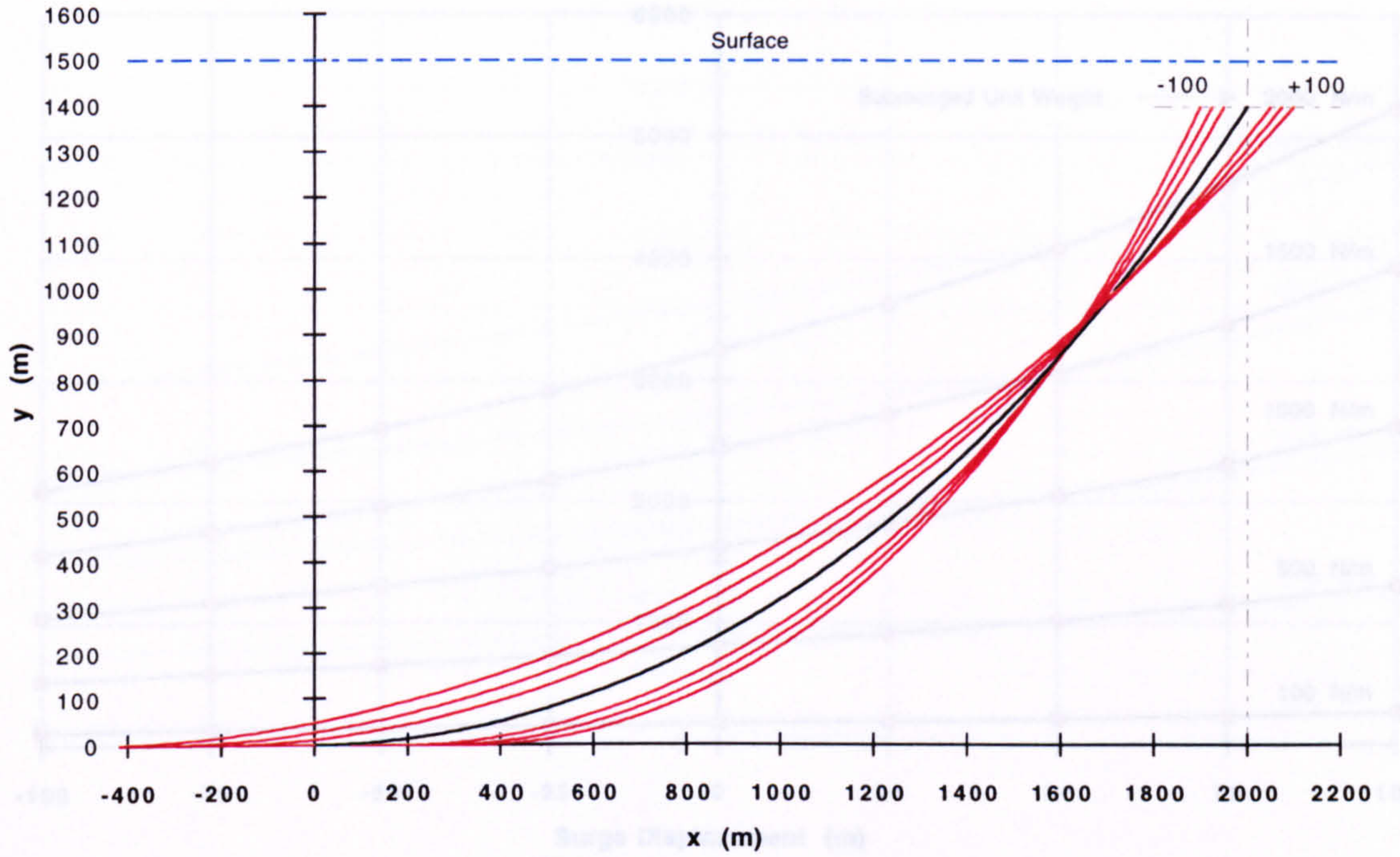

Riser Inclination at the Surface

(b)

Surge Displacement (m)	Surface Inclination (degs) from the Vertical	from the Horizontal
-100	25.3	64.7
-75	27.0	63.0
-50	28.8	61.2
-25	30.6	59.4
0	32.4	57.6
+25	34.4	55.6
+50	36.4	53.6
+75	38.5	51.5
+100	40.7	49.3

Horizontal Surface Offset = 2000 m

Sea Depth = 1500 m

Vertical Offset = 1400 m

Figure 5.57

Horizontal Load at the Surface (H)

(c)

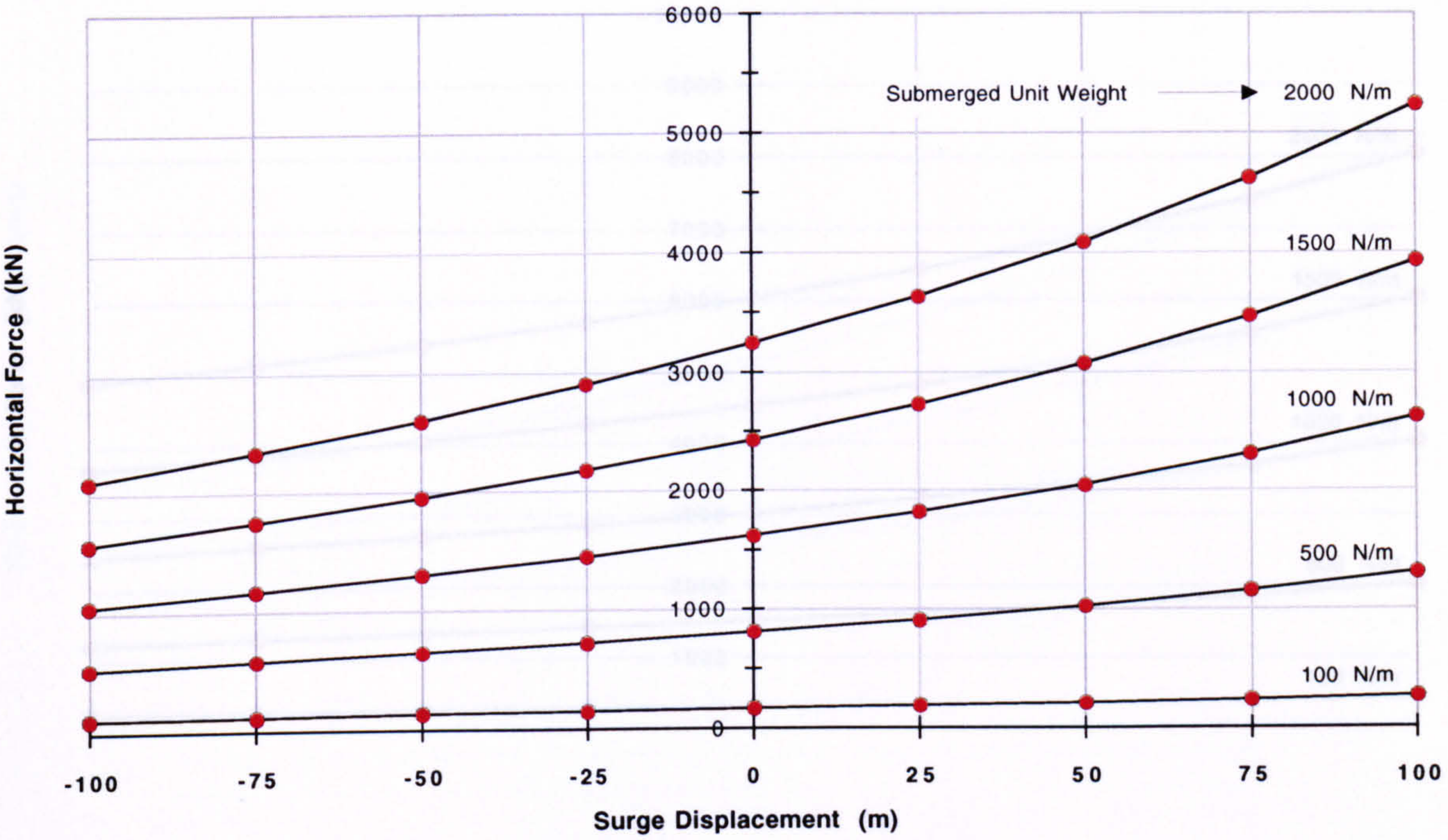

Vertical Load at the Surface (V)

(d)

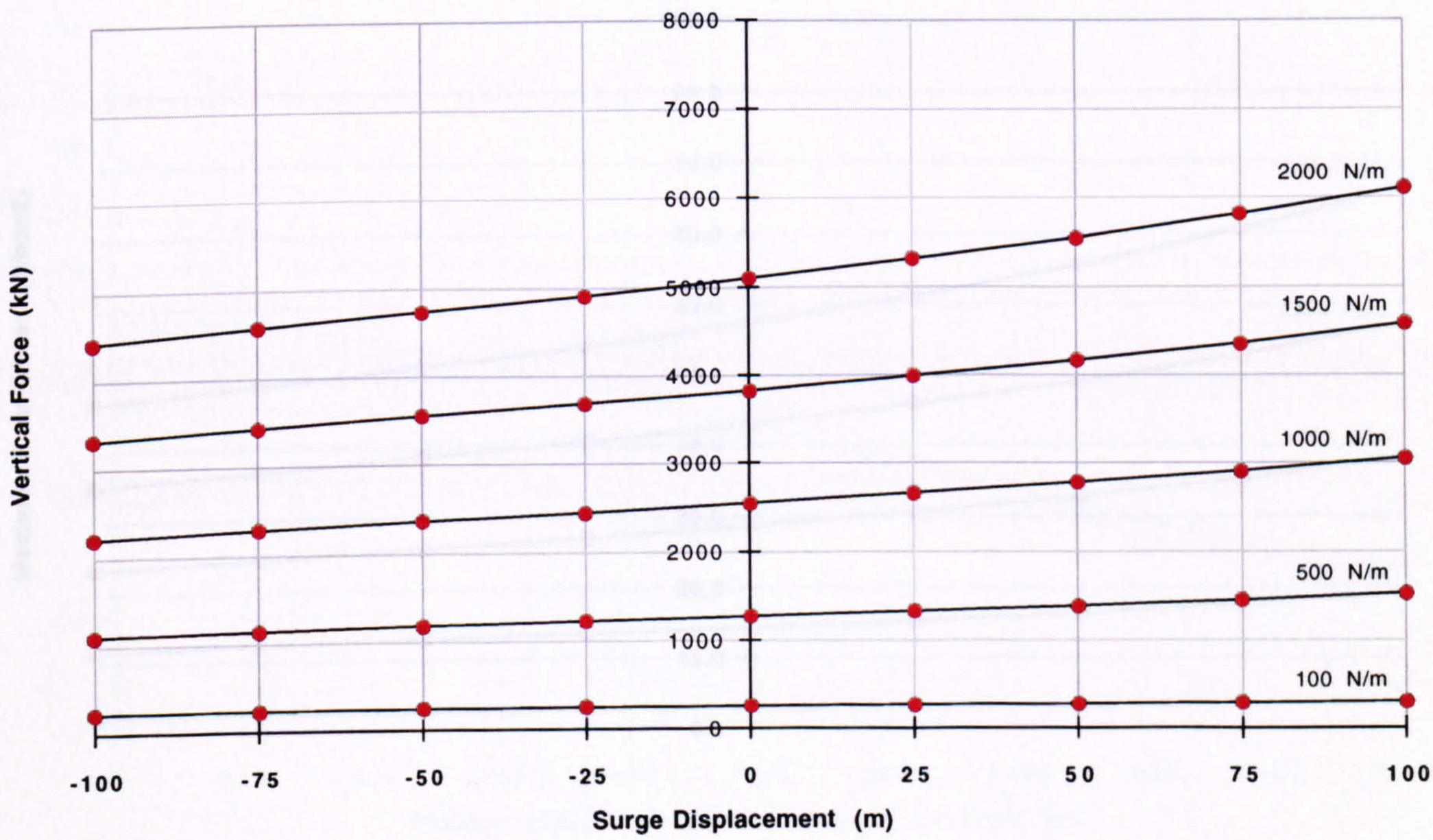

Horizontal Surface Offset = 2000 m

Vertical Offset = 1400 m

Sea Depth = 1500 m

Sea Depth = 1500 m

Figure 5.57

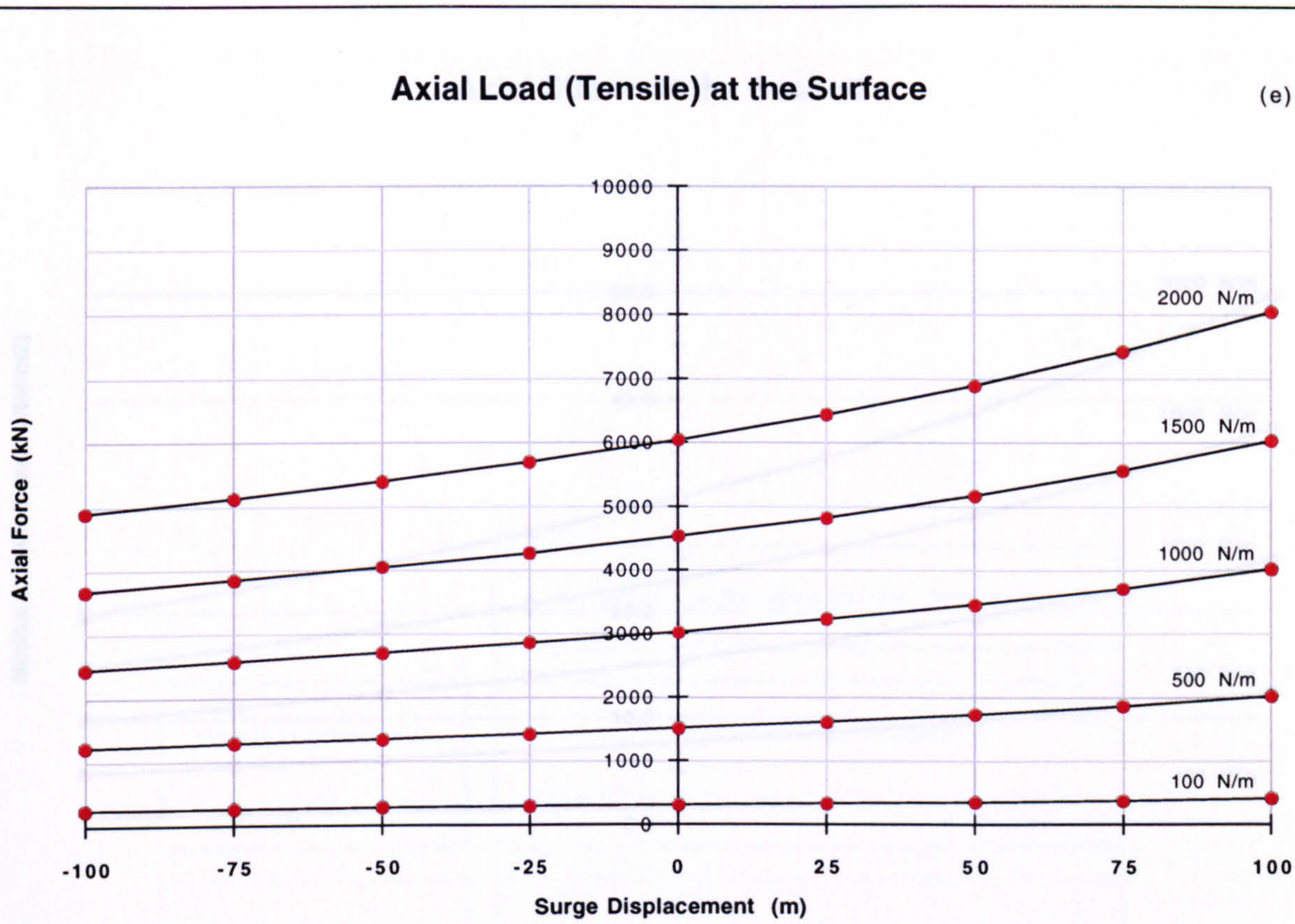

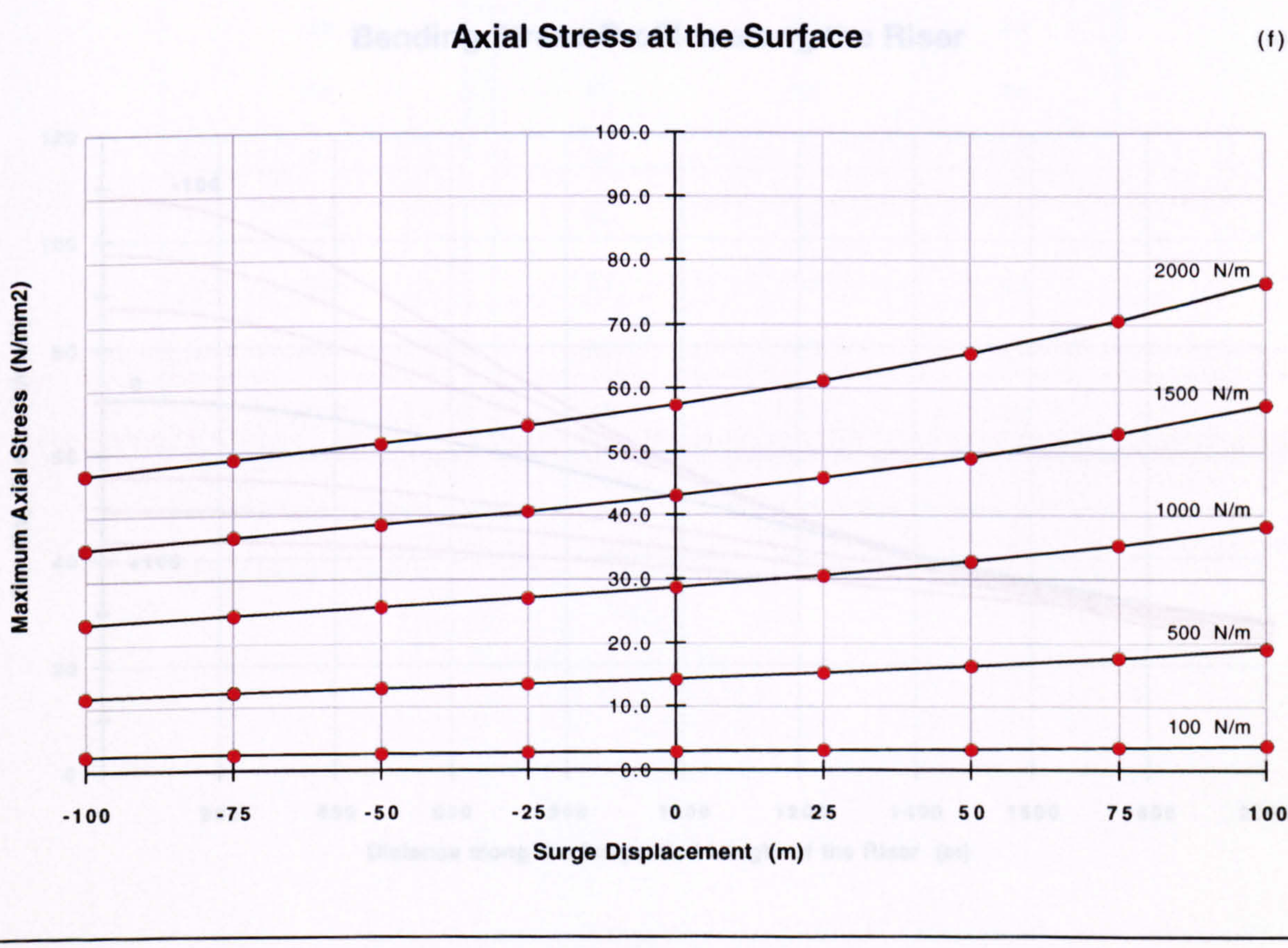

Horizontal Surface Offset = 2000 m

Vertical Offset = 1400 m

Sea Depth = 1500 m

Carrier Pipe Outer Diameter = 1.1 m

Carrier Pipe Wall Thickness = 10 mm

Figure 5.57

Axial Stress at the Seabed

(g)

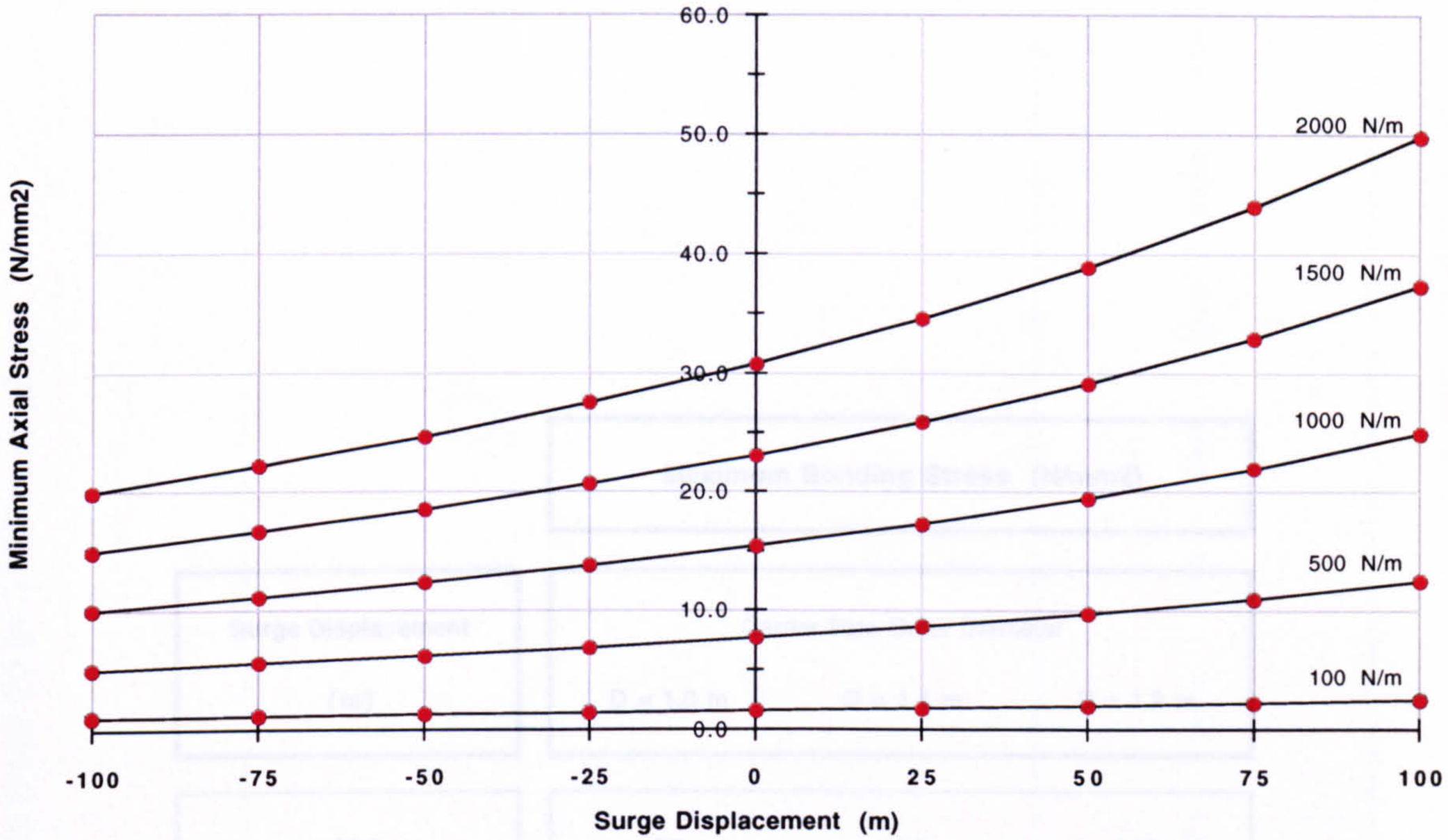

Bending Stress Profiles along the Riser

(h)

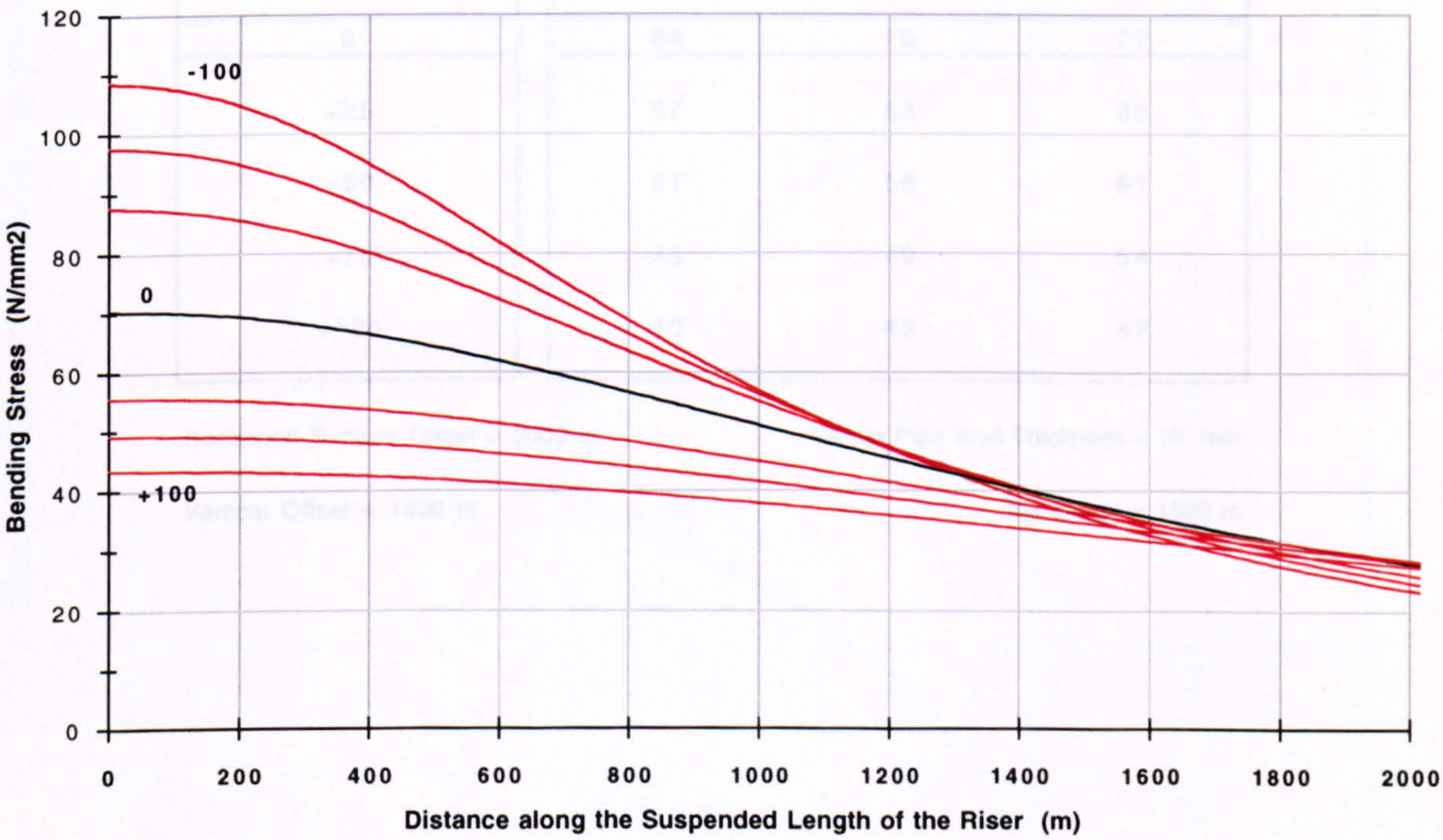

Horizontal Surface Offset = 2000 m

Vertical Offset = 1400 m

Sea Depth = 1500 m

Carrier Pipe Outer Diameter = 1.1 m

Carrier Pipe Wall Thickness = 10 mm

Figure 5.57

Bending Stress at the Seabed - Surge Displacement (a = 2000 m, b = 1400 m)

Surge Displacement (m)	Maximum Bending Stress (N/mm2)		
	Carrier Pipe Outer Diameter		
	D = 1.0 m	D = 1.1 m	D = 1.2 m
-100	99	109	119
-75	89	98	107
-50	80	88	96
-25	71	79	86
0	64	70	77
+25	57	63	68
+50	51	56	61
+75	45	49	54
+100	40	43	47

Horizontal Surface Offset = 2000 m

Vertical Offset = 1400 m

Carrier Pipe Wall Thickness = 10 mm

Sea Depth = 1500 m

Table 5.58

Current Velocity : 1.3 m/s at the surface, 0.2 m/s from 50 to 1400 m depth.

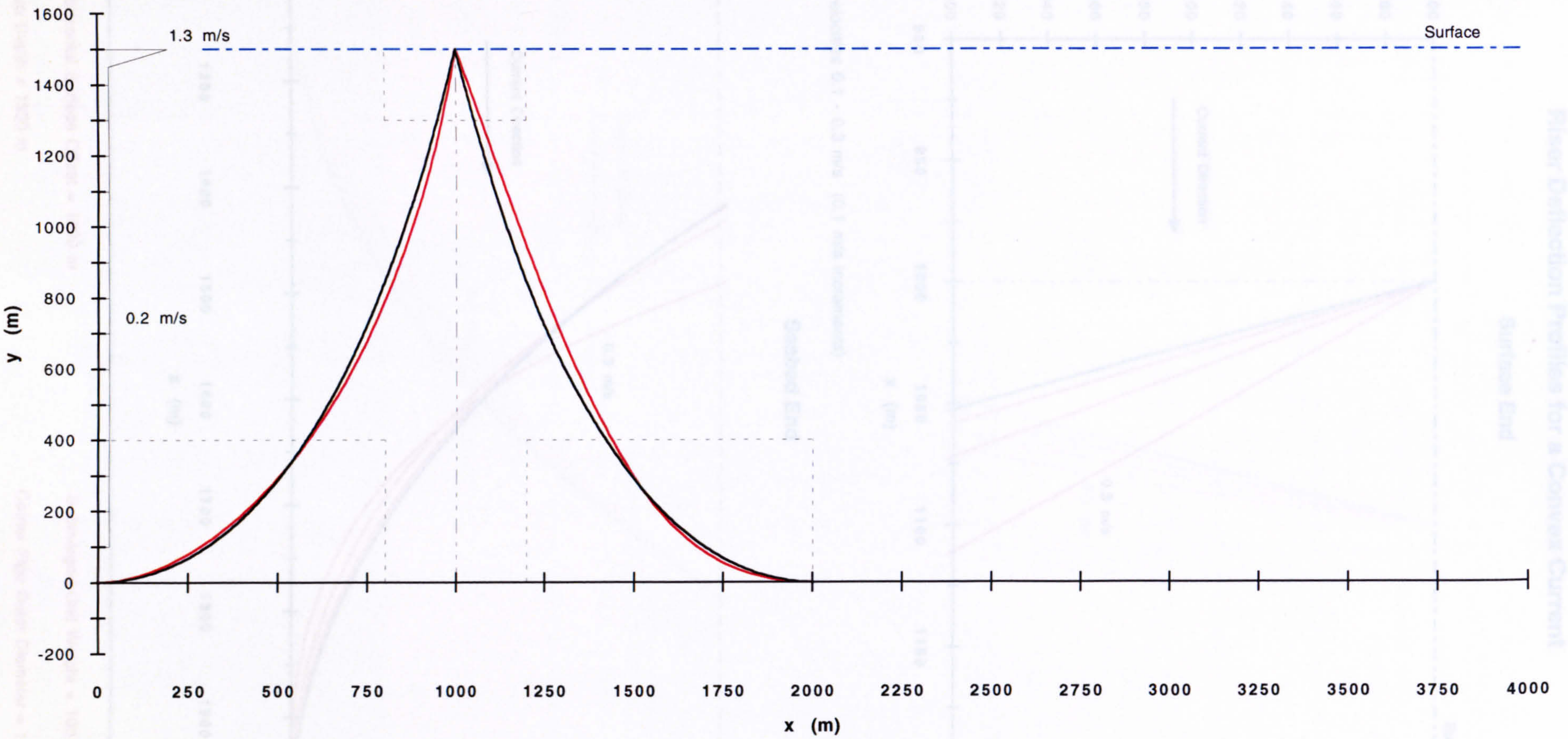

Horizontal Surface Offset = 1000 m

Sea Depth = 1500 m

Submerged Unit Weight = 100 N/m

Carrier Pipe Outer Diameter = 1.1 m

Figure 5.59

Riser Deflection Profiles for a Convex Current

Surface End

(a)

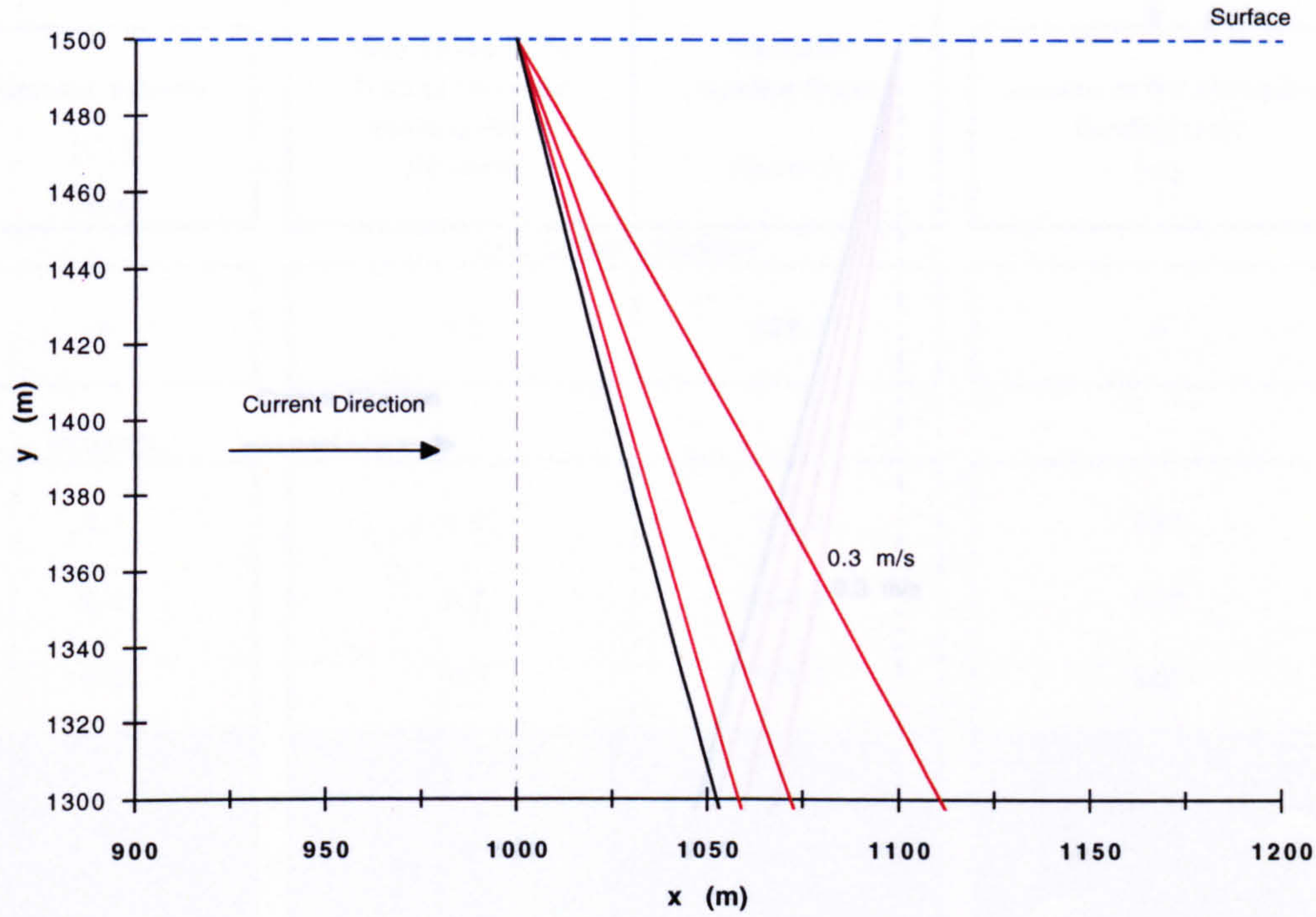

Current velocities 0.1 - 0.3 m/s (0.1 m/s increments)

Seabed End

(b)

Axes to Scale

Horizontal Surface Offset = 1000 m

Sea Depth = 1500 m

Submerged Unit Weight = 100 N/m

Carrier Pipe Outer Diameter = 1.1 m

Figure 5.60

Riser Deflection Profiles for a Concave Current

Surface End

(a)

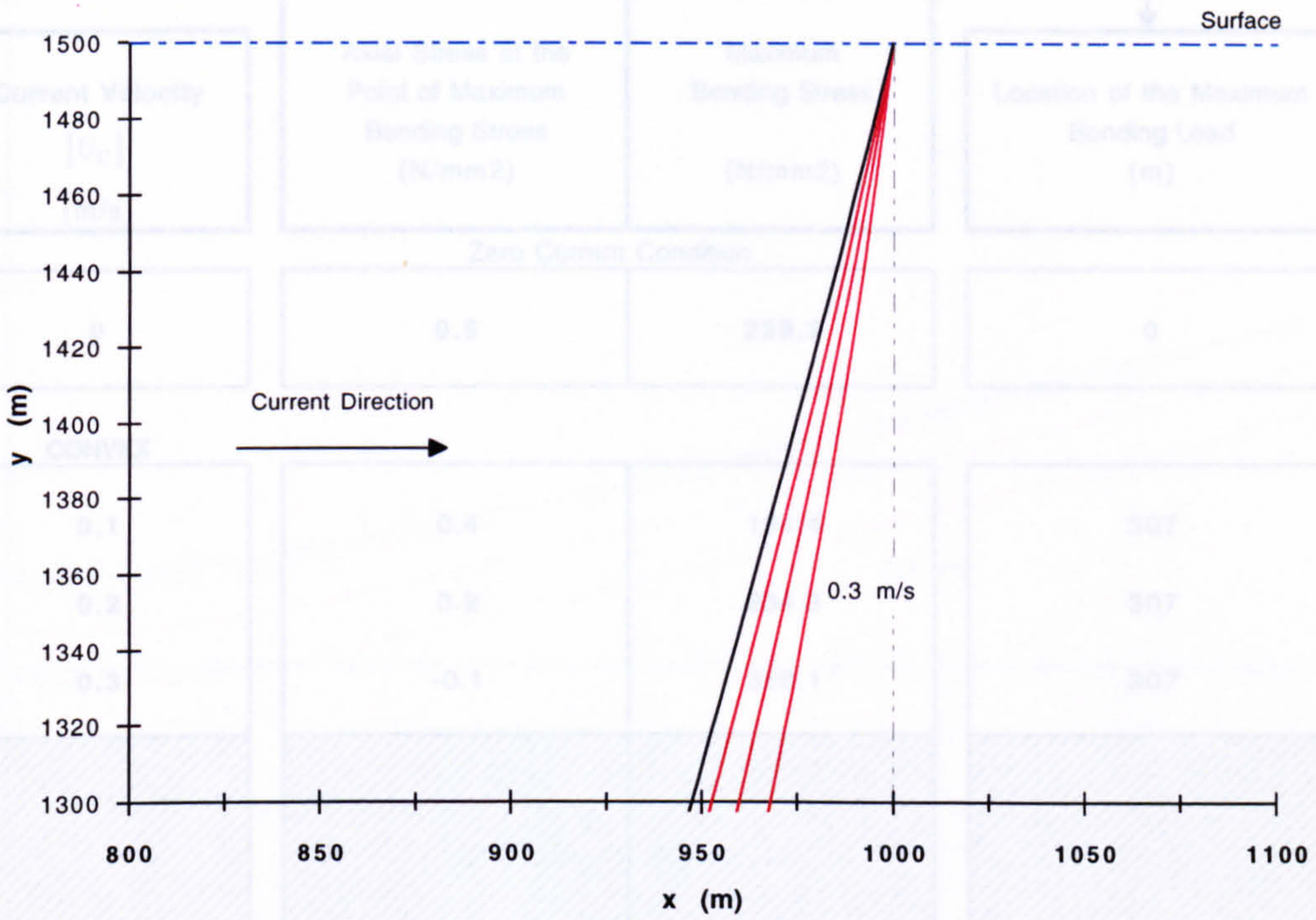

Current velocities 0.1 - 0.3 m/s (0.1 m/s increments)

Seabed End

(b)

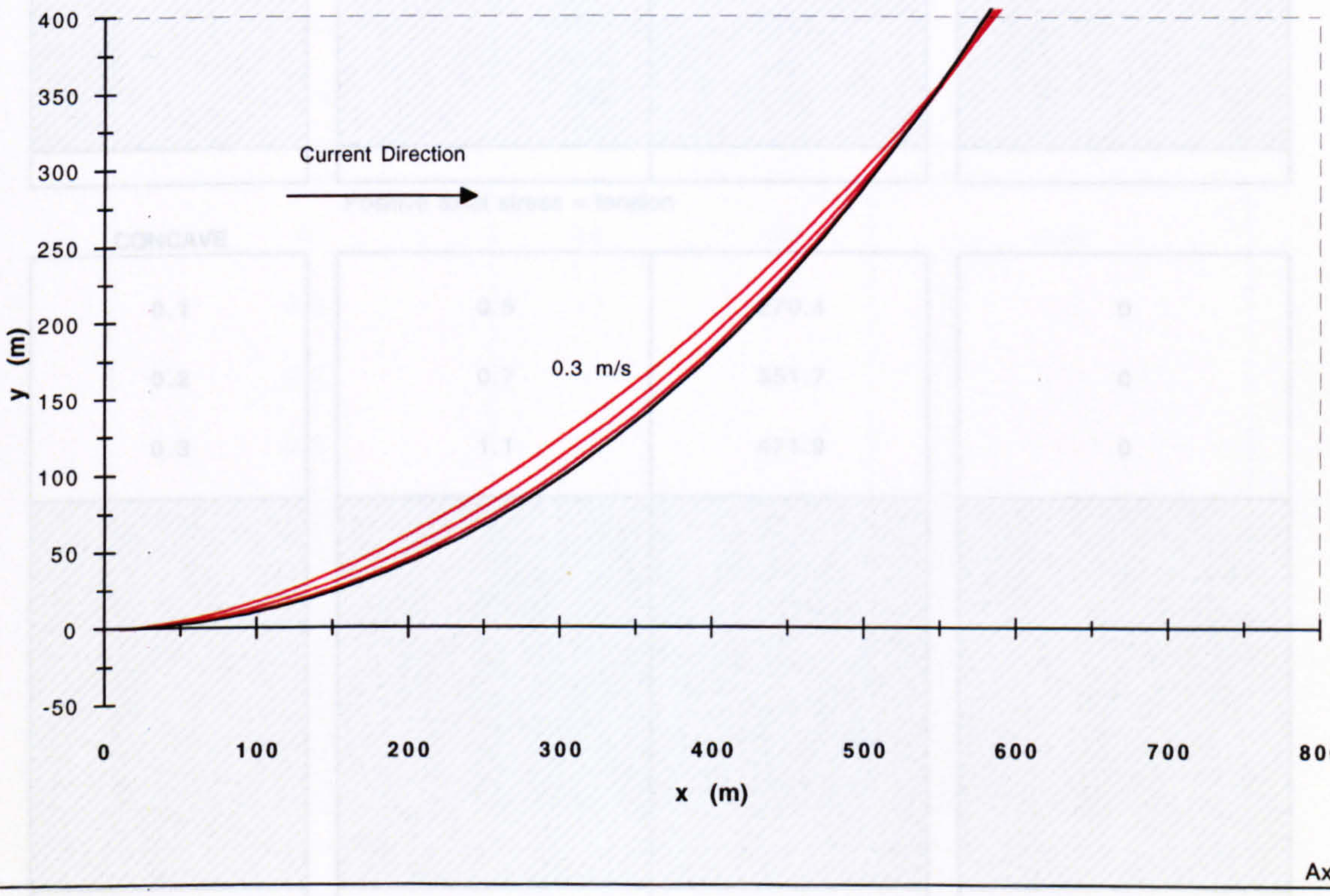

Axes to Scale

Horizontal Surface Offset = 1000 m

Sea Depth = 1500 m

Submerged Unit Weight = 100 N/m

Carrier Pipe Outer Diameter = 1.1 m

Figure 5.61

Maximum Stress Conditions under Current Loading (a = 1000 m)

Submerged Unit Weight = 100 N/m

Current Velocity $[U_C]$ (m/s)	Axial Stress at the Point of Maximum Bending Stress (N/mm2)	Maximum Bending Stress (N/mm2)	Location of the Maximum Bending Load (m)
			Measured along the riser from the seabed end
	Zero Current Condition		
0	0.5	239.3	0
CONVEX			
0.1	0.4	184.4	307
0.2	0.2	234.3	307
0.3	-0.1	356.1	307
	Positive axial stress = tension		
CONCAVE			
0.1	0.5	270.4	0
0.2	0.7	351.7	0
0.3	1.1	471.9	0

Horizontal Surface Offset = 1000 m

Sea Depth = 1500 m

Carrier Pipe Outer Diameter = 1.1 m

Carrier Pipe Wall Thickness = 10 mm

Table 5.62

Axial Stress Distributions for a Convex Current

(a)

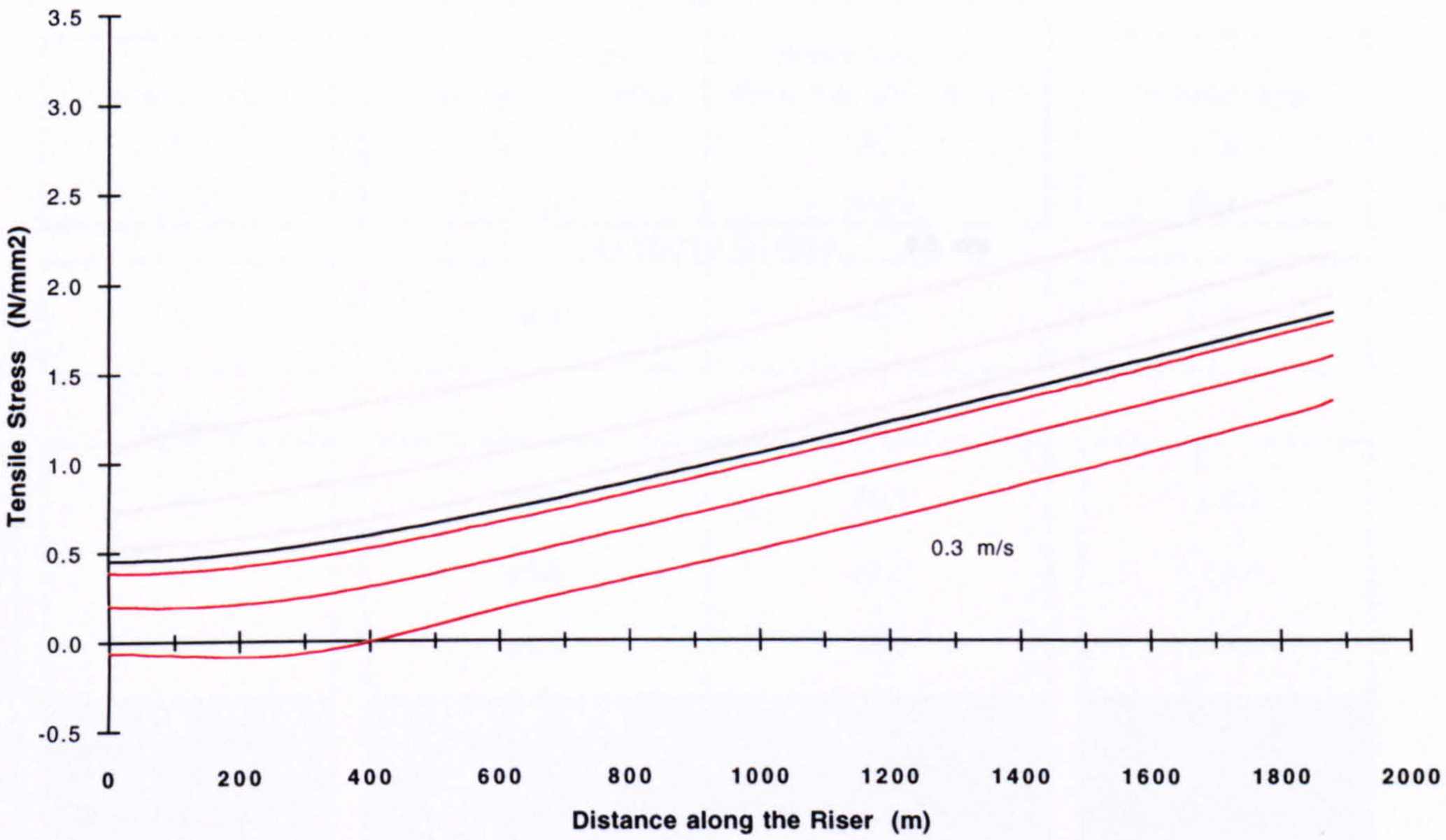

Current velocities 0.1 - 0.3 m/s (0.1 m/s increments)

Surface Forces for a Convex Current

(b)

Current Velocity (m/s)	Horizontal Load (kN)	Vertical Load (kN)	Axial Load (kN)
0	48	192	198
0.1	54	179	187
0.2	68	160	174
0.3	72	134	152

Horizontal Surface Offset = 1000 m

Sea Depth = 1500 m

Submerged Unit Weight = 100 N/m

Carrier Pipe Outer Diameter = 1.1 m

Figure 5.63

Axial Stress Distributions for a Concave Current

(a)

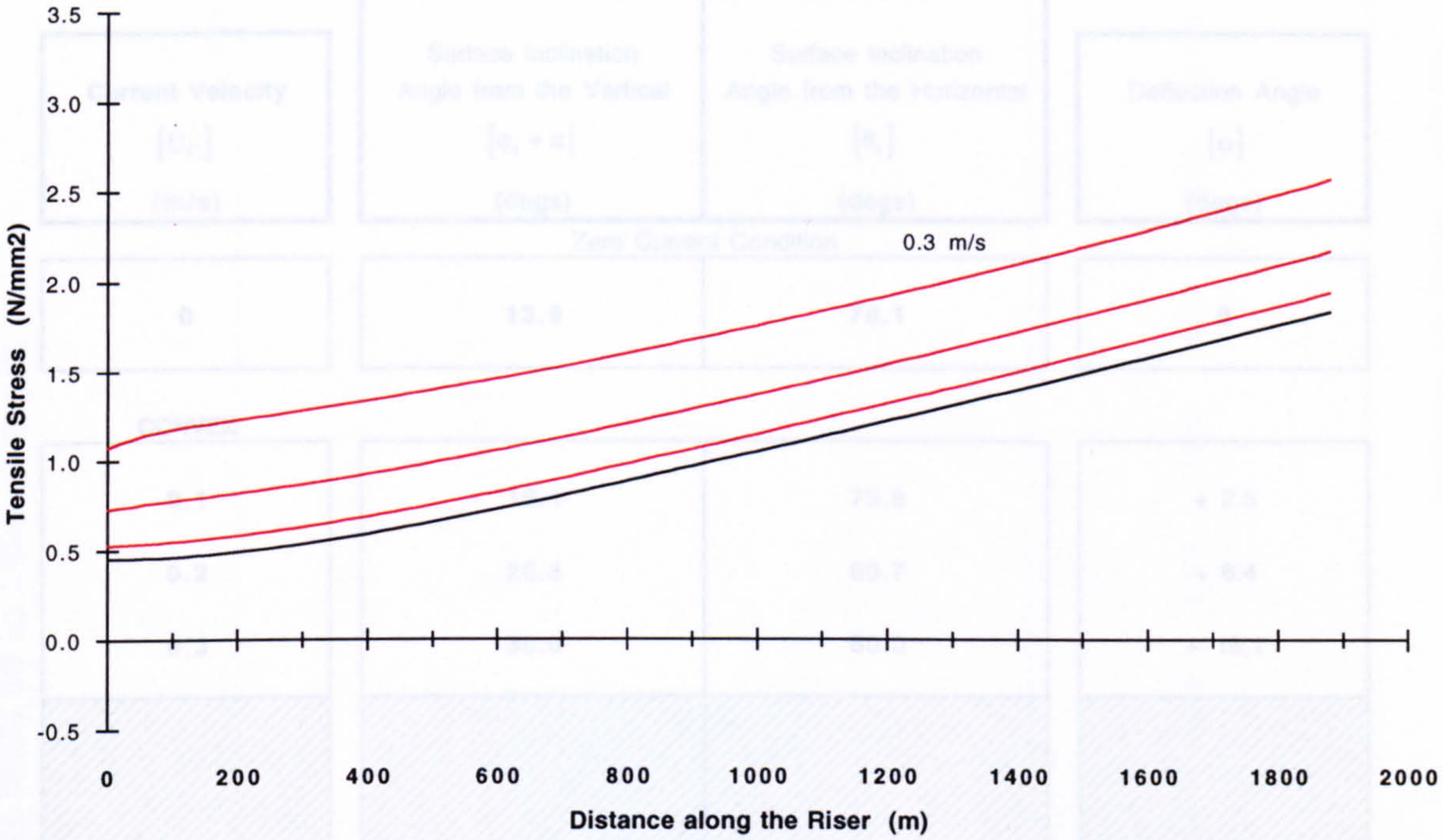

Current velocities 0.1 - 0.3 m/s (0.1 m/s increments)

Surface Forces for a Concave Current

(b)

Current Velocity (m/s)	Horizontal Load (kN)	Vertical Load (kN)	Axial Load (kN)
0	48	192	198
0.1	40	208	212
0.2	31	230	232
0.3	21	260	261

Horizontal Surface Offset = 1000 m

Sea Depth = 1500 m

Submerged Unit Weight = 100 N/m

Carrier Pipe Outer Diameter = 1.1 m

Figure 5.64

Surface Deflection Angles under Current Loading (a = 1000 m)

Submerged Unit Weight = 100 N/m

Current Velocity $[U_C]$ (m/s)	Surface Inclination Angle from the Vertical $[\varphi_s + \alpha]$ (degs)	Surface Inclination Angle from the Horizontal $[\theta_s]$ (degs)	Deflection Angle $[\alpha]$ (degs)
	Zero Current Condition		
0	13.9	76.1	0
CONVEX			
0.1	16.4	73.6	+ 2.5
0.2	20.3	69.7	+ 6.4
0.3	30.0	60.0	+ 16.1
CONCAVE			
0.1	11.7	78.3	- 2.2
0.2	9.6	80.4	- 4.3
0.3	7.1	82.9	- 6.8

Horizontal Surface Offset = 1000 m

Sea Depth = 1500 m

Carrier Pipe Outer Diameter = 1.1 m

Carrier Pipe Wall Thickness = 10 mm

Table 5.65

Current Velocity : 1.3 m/s at the surface, 0.4 m/s from 50 to 1400 m depth.

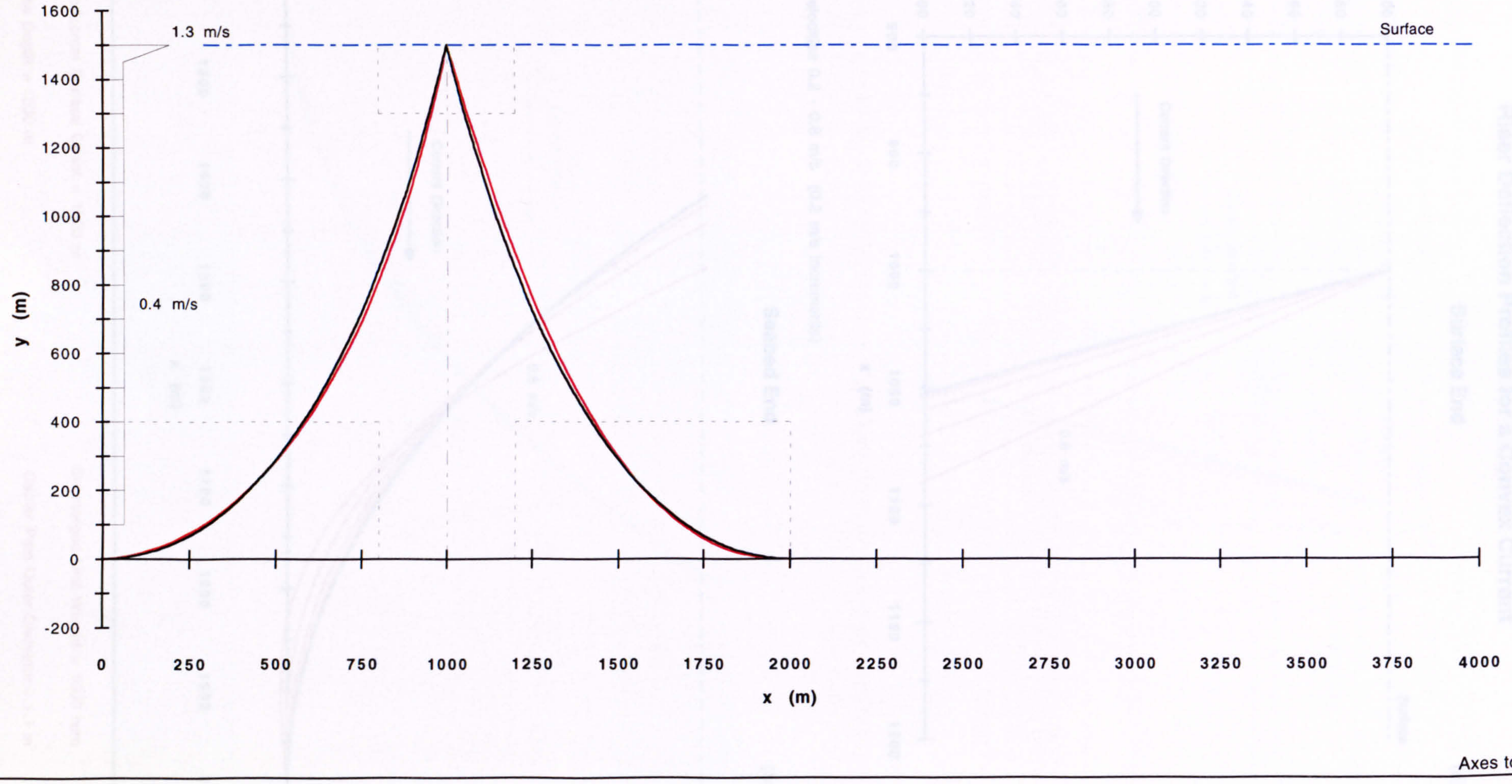

Horizontal Surface Offset = 1000 m

Submerged Unit Weight = 1000 N/m

Sea Depth = 1500 m

Carrier Pipe Outer Diameter = 1.1 m

Figure 5.66

Riser Deflection Profiles for a Convex Current

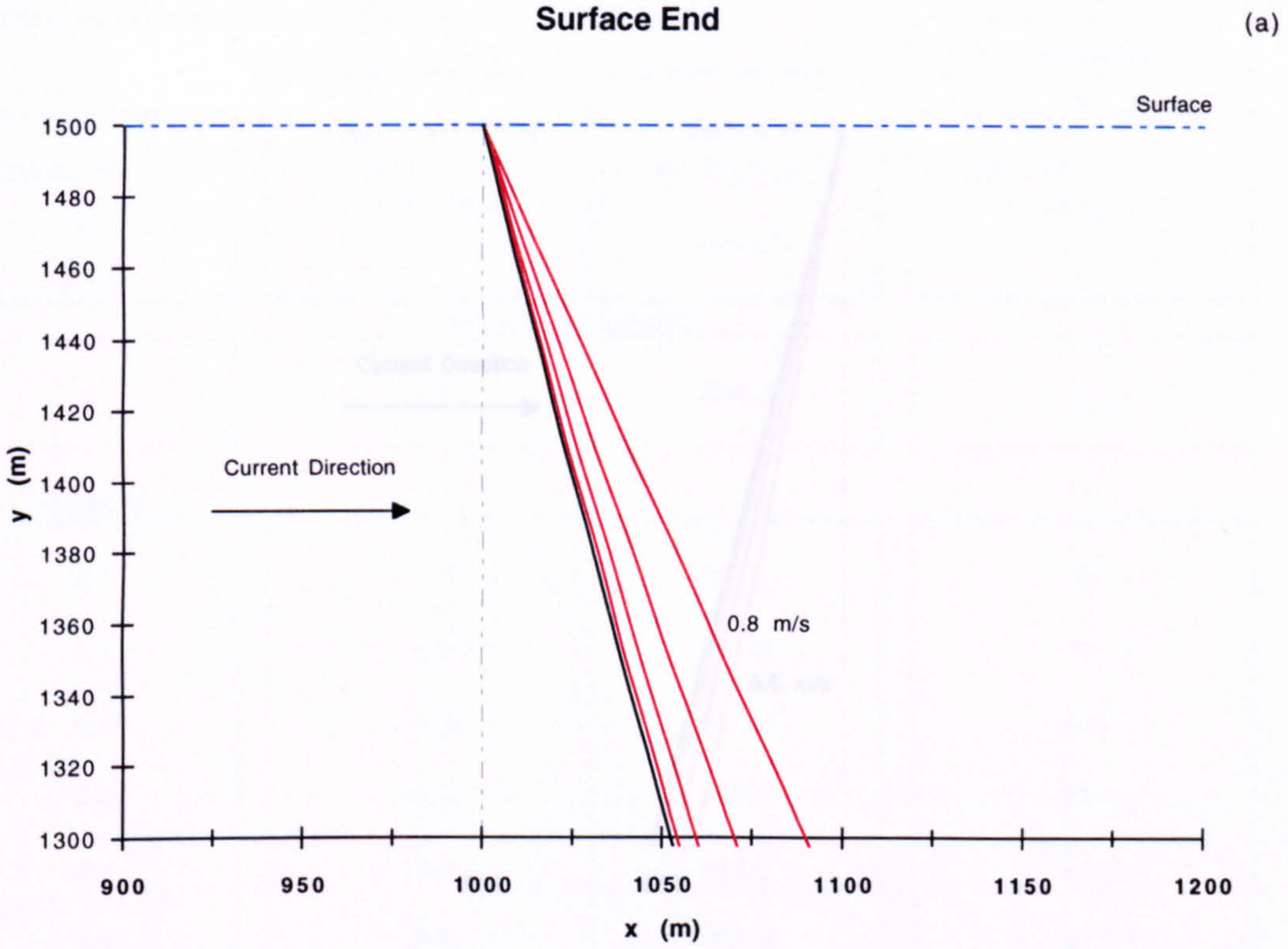

Current velocities 0.2 - 0.8 m/s (0.2 m/s increments)

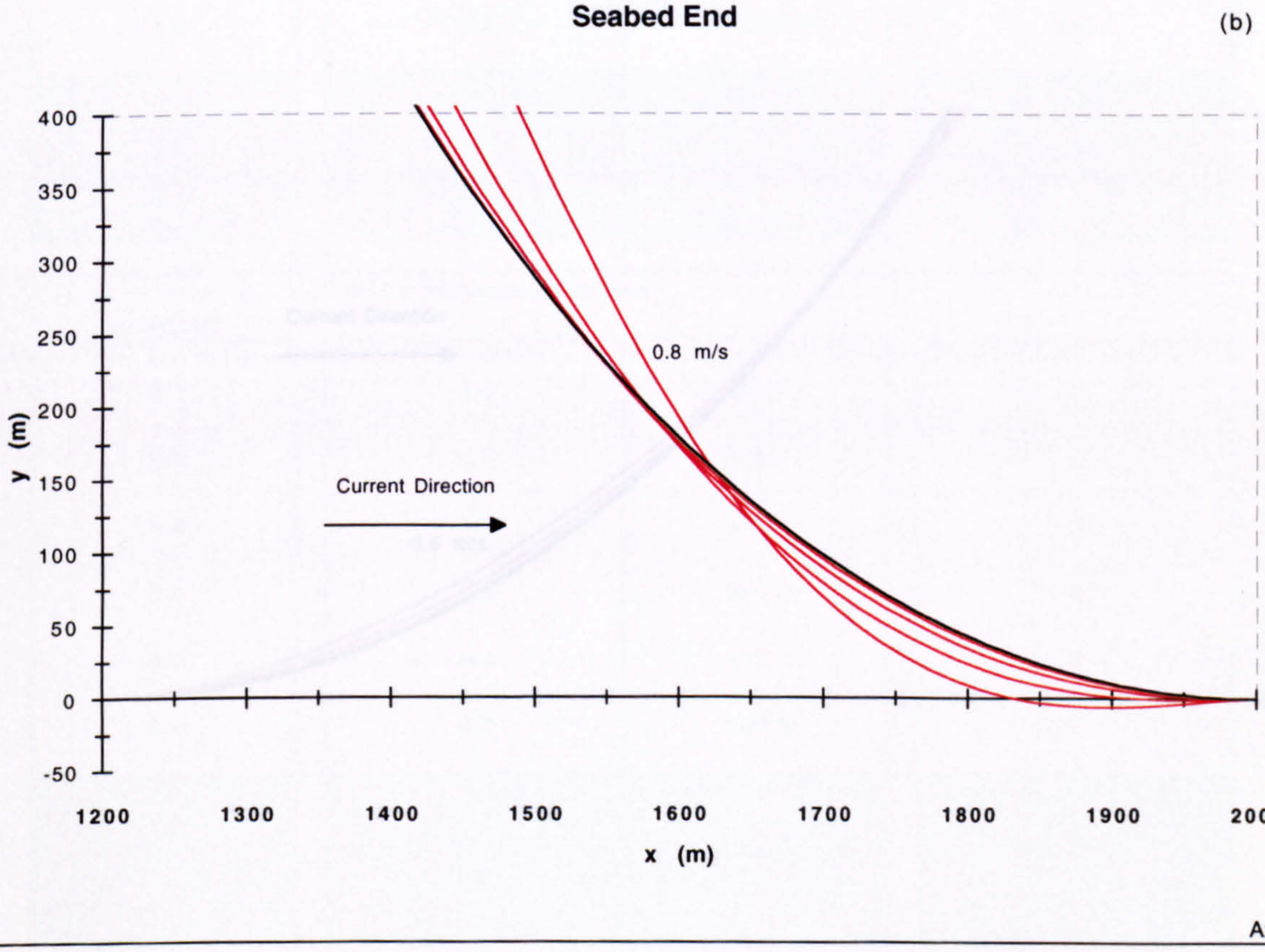

Horizontal Surface Offset = 1000 m

Sea Depth = 1500 m

Submerged Unit Weight = 1000 N/m

Carrier Pipe Outer Diameter = 1.1 m

Figure 5.67

Riser Deflection Profiles for a Concave Current

Surface End

(a)

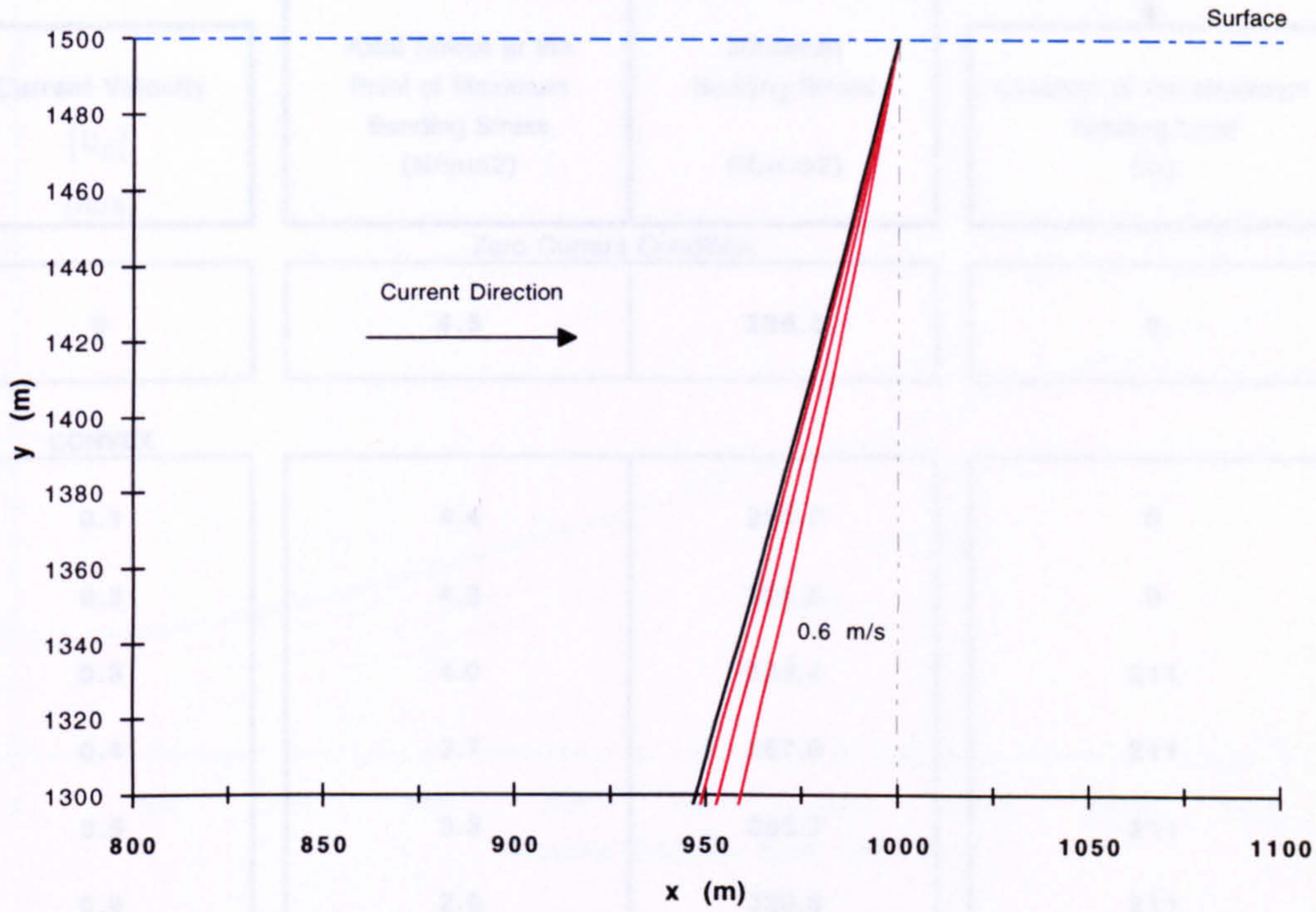

Current velocities 0.2 - 0.6 m/s (0.2 m/s increments)

Seabed End

(b)

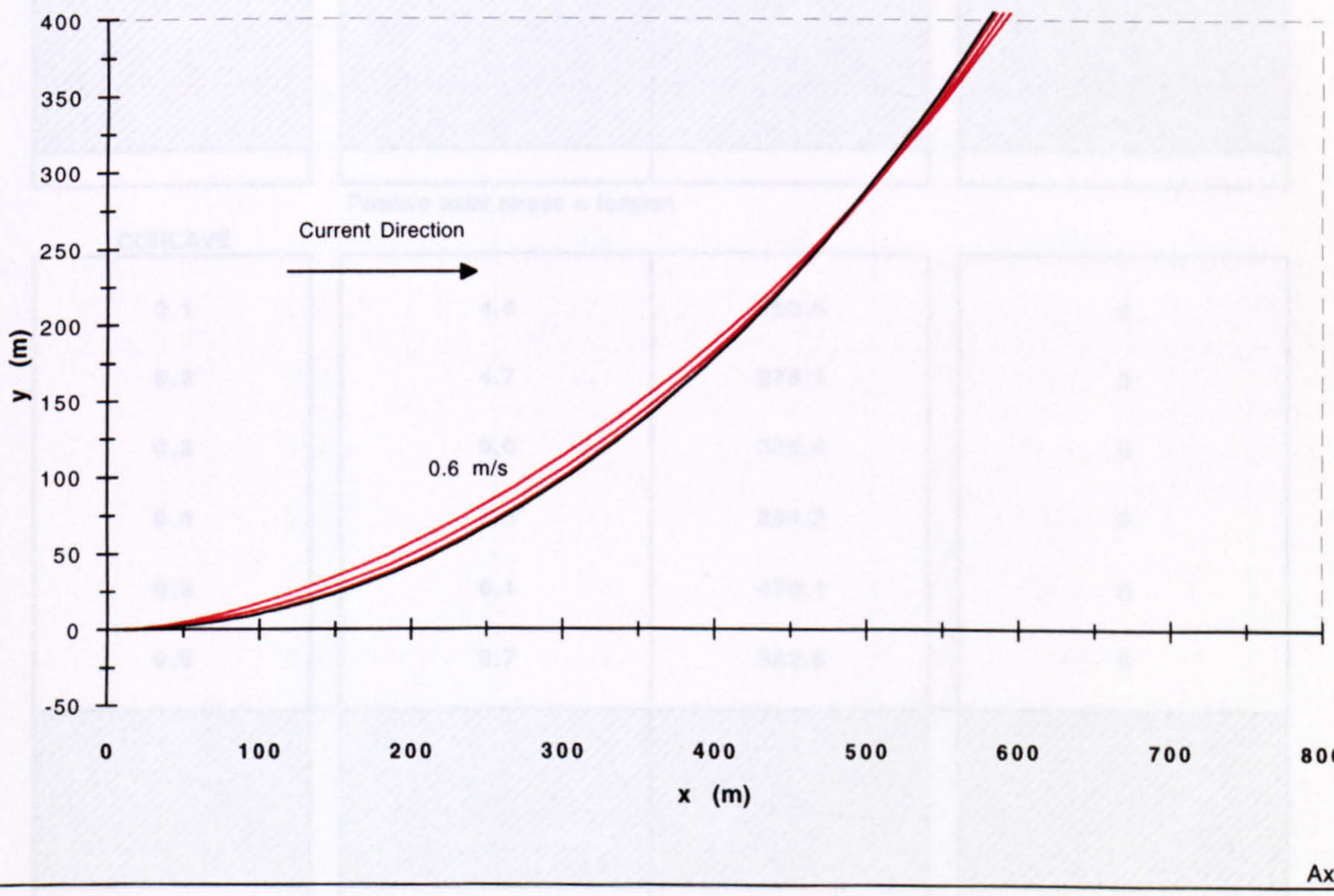

Axes to Scale

Horizontal Surface Offset = 1000 m

Sea Depth = 1500 m

Submerged Unit Weight = 1000 N/m

Carrier Pipe Outer Diameter = 1.1 m

Figure 5.68

Maximum Stress Conditions under Current Loading (a = 1000 m)

Submerged Unit Weight = 1000 N/m

Current Velocity $[U_C]$ (m/s)	Axial Stress at the Point of Maximum Bending Stress (N/mm2)	Maximum Bending Stress (N/mm2)	Location of the Maximum Bending Load (m) (Measured along the riser from the seabed end)
Zero Current Condition			
0	4.5	239.3	0
CONVEX			
0.1	4.4	231.7	0
0.2	4.3	225.6	0
0.3	4.0	233.4	211
0.4	3.7	257.0	211
0.5	3.3	295.7	211
0.6	2.6	338.9	211
0.7	2.2	407.1	211
0.8	1.4	495.3	211
Positive axial stress = tension			
CONCAVE			
0.1	4.6	250.6	0
0.2	4.7	278.1	0
0.3	5.0	325.4	0
0.4	5.5	394.2	0
0.5	6.1	479.1	0
0.6	6.7	582.6	0

Horizontal Surface Offset = 1000 m

Sea Depth = 1500 m

Carrier Pipe Outer Diameter = 1.1 m

Carrier Pipe Wall Thickness = 10 mm

Table 5.69

Axial Stress Distributions for a Convex Current

(a)

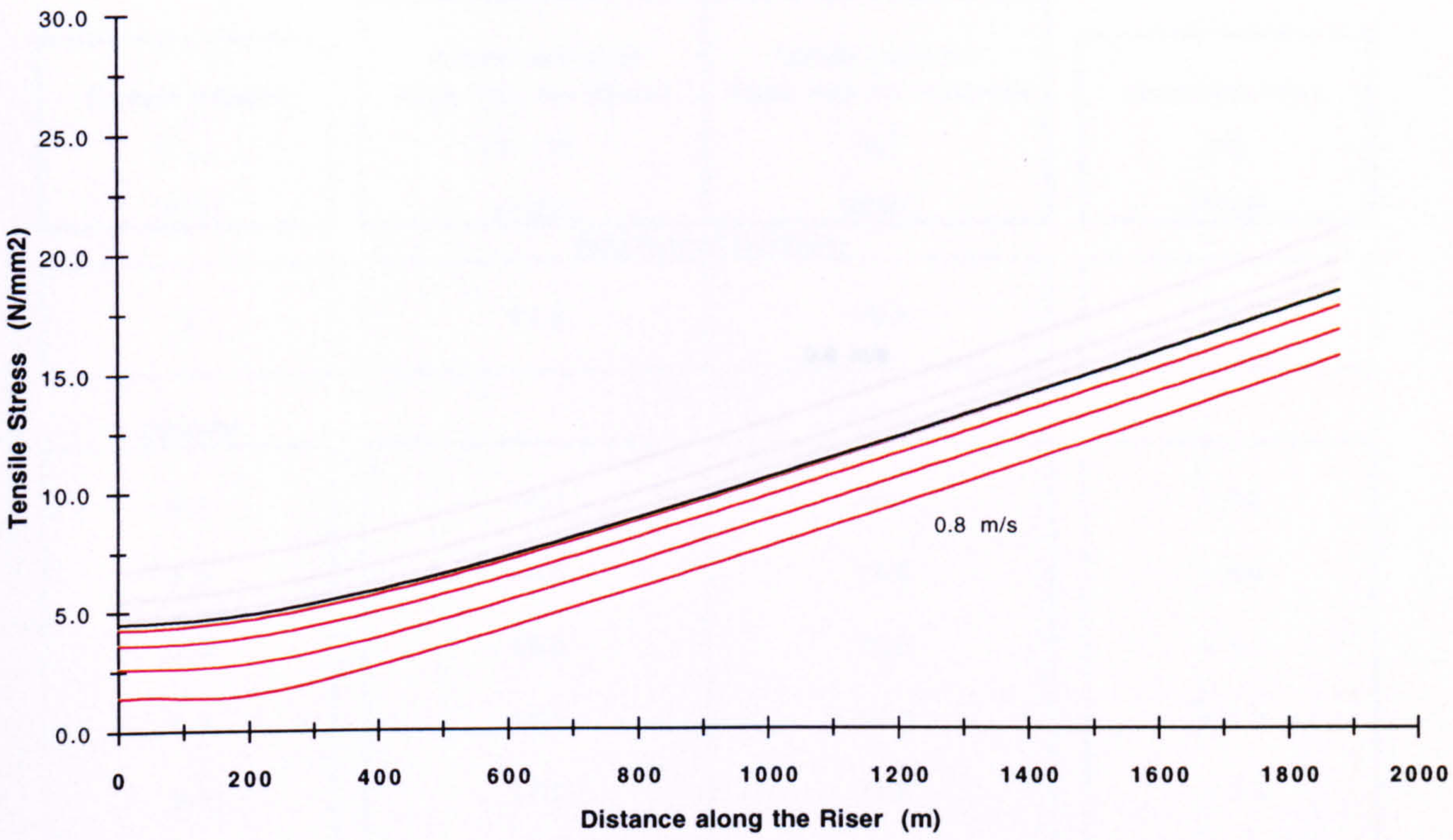

Current velocities 0.2 - 0.8 m/s (0.2 m/s increments)

Surface Forces for a Convex Current

(b)

Current Velocity (m/s)	Horizontal Load (kN)	Vertical Load (kN)	Axial Load (kN)
0	476	1918	1976
0.1	483	1903	1963
0.2	497	1880	1945
0.3	514	1844	1914
0.4	537	1804	1882
0.5	566	1748	1837
0.6	602	1682	1786
0.7	646	1605	1730
0.8	703	1522	1677

Horizontal Surface Offset = 1000 m

Sea Depth = 1500 m

Submerged Unit Weight = 1000 N/m

Carrier Pipe Outer Diameter = 1.1 m

Figure 5.70

Axial Stress Distributions for a Concave Current

(a)

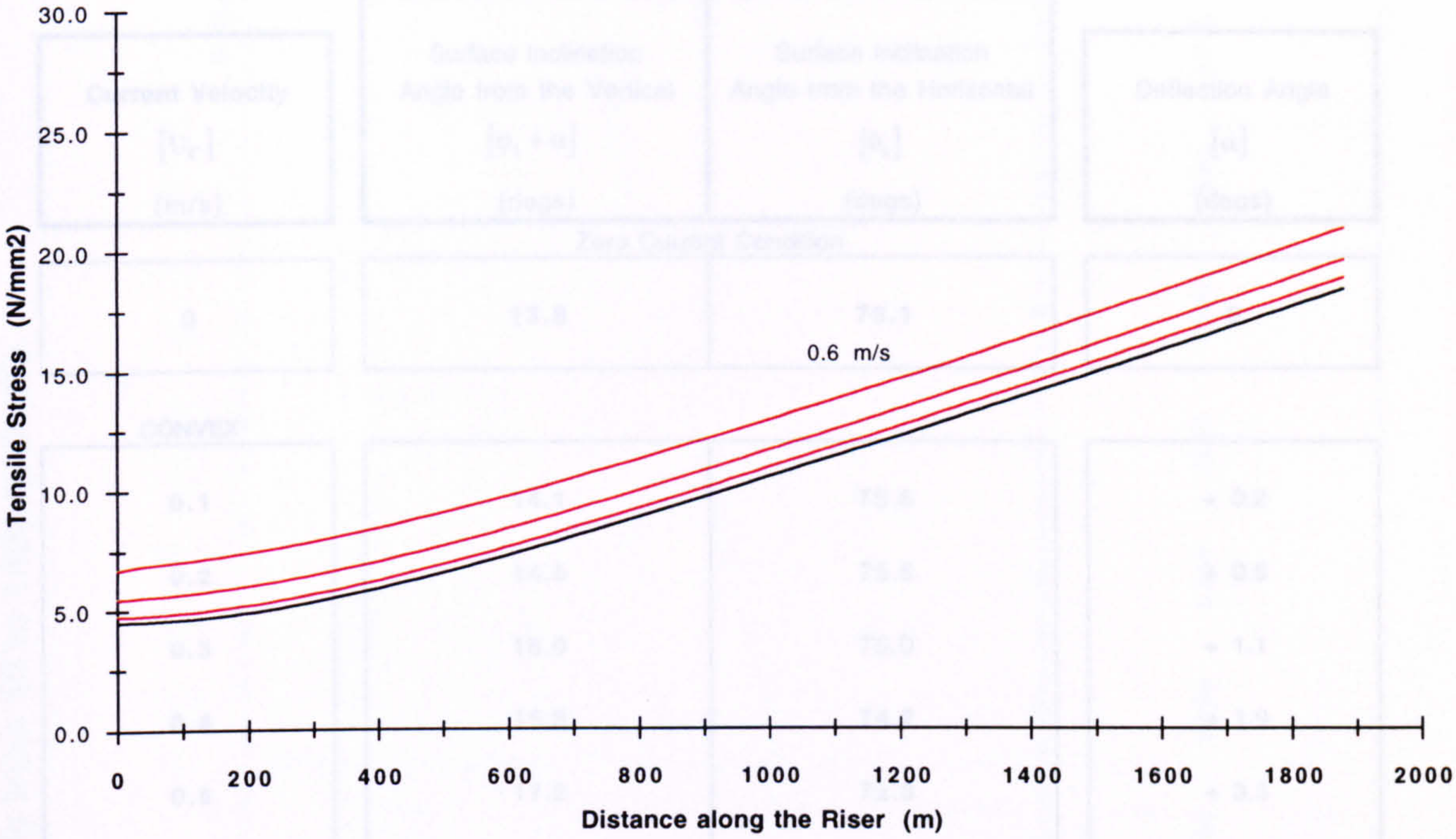

Current velocities 0.2 - 0.6 m/s (0.2 m/s increments)

Surface Forces for a Concave Current

(b)

Current Velocity (m/s)	Horizontal Load (kN)	Vertical Load (kN)	Axial Load (kN)
0	476	1918	1976
0.1	463	1937	1992
0.2	450	1960	2011
0.3	435	1998	2045
0.4	421	2051	2094
0.5	403	2120	2158
0.6	385	2203.6	2237

Horizontal Surface Offset = 1000 m

Sea Depth = 1500 m

Submerged Unit Weight = 1000 N/m

Carrier Pipe Outer Diameter = 1.1 m

Figure 5.71

Surface Deflection Angles under Current Loading (a = 1000 m)

Submerged Unit Weight = 1000 N/m

Current Velocity $[U_C]$ (m/s)	Surface Inclination Angle from the Vertical $[\varphi_s + \alpha]$ (degs)	Surface Inclination Angle from the Horizontal $[\theta_s]$ (degs)	Deflection Angle $[\alpha]$ (degs)
	Zero Current Condition		
0	13.9	76.1	0
CONVEX			
0.1	14.1	75.8	+ 0.2
0.2	14.5	75.5	+ 0.6
0.3	15.0	75.0	+ 1.1
0.4	15.8	74.2	+ 1.9
0.5	17.2	72.8	+ 3.3
0.6	19.3	70.7	+ 5.4
0.7	22.0	68.0	+ 8.1
0.8	25.1	64.9	+ 11.2
CONCAVE			
0.1	13.7	76.3	- 0.2
0.2	13.3	76.7	- 0.6
0.3	12.8	77.2	- 1.1
0.4	12.0	78.0	- 1.9
0.5	11.1	78.9	- 2.8
0.6	10.3	79.7	- 3.6

Horizontal Surface Offset = 1000 m

Sea Depth = 1500 m

Carrier Pipe Outer Diameter = 1.1 m

Carrier Pipe Wall Thickness = 10 mm

Table 5.72

Current Velocity : 1.3 m/s at the surface, 0.6 m/s from 50 to 1400 m depth.

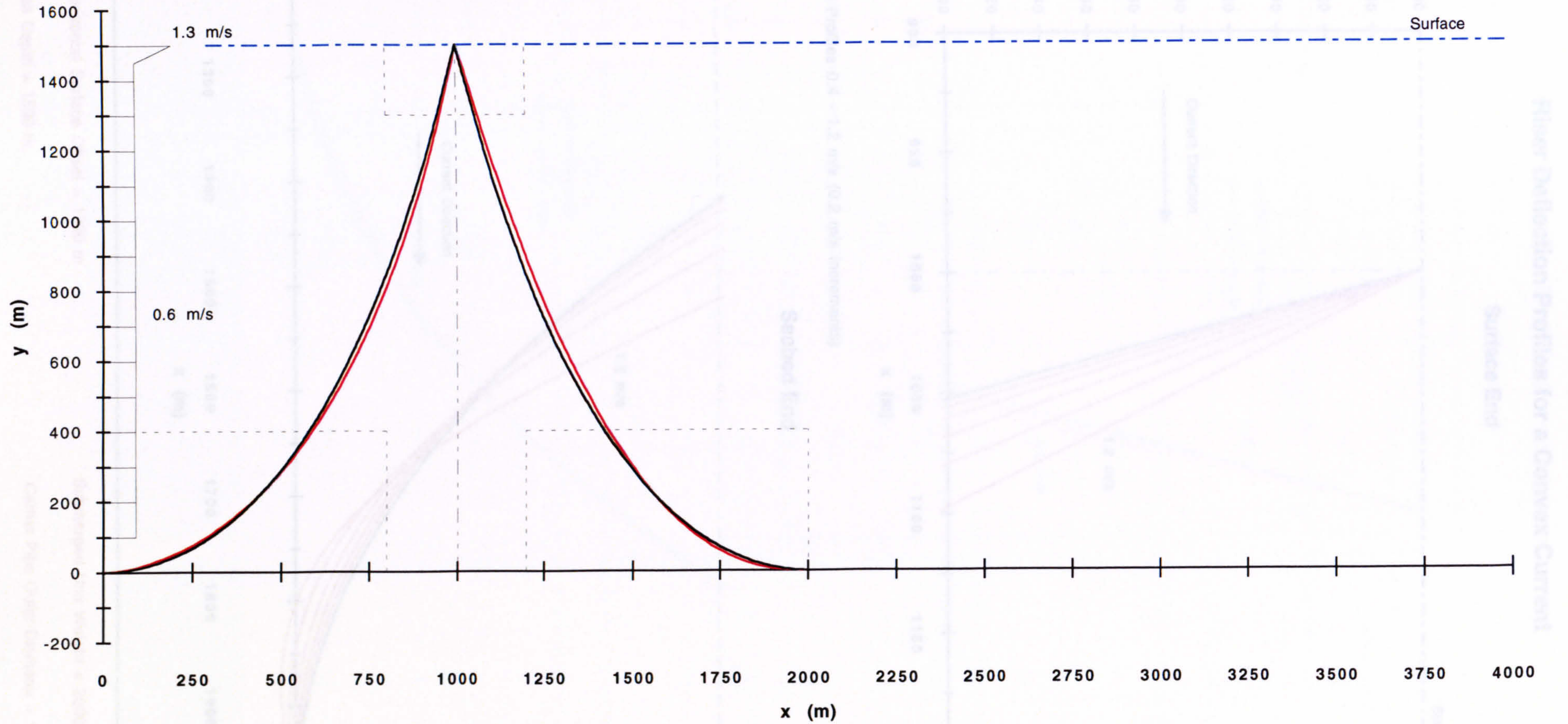

Horizontal Surface Offset = 1000 m

Sea Depth = 1500 m

Submerged Unit Weight = 2000 N/m

Carrier Pipe Outer Diameter = 1.1 m

Figure 5.73

Riser Deflection Profiles for a Convex Current

Surface End

(a)

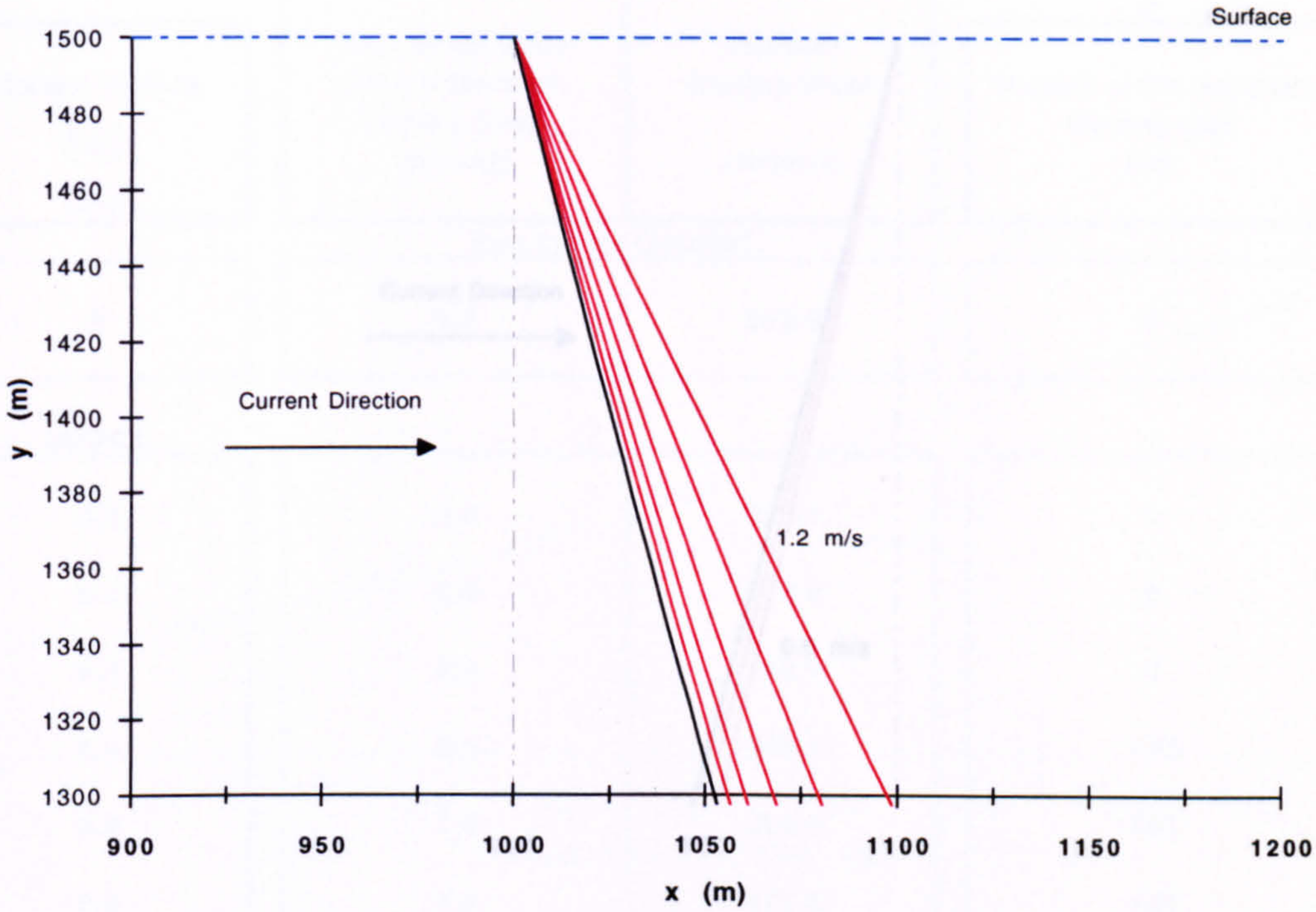

Deflection Profiles 0.4 - 1.2 m/s (0.2 m/s increments)

Seabed End

(b)

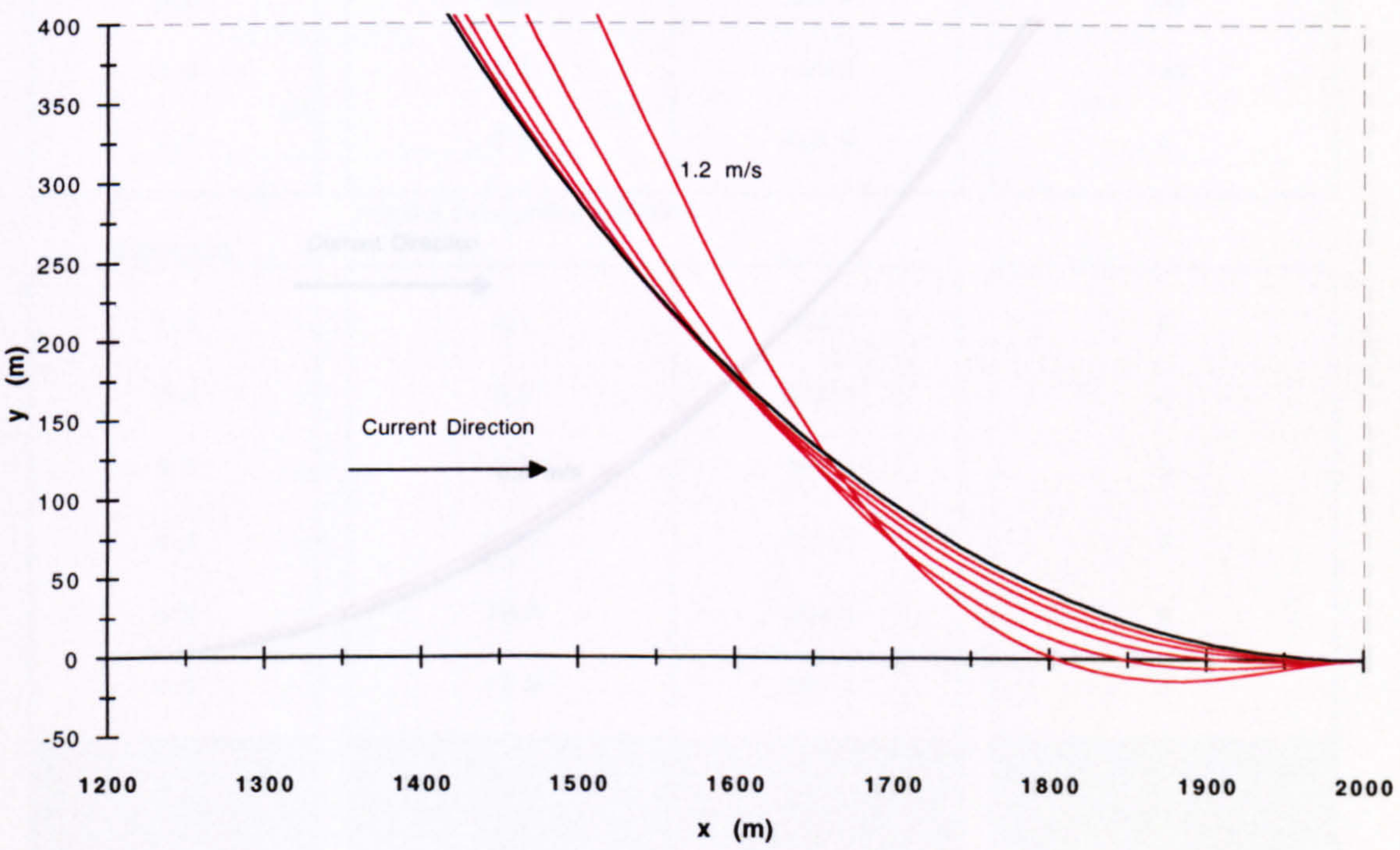

Axes to Scale

Horizontal Surface Offset = 1000 m

Sea Depth = 1500 m

Submerged Unit Weight = 2000 N/m

Carrier Pipe Outer Diameter = 1.1 m

Figure 5.74

Riser Deflection Profiles for a Concave Current

Surface End

(a)

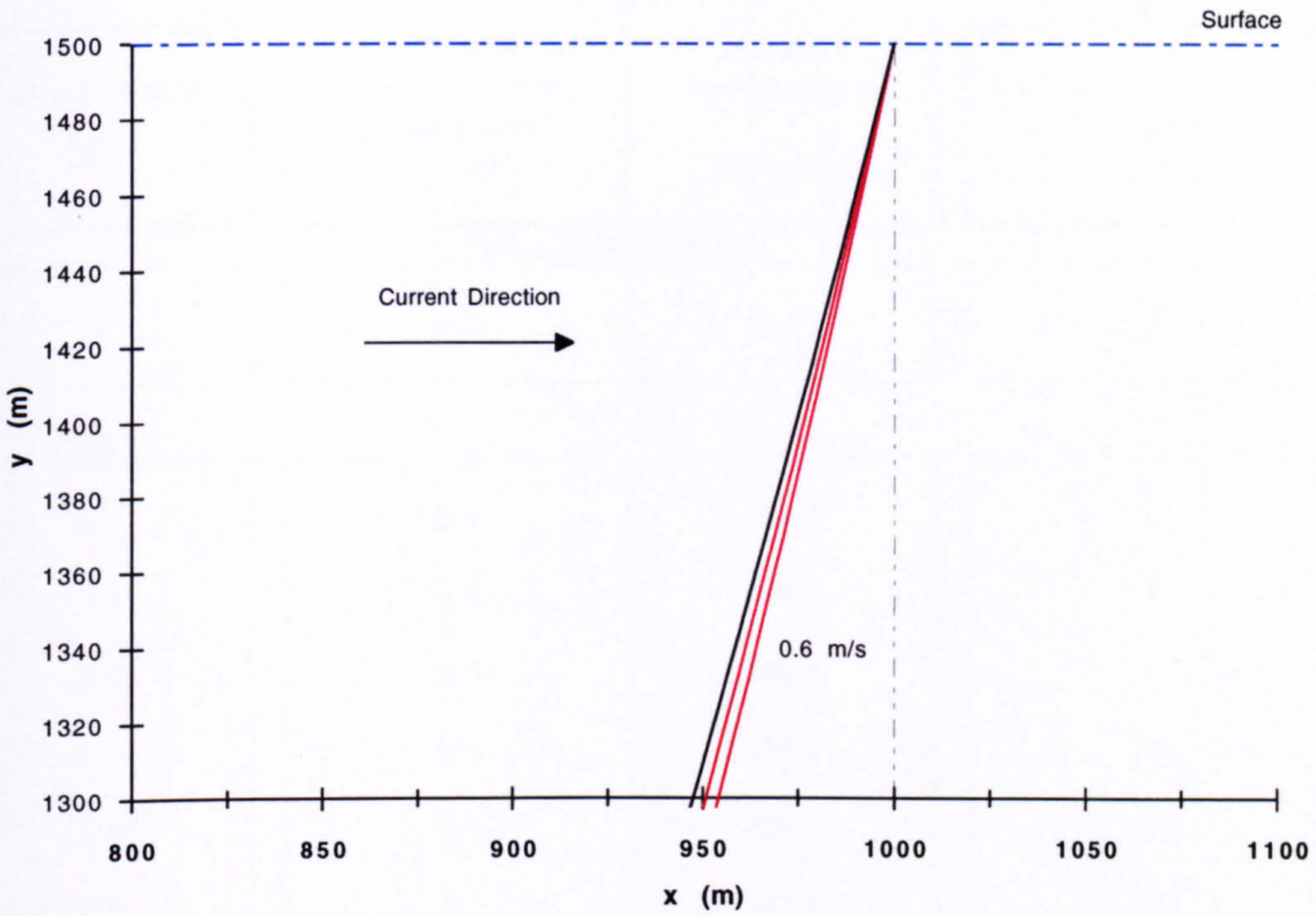

Current velocities 0.4 - 0.6 m/s (0.2 m/s increments)

Seabed End

(b)

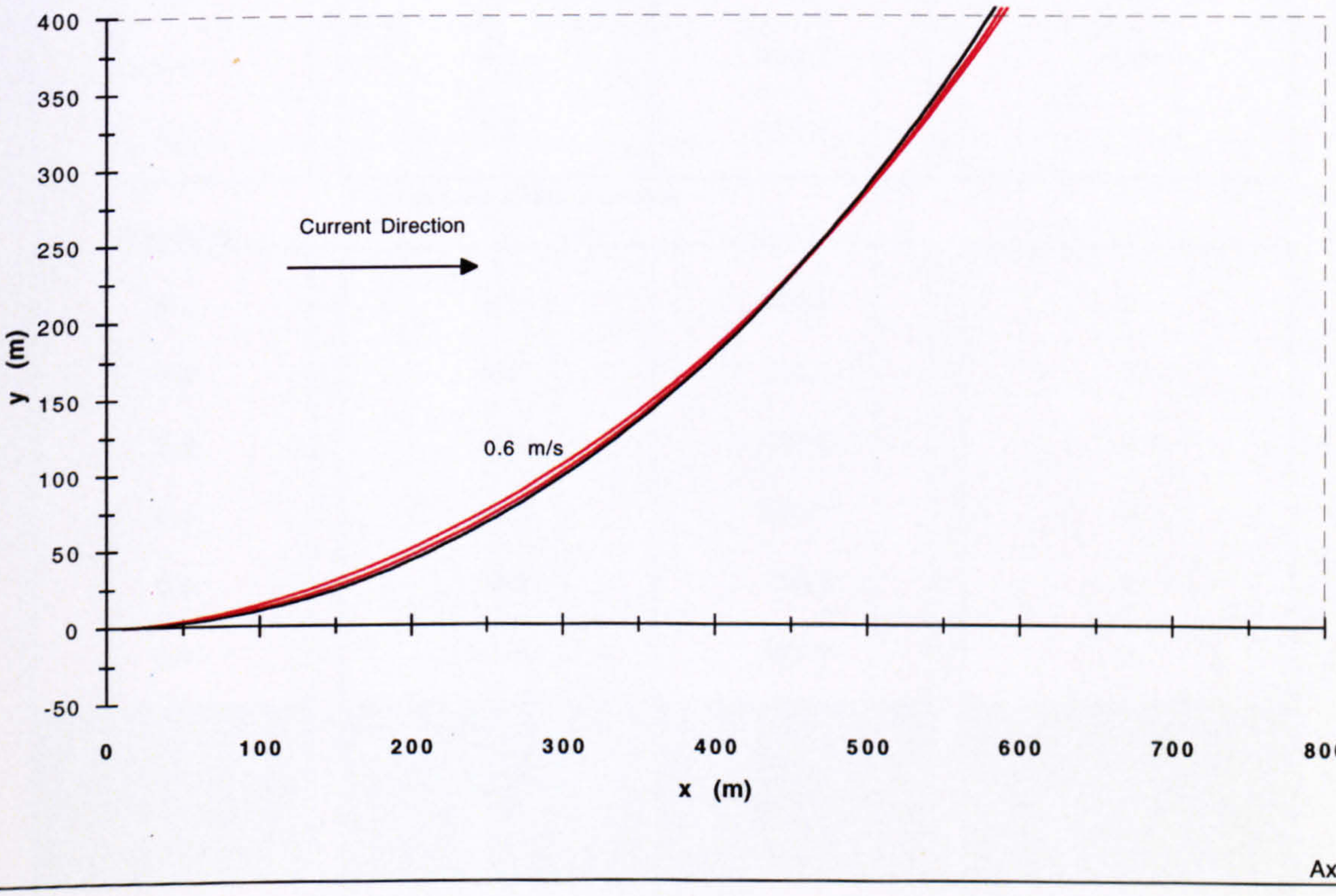

Axes to Scale

Horizontal Surface Offset = 1000 m

Sea Depth = 1500 m

Submerged Unit Weight = 2000 N/m

Carrier Pipe Outer Diameter = 1.1 m

Figure 5.75

Maximum Stress Conditions under Current Loading (a = 1000 m)

Submerged Unit Weight = 2000 N/m

Current Velocity $[U_C]$ (m/s)	Axial Stress at the Point of Maximum Bending Stress (N/mm2)	Maximum Bending Stress (N/mm2)	Location of the Maximum Bending Load (m)
			Measured along the riser from the seabed end
	Zero Current Condition		
0	9.0	239.3	0
CONVEX			
0.1	8.8	238.1	0
0.2	8.6	237.4	0
0.3	8.3	229.7	0
0.4	8.0	225.7	192
0.5	7.6	250.4	192
0.6	7.1	271.8	192
0.7	6.4	302.4	192
0.8	5.8	338.9	192
0.9	5.0	386.4	192
1.0	4.1	450.3	192
1.2	2.5	635.2	0
	Positive axial stress = tension		
CONCAVE			
0.1	9.1	246.3	0
0.2	9.2	264.8	0
0.3	9.6	297.7	0
0.4	10.0	343.1	0
0.5	10.5	408.1	0
0.6	11.2	481.4	0

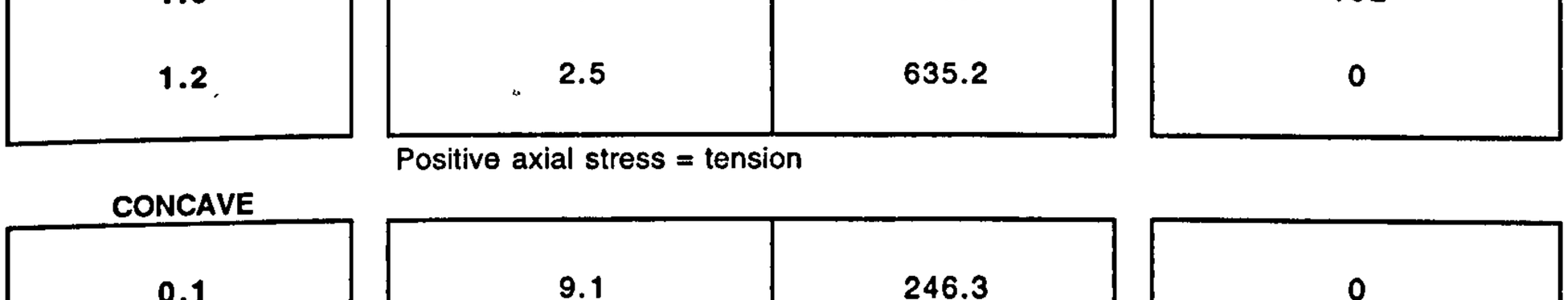

Horizontal Surface Offset = 1000 m

Sea Depth = 1500 m

Carrier Pipe Outer Diameter = 1.1 m

Carrier Pipe Wall Thickness = 10 mm

Table 5.76

Axial Stress Distributions for a Convex Current

(a)

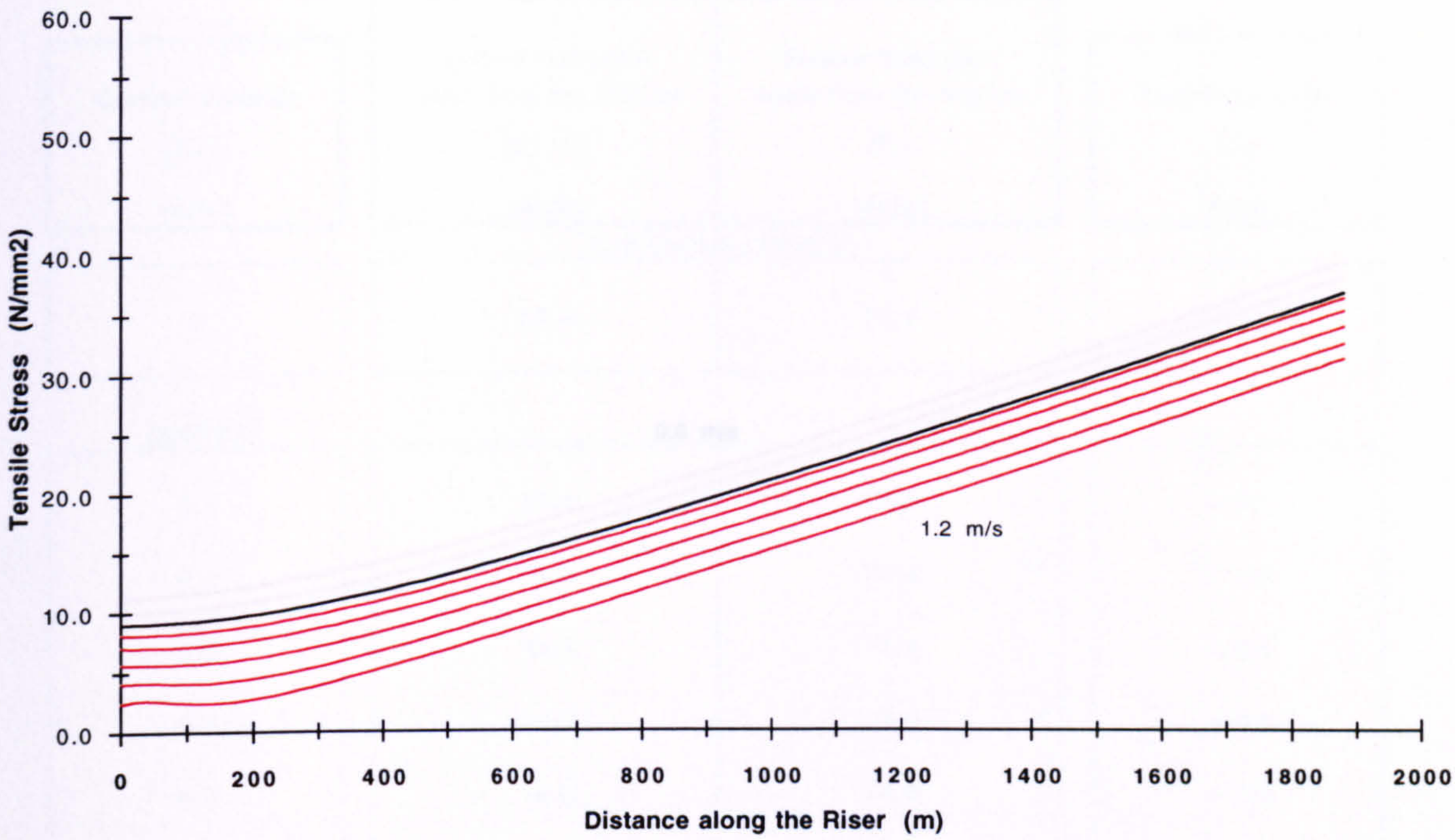

Current velocities 0.4 - 1.2 m/s (0.2 m/s increments)

Surface Forces for a Convex Current

(b)

Current Velocity (m/s)	Horizontal Load (kN)	Vertical Load (kN)	Axial Load (kN)
0	951	3835	3951
0.4	984	3709	3837
0.5	1012	3660	3797
0.6	1047	3585	3735
0.7	1090	3500	3666
0.8	1143	3421	3607
0.9	1210	3325	3538
1.0	1288	3225	3473
1.2	1479	3000	3345

Horizontal Surface Offset = 1000 m

Sea Depth = 1500 m

Submerged Unit Weight = 2000 N/m

Carrier Pipe Outer Diameter = 1.1 m

Figure 5.77

Axial Stress Distributions for a Concave Current

(a)

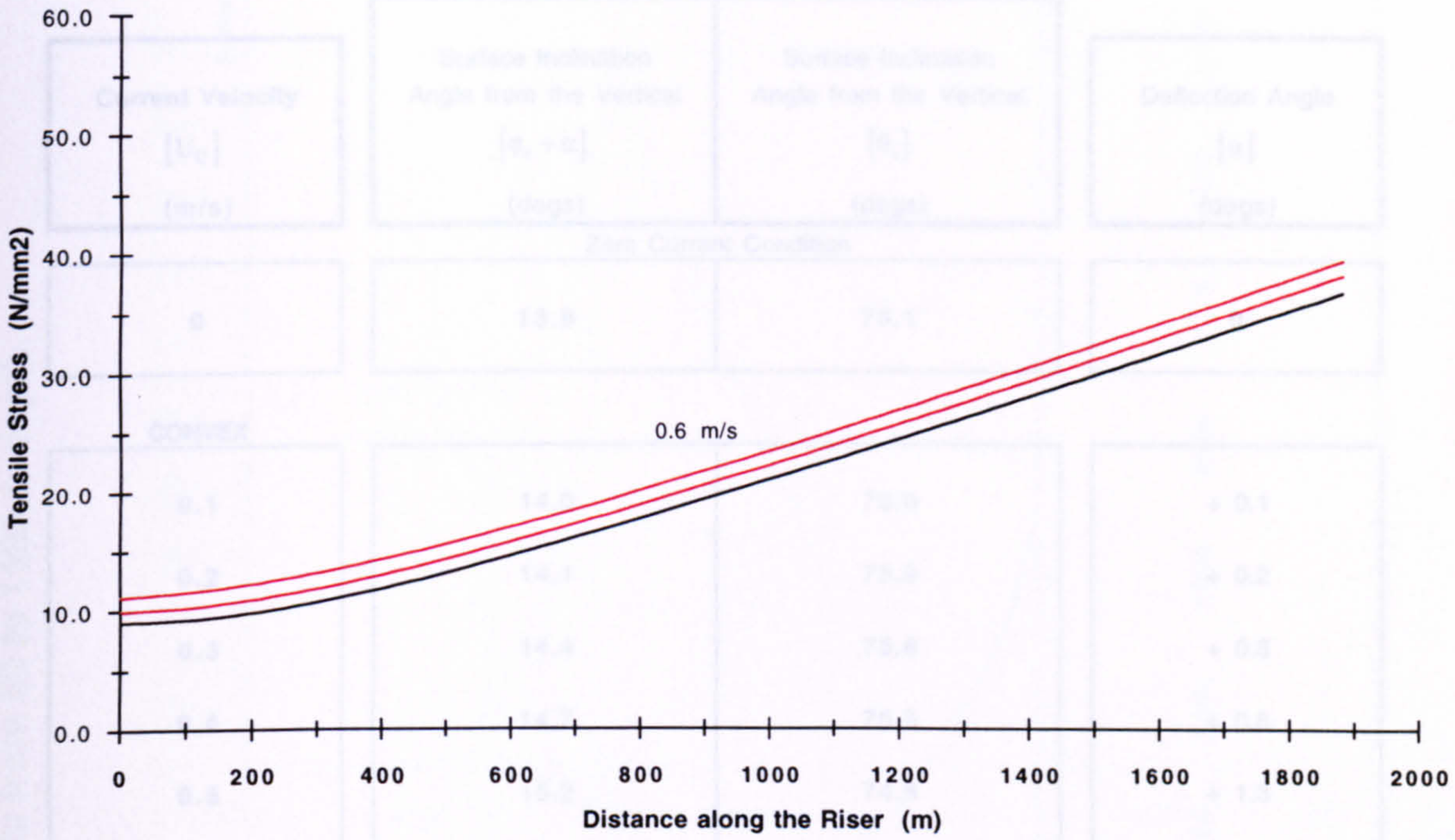

Current velocities 0.4 - 0.6 m/s (0.2 m/s increments)

Surface Forces for a Concave Current

(b)

Current Velocity (m/s)	Horizontal Load (kN)	Vertical Load (kN)	Axial Load (kN)
0	951	3835	3951
0.1	935	3849	3961
0.2	922	3862	3971
0.3	907	3900	4004
0.4	890	3955	4054
0.5	869	4020	4113
0.6	845	4108	4194

Horizontal Surface Offset = 1000 m

Sea Depth = 1500 m

Submerged Unit Weight = 2000 N/m

Carrier Pipe Outer Diameter = 1.1 m

Figure 5.78

Surface Deflection Angles under Current Loading (a = 1000 m)

Submerged Unit Weight = 2000 N/m

Current Velocity $[U_C]$ (m/s)	Surface Inclination Angle from the Vertical $[\varphi_s + \alpha]$ (degs)	Surface Inclination Angle from the Vertical $[\theta_s]$ (degs)	Deflection Angle $[\alpha]$ (degs)
	Zero Current Condition		
0	13.9	76.1	0
CONVEX			
0.1	14.0	76.0	+ 0.1
0.2	14.1	75.9	+ 0.2
0.3	14.4	75.6	+ 0.5
0.4	14.7	75.3	+ 0.8
0.5	15.2	74.8	+ 1.3
0.6	16.0	74.0	+ 2.1
0.7	17.1	72.9	+ 3.2
0.8	18.4	71.6	+ 4.5
0.9	20.0	70.0	+ 6.1
1.0	21.8	68.2	+ 7.9
1.2	26.0	64.0	+ 12.1
CONCAVE			
0.1	13.9	76.1	0
0.2	13.7	76.3	- 0.2
0.3	13.3	76.7	- 0.6
0.4	13.0	77.0	- 0.9
0.5	12.5	77.5	- 1.4
0.6	12.1	77.9	- 1.8

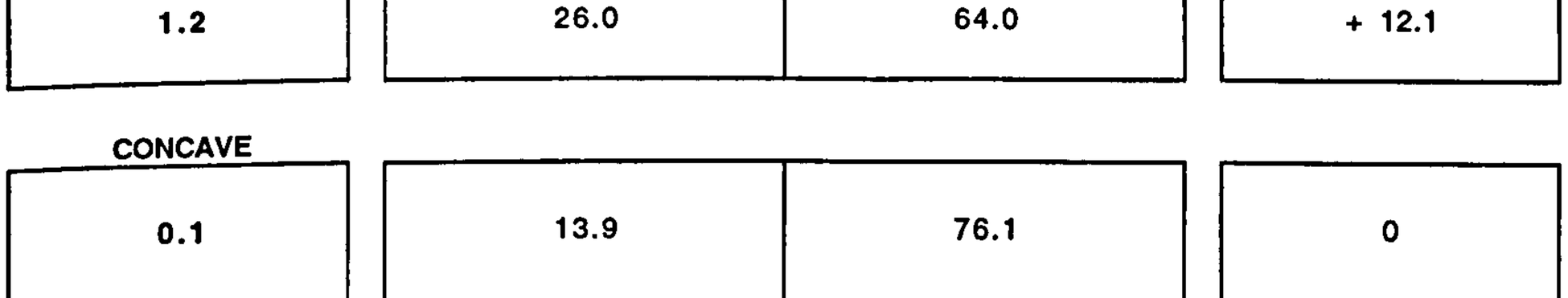

Horizontal Surface Offset = 1000 m

Sea Depth = 1500 m

Carrier Pipe Outer Diameter = 1.1 m

Carrier Pipe Wall Thickness = 10 mm

Table 5.79

Current Velocity : 1.3 m/s at the surface, 0.3 m/s from 50 to 1400 m depth.

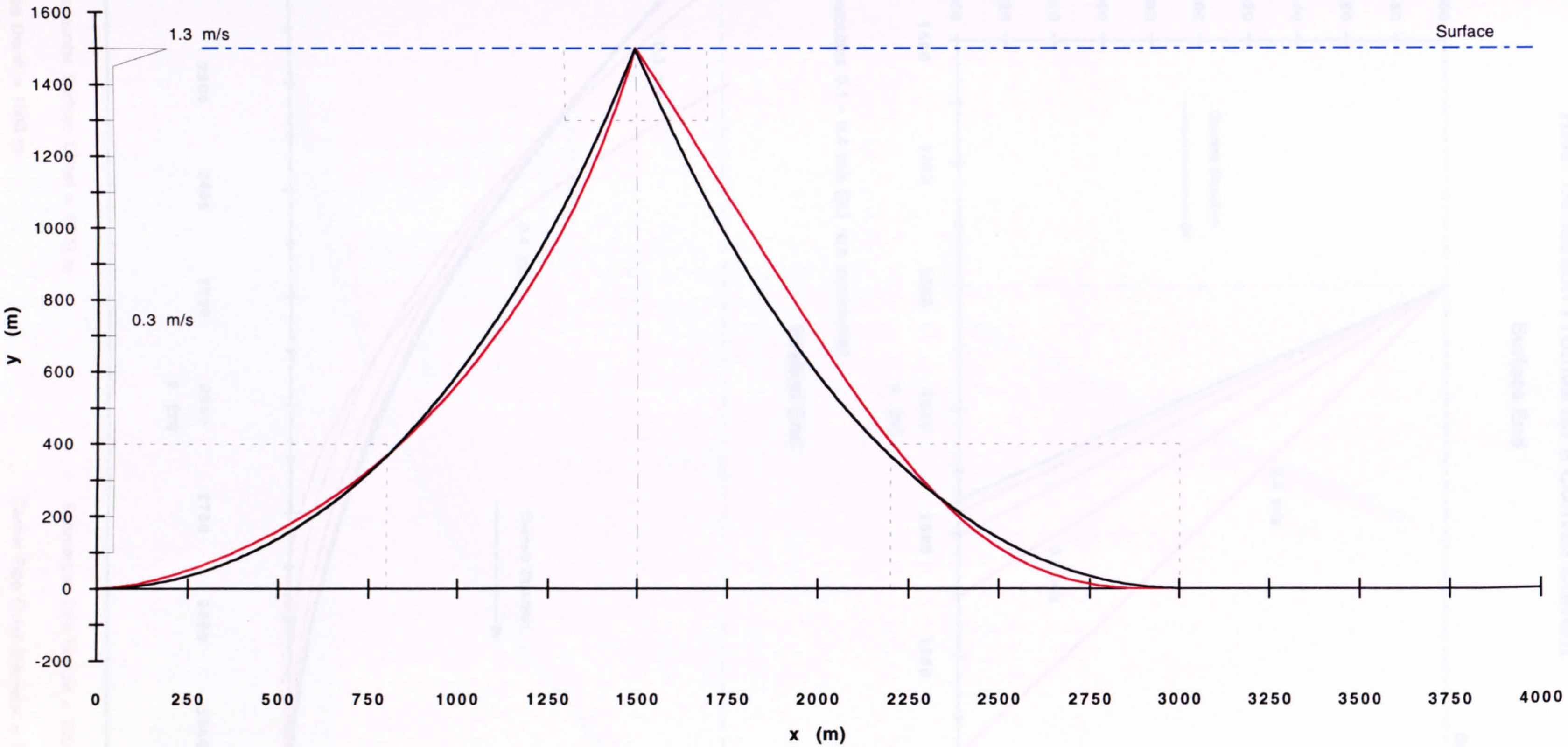

Horizontal Surface Offset = 1500 m

Sea Depth = 1500 m

Submerged Unit Weight = 100 N/m

Carrier Pipe Outer Diameter = 1.1 m

Figure 5.80

Riser Deflection Profiles for a Convex Current

Surface End

(a)

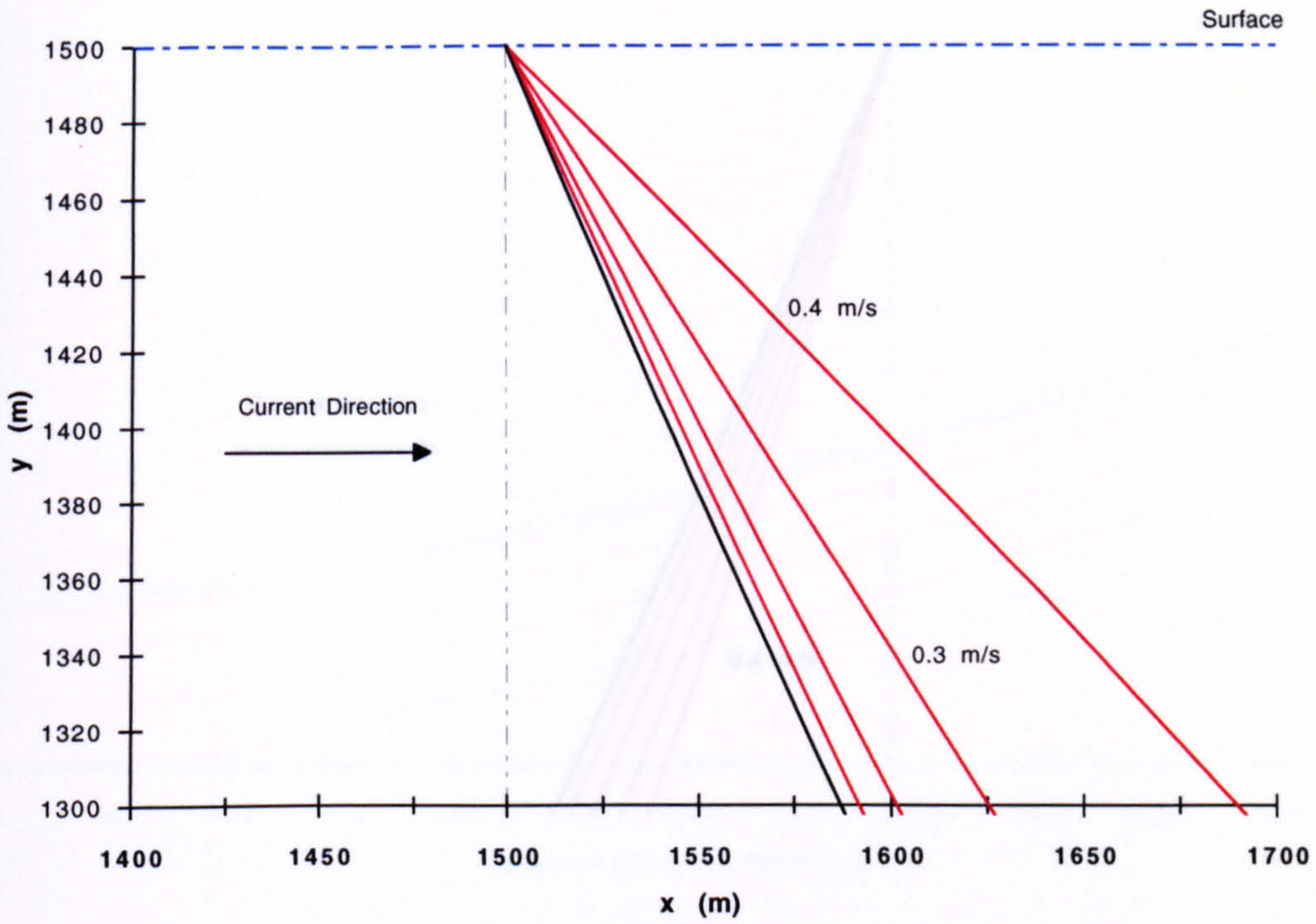

Current velocities 0.1 - 0.4 m/s (0.1 m/s increments)

Seabed End

(b)

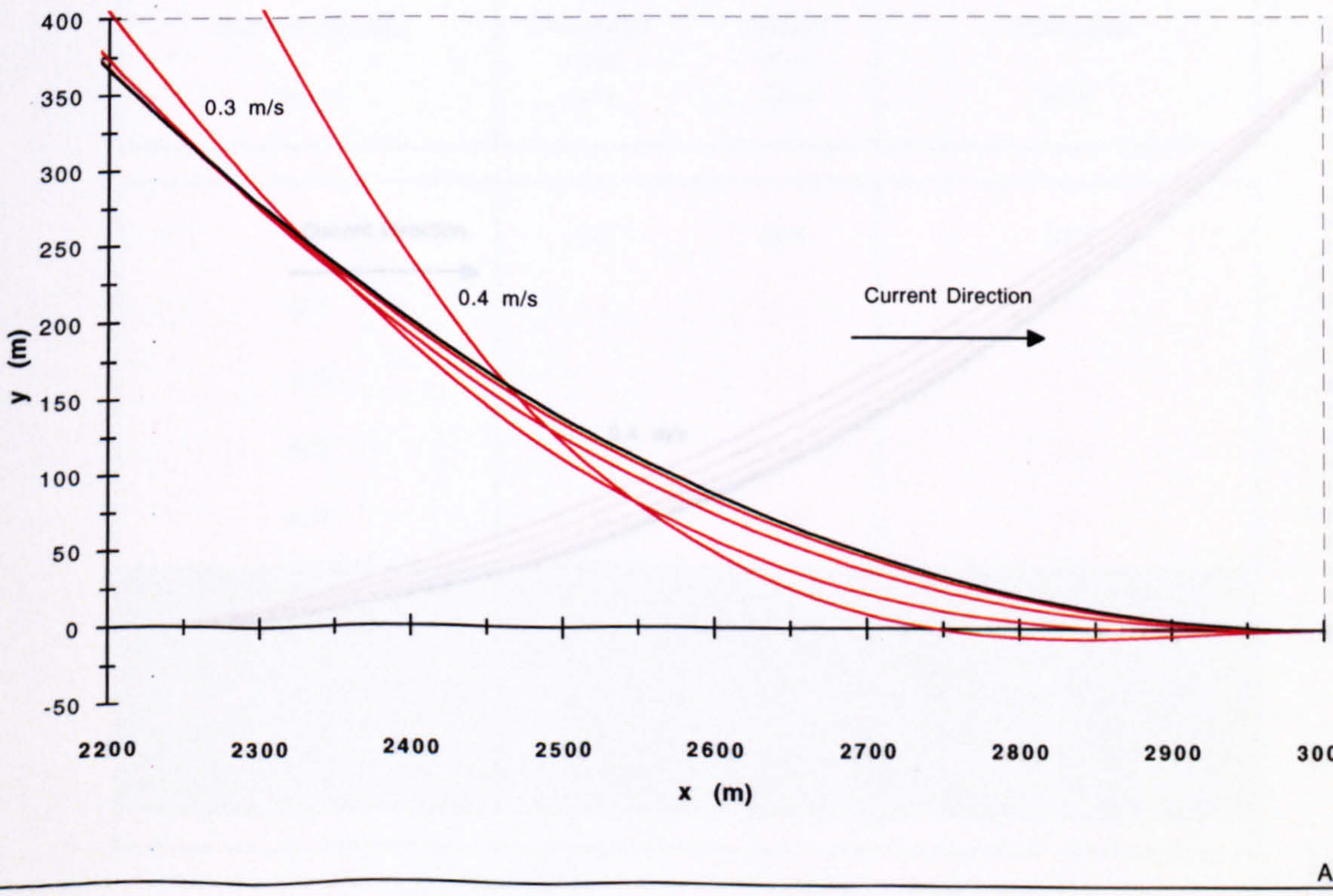

Axes to Scale

Horizontal Surface Offset = 1500 m

Sea Depth = 1500 m

Submerged Unit Weight = 100 N/m

Carrier Pipe Outer Diameter = 1.1 m

Figure 5.81

Riser Deflection Profiles for a Concave Current

Surface End

(a)

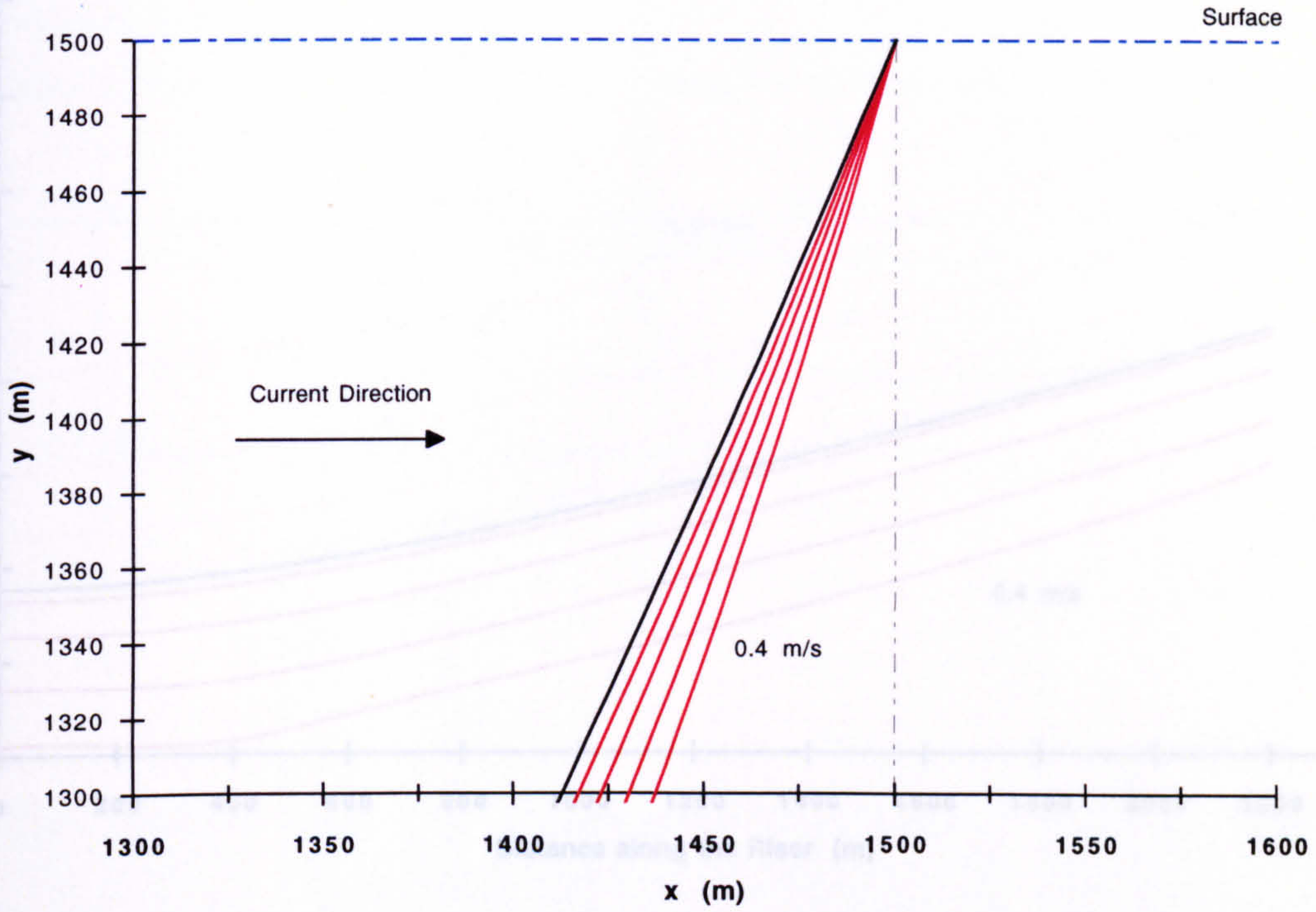

Current velocities 0.1 - 0.4 m/s (0.1 m/s increments)

Seabed End

(b)

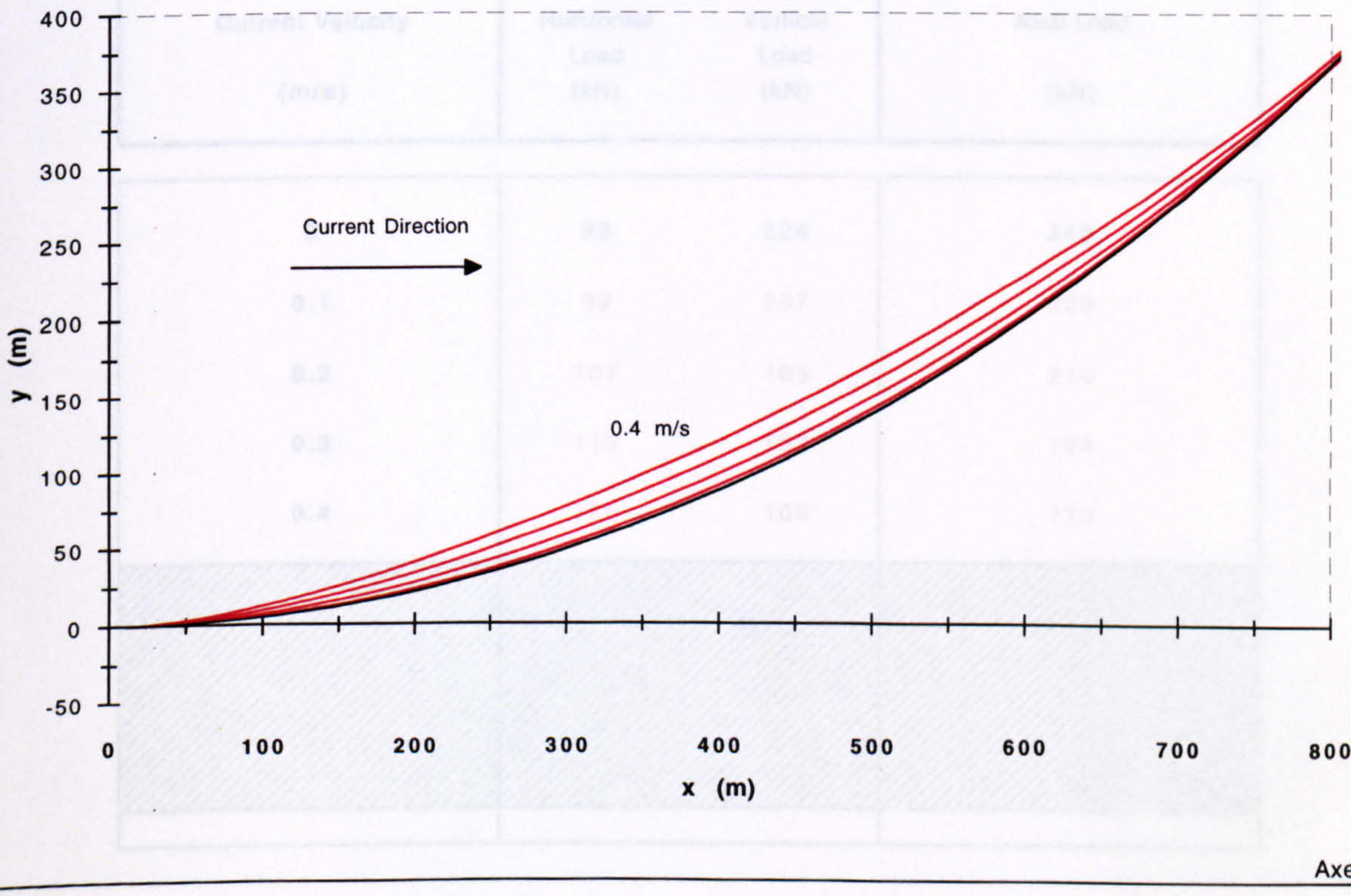

Axes to Scale

Horizontal Surface Offset = 1500 m

Sea Depth = 1500 m

Submerged Unit Weight = 100 N/m

Carrier Pipe Outer Diameter = 1.1 m

Figure 5.82

Axial Stress Distributions for a Convex Current

(a)

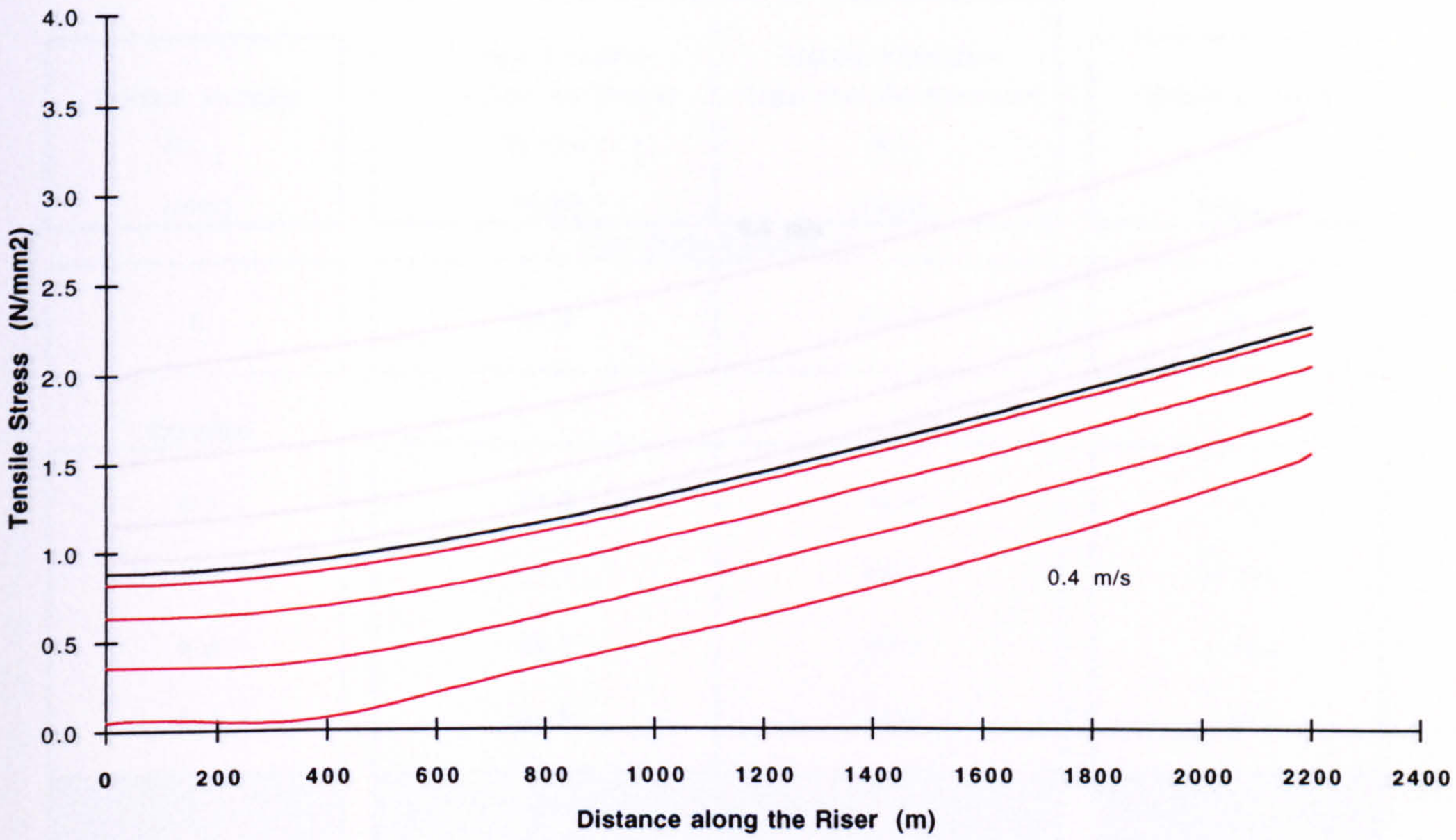

Current velocities 0.1 - 0.4 m/s (0.1 m/s increments)

Surface Forces for a Convex Current

(b)

Current Velocity (m/s)	Horizontal Load (kN)	Vertical Load (kN)	Axial Load (kN)
0	93	224	243
0.1	99	207	229
0.2	107	185	214
0.3	119	153	194
0.4	135	108	173

Horizontal Surface Offset = 1500 m

Sea Depth = 1500 m

Submerged Unit Weight = 100 N/m

Carrier Pipe Outer Diameter = 1.1 m

Figure 5.84

Axial Stress Distributions for a Concave Current

(a)

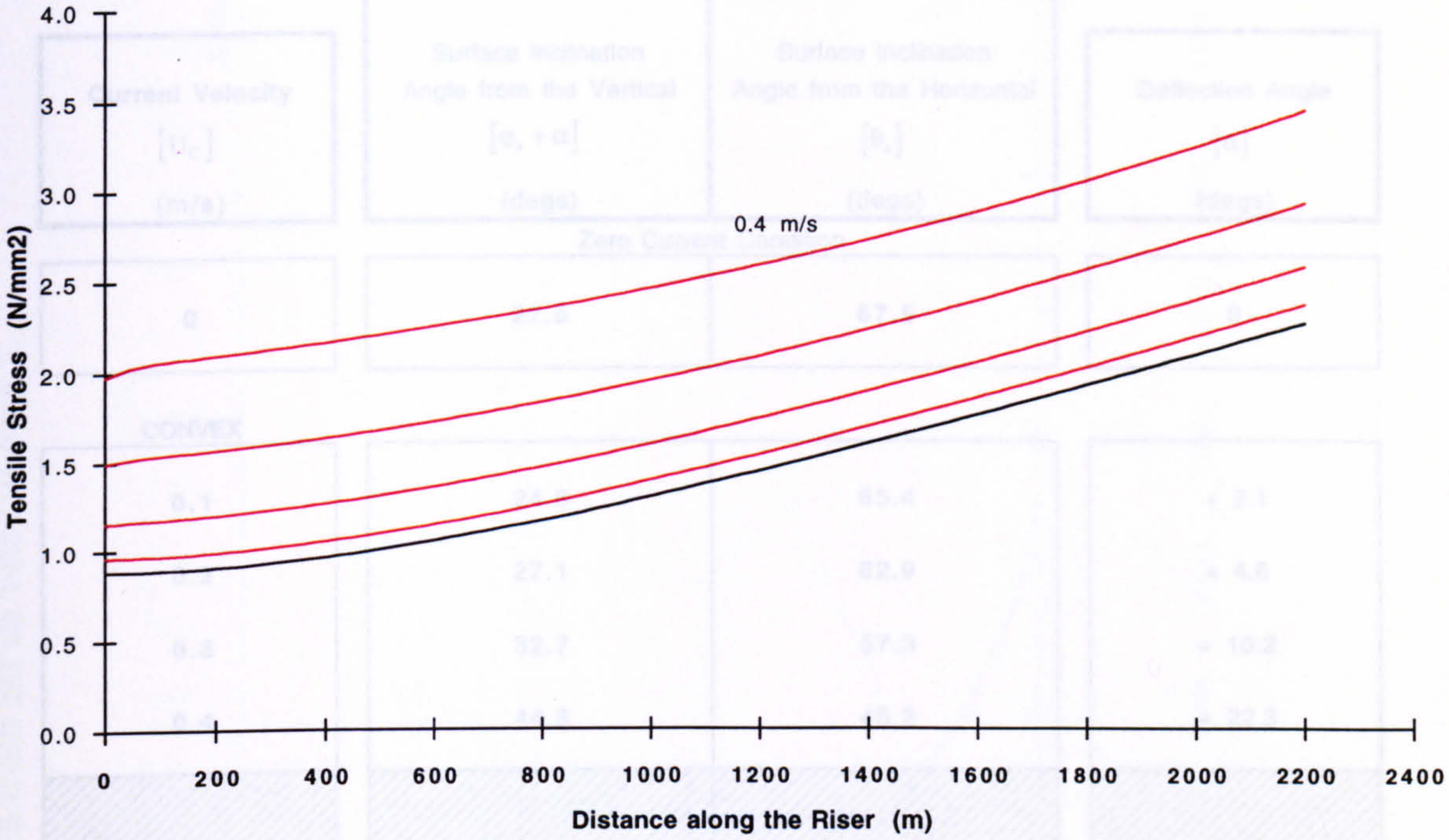

Current velocities 0.1 - 0.4 m/s (0.1 m/s increments)

Surface Forces for a Concave Current

(b)

Current Velocity (m/s)	Horizontal Load (kN)	Vertical Load (kN)	Axial Load (kN)
0	93	224	243
0.1	80	240	253
0.2	76	265	276
0.3	75	303	312
0.4	79	360	369

Horizontal Surface Offset = 1500 m

Sea Depth = 1500 m

Submerged Unit Weight = 100 N/m

Carrier Pipe Outer Diameter = 1.1 m

Figure 5.85

Surface Deflection Angles under Current Loading (a = 1500 m)

Submerged Unit Weight = 100 N/m

Current Velocity $[U_C]$ (m/s)	Surface Inclination Angle from the Vertical $[\varphi_s + \alpha]$ (degs)	Surface Inclination Angle from the Horizontal $[\theta_s]$ (degs)	Deflection Angle $[\alpha]$ (degs)
Zero Current Condition			
0	22.5	67.5	0
CONVEX			
0.1	24.6	65.4	+ 2.1
0.2	27.1	62.9	+ 4.6
0.3	32.7	57.3	+ 10.2
0.4	44.8	45.2	+ 22.3
CONCAVE			
0.1	20.7	69.3	- 1.8
0.2	19.1	70.9	- 3.4
0.3	17.0	73.0	- 5.5
0.4	15.1	74.9	- 7.4

Horizontal Surface Offset = 1500 m

Sea Depth = 1500 m

Carrier Pipe Outer Diameter = 1.1 m

Carrier Pipe Wall Thickness = 10 mm

Table 5.86

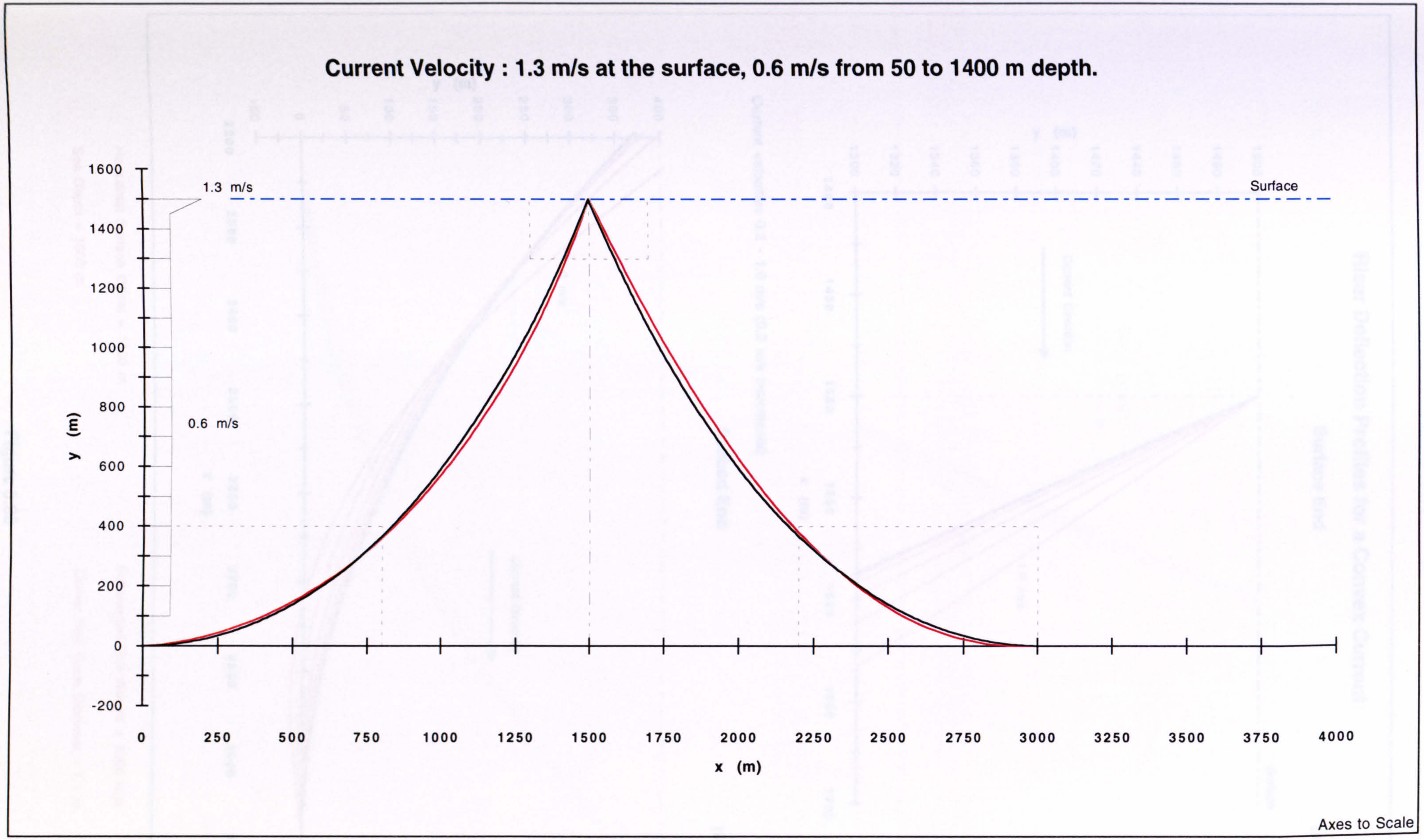

Horizontal Surface Offset = 1500 m

Submerged Unit Weight = 1000 N/m

Sea Depth = 1500 m

Carrier Pipe Outer Diameter = 1.1 m

Figure 5.87

Riser Deflection Profiles for a Convex Current

Surface End

(a)

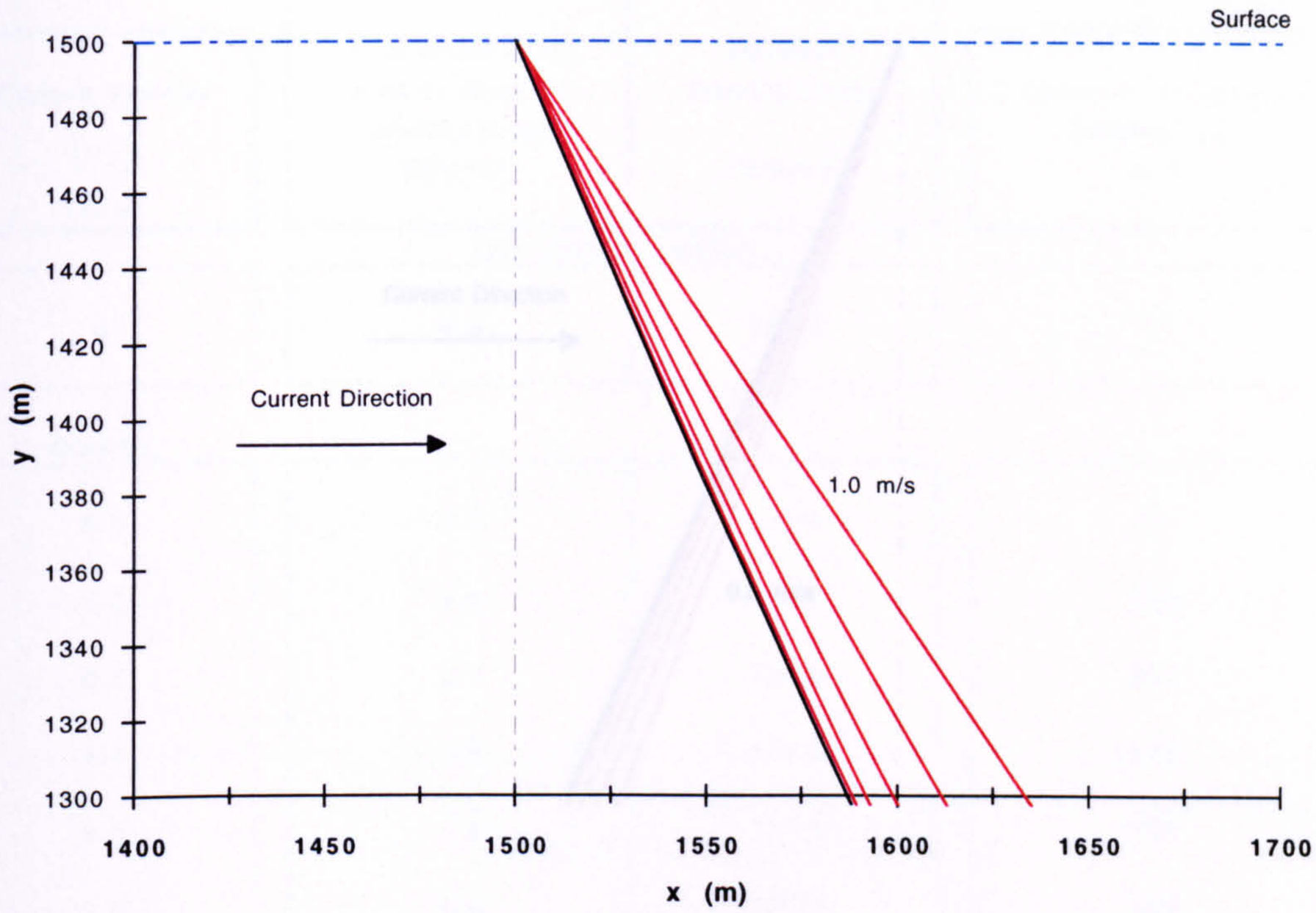

Current velocities 0.2 - 1.0 m/s (0.2 m/s increments)

Seabed End

(b)

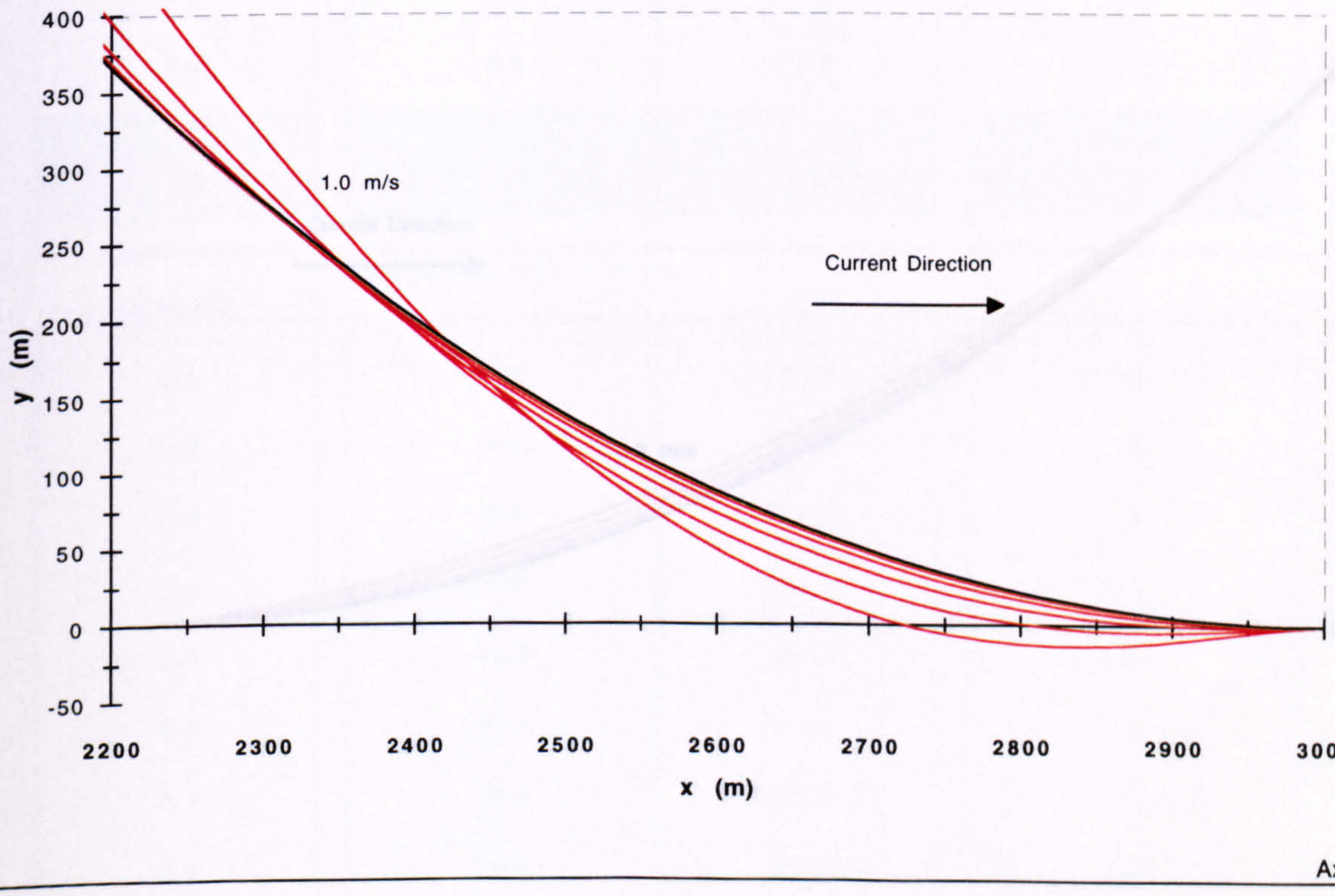

Axes to Scale

Horizontal Surface Offset = 1500 m

Sea Depth = 1500 m

Submerged Unit Weight = 1000 N/m

Carrier Pipe Outer Diameter = 1.1 m

Figure 5.88

Riser Deflection Profiles for a Concave Current

Surface End

(a)

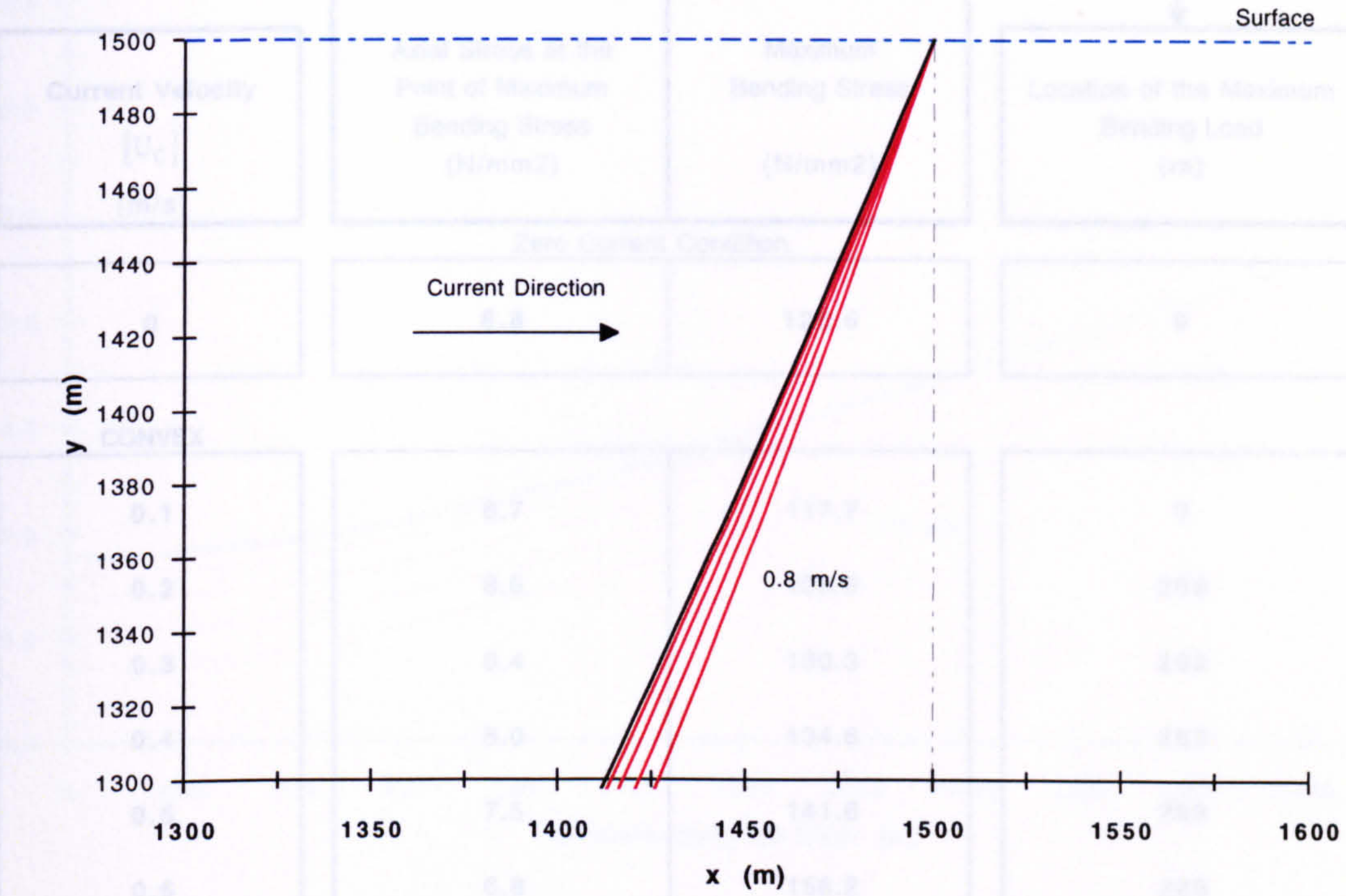

Current velocities 0.2 - 0.8 m/s (0.2 m/s increments)

Seabed End

(b)

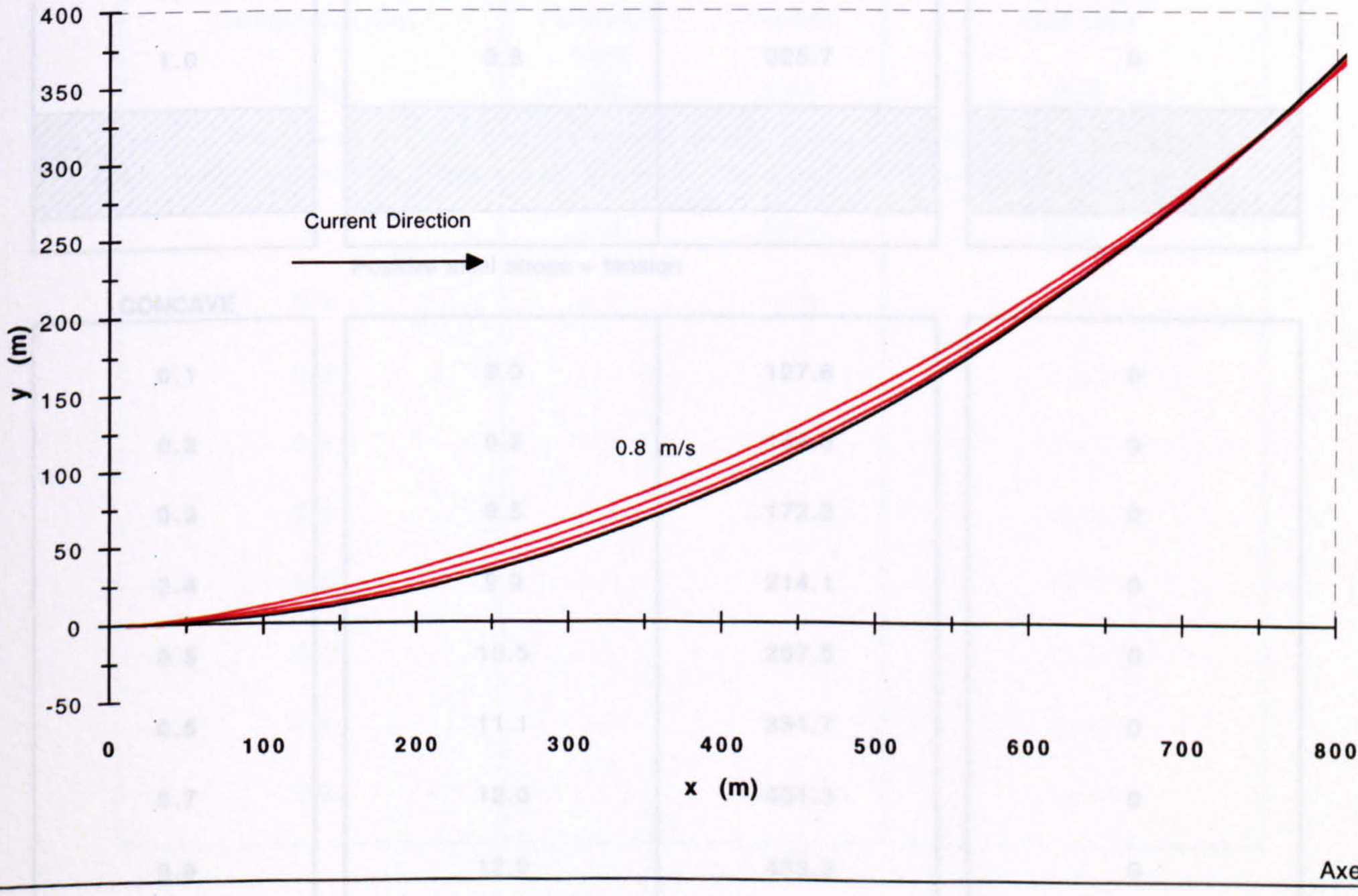

Axes to Scale

Horizontal Surface Offset = 1500 m

Sea Depth = 1500 m

Submerged Unit Weight = 1000 N/m

Carrier Pipe Outer Diameter = 1.1 m

Figure 5.89

Maximum Stress Conditions under Current Loading (a = 1500 m)

Submerged Unit Weight = 1000 N/m

Current Velocity $[U_C]$ (m/s)	Axial Stress at the Point of Maximum Bending Stress (N/mm2)	Maximum Bending Stress (N/mm2)	Location of the Maximum Bending Load (m) (Measured along the riser from the seabed end)
	Zero Current Condition		
0	8.8	122.6	0
CONVEX			
0.1	8.7	117.7	0
0.2	8.6	128.9	269
0.3	8.4	130.3	269
0.4	8.0	134.6	269
0.5	7.5	141.6	269
0.6	6.8	156.2	269
0.7	6.2	178.3	247
0.8	5.4	208.5	247
0.9	4.6	245.8	247
1.0	3.8	325.7	0
	Positive axial stress = tension		
CONCAVE			
0.1	9.0	127.6	0
0.2	9.2	144.8	0
0.3	9.5	172.3	0
0.4	9.9	214.1	0
0.5	10.5	267.5	0
0.6	11.1	331.7	0
0.7	12.0	401.3	0
0.8	12.9	483.3	0

Horizontal Surface Offset = 1500 m

Sea Depth = 1500 m

Carrier Pipe Outer Diameter = 1.1 m

Carrier Pipe Wall Thickness = 10 mm

Table 5.90

Axial Stress Distributions for a Convex Current

(a)

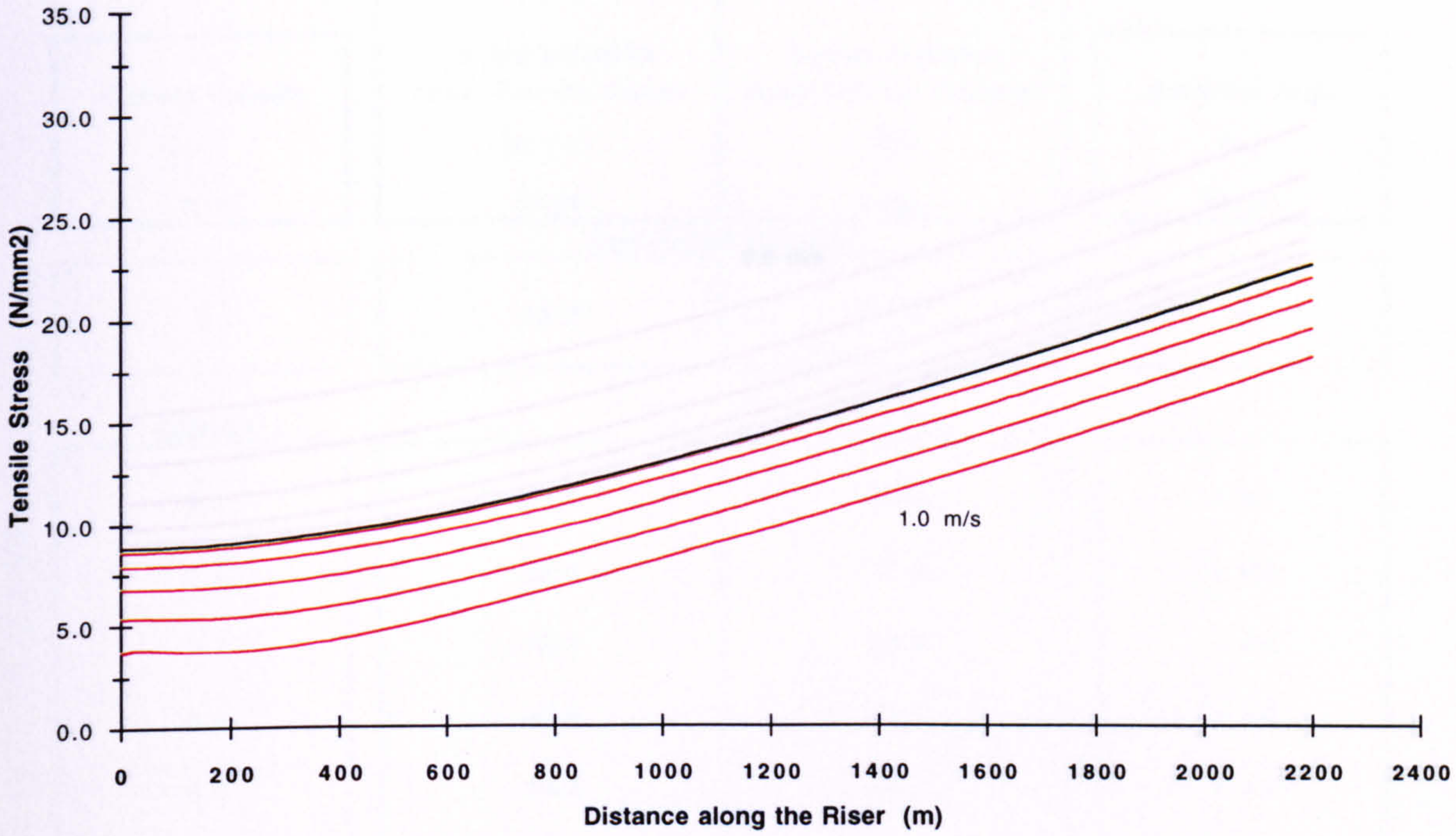

Current velocities 0.2 - 1.0 m/s (0.2 m/s increments)

Surface Forces for a Convex Current

(b)

Current Velocity (m/s)	Horizontal Load (kN)	Vertical Load (kN)	Axial Load (kN)
0	928	2244	2428
0.2	936	2203	2394
0.3	943	2172	2368
0.4	953	2128	2341
0.5	965	2065	2279
0.6	981	1998	2226
0.7	1001	1910	2156
0.8	1025	1817	2086
1.0	1092	1591	1930

Horizontal Surface Offset = 1500 m

Sea Depth = 1500 m

Submerged Unit Weight = 1000 N/m

Carrier Pipe Outer Diameter = 1.1 m

Figure 5.91

Axial Stress Distributions for a Concave Current

(a)

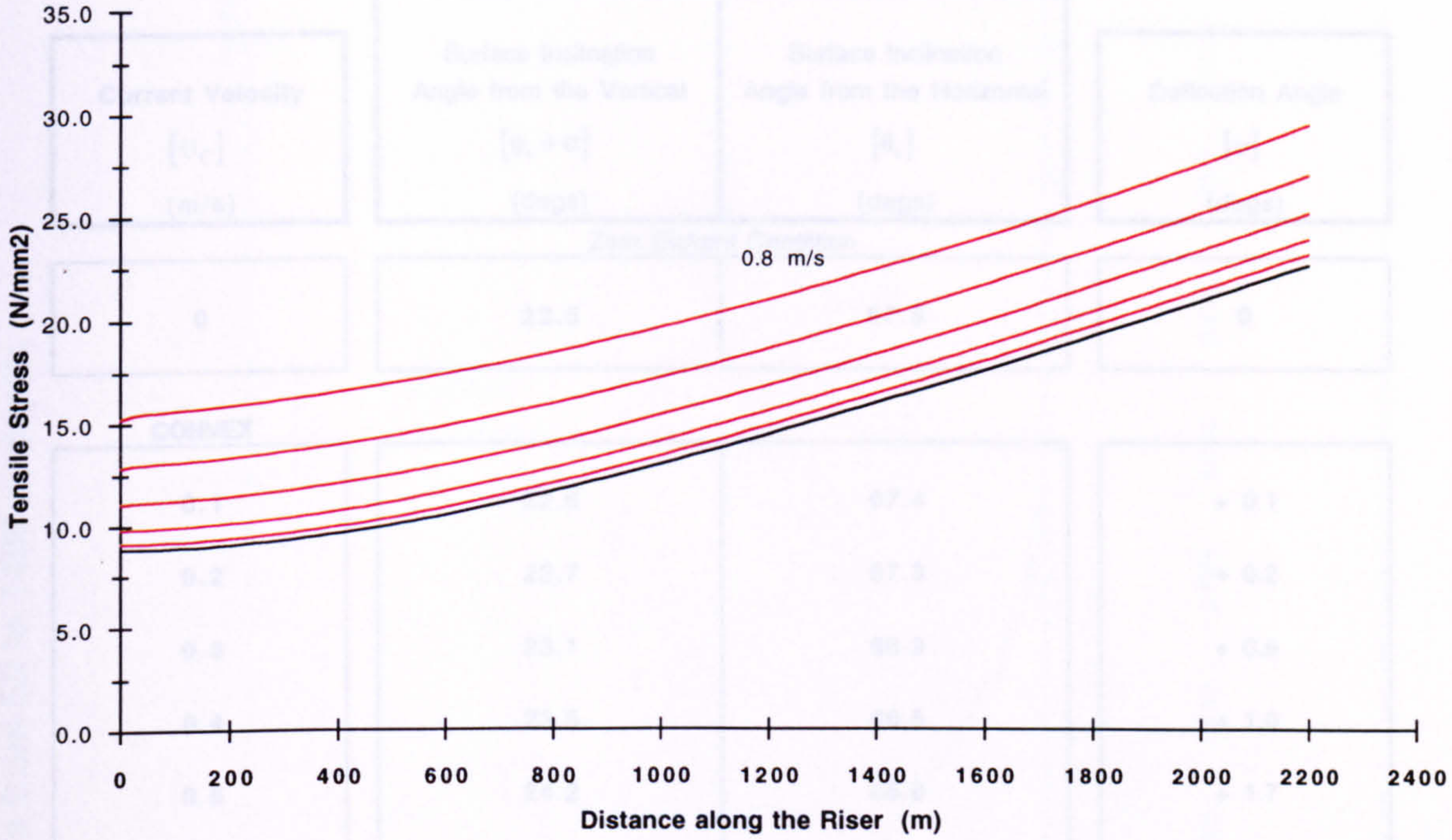

Current velocities 0.2 - 0.8 m/s (0.2 m/s increments)

Surface Forces for a Concave Current

(b)

Current Velocity (m/s)	Horizontal Load (kN)	Vertical Load (kN)	Axial Load (kN)
0	928	2244	2428
0.1	921	2258	2439
0.2	915	2284	2460
0.3	909	2324	2495
0.4	906	2375	2542
0.5	903	2442	2604
0.6	902	2520	2677
0.7	902	2619	2770
0.8	904	2726	2872

Horizontal Surface Offset = 1500 m

Sea Depth = 1500 m

Submerged Unit Weight = 1000 N/m

Carrier Pipe Outer Diameter = 1.1 m

Figure 5.92

Surface Deflection Angles under Current Loading (a = 1500 m)

Submerged Unit Weight = 1000 N/m

Current Velocity $[U_C]$ (m/s)	Surface Inclination Angle from the Vertical $[\varphi_s + \alpha]$ (degs)	Surface Inclination Angle from the Horizontal $[\theta_s]$ (degs)	Deflection Angle $[\alpha]$ (degs)
	Zero Current Condition		
0	22.5	67.5	0
CONVEX			
0.1	22.6	67.4	+ 0.1
0.2	22.7	67.3	+ 0.2
0.3	23.1	66.9	+ 0.6
0.4	23.5	66.5	+ 1.0
0.5	24.2	65.8	+ 1.7
0.6	25.4	64.6	+ 2.9
0.7	27.0	63.0	+ 4.5
0.8	29.0	61.0	+ 6.5
0.9	31.5	58.5	+ 9.0
1.0	34.3	55.7	+ 11.8
CONCAVE			
0.1	22.3	67.7	- 0.2
0.2	22.1	67.9	- 0.4
0.3	21.7	68.3	- 0.8
0.4	21.2	68.8	- 1.3
0.5	20.6	69.4	- 1.9
0.6	20.0	20.0	- 2.5
0.7	19.3	70.7	- 3.2
0.8	18.5	71.5	- 4.0

Horizontal Surface Offset = 1500 m

Sea Depth = 1500 m

Carrier Pipe Outer Diameter = 1.1 m

Carrier Pipe Wall Thickness = 10 mm

Table 5.93

Current Velocity : 1.3 m/s at the surface, 0.8 m/s from 50 to 1400 m depth.

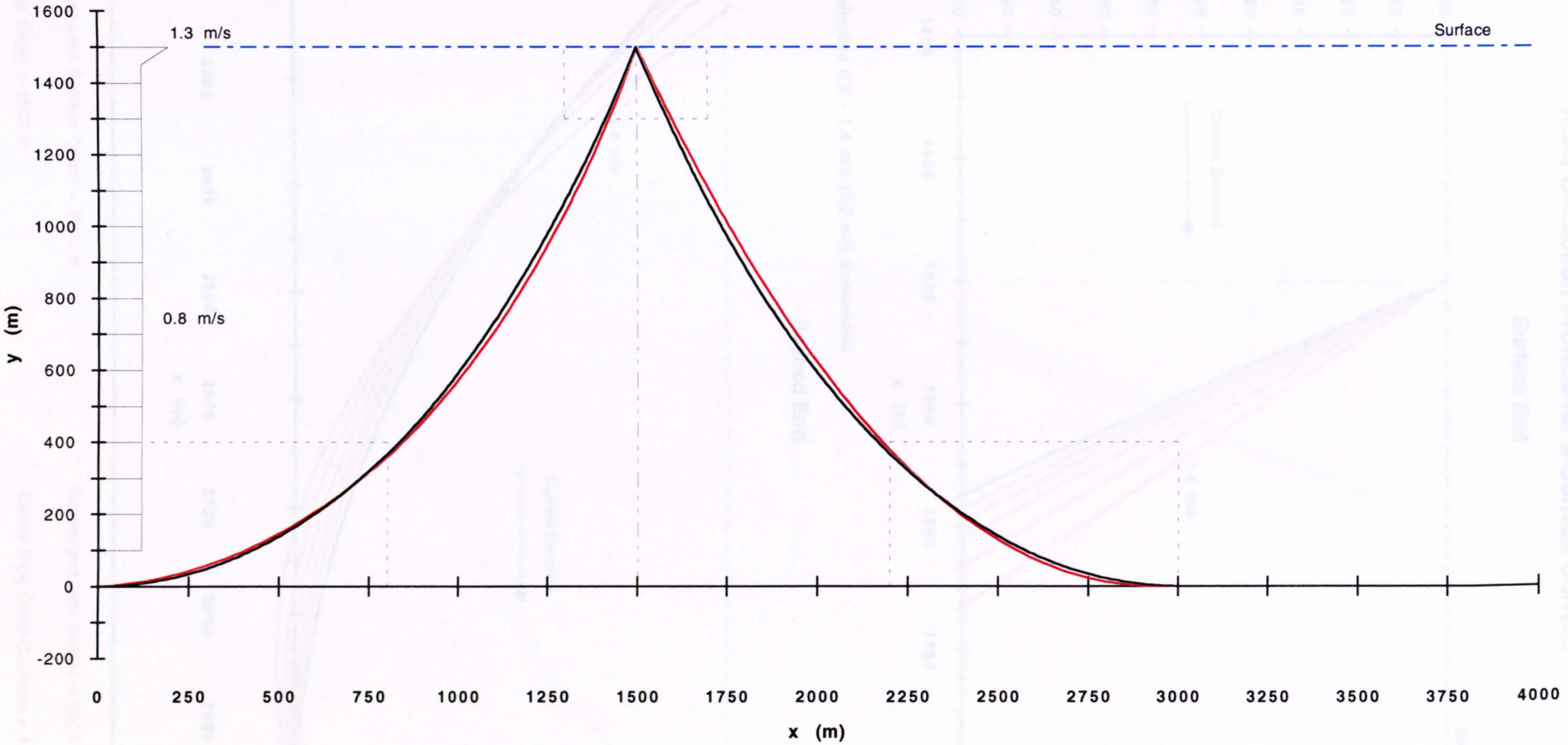

Horizontal Surface Offset = 1500 m

Sea Depth = 1500 m

Submerged Unit Weight = 2000 N/m

Carrier Pipe Outer Diameter = 1.1 m

Figure 5.94

Riser Deflection Profiles for a Convex Current

Surface End

(a)

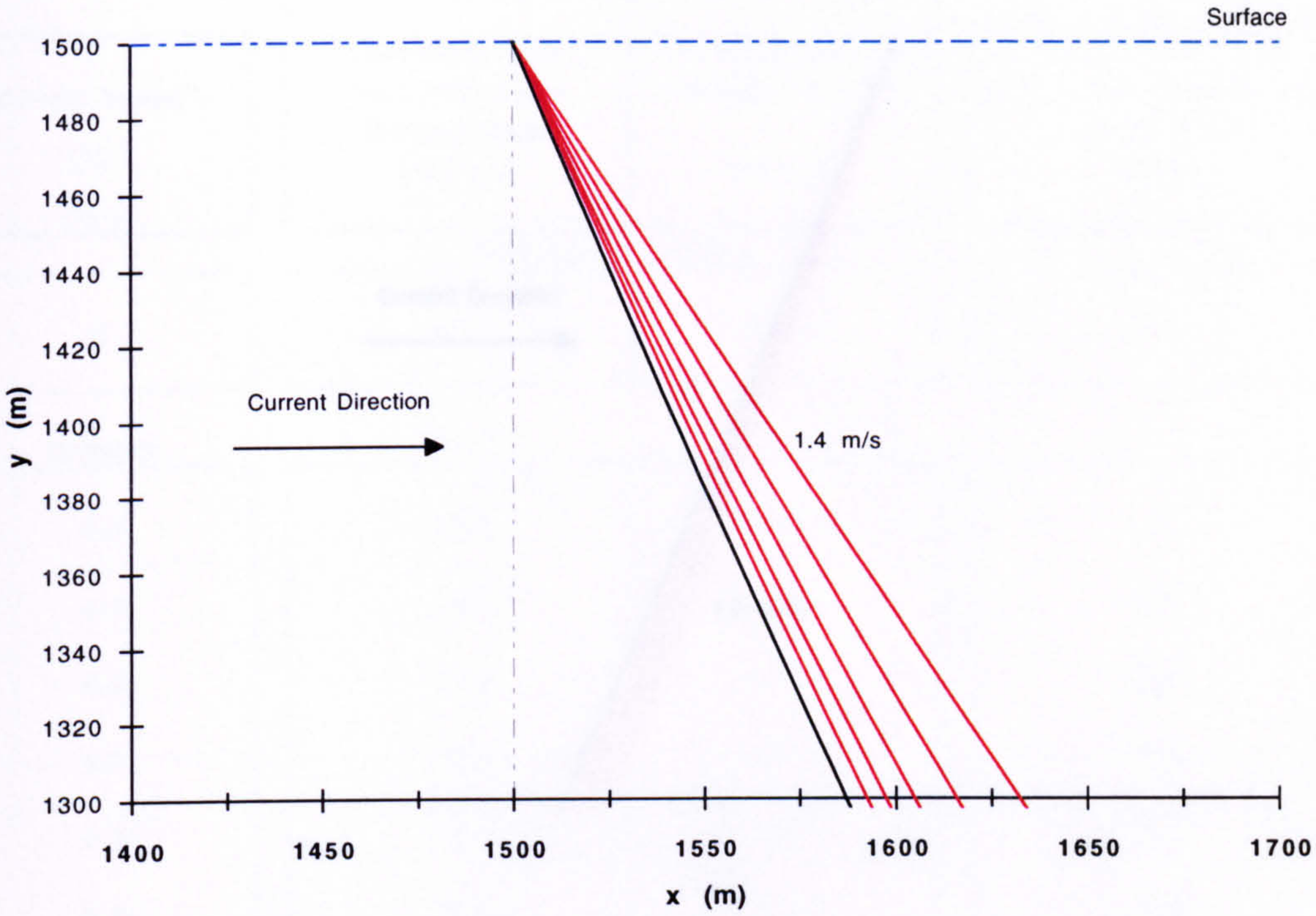

Current velocities 0.6 - 1.4 m/s (0.2 m/s increments)

Seabed End

(b)

Axes to Scale

Horizontal Surface Offset = 1500 m

Sea Depth = 1500 m

Submerged Unit Weight = 2000 N/m

Carrier Pipe Outer Diameter = 1.1 m

Figure 5.95

Riser Deflection Profiles for a Concave Current

Surface End

(a)

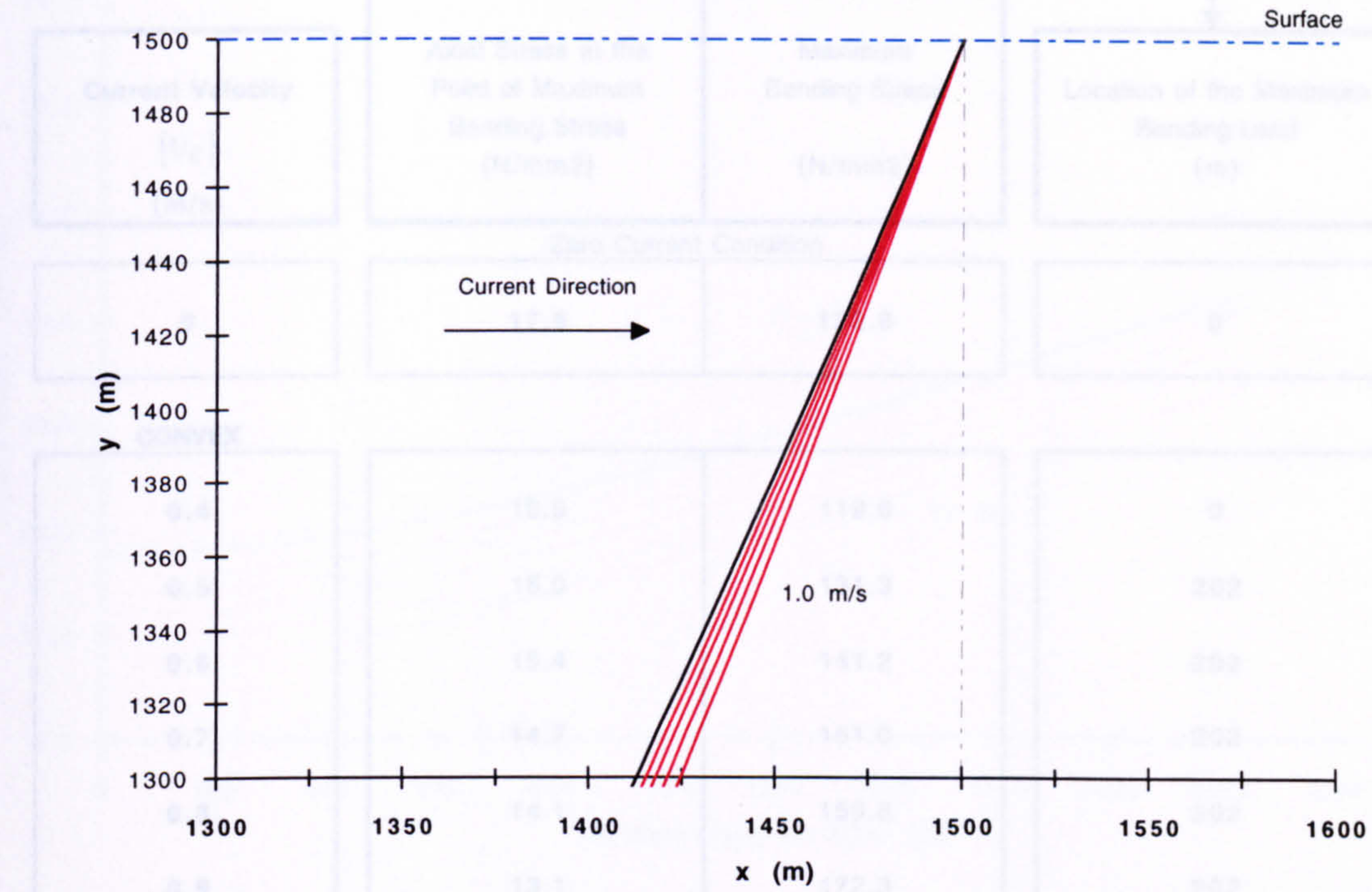

Current velocities 0.4 - 1.0 m/s (0.2 m/s increments)

Seabed End

(b)

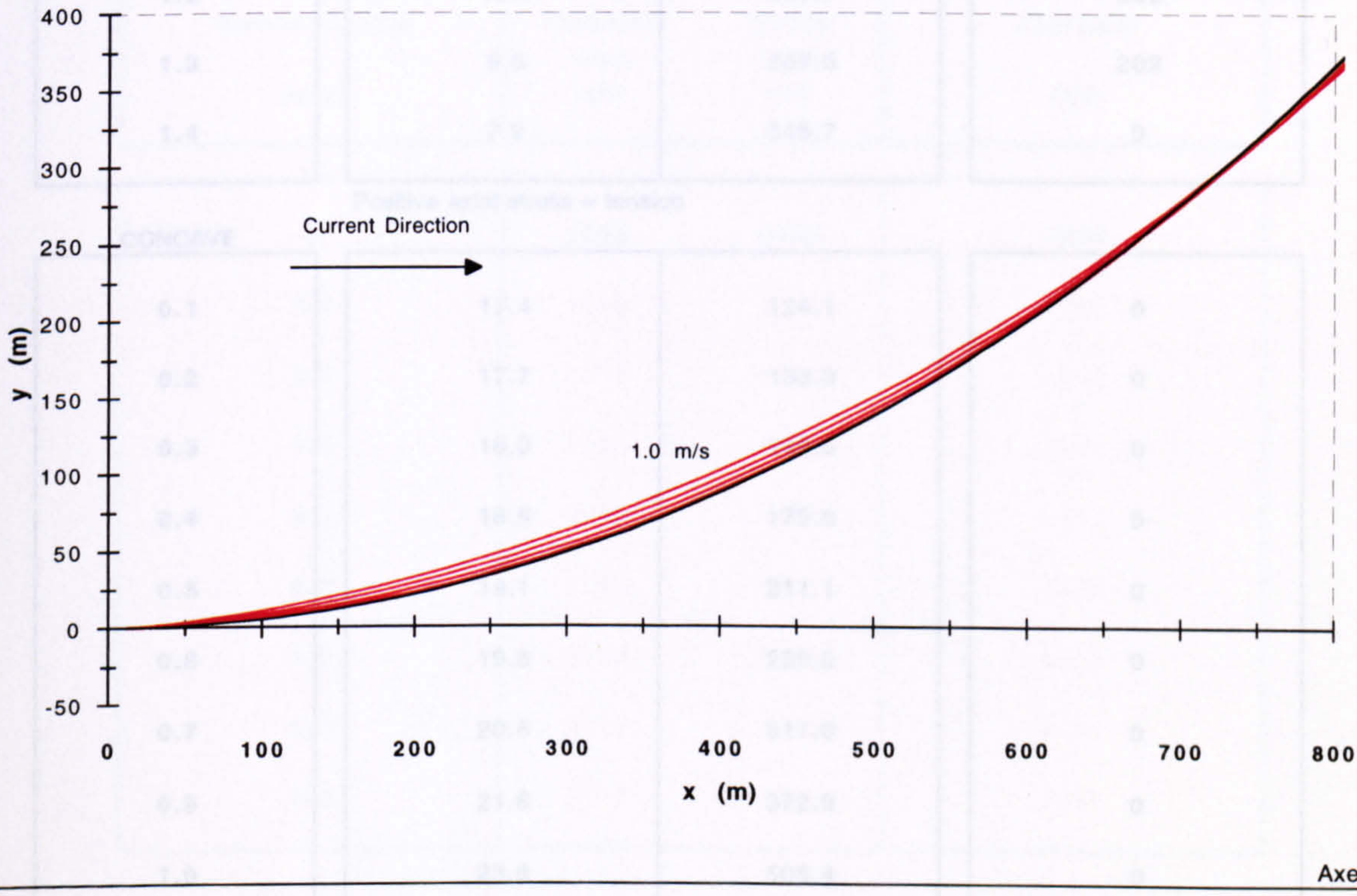

Axes to Scale

Horizontal Surface Offset = 1500 m

Sea Depth = 1500 m

Submerged Unit Weight = 2000 N/m

Carrier Pipe Outer Diameter = 1.1 m

Figure 5.96

Maximum Stress Conditions under Current Loading (a = 1500 m)

Submerged Unit Weight = 2000 N/m

Current Velocity $[U_C]$ (m/s)	Axial Stress at the Point of Maximum Bending Stress (N/mm2)	Maximum Bending Stress (N/mm2)	Location of the Maximum Bending Load (m) (Measured along the riser from the seabed end)
Zero Current Condition			
0	17.6	122.6	0
CONVEX			
0.4	16.5	119.6	0
0.5	16.0	131.3	202
0.6	15.4	141.2	202
0.7	14.7	151.0	202
0.8	14.1	159.6	202
0.9	13.1	172.3	202
1.0	12.2	187.7	202
1.1	11.2	209.1	202
1.2	10.1	235.7	202
1.3	9.0	267.5	202
1.4	7.9	345.7	0
Positive axial stress = tension			
CONCAVE			
0.1	17.4	124.1	0
0.2	17.7	133.3	0
0.3	18.0	149.5	0
0.4	18.5	175.8	0
0.5	19.1	211.1	0
0.6	19.8	258.5	0
0.7	20.6	311.0	0
0.8	21.6	372.9	0
1.0	23.8	508.4	0

Horizontal Surface Offset = 1500 m

Sea Depth = 1500 m

Carrier Pipe Outer Diameter = 1.1 m

Carrier Pipe Wall Thickness = 10 mm

Table 5.97

Axial Stress Distributions for a Convex Current

(a)

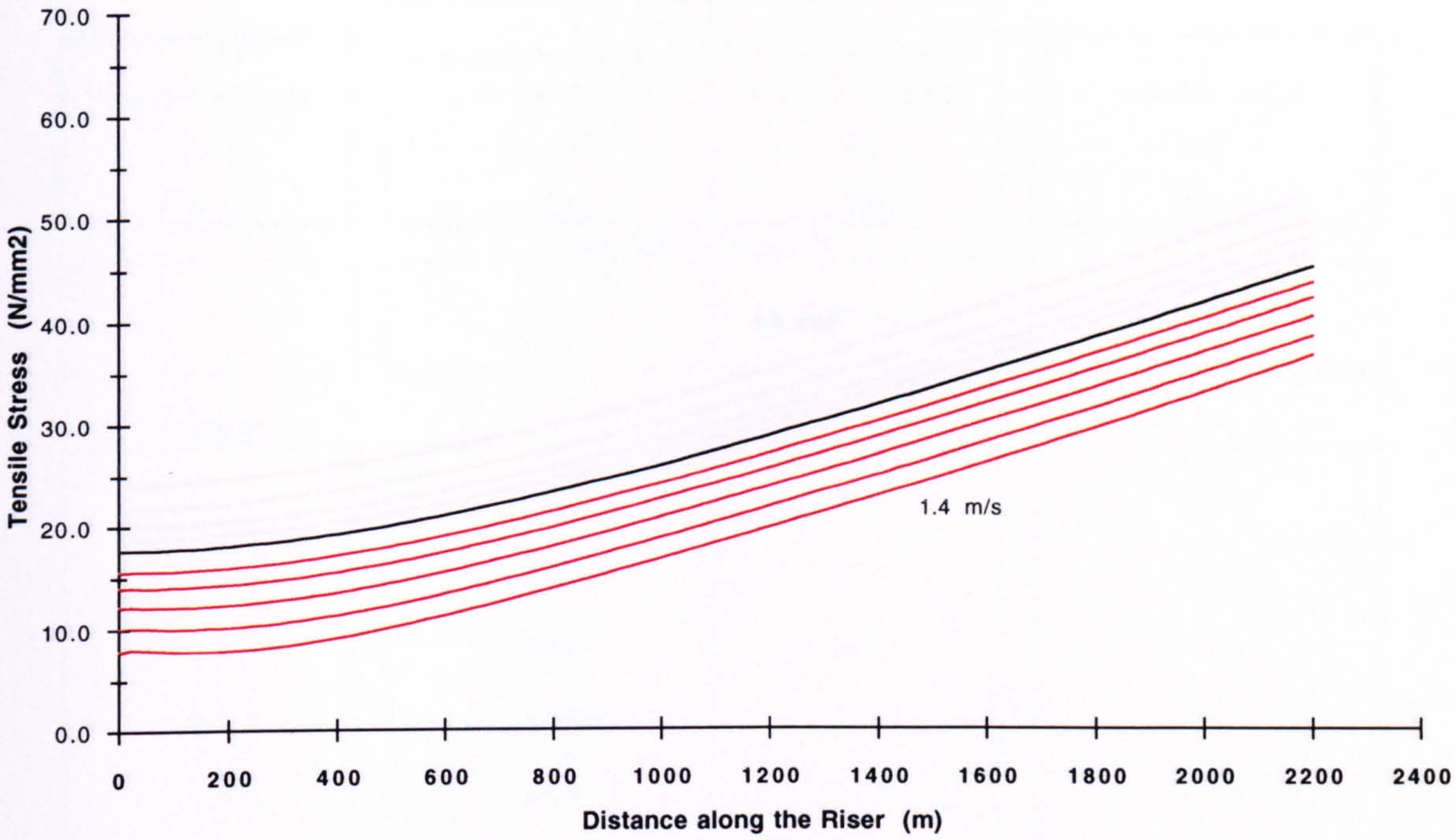

Current velocities 0.6 - 1.4 m/s (0.2 m/s increments)

Surface Forces for a Convex Current

(b)

Current Velocity (m/s)	Horizontal Load (kN)	Vertical Load (kN)	Axial Load (kN)
0	1856	4488	4856
0.4	1866	4370	4752
0.5	1878	4309	4700
0.6	1890	4220	4624
0.7	1908	4157	4574
0.8	1928	4061	4495
1.0	1983	3829	4312
1.2	2060	3558	4111
1.4	2167	3241	3899

Horizontal Surface Offset = 1500 m

Sea Depth = 1500 m

Submerged Unit Weight = 2000 N/m

Carrier Pipe Outer Diameter = 1.1 m

Figure 5.98

Axial Stress Distributions for a Concave Current

(a)

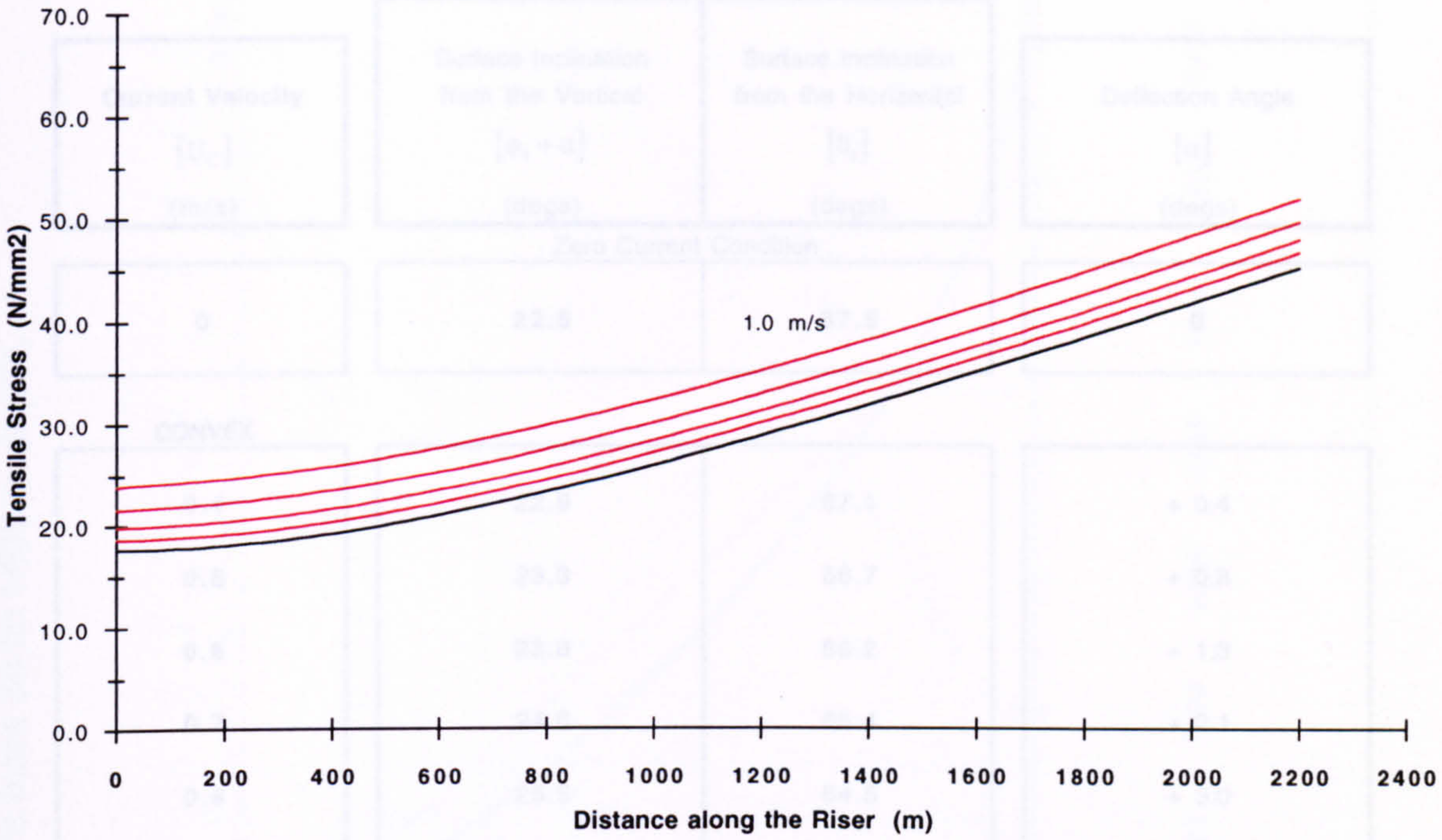

Current velocities 0.4 - 1.0 m/s (0.2 m/s increments)

Surface Forces for a Concave Current

(b)

Current Velocity (m/s)	Horizontal Load (kN)	Vertical Load (kN)	Axial Load (kN)
0	1856	4488	4856
0.2	1837	4520	4879
0.3	1831	4557	4911
0.4	1826	4608	4957
0.5	1823	4672	5015
0.6	1821	4758	5095
0.7	1820	4850	5180
0.8	1818	4964	5286
1.0	1817	5235	5541

Horizontal Surface Offset = 1500 m

Sea Depth = 1500 m

Submerged Unit Weight = 2000 N/m

Carrier Pipe Outer Diameter = 1.1 m

Figure 5.99

Surface Deflection Angles under Current Loading (a = 1500 m)

Submerged Unit Weight = 2000 N/m

Current Velocity $[U_C]$ (m/s)	Surface Inclination from the Vertical $[\varphi_s + \alpha]$ (degs)	Surface Inclination from the Horizontal $[\theta_s]$ (degs)	Deflection Angle $[\alpha]$ (degs)
	Zero Current Condition		
0	22.5	67.5	0
CONVEX			
0.4	22.9	67.1	+ 0.4
0.5	23.3	66.7	+ 0.8
0.6	23.8	66.2	+ 1.3
0.7	24.6	65.4	+ 2.1
0.8	25.5	64.5	+ 3.0
0.9	26.4	63.6	+ 3.9
1.0	27.5	62.5	+ 5.0
1.1	28.7	61.3	+ 6.2
1.2	30.0	60.0	+ 7.5
1.3	31.5	58.5	+ 9.0
1.4	33.5	56.5	+ 11.0
CONCAVE			
0.1	22.5	67.5	0
0.2	22.4	67.6	- 0.1
0.3	22.2	67.8	- 0.3
0.4	21.8	68.2	- 0.7
0.5	21.4	68.6	- 1.1
0.6	21.1	68.9	- 1.4
0.7	20.8	69.2	- 1.7
0.8	20.4	69.6	- 2.1
1.0	19.2	70.8	- 3.3

Horizontal Surface Offset = 1500 m

Sea Depth = 1500 m

Carrier Pipe Outer Diameter = 1.1 m

Carrier Pipe Wall Thickness = 10 mm

Table 5.100

Current Velocity : 1.3 m/s at the surface, 0.4 m/s from 50 to 1400 m depth.

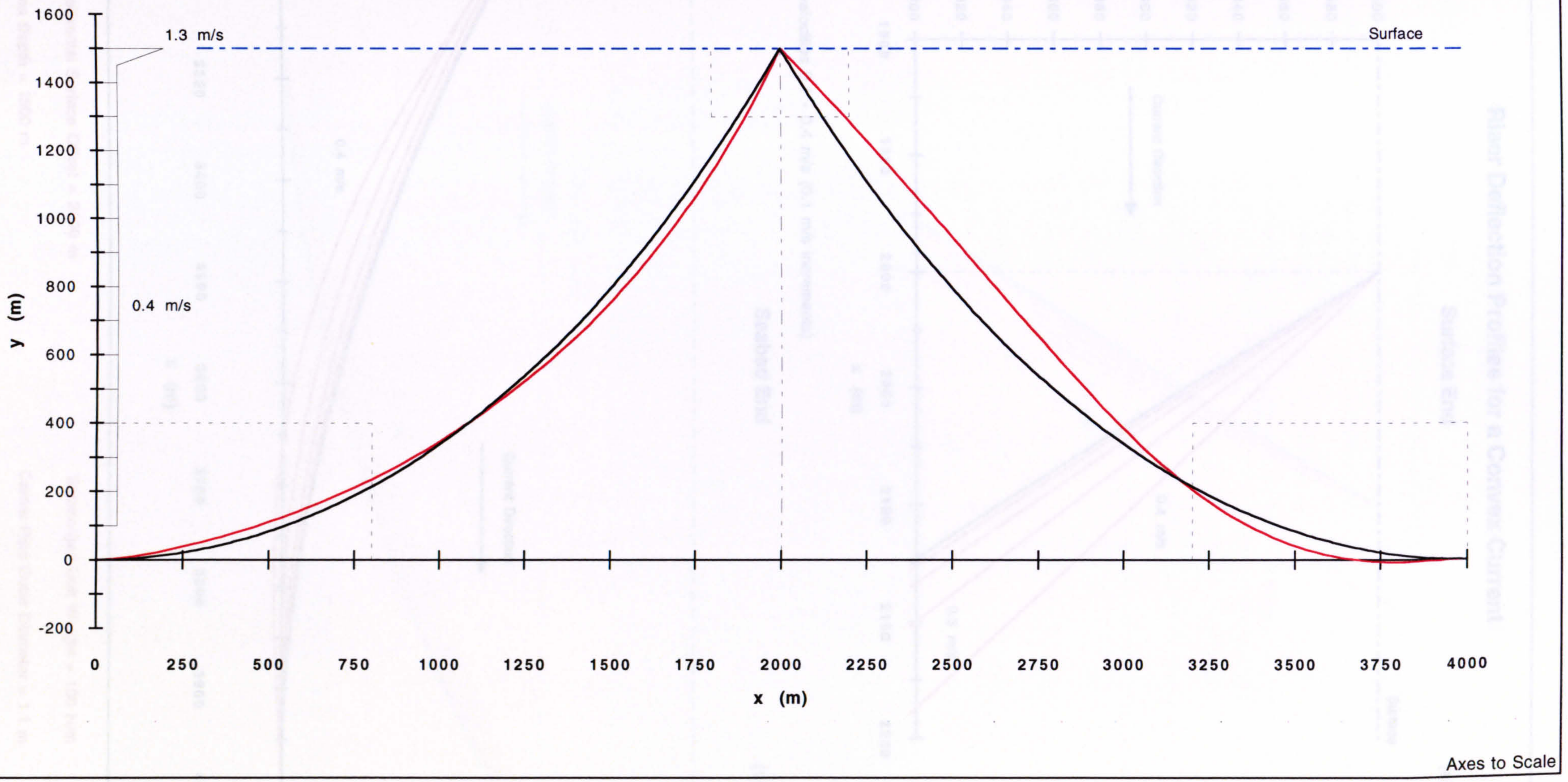

Horizontal Surface Offset = 2000 m

Sea Depth = 1500 m

Submerged Unit Weight = 100 N/m

Carrier Pipe Outer Diameter = 1.1 m

Figure 5.101

Riser Deflection Profiles for a Convex Current

Surface End

(a)

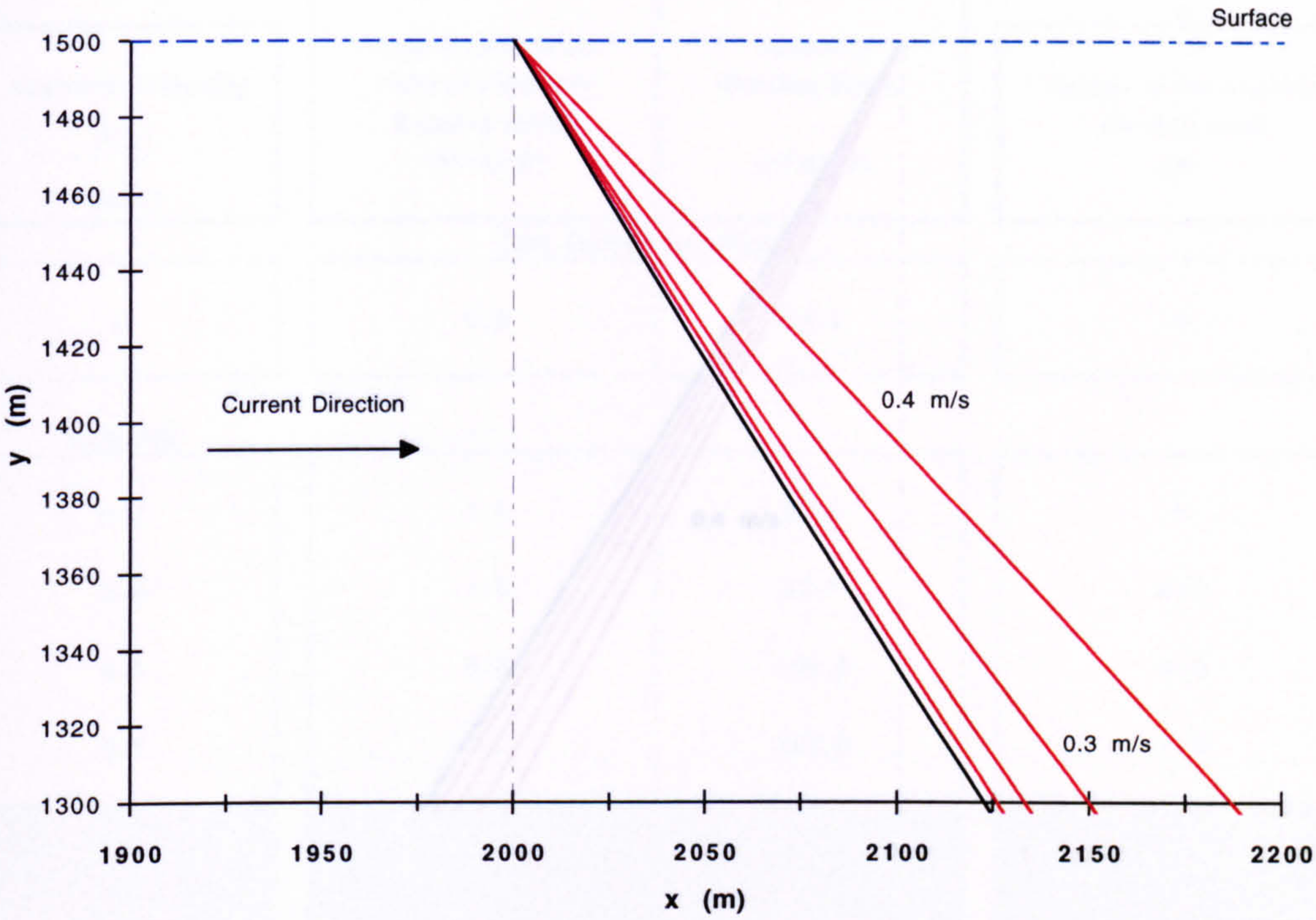

Current velocities 0.1 - 0.4 m/s (0.1 m/s increments)

Seabed End

(b)

Horizontal Surface Offset = 2000 m

Sea Depth = 1500 m

Submerged Unit Weight = 100 N/m

Carrier Pipe Outer Diameter = 1.1 m

Figure 5.102

Riser Deflection Profiles for a Concave Current

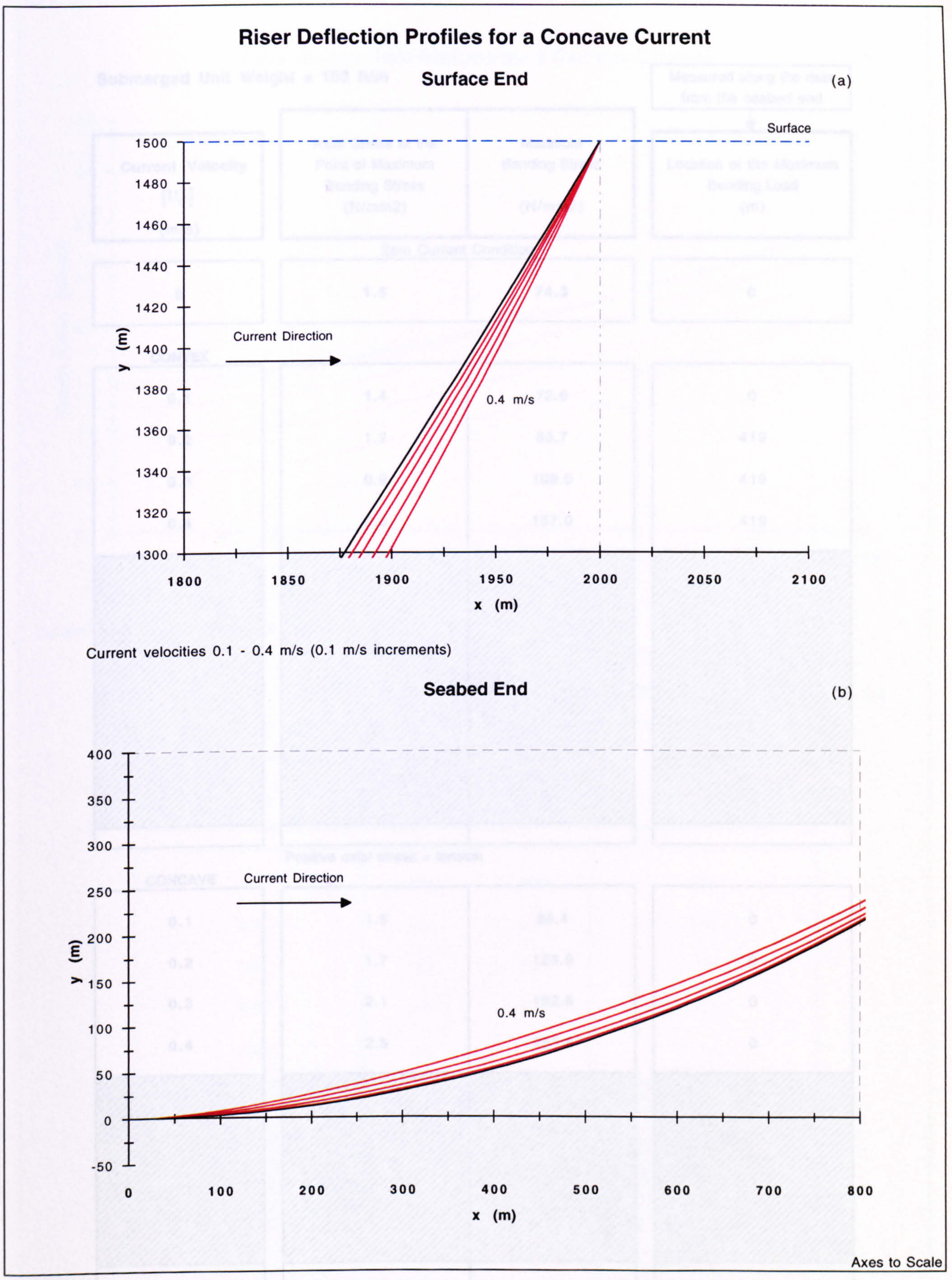

Current velocities 0.1 - 0.4 m/s (0.1 m/s increments)

Horizontal Surface Offset = 2000 m

Sea Depth = 1500 m

Submerged Unit Weight = 100 N/m

Carrier Pipe Outer Diameter = 1.1 m

Figure 5.103

Maximum Stress Conditions under Current Loading (a = 2000 m)

Submerged Unit Weight = 100 N/m

Current Velocity $[U_C]$ (m/s)	Axial Stress at the Point of Maximum Bending Stress (N/mm2)	Maximum Bending Stress (N/mm2)	Measured along the riser from the seabed end → Location of the Maximum Bending Load (m)
	Zero Current Condition		
0	1.5	74.3	0
CONVEX			
0.1	1.4	72.6	0
0.2	1.2	83.7	419
0.3	0.9	108.0	419
0.4	0.6	157.0	419
	Positive axial stress = tension		
CONCAVE			
0.1	1.5	89.4	0
0.2	1.7	125.9	0
0.3	2.1	182.8	0
0.4	2.5	255.6	0

Horizontal Surface Offset = 2000 m

Sea Depth = 1500 m

Carrier Pipe Outer Diameter = 1.1 m

Carrier Pipe Wall Thickness = 10 mm

Table 5.104

Axial Stress Distributions for a Convex Current

(a)

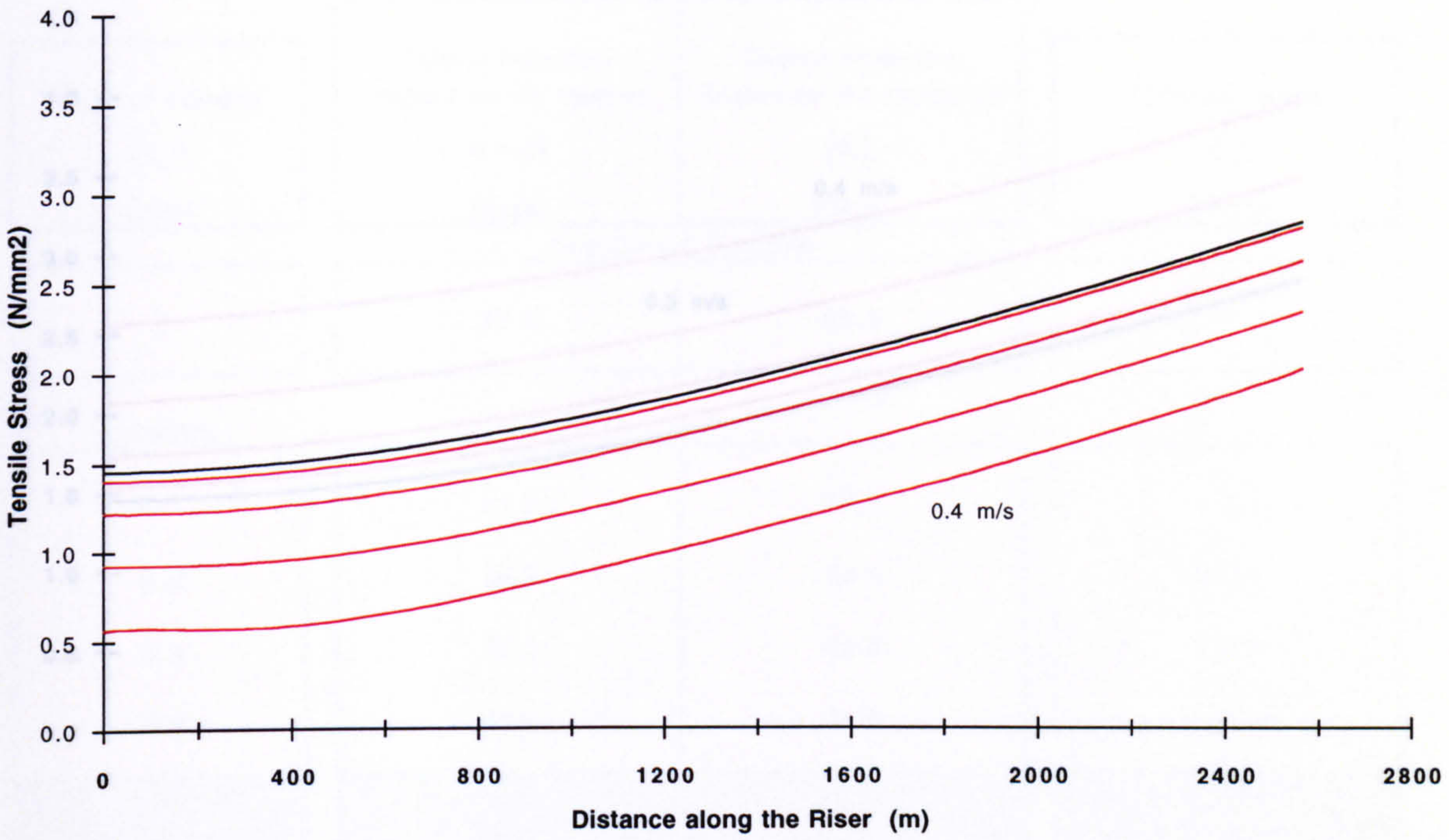

Current velocities 0.1 - 0.4 m/s (0.1 m/s increments)

Surface Forces for a Convex Current

(b)

Current Velocity (m/s)	Horizontal Load (kN)	Vertical Load (kN)	Axial Load (kN)
0	153	262	303
0.1	154	252	295
0.2	157	230	278
0.3	160	193	251
0.4	164	142	217

Horizontal Surface Offset = 2000 m

Sea Depth = 1500 m

Submerged Unit Weight = 100 N/m

Carrier Pipe Outer Diameter = 1.1 m

Figure 5.105

Axial Stress Distributions for a Concave Current

(a)

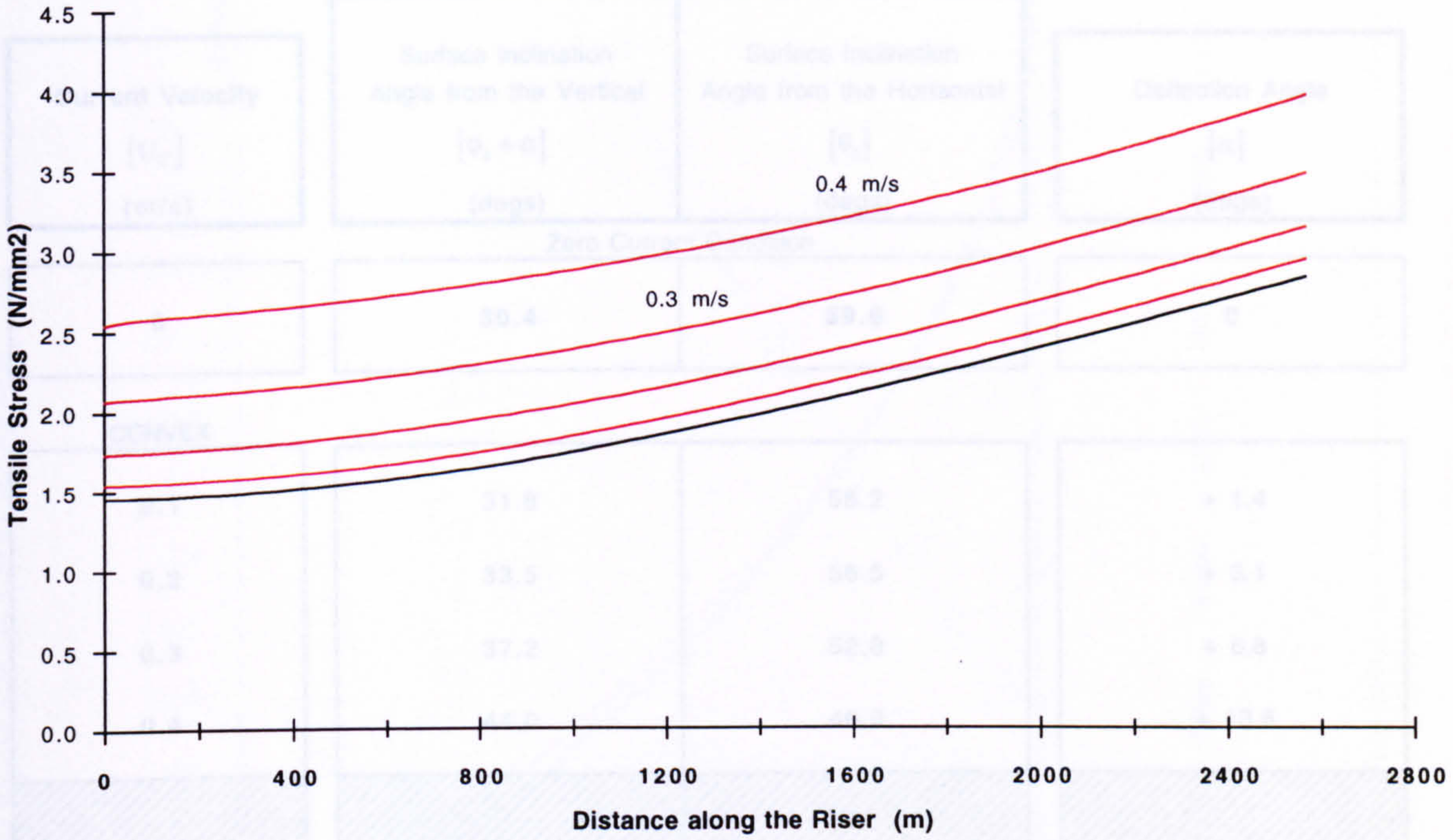

Current velocities 0.1 - 0.4 m/s (0.1 m/s increments)

Surface Forces for a Concave Current

(b)

Current Velocity (m/s)	Horizontal Load (kN)	Vertical Load (kN)	Axial Load (kN)
0	153	262	303
0.1	147	278	314
0.2	146	302	335
0.3	150	339	371
0.4	162	391	423

Horizontal Surface Offset = 2000 m

Sea Depth = 1500 m

Submerged Unit Weight = 100 N/m

Carrier Pipe Outer Diameter = 1.1 m

Figure 5.106

Surface Deflection Angles under Current Loading (a = 2000 m)

Submerged Unit Weight = 100 N/m

Current Velocity $[U_C]$ (m/s)	Surface Inclination Angle from the Vertical $[\varphi_s + \alpha]$ (degs)	Surface Inclination Angle from the Horizontal $[\theta_s]$ (degs)	Deflection Angle $[\alpha]$ (degs)
	Zero Current Condition		
0	30.4	59.6	0
CONVEX			
0.1	31.8	58.2	+ 1.4
0.2	33.5	56.5	+ 3.1
0.3	37.2	52.8	+ 6.8
0.4	44.0	46.0	+ 13.6
CONCAVE			
0.1	28.9	61.1	- 1.5
0.2	27.7	62.3	- 2.7
0.3	26.2	63.8	- 4.2
0.4	24.6	65.4	- 5.8

Horizontal Surface Offset = 2000 m

Sea Depth = 1500 m

Carrier Pipe Outer Diameter = 1.1 m

Carrier Pipe Wall Thickness = 10 mm

Table 5.107

Current Velocity : 1.3 m/s at the surface, 0.8 m/s from 50 to 1400 m depth.

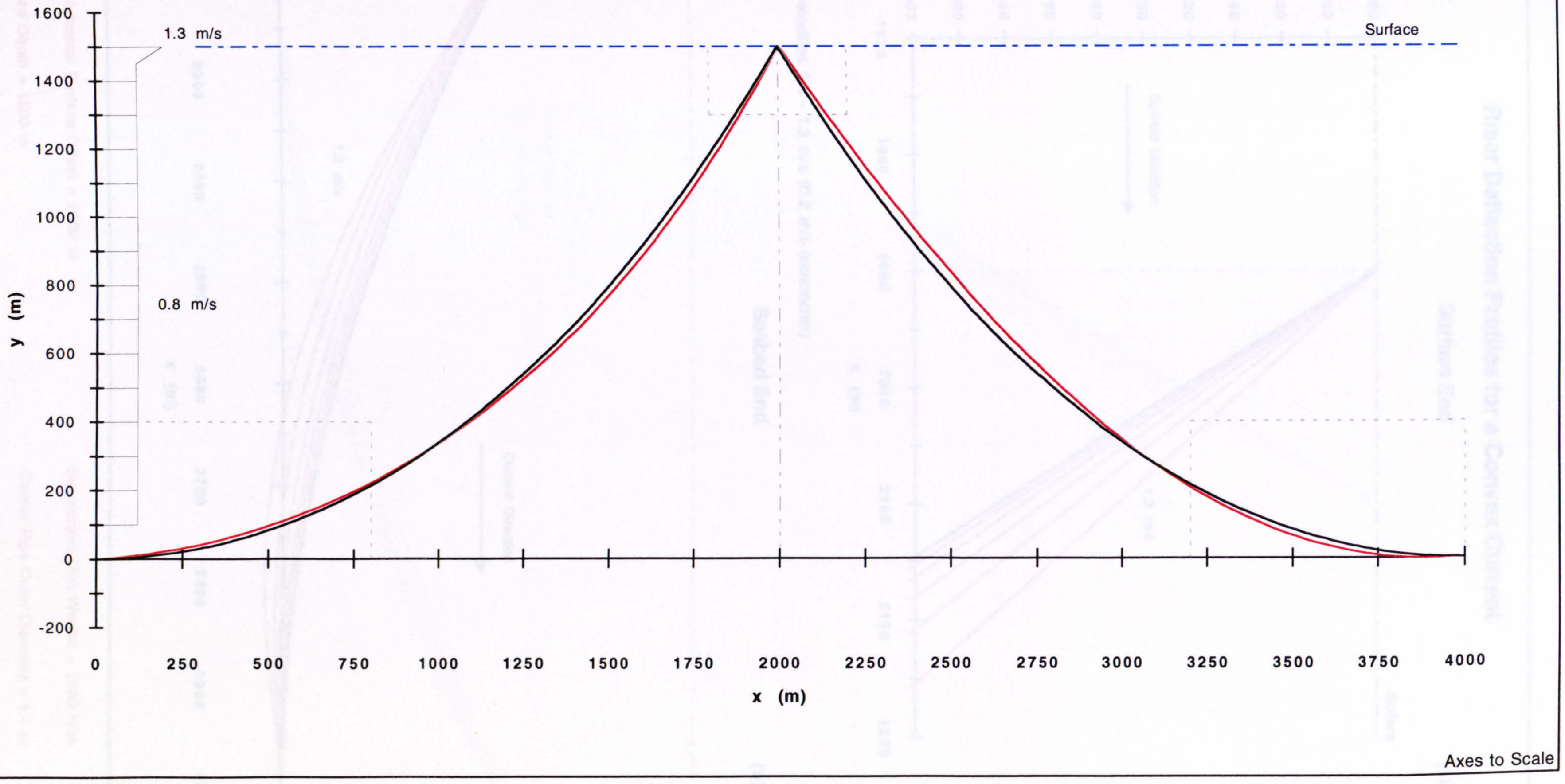

Horizontal Surface Offset = 2000 m

Sea Depth = 1500 m

Submerged Unit Weight = 1000 N/m

Carrier Pipe Outer Diameter = 1.1 m

Figure 5.108

Riser Deflection Profiles for a Convex Current

Surface End

(a)

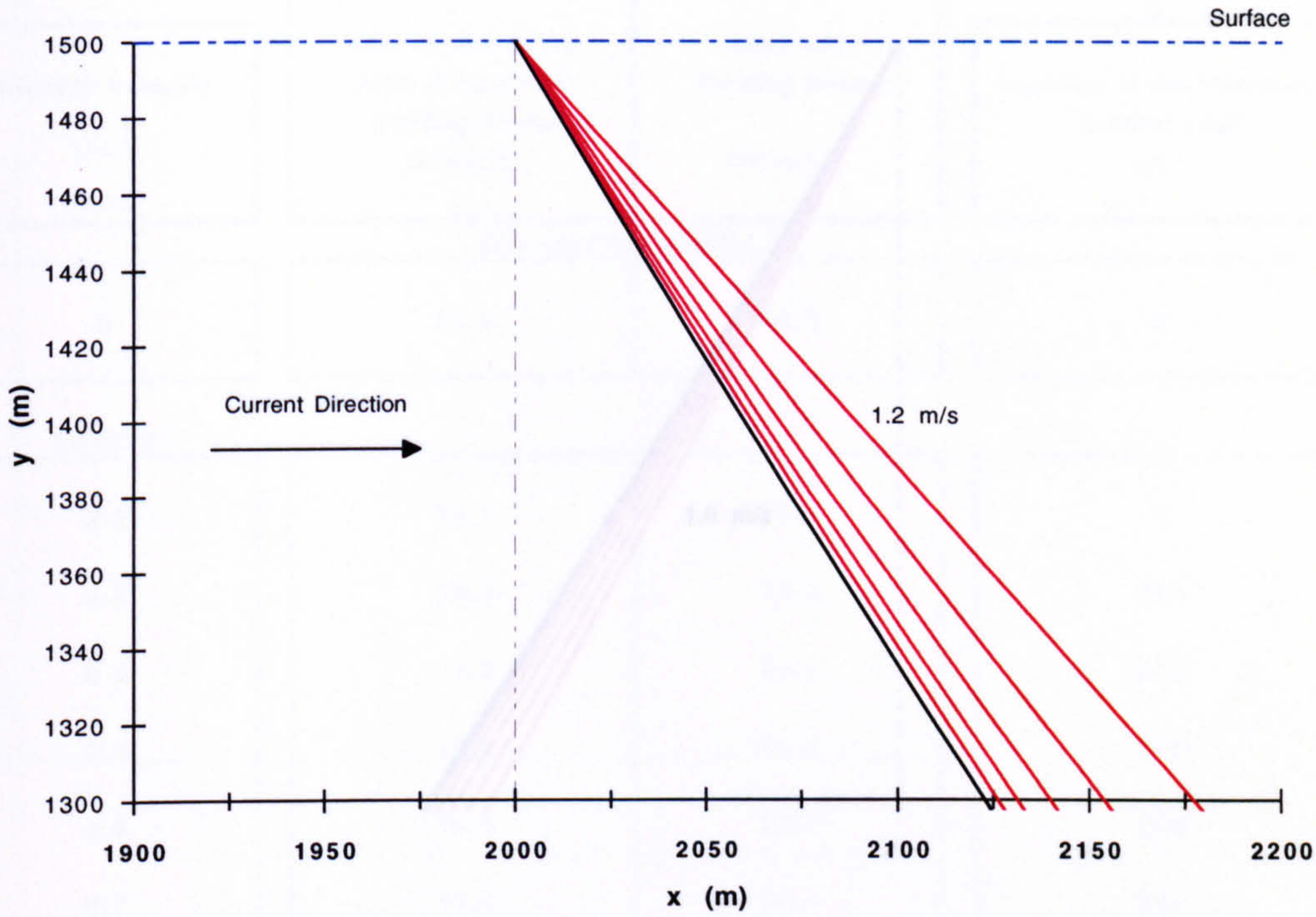

Current velocities 0.4 - 1.2 m/s (0.2 m/s increments)

Seabed End

(b)

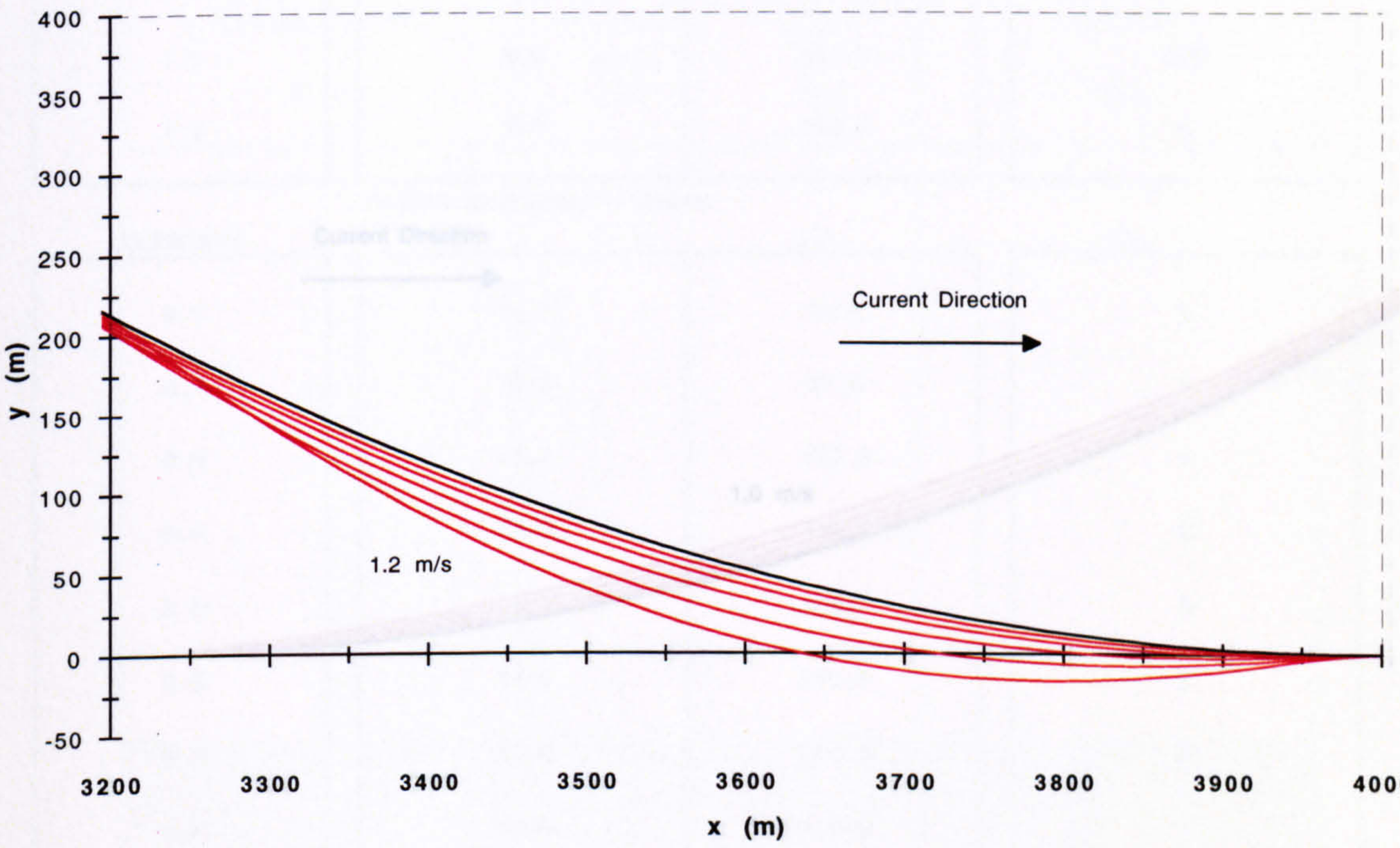

Axes to Scale

Horizontal Surface Offset = 2000 m

Sea Depth = 1500 m

Submerged Unit Weight = 1000 N/m

Carrier Pipe Outer Diameter = 1.1 m

Figure 5.109

Riser Deflection Profiles for a Concave Current

Surface End

(a)

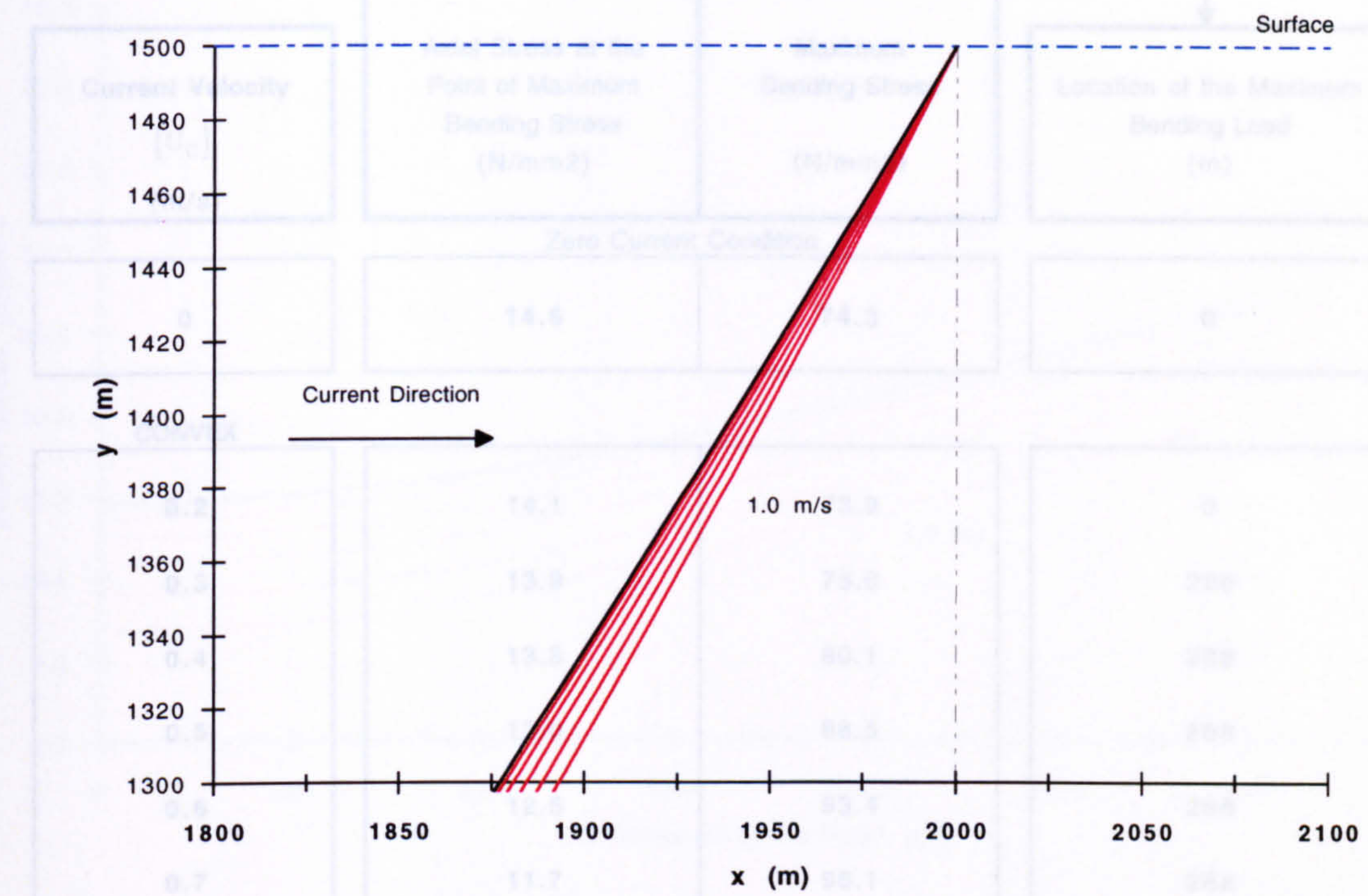

Current velocities 0.2 - 1.0 m/s (0.2 m/s increments)

Seabed End

(b)

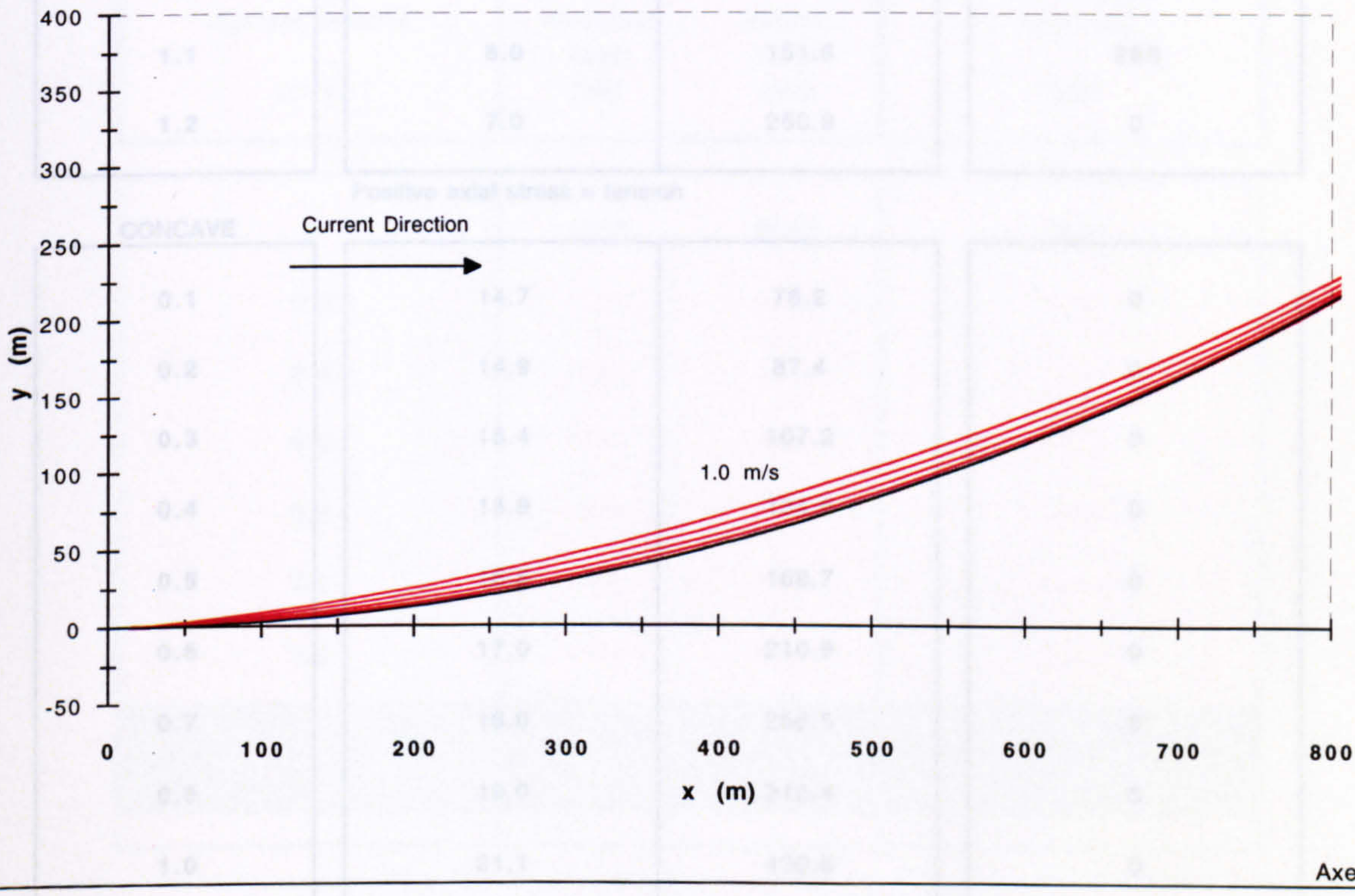

Axes to Scale

Horizontal Surface Offset = 2000 m

Sea Depth = 1500 m

Submerged Unit Weight = 1000 N/m

Carrier Pipe Outer Diameter = 1.1 m

Figure 5.110

Maximum Stress Conditions under Current Loading (a = 2000 m)

Submerged Unit Weight = 1000 N/m

Current Velocity $[U_C]$ (m/s)	Axial Stress at the Point of Maximum Bending Stress (N/mm2)	Maximum Bending Stress (N/mm2)	Location of the Maximum Bending Load (m)
			Measured along the riser from the seabed end
Zero Current Condition			
0	14.6	74.3	0
CONVEX			
0.2	14.1	73.9	0
0.3	13.9	75.6	288
0.4	13.5	80.1	288
0.5	13.0	88.5	288
0.6	12.5	93.4	288
0.7	11.7	98.1	288
0.8	11.0	104.2	288
0.9	10.1	115.8	288
1.0	9.1	131.7	288
1.1	8.0	151.6	288
1.2	7.0	256.9	0
Positive axial stress = tension			
CONCAVE			
0.1	14.7	76.2	0
0.2	14.9	87.4	0
0.3	15.4	107.2	0
0.4	15.9	134.8	0
0.5	16.5	168.7	0
0.6	17.0	210.9	0
0.7	18.0	256.5	0
0.8	19.0	310.4	0
1.0	21.1	430.8	0

Horizontal Surface Offset = 2000 m

Sea Depth = 1500 m

Carrier Pipe Outer Diameter = 1.1 m

Carrier Pipe Wall Thickness = 10 mm

Table 5.111

Axial Stress Distributions for a Convex Current

(a)

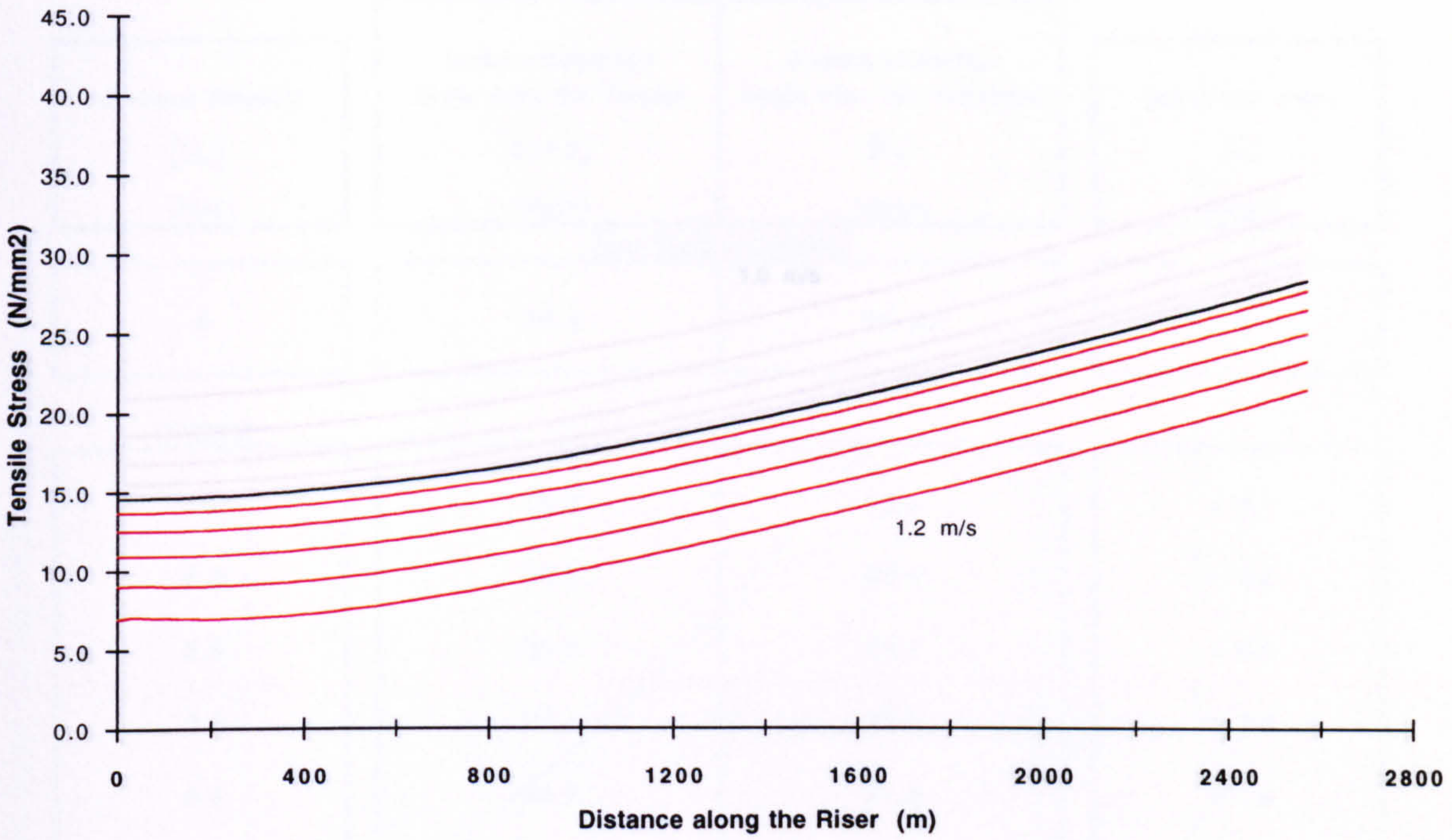

Current velocities 0.4 - 1.2 m/s (0.2 m/s increments)

Surface Forces for a Convex Current

(b)

Current Velocity (m/s)	Horizontal Load (kN)	Vertical Load (kN)	Axial Load (kN)
0	1533	2617	3033
0.2	1527	2563	2983
0.4	1527	2486	2918
0.6	1532	2374	2825
0.8	1542	2192	2680
1.0	1558	1964	2507
1.2	1579	1703	2322

Horizontal Surface Offset = 2000 m

Sea Depth = 1500 m

Submerged Unit Weight = 1000 N/m

Carrier Pipe Outer Diameter = 1.1 m

Figure 5.112

Axial Stress Distributions for a Concave Current

(a)

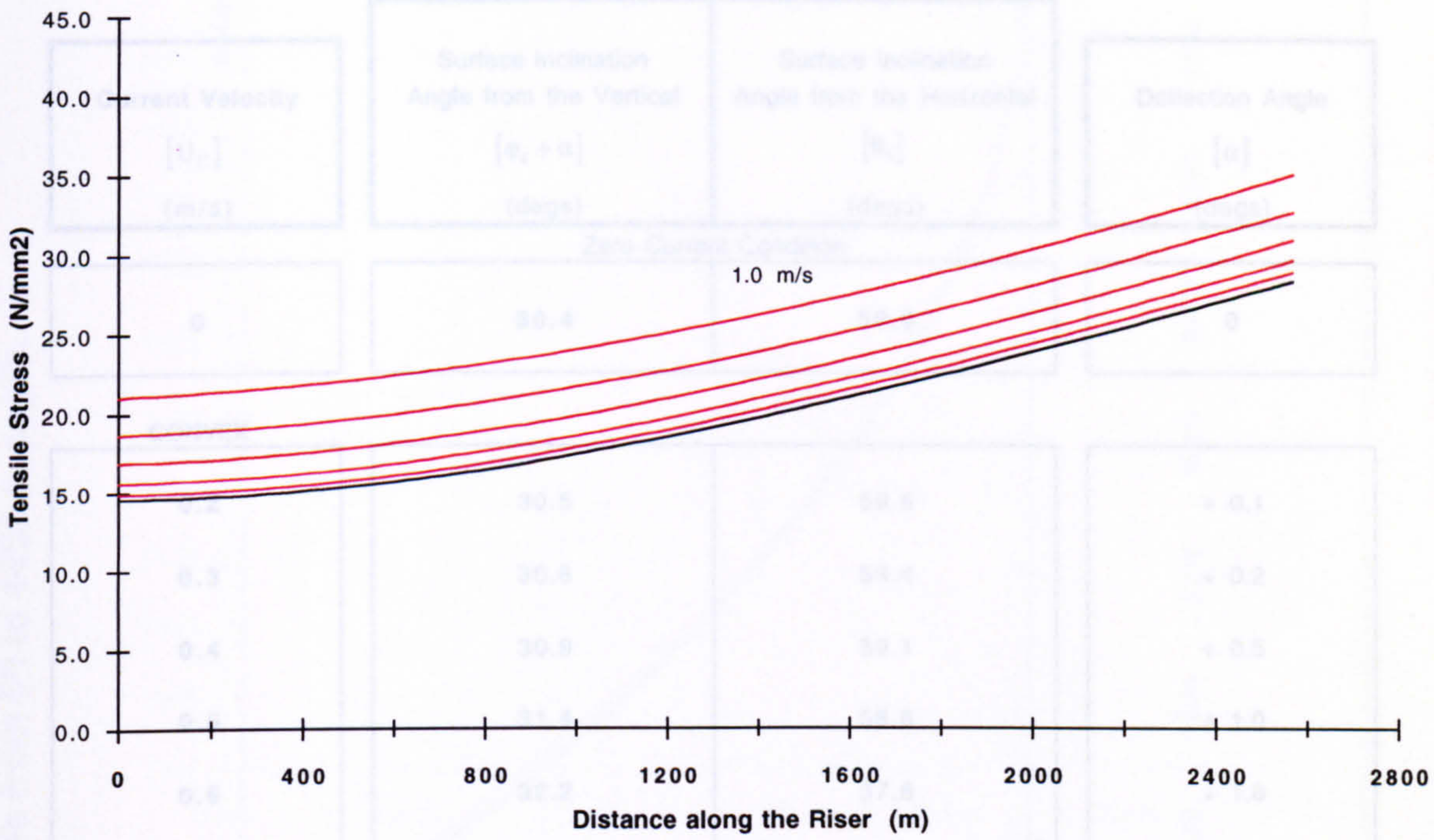

Current velocities 0.2 - 1.0 m/s (0.2 m/s increments)

Surface Forces for a Concave Current

(b)

Current Velocity (m/s)	Horizontal Load (kN)	Vertical Load (kN)	Axial Load (kN)
0	1533	2617	3033
0.2	1534	2672	3081
0.3	1538	2710	3116
0.4	1544	2758	3161
0.5	1552	2818	3217
0.6	1564	2886	3283
0.7	1579	2974	3367
0.8	1598	3081	3471
1.0	1652	3338	3724

Horizontal Surface Offset = 2000 m

Sea Depth = 1500 m

Submerged Unit Weight = 1000 N/m

Carrier Pipe Outer Diameter = 1.1 m

Figure 5.113

Surface Deflection Angles under Current Loading (a = 2000 m)

Submerged Unit Weight = 1000 N/m

Current Velocity $[U_C]$ (m/s)	Surface Inclination Angle from the Vertical $[\varphi_s + \alpha]$ (degs)	Surface Inclination Angle from the Horizontal $[\theta_s]$ (degs)	Deflection Angle $[\alpha]$ (degs)
	Zero Current Condition		
0	30.4	59.6	0
CONVEX			
0.2	30.5	59.5	+ 0.1
0.3	30.6	59.4	+ 0.2
0.4	30.9	59.1	+ 0.5
0.5	31.4	58.6	+ 1.0
0.6	32.2	57.8	+ 1.8
0.7	33.1	56.9	+ 2.7
0.8	34.3	55.7	+ 3.9
0.9	35.8	54.2	+ 5.4
1.0	37.7	52.3	+ 7.3
1.1	39.8	50.2	+ 9.4
1.2	42.2	47.8	+ 11.8
CONCAVE			
0.1	30.2	59.8	- 0.2
0.2	30.0	60.0	- 0.4
0.3	29.7	60.3	- 0.7
0.4	29.4	60.6	- 1.0
0.5	29.0	61.0	- 1.4
0.6	28.6	61.4	- 1.8
0.7	28.1	61.9	- 2.3
0.8	27.5	62.5	- 2.9
1.0	26.5	63.5	- 3.9

Horizontal Surface Offset = 2000 m

Sea Depth = 1500 m

Carrier Pipe Outer Diameter = 1.1 m

Carrier Pipe Wall Thickness = 10 mm

Table 5.114

Current Velocity : 1.3 m/s at the surface, 1.0 m/s from 50 to 1400 m depth.

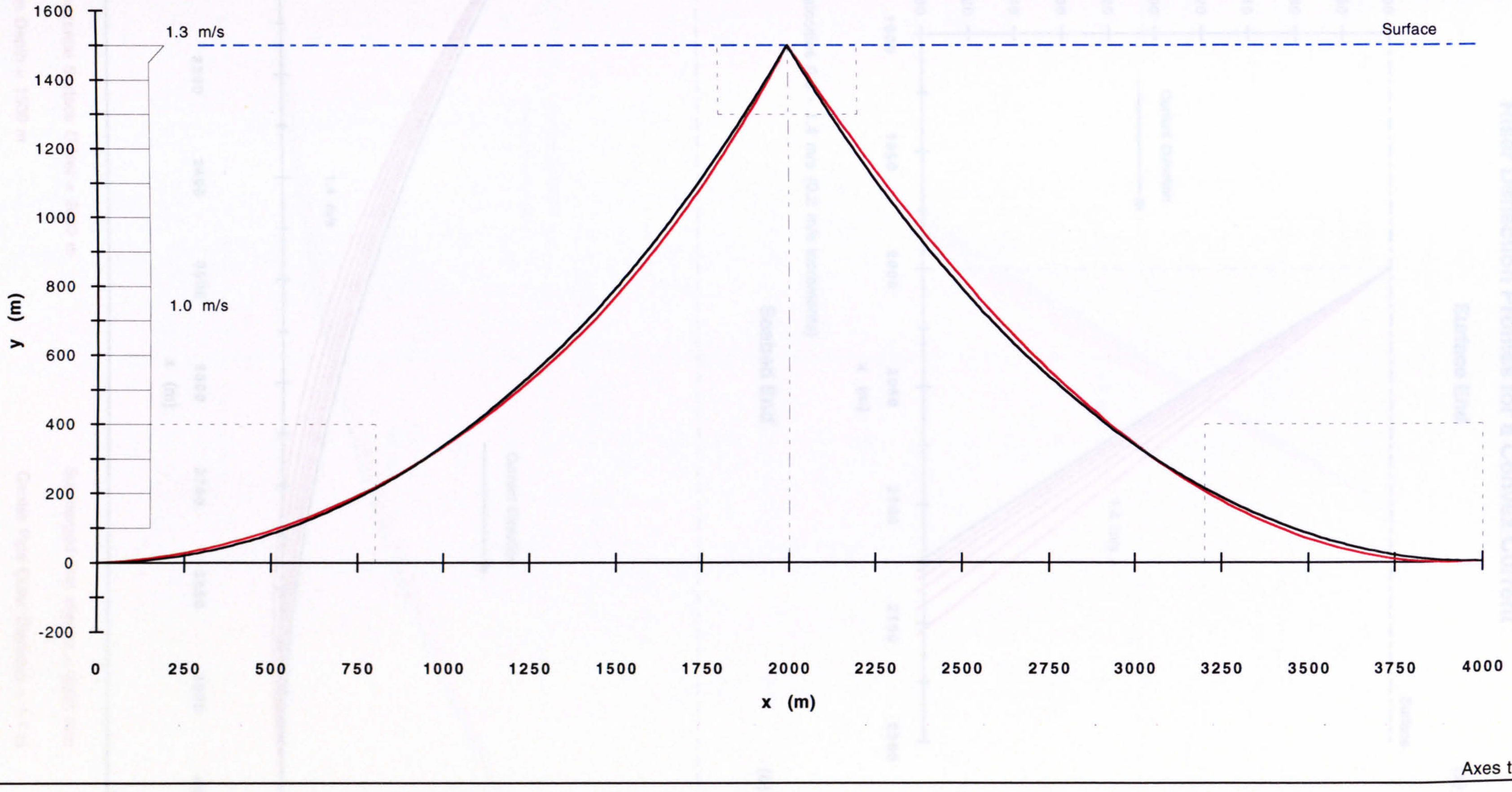

Horizontal Surface Offset = 2000 m

Sea Depth = 1500 m

Submerged Unit Weight = 2000 N/m

Carrier Pipe Outer Diameter = 1.1 m

Figure 5.115

Riser Deflection Profiles for a Convex Current

Surface End

(a)

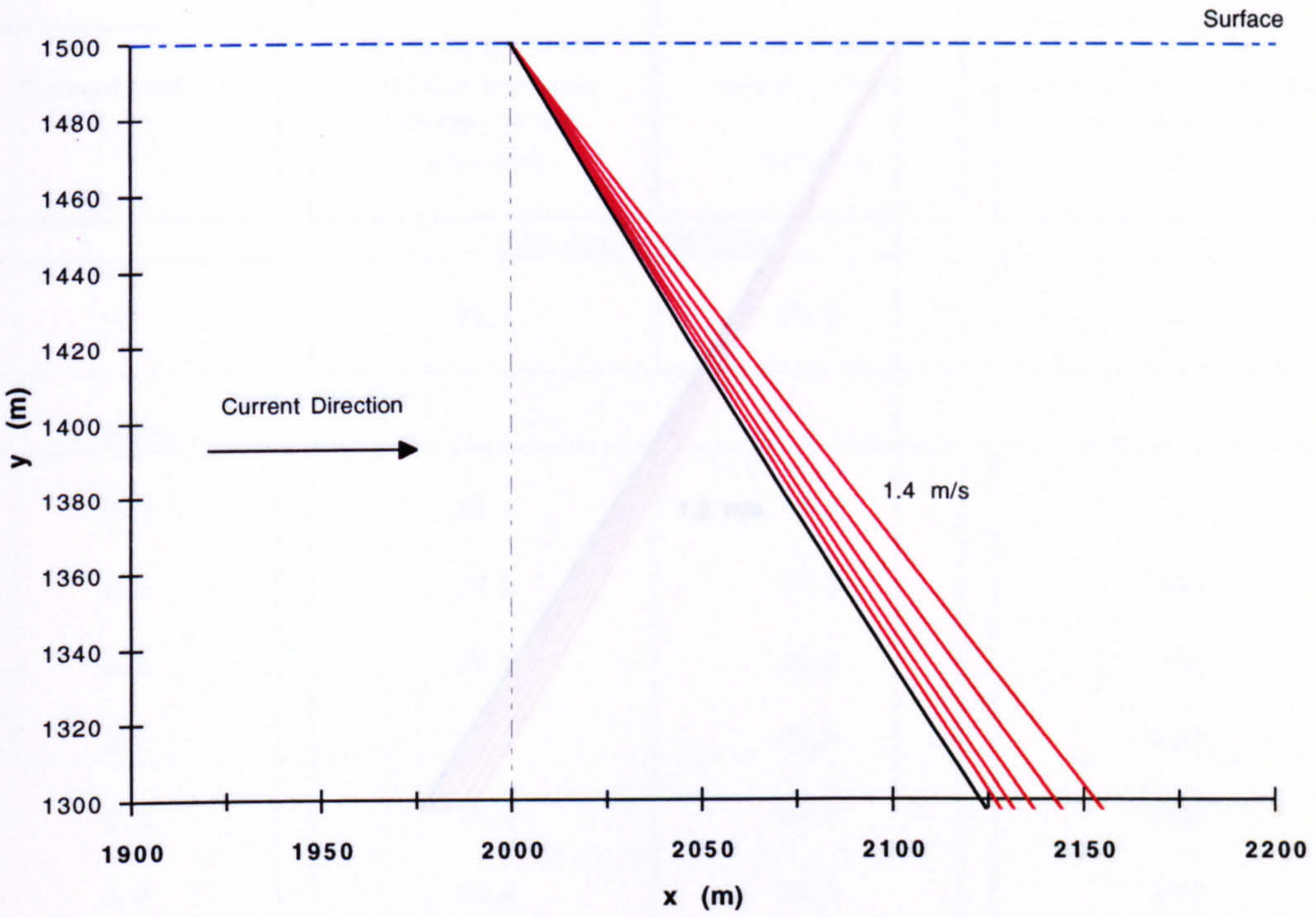

Current velocities 0.6 - 1.4 m/s (0.2 m/s increments)

Seabed End

(b)

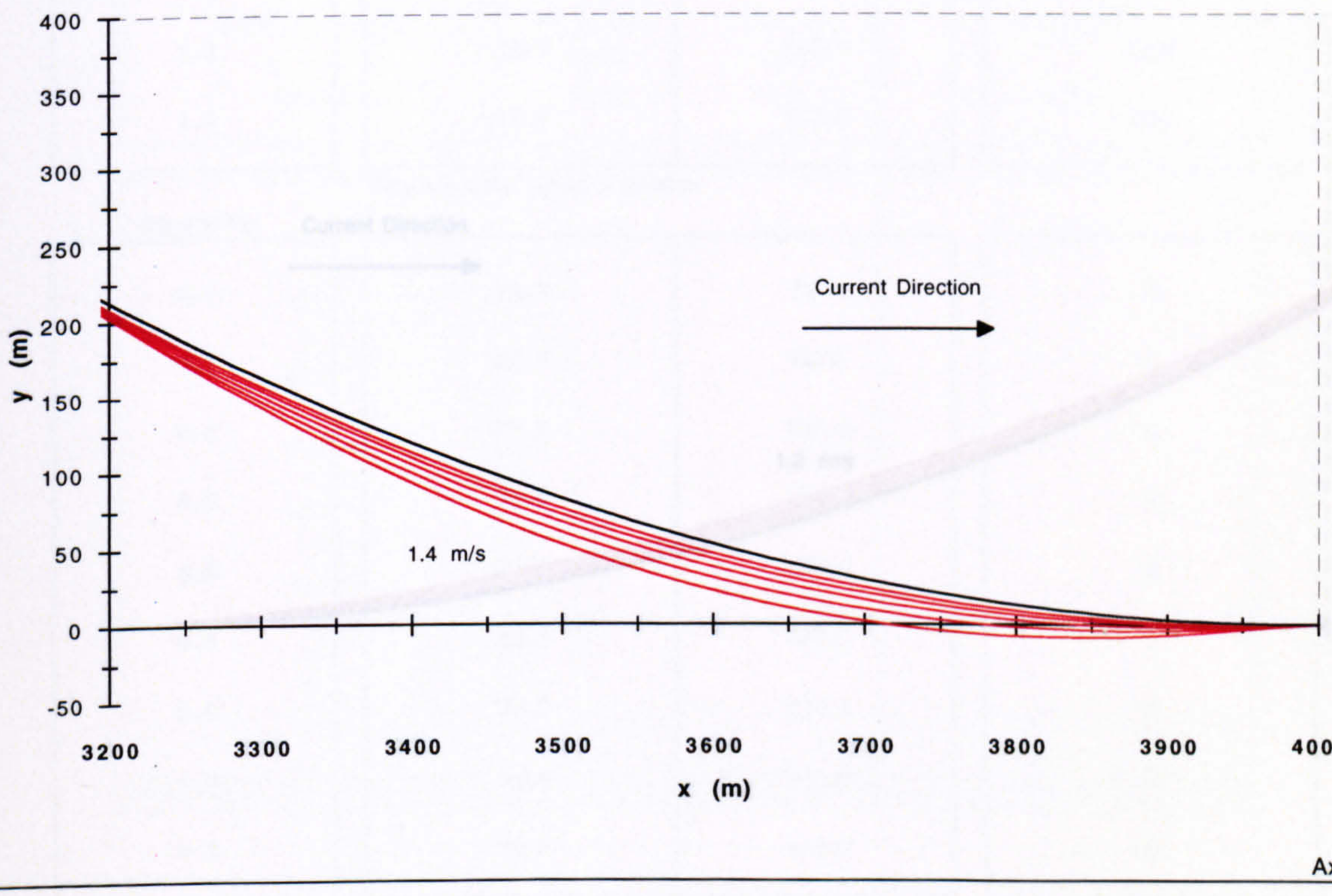

Axes to Scale

Horizontal Surface Offset = 2000 m

Sea Depth = 1500 m

Submerged Unit Weight = 2000 N/m

Carrier Pipe Outer Diameter = 1.1 m

Figure 5.116

Riser Deflection Profiles for a Concave Current

Surface End

(a)

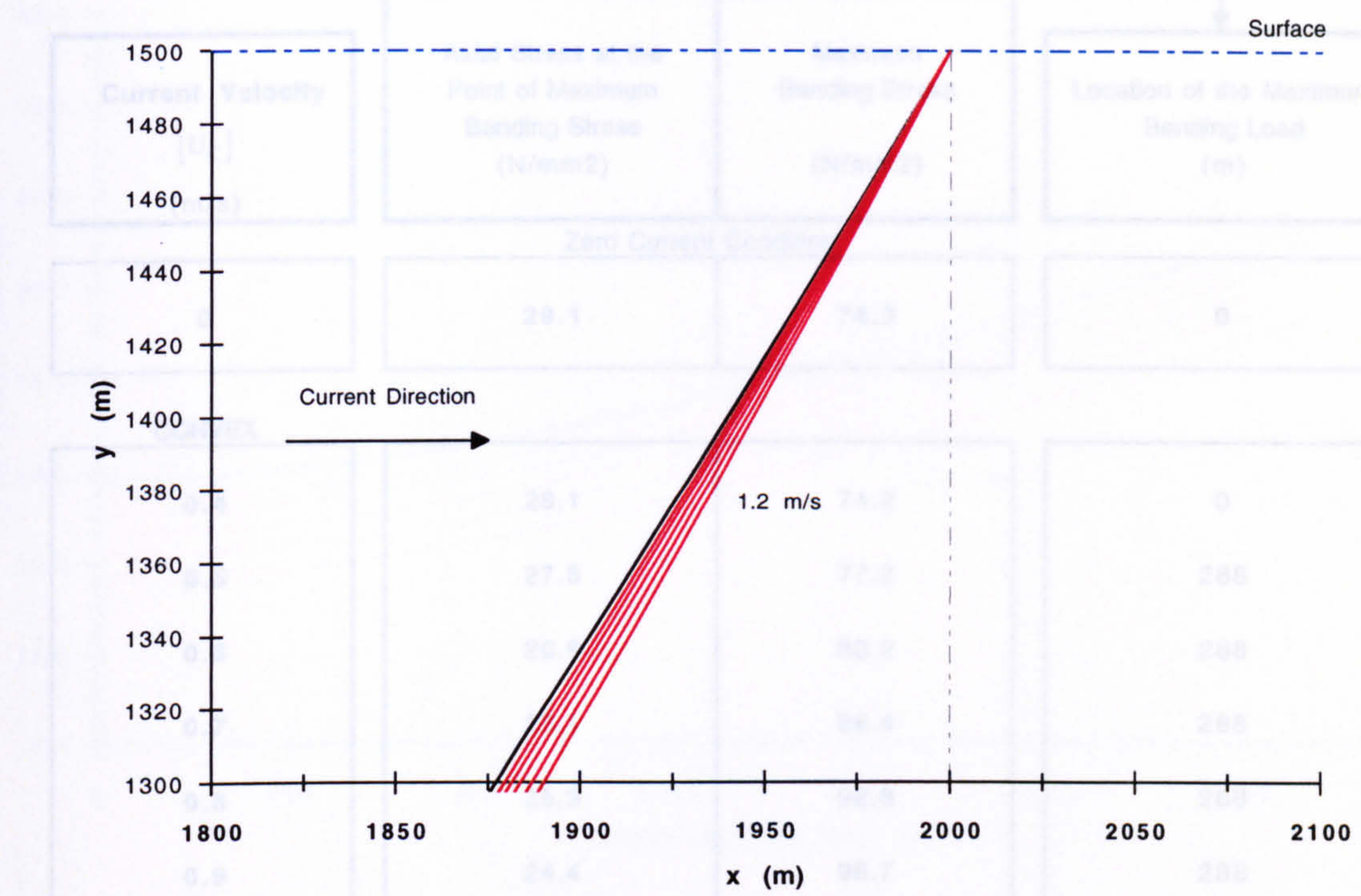

Current velocities 0.4 - 1.2 m/s (0.2 m/s increments)

Seabed End

(b)

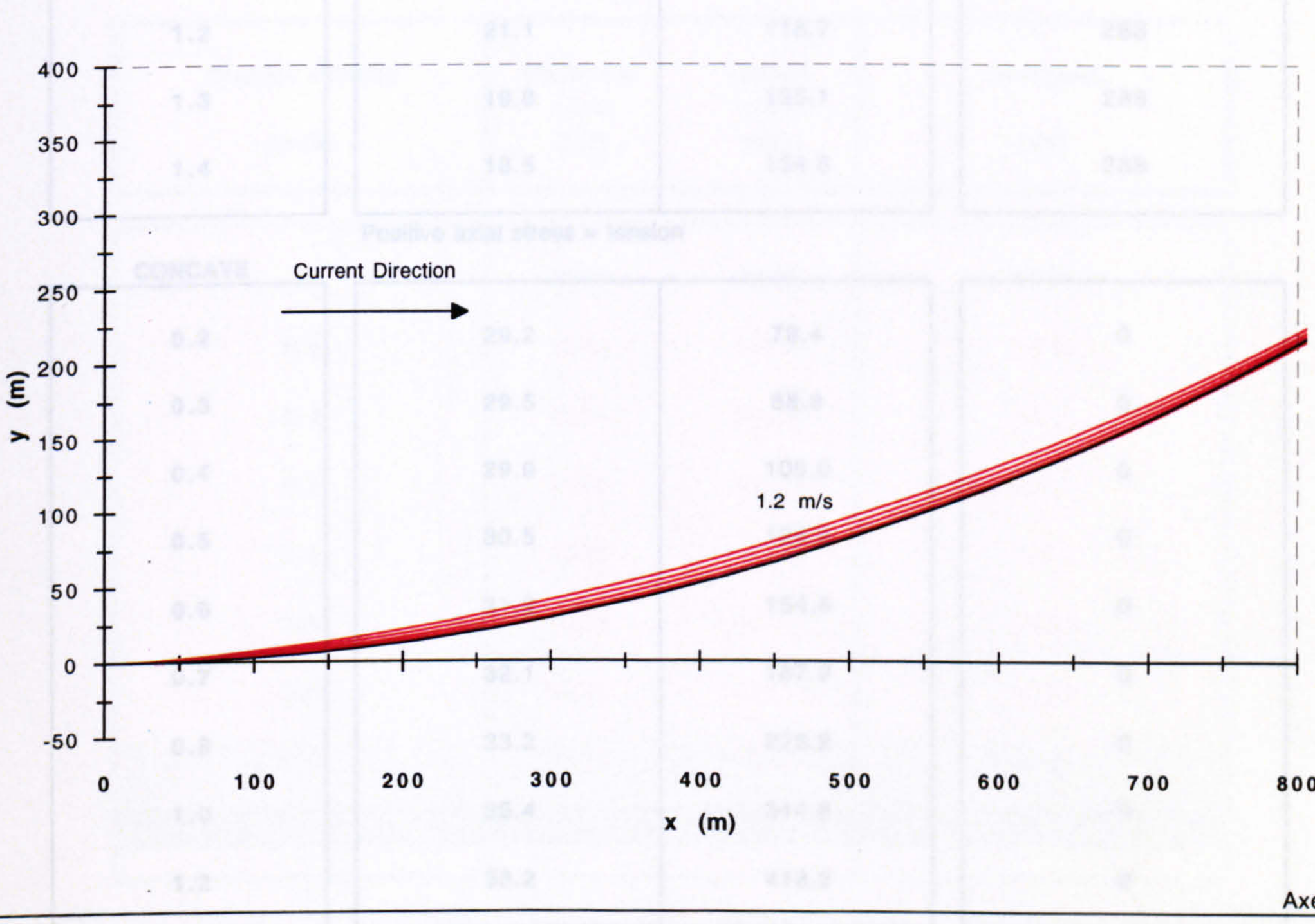

Horizontal Surface Offset = 2000 m

Submerged Unit Weight = 2000 N/m

Sea Depth = 1500 m

Carrier Pipe Outer Diameter = 1.1 m

Figure 5.117

Maximum Stress Conditions under Current Loading (a = 2000 m)

Submerged Unit Weight = 2000 N/m

Current Velocity $[U_C]$ (m/s)	Axial Stress at the Point of Maximum Bending Stress (N/mm2)	Maximum Bending Stress (N/mm2)	Location of the Maximum Bending Load (m)
			Measured along the riser from the seabed end
Zero Current Condition			
0	29.1	74.3	0
CONVEX			
0.4	28.1	74.2	0
0.5	27.5	77.2	288
0.6	26.9	83.2	288
0.7	26.1	88.4	288
0.8	25.3	92.8	288
0.9	24.4	98.7	288
1.0	23.3	105.8	288
1.1	22.2	110.2	288
1.2	21.1	118.7	288
1.3	19.8	125.1	288
1.4	18.5	134.6	288
Positive axial stress = tension			
CONCAVE			
0.2	29.2	78.4	0
0.3	29.5	88.8	0
0.4	29.9	105.0	0
0.5	30.5	126.6	0
0.6	31.2	154.8	0
0.7	32.1	187.9	0
0.8	33.2	225.2	0
1.0	35.4	314.6	0
1.2	38.2	418.2	0

Horizontal Surface Offset = 2000 m

Sea Depth = 1500 m

Carrier Pipe Outer Diameter = 1.1 m

Carrier Pipe Wall Thickness = 10 mm

Table 5.118

Axial Stress Distributions for a Convex Current

(a)

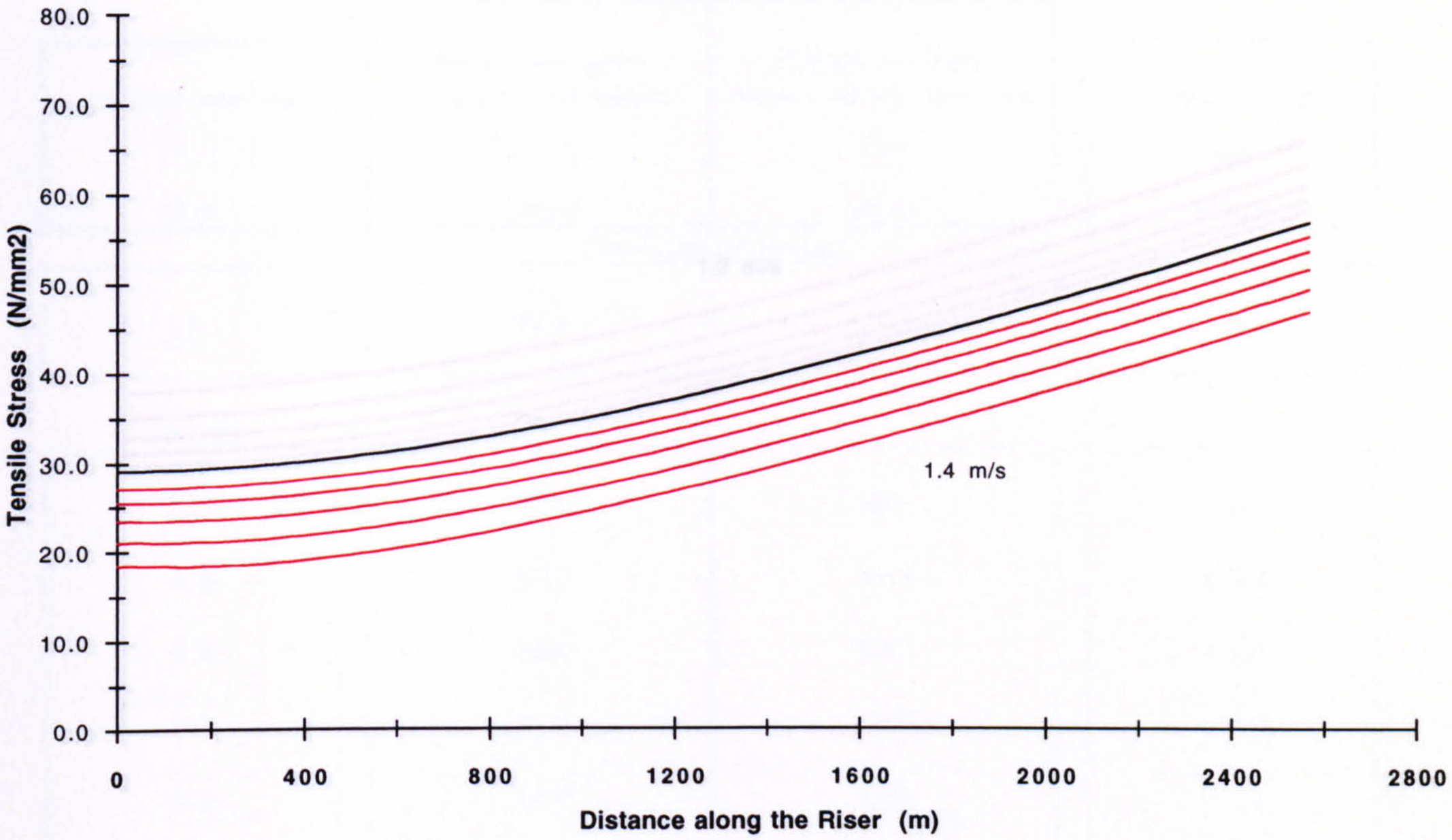

Current velocities 0.6 - 1.4 m/s (0.2 m/s increments)

Surface Forces for a Convex Current

(b)

Current Velocity (m/s)	Horizontal Load (kN)	Vertical Load (kN)	Axial Load (kN)
0	3067	5235	6067
0.2	3046	5187	6015
0.4	3031	5096	5929
0.6	3022	4963	5811
0.8	3020	4788	5661
1.0	3024	4574	5483
1.2	3034	4295	5259
1.4	3051	3968	5005

Horizontal Surface Offset = 2000 m

Sea Depth = 1500 m

Submerged Unit Weight = 2000 N/m

Carrier Pipe Outer Diameter = 1.1 m

Figure 5.119

Axial Stress Distributions for a Concave Current

(a)

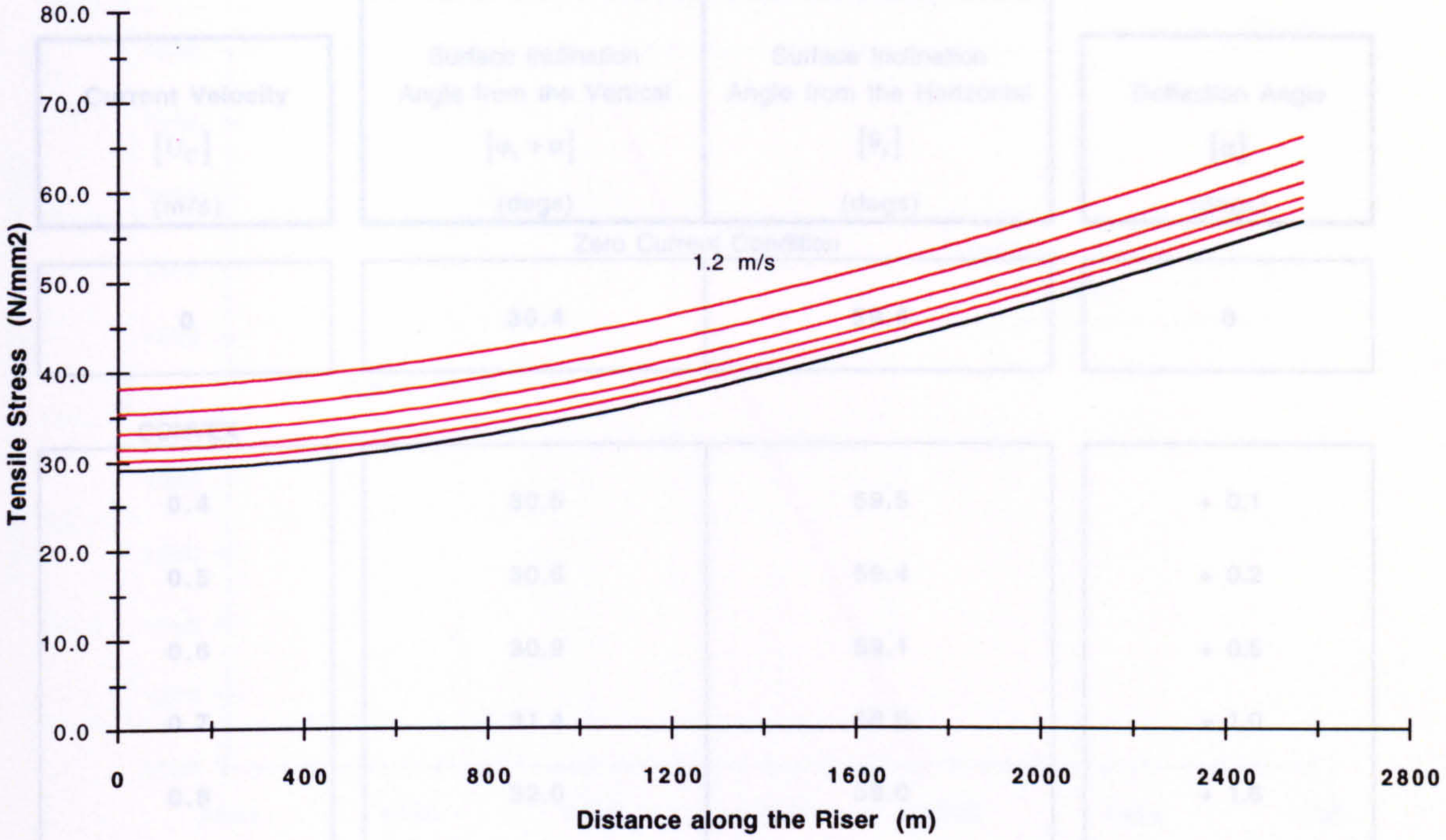

Current velocities 0.4 - 1.2 m/s (0.2 m/s increments)

Surface Forces for a Concave Current

(b)

Current Velocity (m/s)	Horizontal Load (kN)	Vertical Load (kN)	Axial Load (kN)
0	3067	5235	6067
0.2	3069	5278	6105
0.4	3079	5364	6185
0.6	3097	5505	6316
0.8	3126	5699	6500
1.0	3167	5942	6733
1.2	3218	6227	7009

Horizontal Surface Offset = 2000 m

Sea Depth = 1500 m

Submerged Unit Weight = 2000 N/m

Carrier Pipe Outer Diameter = 1.1 m

Figure 5.120

Surface Deflection Angles under Current Loading (a = 2000 m)

Submerged Unit Weight = 2000 N/m

Current Velocity $[U_C]$ (m/s)	Surface Inclination Angle from the Vertical $[\varphi_s + \alpha]$ (degs)	Surface Inclination Angle from the Horizontal $[\theta_s]$ (degs)	Deflection Angle $[\alpha]$ (degs)
	Zero Current Condition		
0	**30.4**	**59.6**	**0**
CONVEX			
0.4	30.5	59.5	+ 0.1
0.5	30.6	59.4	+ 0.2
0.6	30.9	59.1	+ 0.5
0.7	31.4	58.6	+ 1.0
0.8	32.0	58.0	+ 1.6
0.9	32.7	57.3	+ 2.3
1.0	33.3	56.7	+ 2.9
1.1	34.0	56.0	+ 3.6
1.2	34.9	55.1	+ 4.5
1.3	35.9	54.1	+ 5.5
1.4	37.0	53.0	+ 6.6
CONCAVE			
0.2	30.4	59.6	0
0.3	30.3	59.7	- 0.1
0.4	30.1	59.9	- 0.3
0.5	29.7	60.3	- 0.7
0.6	29.5	60.5	- 0.9
0.7	29.2	60.8	- 1.2
0.8	28.8	61.2	- 1.6
1.0	28.0	62.0	- 2.4
1.2	27.2	62.8	- 3.2

Horizontal Surface Offset = 2000 m

Sea Depth = 1500 m

Carrier Pipe Outer Diameter = 1.1 m

Carrier Pipe Wall Thickness = 10 mm

Table 5.121

The Effect of Drag Coefficient on the Deflection Profile

Surface End

(a)

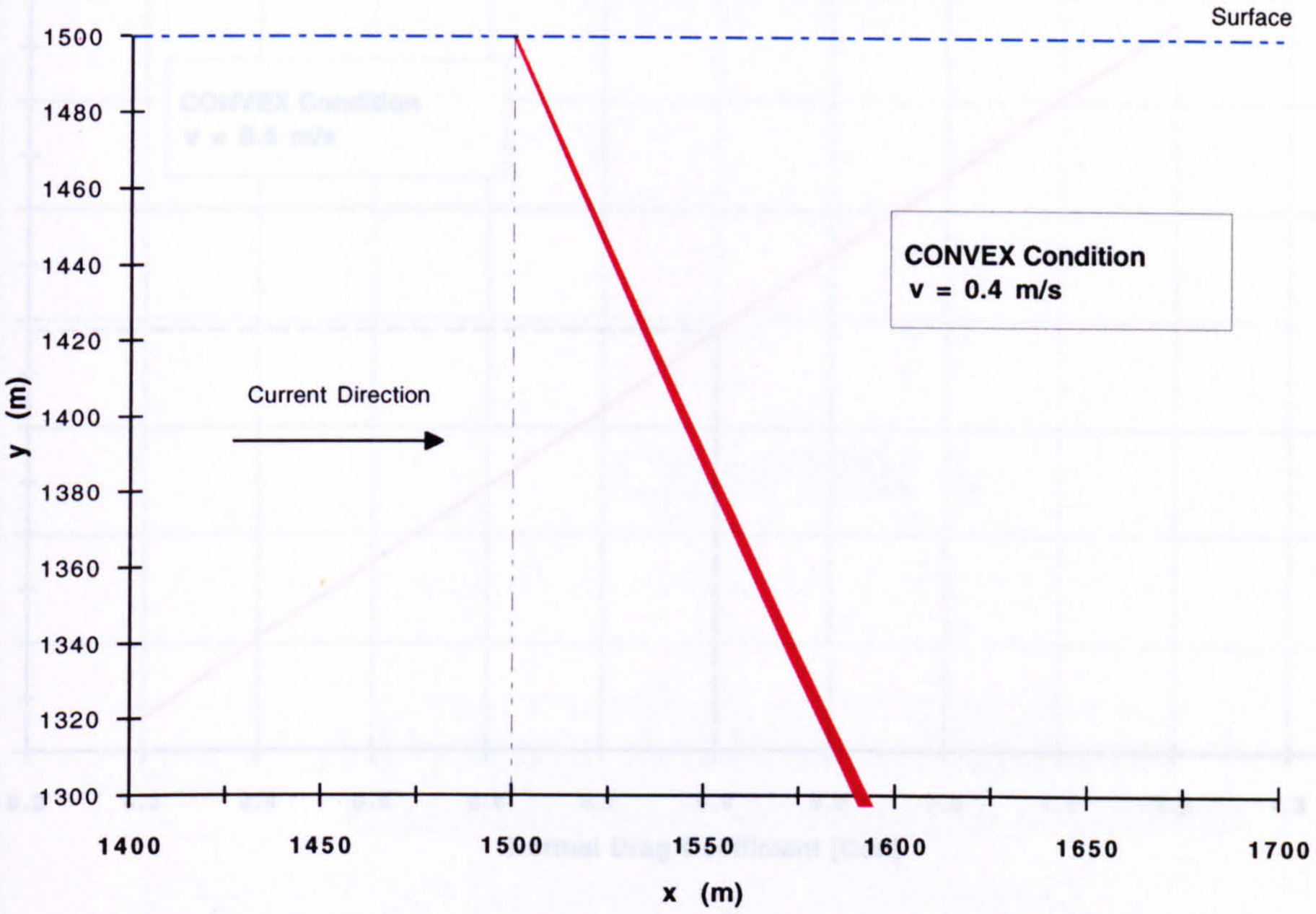

Drag Coefficients 0.3 - 1.2 (0.1 increments)

Seabed End

(b)

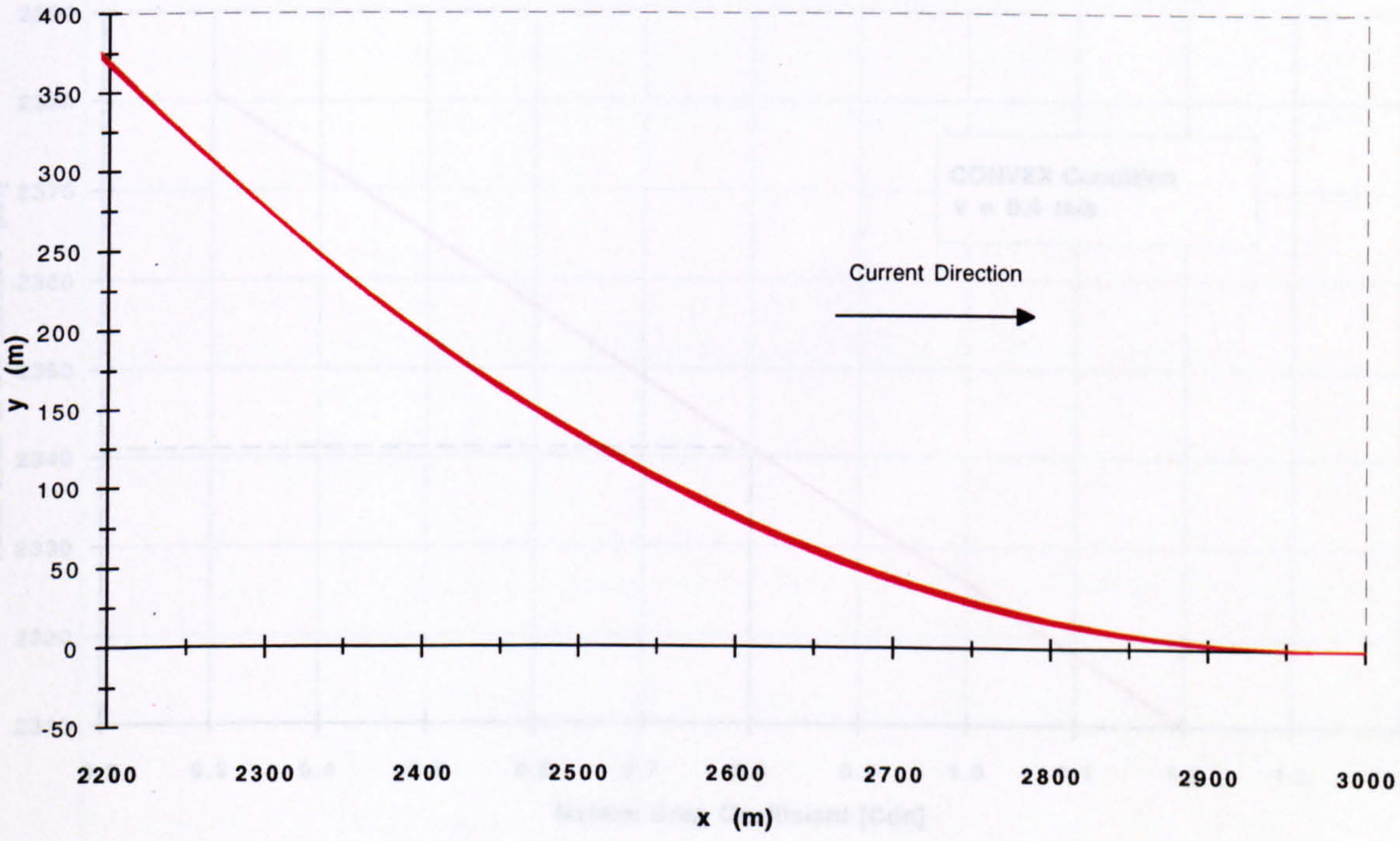

Axes to Scale

Horizontal Surface Offset = 1500 m

Sea Depth = 1500 m

Submerged Unit Weight = 1000 N/m

Carrier Pipe Outer Diameter = 1.1 m

Figure 5.122

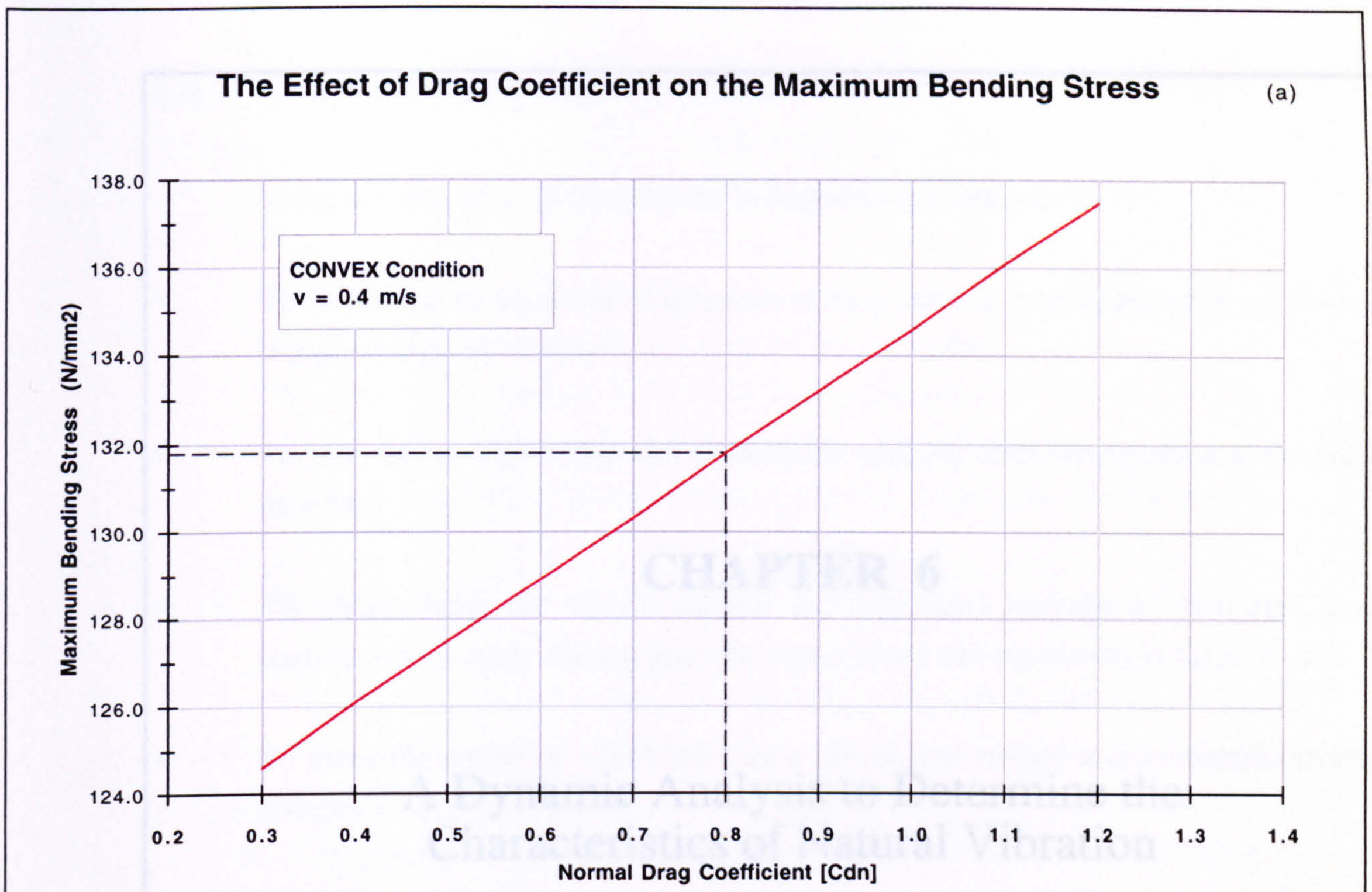

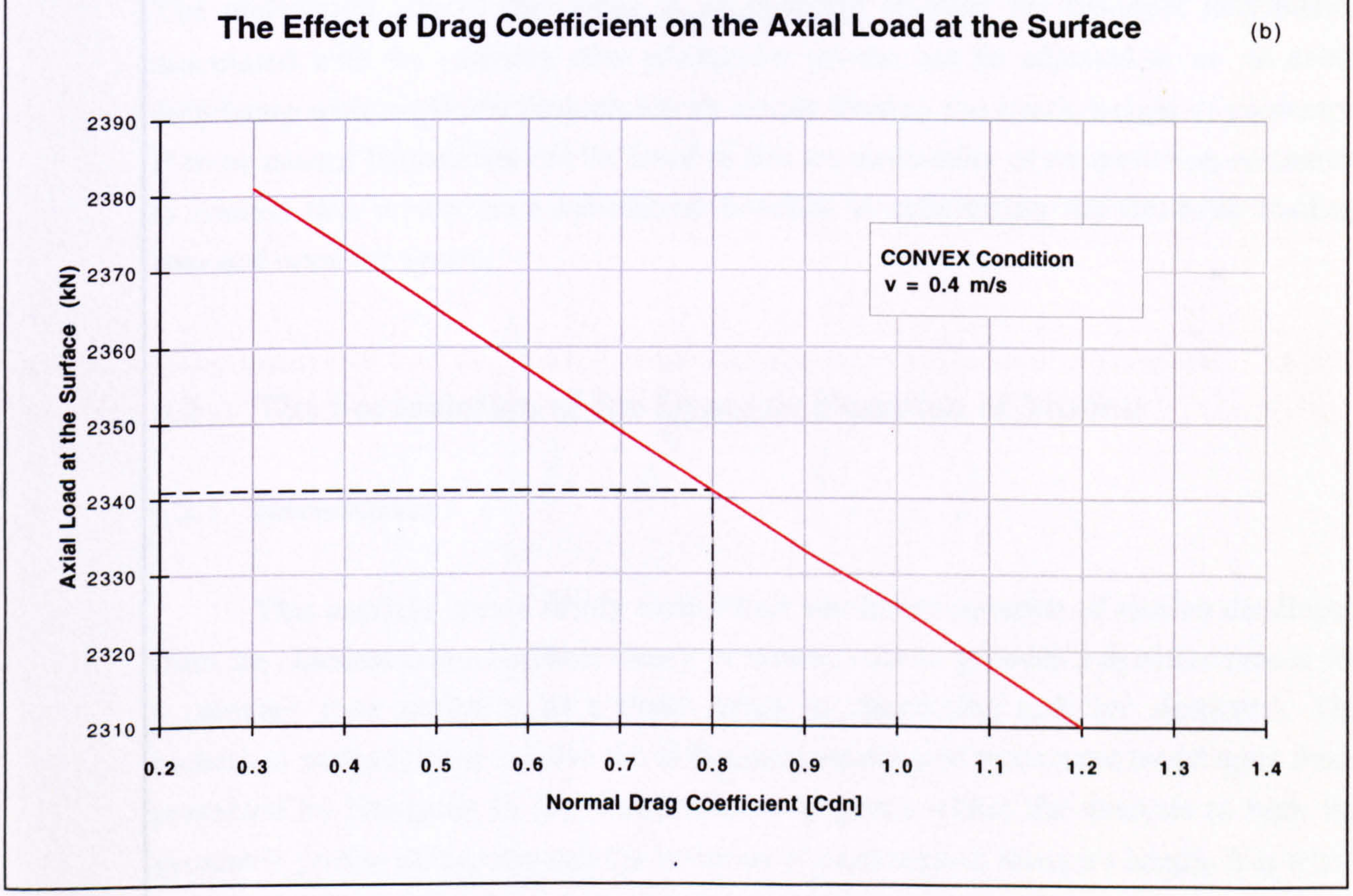

Horizontal Surface Offset = 1500 m

Submerged Unit Weight = 1000 N/m

Sea Depth = 1500 m

Carrier Pipe Outer Diameter = 1.1 m

Figure 5.123

CHAPTER 6

A Dynamic Analysis to Determine the Characteristics of Natural Vibration

6.1 General Description

There are five principle objectives or stages to this analysis:

- To formulate an equation of dynamic motion from a general equation of motion using a numerical method.

- To carry out an eigenvalue and eigenvector analysis from the equation of dynamic motion.

- To obtain both the riser's natural (or resonant) periods of vibration and corresponding mode shapes from the eigenvalues and eigenvectors respectively.

- To asses the extent to which the riser's submerged weight and geometric profile influence the natural periods.

- To verify the results using a published analytical method.

The underlying aim of this study is to establish whether the resonant frequencies associated with the catenary riser production system can be adjusted so as to avoid coinciding with excitation frequencies by simply altering the riser's weight or geometry. If these natural frequencies can be *tuned* so that the probability of encountering resonance is limited this would have substantial benefits in minimising the dynamic loading imposed upon the system.

6.2 The Formulation of the Dynamic Equation of Motion

6.2.1 Introduction

This analysis uses a firmly established non-linear equation of motion developed from the classical Euler-Kirchoff theory of slender rods to generate a dynamic matrix for a catenary riser modelled as a finite series of connecting rods (or elements). The numerical methods used to solve the differential equation of motion are based upon those presented by Nordgren in [3]. Consideration is given within the analysis to both the geometric profile of the riser and the variation of axial tension along it's length. It is worth reiterating that the tension load distribution along the riser (for a zero current condition) is a function of it's submerged unit weight, size and geometric profile.

6.2.2 Assumptions

The following assumptions are adhered to throughout the analysis:

- The catenary riser is inextensible.
- The entire length of riser is subjected to a tension load
- The riser is simply supported at both the seabed and surface ends
- The bending stiffness and torsional rigidity are negligible
- The riser is materially and geometrically uniform along its whole length.

6.2.3 Equation of Motion

In the classical theory of rods, the behaviour of long thin bars is described in terms of the position of the centreline of the bar. The centreline of the rod is a space curve ***r(s,t)*** as illustrated in Figure 6.1. The space curve is defined by the position vector ***r*** which is a function of arc length *s* (measured along the curve) and time *t*. The non-linear equation of motion in vector form can be written as:

$$F' + q = m\ddot{r} \tag{6.1}$$

where: F' = resultant force on the cross-section

q = applied force per unit length

m = mass per unit length (subsequently referred to as the unit mass)

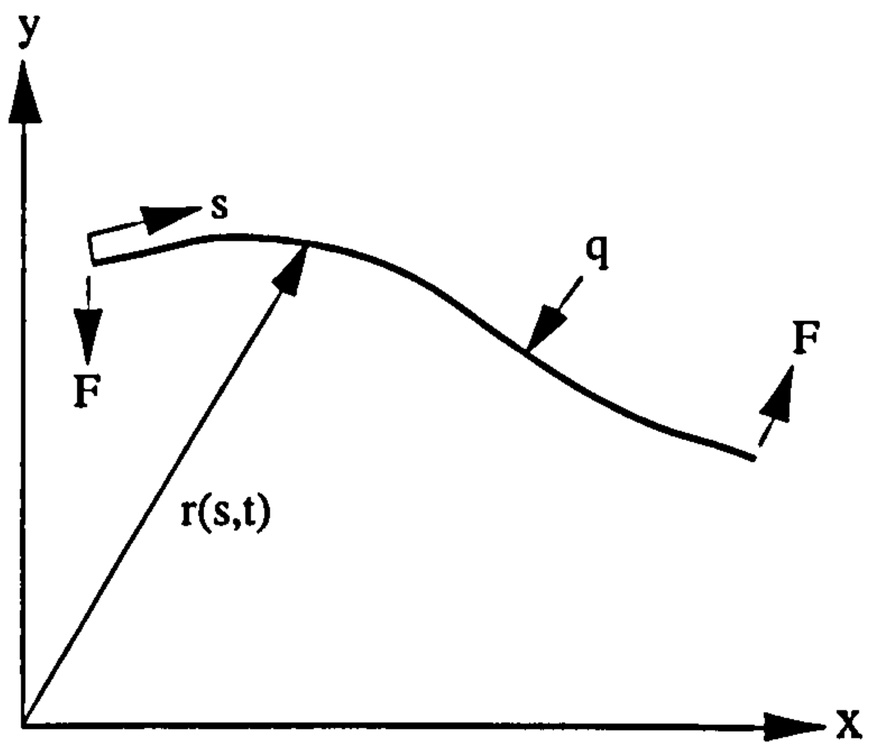

Figure 6.1

Centreline of Rod

The unit tangent to the space curve is r' and the principle normal is directed along r''. A prime denotes differentiation with respect to arc length and a superposed dot denotes differentiation with respect to time i.e.

$$F' \equiv \frac{dF}{ds} \tag{6.2}$$

and

$$\ddot{r} \equiv \frac{d^2r}{dt^2} \tag{6.3}$$

Since this analysis is solely concerned with evaluating the risers natural frequency characteristics the applied force term q can be neglected. Equation (6.1) can therefore be reduced to:

$$F' = m\ddot{r} \tag{6.4}$$

Tension

The axial tension load T exerted upon the riser's cross-section can be defined by:

$$T = F.r' \tag{6.5}$$

Axial Deformation

Stretch of the rod centreline is given by:

$$\frac{1}{2}(r'.r' - 1) = \frac{T}{AE} \tag{6.6}$$

where: AE = axial stiffness

However if the rod is assumed to be inextensible,

$$\frac{1}{2}(r'.r' - 1) = 0 \tag{6.7}$$

or

$$r'.r' = 1 \tag{6.8}$$

Axial stretch is not significant for most riser applications. Inclusion of stretch in numerical models is straight forward, but may introduce high frequency components of the response which, in turn, may be undesirable from a computational point of view.

The scalar product of r' with both sides of Eqn (6.5) followed by the application of Eqn (6.8), results in the following expression:

$$T.r' = F \tag{6.9}$$

If this is substituted into Eqn (6.4), the vector equation of motion becomes:

$$(T.r')' = m\ddot{r} \tag{6.10}$$

6.2.4 Finite Difference Numerical Computation

This analysis uses a Finite-Difference numerical method to solve the second order non-linear differential equation of motion as given by Eqn (6.10).

When differential equations cannot be integrated in closed form, numerical methods must be employed. The method selected for this analysis allows the second order differential equation of motion to be integrated directly without a change in form.

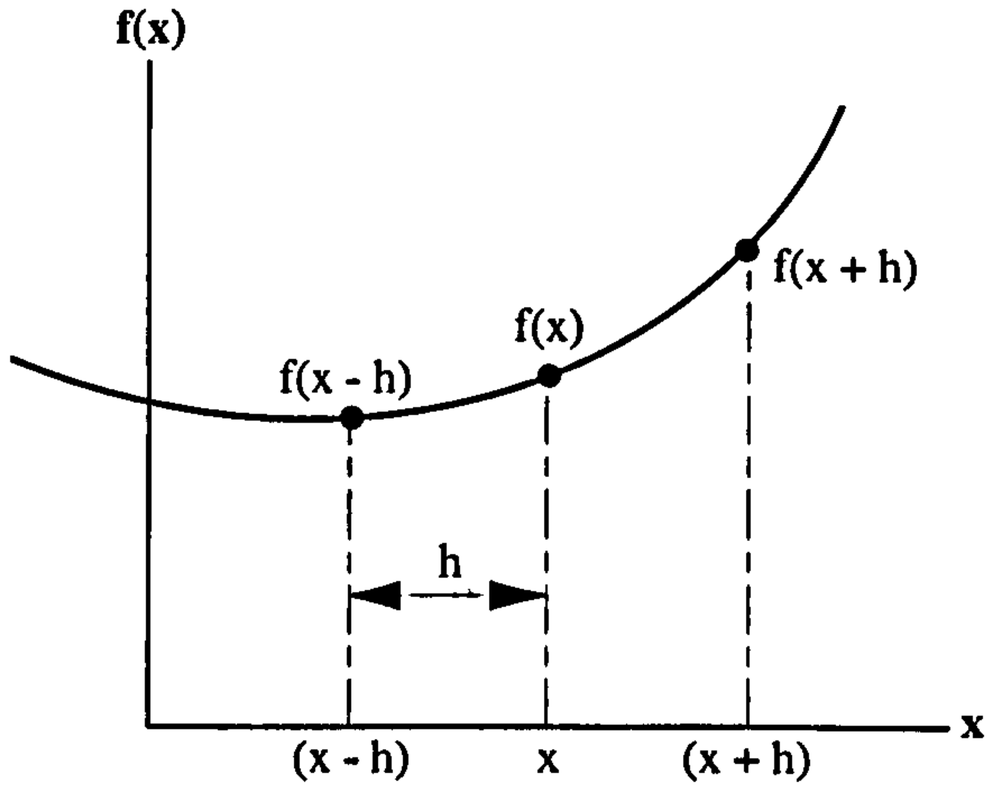

Figure 6.2

Finite-Difference Method

The following procedure is known as the central difference method, the basis of which can be developed from the Taylor expansion of $f(x + h)$ and $f(x - h)$.

$$f(x+h) = f(x) + h f'(x) + \frac{h^2}{2} f''(x) + \frac{h^3}{6} f'''(x) \tag{6.11}$$

$$f(x-h)=f(x)-hf'(x)+\frac{h^2}{2}f''(x)-\frac{h^3}{6}f'''(x) \tag{6.12}$$

Subtracting and ignoring higher order terms results in the following expression

$$f'(x)\approx\frac{f(x+h)-f(x-h)}{2h} \tag{6.13}$$

This equation is referred to as the Central Difference First Derivative Formula.

If Eqns (6.11) and (6.12) are added together

$$f''(x)\approx\frac{f(x+h)-2f(x)+f(x-h)}{h^2} \tag{6.14}$$

a Central Difference Second Derivative Formula is generated.

In both Eqns (6.13) and (6.14) the ignored terms are of order h^2 therefore introducing what is known as truncation errors.

6.2.5 Applying the Equation of Motion to a Simple Vibrating System

The following analysis applies the equation of motion as given by Eqn (6.10) to a stretched string in lateral vibration using the FD method presented, in order to illustrate how the dynamic equation of motion is formulated.

A flexible string as shown in Figure 6.3, of mass m per unit length is stretched under a tension T. By assuming the lateral deflection x of the string to be small, the change in tension with deflection is negligible and can be ignored. The string which is secured at each end, is divided up into four equal length (ds) elements which are connected to one another by the nodes, n = 1, 2 and 3, (see Figure 6.3). The boundary conditions for the system are as follows:

$$x_0=0 \qquad x_4=0$$
$$\ddot{x}_0=0 \qquad \ddot{x}_4=0$$

The equation of motion can be defined as:

$$m\ddot{x}=(Tx')' \tag{6.15}$$

Constant tension string of mass
m per unit length

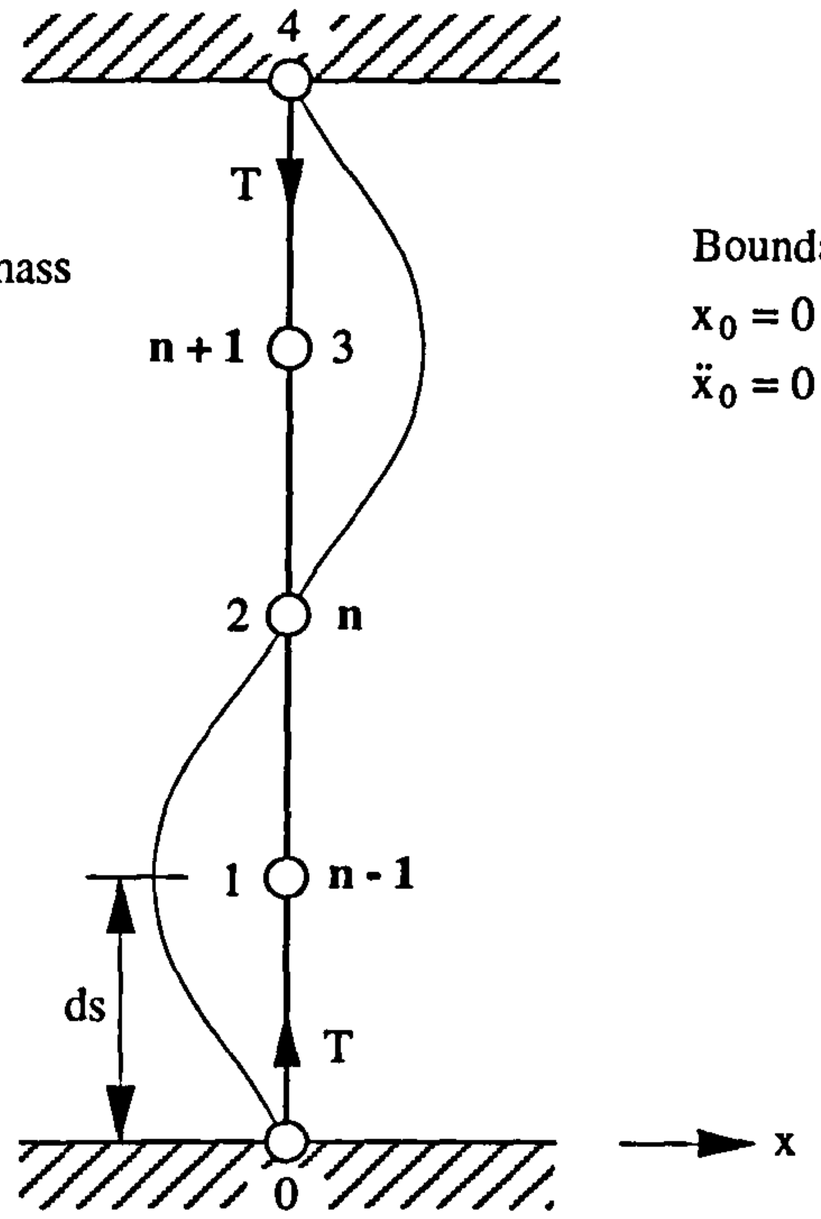

Boundary Conditions

$x_0 = 0 \qquad x_4 = 0$

$\ddot{x}_0 = 0 \qquad \ddot{x}_4 = 0$

Figure 6.3

A Stretched String in Lateral Vibration

Position Vector $r_n = x_n i + y_n j$

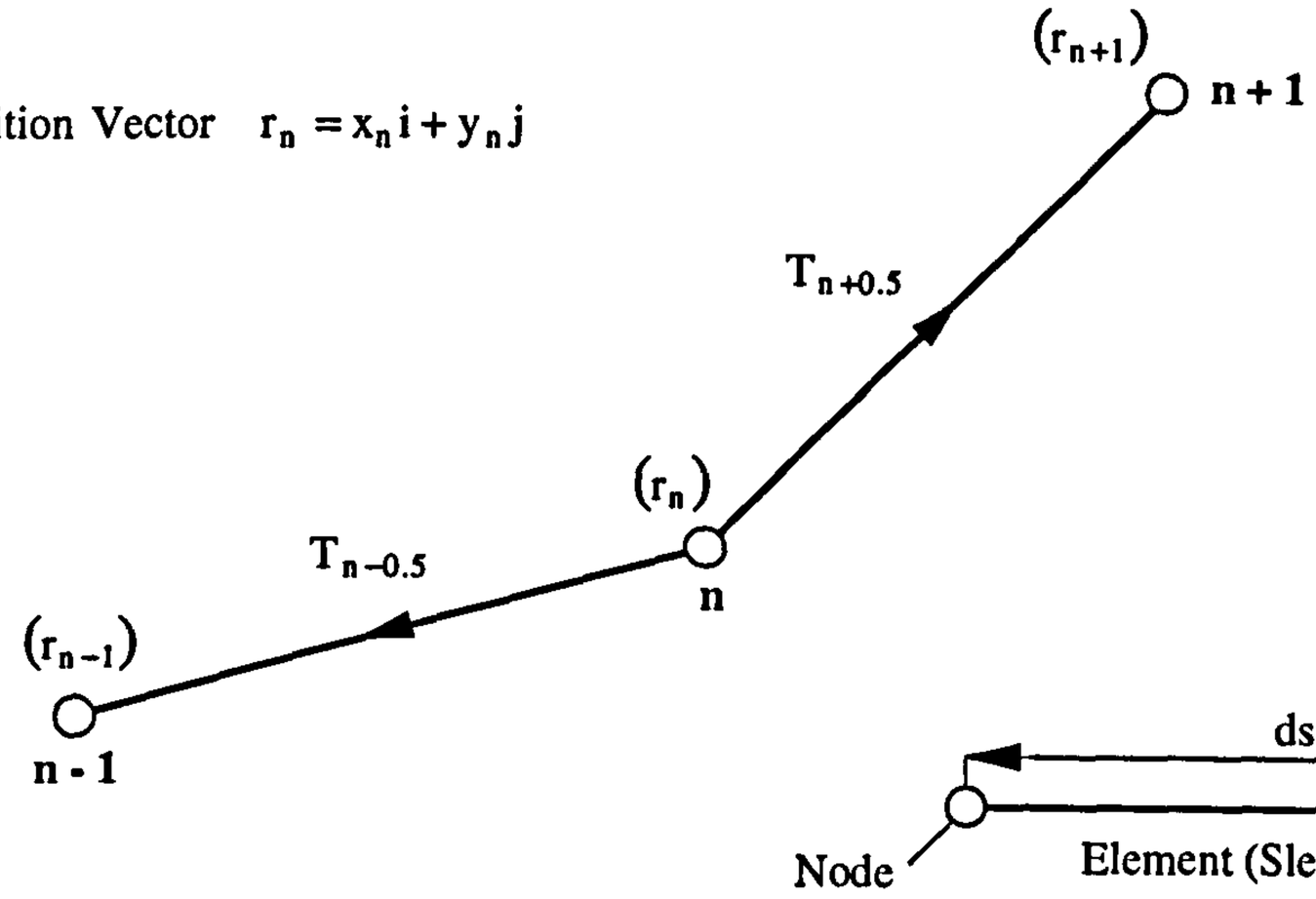

Figure 6.4

Dynamic Model

T is constant along the length of the string and hence:

$$m\ddot{x} = T x'' \tag{6.16}$$

$$\ddot{x} = \left(\frac{T}{m}\right) x'' \tag{6.17}$$

Let:
$$a^2 = \left(\frac{T}{m}\right) \tag{6.18}$$

therefore

$$\ddot{x} = a^2 x'' \tag{6.19}$$

The second derivative central difference formula (see Eqn (6.14)) can be written as follows:

$$x_n'' = \frac{1}{ds^2}\left(x_{n+1} - 2x_n + x_{n-1}\right) \tag{6.20}$$

If this is substituted into Eqn (6.19):

$$\ddot{x}_n = \left(\frac{a}{ds}\right)^2 \left[x_{n+1} - 2x_n + x_{n-1}\right] \tag{6.21}$$

This equation can then be applied to the nodes **n = 1, 2** and **3**.

n = 1
$$\ddot{x}_1 = \left(\frac{a}{ds}\right)^2 \left[x_2 - 2x_1 + x_0\right] = \left(\frac{a}{ds}\right)^2 \left[-2x_1 + x_2\right] \tag{6.22}$$

n = 2
$$\ddot{x}_2 = \left(\frac{a}{ds}\right)^2 \left[x_3 - 2x_2 + x_1\right] = \left(\frac{a}{ds}\right)^2 \left[x_1 - 2x_2 + x_3\right] \tag{6.23}$$

n = 3
$$\ddot{x}_3 = \left(\frac{a}{ds}\right)^2 \left[x_4 - 2x_3 + x_2\right] = \left(\frac{a}{ds}\right)^2 \left[x_2 - 2x_3\right] \tag{6.24}$$

These three equations can be transferred into a matrix format

$$\begin{Bmatrix} \ddot{x}_1 \\ \ddot{x}_2 \\ \ddot{x}_3 \end{Bmatrix} \begin{bmatrix} 1 & 0 & 0 \\ 0 & 1 & 0 \\ 0 & 0 & 1 \end{bmatrix} = \left(\frac{a}{ds}\right)^2 \begin{bmatrix} -2 & 1 & 0 \\ 1 & -2 & 1 \\ 0 & 1 & -2 \end{bmatrix} \begin{Bmatrix} x_1 \\ x_2 \\ x_3 \end{Bmatrix} \tag{6.25}$$

Let
$$-\mathbf{A} = \left(\frac{a}{ds}\right)^2 \begin{bmatrix} -2 & 1 & 0 \\ 1 & -2 & 1 \\ 0 & 1 & -2 \end{bmatrix} \tag{6.26}$$

and
$$\mathbf{I} = \begin{bmatrix} 1 & 0 & 0 \\ 0 & 1 & 0 \\ 0 & 0 & 1 \end{bmatrix} \tag{6.27}$$

The matrix *A* is referred to as the *system matrix*, or the dynamic matrix since the dynamic properties of the system are defined by this matrix. The tri-diagonal or symmetric nature of this matrix is a characterising feature of this FD analysis and should be noted. The matrix *I* is referred to as a *unit matrix*. Eqn (6.25) then becomes

$$\{\ddot{x}\}\mathbf{I} = -\mathbf{A}\{x\} \tag{6.28}$$

or
$$\mathbf{A}\{x\} + \{\ddot{x}\}\mathbf{I} = 0 \tag{6.29}$$

Assuming harmonic motion $\ddot{x} = -\omega^2 x$, where $\lambda = \omega^2$, Eqn (6.29) becomes

$$|\mathbf{A} - \lambda\mathbf{I}|\{X\} = 0 \tag{6.30}$$

The *characteristic* equation of the system is the determinant equated to zero, or

$$|\mathbf{A} - \lambda\mathbf{I}| = 0 \tag{6.31}$$

The roots λ of the characteristic equation are the *eigenvalues* and the natural frequencies of the system are determined from them by the relationship $\lambda = \omega^2$. By substituting λ into Eqn (6.30), enables the *eigenvectors* and hence the mode shapes to be obtained.

Eigen-problems can easily be solved using computer algorithms. These algorithms are usually written for the standard form of the equation written as Eqn (6.30), where the matrix *A* must be symmetric.

6.2.6 Applying the Equation of Motion to a Catenary Riser

The catenary riser is modelled as series of connecting elements or rods in an arrangement similar to that used in the static analysis FE model in Chapter 5. At both ends of all the elements are nodes which lie within an x-y plane and are defined in terms

of their location by a position vector *r* such that $r = x\,i + y\,j$, see Figure 6.4. A small nodal displacement is represented by the vectorial expression $\delta r = \delta x\,i + \delta y\,j$. However the axial tension *T* in the riser is a scalar quantity and is varied along the riser on an elemental basis. Both the tension and the position vector along with its differential derivative can be broken up into their static and dynamic components:

$$r = r_0 + \delta r \tag{6.32}$$

$$r' = r_0' + \delta r' \tag{6.33}$$

$$T = T_0 + \delta T \tag{6.34}$$

$$\ddot{r} = \ddot{r}_0 + \delta\ddot{r} \qquad \ddot{r}_0 = 0 \quad \text{therefore } \ddot{r} = \delta\ddot{r} \tag{6.35}$$

where:

- subscript *0* denotes the static or reference value.
- δ term corresponds to the small amplitude dynamic component

If the equation of motion is applied to a node *n*.

$$m\,\delta\ddot{r}_n = [T\,r']_n \tag{6.36}$$

Expanding the term $[T\,r']_n'$ using Eqns (6.33) and (6.34)

$$m\,\delta\ddot{r}_n = \left[(T_0 + \delta T)(r_0' + \delta r')\right]_n' \tag{6.37}$$

$$m\,\delta\ddot{r}_n = \left[T_0\,r_0' + \delta T\,r_0' + T_0\,\delta r' + \delta T\,\delta r'\right]_n' \tag{6.38}$$

The term $T_0\,r_0'$ is a static tension term and can neglected since $\sum F_{static} = 0$ as required by small amplitude motions about the equilibrium position. The term $\delta T\,\delta r'$ can also be neglected on the basis of it being a second order term. Therefore Eqn (6.38) can be reduced to

$$m\ddot{r}_n = \left[\delta T\,r_0' + T_0\,\delta r'\right]_n' \tag{6.39}$$

The term δT arises from a change in riser geometry and is proportional to $\delta r'$, however this term has to be removed in order to enable an eigenvalue analysis to be carried out.

This is achieved by introducing the extensibility relationship into the analysis as defined previously by Eqn (6.6) i.e.

$$\frac{1}{2}(\mathbf{r}'.\mathbf{r}'-1)=\frac{T}{AE} \tag{6.40}$$

Both sides of this equation can be expanded by substituting in Eqns (6.33) and (6.34)

$$\frac{1}{2}\left[(\mathbf{r}_0'+\delta\mathbf{r}').(\mathbf{r}_0'+\delta\mathbf{r}')\right]=\left(\frac{T_0}{AE}+\frac{\delta T}{AE}\right) \tag{6.41}$$

$$\frac{1}{2}\left[\mathbf{r}_0'.\mathbf{r}_0'+2\,\mathbf{r}_0'.\delta\mathbf{r}'+\delta\mathbf{r}'.\delta\mathbf{r}'-1\right]=\frac{T_0}{AE}+\frac{\delta T}{AE} \tag{6.42}$$

The term $\delta\mathbf{r}.\delta\mathbf{r}$ can be eliminated due to it's second order property. This allows Eqn (6.42) to be re-arranged as follows

$$(\mathbf{r}_0'.\mathbf{r}_0'-1)+2\,\mathbf{r}_0'.\delta\mathbf{r}'=\frac{2T_0}{AE}+\frac{2\delta T}{AE} \tag{6.43}$$

Since $$(\mathbf{r}_0'.\mathbf{r}_0'-1)=\frac{2T_0}{AE}$$ (from Eqn (6.40)) (6.44)

$$2\,\mathbf{r}_0'.\delta\mathbf{r}'=\frac{2\delta T}{AE} \tag{6.45}$$

therefore

$$\delta T=AE(\mathbf{r}_0'.\delta\mathbf{r}') \tag{6.46}$$

This expression can be checked by applying inextensibility and letting $AE\Rightarrow\infty$. By definition δT is small (small amplitudes) and so the term $\mathbf{r}_0'.\delta\mathbf{r}'$ must therefore equal zero. If the inextensibility condition as defined by Eqn (6.7) is expanded using Eqn (6.33)

$$\frac{1}{2}(\mathbf{r}'.\mathbf{r}'-1)=0 \tag{6.47}$$

$$(\mathbf{r}_0'+\delta\mathbf{r}').(\mathbf{r}_0'+\delta\mathbf{r}')-1=0 \tag{6.48}$$

$$\mathbf{r}_0'.\mathbf{r}_0'+2\,\mathbf{r}_0'.\delta\mathbf{r}'+\delta\mathbf{r}'.\delta\mathbf{r}'-1=0 \tag{6.49}$$

Since $\mathbf{r}_0'.\mathbf{r}_0' - 1 = 0$ and $\delta\mathbf{r}'.\delta\mathbf{r}' \approx 0$ (2nd order)

$$\mathbf{r}_0'.\delta\mathbf{r}' = 0 \tag{6.50}$$

i.e. the same answer as before!

If the term δT is removed from Eqn (6.39) by substituting in Eqn (6.46), the following formulation is obtained

$$m\delta\ddot{\mathbf{r}}_n = \underset{1}{\left[AE\left(\mathbf{r}_0'.\delta\mathbf{r}'\right)\mathbf{r}_0'\right]_n'} + \underset{2}{\left[T_0\,\delta\mathbf{r}'\right]_n'} \tag{6.51}$$

It should be noted that the inextensibility condition can still be maintained despite the presence of the axial stiffness term AE by simply letting elasticity modulus E equal a very large number. Further details on this are given in a later section.

Both terms (1 and 2) on the RHS of the above equation can be integrated using the *central difference, first derivative formula* as defined by Eqn (6.14).

Integrating Term 1

$$\left[AE\left(\mathbf{r}_0'.\delta\mathbf{r}'\right)\mathbf{r}_0'\right]_n' = AE\left[\left(\mathbf{r}_0'.\delta\mathbf{r}'\right)\mathbf{r}_0'\right]_n' \tag{6.52}$$

$$= \frac{AE}{ds}\left[\left(\left(\mathbf{r}_0'.\delta\mathbf{r}'\right)\mathbf{r}_0'\right)_{n+1/2} - \left(\left(\mathbf{r}_0'.\delta\mathbf{r}'\right)\mathbf{r}_0'\right)_{n-1/2}\right] \tag{6.53}$$

(a) (b)

By definition

$$\mathbf{r}_0' = x_0'\,\mathbf{i} + y_0'\,\mathbf{j} \tag{6.54}$$

$$\delta\mathbf{r}' = \delta x'\,\mathbf{i} + \delta y'\,\mathbf{j} \tag{6.55}$$

Before numerical integration is carried out these two vector component equations can be substituted into both the RHS terms of Eqn (6.53).

(a) $$\left(\left(\mathbf{r}_0'.\delta\mathbf{r}'\right)\mathbf{r}_0'\right)_{n+1/2} = \left[\left(x_0'\,\delta x' + y_0'\,\delta y'\right).\left(x_0'\,\mathbf{i} + y_0'\,\mathbf{j}\right)\right]_{n+1/2} \tag{6.56}$$

$$= \left[x_0'\left(x_0'\,\delta x' + y_0'\,\delta y'\right)\mathbf{i} + y_0'\left(x_0'\,\delta x' + y_0'\,\delta y'\right)\mathbf{j}\right]_{n+1/2} \tag{6.57}$$

$$= \left[\left(x_0'^2 \, \delta x' + x_0 \, y_0' \, \delta y' \right) i + \left(x_0' y_0' \, \delta x' + y_0'^2 \, \delta y' \right) j \right]_{n+1/2} \tag{6.58}$$

From the central difference, first derivative formula

$$\delta x'_{n+1/2} = \frac{1}{ds} \left(\delta x_{n+1} - \delta x_n \right) \tag{6.59}$$

$$\delta y'_{n+1/2} = \frac{1}{ds} \left(\delta y_{n+1} - \delta y_n \right) \tag{6.60}$$

Substituting Eqns (6.59) and (6.60) into Eqn (6.58)

$$\left(\left(r_0' . \delta r' \right) r_0' \right)_{n+1/2} = \left(x_0'^2 \right)_{n+1/2} \frac{1}{ds} \left(\delta x_{n+1} - \delta x_n \right) i$$

$$+ \left(x_0' \, y_0' \right)_{n+1/2} \frac{1}{ds} \left(\delta y_{n+1} - \delta y_n \right) i + \left(x_0' \, y_0' \right)_{n+1/2} \frac{1}{ds} \left(\delta y_{n+1} - \delta y_n \right) j$$

$$= \left(y_0'^2 \right)_{n+1/2} \frac{1}{ds} \left(\delta y_{n+1} - \delta y_n \right) j \tag{6.61}$$

$$\left(\left(r_0' . \delta r' \right) r_0' \right)_{n+1/2} = \frac{1}{ds} \left[\left(x_0'^2 \right)_{n+1/2} \delta x_{n+1} \, i - \left(x_0'^2 \right)_{n+1/2} \delta x_n \, i \right.$$

$$+ \left(x_0' \, y_0' \right)_{n+1/2} \delta y_{n+1} \, i - \left(x_0' \, y_0' \right)_{n+1/2} \delta y_n \, i$$

$$+ \left(x_0' \, y_0' \right)_{n+1/2} \delta x_{n+1} \, j - \left(x_0' \, y_0' \right)_{n+1/2} \delta x_n \, j$$

$$\left. + \left(y_0'^2 \right)_{n+1/2} \delta y_{n+1} \, j - \left(y_0'^2 \right)_{n+1/2} \delta y_n \, j \right] \tag{6.62}$$

Therefore

$$\left(\left(r_0' . \delta r' \right) r_0' \right)_{n+1/2} = \frac{1}{ds} \left[\left(x_0'^2 \, i + x_0' \, y_0' \, j \right)_{n+1/2} \delta x_{n+1} \right.$$

$$+ \left(x_0' \, y_0' \, i + y_0'^2 \, j \right)_{n+1/2} \delta y_{n+1} - \left(x_0'^2 \, i + x_0' \, y_0' \, j \right)_{n+1/2} \delta x_n$$

$$\left. - \left(x_0' \, y_0' \, i + y_0'^2 \, j \right)_{n+1/2} \delta y_n \right] \tag{6.63}$$

(b)
$$\left((r_0'.\delta r')r_0'\right)_{n-1/2} = \left[(x_0'\,\delta x' + y_0'\,\delta y').(x_0'\,i + y_0'\,j)\right]_{n-1/2} \tag{6.64}$$

$$= \left[x_0'\left(x_0'\,\delta x' + y_0'\,\delta y'\right)i + y_0'\left(x_0'\,\delta x' + y_0'\,\delta y'\right)j\right]_{n-1/2} \tag{6.65}$$

$$= \left[\left(x_0'^2\,\delta x' + x_0\,y_0'\,\delta y'\right)i + \left(x_0'y_0'\,\delta x' + y_0'^2\,\delta y'\right)j\right]_{n-1/2} \tag{6.66}$$

From the central difference, first derivative formula

$$\delta x'_{n-1/2} = \frac{1}{ds}\left(\delta x_n - \delta x_{n-1}\right) \tag{6.67}$$

$$\delta y'_{n-1/2} = \frac{1}{ds}\left(\delta y_n - \delta y_{n-1}\right) \tag{6.68}$$

Substituting Eqns (6.67) and (6.68) into Eqn (6.66) yields

$$\left((r_0'.\delta r')r_0'\right)_{n-1/2} = \frac{1}{ds}\Big[\left(x_0'^2\,i + x_0'\,y_0'\,j\right)_{n-1/2}\delta x_n$$

$$+\left(x_0'\,y_0'\,i + y_0'^2\,j\right)_{n-1/2}\delta y_n - \left(x_0'^2\,i + x_0'\,y_0'\,j\right)_{n-1/2}\delta x_{n-1}$$

$$-\left(x_0'\,y_0'\,i + y_0'^2\,j\right)_{n-1/2}\delta y_{n-1}\Big] \tag{6.69}$$

The expansion and preliminary integration of term 1 in Eqn (6.51) is therefore completed when Eqns (6.63) and (6.69) (*a* and *b* respectively) are added together.

$$\left[AE\left(r_0'.\delta r'\right)r_0'\right]_n' = \frac{AE}{ds^2}\Big[\left(x_0'^2\,i + x_0'\,y_0'\,j\right)_{n+1/2}\delta x_{n+1}$$

$$+\left(x_0'\,y_0'\,i + y_0'^2\,j\right)_{n+1/2}\delta y_{n+1} - \left(x_0'^2\,i + x_0'\,y_0'\,j\right)_{n+1/2}\delta x_n$$

$$-\left(x_0'\,y_0'\,i + y_0'^2\,j\right)_{n+1/2}\delta y_n - \left(x_0'^2\,i + x_0'\,y_0'\,j\right)_{n-1/2}\delta x_n$$

$$-\left(x_0'\,y_0'\,i + y_0'^2\,j\right)_{n-1/2}\delta y_n + \left(x_0'^2\,i + x_0'\,y_0'\,j\right)_{n-1/2}\delta x_{n-1}$$

$$+\left(x_0'\,y_0'\,i + y_0'^2\,j\right)_{n-1/2}\delta y_{n-1}\Big] \tag{6.70}$$

Integrating Term 2

$$\left[T_0\,\delta r'\right]_n' = \frac{1}{ds}\left[\left(T_0\,\delta r'\right)_{n+1/2} - \left(T_0\,\delta r'\right)_{n-1/2}\right] \tag{6.71}$$

$$= \frac{1}{ds^2}\left[T_{0\,n+1/2}\left(\delta r_{n+1} - \delta r_n\right) - T_{0\,n-1/2}\left(\delta r_n - \delta r_{n-1}\right)\right] \tag{6.72}$$

The vector term δr can be replaced by it's directional components by substituting in Eqn (6.55)

$$\left[T_0\,\delta r'\right]_n' = \frac{1}{ds}\left[T_{0\,n+1/2}\left(\delta x' i + \delta y' j\right)_{n+1/2}\right.$$

$$\left. - T_{0\,n-1/2}\left(\delta x' i + \delta y' j\right)_{n-1/2}\right] \tag{6.73}$$

This equation can now be numerically integrated by using the first derivative formulas as defined by Eqns (6.59), (6.60), (6.67) and (6.68)

$$\left[T_0\,\delta r'\right]_n' = \frac{1}{ds^2}\left[T_{0\,n+1/2}\left(\delta x_{n+1} - \delta x_n\right)i + T_{0\,n+1/2}\left(\delta y_{n+1} - \delta y_n\right)j\right.$$

$$\left. - T_{0\,n-1/2}\left(\delta x_n - \delta x_{n-1}\right)i + T_{0\,n-1/2}\left(\delta y_n - \delta y_{n-1}\right)j\right] \tag{6.74}$$

$$\left[T_0\,\delta r'\right]_n' = \frac{1}{ds^2}\left[T_{0\,n+1/2}\,i\,\delta x_{n+1} + \left(T_{0\,n+1/2} + T_{0\,n-1/2}\right)i\,\delta x_n\right.$$

$$+ \left(T_{0\,n+1/2} + T_{0\,n-1/2}\right)j\,\delta y_n + T_{0\,n+1/2}\,j\,\delta y_{n+1}$$

$$\left. + T_{0\,n-1/2}\,i\,\delta x_{n-1} + T_{0\,n-1/2}\,\delta y_{n-1}\right] \tag{6.75}$$

The equation of motion (Eqn (6.51)) can now be written as follows

$$m\,\delta\ddot{r}_n = m\left(\delta\ddot{x}_n\,i + \delta\ddot{y}_n\,j\right) = \text{Eqn}(6.70) + \text{Eqn}(6.75) \tag{6.76}$$

Therefore

$$m\,ds^2\left(\delta\ddot{x}_n\,i+\delta\ddot{y}_n\,j\right)=$$

$$\left[\left(AE\,x_0'^2\right)_{n+1/2}\delta x_{n+1}+\left(AE\,x_0'\,y_0'\right)_{n+1/2}\delta y_{n+1}\right.$$

$$-\left(AE\,x_0'^2\right)_{n+1/2}\delta x_n-\left(AE\,x_0'\,y_0'\right)_{n+1/2}\delta y_n$$

$$-\left(AE\,x_0'^2\right)_{n-1/2}\delta x_n-\left(AE\,x_0'\,y_0'\right)_{n-1/2}\delta y_n$$

$$+\left(AE\,x_0'^2\right)_{n-1/2}\delta x_{n-1}+\left(AE\,x_0'\,y_0'\right)_{n-1/2}\delta y_{n-1}$$

$$\left.+T_{0\,n+1/2}\,\delta x_{n+1}-\left(T_{0\,n+1/2}+T_{0\,n-1/2}\right)\delta x_n+T_{0\,n-1/2}\,\delta x_{n-1}\right]i$$

$$+\left[\left(AE\,x_0'\,y_0'\right)_{n+1/2}\delta x_{n+1}+\left(AE\,y_0'^2\right)_{n+1/2}\delta y_{n+1}\right.$$

$$-\left(AE\,x_0'\,y_0'\right)_{n+1/2}\delta x_n-\left(AE\,y_0'^2\right)_{n+1/2}\delta y_n$$

$$-\left(AE\,x_0'\,y_0'\right)_{n-1/2}\delta x_n-\left(AE\,y_0'^2\right)_{n-1/2}\delta y_n$$

$$+\left(AE\,x_0'\,y_0'\right)_{n-1/2}\delta x_{n-1}+\left(AE\,y_0'^2\right)_{n-1/2}\delta y_{n-1}$$

$$\left.+T_{0\,n+1/2}\,\delta y_{n+1}-\left(T_{0\,n+1/2}+T_{0\,n-1/2}\right)\delta y_n+T_{0\,n-1/2}\,\delta y_{n-1}\right]j \qquad (6.77)$$

This equation can be sub divided into it's two constituent components in the x and y directions as defined by the unit vectors $\boldsymbol{i}$ and $\boldsymbol{j}$, respectively.

$$\left(m\,ds^2\right)\ddot{x}_n=ax_{1,n}\,\delta x_{n-1}+ax_{2,n}\,\delta y_{n-1}+ax_{3,n}\,\delta x_n+ax_{4,n}\,\delta y_n$$

$$+ax_{5,n}\,\delta x_{n+1}+ax_{6,n}\,\delta y_{n+1} \qquad (6.78)$$

and

$$\left(m\,ds^2\right)\ddot{y}_n=ay_{1,n}\,\delta x_{n-1}+ay_{2,n}\,\delta y_{n-1}+ay_{3,n}\,\delta x_n+ay_{4,n}\,\delta y_n$$

$$+ay_{5,n}\,\delta x_{n+1}+ay_{6,n}\,\delta y_{n+1} \qquad (6.79)$$

where the coefficients can be defined as follows

$$ax_{1,n} = \left(T_0 + AE x_0'^2\right)_{n-1/2}$$

$$ax_{2,n} = \left(AE x_0' y_0'\right)_{n-1/2}$$

$$ax_{3,n} = -\left(T_0 + AE x_0'^2\right)_{n+1/2} - \left(T_0 + AE x_0'^2\right)_{n-1/2}$$

$$ax_{4,n} = -\left(AE x_0' y_0'\right)_{n+1/2} - \left(AE x_0' y_0'\right)_{n-1/2}$$

$$ax_{5,n} = \left(T_0 + AE x_0'^2\right)_{n+1/2}$$

$$ax_{6,n} = \left(AE x_0' y_0'\right)_{n+1/2}$$

$$ay_{1,n} = \left(AE x_0' y_0'\right)_{n-1/2}$$

$$ay_{2,n} = \left(T_0 + AE y_0'^2\right)_{n-1/2}$$

$$ay_{3,n} = -\left(AE x_0' y_0'\right)_{n+1/2} - \left(AE x_0' y_0'\right)_{n-1/2}$$

$$ay_{4,n} = -\left(T_0 + AE y_0'^2\right)_{n+1/2} - \left(T_0 + AE y_0'^2\right)_{n-1/2}$$

$$ay_{5,n} = \left(AE x_0' y_0'\right)_{n+1/2}$$

$$ay_{6,n} = \left(T_0 + AE y_0'^2\right)_{n+1/2}$$

From these equations the following features should be noted

$$ax_{2,n} = ay_{1,n}$$

$$ax_{4,n} = ay_{3,n}$$

$$ax_{6,n} = ay_{5,n}$$

If Eqns (6.78) and (6.79) are placed into a matrix format it can be seen that the equalities above have a diagonal characteristic (shown in bold type). This is a distinguishing feature of this type of analysis and can be used as a simple check

$$\begin{bmatrix} & & & & & \\ \mathbf{ax_{1,n}} & \mathbf{ax_{2,n}} & \mathbf{ax_{3,n}} & \mathbf{ax_{4,n}} & \mathbf{ax_{5,n}} & \mathbf{ax_{6,n}} \\ \mathbf{ay_{1,n}} & \mathbf{ay_{2,n}} & \mathbf{ay_{3,n}} & \mathbf{ay_{4,n}} & \mathbf{ay_{5,n}} & \mathbf{ay_{6,n}} \\ & & & & & \end{bmatrix} \begin{Bmatrix} \delta x_{n-1} \\ \delta y_{n-1} \\ \delta x_n \\ \delta y_n \\ \delta x_{n+1} \\ \delta y_{n+1} \end{Bmatrix} \tag{6.80}$$

The coefficients ($ax_{1,n}$, $ay_{1,n}$, $ax_{2,n}$, ...) can be integrated further using the FD method. The outcome of this process is shown below. It should be reiterated the axial stiffness, denoted by the term *AE* is assumed constant along the riser's length.

$$ax_{1,n} = T_{0n-1/2} + \frac{AE}{ds^2}\left(x_{0n} - x_{0n-1}\right)^2 \tag{6.81}$$

$$ax_{2,n} = \frac{AE}{ds^2}\left(x_{0n} - x_{0n-1}\right)\left(y_{0n} - y_{0n-1}\right) \tag{6.82}$$

$$ax_{3,n} = -\left(T_{0n-1/2} + T_{0n+1/2}\right) - \frac{AE}{ds^2}\left(x_{0n+1} - x_{0n}\right)^2 \tag{6.83}$$

$$-\frac{AE}{ds^2}\left(x_{0n} - x_{0n-1}\right)^2$$

$$ax_{4,n} = -\frac{AE}{ds^2}\left(x_{0n+1} - x_{0n}\right)\left(y_{0n+1} - y_n\right) \tag{6.84}$$

$$-\frac{AE}{ds^2}\left(x_{0n} - x_{0n-1}\right)\left(y_{0n} - y_{n-1}\right)$$

$$ax_{5,n} = T_{0n+1/2} + \frac{AE}{ds^2}\left(x_{0n+1} - x_{0n}\right)^2 \tag{6.85}$$

$$ax_{6,n} = \frac{AE}{ds^2}\left(x_{0n+1} - x_{0n}\right)\left(y_{0n+1} - y_{0n}\right) \tag{6.86}$$

$$ay_{1,n} = \frac{AE}{ds^2}\left(x_{0n} - x_{0n-1}\right)\left(y_{0n} - y_{0n-1}\right) \tag{6.87}$$

$$ay_{2,n} = T_{0n-1/2} + \frac{AE}{ds^2}\left(y_{0n} - y_{0n-1}\right)^2 \tag{6.88}$$

$$ay_{3,n} = -\frac{AE}{ds^2}\left(x_{0n+1} - x_{0n}\right)\left(y_{0n+1} - y_n\right)$$

$$-\frac{AE}{ds^2}\left(x_{0n} - x_{0n-1}\right)\left(y_{0n} - y_{n-1}\right) \tag{6.89}$$

$$ay_{4,n} = -\left(T_{0n+1/2} + T_{0n-1/2}\right) - \frac{AE}{ds^2}\left(y_{0n+1} - y_{0n}\right)^2$$

$$-\frac{AE}{ds^2}\left(y_{0n} - y_{0n-1}\right)^2 \tag{6.90}$$

$$ay_{5,n} = \frac{AE}{ds^2}\left(x_{0n+1} - x_{0n}\right)\left(y_{0n+1} - y_{0n}\right) \tag{6.91}$$

$$ay_{6,n} = T_{0n+1/2} + \frac{AE}{ds^2}\left(y_{0n+1} - y_n\right)^2 \tag{6.92}$$

The next part of the analysis is best demonstrated if it is applied to an example system such as that illustrated in Figure 6.5. The diagram shows a riser of circular profile which has been divided up into just four elements so as to allow the dynamic matrices to be presented.

Eqns (6.78) and (6.79) can be applied to the three *free* nodes, **n = 1, 2** and **3** as follows

n=1

$$\left(m\,ds^2\right)\ddot{x}_1 = ax_{1,1}\,\delta x_0 + ax_{2,1}\,\delta y_0 + ax_{3,1}\,\delta x_1 + ax_{4,1}\,\delta y_1$$

$$+ ax_{5,1}\,\delta x_2 + ax_{6,1}\,\delta y_2 \tag{6.93}$$

$$\left(m\,ds^2\right)\ddot{y}_1 = ay_{1,1}\,\delta x_0 + ay_{2,1}\,\delta y_0 + ay_{3,1}\,\delta x_1 + ay_{4,1}\,\delta y_1$$

$$+ ay_{5,1}\,\delta x_2 + ay_{6,1}\,\delta y_2 \tag{6.94}$$

The unit mass **m** is constant along the length of the riser

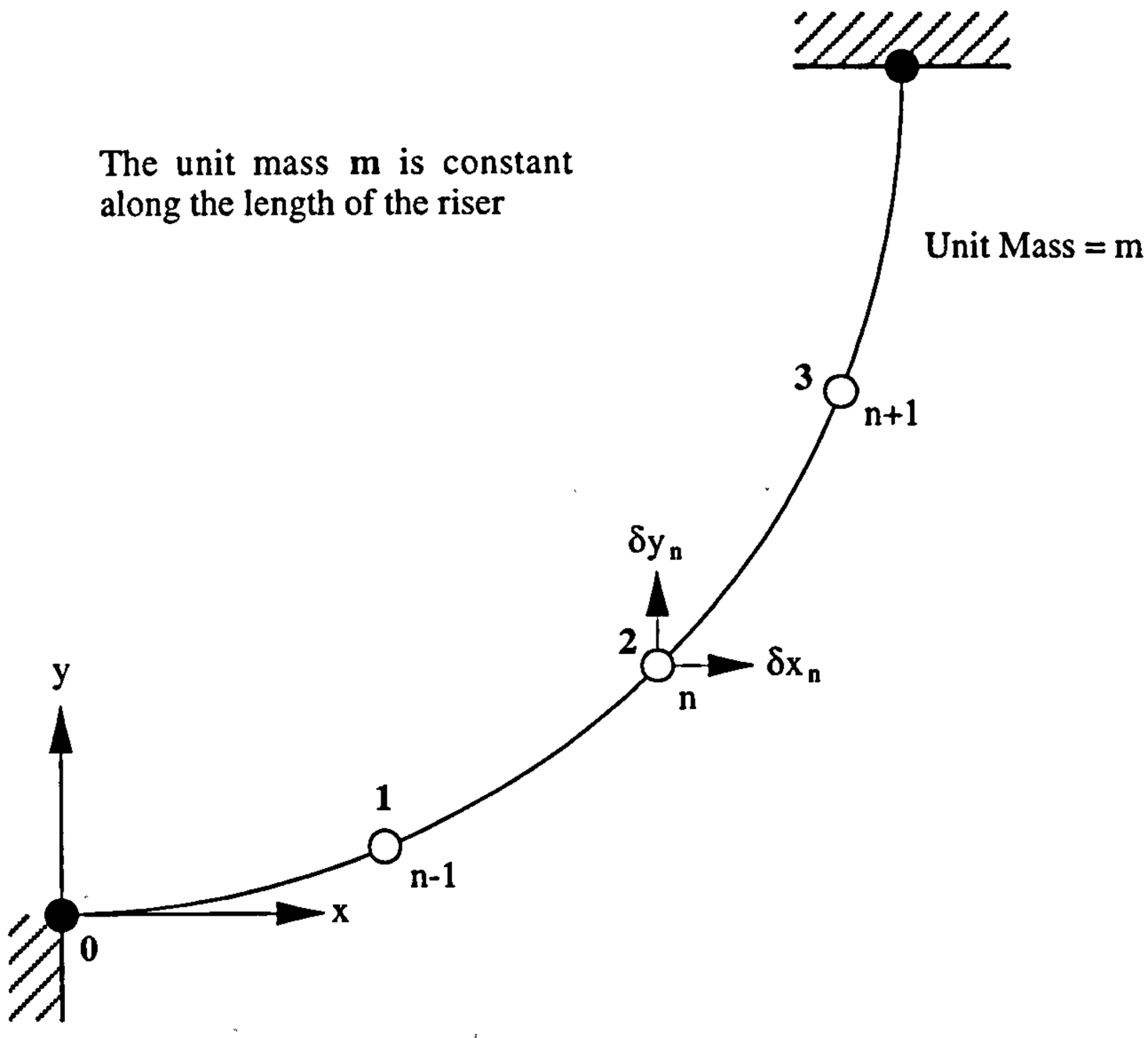

The axial stiffness term **AE** is constant along the length of the riser

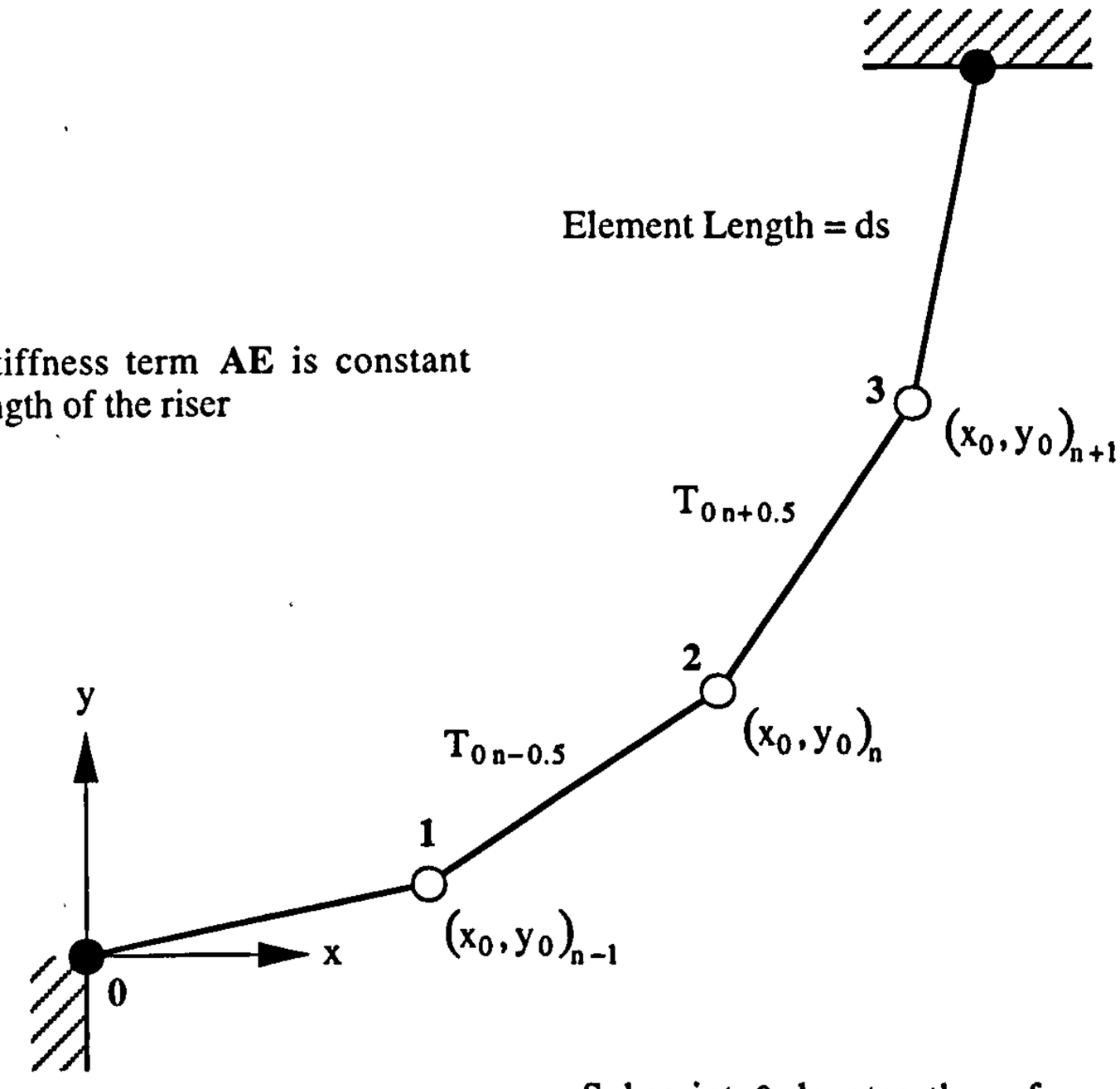

Subscript *0* denotes the references or static condition

Figure 6.5

Dynamic Example

n=2

$$\left(m\,ds^2\right)\ddot{x}_2 = ax_{1,2}\,\delta x_1 + ax_{2,2}\,\delta y_1 + ax_{3,2}\,\delta x_2 + ax_{4,2}\,\delta y_2$$

$$+ ax_{5,2}\,\delta x_3 + ax_{6,2}\,\delta y_3 \qquad (6.95)$$

$$\left(m\,ds^2\right)\ddot{y}_2 = ay_{1,2}\,\delta x_1 + ay_{2,2}\,\delta y_1 + ay_{3,2}\,\delta x_2 + ay_{4,2}\,\delta y_2$$

$$+ ay_{5,2}\,\delta x_3 + ay_{6,2}\,\delta y_3 \qquad (6.96)$$

n=3

$$\left(m\,ds^2\right)\ddot{x}_3 = ax_{1,3}\,\delta x_2 + ax_{2,3}\,\delta y_2 + ax_{3,3}\,\delta x_3 + ax_{4,3}\,\delta y_3$$

$$+ ax_{5,3}\,\delta x_4 + ax_{6,3}\,\delta y_4 \qquad (6.97)$$

$$\left(m\,ds^2\right)\ddot{y}_3 = ay_{1,3}\,\delta x_2 + ay_{2,3}\,\delta y_2 + ay_{3,3}\,\delta x_3 + ay_{4,3}\,\delta y_3$$

$$+ ay_{5,3}\,\delta x_4 + ay_{6,3}\,\delta y_4 \qquad (6.98)$$

Boundary conditions state that $\delta x_0 = \delta y_0 = \delta x_4 = \delta y_4 = 0$.

Eqns (6.93) to (6.98) can be transplanted into a matrix formation as shown below

$$\begin{Bmatrix} \ddot{x}_1 \\ \ddot{y}_1 \\ \ddot{x}_2 \\ \ddot{y}_2 \\ \ddot{x}_3 \\ \ddot{y}_3 \end{Bmatrix} \mathbf{I} = \frac{1}{m\,ds^2} \begin{bmatrix} ax_{3,1} & ax_{4,1} & ax_{5,1} & ax_{6,1} & 0 & 0 \\ ay_{3,1} & ay_{4,1} & ay_{5,1} & ay_{6,1} & 0 & 0 \\ ax_{1,2} & ax_{2,2} & ax_{3,2} & ax_{4,2} & ax_{5,2} & ax_{6,2} \\ ay_{1,2} & ay_{2,2} & ay_{3,2} & ay_{4,2} & ay_{5,2} & ay_{6,2} \\ 0 & 0 & ax_{1,3} & ax_{2,3} & ax_{3,3} & ax_{4,3} \\ 0 & 0 & ay_{1,3} & ay_{2,3} & ay_{3,3} & ay_{4,3} \end{bmatrix} \begin{Bmatrix} \delta x_1 \\ \delta y_1 \\ \delta x_2 \\ \delta y_2 \\ \delta x_3 \\ \delta y_3 \end{Bmatrix}$$

(6.99)

where $\boldsymbol{I}$ is a unit matrix (see Eqn (6.27)). The dynamic matrix is characterised by a six band diagonal and is both real and symmetric in nature.

If

$$-\mathbf{A} = \frac{1}{m\,ds^2}\begin{bmatrix} ax_{3,1} & ax_{4,1} & ax_{5,1} & ax_{6,1} & 0 & 0 \\ ay_{3,1} & ay_{4,1} & ay_{5,1} & ay_{6,1} & 0 & 0 \\ ax_{1,2} & ax_{2,2} & ax_{3,2} & ax_{4,2} & ax_{5,2} & ax_{6,2} \\ ay_{1,2} & ay_{2,2} & ay_{3,2} & ay_{4,2} & ay_{5,2} & ay_{6,2} \\ 0 & 0 & ax_{1,3} & ax_{2,3} & ax_{3,3} & ax_{4,3} \\ 0 & 0 & ay_{1,3} & ay_{2,3} & ay_{3,3} & ay_{4,3} \end{bmatrix} \tag{6.100}$$

then (see Section 6.2.5)

$$\mathbf{A}\begin{Bmatrix} x \\ y \end{Bmatrix} + \begin{Bmatrix} \ddot{x} \\ \ddot{y} \end{Bmatrix}\mathbf{I} = 0 \tag{6.101}$$

Assuming harmonic motion $\ddot{x} = -\omega^2 x$ and $\ddot{y} = -\omega^2 y$, where $\lambda = \omega^2$, Eqn (6.101) becomes

$$\mathbf{A}\begin{Bmatrix} x \\ y \end{Bmatrix} = \lambda\begin{Bmatrix} x \\ y \end{Bmatrix}\mathbf{I} \tag{6.102}$$

This dynamic equation is now in a configuration whereby it can be solved in terms of it's eigenvalues and eigenvectors by standard computer algorithms.

Natural periods of vibration are obtained from the eigenvalues λ using the following expression

$$Tp = \frac{2\pi}{\sqrt{\lambda}} \tag{6.103}$$

6.3 Analysis Implementation Using a Computational Program

The dynamic theory presented in the previous section is applied to the catenary riser using a computer program written in FORTRAN. This program is summarised in Figure 6.6 in block diagram format and is listed in Appendix C.

From a range of input parameters the program calculates the all important horizontal tension using the iterative method developed in Section 2.4. In the next stage this parameter is used within catenary equations formulated in Section 2.3 to define the riser's profile in terms of a series of equally spaced nodes with co-ordinates x_0 and y_0.

Program Input

1. Horizontal Surface Offset

2. Sea Depth/Vertical Offset

3. Length of the Riser

4. Outer Diameter of the Carrier Pipe

5. Unit Mass

6. Submerged Unit Mass

7. Cross-Sectional Area

8. Number of Nodes

The horizntal tension (H) is calculated using the iteration method developed in Section 2.4

The catenary riser is broken up a series of elements. The number of elements is determined by the number of nodes inputted. The nodal coordinates are calculated using the catenary equations formulated in Section 2.3

An axial tension is calculated for each element based upon the horizontal tension and slope of each element

The axial stiffness term (AE) is calculated

T_0

(x_0, y_0)

AE

Figure 6.6(a)
Block Diagram of the Vibration Analysis FORTRAN Computer Program

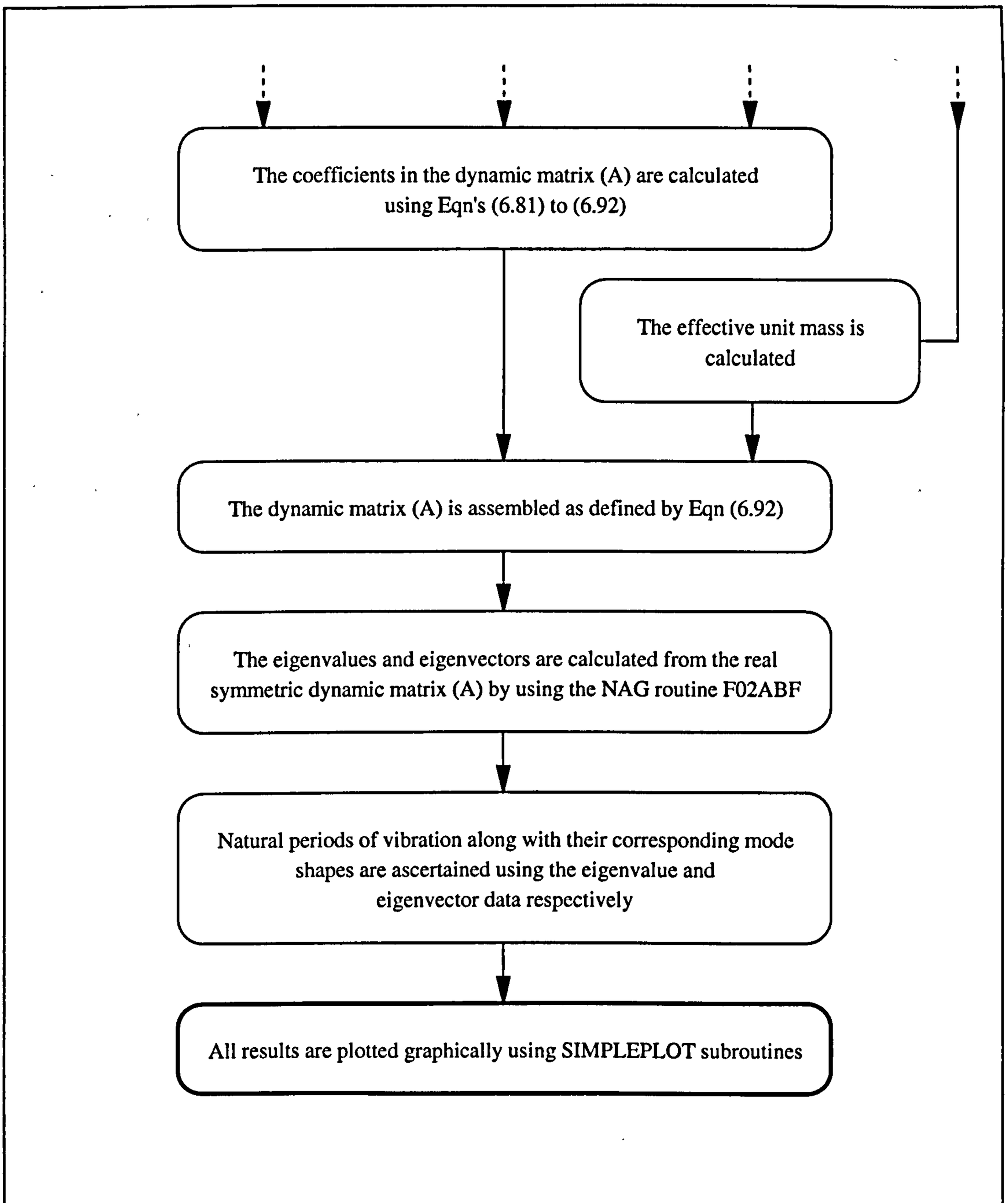

Figure 6.6(b)
Block Diagram of the Vibration Analysis FORTRAN Computer Program

The calculated axial tension at a point midway between nodes is then applied to the corresponding element. The catenary riser has now been sufficiently modelled so as to allow the coefficients in the dynamic matrix to be evaluated using Eqns (6.81) to (6.92).

For any structure which is submerged and undergoing oscillation, a certain amount of water becomes entrained and moves with the structure. This mass of water must be included when considering the dynamics of the structure. Therefore the riser has an effective unit mass (sometimes referred to as virtual unit mass) based upon

- The structural unit mass of the member (m_s)
- The unit mass of the externally entrained water or added unit mass (m_{am})

The next section of the program calculates this property using the following expression

$$m = m_s + m_{am} \qquad (6.104)$$

where m = effective unit mass

Added mass is dependent upon the direction of movement as demonstrated below for a circular cylinder

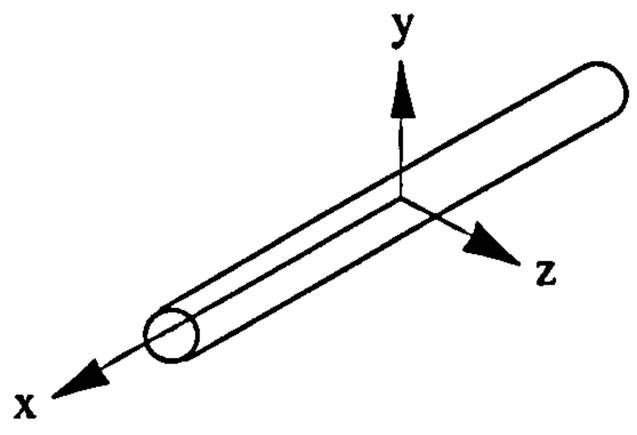

$$m_{am} = \frac{\pi}{4} D^2 \rho_{sw} \qquad \text{in the y and z direction} \qquad (6.105)$$

$$m_{am} = 0 \qquad \text{in the x direction (approximately)}$$

where D = outer diameter of the cylinder
ρ_{sw} = density of the *entrained* seawater

The added-mass for arbitrary directions can be determined by suitable vectoring, however in an attempt to simplify the vector analysis it is assumed that the riser elements oscillate perpendicular to their longitudinal axis. This is a conservative assumption as it will result in the effective mass being overestimated and will therefore give the lowest natural frequency (or highest natural period) likely to occur. Once the effective mass has been

calculated the system or dynamic matrix A can then be determined as defined by Eqn (100).

The evaluation of eigenvalues and eigenvectors from an n by n matrix is achieved by using a NAG (Numerical Algorithm Group) routine. The routine selected (F02ABF) is based upon an eigenvalue problem as defined by the equation below

$$A x = \lambda x \tag{6.106}$$

where A = real symmetric matrix
λ = eigenvalue
x = eigenvector ($x \neq 0$)

The F02ABF routine reduces the real symmetric matrix A to a real symmetric tridiaganol matrix by Householder's method. The eigenvalues and eigenvectors are calculated using the QL algorithm.

The program uses Eqn (6.103) in conjunction with SIMPLEPLOT to create a natural period spectrum. SIMPLEPLOT is a library of FORTRAN subroutines for plotting graphs and is further utilised within the program to plot vibration mode shapes which are generated by normalising the eigenvectors to unity.

6.4 Analysis Input

A natural period and vibration mode shape analysis is conducted upon a range catenary risers with varying horizontal surface offsets and carrier pipe diameters. The reason for using the diameter of the carrier pipe as a variable is because it establishes both the effective unit mass and submerged unit weight for a given type of buoyancy material and as previously demonstrated the submerged unit weight in conjunction with the riser profile determines the axial tension.

Figures 6.10 and 6.11 illustrate the effects of diameter on both the riser's effective mass and horizontal tension for syntactic foam and nitrogen gas buoyancy cases respectively. These graphs have been derived using the buoyancy spreadsheets presented in Chapter 3.

A selection of conditions representing a practical range have been extracted from these graphs and tabulated below in Table 6.1

Carrier Pipe Outer Diameter (m)	Submerged Unit Weight (N/m)	Effective Unit Mass (kg/m)
Syntactic Foam		
1.10	2128	2165.1
1.20	1222	2443.2
1.30	219	2743.5
Nitrogen Gas		
1.00	1887	1802.0
1.10	745	2024.1

Table 6.1

Properties Influencing Vibrational Performance

The dynamic study is conducted using each one of the five conditions listed above with horizontal surface offsets of 1000, 1500 and 2000 m.

The results of this analysis are all based upon a riser model using 200 nodes and therefore 201 elements (or slender rods). This generates a 400 by 400 dynamic matrix (i.e. n = 400) in which the computing time taken by the F02ABF routine is approximately proportional to n^3. This size of matrix represents an optimum value based upon computing time and model accuracy.

6.5 Discussion of the Results

The results corresponding to a horizontal surface offset of 1000 m are presented in Figures 6.12 to 6.17. The natural period spectrums (Figures 6.12 to 6.16) are shown in order of increasing diameter for both syntactic foam (shown first) and nitrogen gas buoyancy cases. The last diagram (Figure 6.17) illustrates the riser's vibrational profile (as depicted by the plain line) for the first six modes of vibration. Over the selected range the effects of diameter on the riser's vibrational mode shape is negligible and it is for this reason that only one set of mode shape profiles is shown. The main characteristics ascertained from the dynamic data can be summarised as follows

- The resonant periods of vibration rapidly converge as the mode number is increased. All the high frequencies (low periods) appear within a convergence

block as opposed to the low frequencies of vibration (high periods) which are well spaced out.

- The range of natural periods increase with an increase in diameter. For the syntactic foam buoyancy condition the effect of increasing the riser diameter from 1.10 m to 1.30 m is to increase the natural periods by an average of 250% for all modes of vibration. This equates to a significant shift with respect to the fundamental and lower modes of vibration and a small to negligible shift in the case of the higher modes. The implications of this in terms of *tuning the system* are discussed later.

The first characteristic is a common feature of a vibrating system and it's appearance is encouraging in terms creating confidence in the dynamic analysis. The second characteristic provides evidence to suggest that the natural period is a to a certain extent a function of the riser's *Unit Mass/Tension* ratio. From Figures 6.10 and 6.11 it is shown that increasing the riser's diameter, reduces the tension and increases the effective unit mass and when combined these two changes ultimately increase the *m/T* ratio.

The results corresponding to a horizontal surface offset of 1500 m are shown in Figures 6.18 to 6.23 using the same format as applied in the previous case. When these results are compared to those obtained for the a = 1000 m case it is clear that the same characteristics are present, however the natural period values are all slightly lower. Changing the riser profile has reduced the fundamental periods by approximately 10%, however this percentage reduction progressively decreases as the mode number is increased to a point where the differences become insignificant for the lower periods of vibration. The vibration mode shapes for modes 1 to 6 are illustrated in Figure 6.23.

The results corresponding to a horizontal surface offset of 2000 m are shown in Figures 6.24 to 6.29. For this condition fundamental periods are only about 5% less than those calculated for the a = 1500 m case.

Overall the results suggest that the riser's high natural periods are substantially influenced by carrier pipe diameter and can therefore be positioned so as not to coincide with external excitation by selecting the appropriate diameter i.e. low frequency resonance can be avoided by good design. However as the mode number is increased the diameters influence reduces and spectrum converges towards the roughly the same value irrespective of diameter. Therefore at this end of the spectrum the diameter cannot be used to move the low natural periods of vibration and hence high frequency resonance is always inevitable.

The natural period results are summarised in Figures 6.30 to 6.35 in which the natural periods corresponding to the first six modes of vibration are plotted against carrier pipe diameter. They clearly show a non-linear relationship between diameter and natural period, a characteristic that is created by the effective mass being directly proportional to the diameter squared (D^2).

6.6 Verification

6.6.1 Introduction

The aim of this exercise is to validate the dynamic FD analysis which was used to obtain the results presented in Section 6.4. This validation uses an analytical approach originally developed to assess the vibrational behaviour of inclined suspended cables which sag to support their own weight. The profile of an inclined cable is defined in Figure 6.7.

6.6.2 Assumptions

The general assumptions used in the analysis of cables are

- The cables are uniform and elastic.
- Cables only support tension loads. The mean tension in the cable is much greater than the fluctuating component of tension during vibration.
- The maximum depth of the sag is no greater than *1/8* of the cable span.
- The vibrational amplitude is small compared with the sag of the cable and the distance between vibration nodes.
- The cables are supported at both ends by rigid tie-downs.

It should be noted that all these assumptions (with the exception of the third) are in full agreement with those established in Section 6.2.2 concerning the equation of motion.

6.6.3 Expressions for Natural Periods and Mode Shapes

If a suspended cable is given a small in-plane displacement from it's static equilibrium, the resulting vibrational mode shape will be either antisymmetric or symmetric about the cable midpoint as defined by Figure 6.8. This characterisation is important in terms of defining an expression that can be used to calculate the corresponding natural frequency or period.

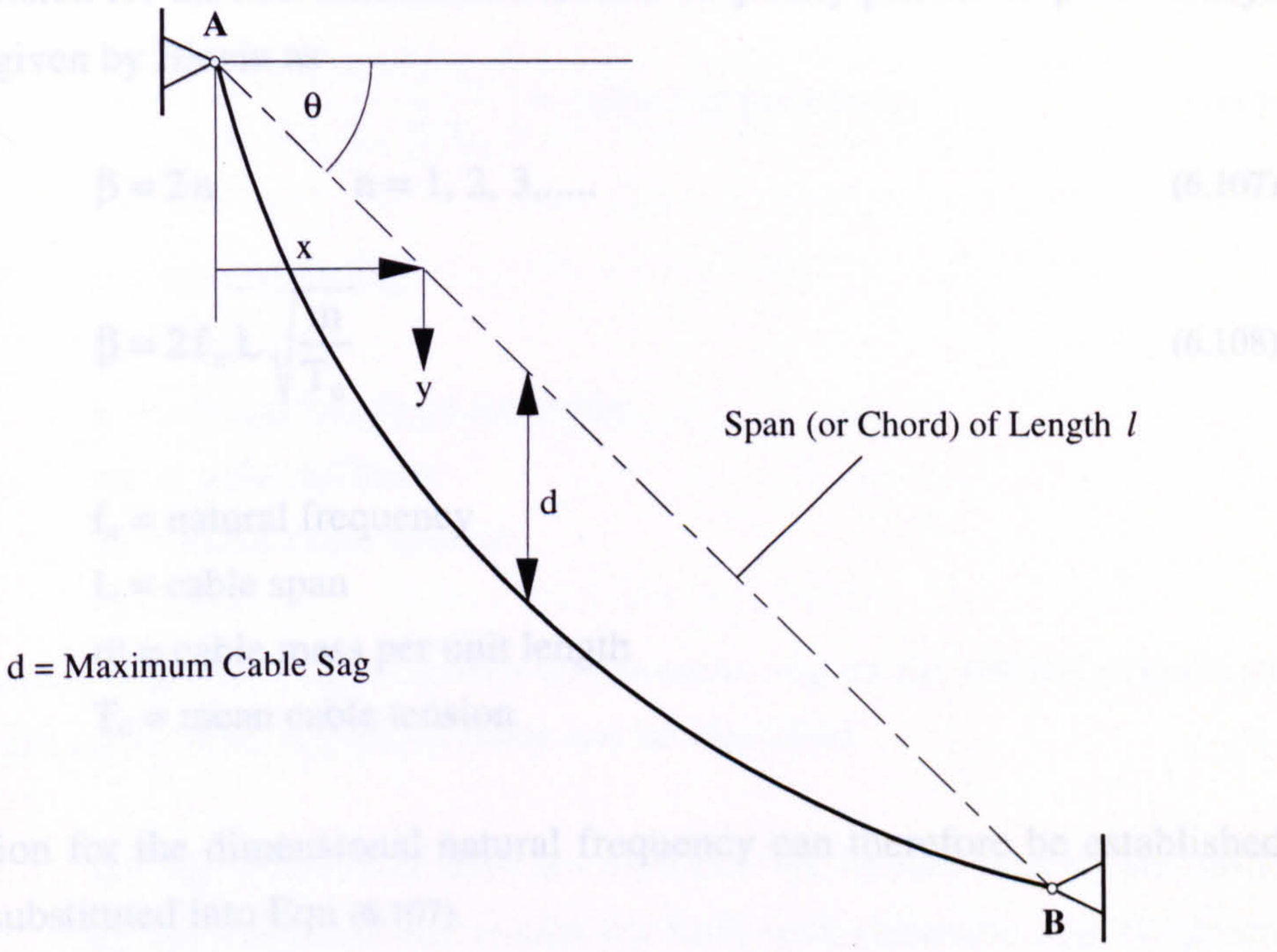

Figure 6.7

Definition Diagram for a Profile of an Inclined Cable

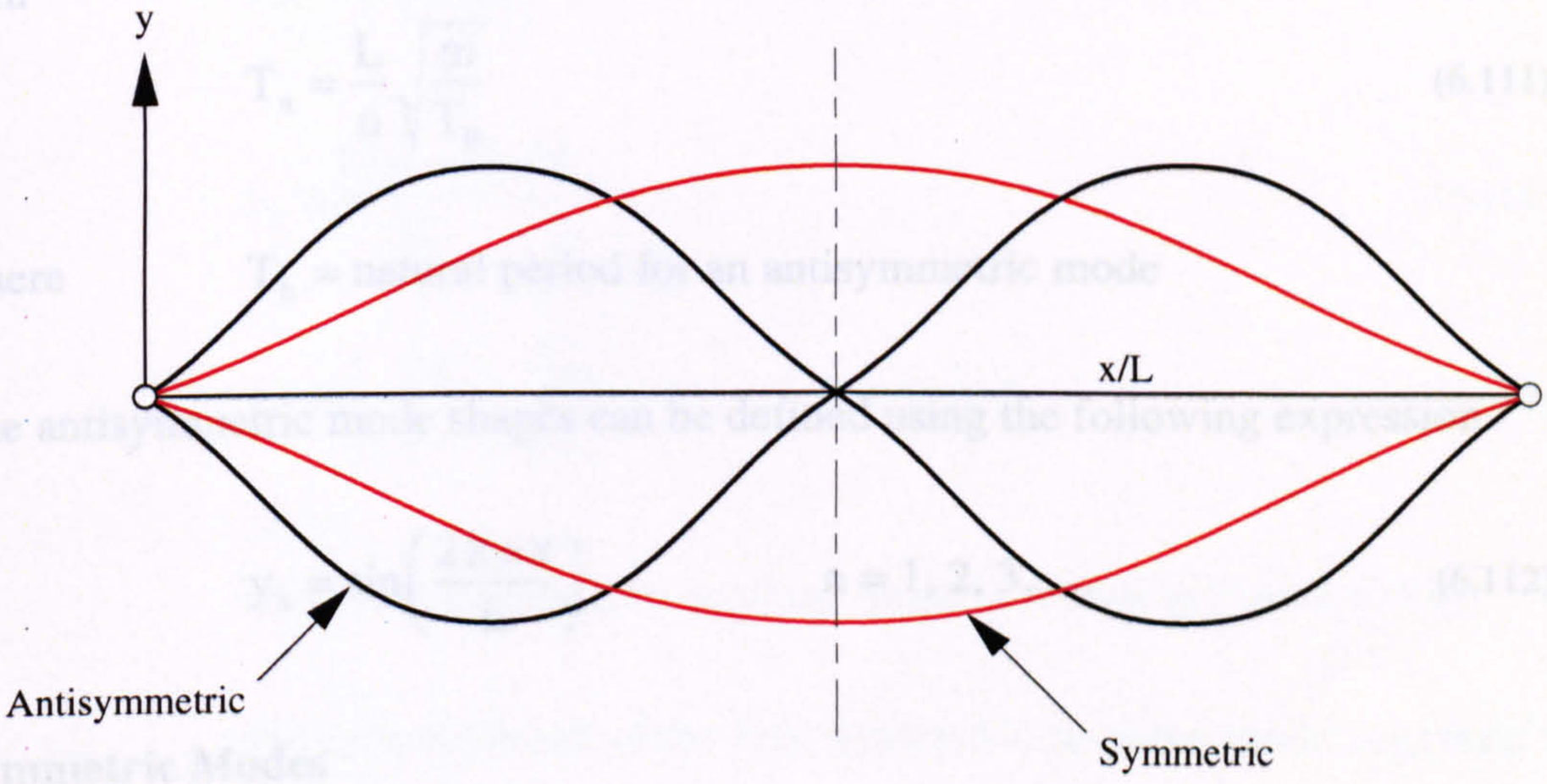

Figure 6.8

Symmetric and Antisymmetric In-Plane Cable Modes

Antisymmetric Modes

The expression for the non-dimensional natural frequency parameter β for antisymmetric modes is given by Blevin as

$$\beta = 2n \qquad n = 1, 2, 3,..... \tag{6.107}$$

where $$\beta = 2 f_n L \sqrt{\frac{m}{T_0}} \tag{6.108}$$

f_n = natural frequency
L = cable span
m = cable mass per unit length
T_0 = mean cable tension

An equation for the dimensional natural frequency can therefore be established if Eqn (6.108) is substituted into Eqn (6.107)

$$f_n = \frac{n}{L}\sqrt{\frac{T_0}{m}} \tag{6.109}$$

Since $$f_n = \frac{1}{T_n} \tag{6.110}$$

then

$$T_n = \frac{L}{n}\sqrt{\frac{m}{T_0}} \tag{6.111}$$

where T_n = natural period for an antisymmetric mode

The antisymmetric mode shapes can be defined using the following expression

$$y_n = \sin\left(\frac{2\pi n x}{L}\right) \qquad n = 1, 2, 3,..... \tag{6.112}$$

Symmetric Modes

The expression for the non-dimensional natural frequency parameter β for symmetric modes is given by Blevin as the positive non-zero solution of the following transcendental equation

$$\tan\left(\frac{\pi\beta}{2}\right)=\left(\frac{\pi\beta}{2}\right)-\frac{4}{\alpha^2}\left(\frac{\pi\beta}{2}\right)^3 \qquad (6.113)$$

where $$\alpha^2=\left(\frac{8d}{L}\right)^2\left(\frac{AE}{T_0}\right)\left(\frac{L}{L_e}\right)=\text{cable sag parameter} \qquad (6.114)$$

d = maximum sag

L = cable span

L_e = virtual length of the cable

AE = axial stiffness

T_0 = mean cable tension

The parameter α governs the influence of the mean sag on the natural periods and mode shapes of the cable. Four important cases can be identified

$\alpha \Rightarrow 0$ the sag in the cable does not influence the natural periods and mode shapes of the cable and the results for both antisymmetric and symmetric cases approach the taut cable condition as defined by the equation below

$$\text{if } \alpha\Rightarrow 0 \qquad \tan\left(\frac{\pi\beta}{2}\right)\Rightarrow -\infty \qquad \beta=2n-1 \qquad (6.114)$$

$$\beta_n=2f_nL\sqrt{\frac{m}{T_0}}=2n-1 \qquad (6.115)$$

$$f_n=\frac{[2n-1]}{2L}\sqrt{\frac{T_0}{m}} \qquad (6.116)$$

$$T_n=\frac{2L}{[2n-1]}\sqrt{\frac{m}{T_0}} \qquad n=1,2,3,..... \qquad (6.117)$$

The profile of the first in-plane mode is shown in Figure 6.9(a).

$\alpha < \pi\beta$ the natural period of the first symmetric in-plane mode is greater than the natural period of the first antisymmetric in-plane mode.

$\alpha = \pi\beta$ the first symmetric and first antisymmetric in-plane modes have the same natural periods and the first symmetric in-plane mode is tangent to the mean cable catenary at the end points as shown in Figure 6.9(b).

$$\text{if } \alpha = \pi\beta \qquad \tan\left(\frac{\pi\beta}{2}\right) = 0 \qquad \beta = 2n \tag{6.118}$$

$\alpha \Rightarrow \infty$ the natural frequency of the first symmetric in-plane mode is less than the natural period of the first antisymmetric in-plane mode and the first symmetric mode has two internal modes (see Figure 6.9(c)). This condition is a characteristic of a inextensible case i.e.

$$\text{if } \left(\frac{AE}{T_0}\right) \Rightarrow \infty \text{ then from Eqn (6.114) } \alpha \Rightarrow \infty$$

and if this is substituted back into Eqn (6.113)

$$\tan\left(\frac{\pi\beta}{2}\right) - \left(\frac{\pi\beta}{2}\right) = 0 \tag{6.119}$$

Since the catenary riser is assumed to be inextensible for the purposes of the finite difference method it's verification is also based upon the same assumption and therefore Eqn (6.119) is used. Beta must be obtained by iteration, however Eqn (6.119) is not a nice equation to iterate due to the presence of the *tan* function. It's user friendliness can however be improved by multiplying through by

$$\cos\left(\frac{\pi\beta}{2}\right)$$

to give

$$\sin\left(\frac{\pi\beta}{2}\right) - \left(\frac{\pi\beta}{2}\right)\cos\left(\frac{\pi\beta}{2}\right) = 0 \tag{6.120}$$

Noting that for large $\left(\frac{\pi\beta}{2}\right)$

$$\cos\left(\frac{\pi\beta}{2}\right) = 0 \qquad \beta = 2n+1 \qquad n = 1, 2, 3,..... \tag{6.121}$$

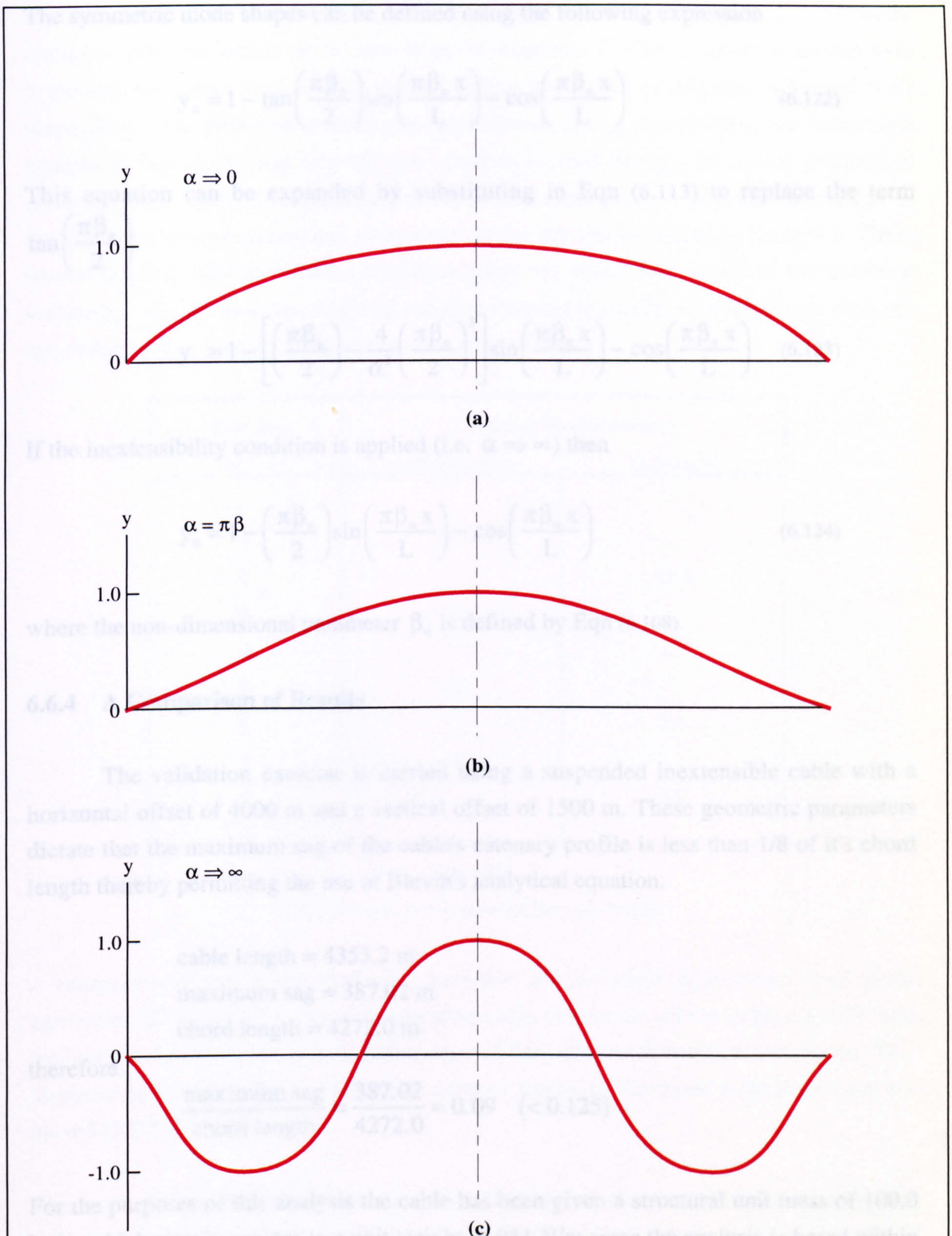

Figure 6.9

Mode Shapes of First Symmetric In-Plane Cable Mode

The symmetric mode shapes can be defined using the following expression

$$y_n = 1 - \tan\left(\frac{\pi\beta_n}{2}\right)\sin\left(\frac{\pi\beta_n x}{L}\right) - \cos\left(\frac{\pi\beta_n x}{L}\right) \qquad (6.122)$$

This equation can be expanded by substituting in Eqn (6.113) to replace the term $\tan\left(\frac{\pi\beta_n}{2}\right)$

$$y_n = 1 - \left[\left(\frac{\pi\beta_n}{2}\right) - \frac{4}{\alpha^2}\left(\frac{\pi\beta_n}{2}\right)^3\right]\sin\left(\frac{\pi\beta_n x}{L}\right) - \cos\left(\frac{\pi\beta_n x}{L}\right) \qquad (6.123)$$

If the inextensibility condition is applied (i.e. $\alpha \Rightarrow \infty$) then

$$y_n = 1 - \left(\frac{\pi\beta_n}{2}\right)\sin\left(\frac{\pi\beta_n x}{L}\right) - \cos\left(\frac{\pi\beta_n x}{L}\right) \qquad (6.124)$$

where the non-dimensional parameter β_n is defined by Eqn (6.108)

6.6.4 A Comparison of Results

The validation exercise is carried using a suspended inextensible cable with a horizontal offset of 4000 m and a vertical offset of 1500 m. These geometric parameters dictate that the maximum sag of the cable's catenary profile is less than 1/8 of it's chord length thereby permitting the use of Blevin's analytical equation.

cable length = 4353.2 m
maximum sag = 387.02 m
chord length = 4272.0 m

therefore

$$\frac{\text{maximum sag}}{\text{chord length}} = \frac{387.02}{4272.0} = 0.09 \quad (< 0.125)$$

For the purposes of this analysis the cable has been given a structural unit mass of 100.0 kg/m which simply equates to a unit weight of 981 N/m since the analysis is based within air rather than in water (i.e. no buoyancy or added mass effects).

The natural frequencies and periods corresponding to the antisymmetric modes can easily be attained using Eqns (6.109) and (6.111) respectively. However the symmetric modes

require an equation to be solved by iteration and this achieved using a FORTRAN computer program which can be seen listed in Appendix C. This program generates both a natural frequency and natural period output as shown in Figures 6.36 and 6.37 respectively. The plain line on both plots corresponds to Eqn (6.119) whilst the dashed line equates to Eqn (6.120) and it is this plot which is iterated (using a bi-section method) in order to obtain symmetric mode natural frequencies and periods. The natural periods of the first four antisymmetric and symmetric modes are shown below in Table 6.2. These results confirm the inextensible condition ($\alpha \Rightarrow \infty$) which was stated in the previous section i.e. *the natural frequency of the first symmetric in-plane mode is less than the natural period of the first antisymmetric in-plane mode.*

Mode No.	**Natural Period (secs)**	
	Antisymmetric	Symmetric
1	17.7	
2		12.4
3	8.8	
4		7.2
5	5.9	
6		5.1
7	4.4	
8		3.9

Table 6.2

Antisymmetric and Symmetric Natural Periods

A comparison of results obtained using both Blevin's analytical expression as well as the numerical FD analysis for the same vibrating cable system are shown in Figure 6.39. The two sets of data compare with a discrepancy of only 5% in the fundamental period. This disparity however declines as the mode number increases, for mode 8 the difference has halved to 2.5%.

The mode shapes for both antisymmetric and symmetric cases as are defined in Figures 6.38(a) and 6.38(b) respectively. These have been plotted using Eqns (6.112) and (6.124). If these shapes are compared to those obtained using the finite difference method (see Figures 6.17, 6.23 and 6.29) it can be seen that in terms of the number of internal nodes the mode shapes do correspond with one another. This can be used to further validate the numerical approach.

References

1. Turner, P.R. (1994) *Numerical Analysis*, Macmillan College Work Out Series.

2. Thomson, W.T. (1989) *Theory of Vibration with Applications*, Third Edition, Unwin Hyman Ltd.

3. Nordgren, R.P. (1974) *On Computation of the Motion of Elastic Rods*, Shell Development Company, Pres Seventh U.S. National Congress of Applied Mechanics, University of Colorado, 1974.

4. Blevin, R.D. (1979) *Formulas for Natural Frequency and Mode Shape*, Robert E. Krieger Publishing Company.

CHAPTER 6

Results

Figures 6.10 - 6.39

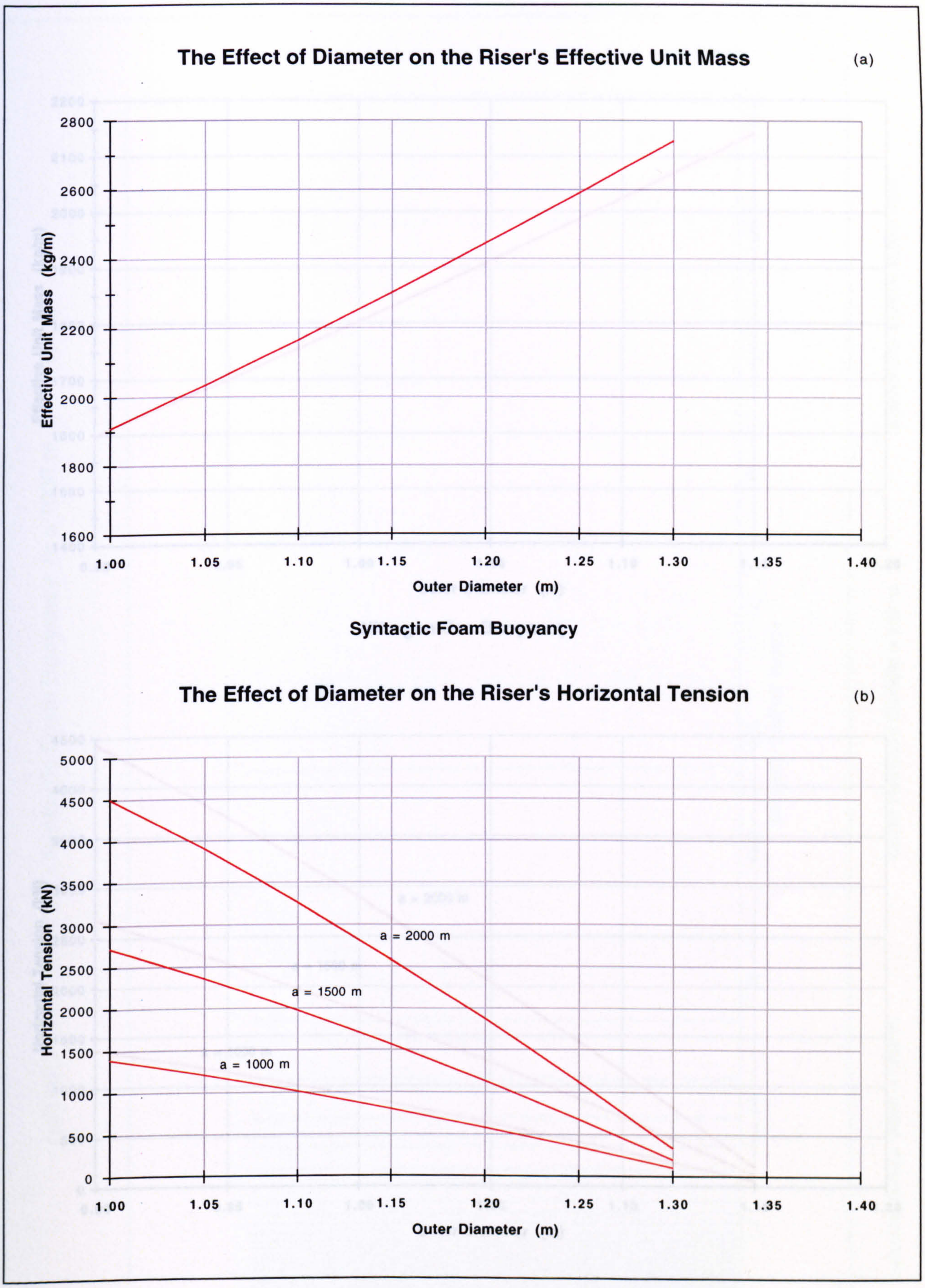

Effective Unit Mass = Structural Unit Mass + Added Unit Mass

Figure 6.10

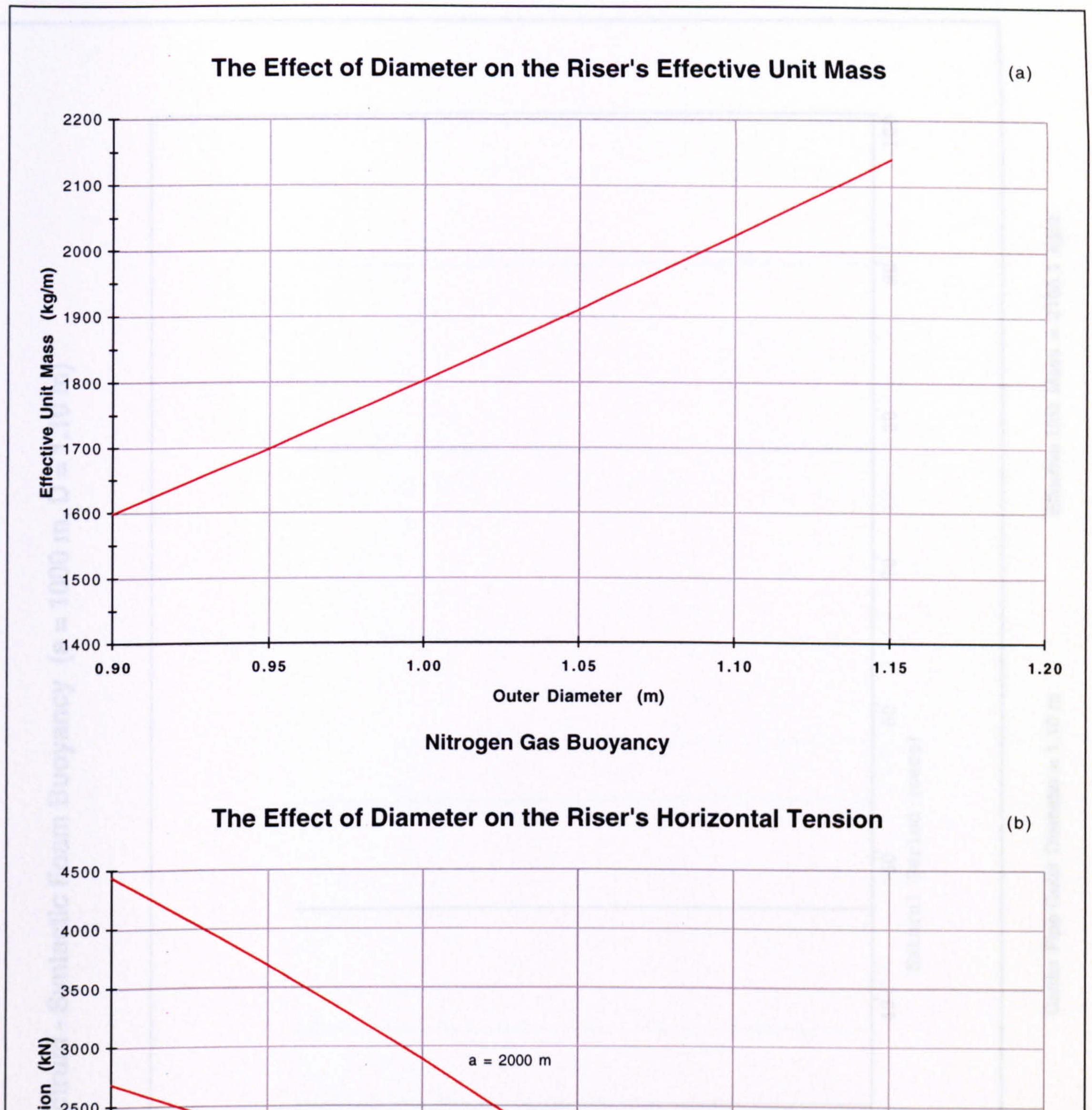

Effective Unit Mass = Structural Unit Mass + Added Unit Mass

Figure 6.11

Natural Period Spectrum - Syntactic Foam Buoyancy (a = 1000 m, D = 1.10 m)

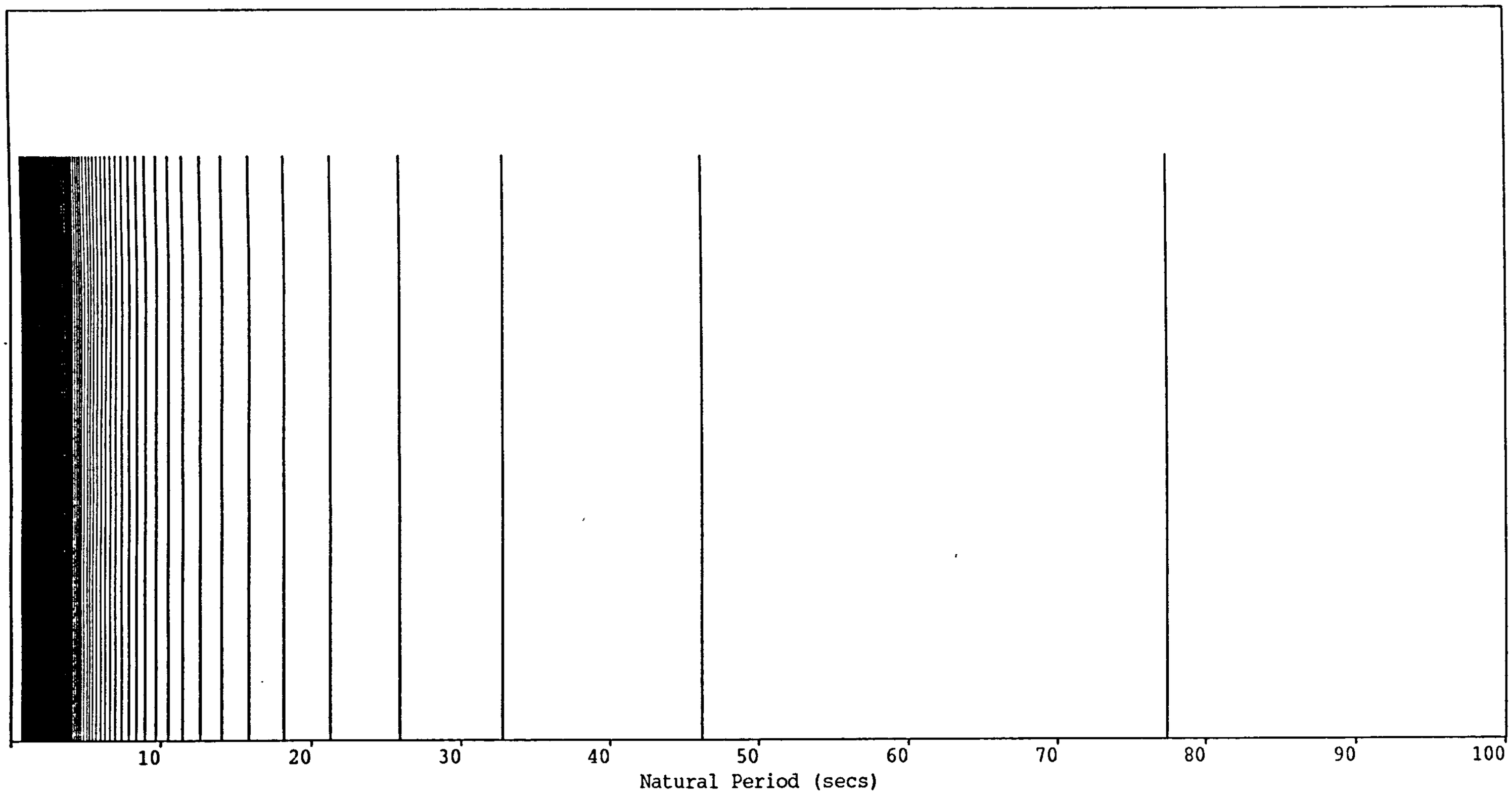

Horizontal Surface Offset = 1000 m

Carrier Pipe Outer Diameter = 1.10 m

Effective Unit Mass = 2165.1 kg/m

Sea Depth = 1500 m

Submerged Unit Weight = 2128 N/m

Figure 6.12

Natural Period Spectrum - Syntactic Foam Buoyancy (a = 1000 m, D = 1.20 m)

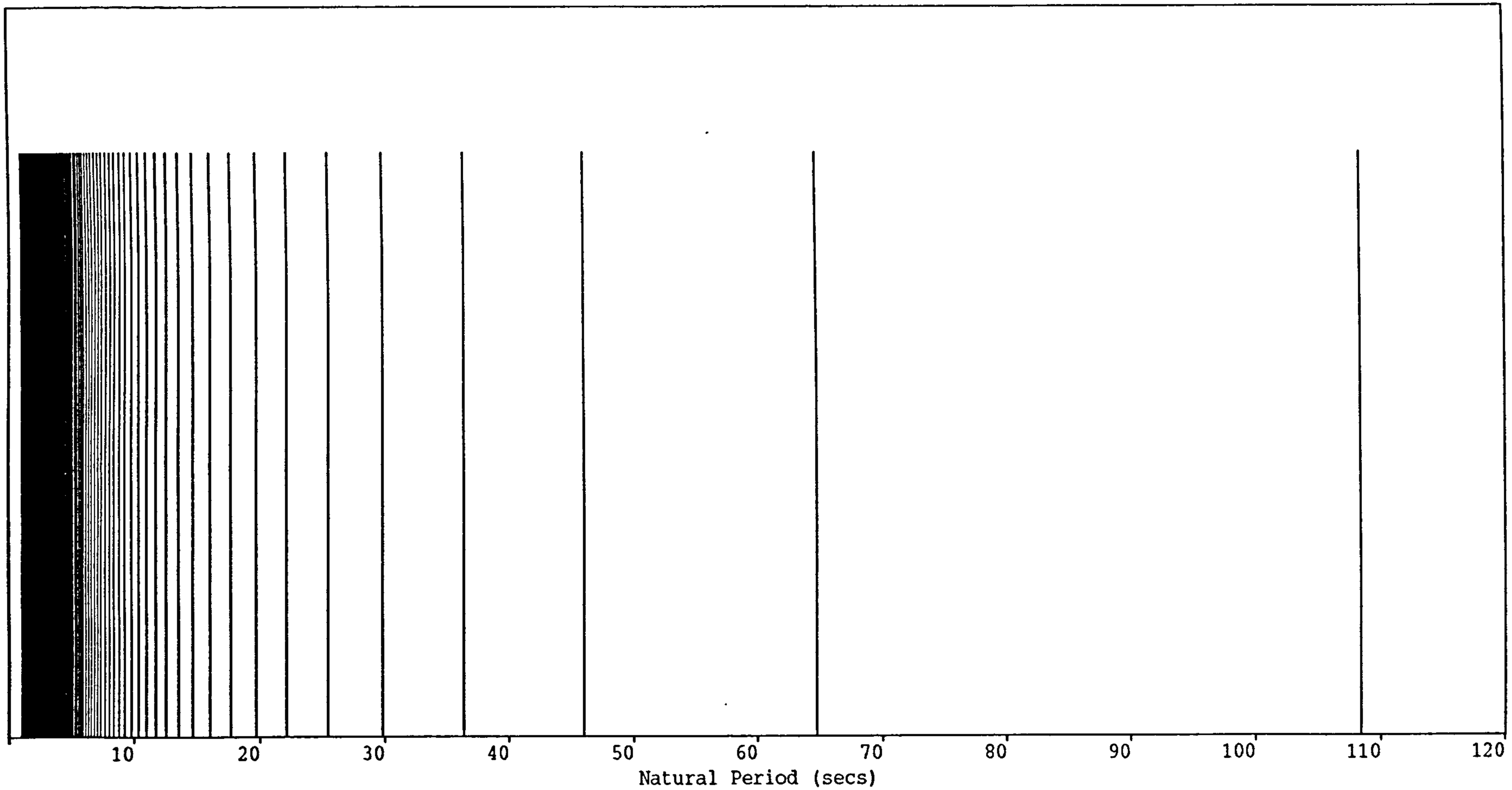

Horizontal Surface Offset = 1000 m

Carrier Pipe Outer Diameter = 1.20 m

Effective Unit Mass = 2443.2 kg/m

Sea Depth = 1500 m

Submerged Unit Weight = 1222 N/m

Figure 6.13

Natural Period Spectrum - Syntactic Foam Buoyancy (a = 1000 m, D = 1.30 m)

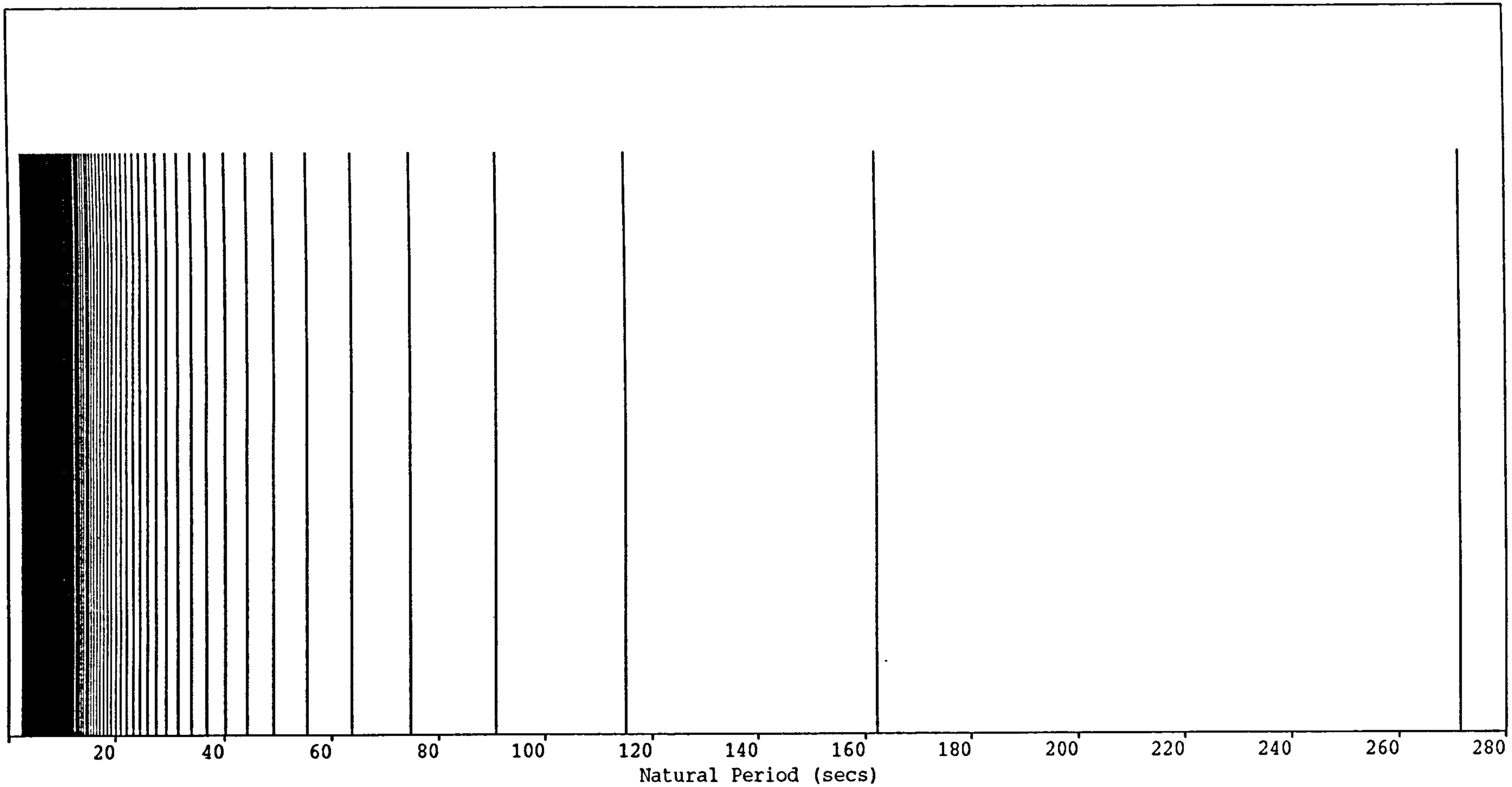

Horizontal Surface Offset = 1000 m

Carrier Pipe Outer Diameter = 1.30 m

Effective Unit Mass = 2743.5 kg/m

Sea Depth = 1500 m

Submerged Unit Weight = 219 N/m

Figure 6.14

Natural Period Spectrum - Nitrogen Gas Buoyancy (a = 1000 m, D = 1.0 m)

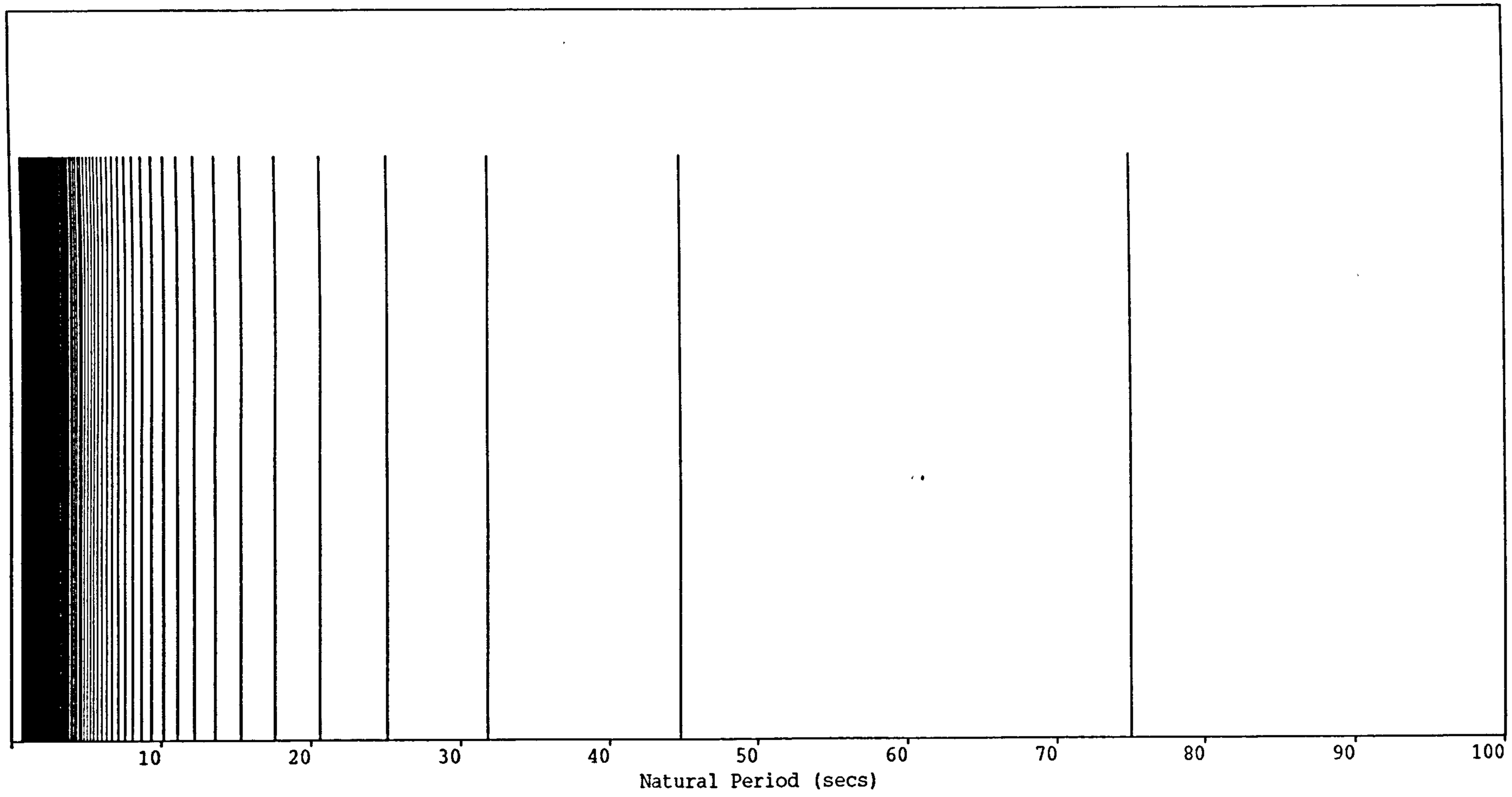

Horizontal Surface Offset = 1000 m

Carrier Pipe Outer Diameter = 1.0 m

Effective Unit Mass = 1802.0 kg/m

Sea Depth = 1500 m

Submerged Unit Weight = 1887 N/m

Figure 6.15

Natural Period Spectrum - Nitrogen Gas Buoyancy (a = 1000 m, D = 1.10 m)

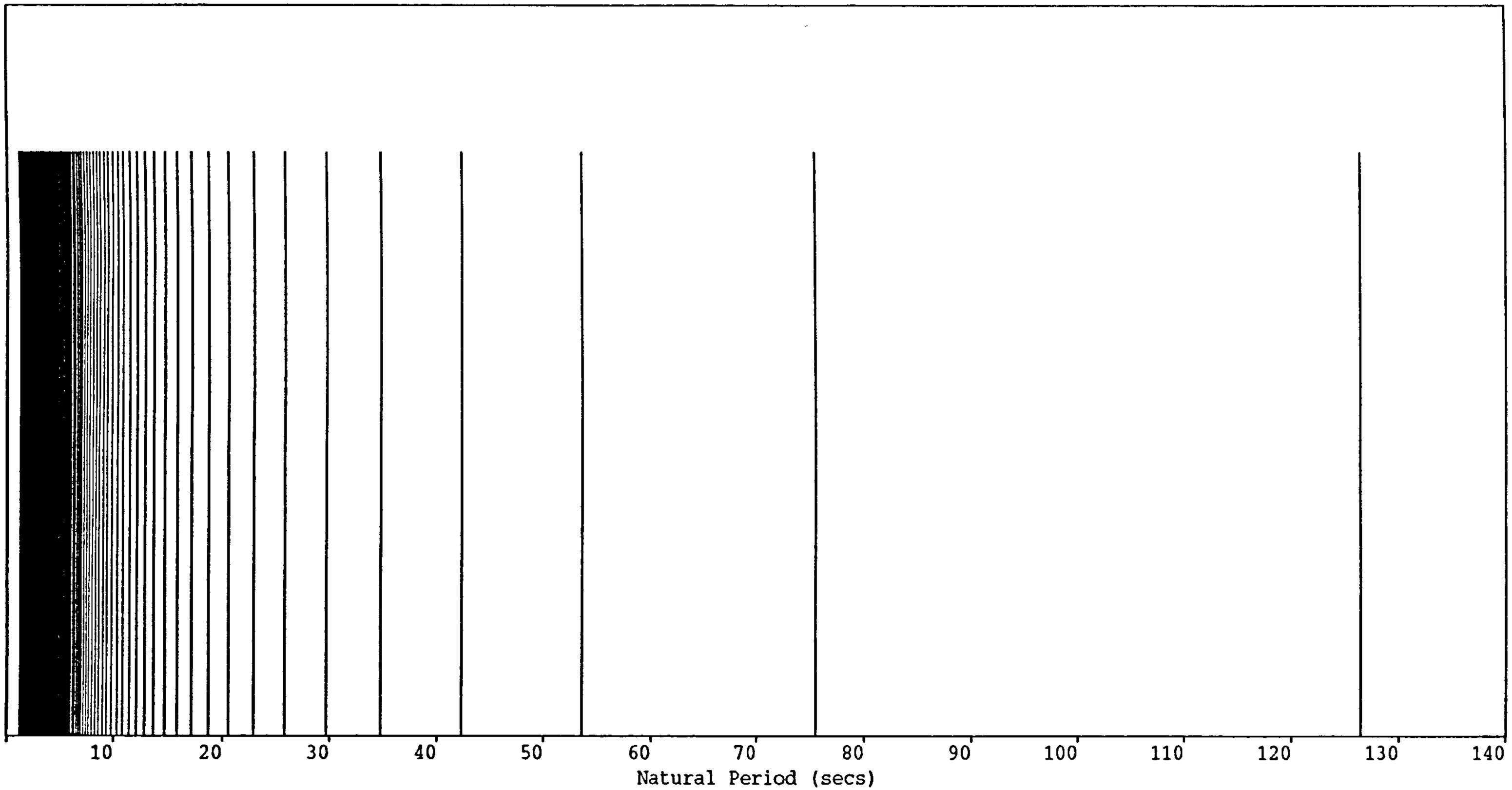

Horizontal Surface Offset = 1000 m

Carrier Pipe Outer Diameter = 1.10 m

Effective Unit Mass = 2024.1 kg/m

Sea Depth = 1500 m

Submerged Unit Weight = 745 N/m

Figure 6.16

Mode 1 - Fundamental

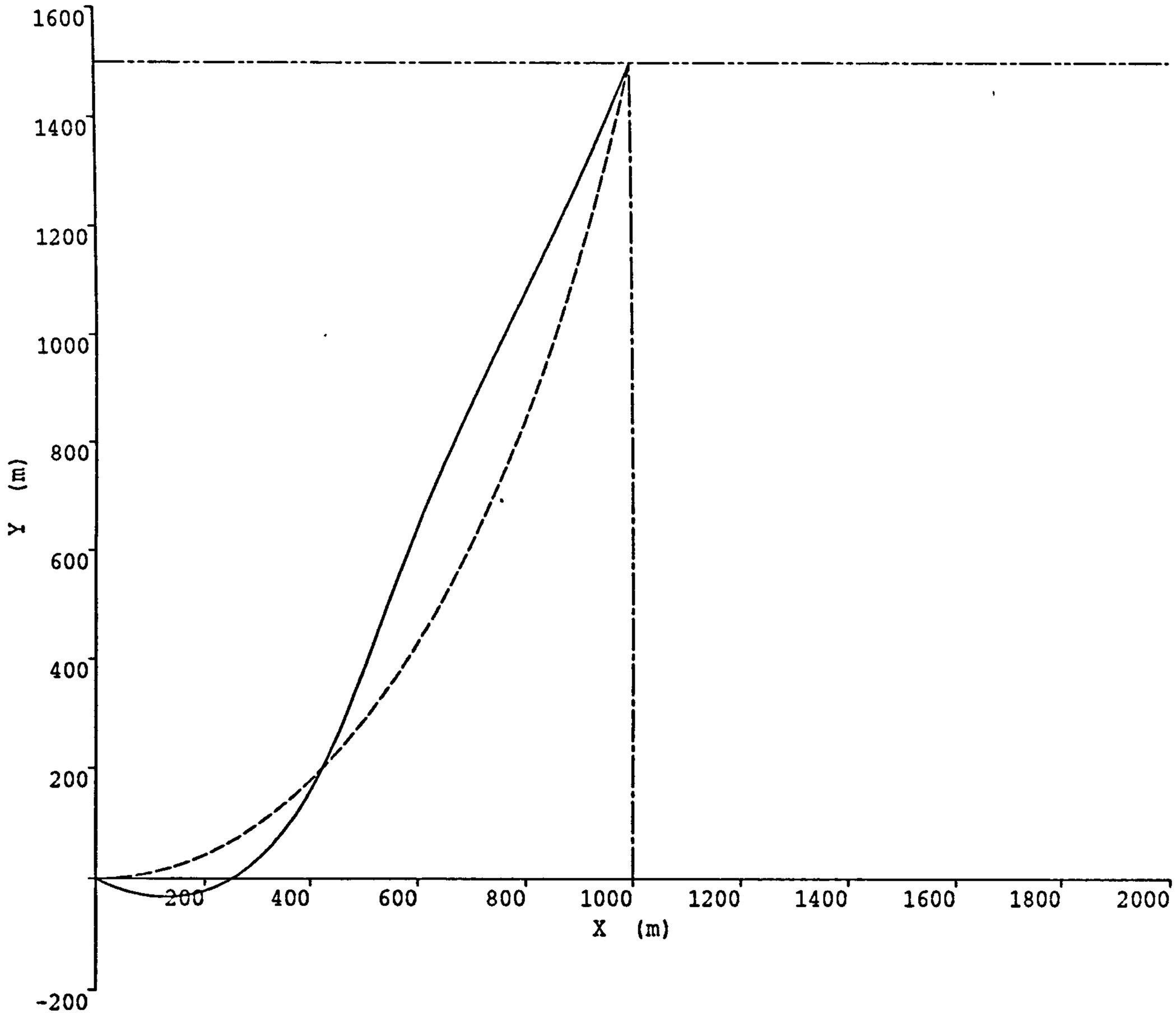

Figure 6.17(a)

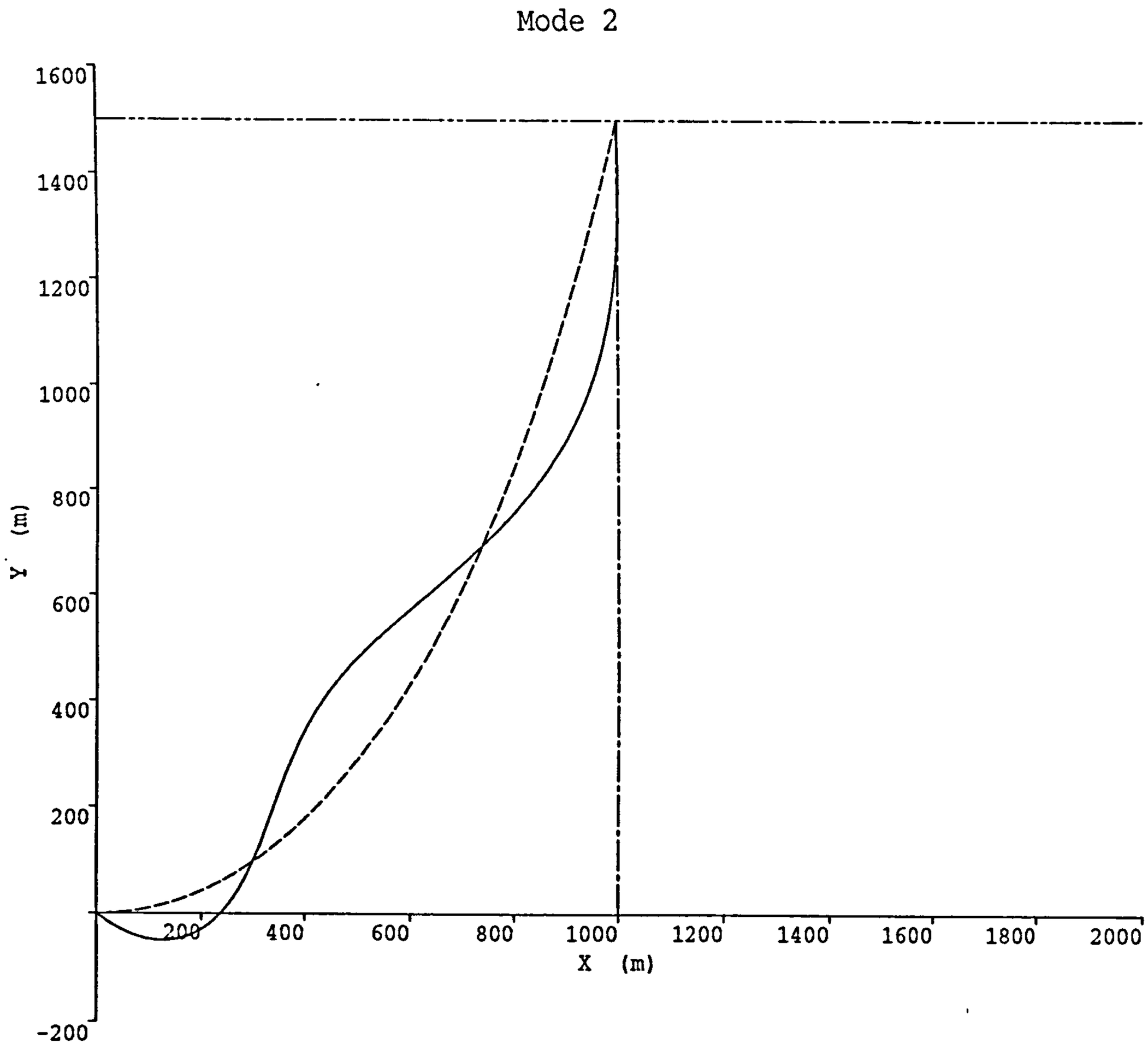
Mode 2
1600
1400
1200
1000
800
600
400
200
-200
Y (m)
200
400
600
800
1000
1200
1400
1600
1800
2000
X (m)

Figure 6.17(b)

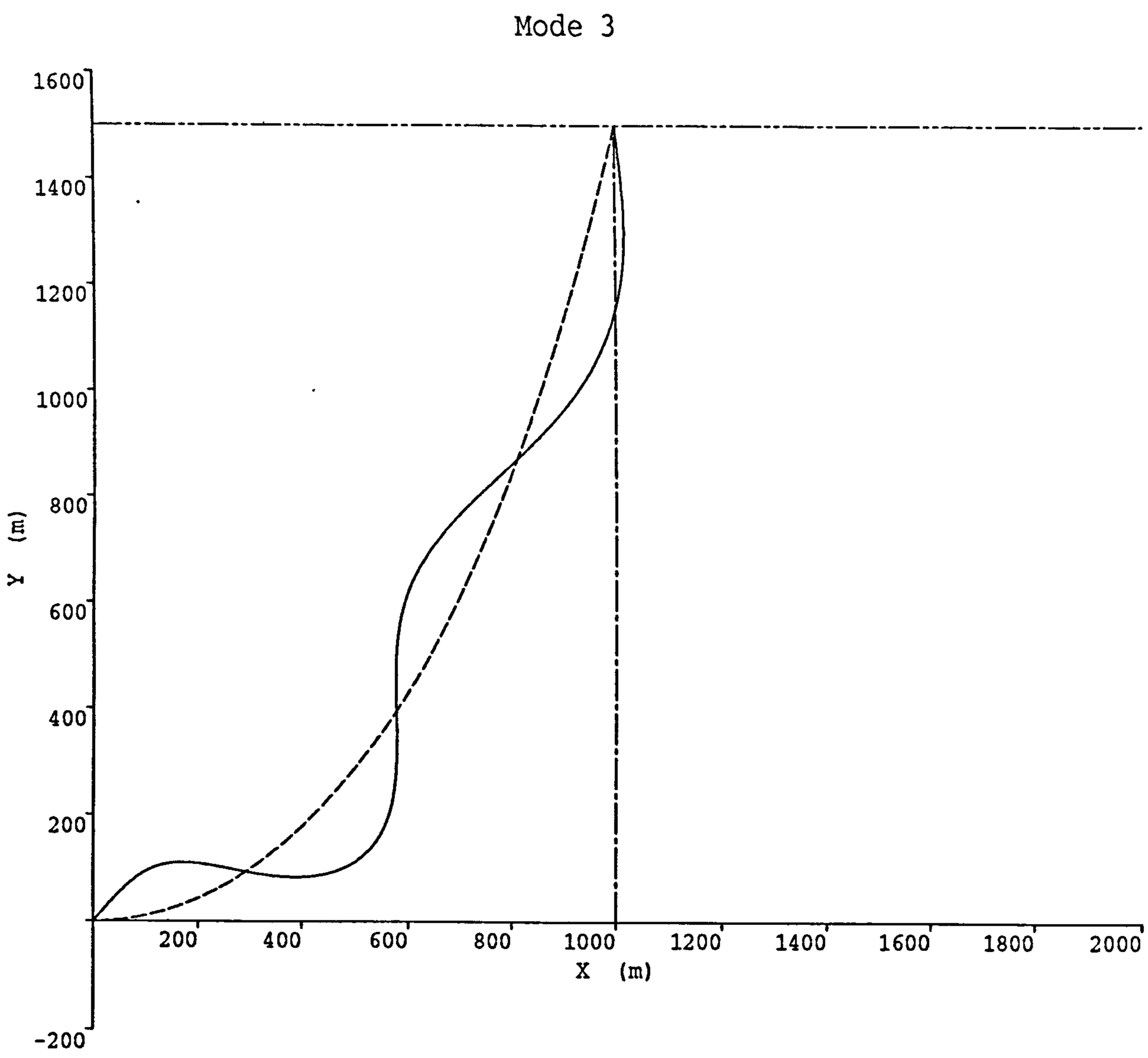
Mode 3
1600
1400
1200
1000
800
600
400
200
-200
Y (m)
200
400
600
800
1000
1200
1400
1600
1800
2000
X (m)

Figure 6.17(c)

Mode 4

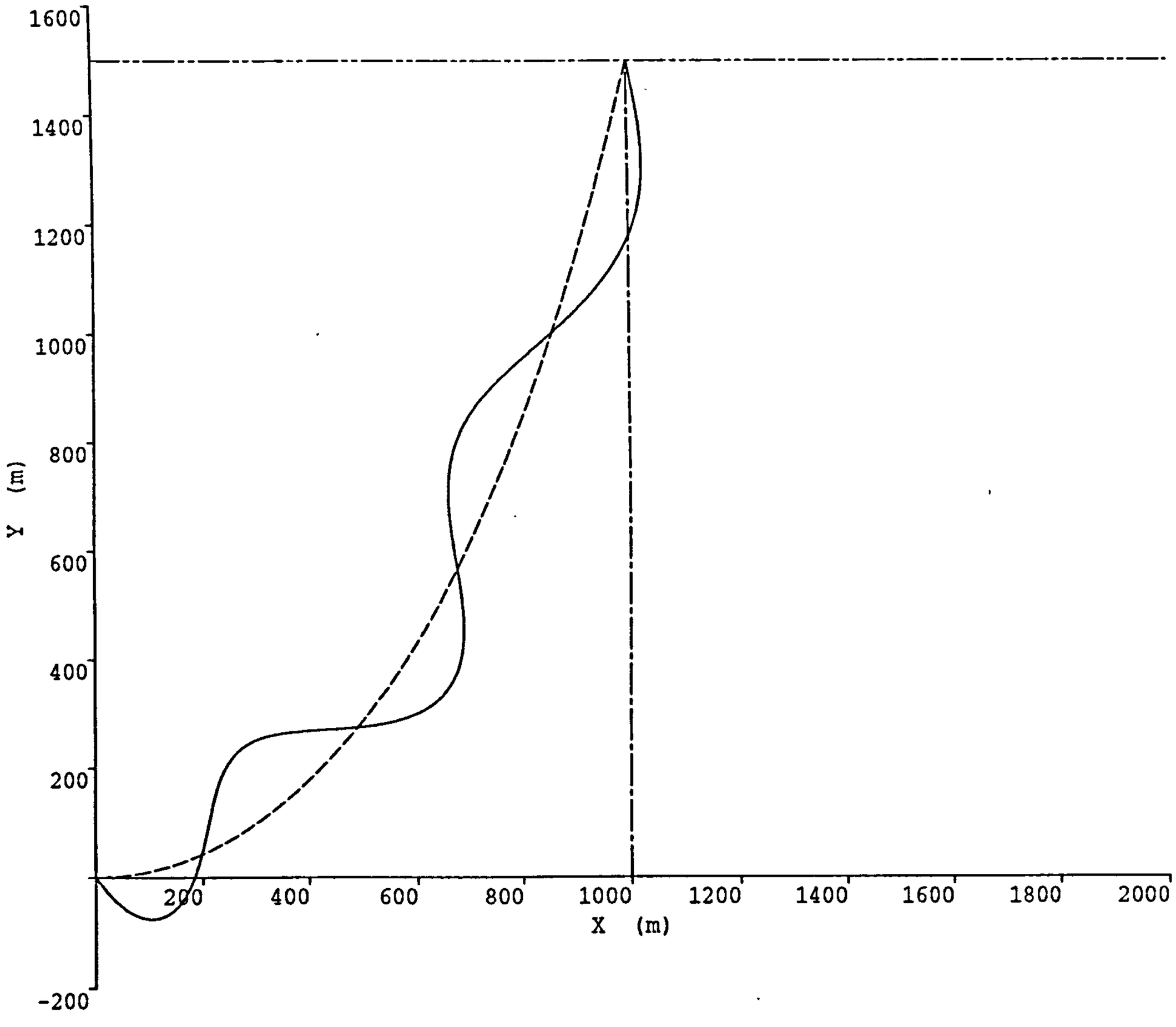

Figure 6.17(d)

Mode 5

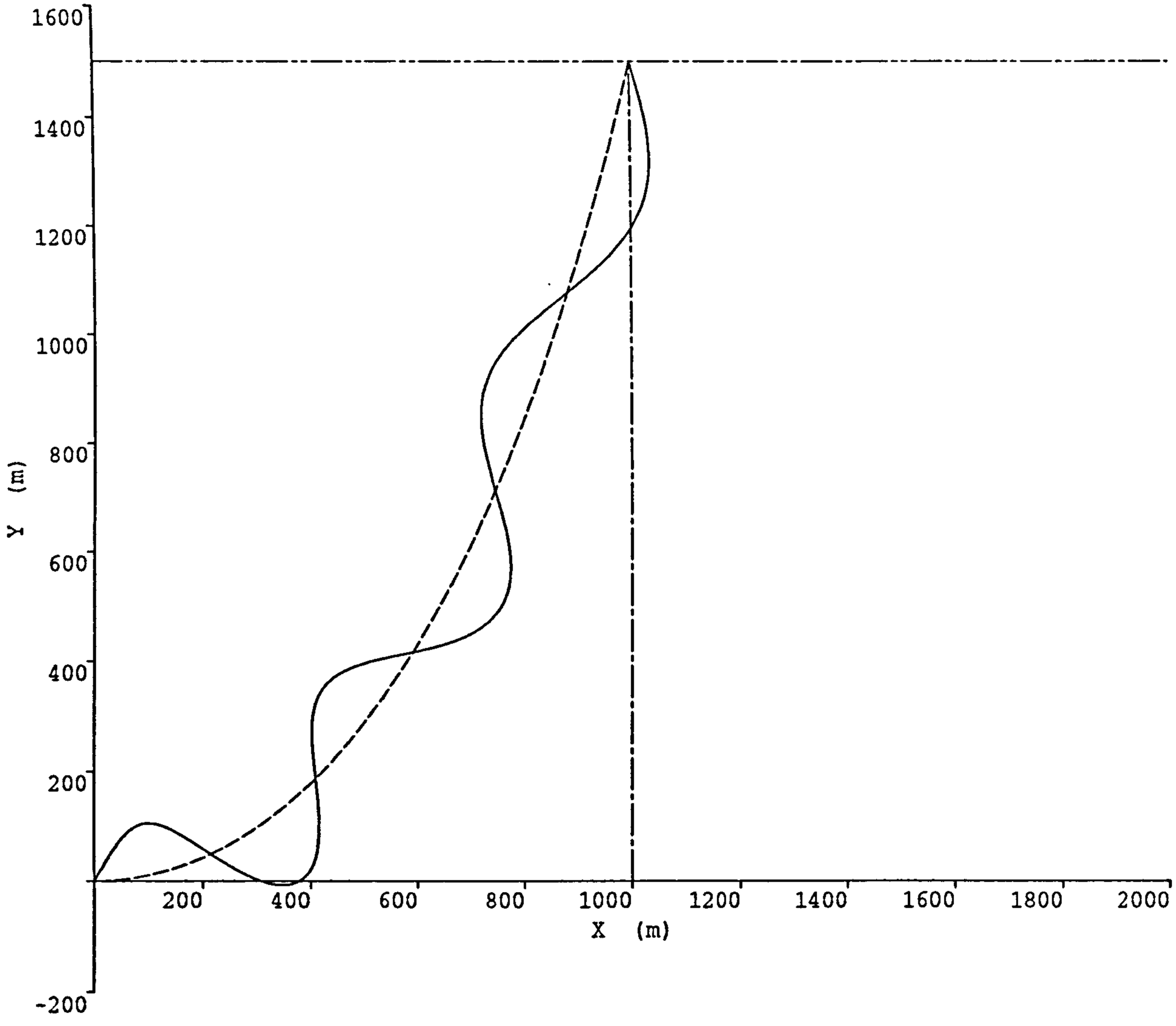

Figure 6.17(e)

Mode 6

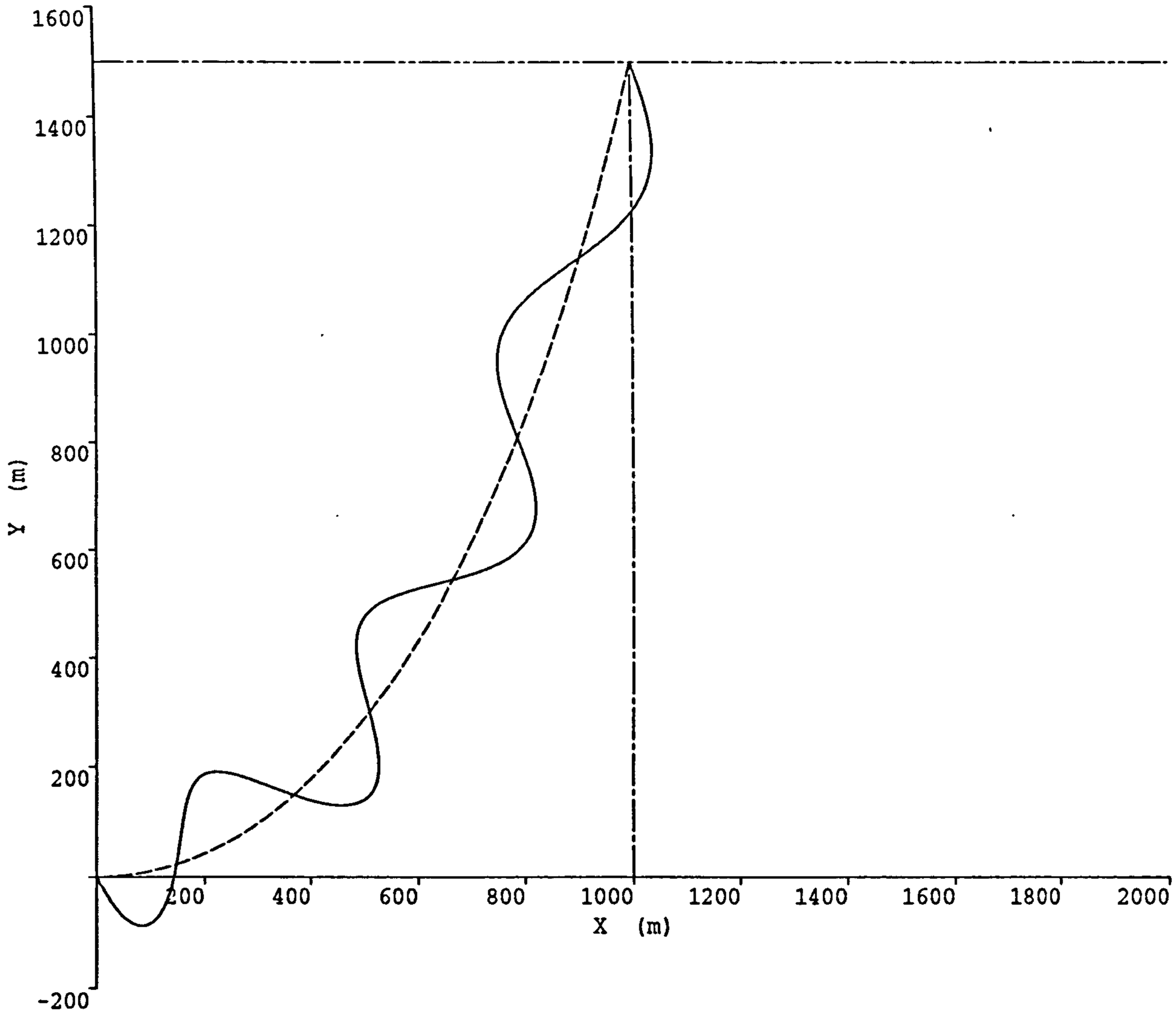

Figure 6.17(f)

Natural Period Spectrum - Syntactic Foam Buoyancy (a = 1500 m, D = 1.10 m)

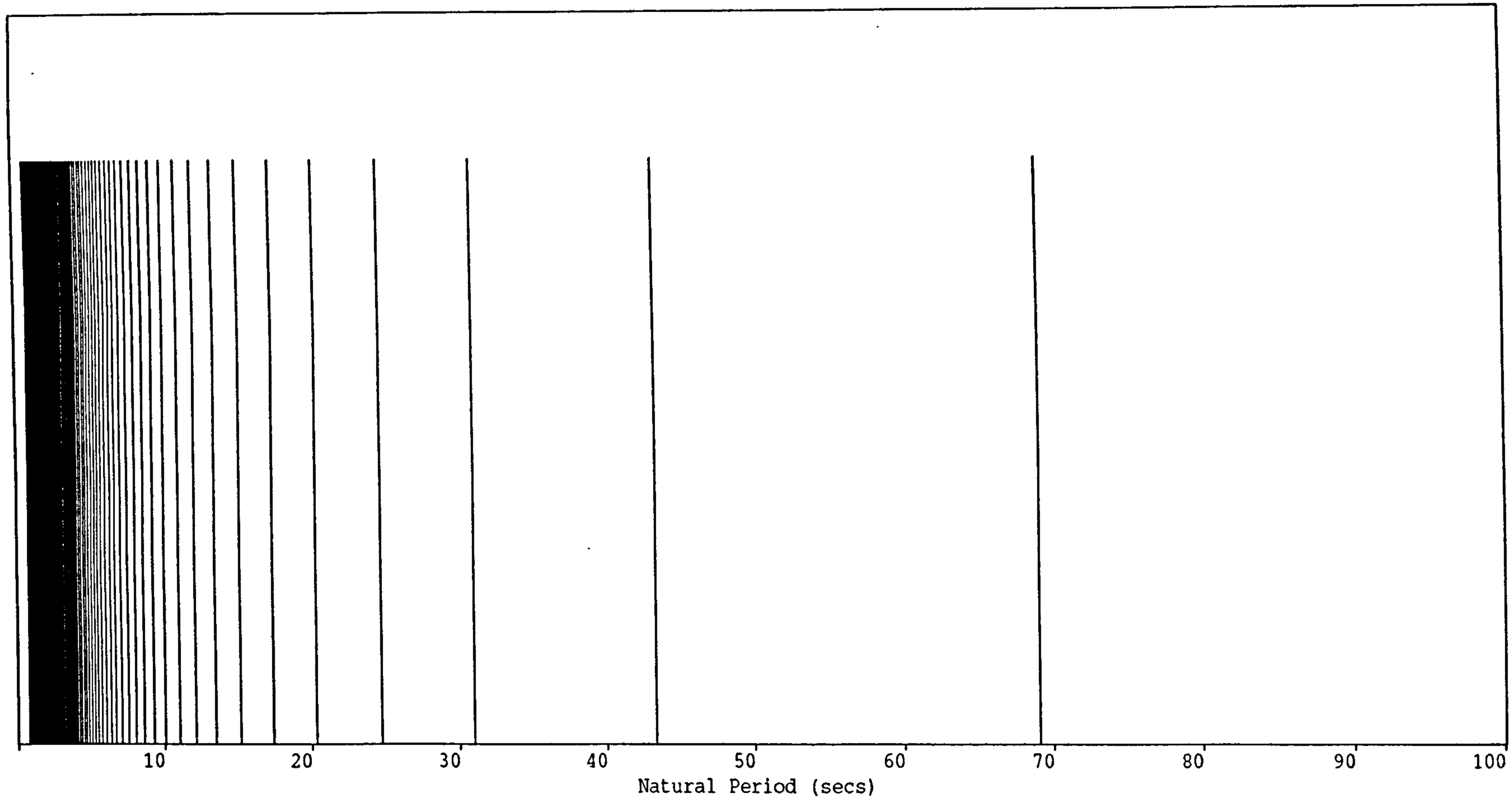

Horizontal Surface Offset = 1500 m

Carrier Pipe Outer Diameter = 1.10 m

Effective Unit Mass = 2165.1 kg/m

Sea Depth = 1500 m

Submerged Unit Weight = 2128 N/m

Figure 6.18

Natural Period Spectrum - Syntactic Foam Buoyancy (a = 1500 m, D = 1.20 m)

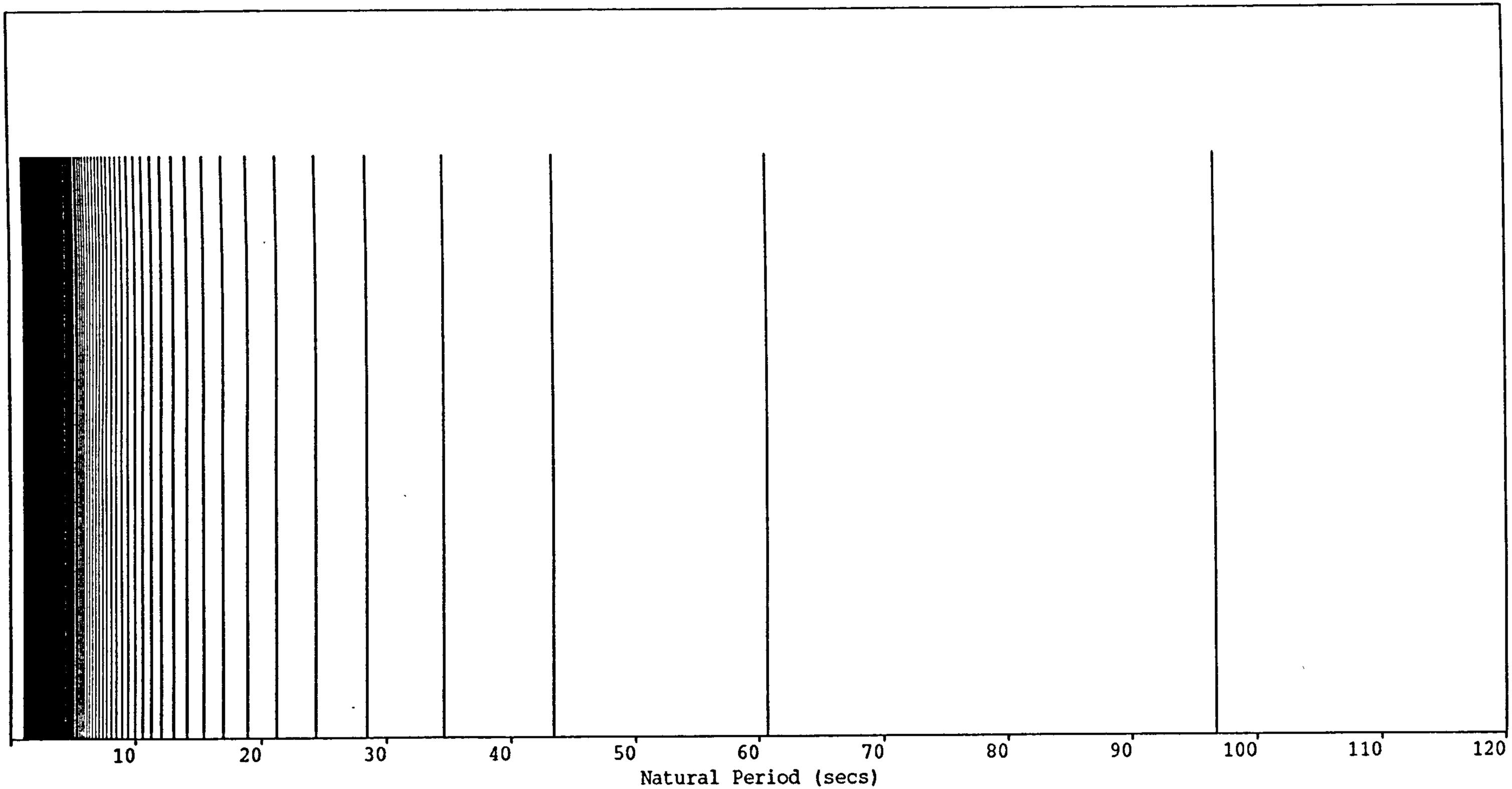

Horizontal Surface Offset = 1500 m

Carrier Pipe Outer Diameter = 1.20 m

Effective Unit Mass = 2443.2 kg/m

Sea Depth = 1500 m

Submerged Unit Weight = 1222 N/m

Figure 6.19

Natural Period Spectrum - Syntactic Foam Buoyancy (a = 1500 m, D = 1.30 m)

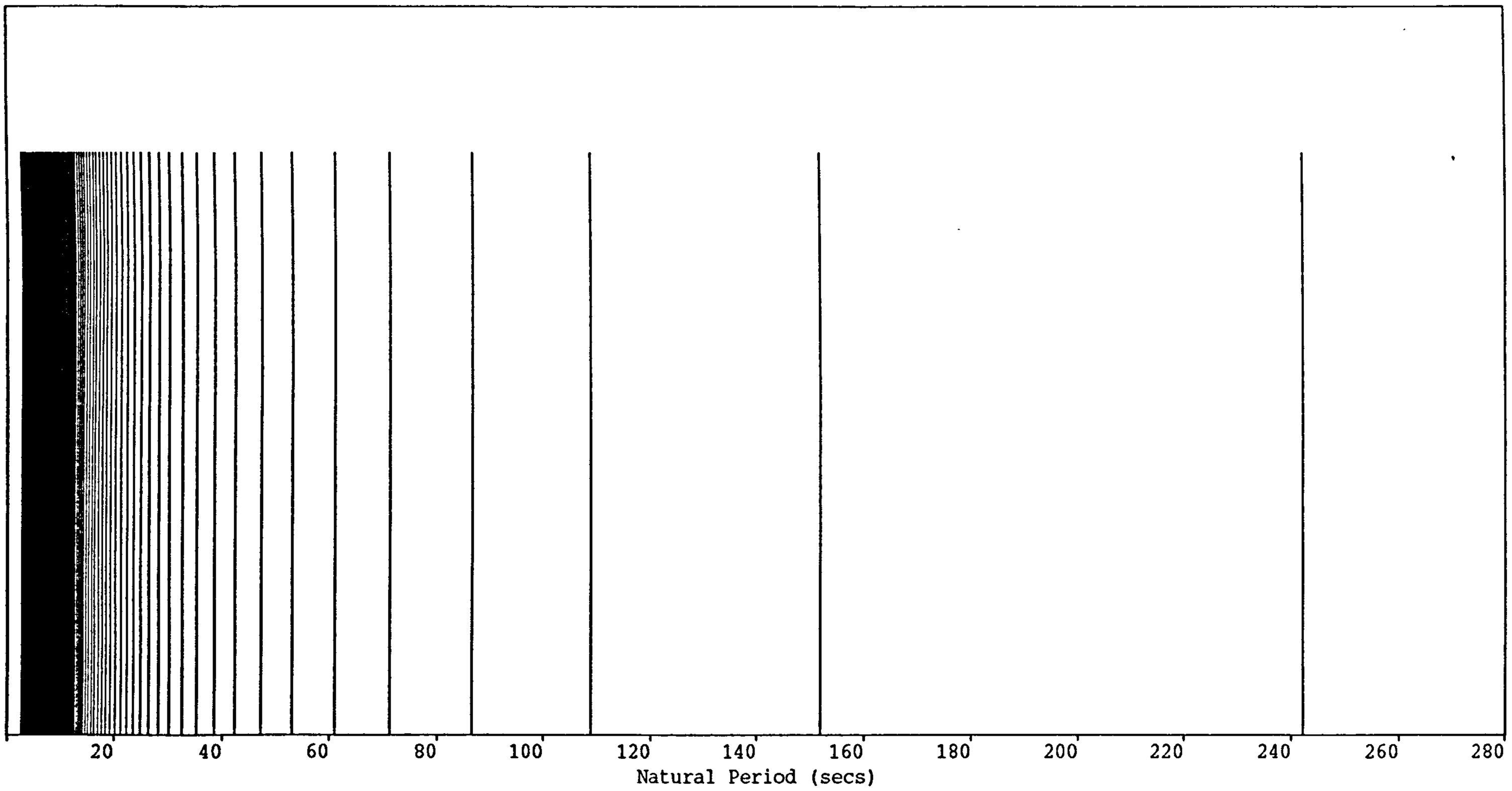

Horizontal Surface Offset = 1500 m

Carrier Pipe Outer Diameter = 1.30 m

Effective Unit Mass = 2743.5 kg/m

Sea Depth = 1500 m

Submerged Unit Weight = 219 N/m

Figure 6.20

Natural Period Spectrum - Nitrogen Gas Buoyancy (a = 1500 m, D = 1.0 m)

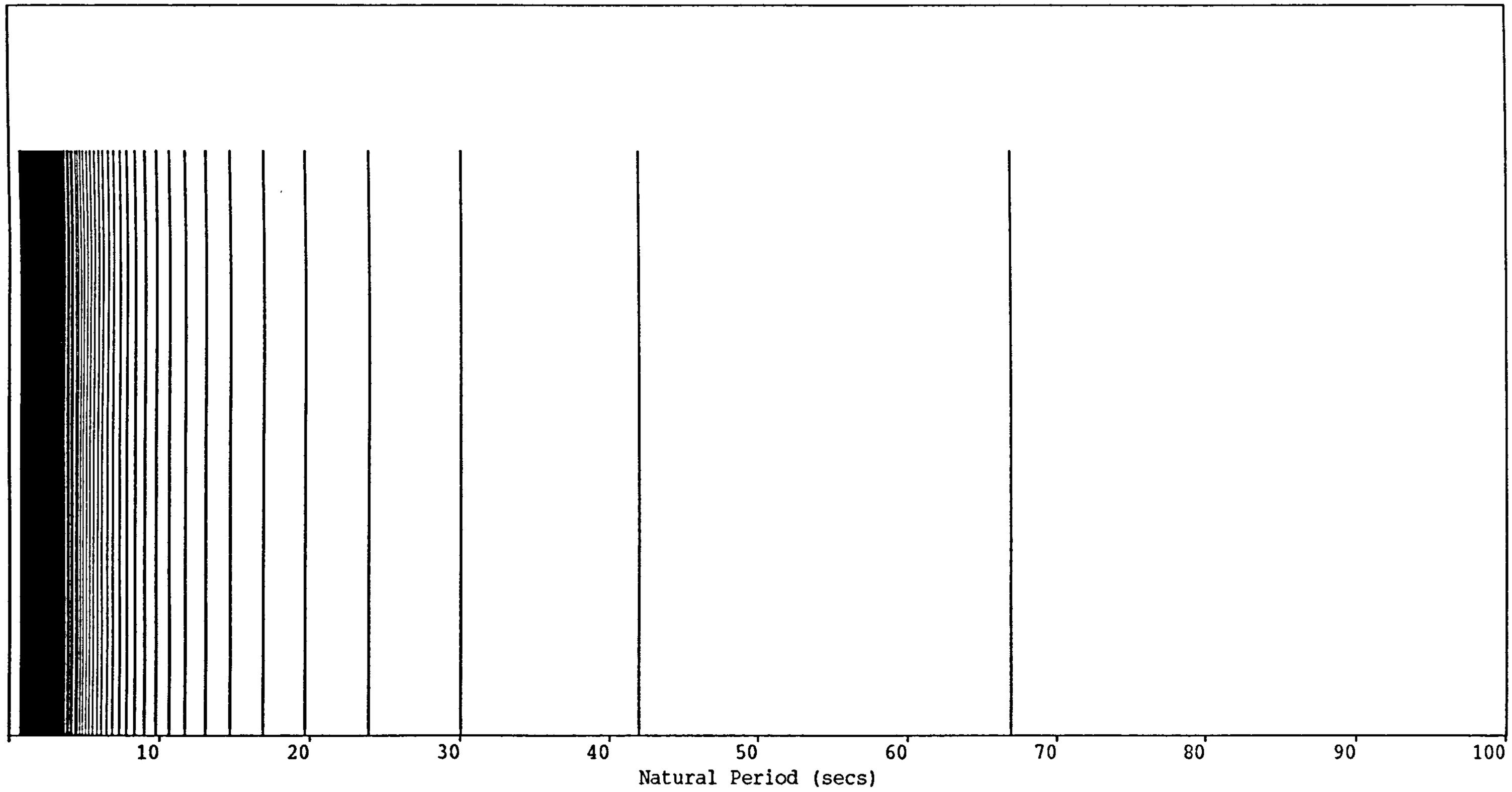

Horizontal Surface Offset = 1500 m

Carrier Pipe Outer Diameter = 1.0 m

Effective Unit Mass = 1802.0 kg/m

Sea Depth = 1500 m

Submerged Unit Weight = 1887 N/m

Figure 6.21

Natural Period Spectrum - Nitrogen Gas Buoyancy (a = 1500 m, D = 1.10 m)

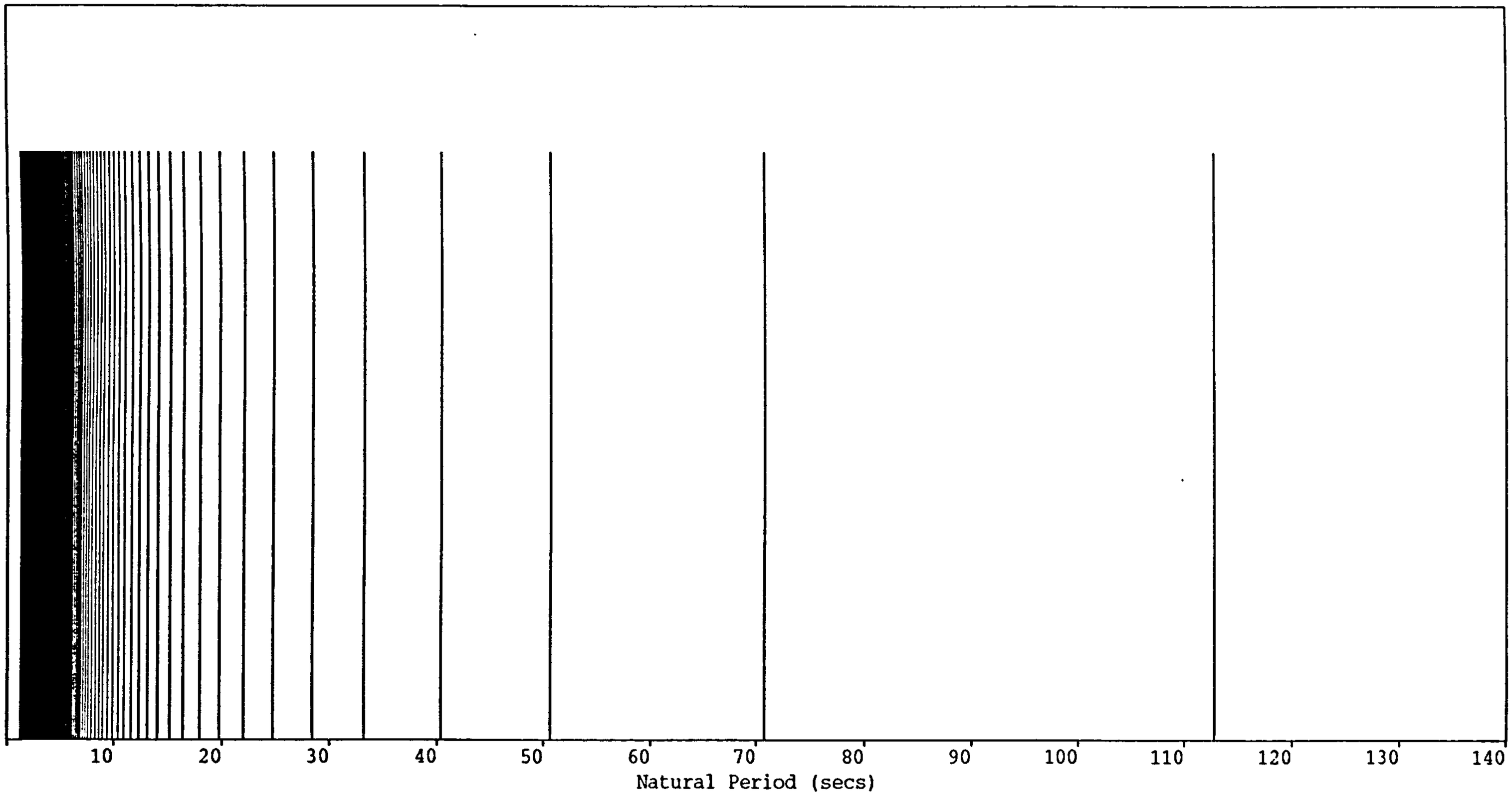

Horizontal Surface Offset = 1500 m

Carrier Pipe Outer Diameter = 1.10 m

Effective Unit Mass = 2024.1 kg/m

Sea Depth = 1500 m

Submerged Unit Weight = 745 N/m

Figure 6.22

Mode 1 - Fundamental

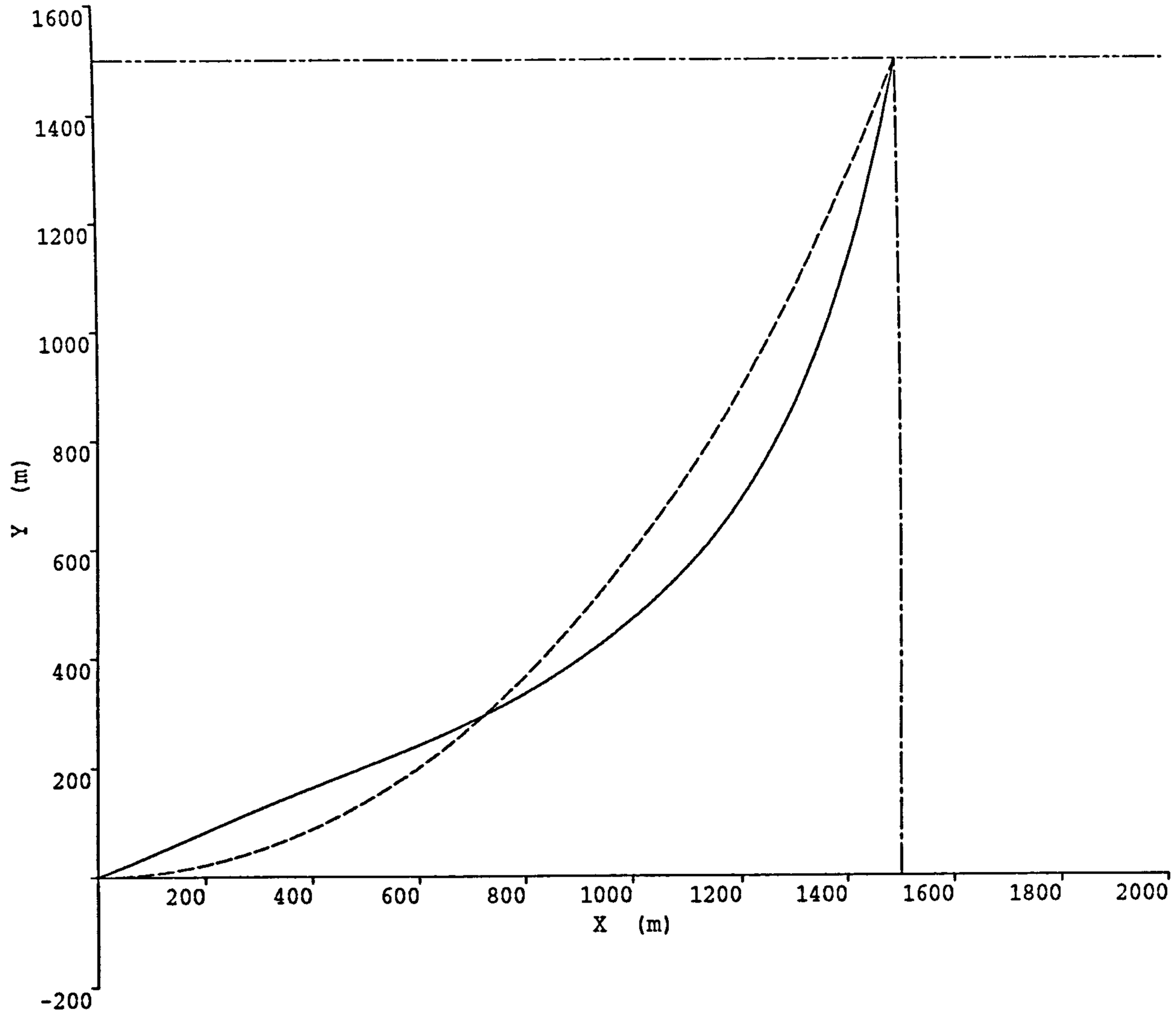

Figure 6.23(a)

Mode 2

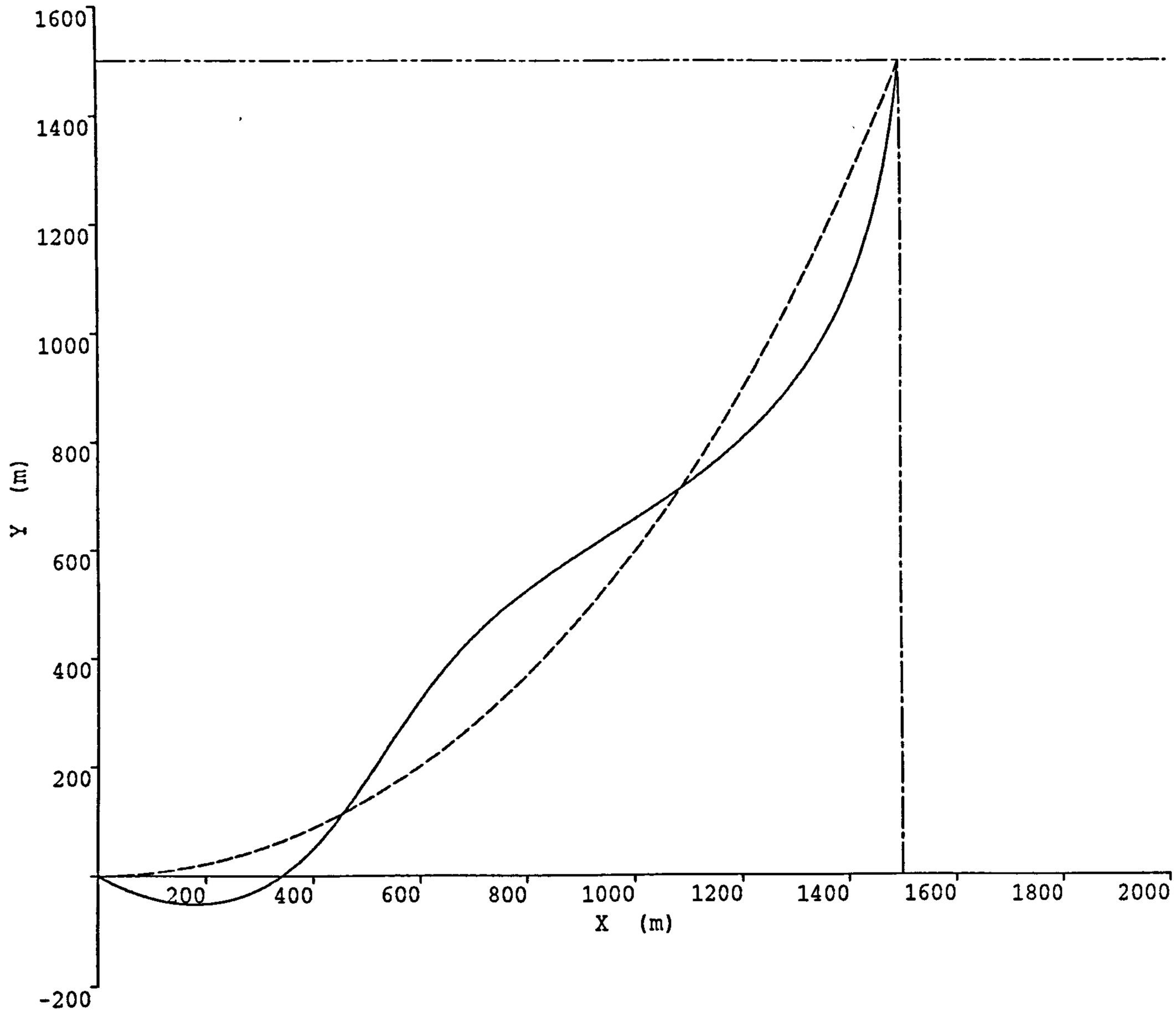

Figure 6.23(b)

Mode 3

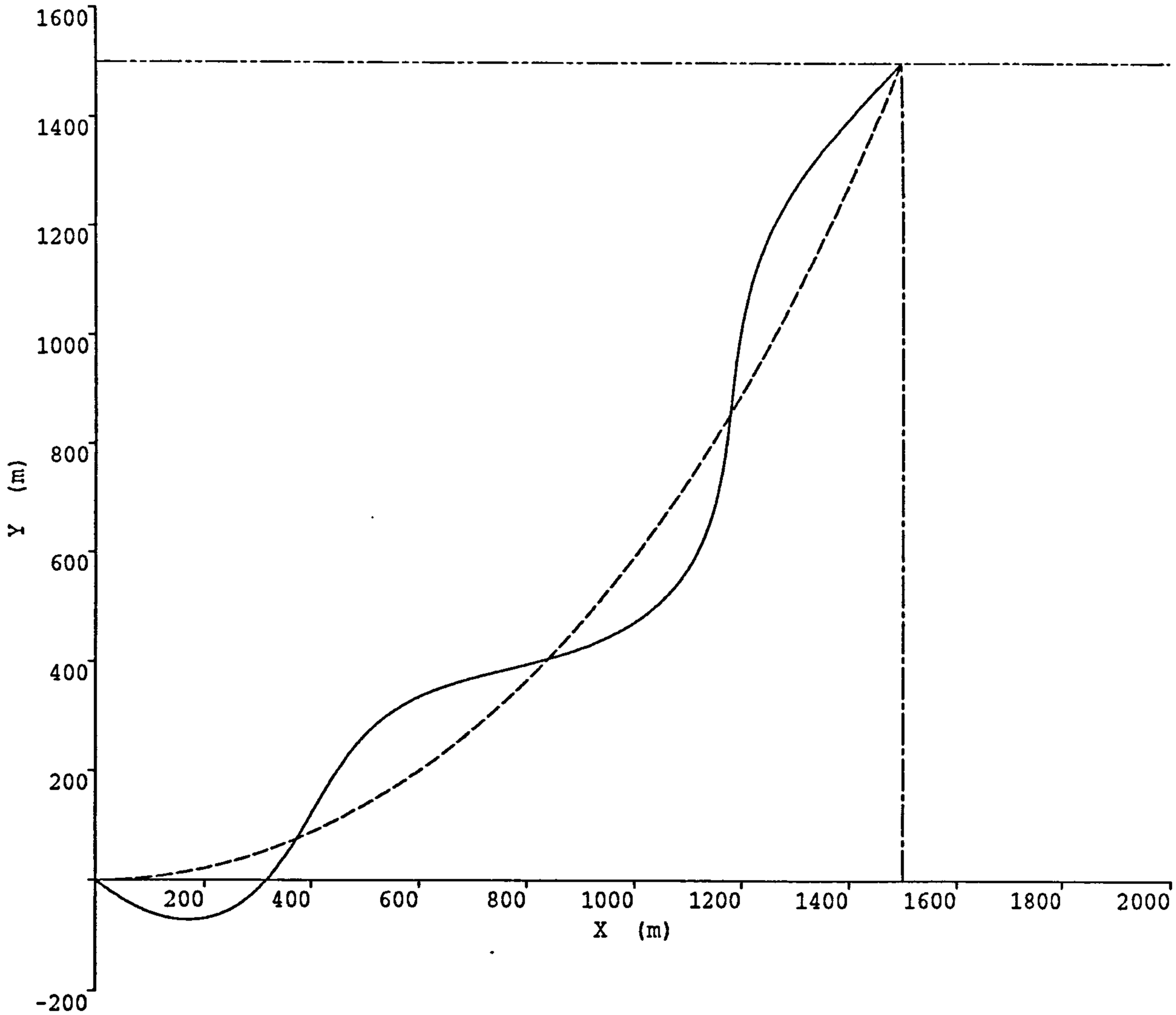

Figure 6.23(c)

Mode 4

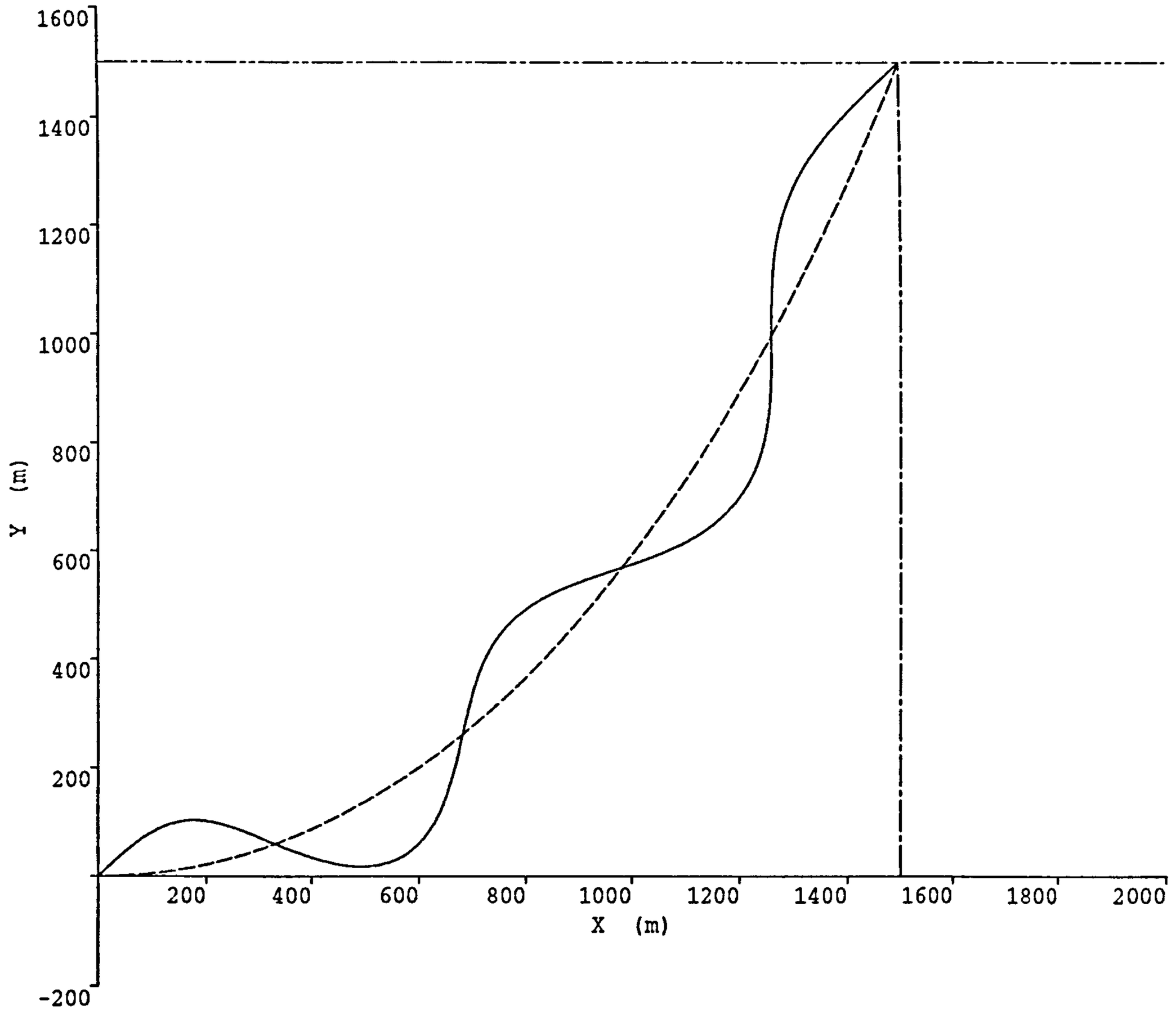

Figure 6.23(d)

Mode 5

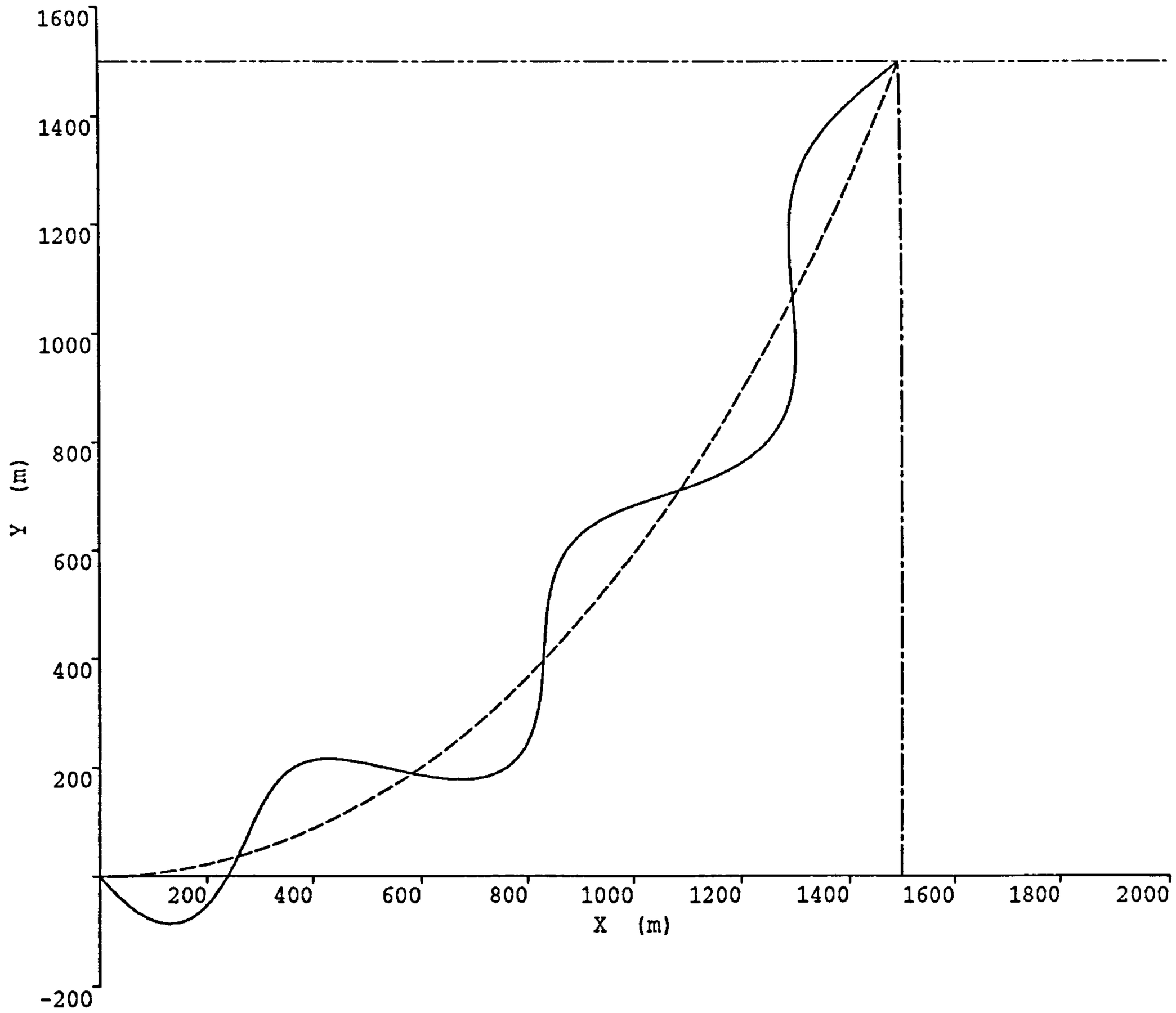

Figure 6.23(e)

Mode 6

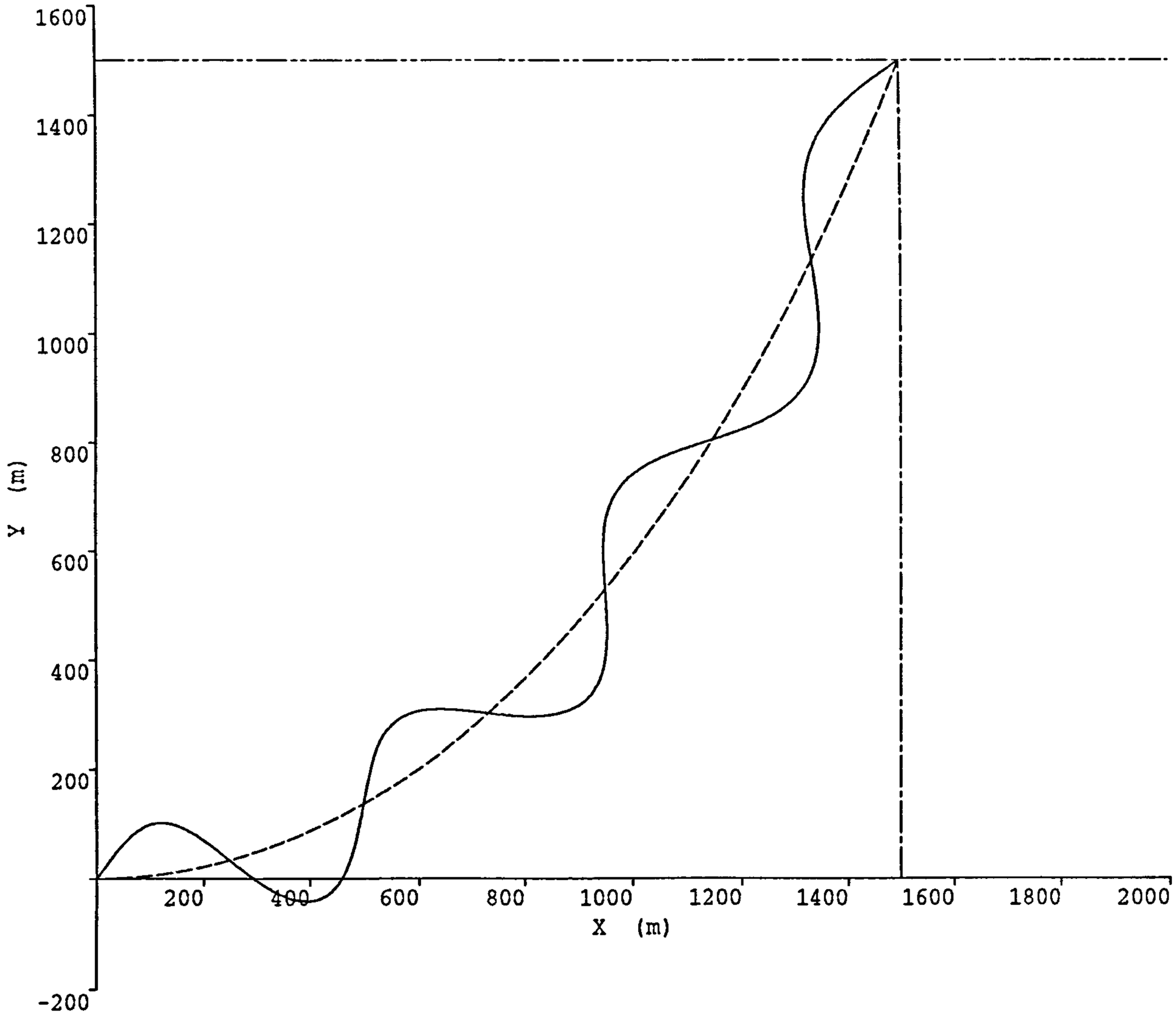

Figure 6.23(f)

Natural Period Spectrum - Syntactic Foam Buoyancy (a = 2000 m, D = 1.10 m)

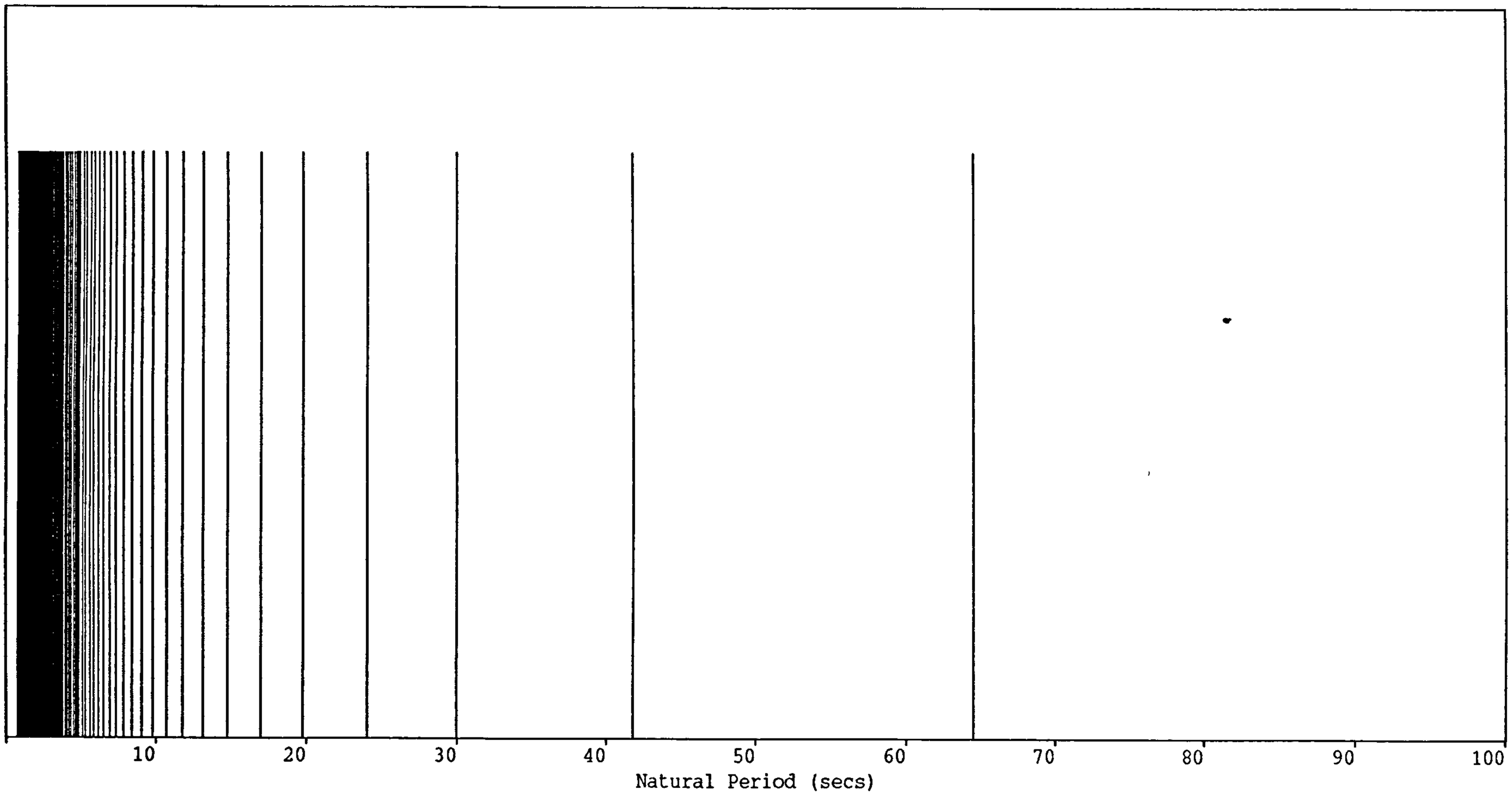

Horizontal Surface Offset = 2000 m

Carrier Pipe Outer Diameter = 1.10 m

Effective Unit Mass = 2165.1 kg/m

Sea Depth = 1500 m

Submerged Unit Weight = 2128 N/m

Figure 6.24

Natural Period Spectrum - Syntactic Foam Buoyancy (a = 2000 m, D = 1.20 m)

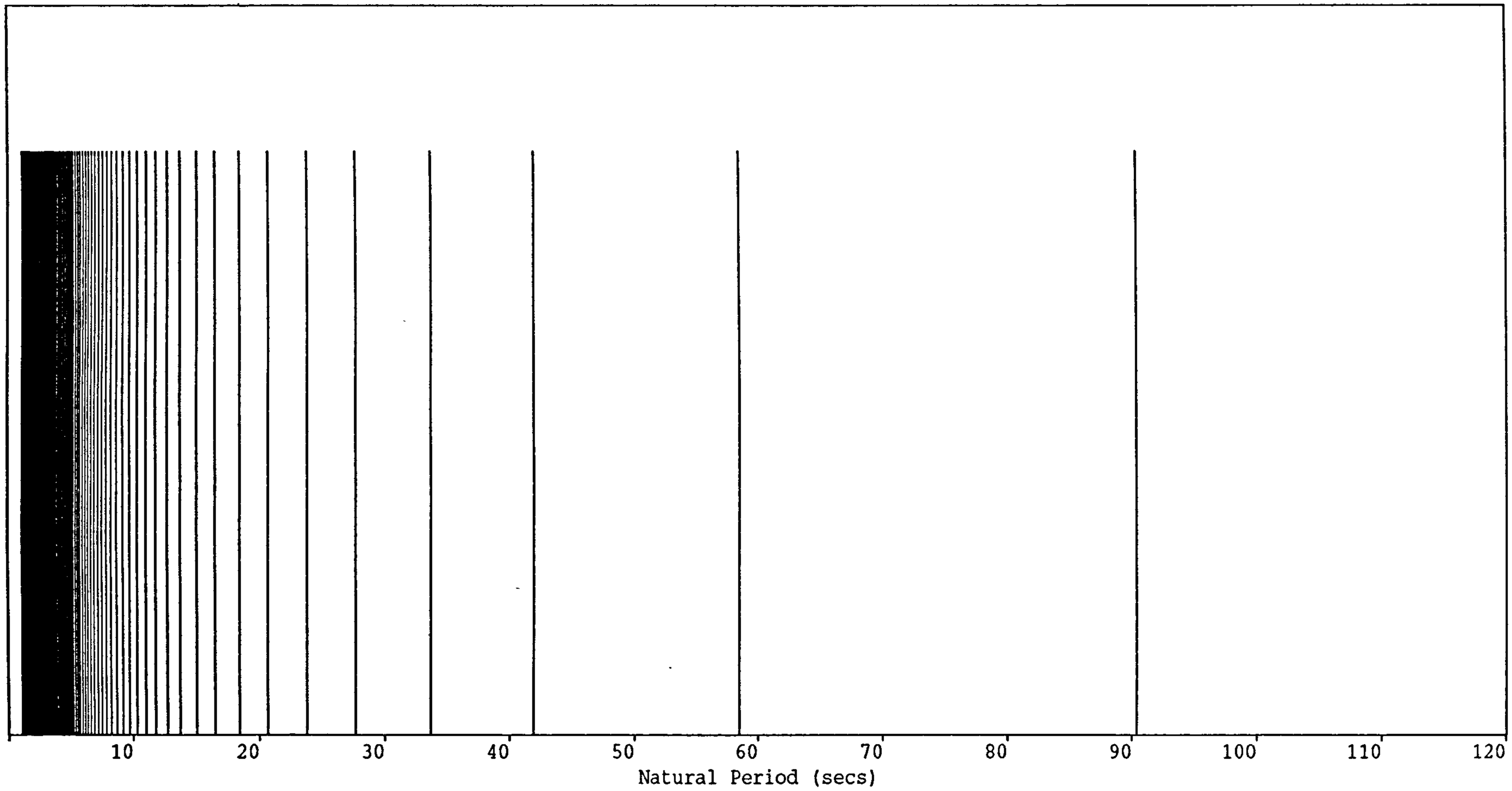

Horizontal Surface Offset = 2000 m

Carrier Pipe Outer Diameter = 1.20 m

Effective Unit Mass = 2443.2 kg/m

Sea Depth = 1500 m

Submerged Unit Weight = 1222 N/m

Figure 6.25

Natural Period Spectrum - Syntactic Foam Buoyancy (a = 2000 m, D = 1.30 m)

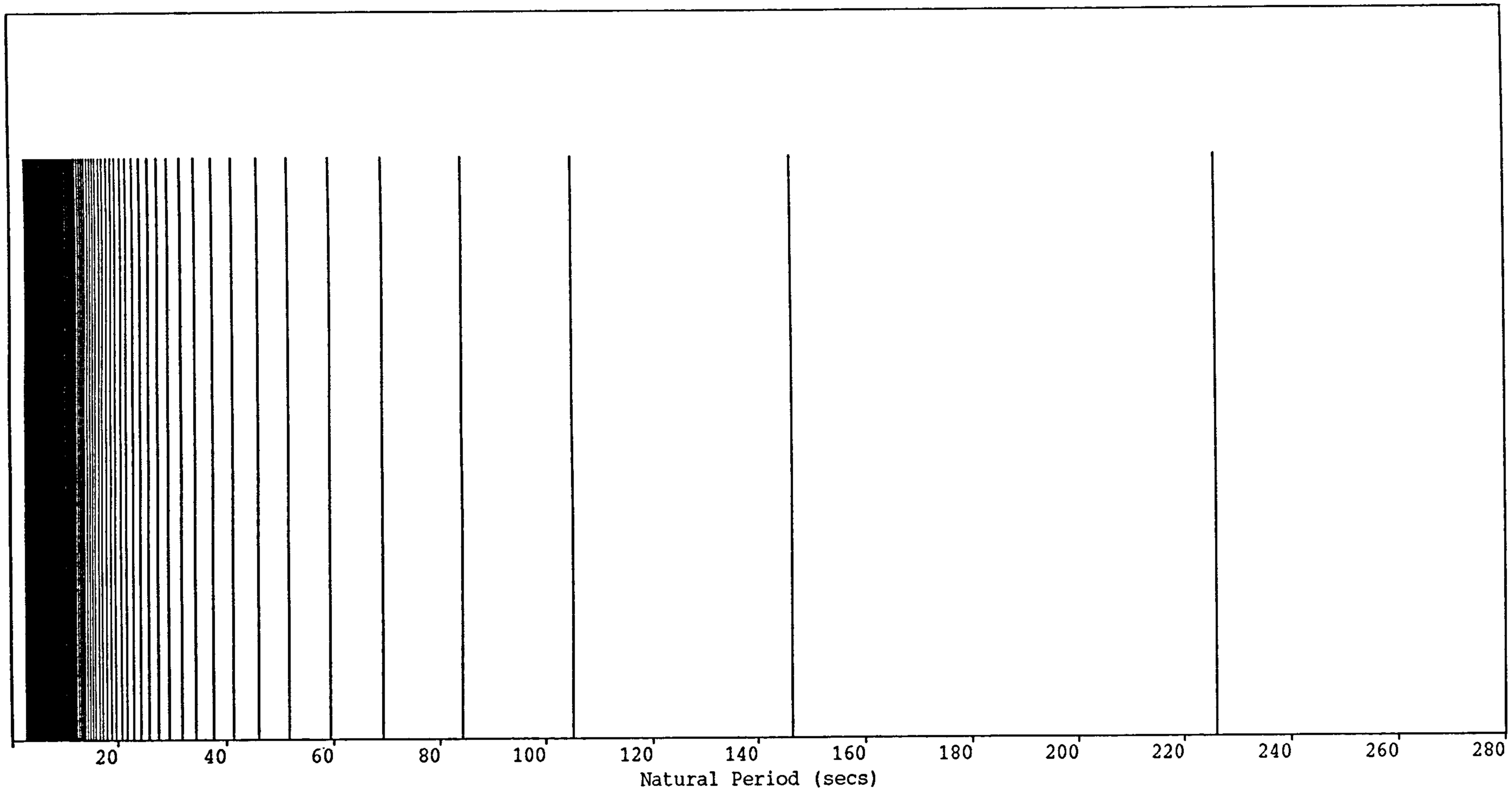

Horizontal Surface Offset = 2000 m

Carrier Pipe Outer Diameter = 1.30 m

Effective Unit Mass = 2743.5 kg/m

Sea Depth = 1500 m

Submerged Unit Weight = 219 N/m

Figure 6.26

Natural Period Spectrum - Nitrogen Gas Buoyancy (a = 2000 m, D = 1.0 m)

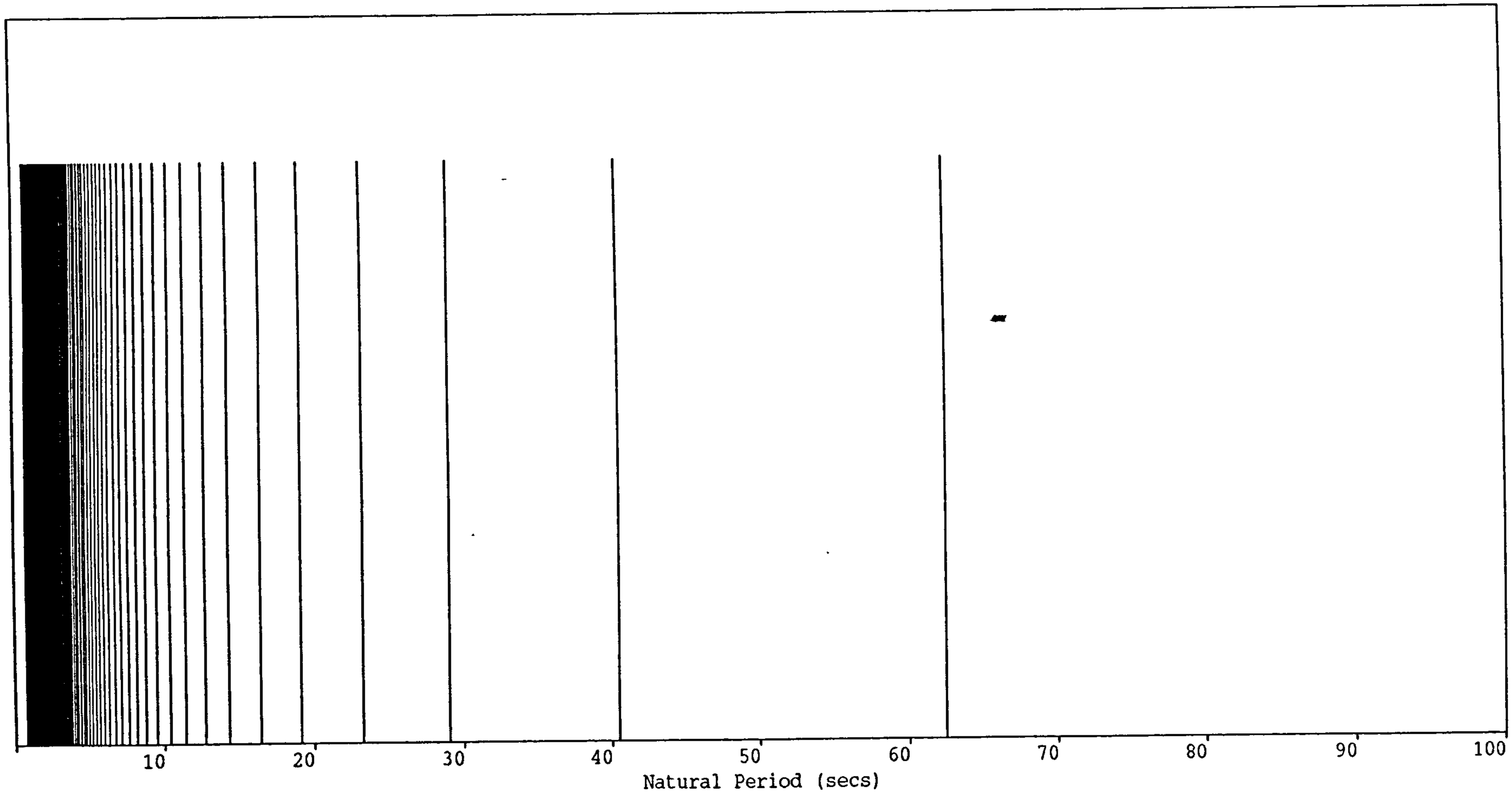

Horizontal Surface Offset = 2000 m

Carrier Pipe Outer Diameter = 1.0 m

Effective Unit Mass = 1802.0 kg/m

Sea Depth = 1500 m

Submerged Unit Weight = 1887 N/m

Figure 6.27

Natural Period Spectrum - Nitrogen Gas Buoyancy (a = 2000 m, D = 1.10 m)

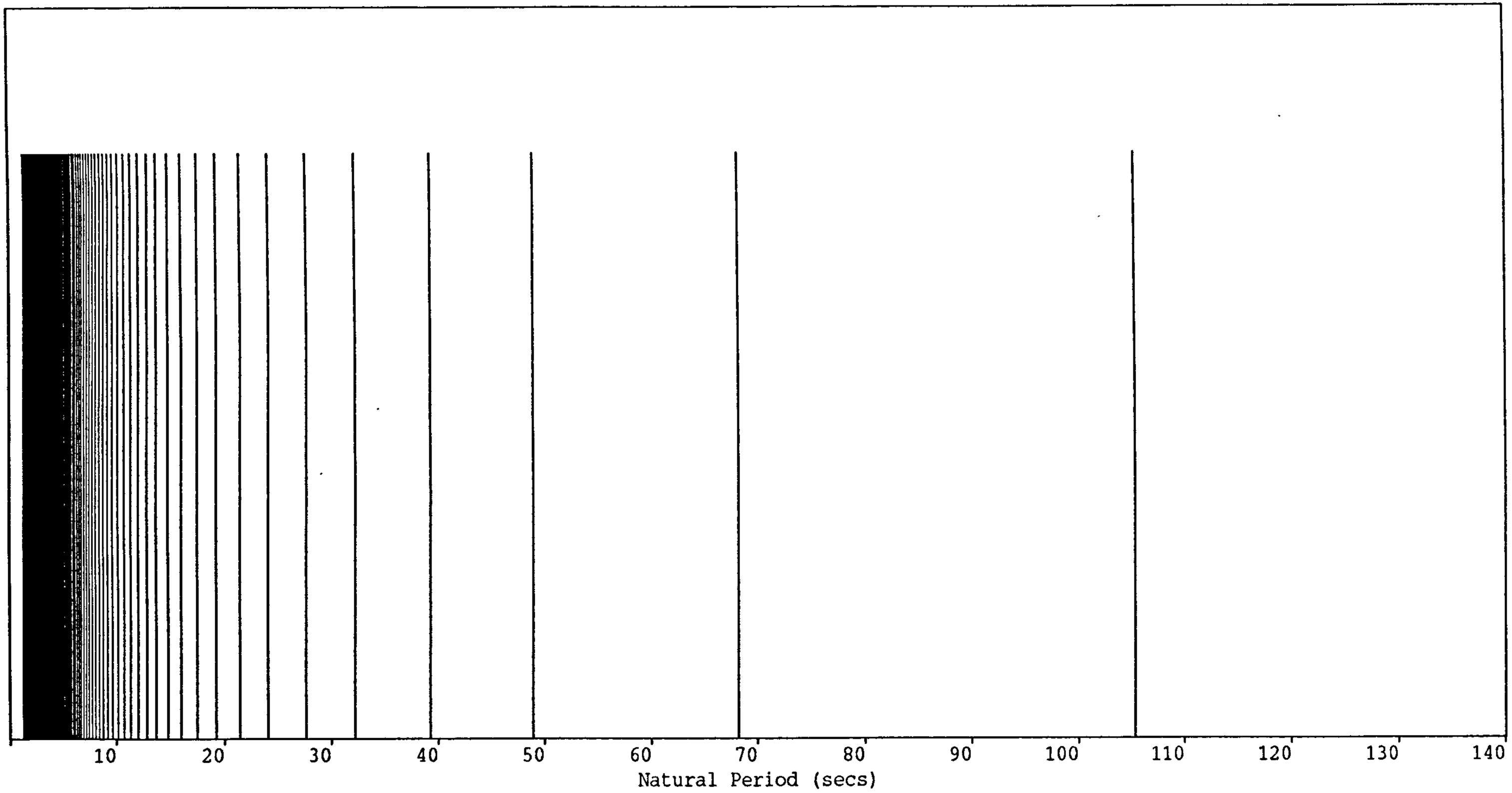

Horizontal Surface Offset = 2000 m

Carrier Pipe Outer Diameter = 1.10 m

Effective Unit Mass = 2024.1 kg/m

Sea Depth = 1500 m

Submerged Unit Weight = 745 N/m

Figure 6.28

Mode 1 - Fundamental

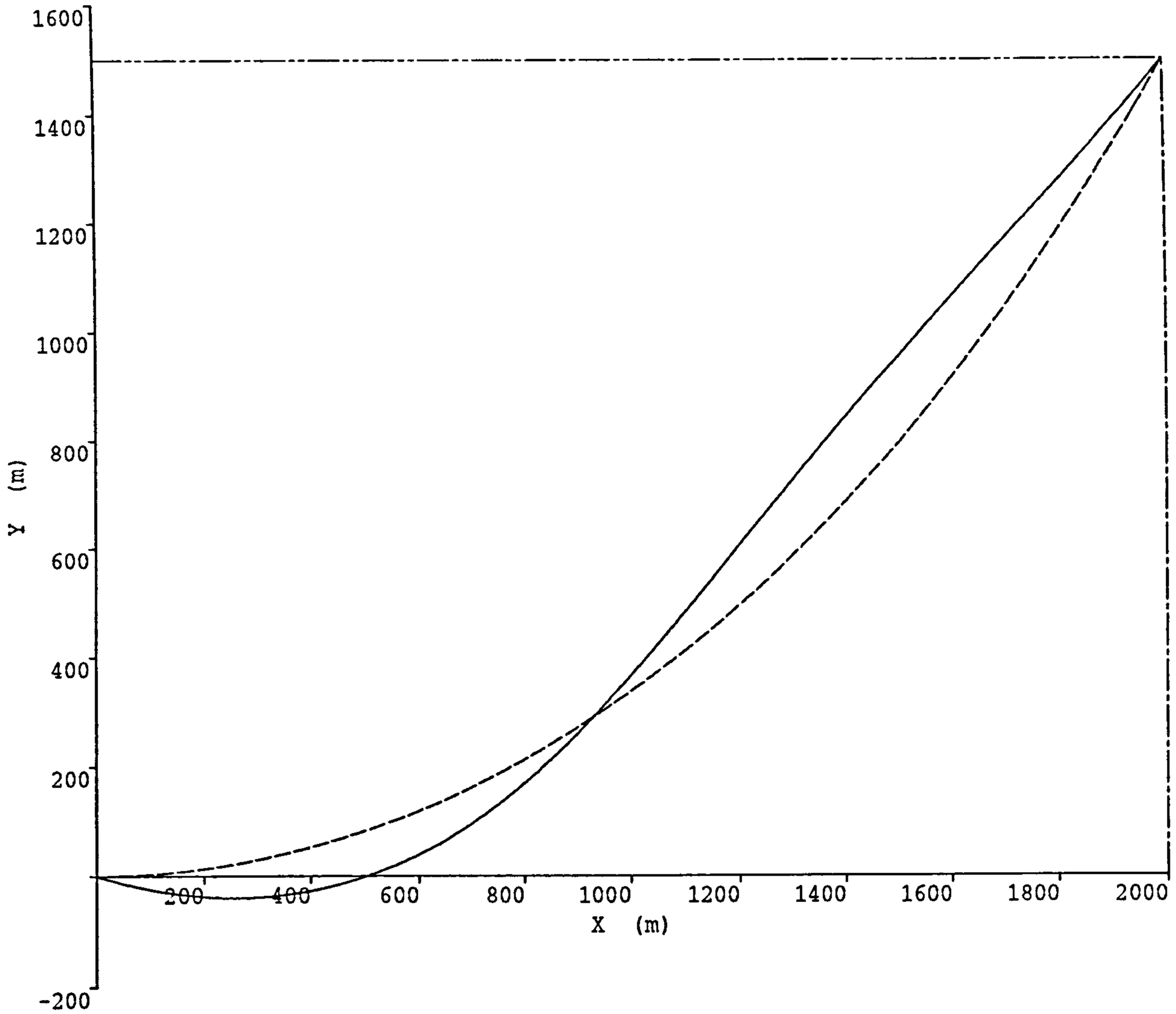

Figure 6.29(a)

Mode 2

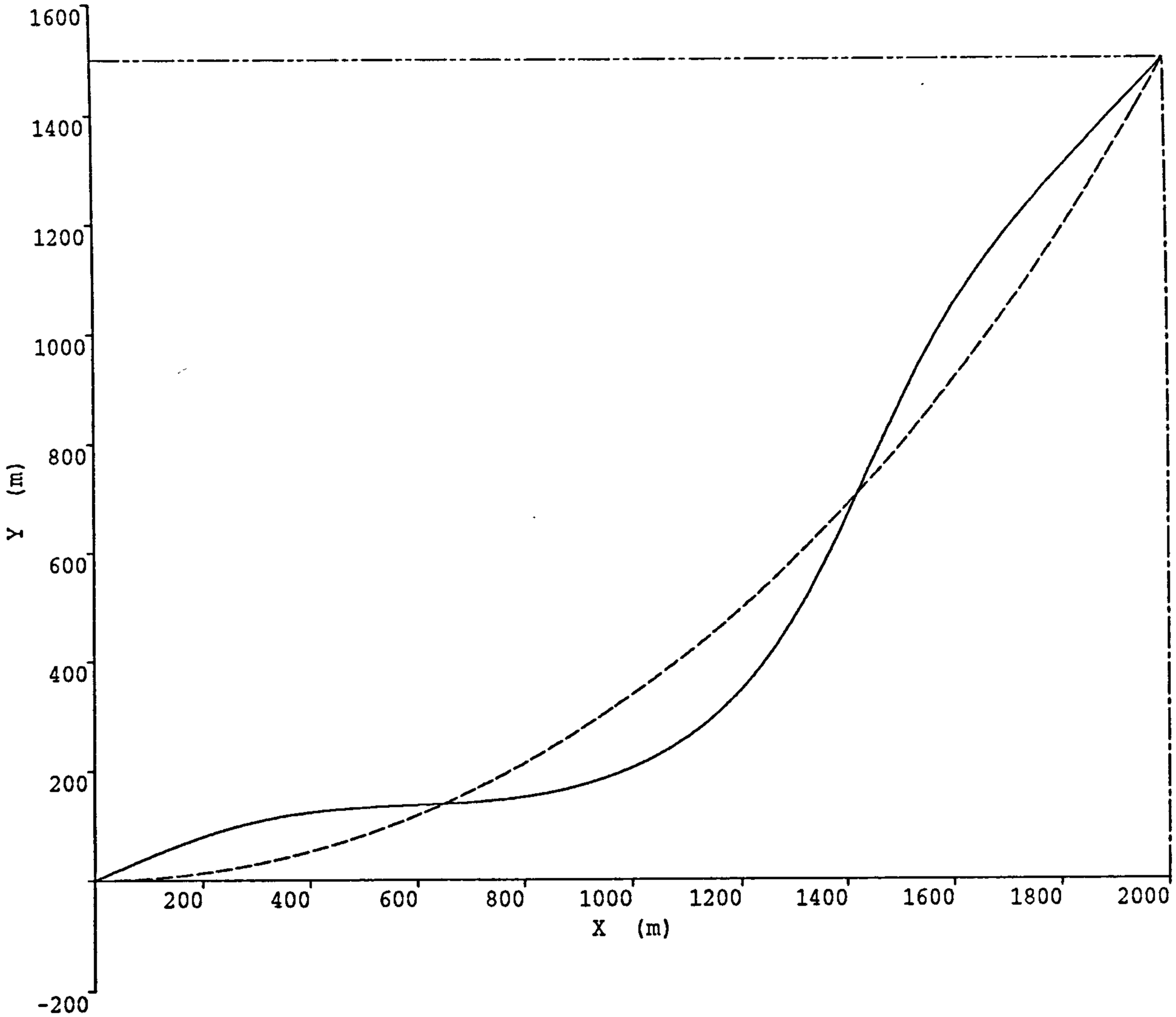

Figure 6.29(b)

Mode 3

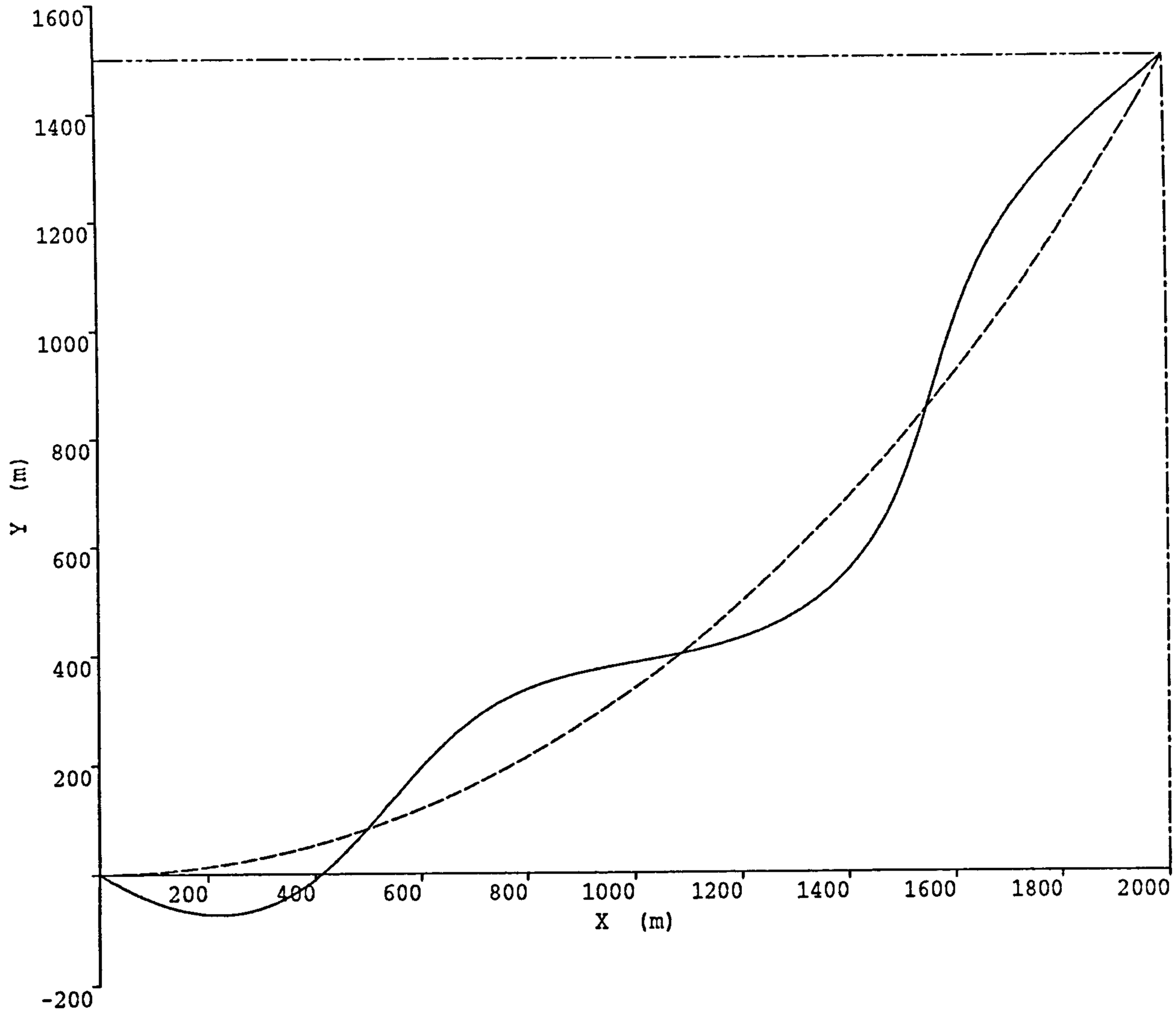

Figure 6.29(c)

Mode 4

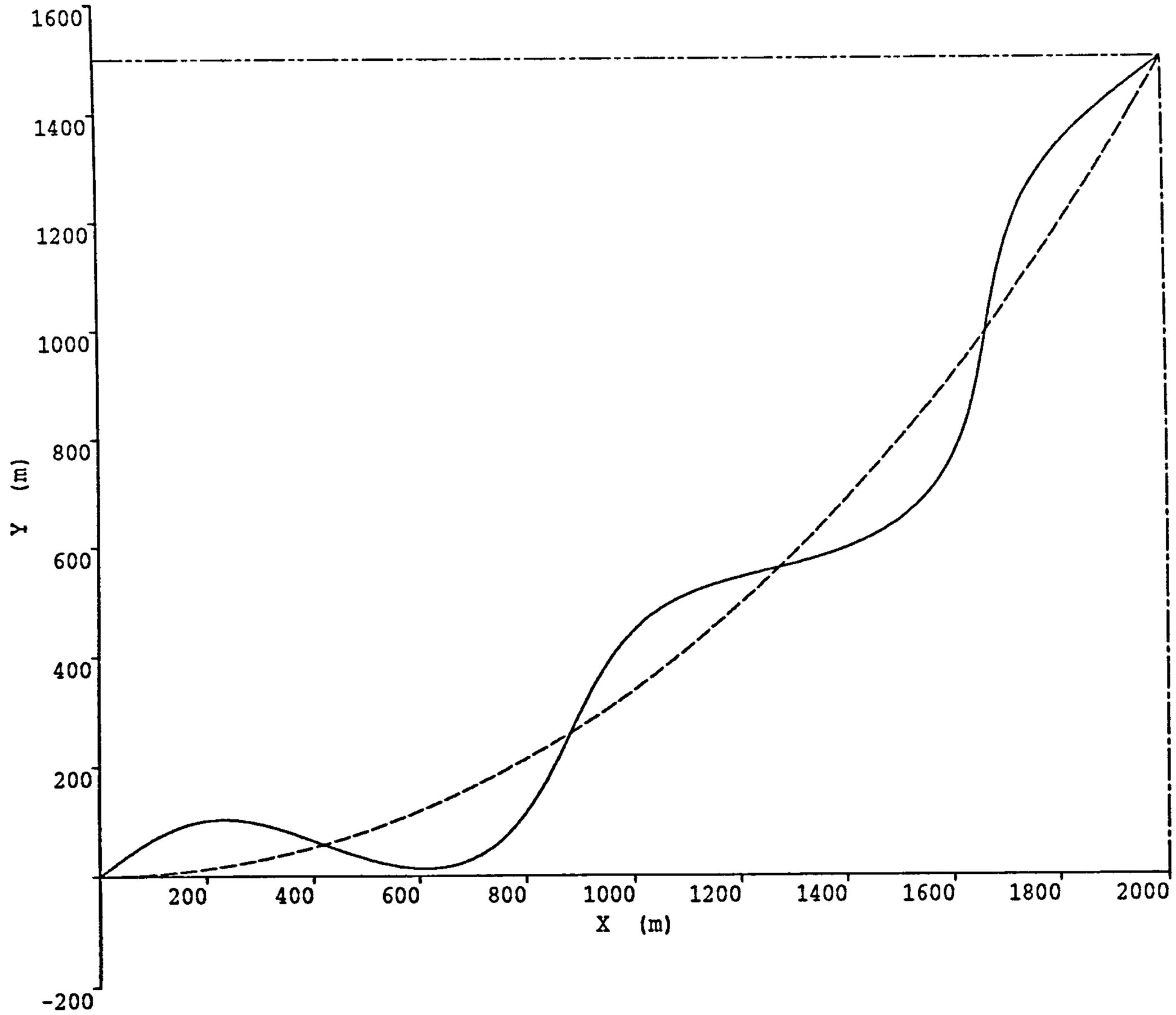

Figure 6.29(d)

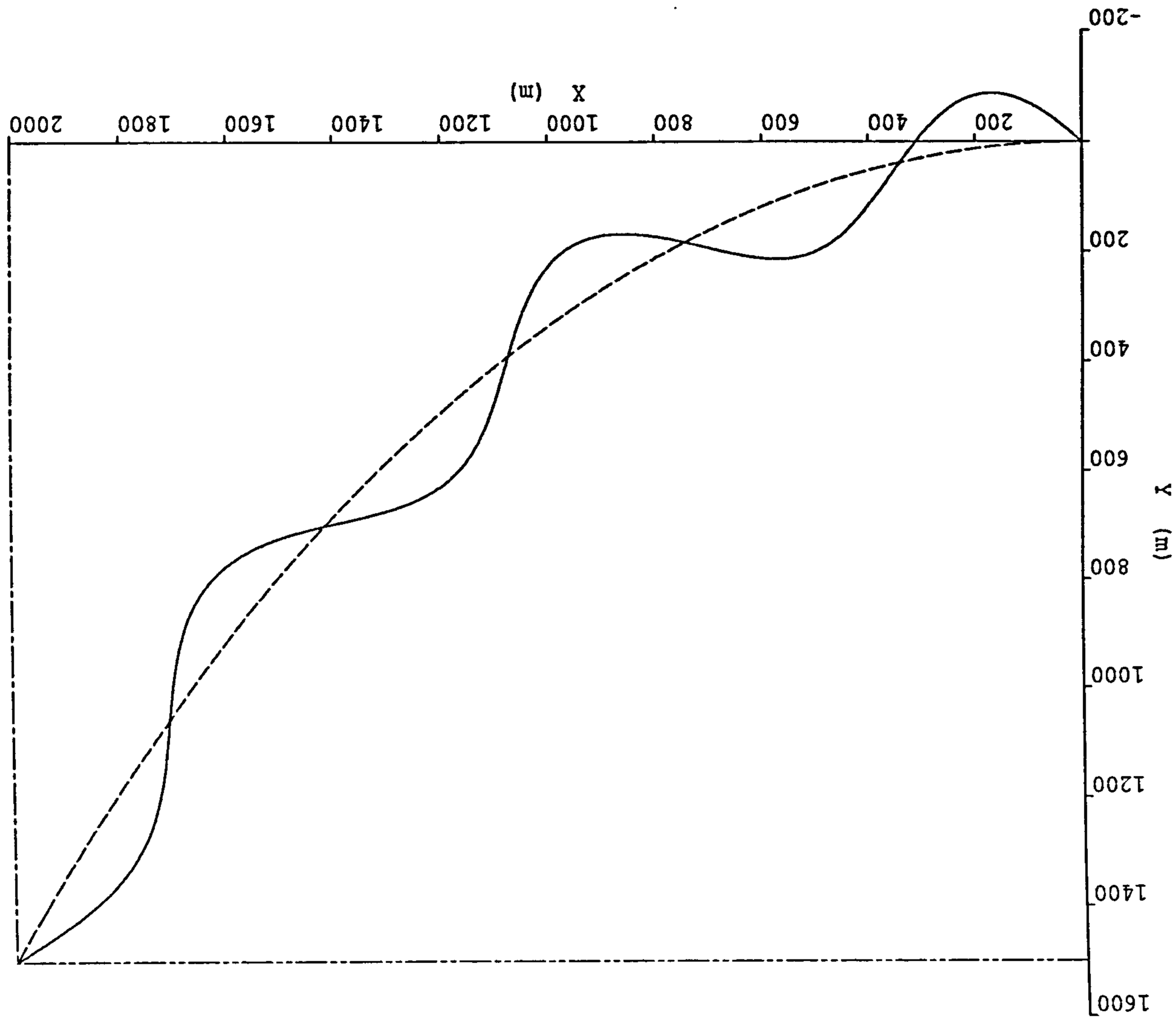
Mode 5
Y (m)
-200
200
400
600
800
1000
1200
1400
1600
X (m)
200
400
600
800
1000
1200
1400
1600
1800
2000

Figure 6.29(e)

Mode 6

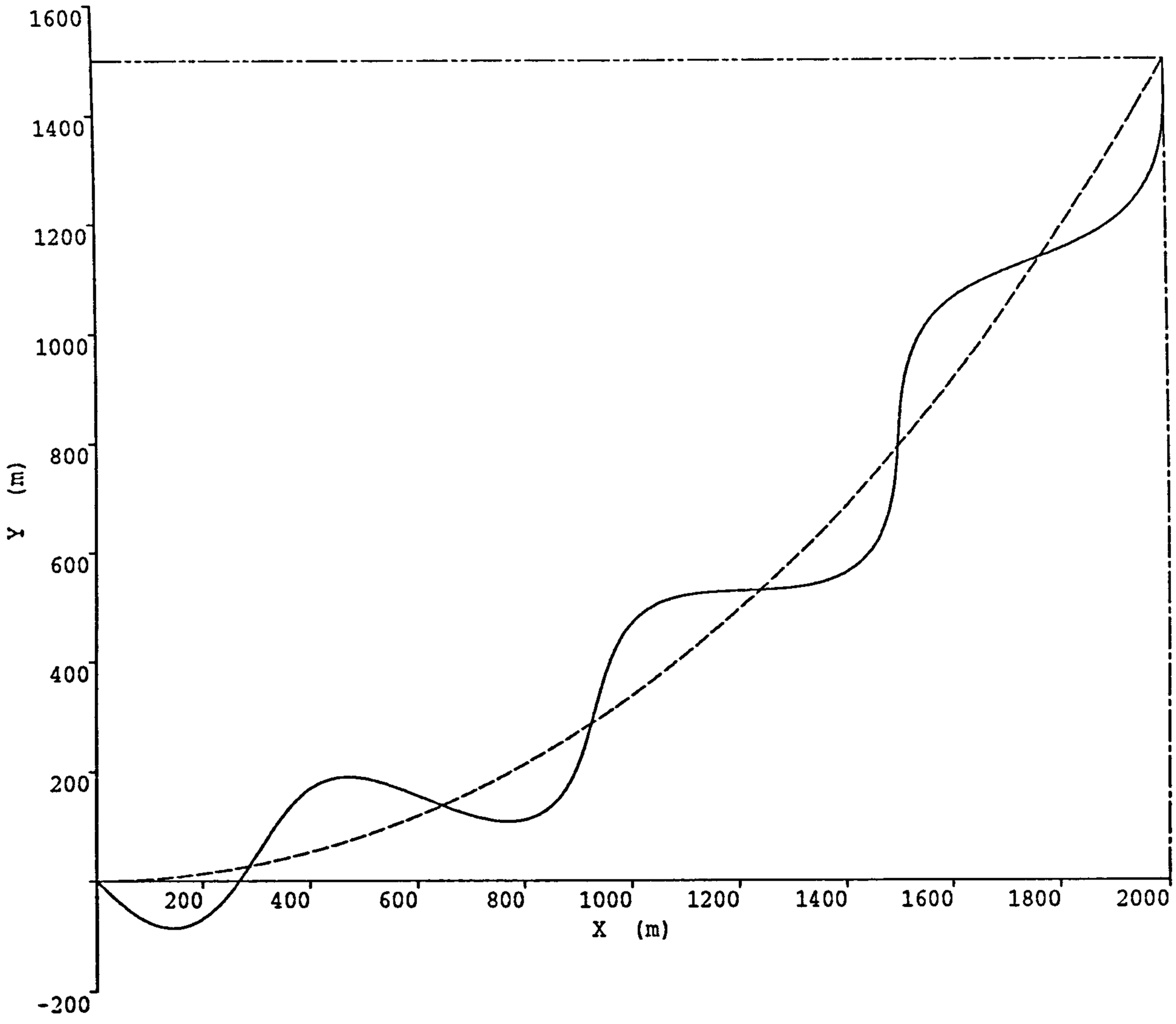

Figure 6.29(f)

The Effect of Riser Diameter on the Natural Period of Vibration

Syntactic Foam Buoyancy (a = 1000 m)

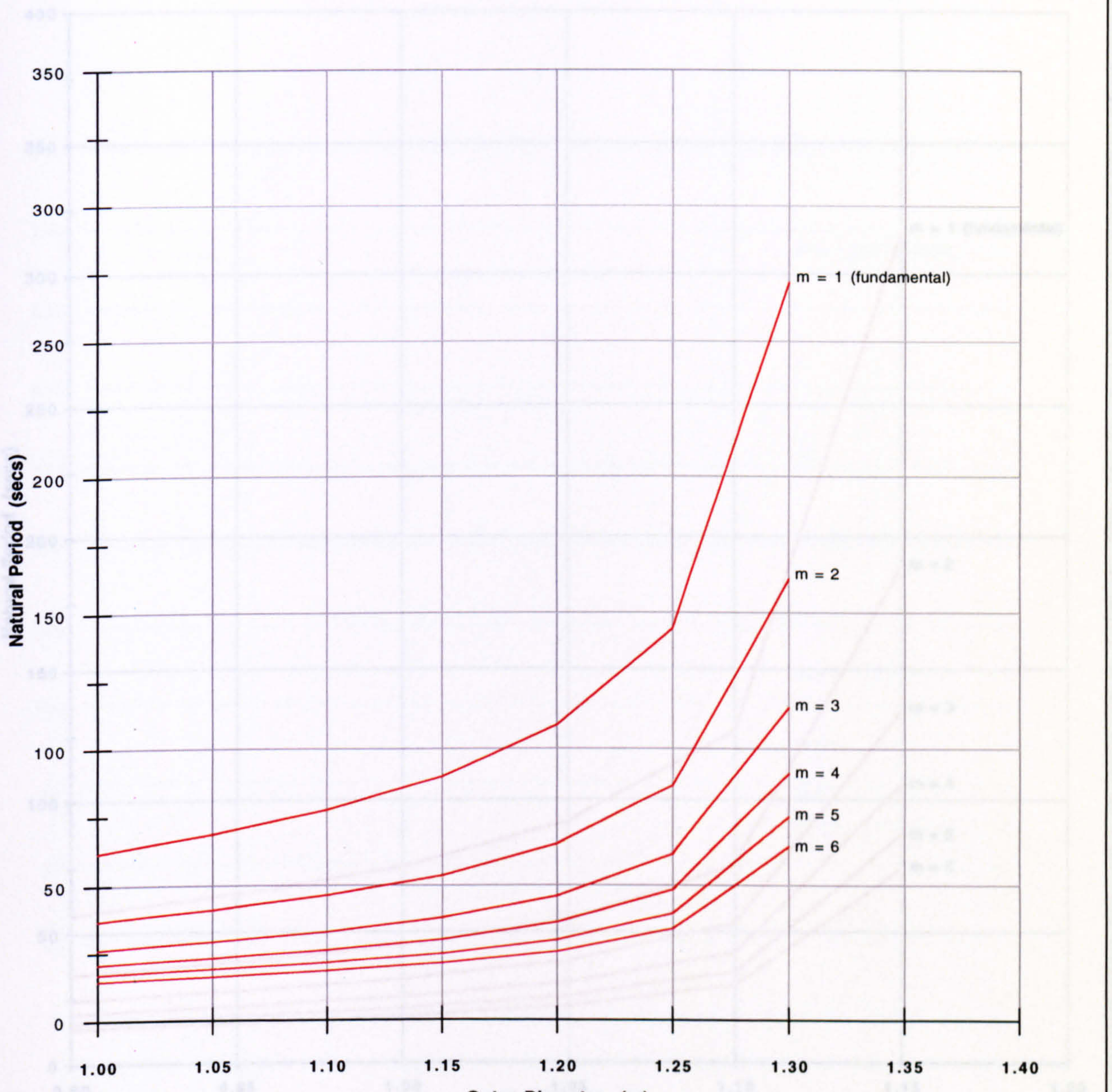

Horizontal Surface Offset = 1000 m

Sea Depth = 1500 m

m = Mode Number

Figure 6.30

The Effect of Riser Diameter on the Natural Period of Vibration

Nitrogen Gas Buoyancy (a = 1000 m)

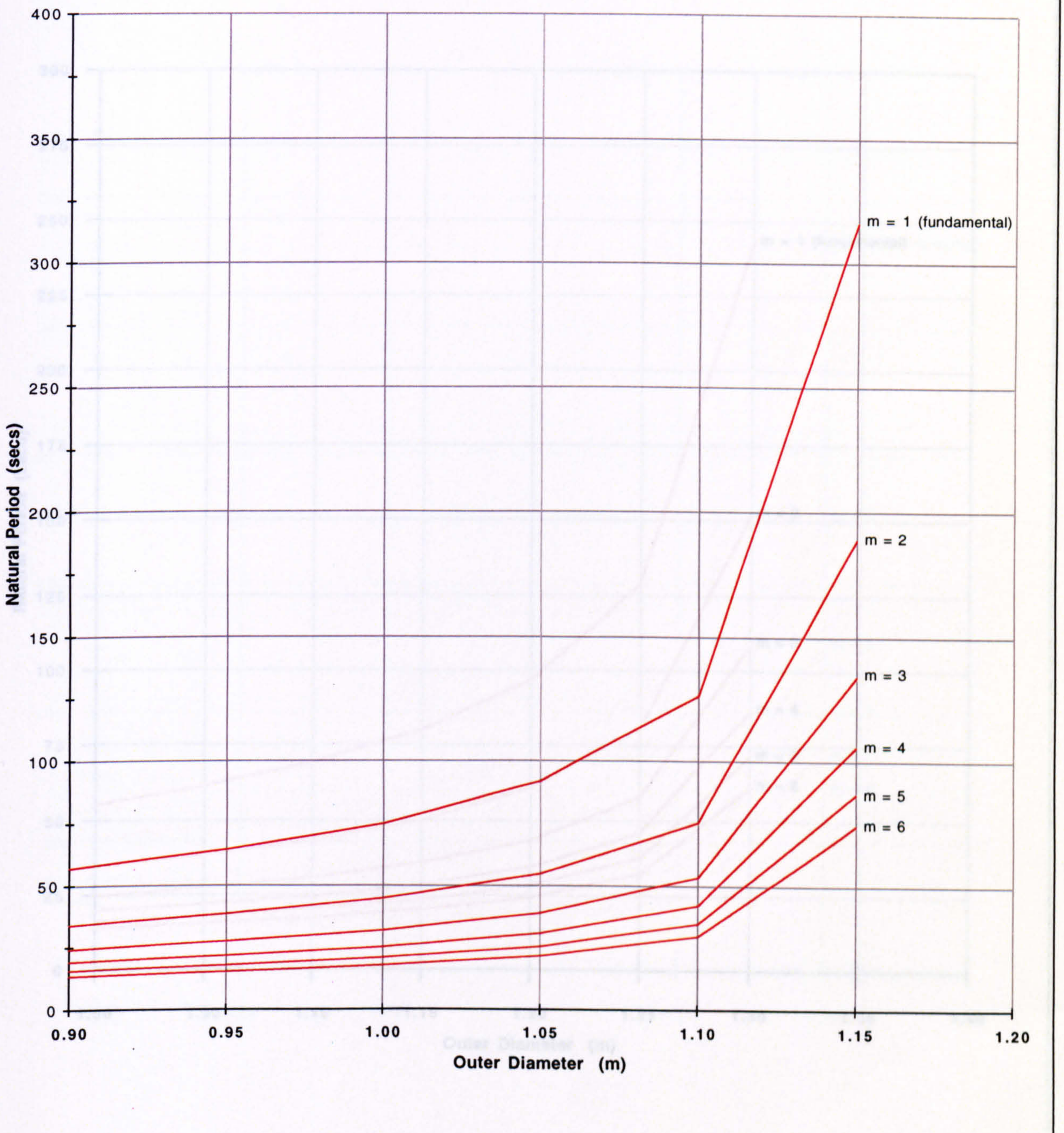

Horizontal Surface Offset = 1000 m

Sea Depth = 1500 m

m = Mode Number

Figure 6.31

The Effect of Riser Diameter on the Natural Period of Vibration

Syntactic Foam Buoyancy (a = 1500 m)

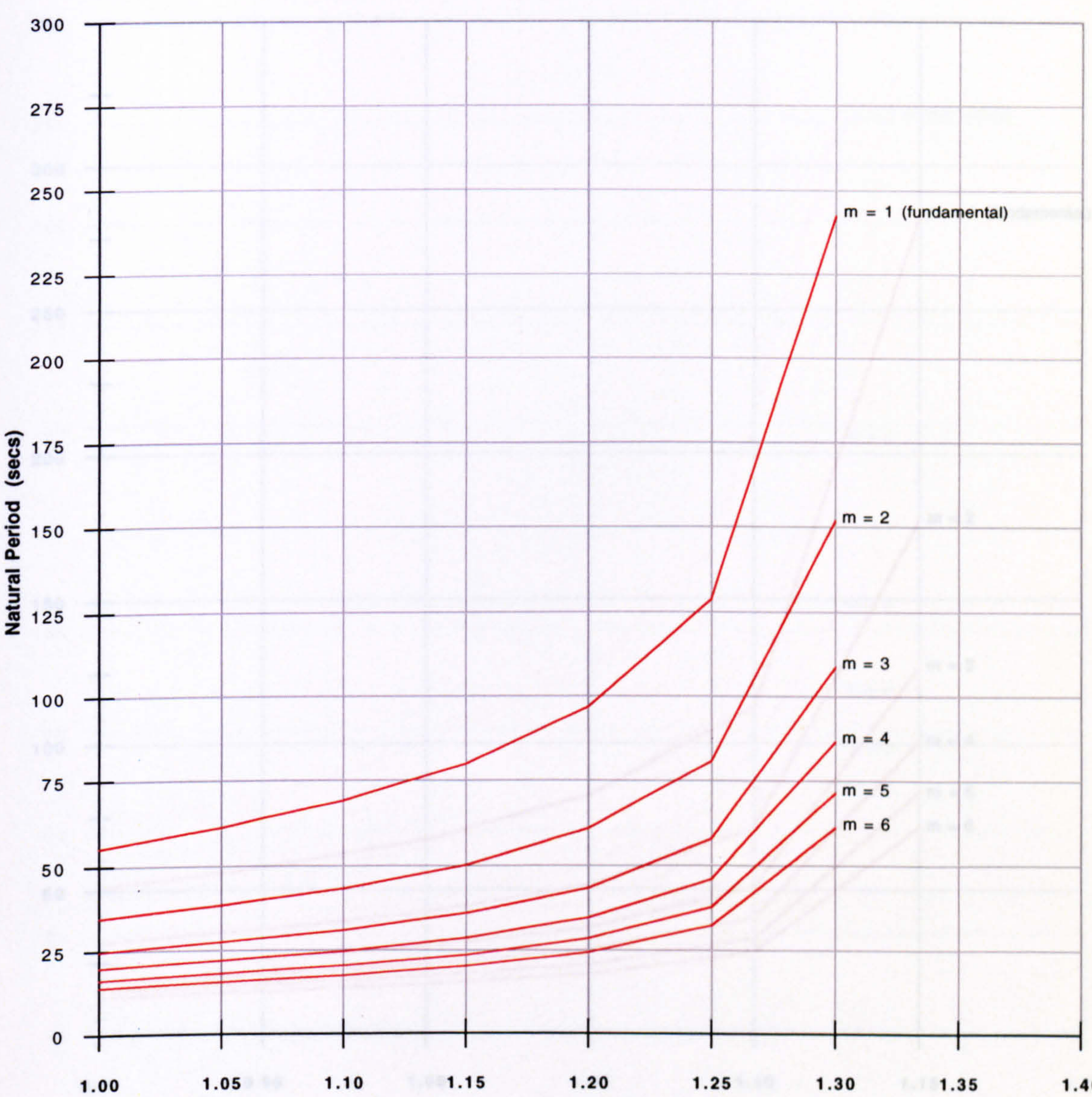

Horizontal Surface Offset = 1500 m

Sea Depth = 1500 m

m = Mode Number

Figure 6.32

The Effect of Riser Diameter on the Natural Period of Vibration

Nitrogen Gas Buoyancy (a = 1500 m)

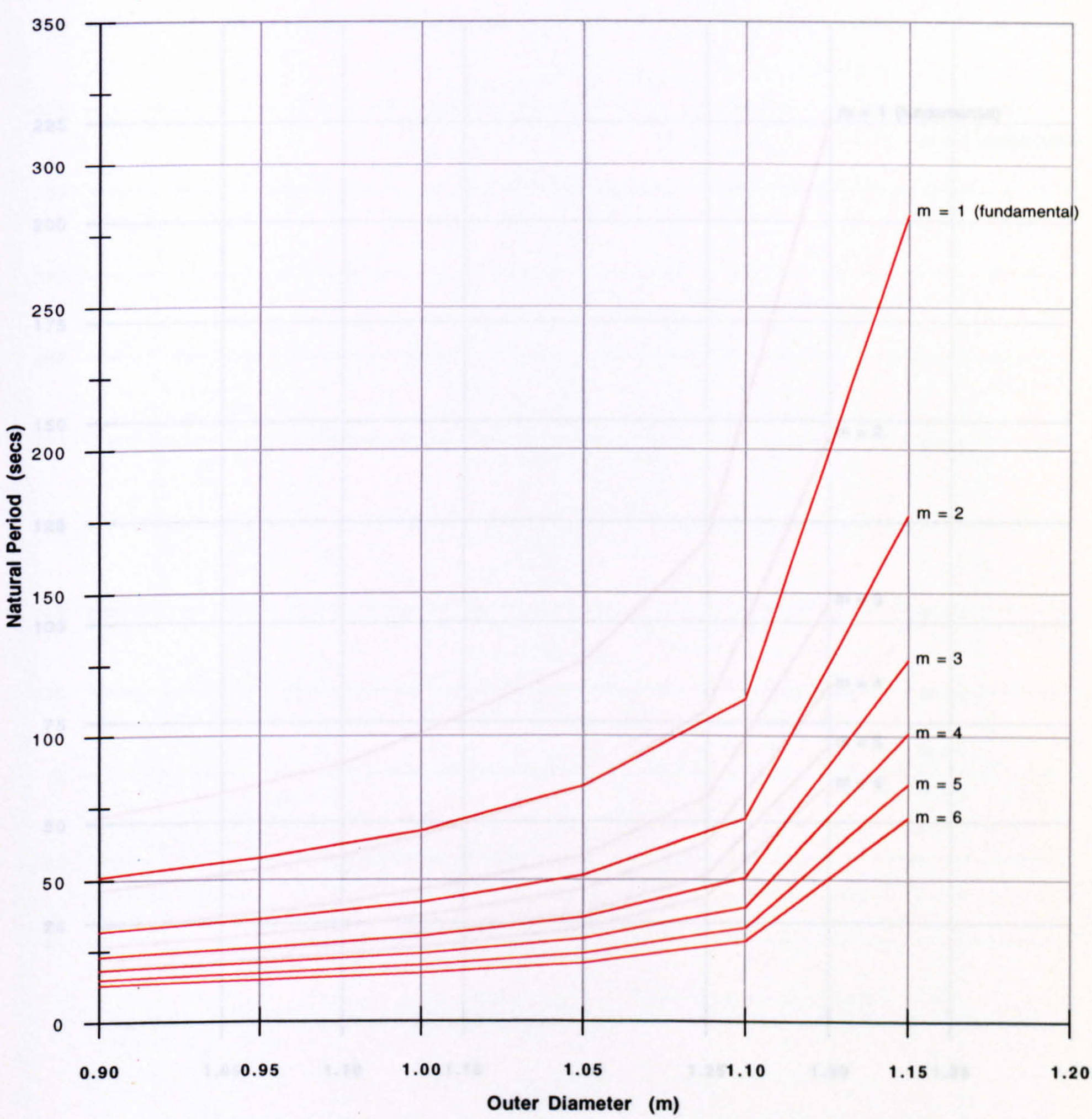

Horizontal Surface Offset = 1500 m

Sea Depth = 1500 m

m = Mode Number

Figure 6.33

The Effect of Riser Diameter on the Natural Period of Vibration

Syntactic Foam Buoyancy (a = 2000 m)

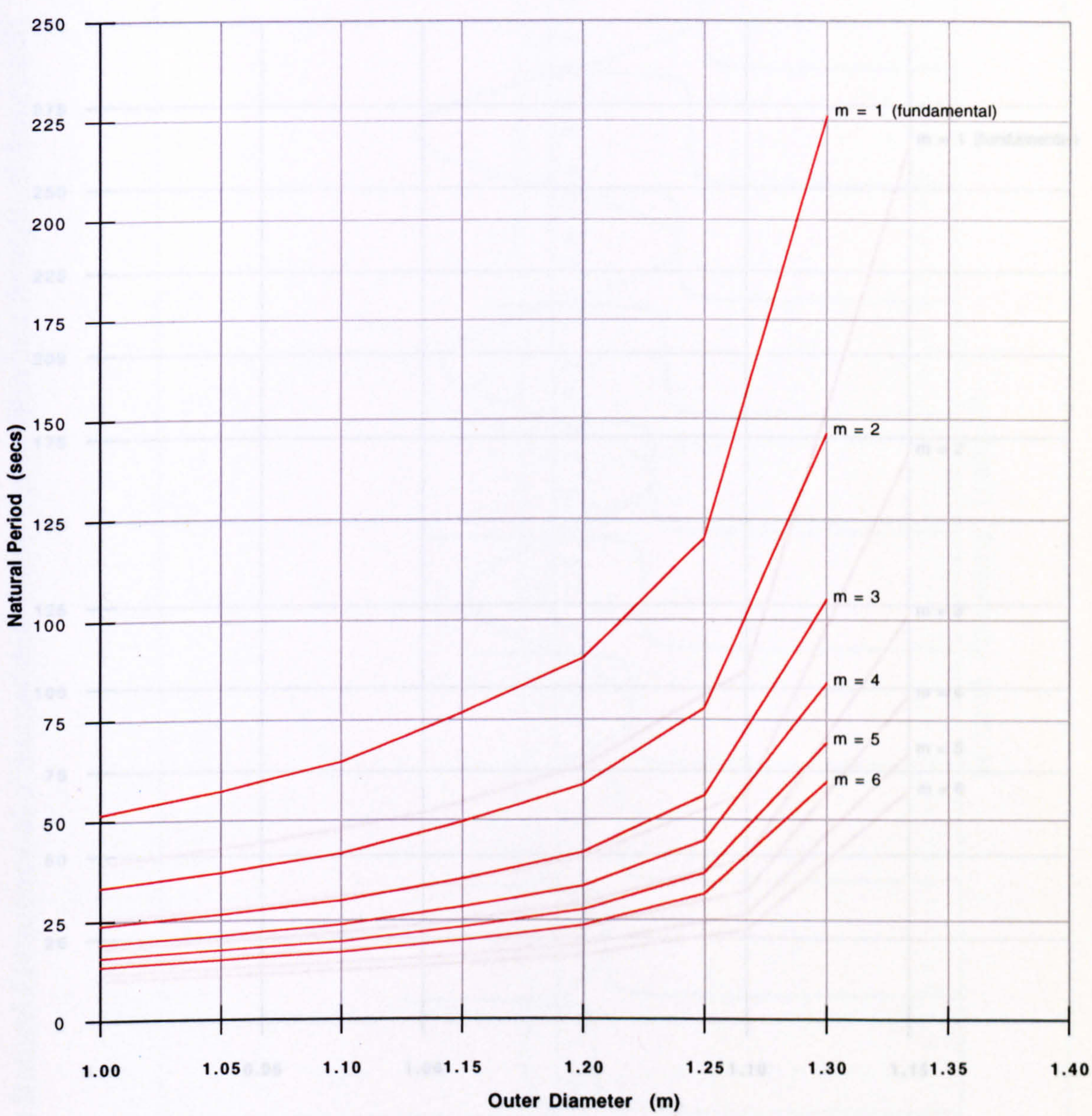

Horizontal Surface Offset = 2000 m

Sea Depth = 1500 m

m = Mode Number

Figure 6.34

The Effect of Riser Diameter on the Natural Period of Vibration

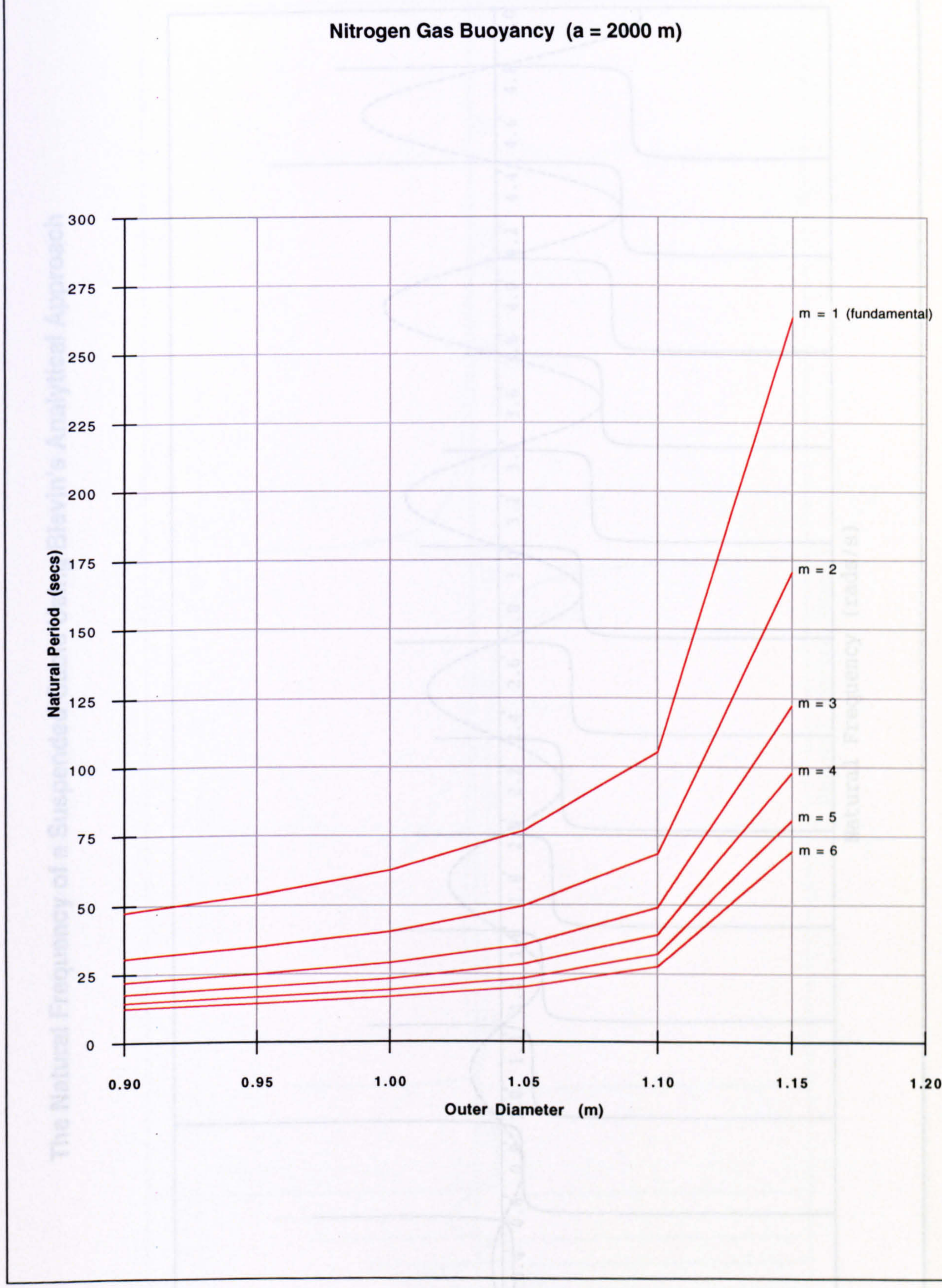

Horizontal Surface Offset = 2000 m

Sea Depth = 1500 m

m = Mode Number

Figure 6.35

The Natural Frequency of a Suspended Cable Using Blevin's Analytical Approach

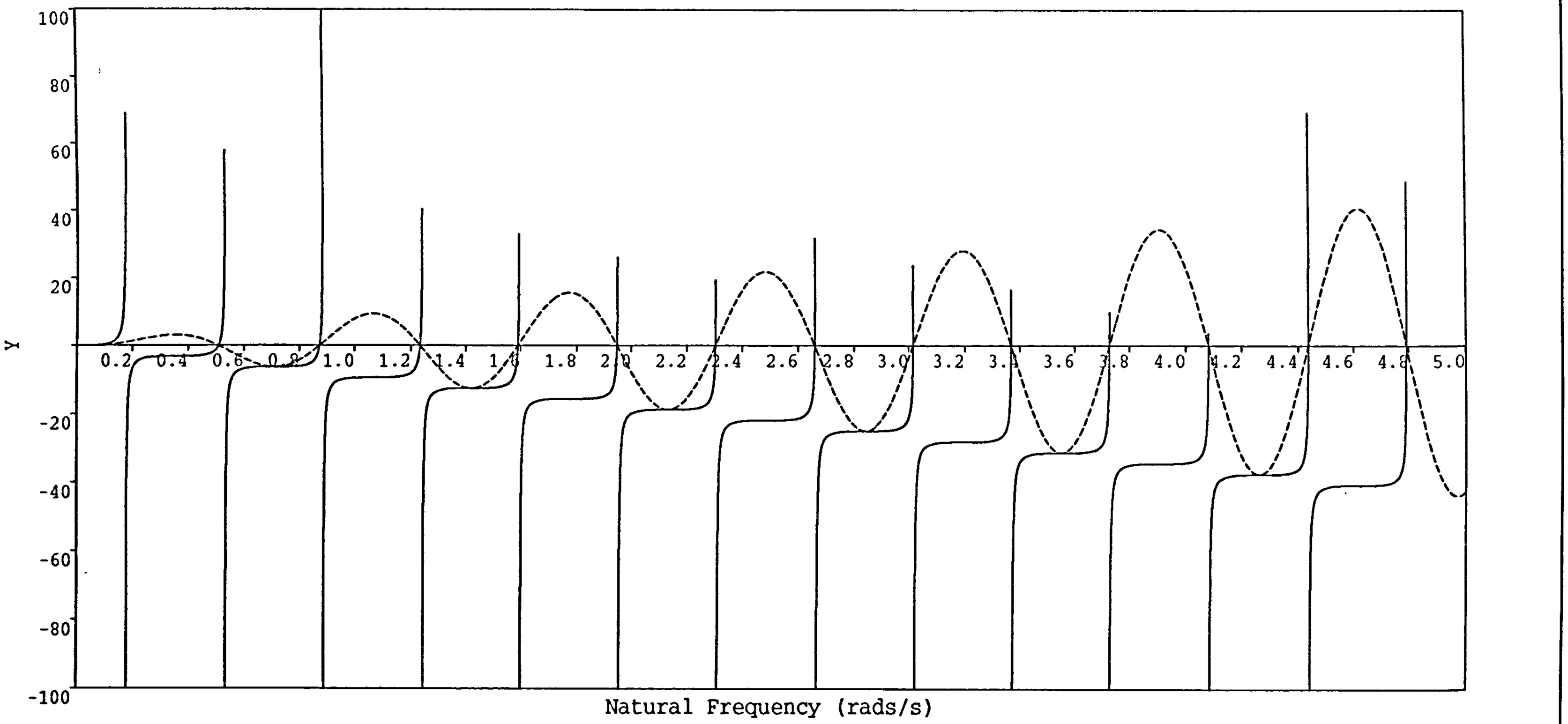

Horizontal Offset = 4000 m

Cable Length = 4353.2 m

Structural Unit Mass = 100.0 kg/m

Vertical Offset = 1500 m

Unit Weight = 981 N/m

Figure 6.36

The Natural Period of a Suspended Cable Using Blevin's Analytical Approach

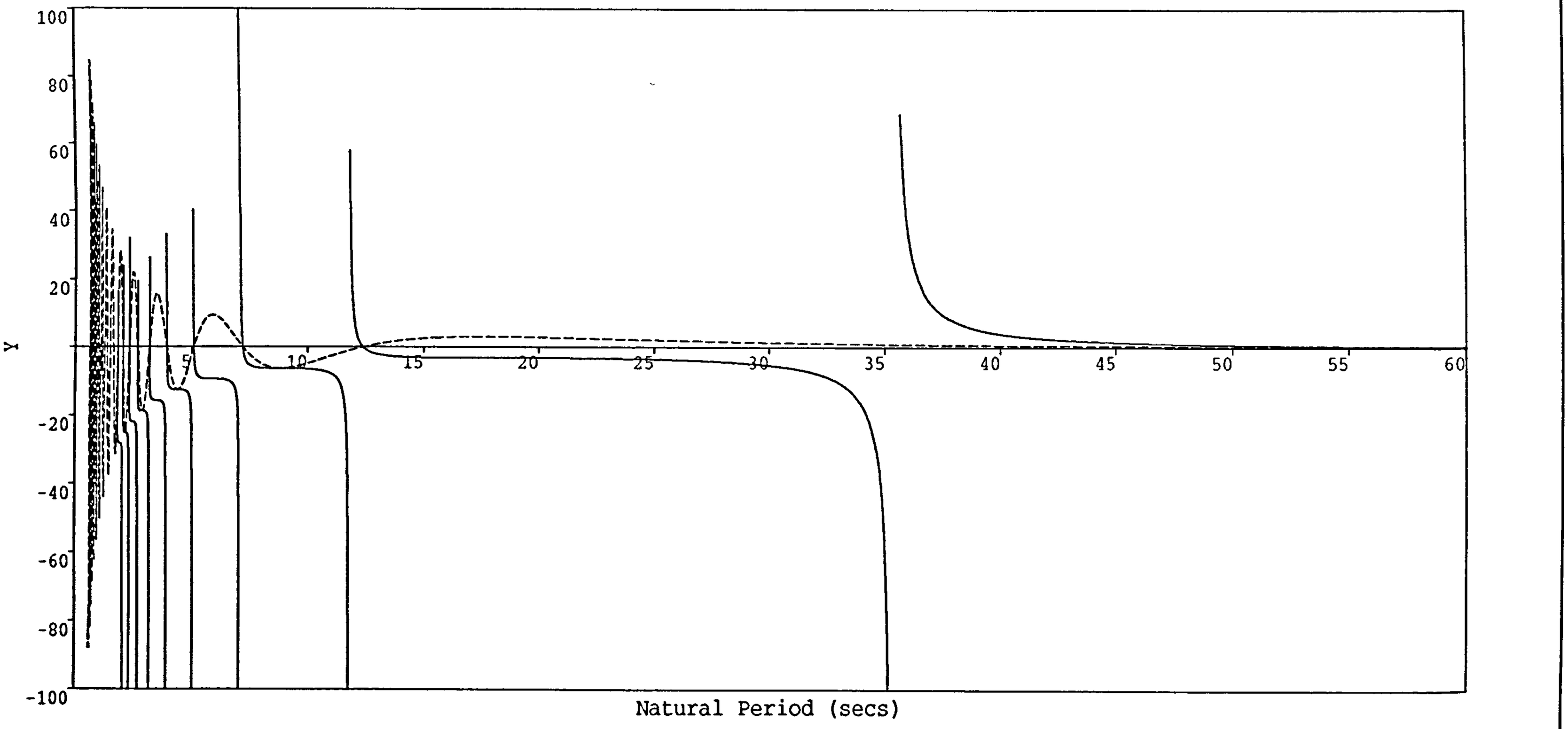

Horizontal Offset = 4000 m

Vertical Offset = 1500 m

Cable Length = 4353.2 m

Structural Unit Mass = 100.0 kg/m

Unit Weight = 981 N/m

Figure 6.37

Antisymmetric Modes

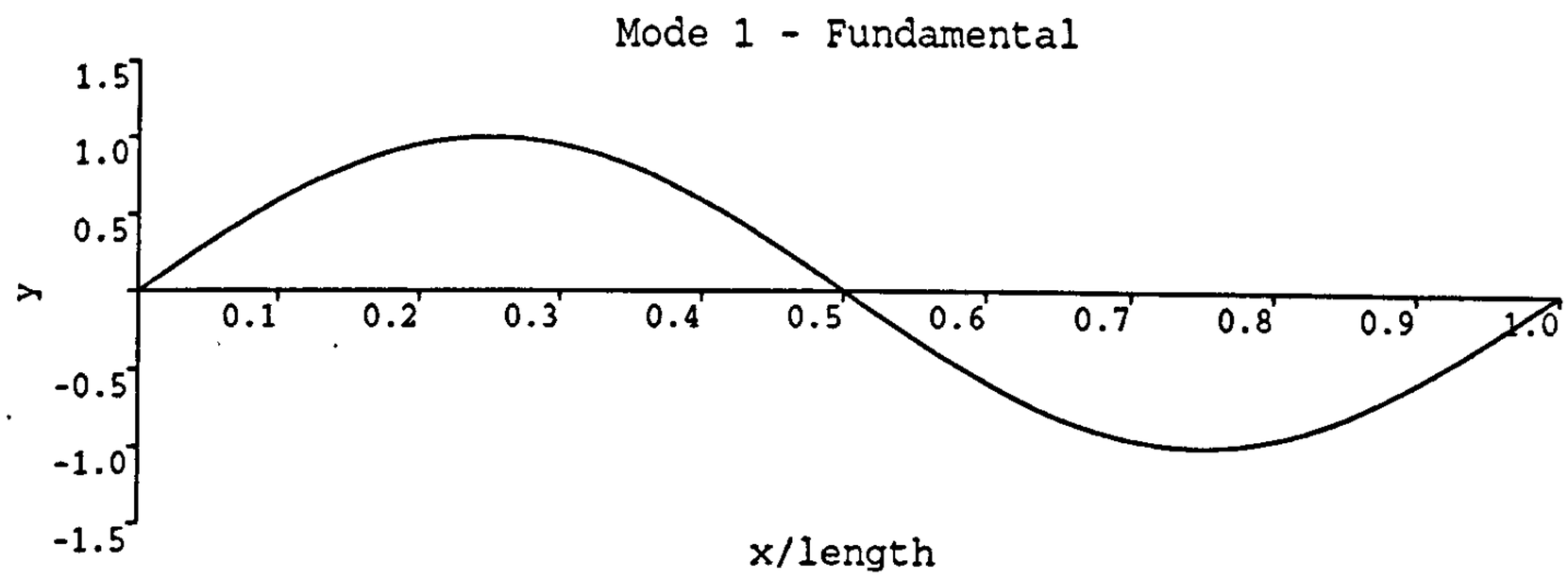

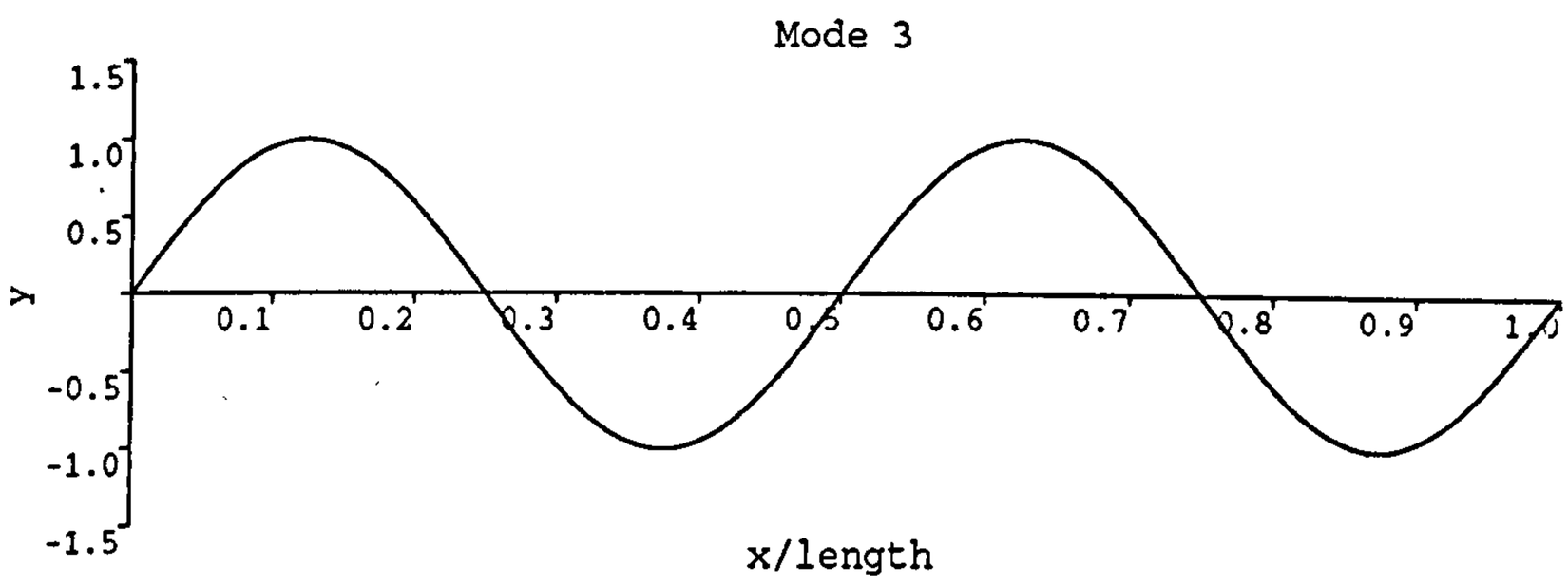

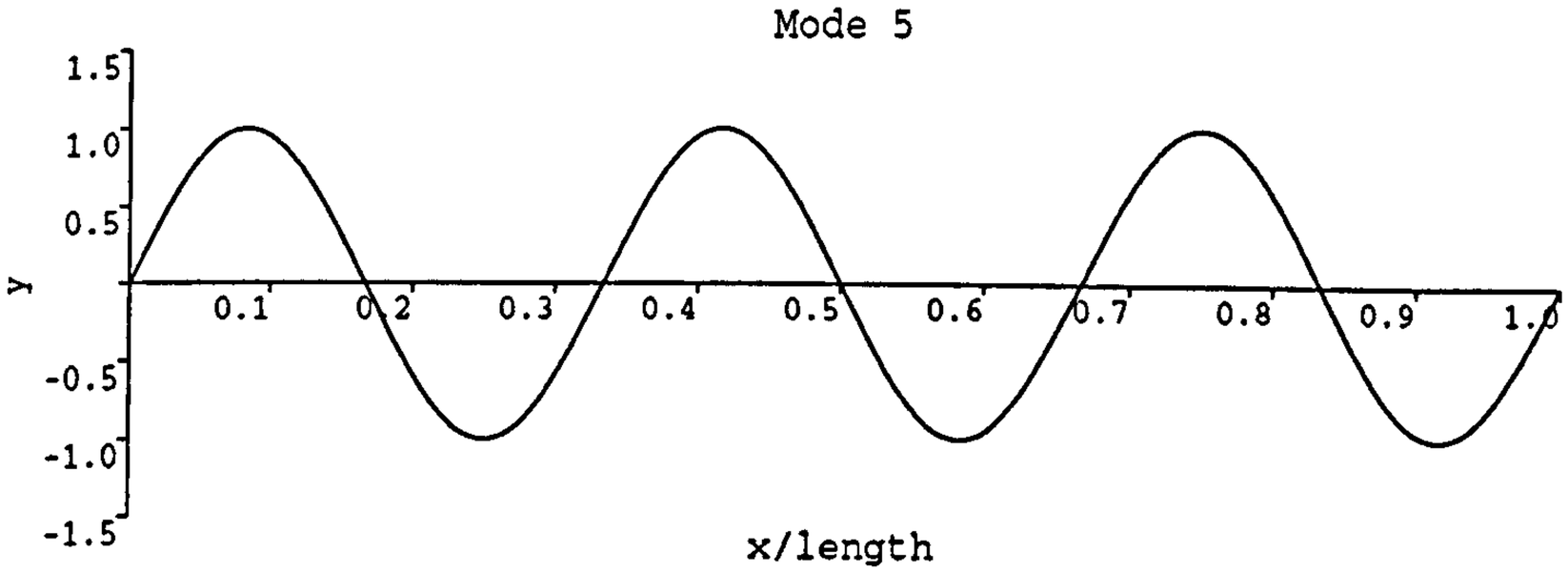

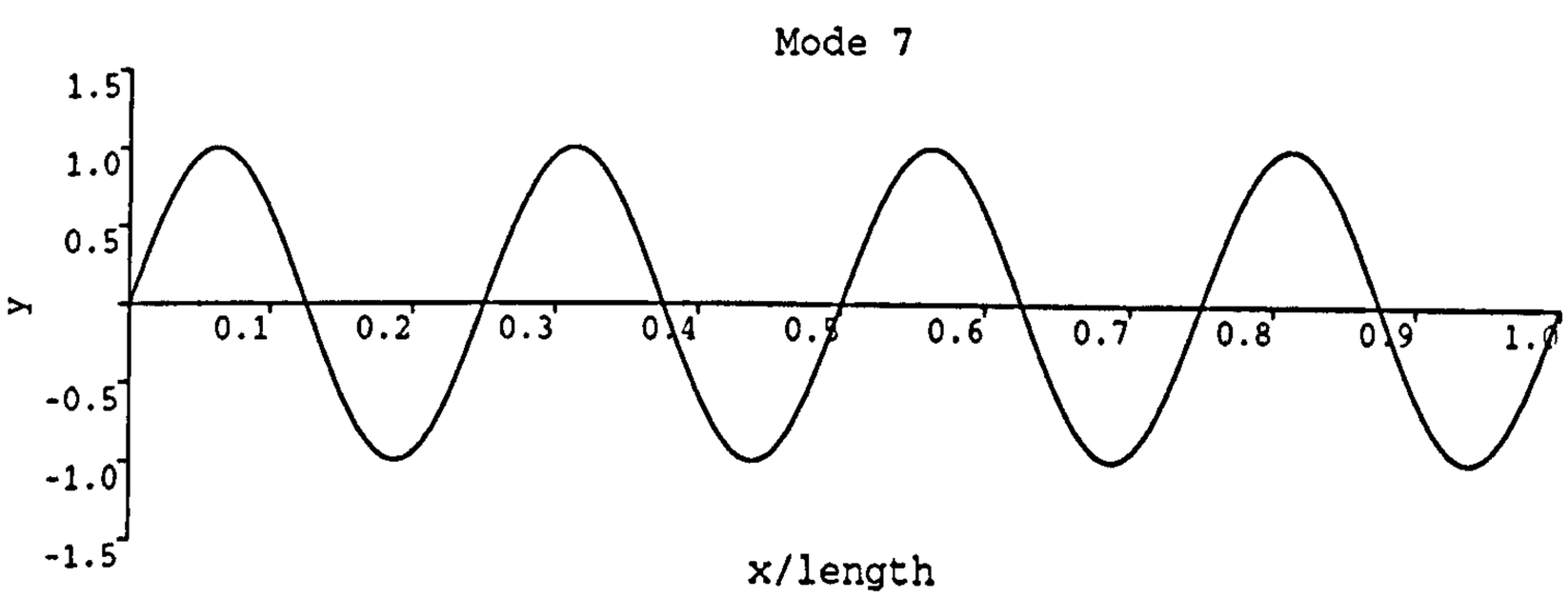

Figure 6.38(a)

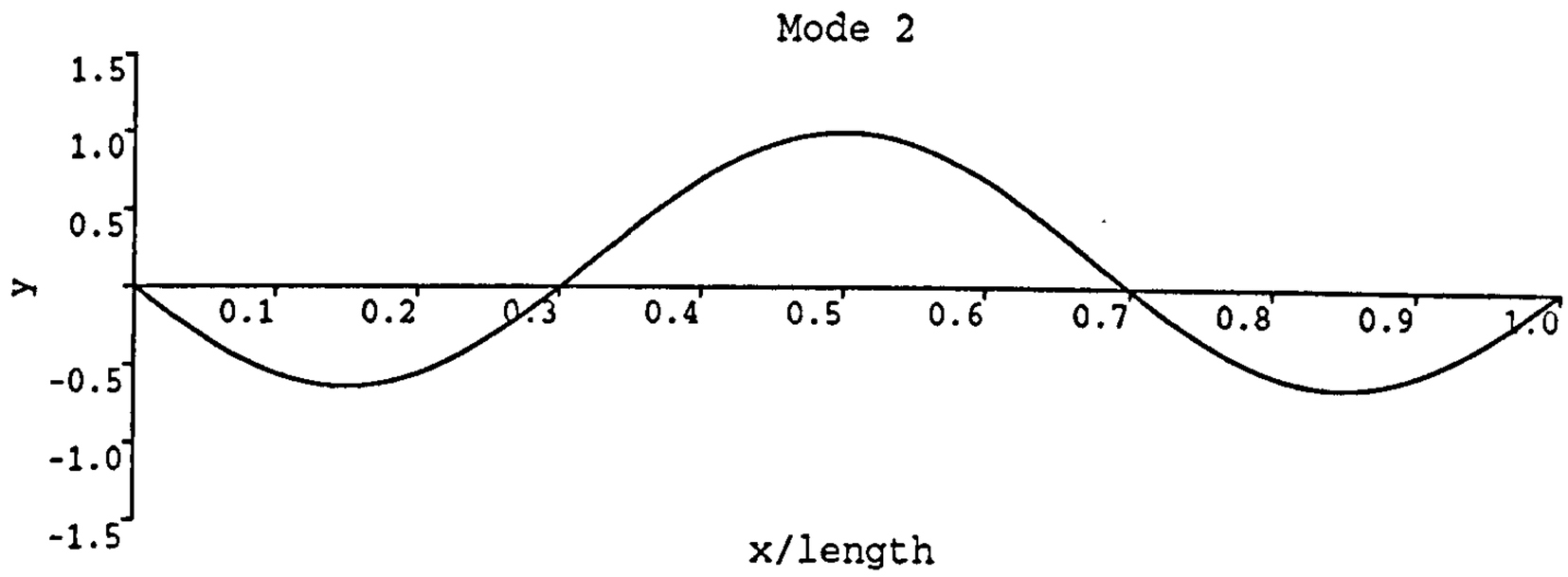
Mode 2
1.5
1.0
0.5
-0.5
-1.0
-1.5
y
0.1
0.2
0.3
0.4
0.5
0.6
0.7
0.8
0.9
1.0
x/length

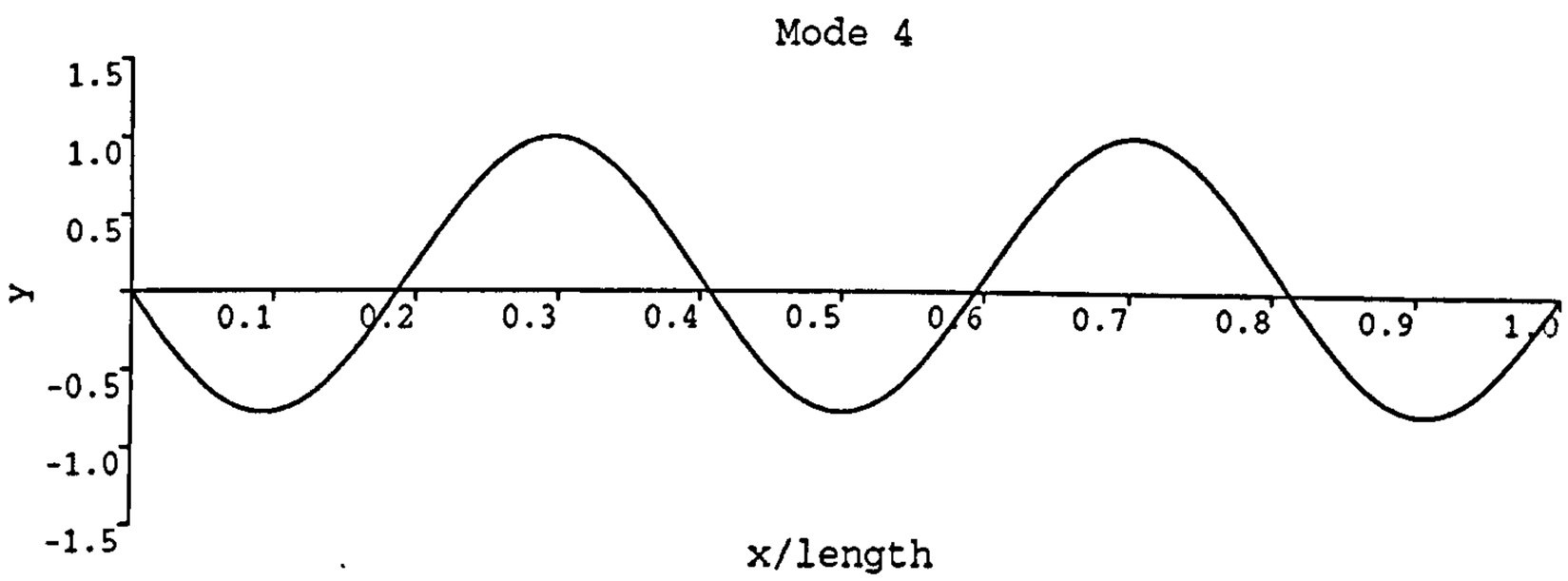
Mode 4
1.5
1.0
0.5
-0.5
-1.0
-1.5
y
0.1
0.2
0.3
0.4
0.5
0.6
0.7
0.8
0.9
x/length

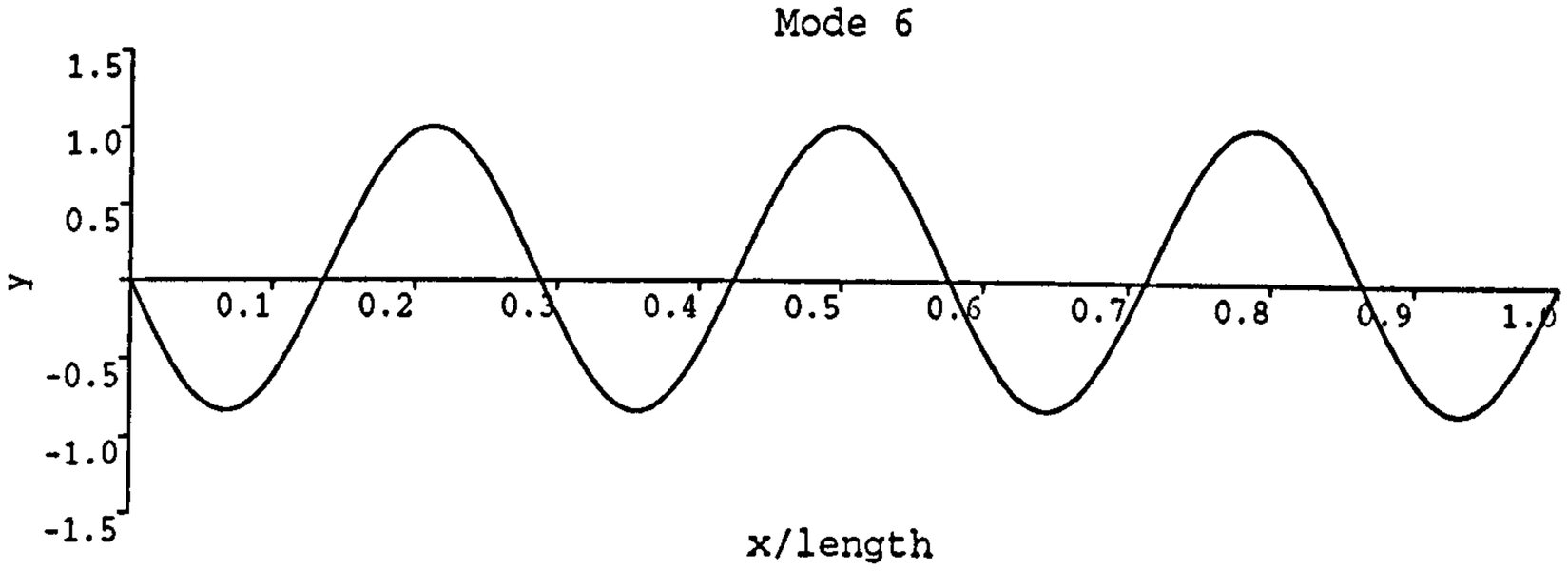
Mode 6
1.5
1.0
0.5
-0.5
-1.0
-1.5
y
0.1
0.2
0.3
0.4
0.5
0.6
0.7
0.8
0.9
x/length

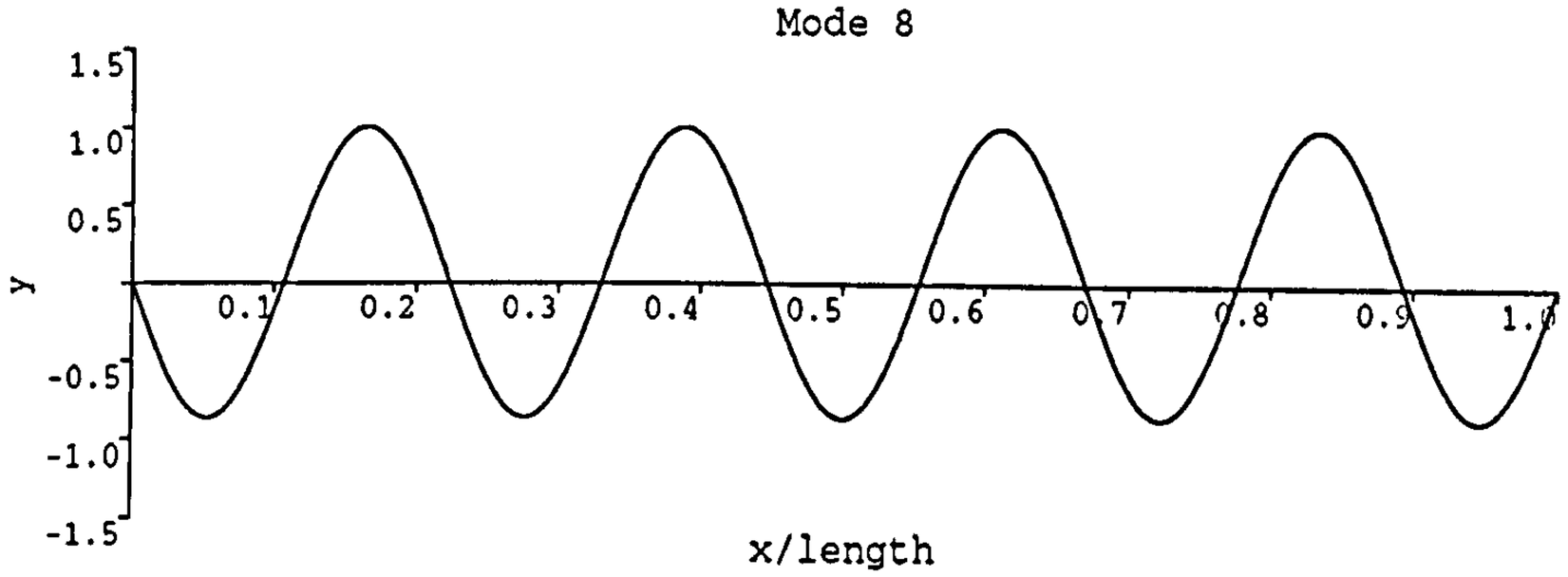
Mode 8
1.5
1.0
0.5
-0.5
-1.0
-1.5
y
0.1
0.2
0.3
0.4
0.5
0.6
0.7
0.8
0.9
x/length

Figure 6.38(b)

A Comparison of Results

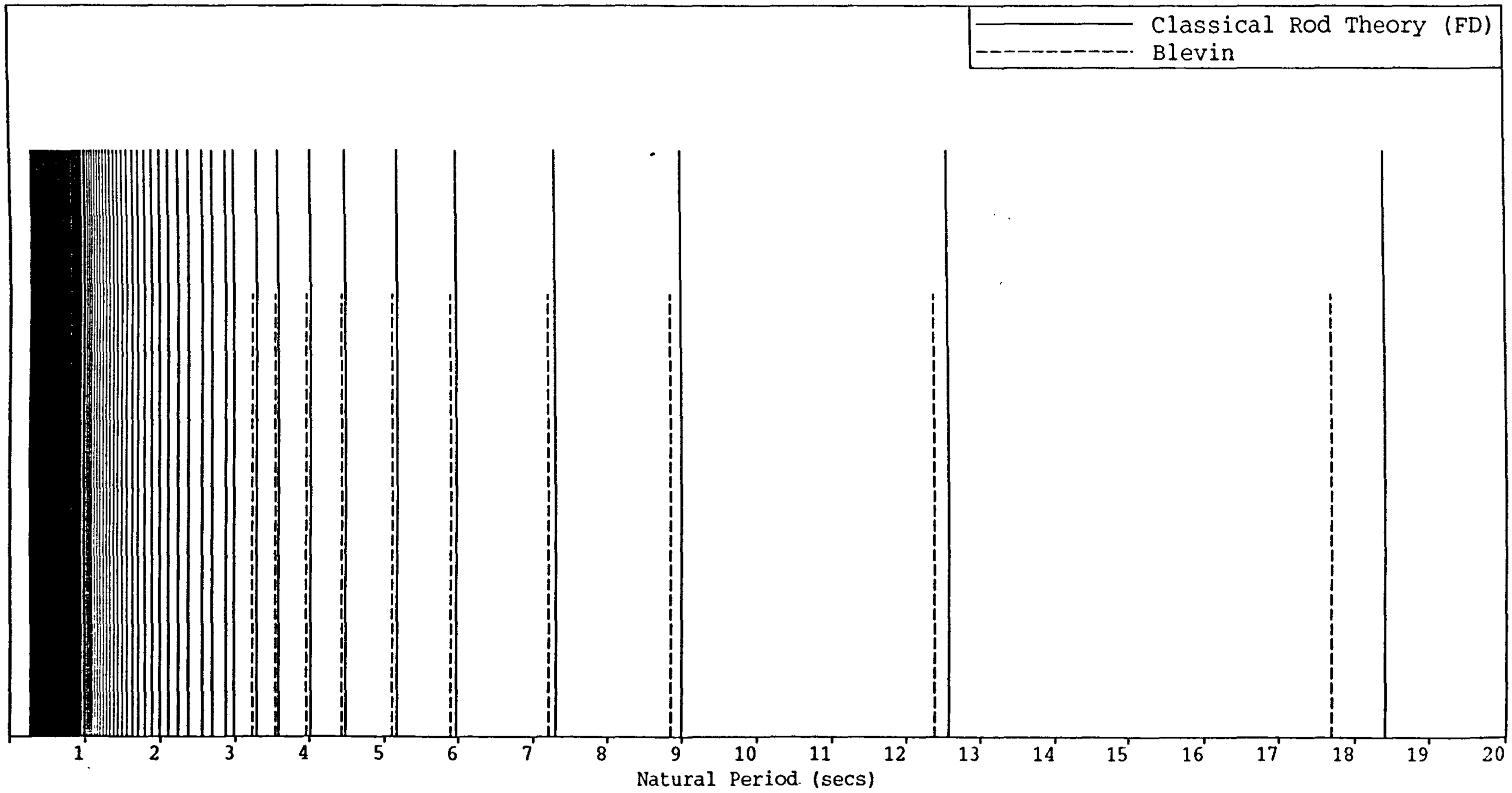

Horizontal Offset = 4000 m

Cable Length = 4353.2 m

Structural Unit Mass = 100.0 kg/m

Vertical Offset = 1500 m

Unit Weight = 981 N/m

Figure 6.39

CHAPTER 7

Sub-Surface Buoy Conceptual Design Study

7.1 General Description

The work conducted so far in this study has been solely concerned with the design of the catenary riser in isolation, however just as much consideration has to be given to the support system at the surface if the entire production system is to be demonstrated as being technically feasible. This study has put forward two proposals which can be summarised as follows:

- *FPSO Based System* - in which the catenary risers are suspended from a swivel stack or turret located within a moored FPSO.

- *Sub-Surface Buoy Based System* - in which the catenary risers are suspended from a sub-surface buoy which is vertical tethered just below the surface. Flexible risers would then form the hydraulic connection between the buoy and a moored FPSO whilst ensuring that the two vessels are effectively de-coupled. This type of arrangement is commonly referred to as a Hybrid System.

The main advantages which result from a Hybrid system as opposed to a system based upon direct coupling to an FPSO are:

- Reduced displacement offsets for the riser's upper end, in both the vertical and horizontal planes. As already demonstrated the main impact of this is to decrease the riser bending loads at the seabed.

- Decrease in wave disturbance which reduces the possibility of fatigue loading.

- Allows the FPSO to be disconnected from the riser system easily and quickly.

- Ensures that the installation of the riser system is quick and simple (a proposed installation procedure is described in detail in Section 7.6).

The work presented in this chapter is concerned with the sub-surface buoy concept in terms of the design of the buoy. However before this can be carried out there are several aspects that have to be established

- The function of the buoy.
- The major influences on the design.

This information then provides the basis for an analytical analysis to be conducted with the objective of calculating the required upthrust. This dictates the size of the buoy as well as the inherent loading imposed upon it. Finally a conceptual design is proposed and discussed.

7.2 Buoy Function

The primary functions of the buoy are twofold:

- To provide support for the risers.
- To limit the watch circle radius (or surface displacement) of the riser system by providing sufficient buoyancy to resist the lateral current loadings exerted both on itself and the risers.

7.3 Influencing Design Factors

7.3.1 Maximum Watch Circle Diameter

The maximum allowable lateral offset (or watch circle radius) is to be 50 m for a given current design velocity. It's value is based upon a compromise between various factors:

- The bending loads imposed upon the catenary risers at the seabed.
- The lengths (and cost) of the flexible risers between the buoy and FPSO.
- The size (and cost) of the buoy.

It was clearly shown in Chapter 5 that the extent of displacement at the surface or near surface dictates the level of additional bending imposed upon the riser. The critical area in terms of maximum bending load occurs at the seabed and therefore limiting the watch circle diameter reduces the possibility of localised buckling at this point.

The overall field development assumes a large FPSO, which is turret moored by a number of catenary lines. It is essential that none of these lines comes into contact with either the buoy or risers during normal operations or any of the failure modes accepted by

the classification societies, such as a failed mooring line. For this to be attainable the individual watch circles must not overlap and if possible they should be separated by a given distance. For the purposes of this study this gap is set at 50 m with a watch circle diameter of 27% of the water depth (400 m) being assumed for the FPSO (accommodates failure modes). Together with the watch circle of the buoy these operating conditions determine the catenary length (and hence cost) of the flexible risers. The relative positioning of the watch circles is shown diagramatically in Figure 7.1. Two conditions of interest concerning the relative positioning of the buoy and the FPSO are:

- Minimum separation *(A-A')* - the current takes the buoy towards the FPSO whilst the wind and waves take the FPSO towards the buoy.

- Maximum separation *(B-B')* - the current takes the buoy away from the FPSO whilst the wind and waves take the FPSO away from the buoy.

For a given current design velocity, the volume (and cost) of the buoy is a direct function of the maximum allowable offset or watch circle. Decreasing the watch circle increases the required buoyancy needed in order to resist a specified current velocity. Greater buoyancy necessitates a greater size of buoy and hence an increase in overall cost.

7.3.2 Depth of the Buoy Below the Surface

The main factors which have to be considered in selecting the depth of the top of the buoy below the surface are:

- The wave induced heave, roll and pitch motions.

- Avoidance of contact between the buoy or the flexibles and any of the FPSO's moorings, as discussed earlier in connection with the FPSO watch circle.

- Minimising the length of the flexibles.

To avoid fatigue problems at the riser surface connection assembly, the top of the buoy should be below a level where 95% of the waves have little or no energy. The wave forces on the buoy are principally due to inertia effects so that the wave particle acceleration gives a direct measure of the force on a constant cross-section circular buoy. The vertical wave particle acceleration can be calculated using the following expressions:

$$a_y = 0.5 H_w \omega^2 e^{ky} \sin(kx - \omega t) \qquad (7.1)$$

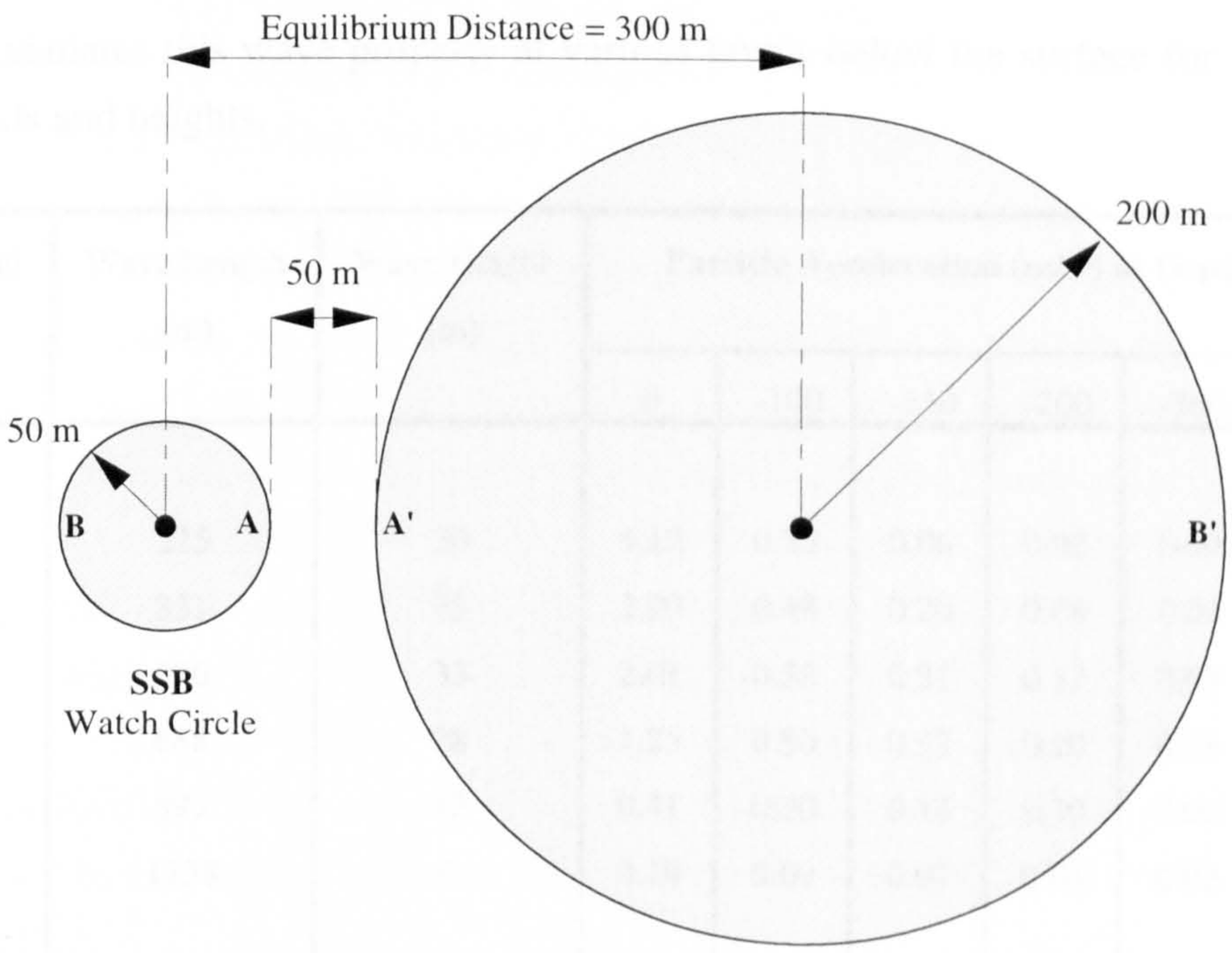

Figure 7.1

Relative Positioning of Buoy and FPSO Watch Circles

$$\omega = \frac{2\pi}{Tp} \tag{7.2}$$

$$k = \frac{2\pi}{\lambda} \tag{7.3}$$

where: H_w = wave height

k = wave number

y = depth below surface

Tp = wave period

λ = wave length

Table 7.1 tabulates this wave property at various levels below the surface for a range of wave periods and heights.

Wave Period (secs)	Wave Length (m)	Wave Height (m)	**Particle Acceleration (m/s^2) at Depth (m)**					
			0	-100	-150	-200	-300	-400
12	225	30	4.12	0.25	0.06	0.02	0.00	0.00
15	351	33	2.90	0.48	0.20	0.08	0.01	0.00
18	506	33	2.01	0.58	0.31	0.17	0.05	0.01
21	688	28	1.25	0.50	0.32	0.20	0.08	0.03
24	899	12	0.41	0.20	0.14	0.10	0.05	0.02
27	1138	6	0.16	0.09	0.07	0.05	0.03	0.02

Table 7.1

Wave Particle Acceleration Versus Depth for a Range of Wave Periods

The wave heights in Table 7.1 have been taken as the maximum in the North East Atlantic at 15 and 18 second period and dropping away either side of these values. There may be some argument about the precise values chosen but they reflect the general trend. The column of accelerations at the surface shows that the reducing frequency has more effect than the increasing wave height between 12 and 15 seconds and the acceleration declines rapidly at the longer periods. However, at -100 m the acceleration at the 12 second period has decayed exponentially (see Eqn (7.1)) to just 6% of its surface value and has almost disappeared at -150 m. Thus all waves with periods less than this will have little or no effect on the buoy which removes a large part of any seaway spectrum and greatly reduces the possibility of fatigue loading. As the wave periods and lengths

increase, the particle acceleration values persist to much greater depths and are certainly significant at -200 m.

A depth below the surface of 100 m to the top of the buoy would appear to offer the optimum condition on the basis of the data given in Table 7.1, the required length (and hence cost) of the flexible risers and the ease of buoy installation (more difficult with increased depth). Therefore for the purposes of this study subsequent design calculations will be based upon this value.

7.3.3 Hydrostatic Pressure

Designing the sub-surface buoy on the basis of utilising syntactic foam to provide buoyancy is inherently expensive as a consequence of the large external volumes needed in order to generate sufficient buoyancy. Designing the buoy as a pressure hull is also expensive as well as being difficult to manufacture. Trying to maintain the structures water tight integrity over it's operational lifetime would also cause problems. However if the buoy is designed on the same pressure can principle that was used for the riser, many of the problems above can be solved. The pressure can principle is based upon an internal gas pressure that largely offsets the external hydrostatic pressure. Under this arrangement, the highest internal pressure to which any compartment within the buoy is subjected is equal to the water head corresponding to the height of the compartment. As in the case of the riser the main benefit over the syntactic foam based system is a greater buoyancy to weight ratio and of course a greater buoyancy to cost ratio. Multiple compartmentalisation of the buoy is adopted in order to both minimises the effects of buoyancy loss in any one compartment and to limit the pressure differentials across the external walls.

7.3.4 Installation

The problems associated with installation provide a further input into the design of the buoy especially in terms of it's shape. If the buoy is a long slender cylinder then resonant problems (and hence dynamic stressing) can exist during either surface sub-surface tow-out with the buoy lying on its side. Once the buoy has reached the field location it then has to be up-ended through 90° which can often involve a complex ballasting procedure. However a short fat buoy eliminates these problem by virtue of it's shape. The structure is a lot stiffer and compact (volume more concentrated) thereby reducing the problem of resonance during tow-out. The buoy also remains in the same attitude all the way through the installation process (see Figure 7.9) and therefore doesn't require upending.

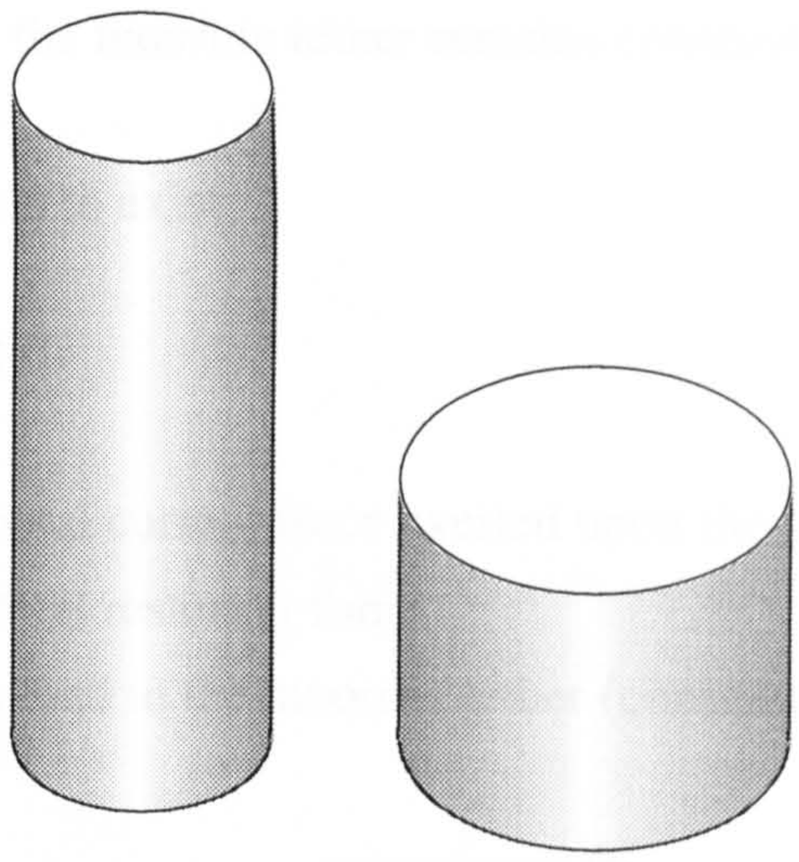

Figure 7.2

Buoy Shape: Long and Slender or Short and Fat

7.4 Lateral Displacement Stiffness

In order to resist the effects of a lateral load imposed upon both the buoy and risers by a current the system must posses a certain amount of lateral stiffness. This is provided by both the buoy and the catenary risers.

In Chapter 2 it was demonstrated that the riser basically act as catenary mooring line. Restoring forces at the surface are generated as a result of a change in line tension as it either lifts off or settles on the seabed. A spread of catenary lines or risers therefore generates a non-linear restoring force that increases with surface or sub-surface displacement and resists steady environmental forces.

In the case of a vertically tethered sub-surface buoy, lateral stiffness is achieved by virtue of the tension that exists within the tethers. This tension is created as a result of the net upthrust generated by the buoy i.e. *buoyancy - weight*.

The lateral stiffness calculations are based upon several assumptions:

- The buoy is only displaced a small distance relative to the mooring tether length.

$$\frac{x}{L} \leq 0.1 \tag{7.4}$$

- The tether does not stretch under tension i.e. elongation can be neglected.

- The tension load in the mooring tether remains constant for all x displacements.

For an equilibrium condition to exist

$$F_C = T \sin\theta \tag{7.5}$$

where: F_C = horizontal current force exerted upon the buoy
$T \sin\theta$ = lateral restoring force
T = tension load in the mooring tether (constant)

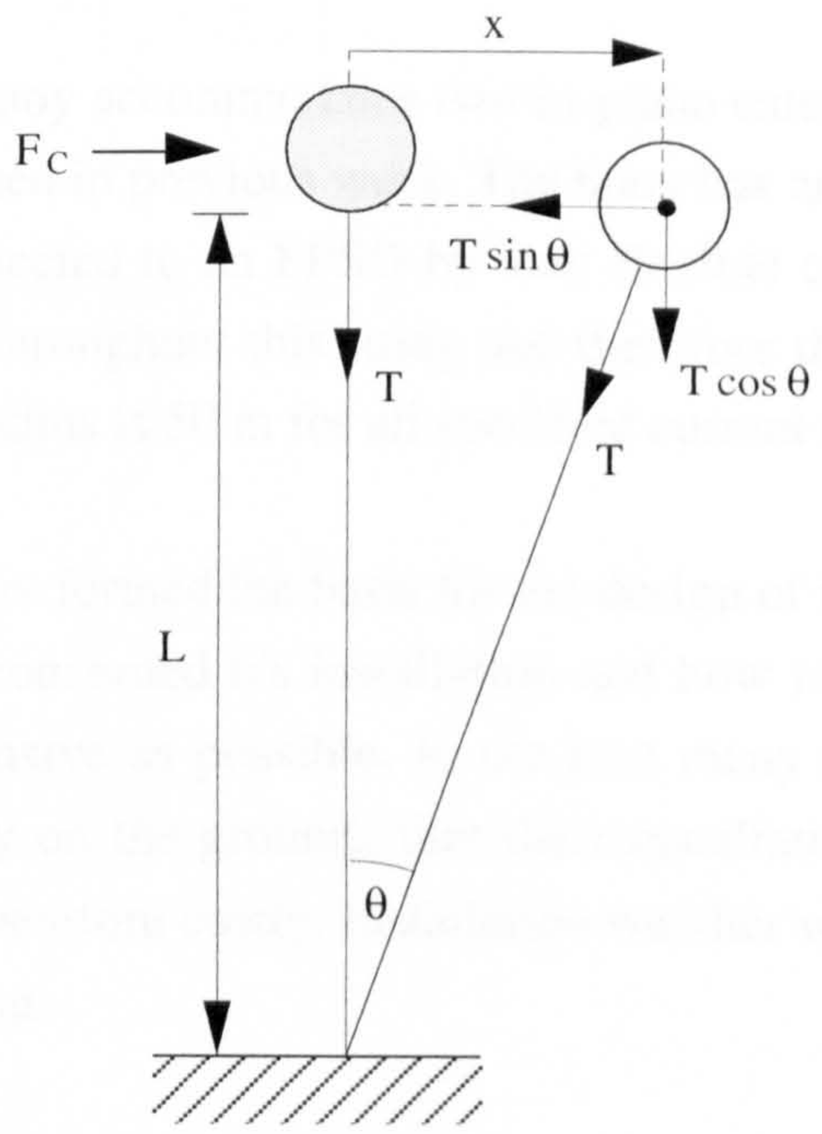

Figure 7.3

Tether Load Components

On the basis of Eqn (7.4) the angle θ can be considered as being small and hence:

$$\sin\theta \approx \frac{x}{L} \tag{7.6}$$

If this is substituted into Eqn (7.5):

$$F_C = T \frac{x}{L} \tag{7.7}$$

It can therefore be concluded that the lateral stiffness of the above arrangement can be obtained using the following expression:

$$k = \frac{T}{L} \tag{7.8}$$

7.5 General Description of the Design Proposal

7.5.1 Operating Parameters

The sub-surface buoy accommodates two in-plane catenary risers of a design that has already been established in previous work. The buoy has an operating depth of 100 m and is hydraulically connected to an FPSO by way flexible catenary risers. The design depth is 1500 m as used throughout this study and therefore the tether length is 1400 m. The buoy's watch circle radius is 50 m for all specified current design velocities.

These operating parameters formed the basis for the design of the buoy, however another important consideration concerned it's installation and how to make it as quick, simple and ultimately as inexpensive as possible. In the past many ingenious subsea systems have been rejected purely on the grounds that their installation is inherently complex, takes a long time and is therefore costly. Installation weather windows in areas like West of Shetland aren't very long.

The main components of the sub-surface buoy are:

- Multiple gas buoyancy compartments which can also be flooded in order to provide ballast during installation.

- Riser connection assembly incorporating two inclined flex-joints

- Vertical mooring tethers

- Rigid flowlines providing a connection between the risers own flowlines and the flexibles going to the FPSO.

- Flexible risers suspended between the buoy and the FPSO

The sub-surface buoy is illustrated in Figures 7.4 to 7.7.

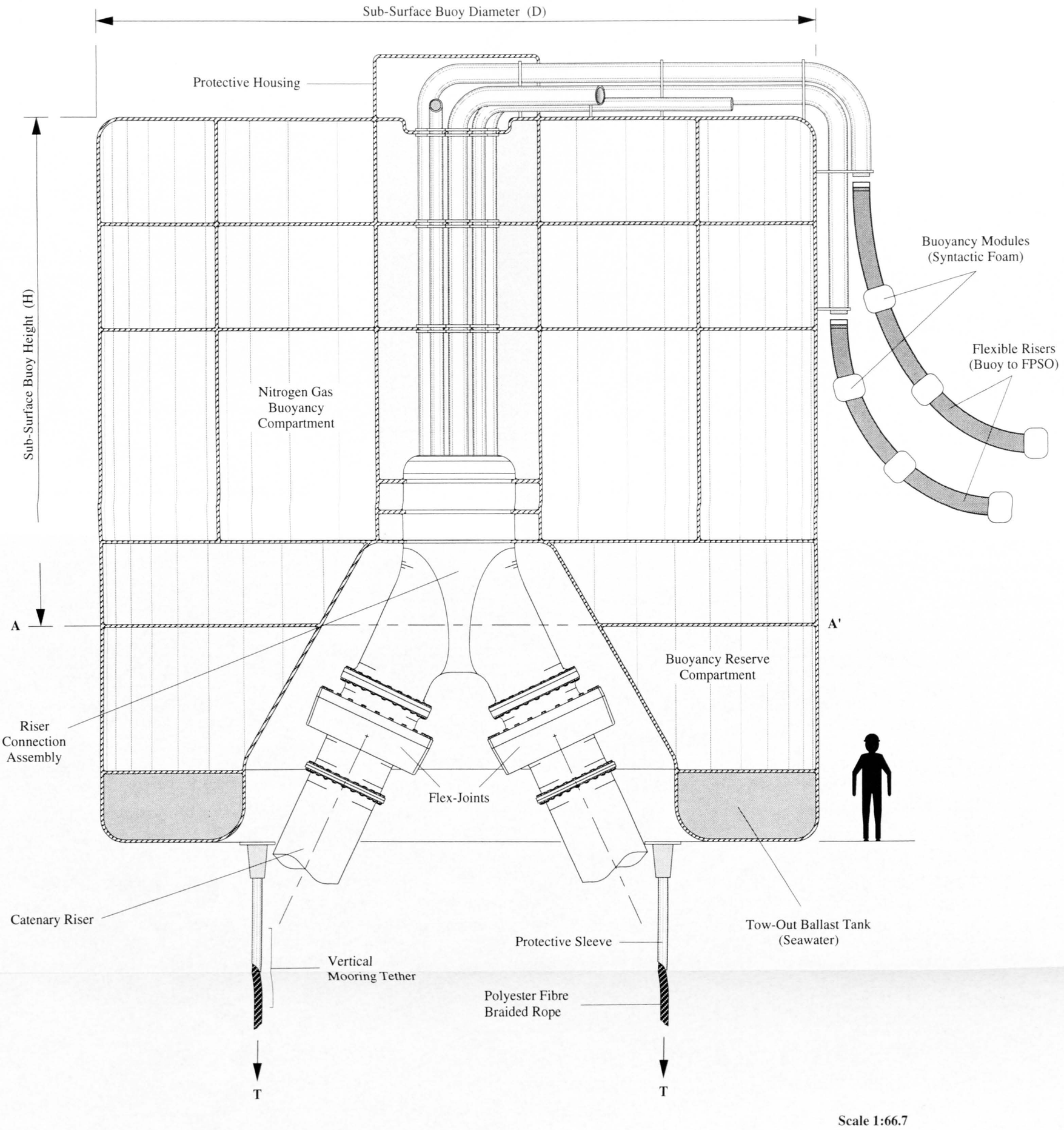

Figure 7.4

Sub-Surface Buoy (Cross-Sectional Side View)

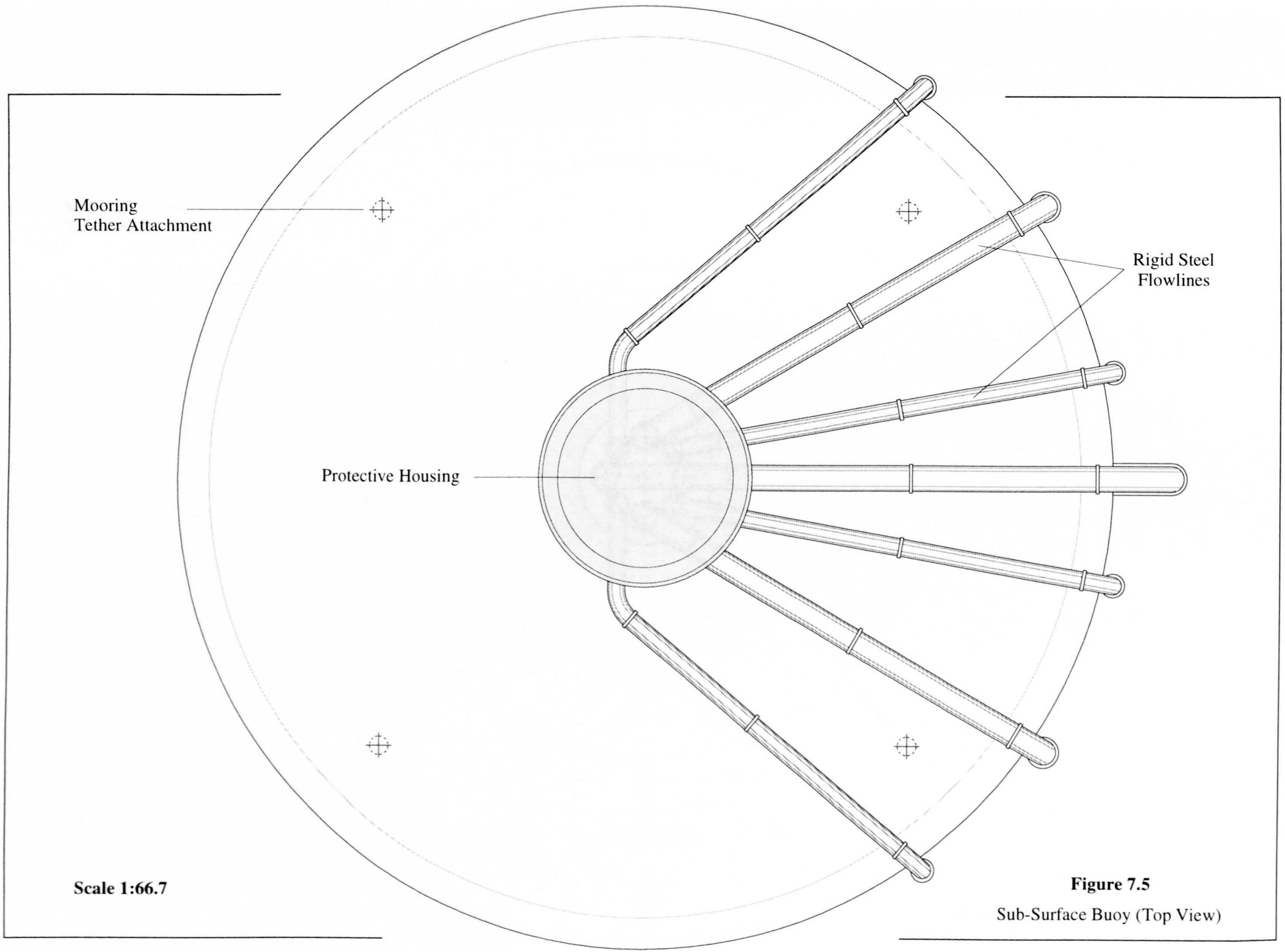

Scale 1:66.7

Figure 7.5

Sub-Surface Buoy (Top View)

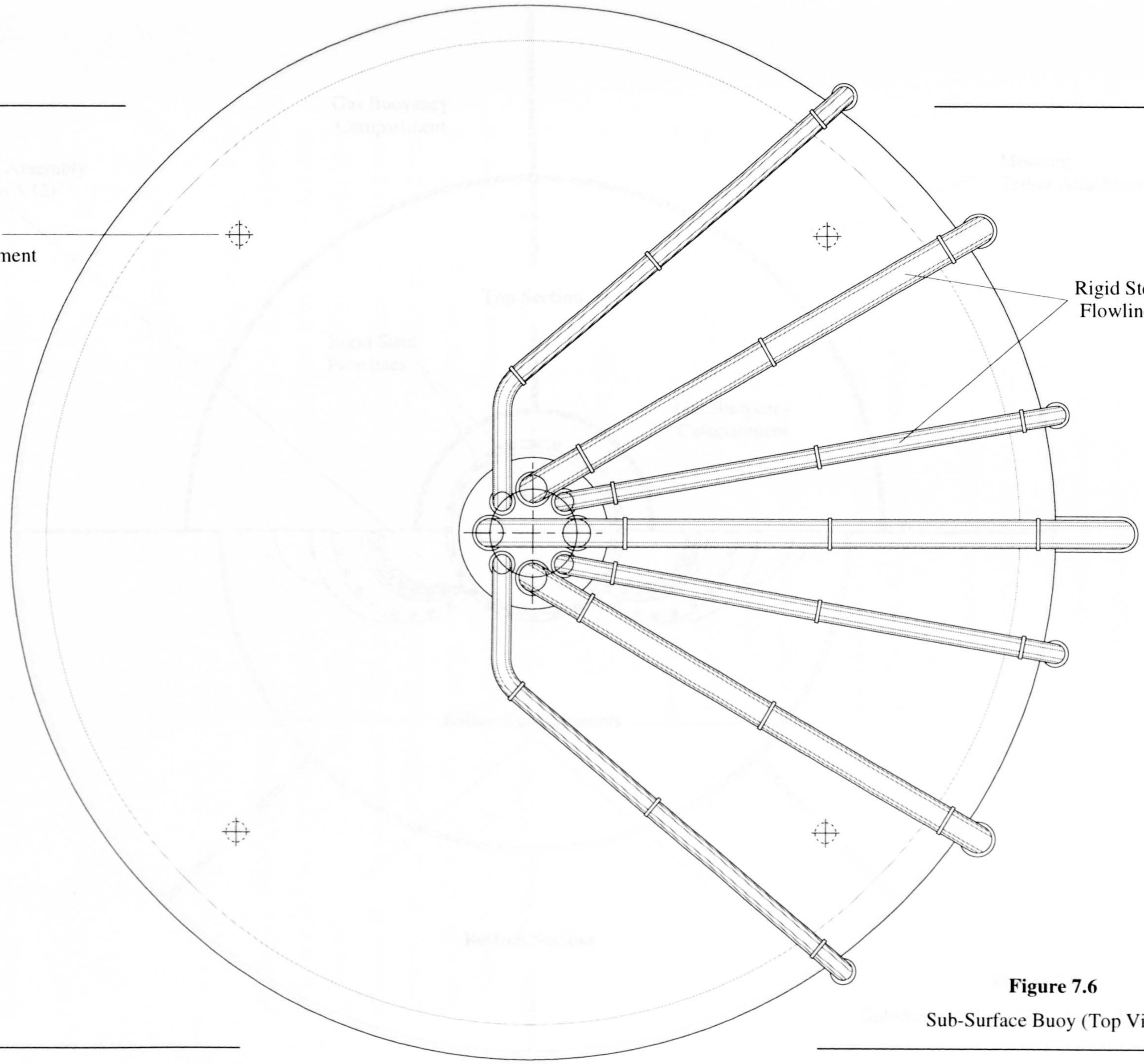

Scale 1:66.7

Figure 7.6

Sub-Surface Buoy (Top View)

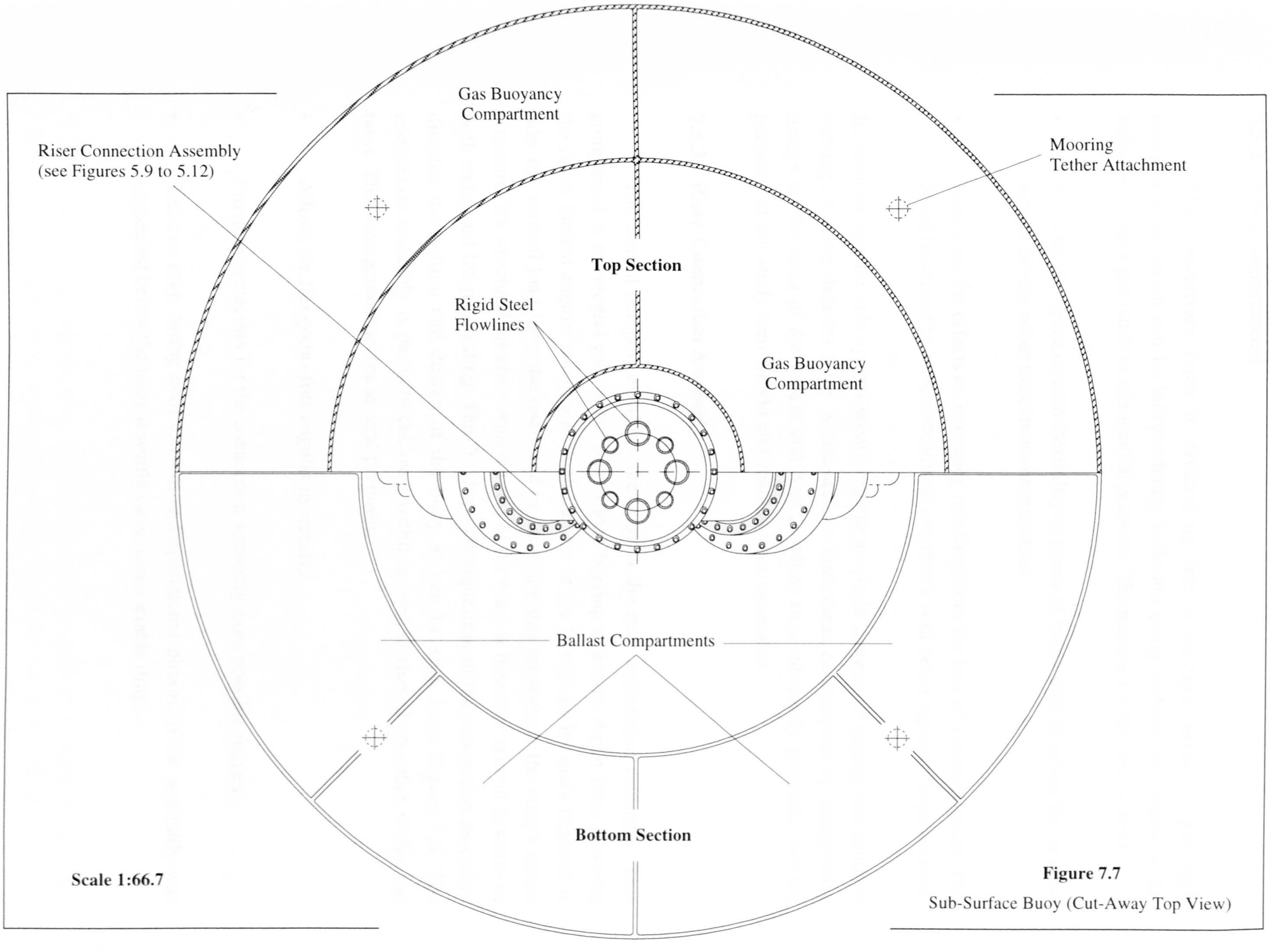

Scale 1:66.7

Figure 7.7

Sub-Surface Buoy (Cut-Away Top View)

7.5.2 The Compartments

The sub-surface buoy is divided up into a multiple array of gas tight compartments which can be independently ballasted using ambient sea water or de-ballasted using a gas (such as nitrogen) at pressure. The reasons for this are twofold:

- Provides the operator with flexibility in terms of being able to adjust the systems weight during either installation or operation.
- Minimises the effects on buoyancy resulting from the loss of a compartment. This could be caused by either a bulkhead or outside wall being ruptured or penetrated.

In order to operate, this system would require a certain amount of piping and actuated valving. A more detailed study would seek to limit these components by imaginative design on the basis of the weight and cost penalties they inherently generate. For the purposes of this study their weight and cost has been estimated.

7.5.3 Riser Connection Assembly

The central component within the buoy is the riser connection assembly. This component is an integral part of the buoy's load bearing structure. Apart from allowing the risers limited angular rotation through the use of the flex-joints it's main function is take the vertical load from the risers and to distribute this throughout the buoy's entire structure. It's structural interface with the rest of the buoy is therefore critical in terms of both static and fatigue loading. The 'Y' shape configuration of the connection assembly dictates the bottom end design of the buoy as can be seen from Figure 7.4. The connection assembly is partially enclosed within a conical shaped chamber within the buoy. This arrangement serves several purposes:

- Allows the flex-joints free angular movement
- Provides protection for the connection assembly from possible impact.
- Reduces drag during both tow-out and operational phases. If the assembly was suspended below the buoy it would cause considerable drag.

7.5.4 Vertical Mooring Tethers

The sub-surface buoy is attached to the seabed by way of four vertical mooring tethers which are constructed using high performance polyester fibre. These ropes are specifically designed for use in deep water mooring applications where a traditional steel cable system would not be possible. In deep water (beyond 1000 m) weight becomes a great disadvantage and may become a significant proportion of the mooring lines breaking load. In the case of a tethered sub-surface buoy a greater line weight necessitates more buoyancy and hence a larger buoy. It therefore seemed appropriate to utilise a lighter weight material especially as their performance in terms of tensile strength has been substantially improved over the last few years. The table below provides some performance data on a currently available range of polyester rope produced by BRIDON.

Jacketed Diameter (mm)	**Weight in Air** (kg/m)	**Minimum Braking Load** (kN)
132	12.6	5000
152	16.7	7000
162	18.9	8000
180	23.4	10000

Table 7.2

The Performance of Fibre Rope From the VIKING 7 STANDARD RANGE

Each rope is made up of a parallel array of seven long braided rope secured within a protective overbraid. The entire length is then enclosed within a polyethylene sleeve which further protects it from both abrasion and marine fouling. Some other benefits attributed to using fibre rope instead of steel cable are outlined below:

- They do not corrode or deteriorate appreciably in sea water
- They are easier to transport handle and install due to their inherent flexibility and light weight.
- They are easier to terminate

The proposed design uses the 132 mm rope (as given in Table 7.2) to tether the buoy. Four tethers are employed so as to provide a high degree of mooring redundancy.

7.5.5 Rigid Flowlines

These flowlines connect the flowlines within the risers to the flexible risers suspended between buoy and FPSO. Bundled together they run vertically upwards through the centre of the buoy from the riser connection assembly to the top of the buoy. At this point they are bent to the horizontal and then splayed out to the circular edge of the buoy, where they are subsequently dropped down the side. This is where the connections with the flexibles are made. As in the case of the riser connection assembly they are also an integral part of the buoy's load bearing structure.

7.5.6 Flexible Risers

Flexible risers are provided between the buoy and FPSO in order to de-couple the two vessels. The length flexible piping needed in order to meet the watch circle requirements as set out in Figure 7.1 is approximately 560 m. If eight flexibles are used this represents a considerable weight that needs to be supported by both buoy and FPSO. In order to limit the extra weight exerted upon the buoy in particular it is suggested that foam buoyancy modules are attached to the flexible risers as illustrated in Figure 7.4.

7.6 Calculations to Determine Size and Loading

7.6.1 Introduction

The size of the buoy is based upon two aspects:

- The total weight it has to support *(buoy + risers)*
- The environmental loading imposed upon it (in this case current).

The aim of these analytical calculations is to determine the size of buoy required in order that it can carry out it's primary functions as set out in Section 7.2 over an operational life span. This evaluation is conducted using a range of riser weights and maximum current velocities. Once the size of the buoy has been determined the tensile loads in the tethers can then be calculated.

7.6.2 Buoy Size Calculation

It was established in Section 7.4 that the lateral stiffness of the tethered sub-surface buoy system could be determined using the following expression:

$$k_x = \frac{T_T}{L} \tag{7.9}$$

where: T_T = total mooring tether load = n T

n = number of mooring tethers

T = tension load in each tether

L = length of the mooring tether

If $$F_{xT} = k_x X_{max} \tag{7.10}$$

then $$X_{max} = \frac{F_{xT}}{T_T} L \tag{7.11}$$

where: X_{max} = maximum allowable displacement (max watch circle radius)

F_{xT} = total horizontal load exerted upon the buoy.

Eqn (7.11) can therefore be expanded as follows:

$$X_{max} = \frac{F_{xT}}{T_T} L = \frac{\left(F_{xR} + F_{xB}\right)}{\left(B - W_B - F_{yR}\right)} L \tag{7.12}$$

where: F_{xR} = resultant horizontal reaction load exerted by the risers on the buoy

F_{xB} = horizontal current load exerted upon the buoy

F_{yR} = resultant vertical reaction load exerted by the risers on the buoy

B = buoyancy force exerted upon the buoy

W_B = weight (in air) of the buoy

Eqn (7.12) can be broken up further into it's constituent parameters by substituting in the following equations:

$$B = \frac{\pi}{4} D^2 \rho_{sw} g H \tag{7.13}$$

$$F_{xB} = \frac{1}{2}\rho_{sw} C_D D H U_C^2 \qquad (7.14)$$

(Morrison Equation)

$$X_{max}\left(B - W_B - F_{yR}\right) = \left(F_{xR} + 0.5\rho_{sw} C_D D H U_C^2\right)L \qquad (7.15)$$

$$\left(\frac{\pi}{4}D^2 \rho_{sw} gH - W_B - F_{yR}\right) = \frac{\left(F_{xR} + 0.5\rho_{sw} C_D D H U_C^2\right)L}{X_{max}} \qquad (7.16)$$

Re-arranging to find *H*:

$$\left(\frac{\pi}{4}D^2 \rho_{sw} gH\right)X_{max} = \left(F_{xR} + 0.5\rho_{sw} C_D D H U_C^2\right)L + \left(W_B + F_{yR}\right)X_{max}$$

$$\frac{\pi}{4}D^2 \rho_{sw} gHX_{max} - 0.5\rho_{sw} C_D D H U_C^2 L = F_{xR} L + \left(W_B + F_{yR}\right)X_{max}$$

$$\rho_{sw} H\left(\frac{\pi}{4}D^2 gX_{max} - 0.5C_D D U_C^2 L\right) = F_{xR} L + \left(W_B + F_{yR}\right)X_{max}$$

$$H = \frac{F_{xR} L + \left(W_B + F_{yR}\right)X_{max}}{\rho_{sw}\left(\frac{\pi}{4}D^2 gX_{max} - 0.5C_D D U_C^2 L\right)} \qquad (7.17)$$

where:
- H = buoy height
- D = buoy diameter
- ρ_{sw} = density of sea water
- g = gravitational acceleration
- U_C = current design velocity

The equation above allows the designer to select the required buoy height (H) for a given diameter (D) on the basis that its lateral displacement (X) never exceeds the value permitted (X_{max}) up to a specified current design velocity (U_C). The buoy's height and diameter dimensions are clearly defined in Figure 7.4 from where it can be observed that *H* does not extend the full height of the buoy. The reason for this is that the compartments below the level *A-A'* would normally be filled with sea water (i.e. ballasted) and would therefore not contribute to the overall buoyancy. If a situation arose in which additional buoyancy was required these compartments could then be evacuated or de-ballasted by filling them with a gas at pressure. These a compartments effectively act as a buoyancy reserve for the system.

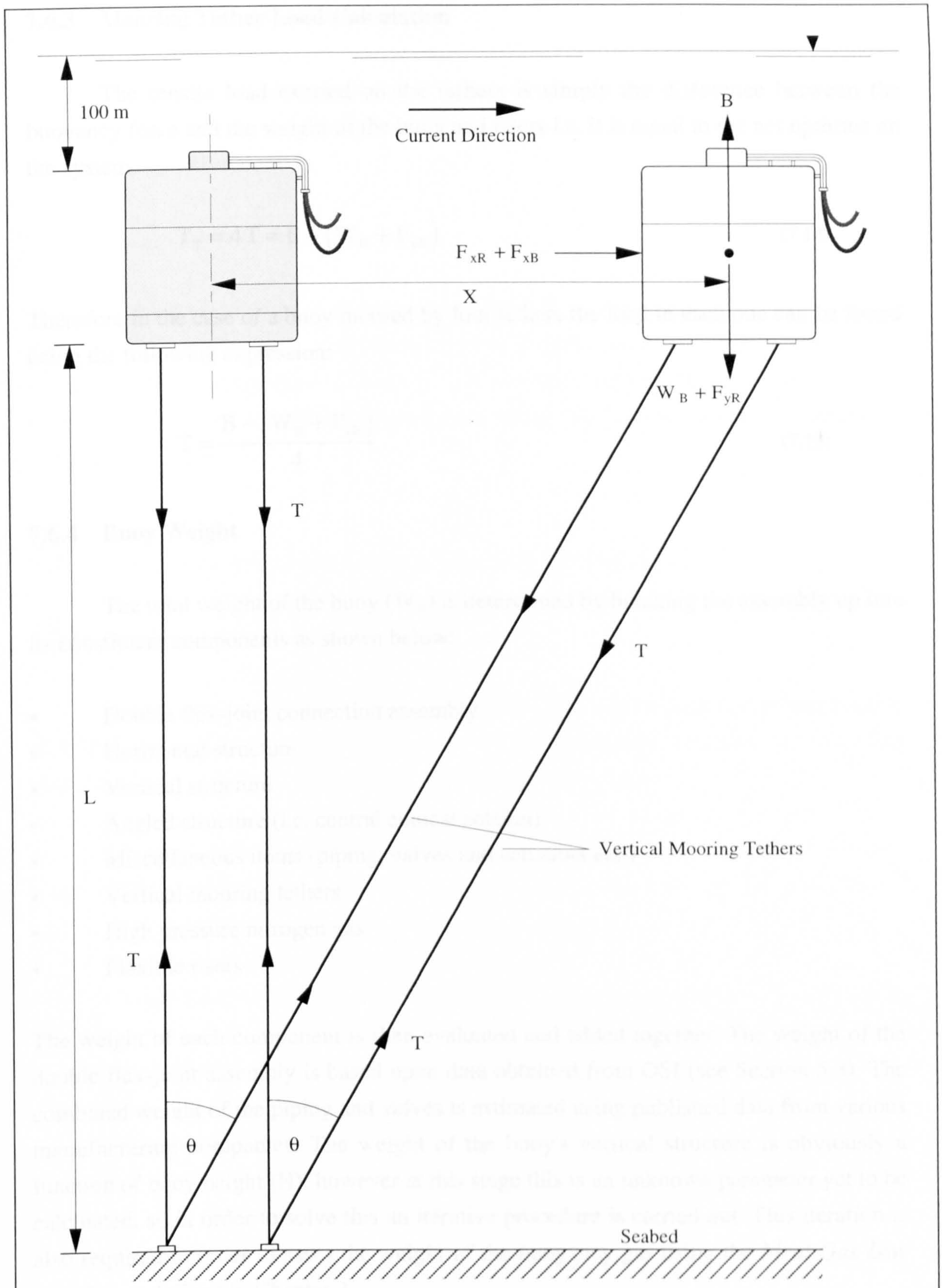

Figure 7.8

Sub-Surface Buoy Displacement

7.6.3 Mooring Tether Load Calculation

The tensile load exerted on the tethers is simply the difference between the buoyancy force and the weight of the buoy and risers i.e. it is equal to the net upthrust on the system

$$T_T = 4T = B - \left(W_B + F_{yR}\right) \tag{7.18}$$

Therefore in the case of a buoy moored by four tethers the load in each one can be found using the following expression:

$$T = \frac{B - \left(W_B + F_{yR}\right)}{4} \tag{7.19}$$

7.6.4 Buoy Weight

The total weight of the buoy (W_B) is determined by breaking the assembly up into its constituent components as shown below:

- Double flex-joint connection assembly
- Horizontal structure
- Vertical structure
- Angled structure (i.e. central conical section)
- Miscellaneous items (piping, valves and actuators etc.)
- Vertical mooring tethers
- High pressure nitrogen gas
- Flexible risers

The weight of each component is then evaluated and added together. The weight of the double flex-joint assembly is based upon data obtained from OSI (see Section 5.3). The combined weight of the piping and valves is estimated using published data from various manufacturing companies. The weight of the buoy's vertical structure is obviously a function of buoy height (H), however at this stage this is an unknown parameter yet to be calculated, so in order to solve this an iterative procedure is carried out. This iteration is also required in order to asses the weight of the buoyancy gas using the *Ideal Gas Law* equation as defined in Chapter 3.

7.6.5 Loads Imposed by the Risers

The loads imposed upon the buoy by the risers have two components:

- Riser self-weight
- Current loads acting on the riser

These combine to generate surface reaction forces in both horizontal (F_{xR}) and vertical (F_{yR}) directions which are a function of riser length, submerged unit weight, riser orientation to the current flow (Convex or Concave) and current velocity. Their values are determined from an FE analysis carried out using the LUSAS software package as described in Chapter 5.

7.7 An Overview of the Design Analysis Spreadsheet

7.7.1 Introduction

The analysis to determine sub-surface buoy size and loading is conducted using an EXCEL spreadsheet (see Spreadsheet 7.1). This spreadsheet generates the following output by utilising Eqns (7.17) and (7.19) within an iterative loop.

- Sub-Surface Buoy (SSB) Height
- SSB Buoyancy
- Lateral Stiffness
- Tension Load in Each Tether
- Current Load on SSB (F_{xB})

A number of other parameters are also calculated:

- Component Weights
  - horizontal structure
  - vertical structure
  - angled structure
  - vertical tethers
  - buoyancy gas
  - flexible risers

- Ambient Sea water Pressure (calculated at the top of the buoy)
- SSB Internal Volume

The spreadsheet input required in order for the preceding parameters to be determined is described below.

7.7.2 Spreadsheet Input

Spreadsheet 7.1 requires the following input:

- Sea Depth
- SSB Tether Length
- No. of Tethers
- SSB Diameter
- Drag Coefficient
- Max Design Current Velocity
- Max Allowable Lateral Displacement
- Resultant Horizontal Riser Load (F_{xR})
- Resultant Vertical Riser Load (F_{yR})
- Depth Below the Surface
- Sea water Temperature

The drag coefficient for the buoy is taken as 0.8. This value is based upon a Reynolds no. range of between 6.0×10^5 and 9.0×10^6 with an allowance for marine fouling taken into consideration (see Figure 5.32). This range accommodates current of velocities of between 0.1 and 0.8 m/s and buoy diameters of between 8 and 16 m.

The loads exerted upon the buoy by the suspended risers in both horizontal and vertical directions are presented graphically in Figures 7.11 to 7.15. These results are obtained using LUSAS and clearly show the sensitivity of the load to current velocity for two in-plane risers with a horizontal offset of 1500 m and submerged unit weights of 100, 500, 1000, 1500 and 2000 N/m. It is shown that in most cases current velocity has a negligible effect on either the resultant horizontal or vertical load. This is due to the different current loading characteristics associated with the Convex and Concave riser conditions cancelling one another out.

7.8 Discussion of the Results

7.8.1 Introduction

The results from the design analysis are presented using both tabular and graphical formats in EXCEL. The following data is given:

Tables 7.4 to 7.8	SSB Height and External Volume for 3 buoy diameters
Tables 7.9 to 7.13	SSB Weight (air) and Buoyancy for 3 buoy diameters
Figures 7.16(a) to 7.20(a)	Maximum Load Exerted Upon Each Mooring Tether
Figures 7.16(b) to 7.20(b)	Maximum Current Load Exerted Upon the SSB

All the data above is based upon a specified current design velocity which is varied in 0.1 m/s increments. For instance, in the case of a 12.0 m diameter buoy supporting risers with a submerged unit weight of 1000 N/m the following results apply for a current design velocity of 0.6 m/s.

Required Height = 8.3 m
Corresponding Parameters: External Volume = 939 m^3
SSB Weight = 2297 kN (or 234.1 tonnes)
SSB Buoyancy = 9439 kN (or 962.2 tonnes)
Max Tether Load = 656 kN
Max Current Load Exerted Upon the Buoy = 21.1 kN

As previously stated these results are based upon a maximum allowable SSB displacement of 50 m from the design condition.

7.8.2 SSB Height and External Volume

Two trends can be identified from the results tabulated in Tables 7.4 to 7.8:

- The required size of buoy increases with an increase in current design velocity. In order for the SSB to resist higher current velocities it must posses a greater lateral stiffness and this is achieved by increasing the tension in the tethers. Increasing the buoyancy - weight ratio provides a means of doing this.

- For a given design velocity buoy size increases with an increase in riser weight. Increasing the weight of the risers has the effect of decreasing the systems buoyancy to weight ratio thereby ultimately reducing the systems lateral stiffness and resistance to current loading. Increasing the buoyancy by increasing the buoys external volume rectifies this problem.

7.8.3 SSB Weight and Buoyancy

The data presented in Tables 7.9 to 7.13 relates to the work above in that it illustrates the consequences in terms of weight and buoyancy of increasing the size or volume of the buoy. Increasing the volume of the buoy has the effect of dramatically increasing the buoyancy to weight ratio i.e. the buoyancy is more sensitive to a change in volume than weight.

7.8.4 Maximum Load Exerted Upon Each Mooring Tether

The graphs in Figures 7.16(a) to 7.20(a) seek to re-affirm the statement made in Section 7.8.2 that an increase in mooring tether load is required in order to accommodate a higher current velocity.

7.8.5 Maximum Current Load Exerted Upon the SSB

The results displayed graphically in Figures 7.16(b) to 7.20(b) show how the current load exerted upon the buoy increases with current velocity. Buoy drag is calculated using the Morrison equation and therefore the increase is a function of the velocity squared.

7.8.6 Component Weights

The calculated weights of the various components which make up a typical sub-surface buoy are tabulated below in Table 7.3.

Constituent Components	Weight in air	
	(kN)	(tonnes)
Double Flex-Joint Connection Assembly	70	7.1
Horizontal Structure	641	65.3
Vertical Structure	697	71.1
Angled Structure	65	6.6
Piping, Valves and Actuators	10	3.0
Vertical Mooring Tethers (4)	659	67.2
Buoyancy Gas (Nitrogen)	14	1.4
Flexible Risers	141	14.3

Table 7.3

The SSB's Constituent Component Weights

These weights relate to a 12.0 m diameter buoy supporting risers with a submerged unit weight of 1000 N/m. The current design velocity is 0.6 m/s.

7.9 Riser Installation Using a Sub-Surface Buoy

7.9.1 Introduction

The aim of this section is to put forward a proposed riser installation procedure based upon the sub-surface buoy system in a format similar to that utilised in Chapter 5 to describe the installation sequence involving the direct connection of the risers to an FPSO. The installation procedure is broken up in six steps which are sequentially illustrated in Figure 7.9.

7.9.2 Installation Procedure

Step 1 — The risers are towed out to the offshore field using the Controlled Depth Tow Method (CDTM). This method of tow-out was described in detail in Chapter 5.

Step 2 — The risers are lowered to the seabed. This is achieved by both reducing the tow speed (which reduces the hydrodynamic lift force acting upon the riser) and adjusting the risers weight through ballasting.

Step 3 — The sub-surface buoy is towed out to the offshore field using a support vessel. In order to generate enough stability to resist environmental forces during tow out the bottom compartments of the buoy are ballasted with either sea water or drilling mud, see Figure 7.10. The support vessel is also used to transport the mooring tethers.

Step 4 — Whilst the buoy is held in position by the support vessel the vertical mooring tethers are off-loaded and attached to the underside of the buoy. This operation will require the use of an offshore crane. A seabed connection template is also lowered on to the seabed and secured using a device appropriate to the seabed geology, suction piles could provide a solution. On the end of each tether are connection units which locate into the seabed template with the assistance of an ROV.

Step 5 — The risers are lifted off the seabed using an offshore crane and connected to the flex-joints within the buoy which at this stage is still floating on the surface.

Step 6 — The buoy submerged down to its operating depth by flooding the appropriate number of compartments with sea water. The lower end of each tether is then located into the seabed template using the ROV. A tension load is applied to the vertical mooring tethers by evacuating the buoy's compartments of sea water. This is achieved by pumping in buoyancy gas at pressure thereby forcing the sea water out through outlet valves. As tension is applied to the tethers the lower end connection units lock into place.

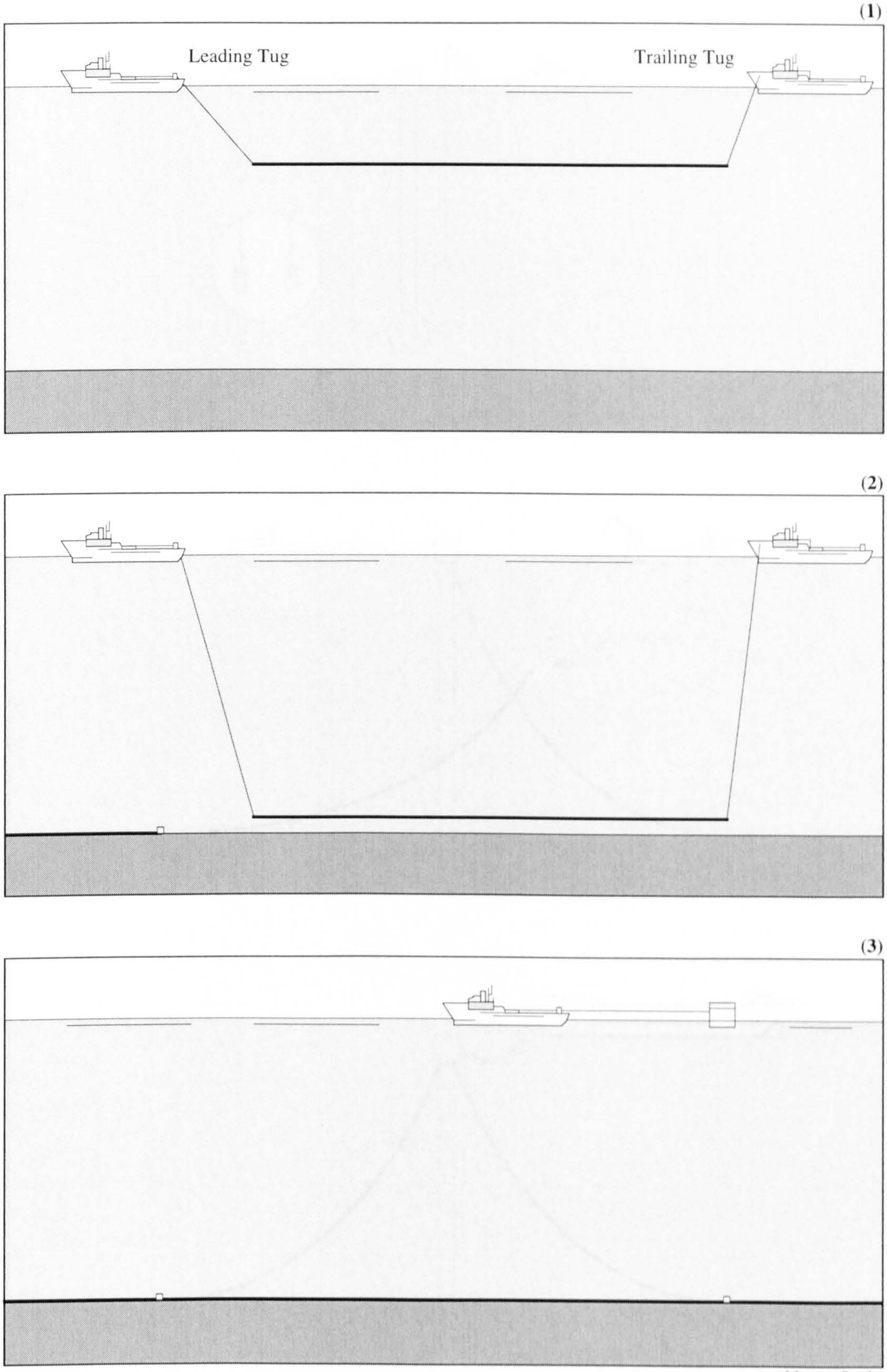

Figure 7.9(a)

Catenary Riser Installation Using a Sub-Surface Buoy

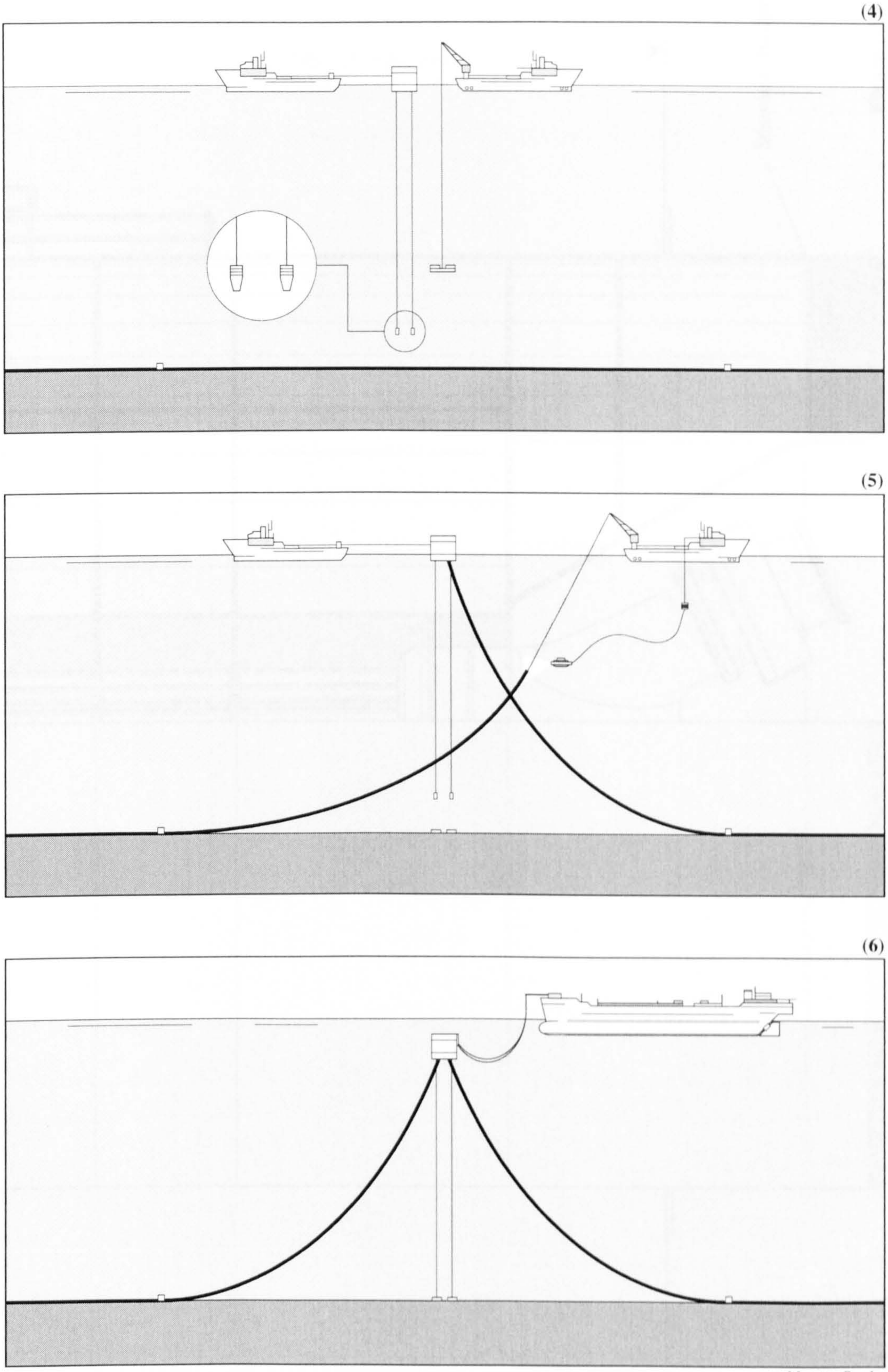

Not to Scale

Figure 7.9(b)

Catenary Riser Installation Using a Sub-Surface Buoy

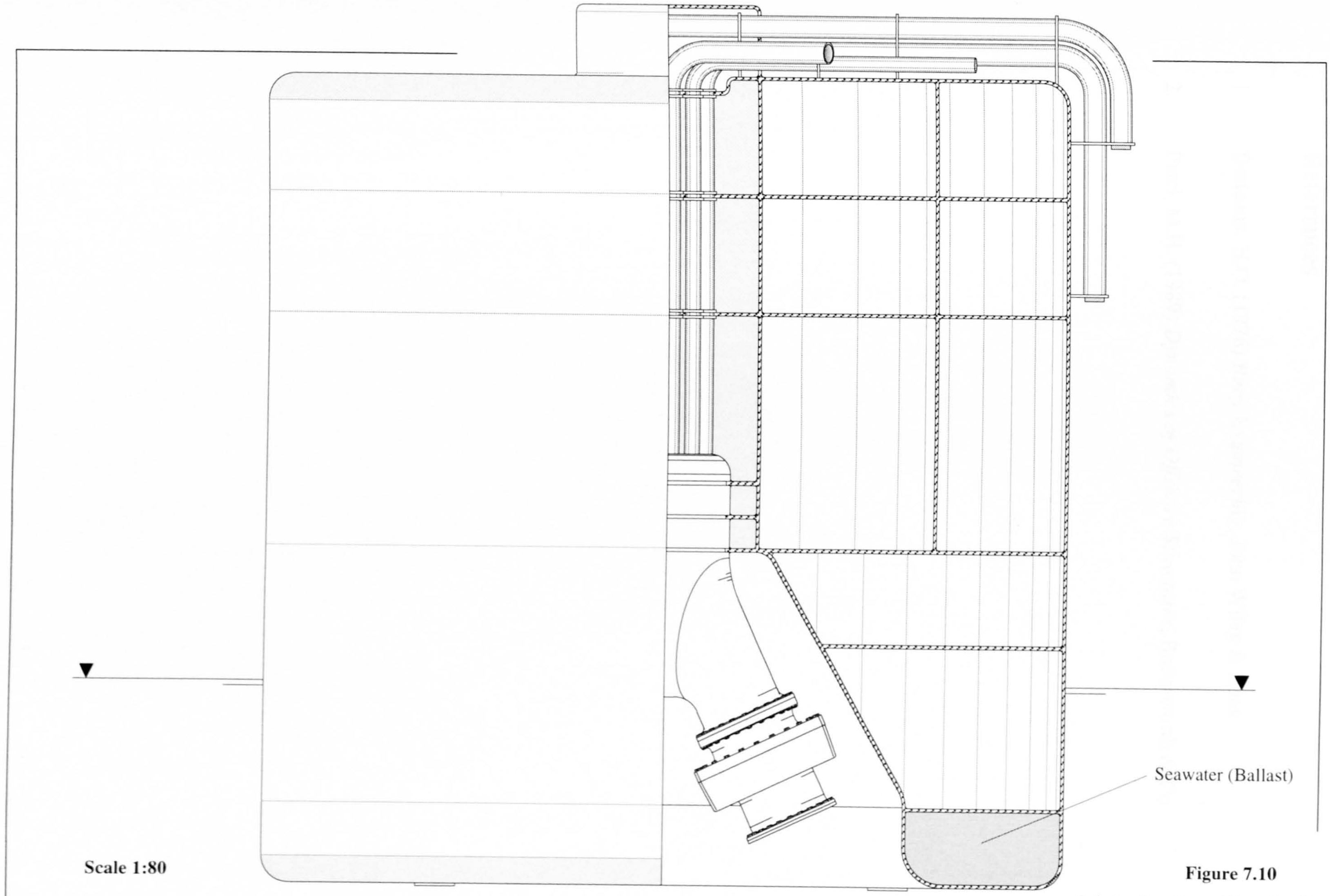

Scale 1:80

Figure 7.10

Sub-Surface Buoy (Tow-Out Condition)

References

1. Berteaux, H.O. (1976) *Buoy Engineering*, John Wiley & Sons.

2. Patel, M.H. (1989) *Dynamics of Offshore Structures*, Butterworth & Co.

CHAPTER 7

Analysis Spreadsheets

Spreadsheet 7.1

Sub-Surface Buoy Design Calculations

SSB and Riser Design Parameters

Sea Depth =	1500	m
SSB Tether Length =	1400	m
No. of Tethers =	4	
SSB Diameter =	12	m
Drag Coefficient =	0.8	
Current Design Velocity =	0.6	m/s

Maximum Allowable Lateral Displacement =	50	m

Resultant Horizontal Riser Load =	79	kN
Resultant Vertical Riser Load =	4518	kN

SSB Height =	8.3	m
SSB Buoyancy =	9439	kN
Lateral Stiffness =	1.9	kN/m
Tension Load in Each Tether =	656	kN
Current Load on SSB =	21.1	kN

Notes:

Minimum tether braking load = 5000 kN

The vertical tethers are a high performance synthetic fibre rope

Sub-Surface Buoy Component Weights (in air)

Double Flex-Joint Connection Assembly =	70	kN
	7.1	*tonnes*
Horizontal Structure =	641	kN
	65.3	*tonnes*
Vertical Structure =	697	kN
	71.1	*tonnes*
Angled Structure =	65	kN
	6.6	*tonnes*
Miscellaneous Items =	10	kN
(Piping, Valves etc)	*1.0*	*tonnes*
Vertical Tethers =	659	kN
	67.2	*tonnes*
Buoyancy Gas (Nitrogen) =	14	kN
	1.4	*tonnes*
Flexible Risers =	141	kN
	14.3	*tonnes*
Total SSB Weight (in air) =	2297	kN
	234.1	*tonnes*

Iteration Loop

Depth Below the Surface =	100	m
Seawater Temperature =	5	degs
Hydrostatic Pressure =	10.1	bar
SSB Internal Volume =	1131	m3

Spreadsheet 7.1

CHAPTER 7

Results

Figures 7.11 - 7.20

Tables 7.4 - 7.13

Horizontal Riser Loads Exerted Upon the Sub-Surface Buoy (a)

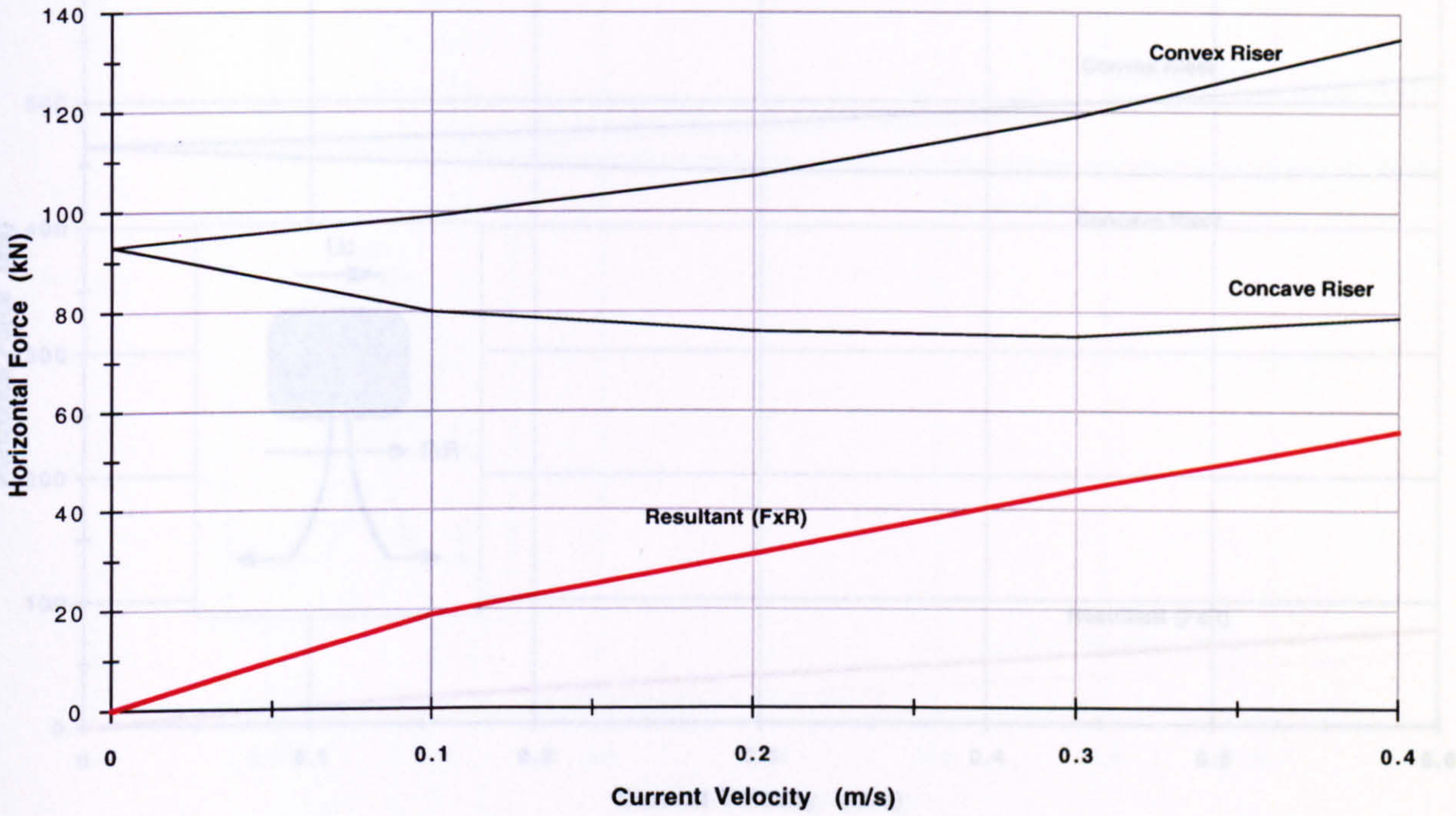

Riser Submerged Unit Weight = 100 N/m

Vertical Riser Loads Exerted Upon the Sub-Surface Buoy (b)

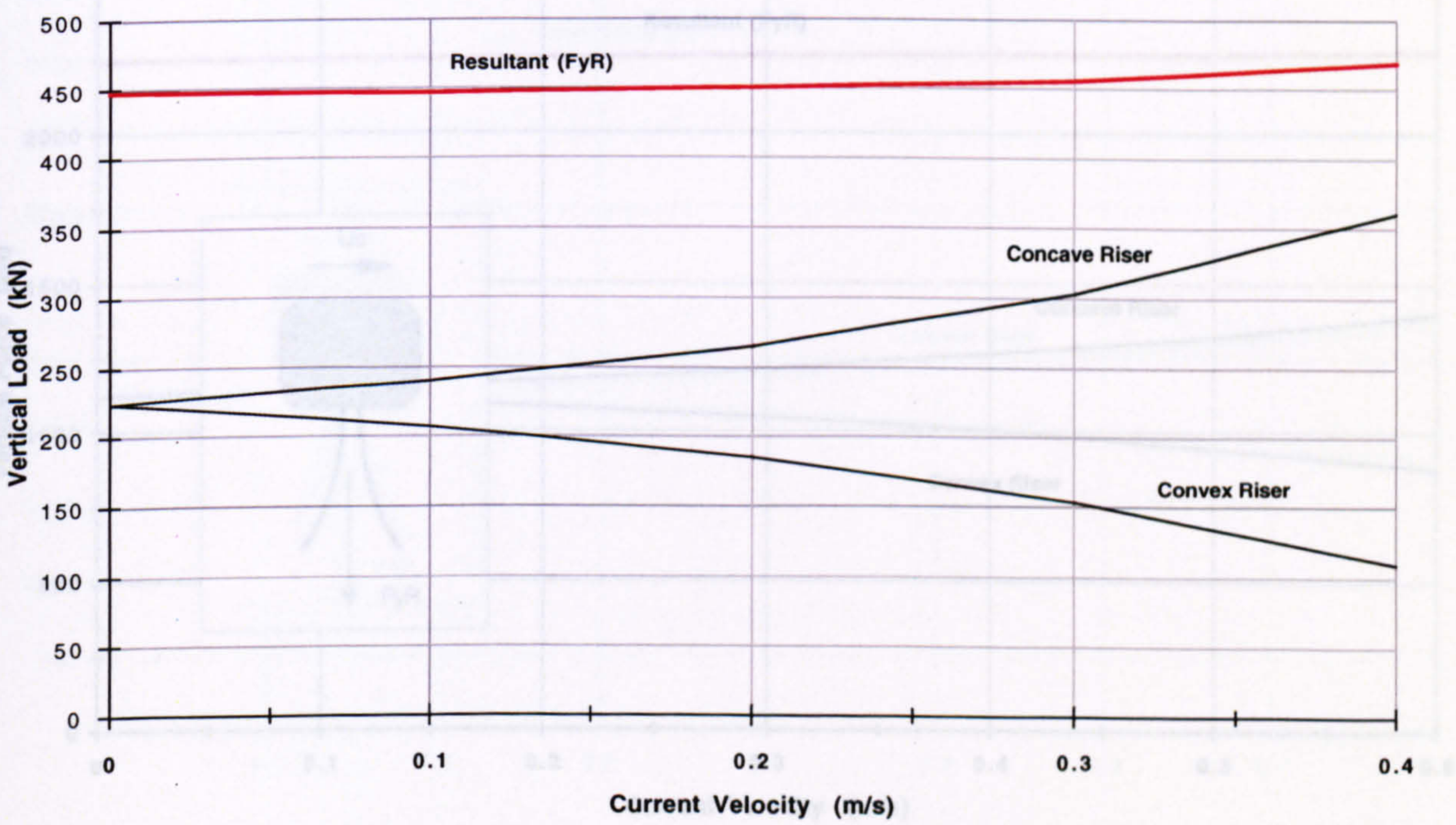

Horizontal Surface Offset = 1500 m

Vertical Offset = 1400 m

Submerged Unit Weight = 100 N/m

Sea Depth = 1500 m

Figure 7.11

Horizontal Riser Loads Exerted Upon the Sub-Surface Buoy (a)

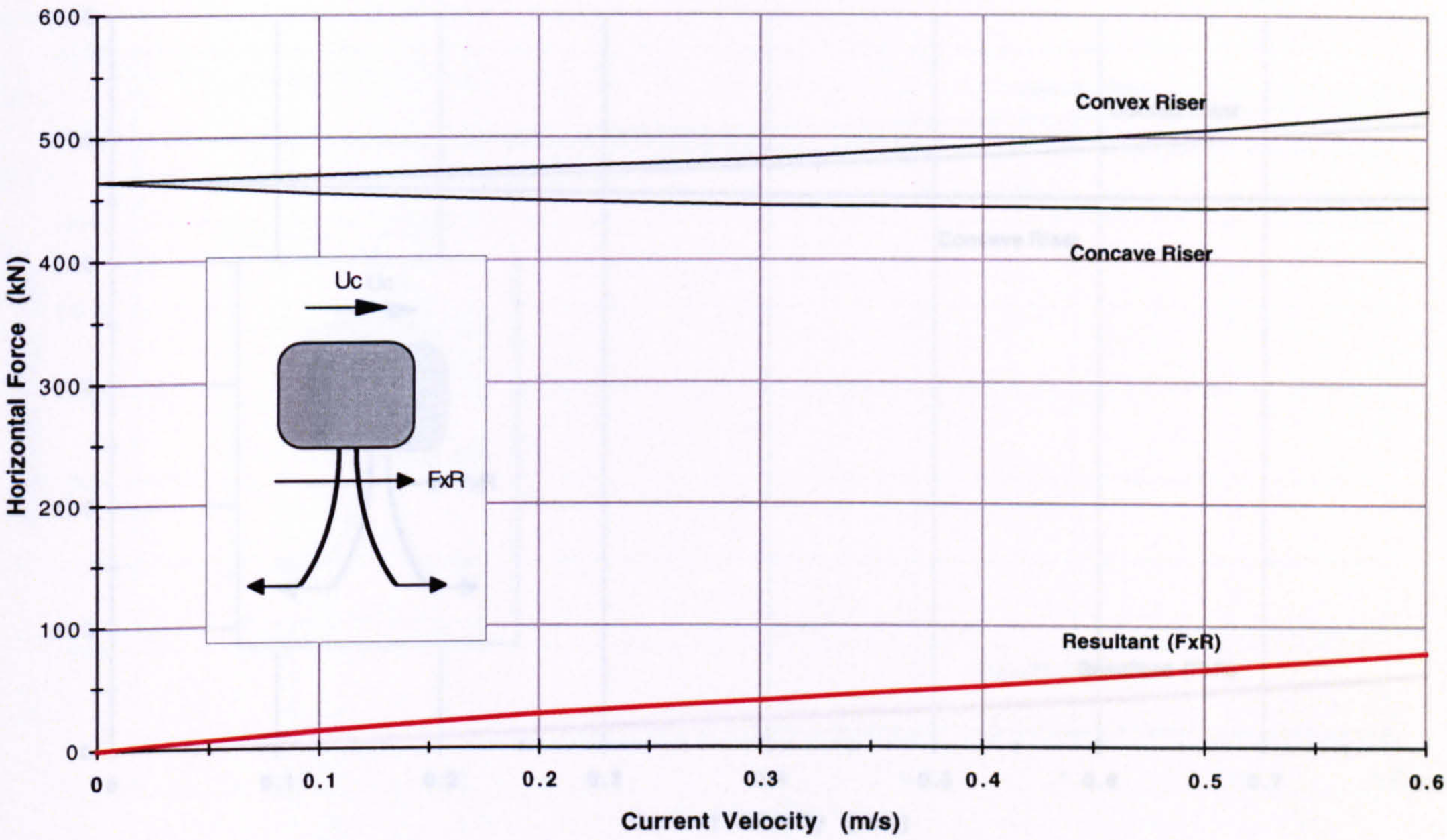

Riser Submerged Unit Weight = 500 N/m

Vertical Riser Loads Exerted Upon the Sub-Surface Buoy (b)

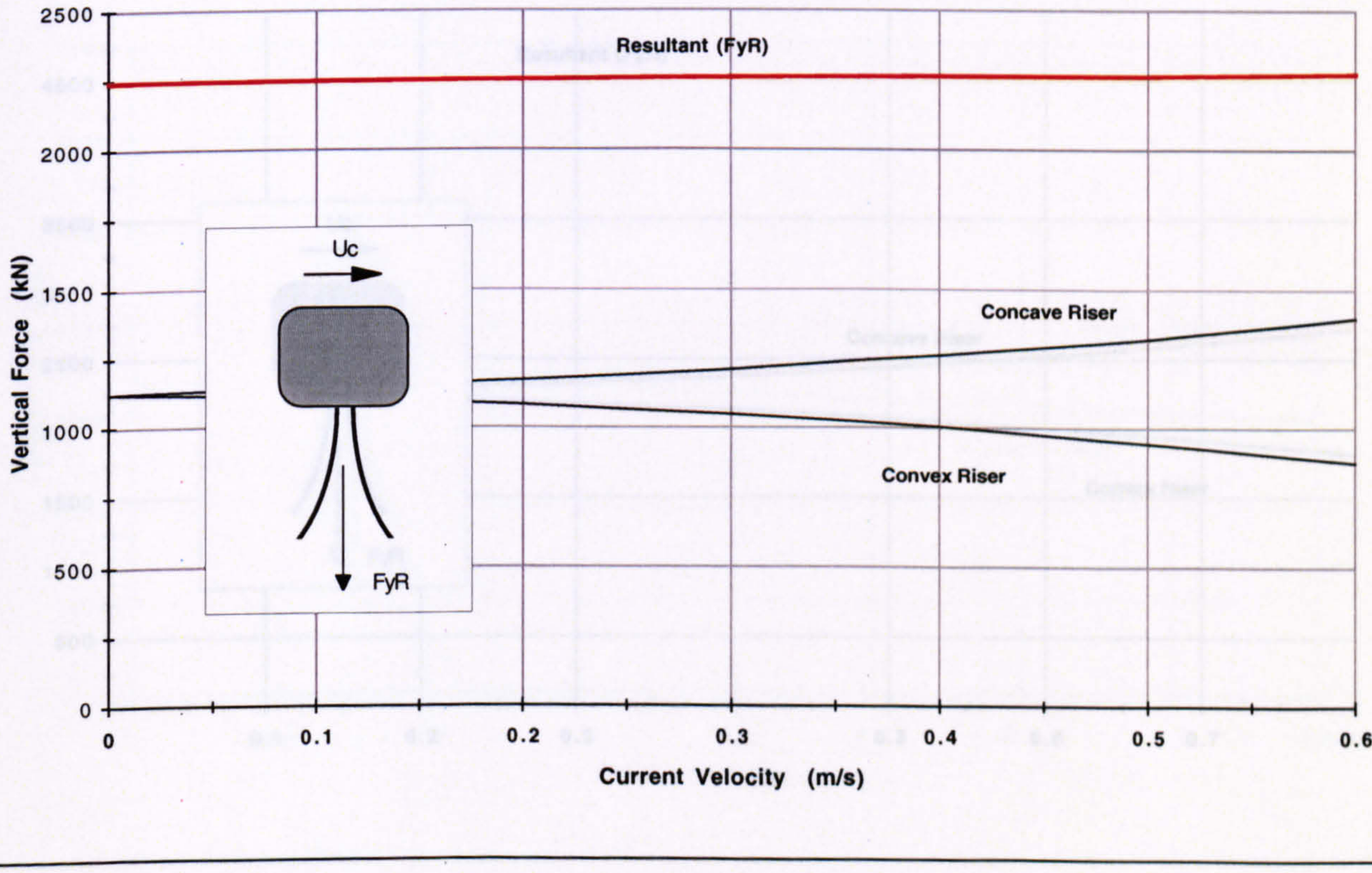

Horizontal Surface Offset = 1500 m

Vertical Offset = 1400 m

Submerged Unit Weight = 500 N/m

Sea Depth = 1500 m

Figure 7.12

Horizontal Riser Loads Exerted Upon the Sub-Surface Buoy (a)

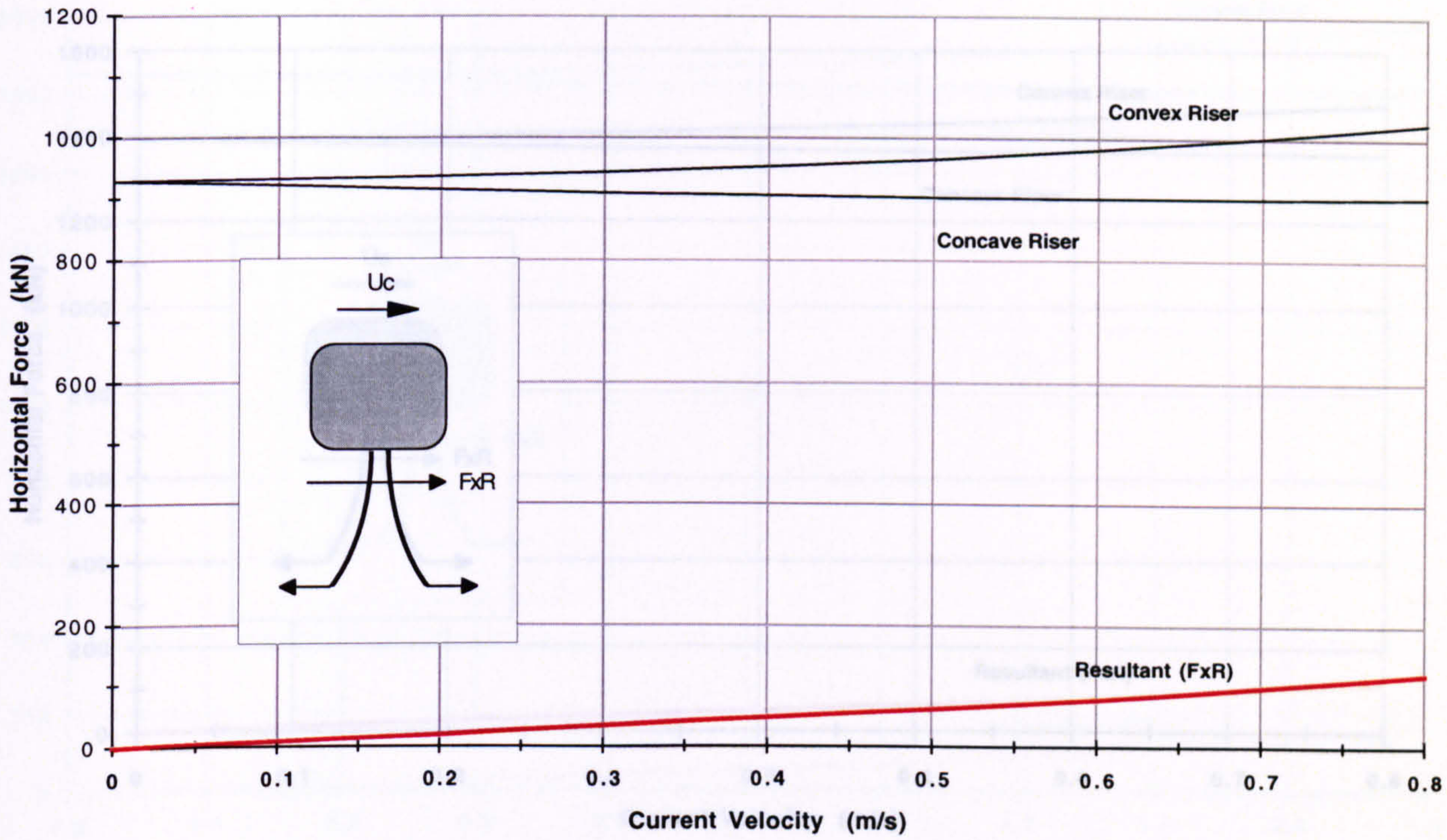

Riser Submerged Unit Weight = 1000 N/m

Vertical Riser Loads Exerted Upon the Sub-Surface Buoy (b)

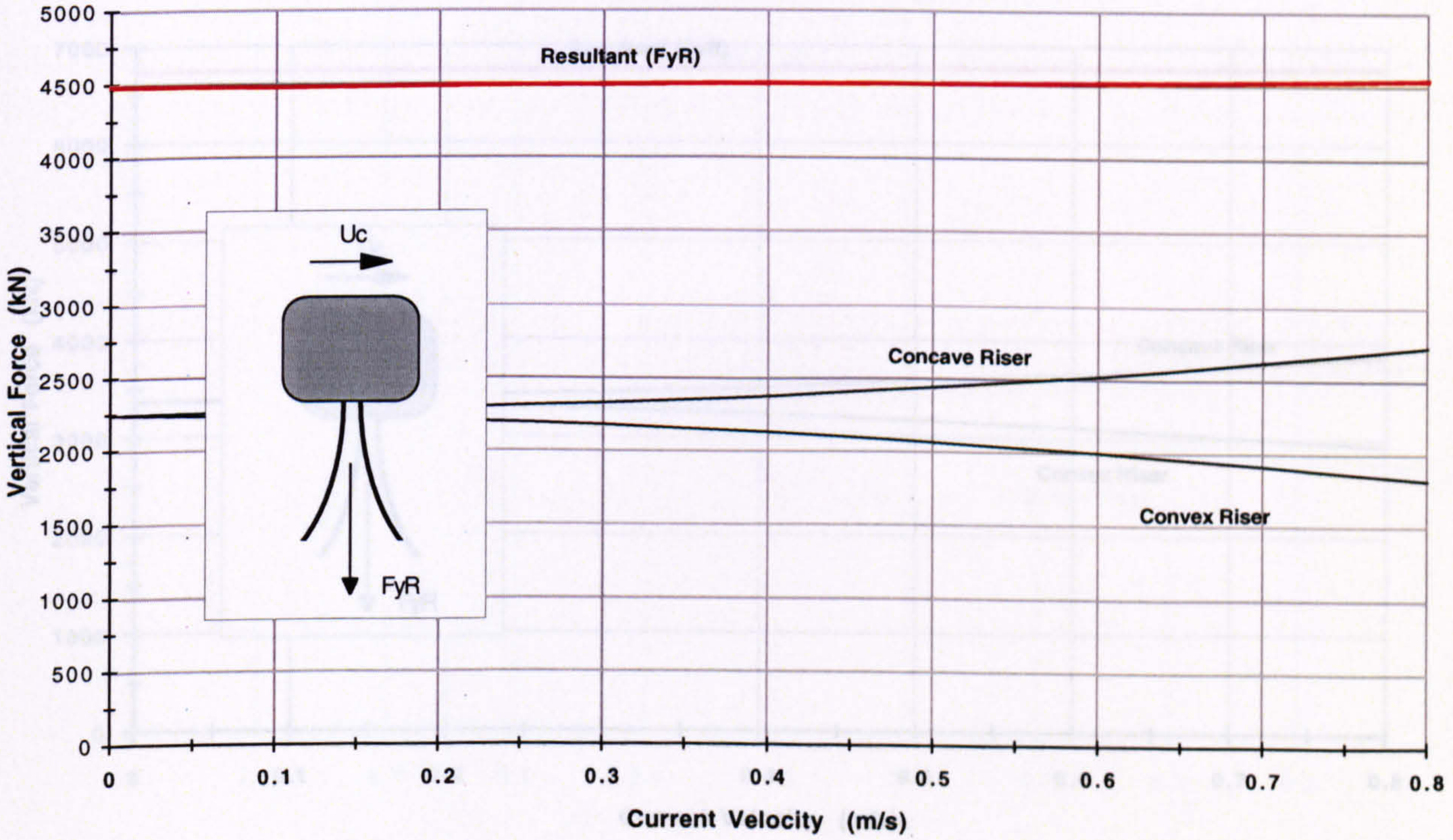

Horizontal Surface Offset = 1500 m

Vertical Offset = 1400 m

Submerged Unit Weight = 1000 N/m

Sea Depth = 1500 m

Figure 7.13

Horizontal Riser Loads Exerted Upon the Sub-Surface Buoy (a)

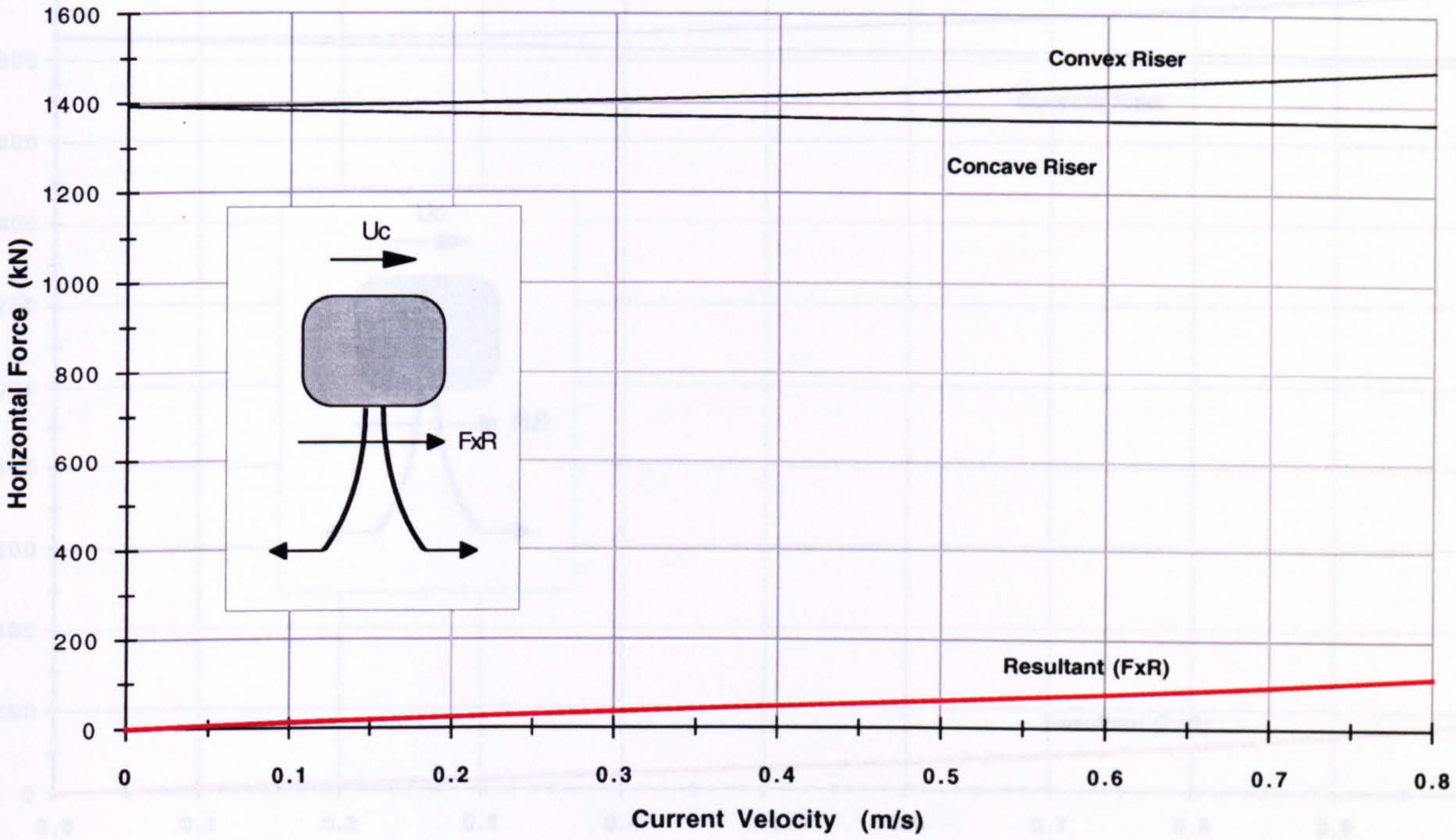

Riser Submerged Unit Weight = 1500 N/m

Vertical Riser Loads Exerted Upon the Sub-Surface Buoy (b)

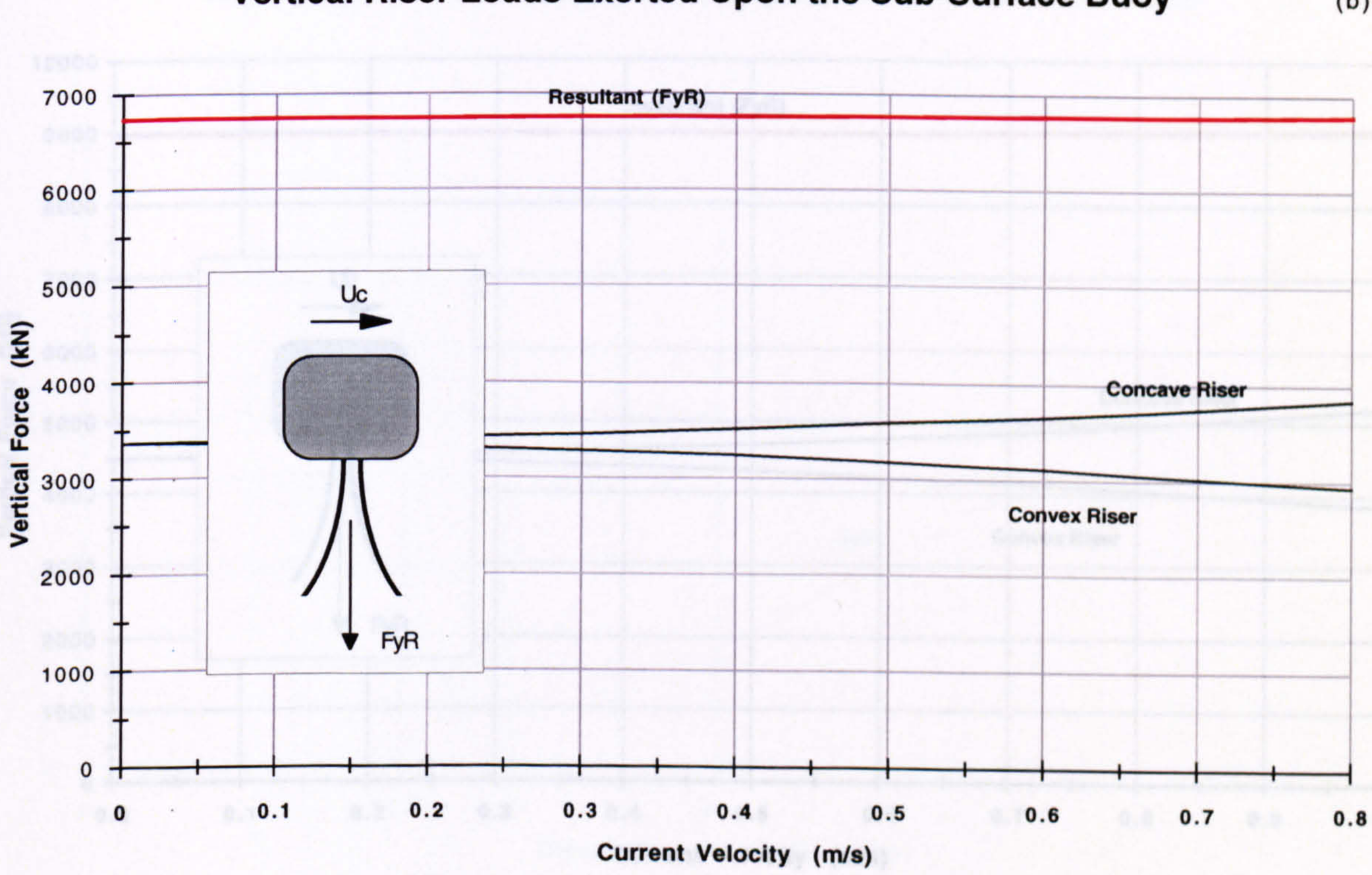

Horizontal Surface Offset = 1500 m

Vertical Offset = 1400 m

Submerged Unit Weight = 1500 N/m

Sea Depth = 1500 m

Figure 7.14

Horizontal Riser Loads Exerted Upon the Sub-Surface Buoy (a)

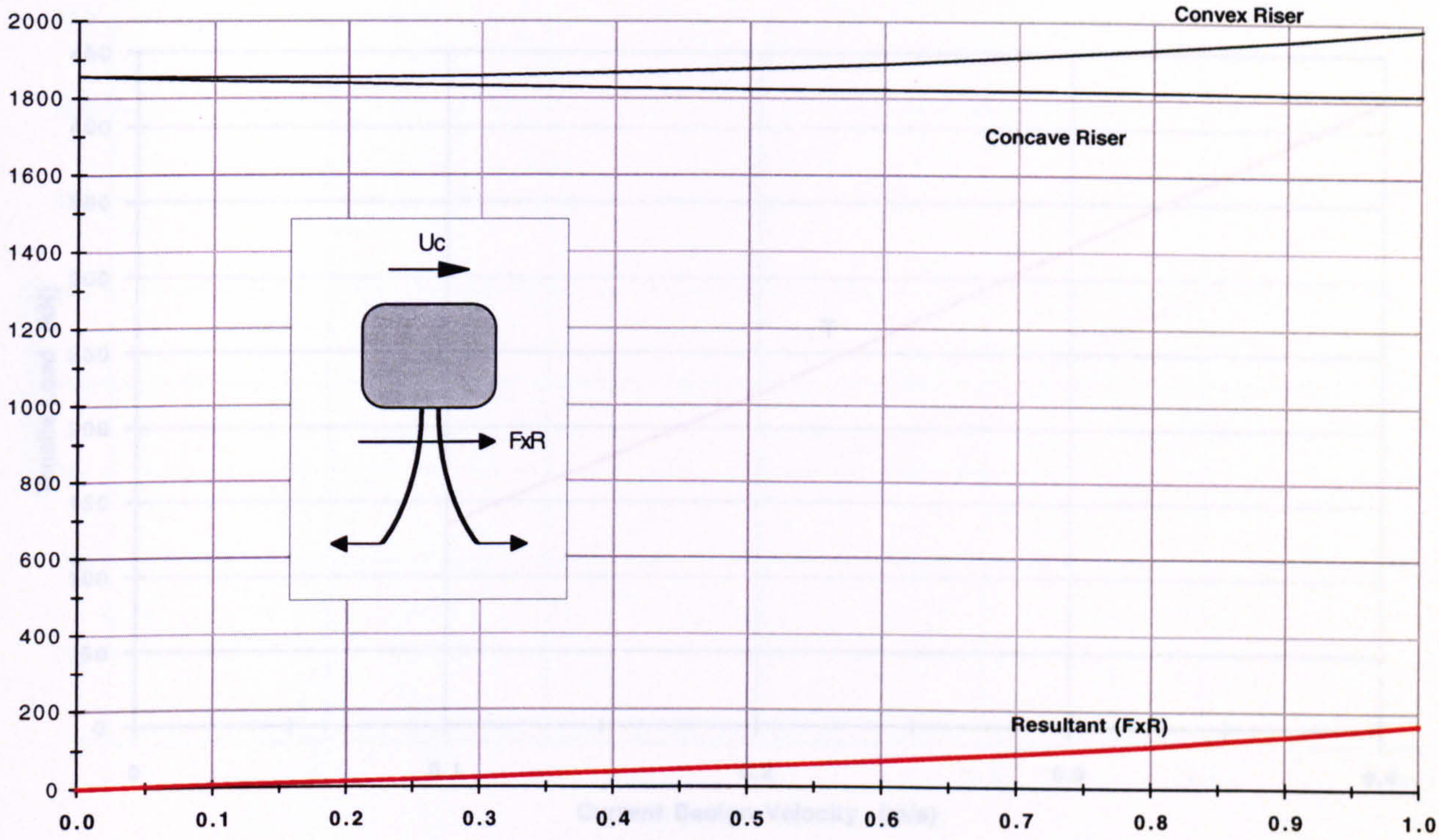

Riser Submerged Unit Weight = 2000 N/m

Vertical Riser Loads Exerted Upon the Sub-Surface Buoy (b)

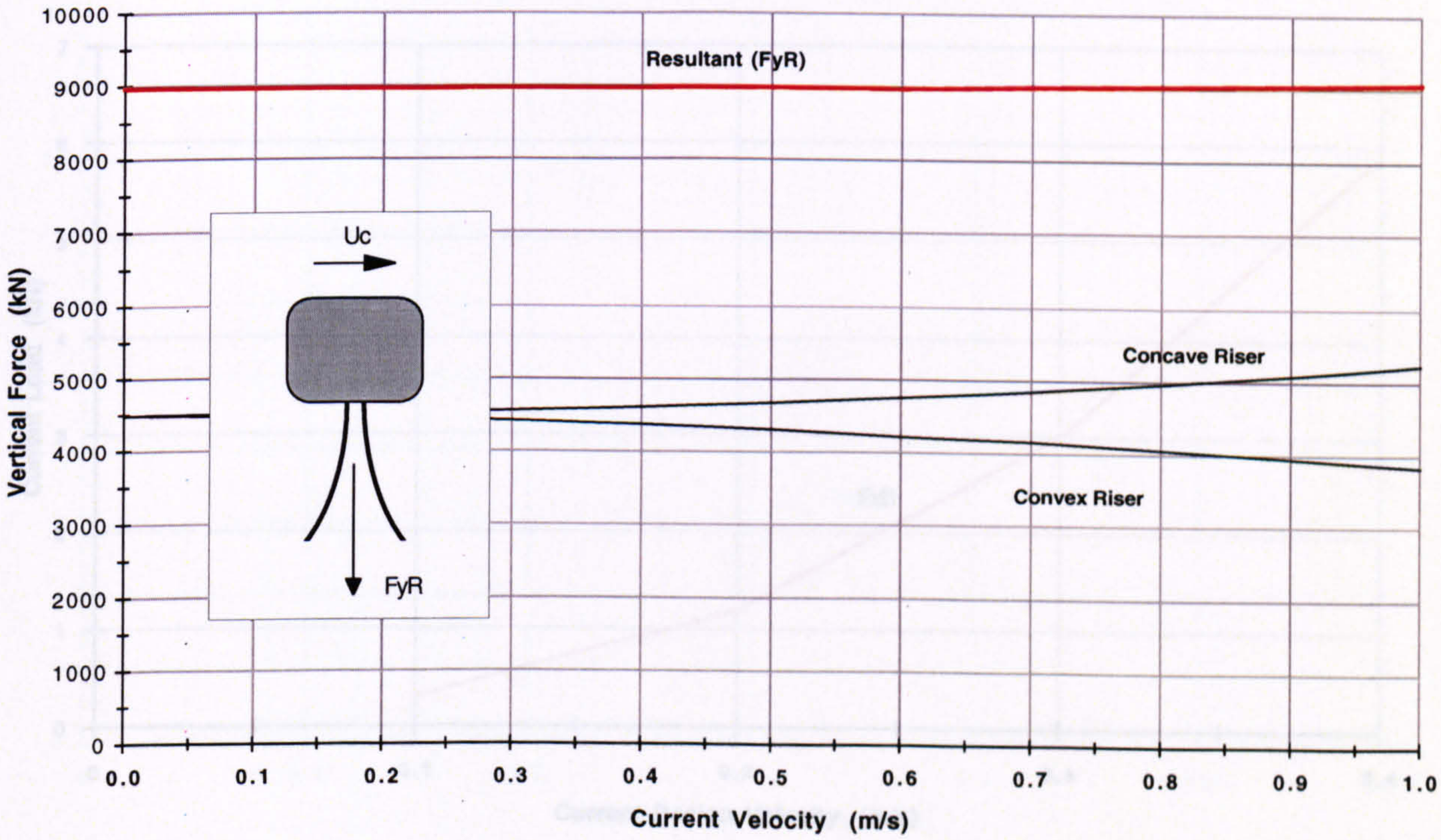

Horizontal Surface Offset = 1500 m

Vertical Offset = 1400 m

Submerged Unit Weight = 2000 N/m

Sea Depth = 1500 m

Figure 7.15

Maximum Load Exerted Upon Each Mooring Tether

(a)

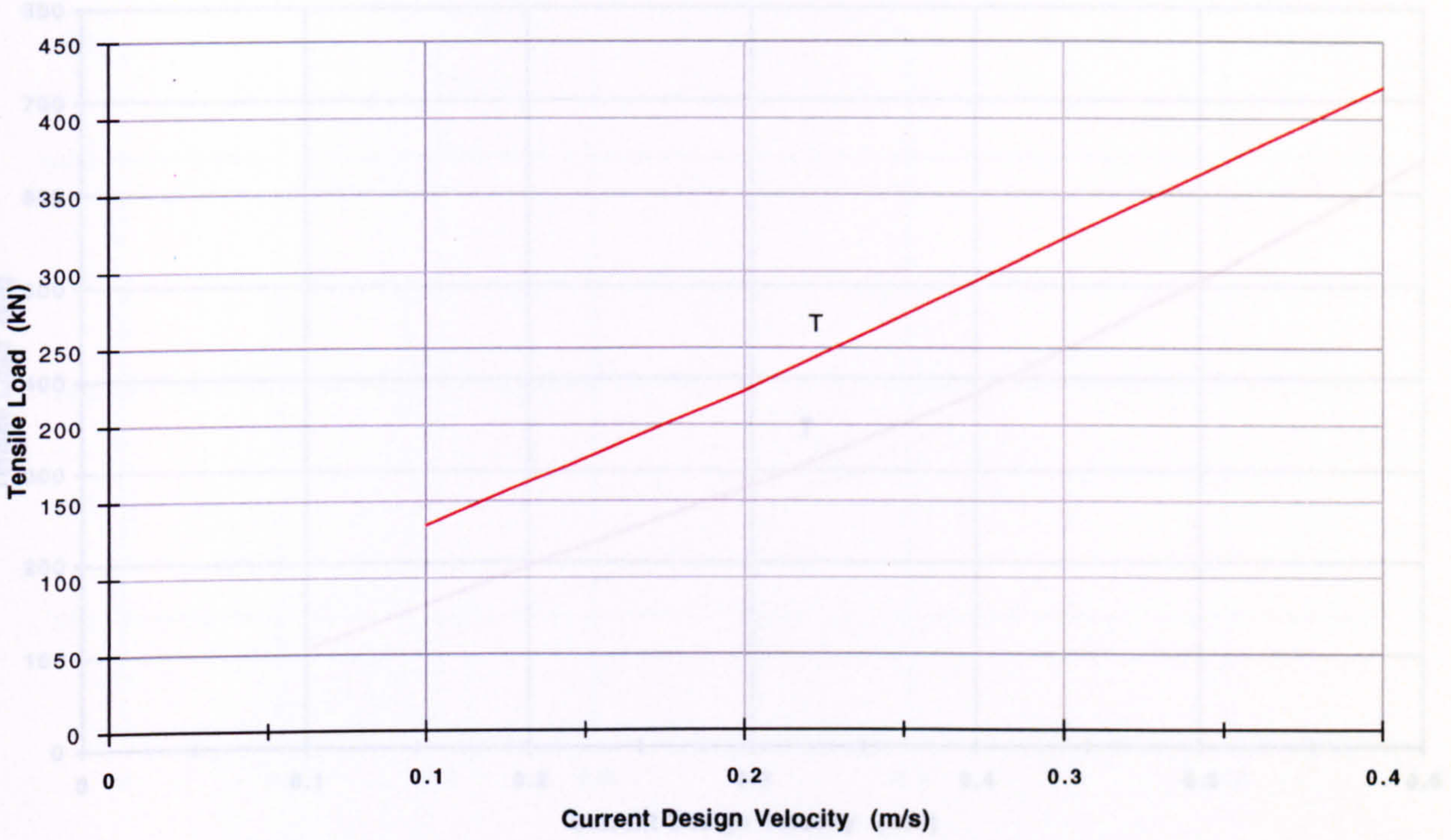

Riser Submerged Unit Weight = 100 N/m

Maximum Current Load Exerted Upon the Sub-Surface Buoy

(b)

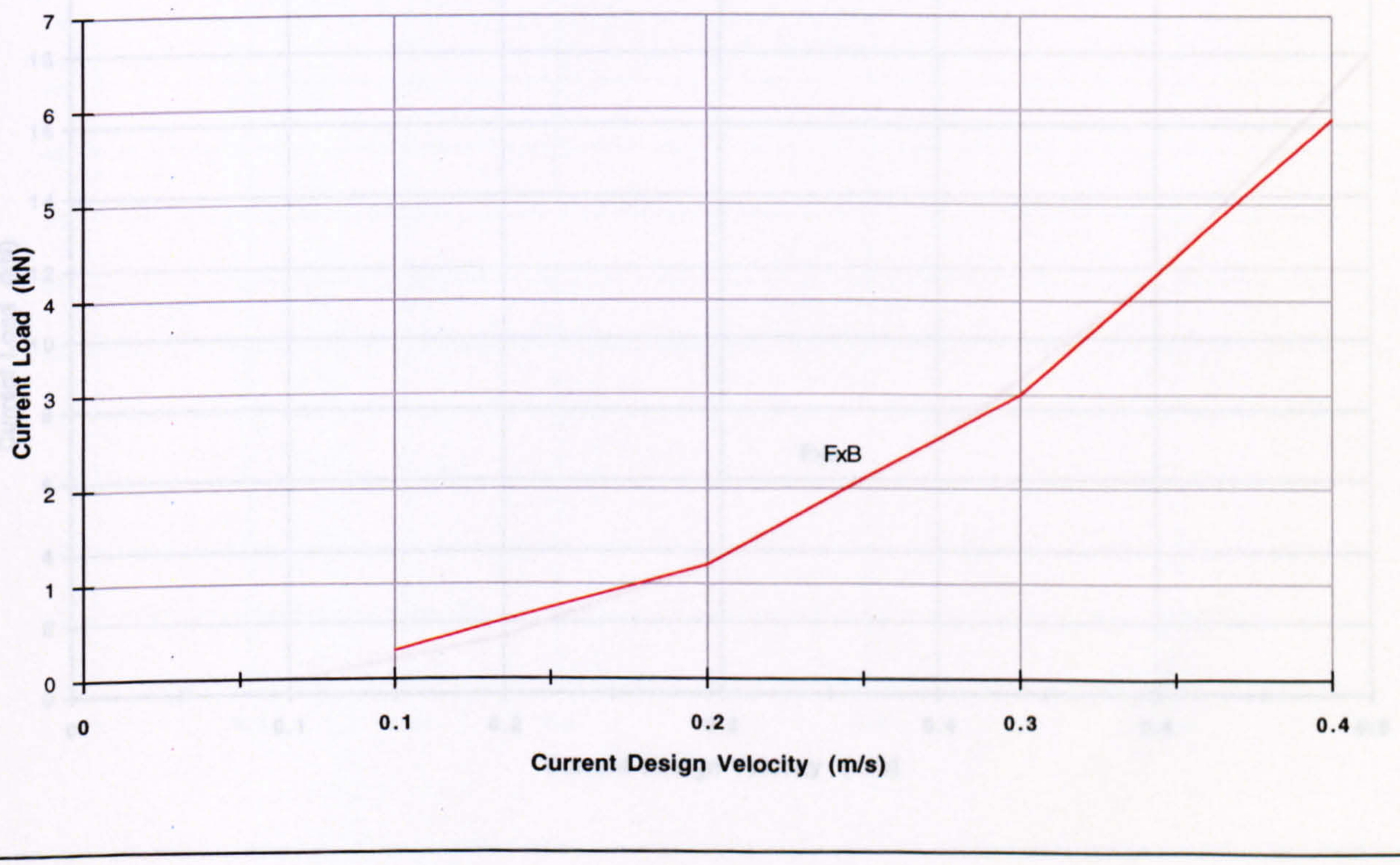

Riser

Horizontal Surface Offset = 1500 m

Vertical Offset = 1400 m

Sub-Surface Buoy

Depth Below Surface = 100 m

Diameter = 8.0 m

Figure 7.16

Maximum Load Exerted Upon Each Mooring Tether

(a)

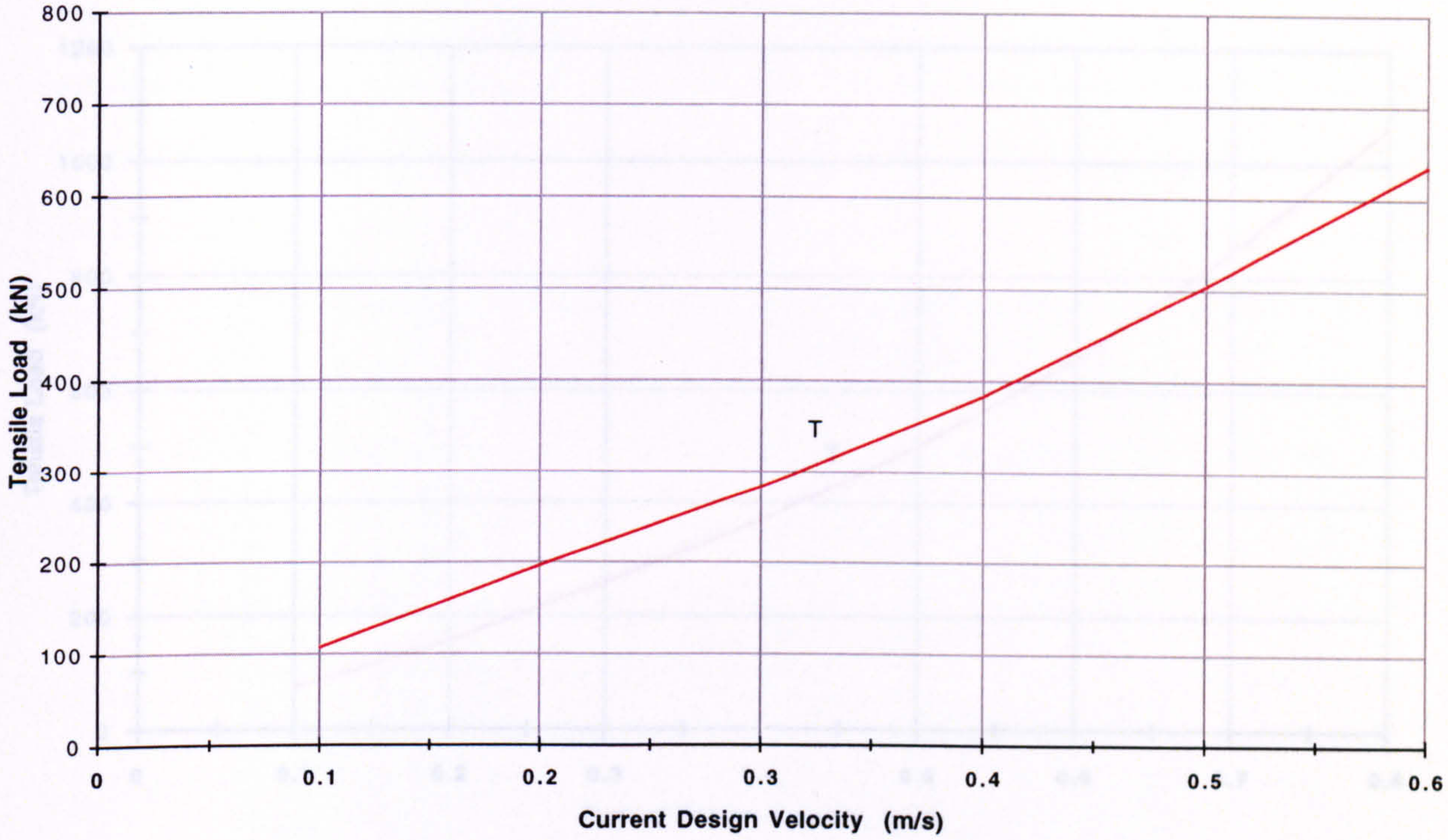

Riser Submerged Unit Weight = 500 N/m

Maximum Current Load Exerted Upon the Sub-Surface Buoy

(b)

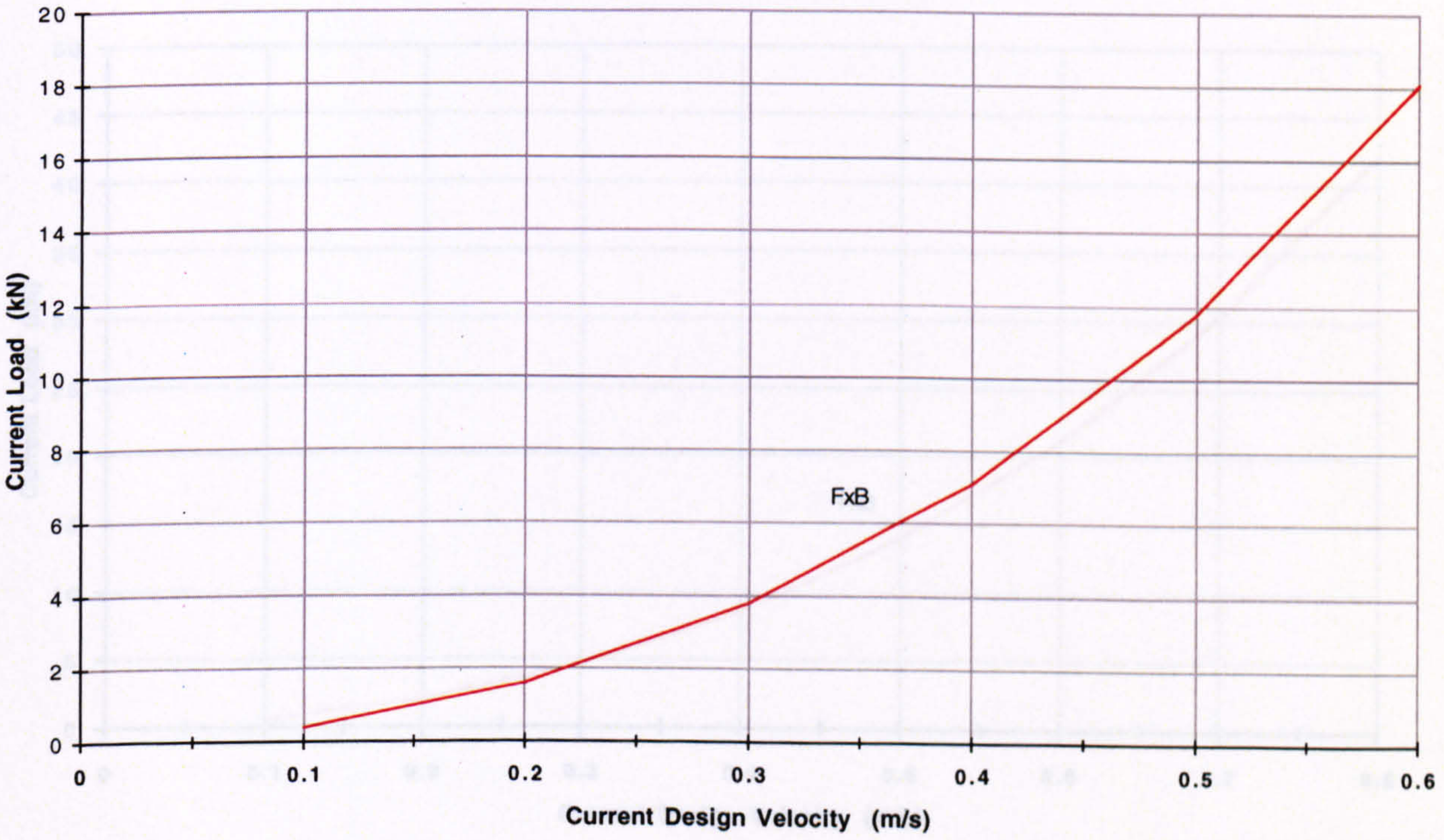

Riser

Horizontal Surface Offset = 1500 m

Vertical Offset = 1400 m

Sub-Surface Buoy

Depth Below Surface = 100 m

Diameter = 10.0 m

Figure 7.17

Maximum Load Exerted Upon Each Mooring Tether

(a)

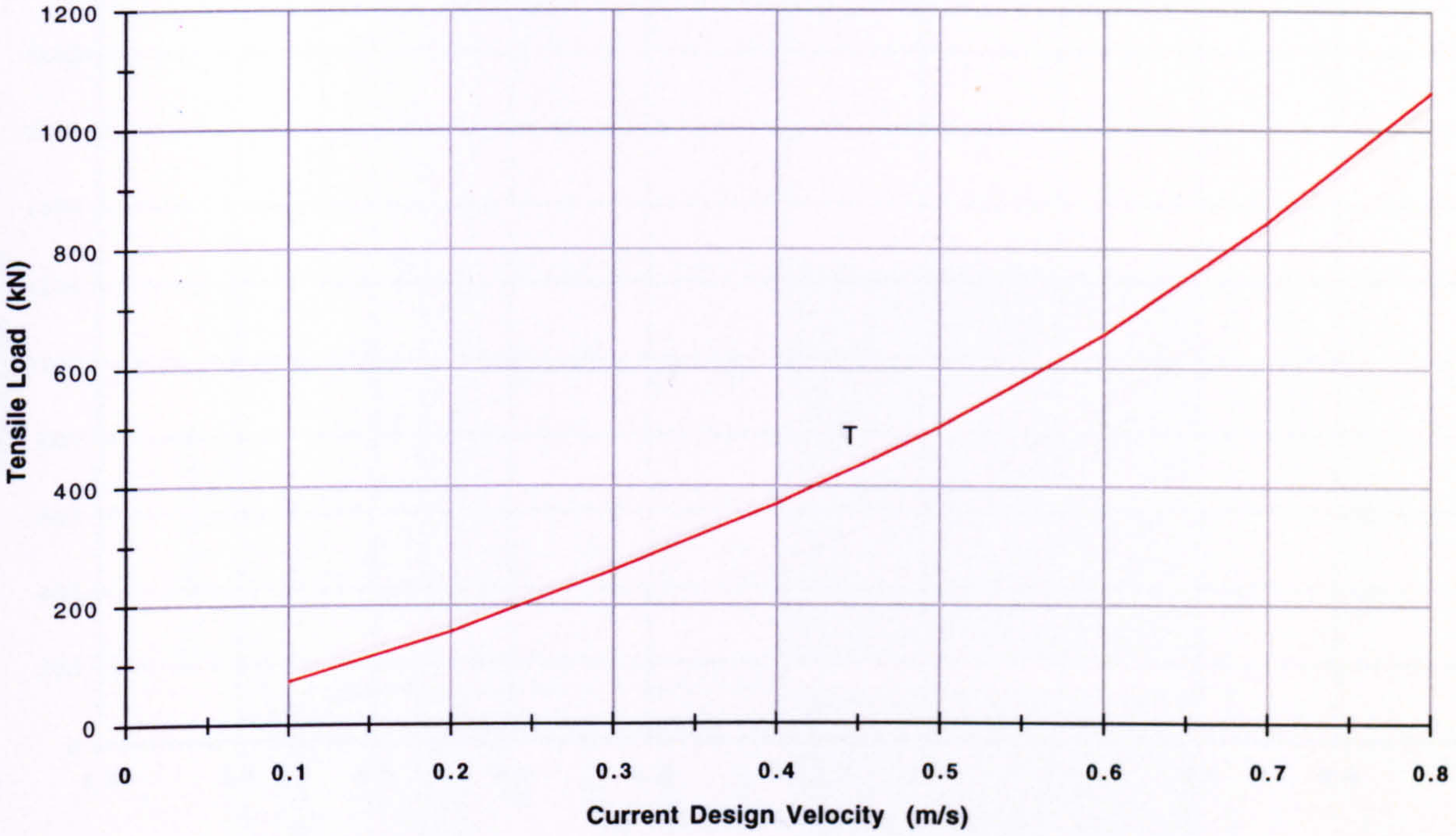

Riser Submerged Unit Weight = 1000 N/m

Maximum Current Load Exerted Upon the Sub-Surface Buoy

(b)

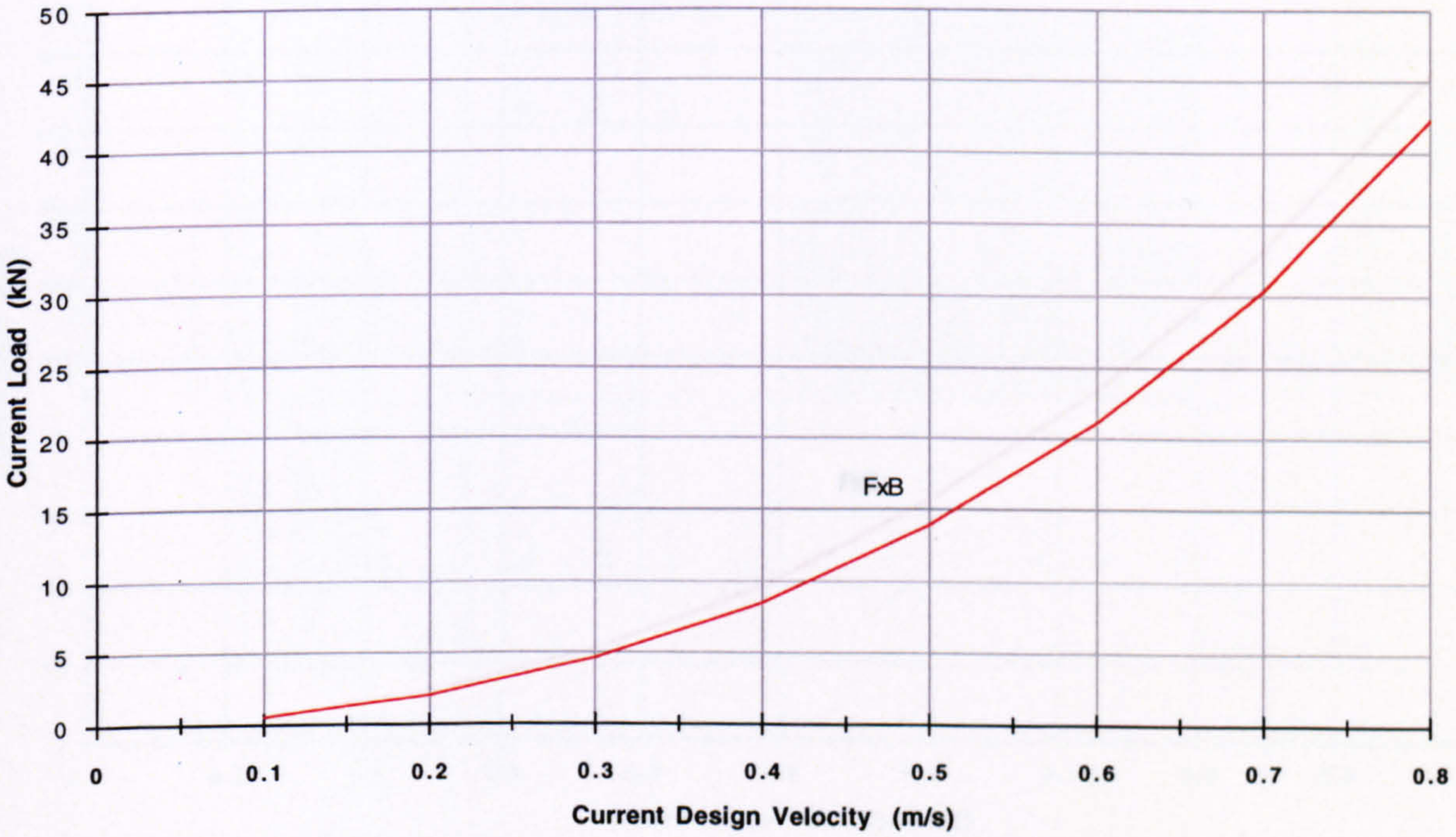

Riser

Horizontal Surface Offset = 1500 m

Vertical Offset = 1400 m

Sub-Surface Buoy

Depth Below Surface = 100 m

Diameter = 12.0 m

Figure 7.18

Maximum Load Exerted Upon Each Mooring Tether

(a)

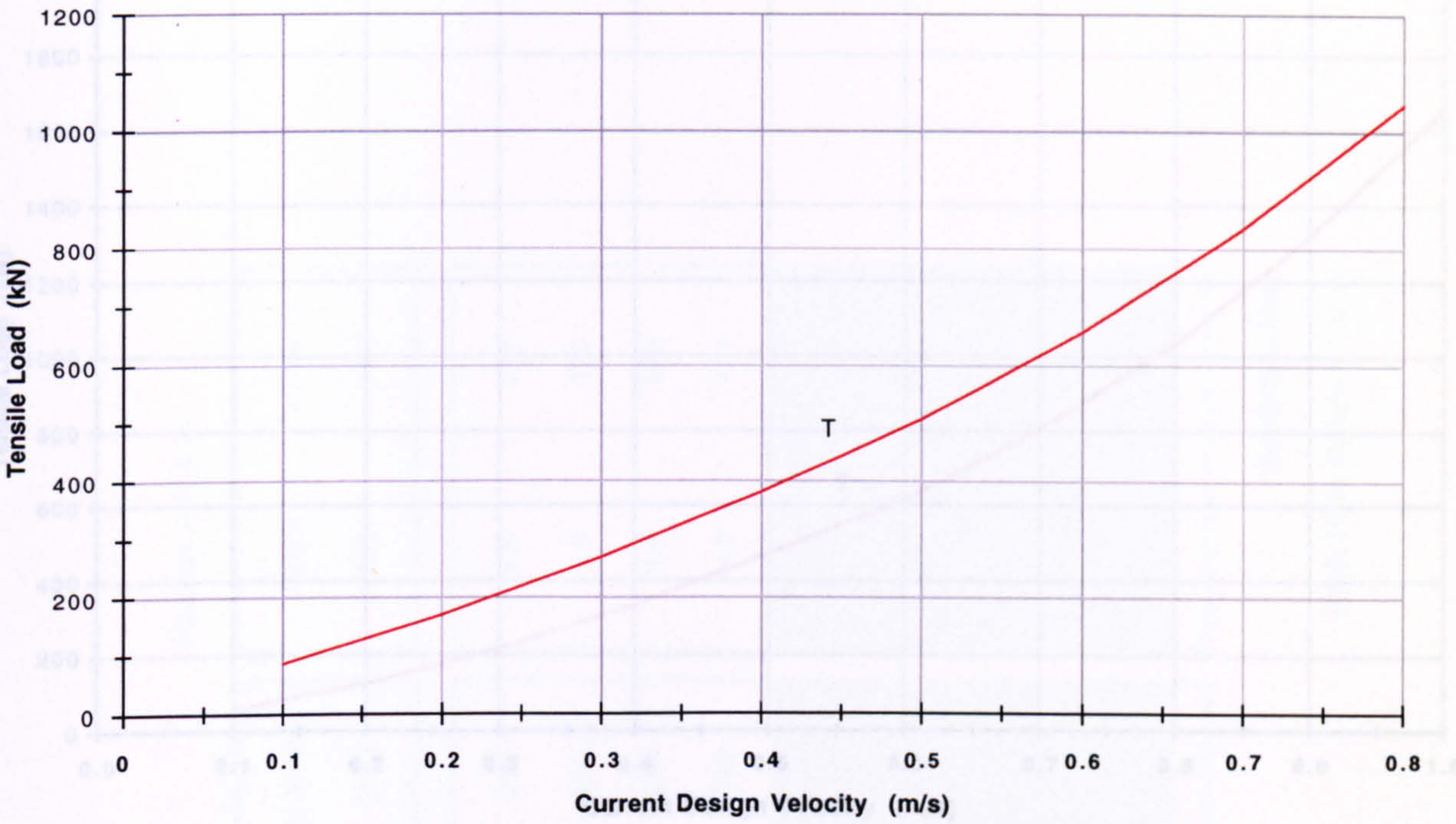

Riser Submerged Unit Weight = 1500 N/m

Maximum Current Load Exerted Upon the Sub-Surface Buoy

(b)

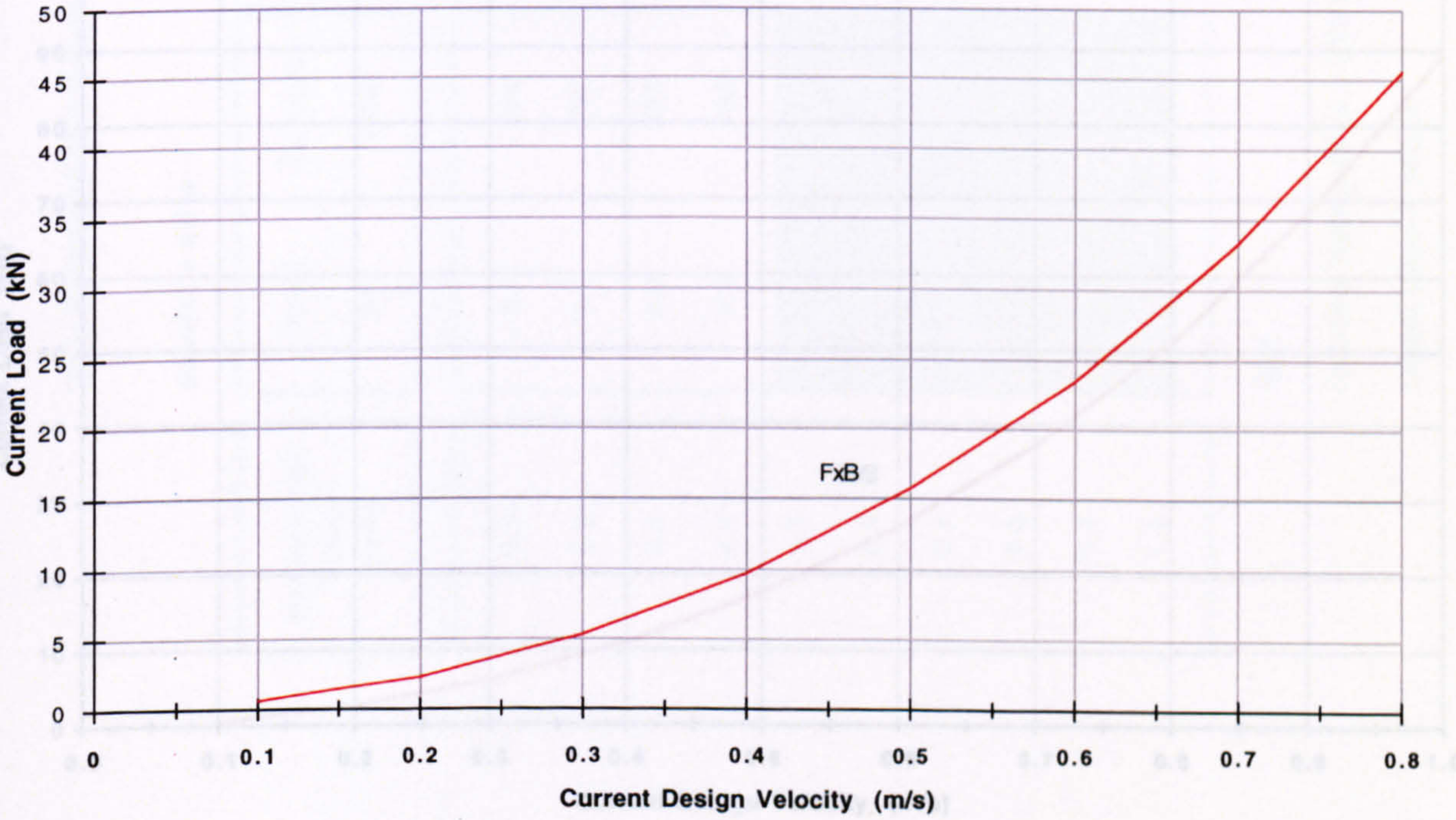

Riser

Horizontal Surface Offset = 1500 m

Vertical Offset = 1400 m

Sub-Surface Buoy

Depth Below Surface = 100 m

Diameter = 14.0 m

Figure 7.19

Maximum Load Exerted Upon Each Mooring Tether

(a)

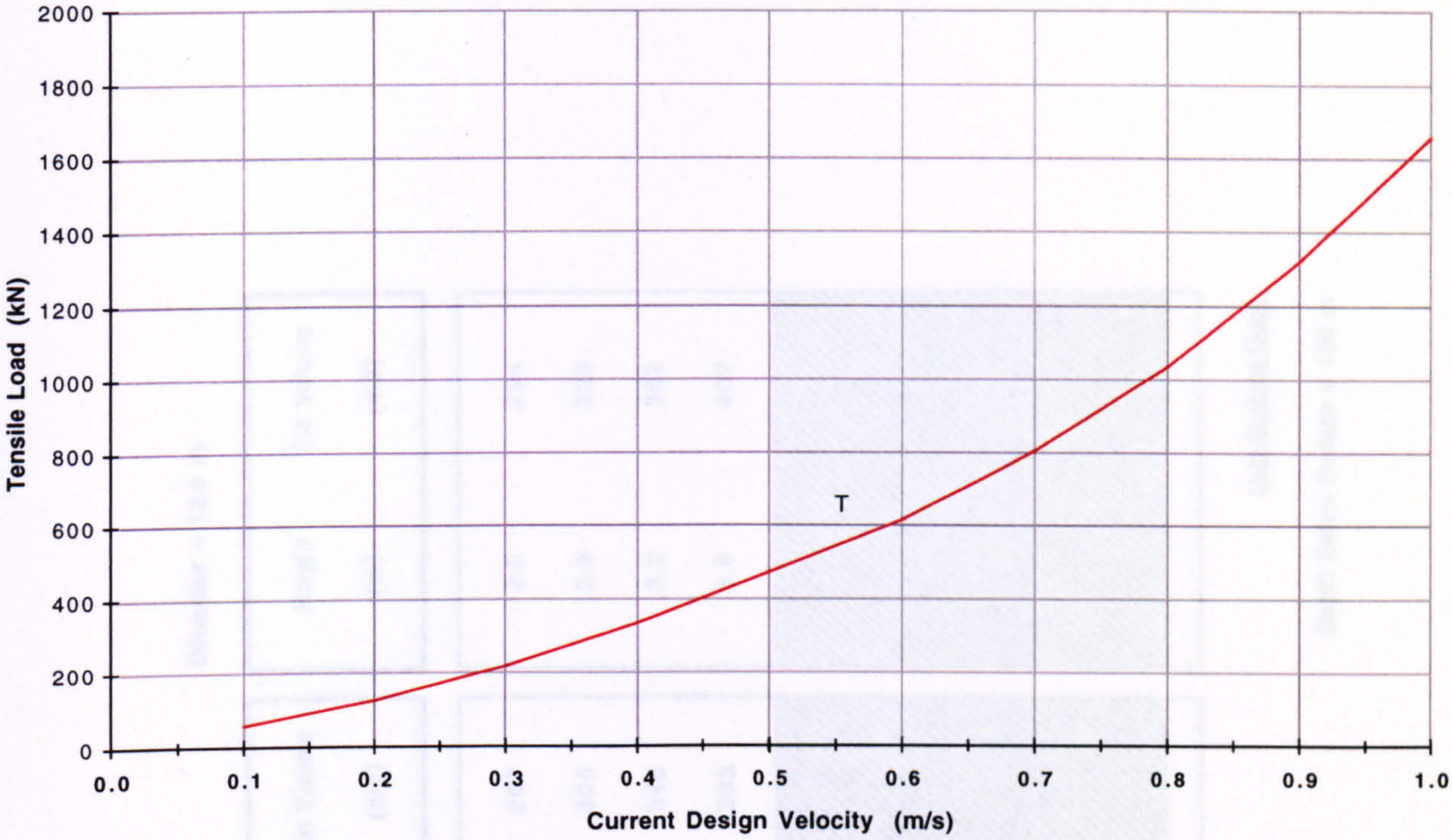

Riser Submerged Unit Weight = 2000 N/m

Maximum Current Load Exerted Upon the Sub-Surface Buoy

(b)

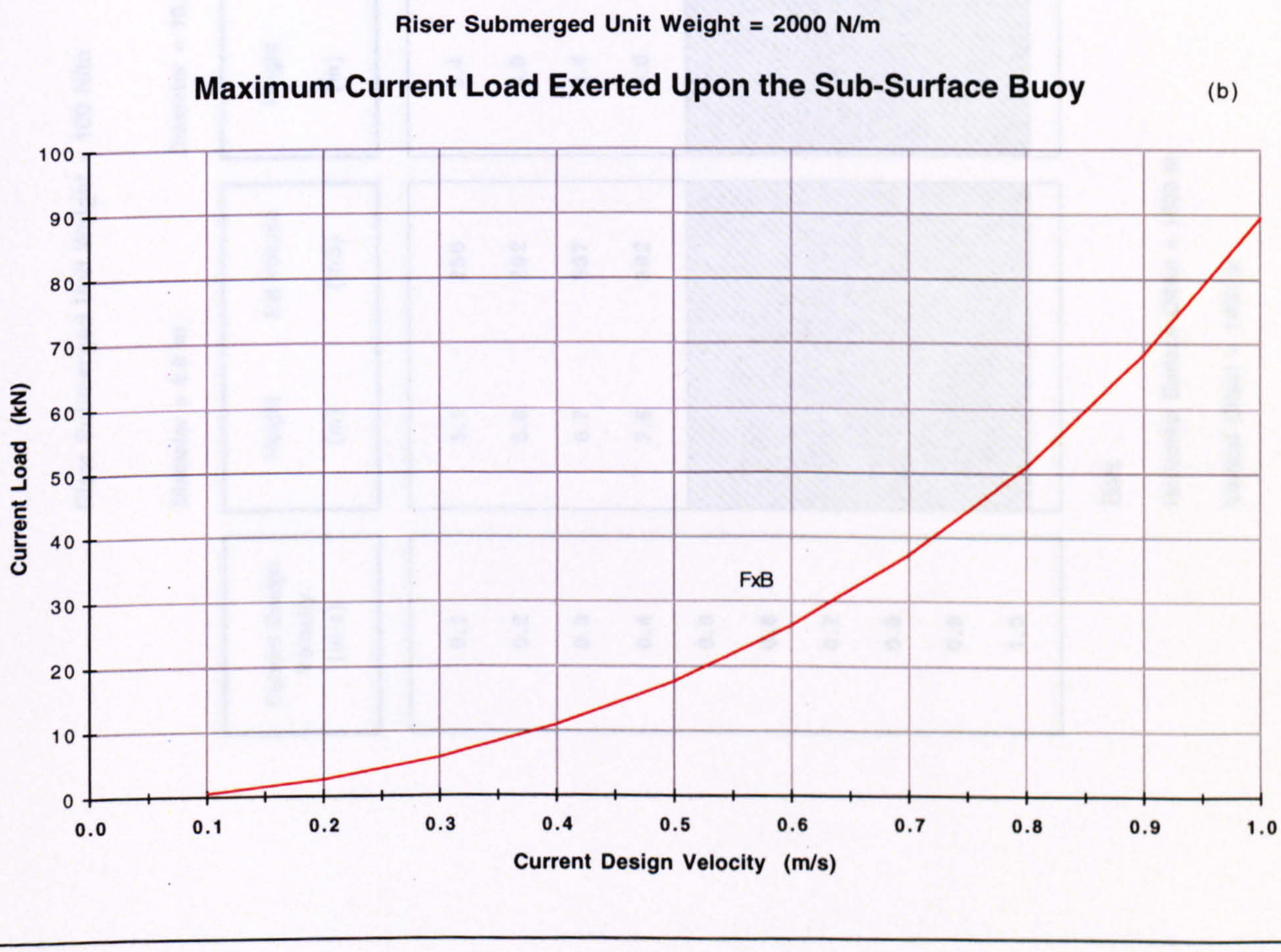

Riser

Horizontal Surface Offset = 1500 m

Vertical Offset = 1400 m

Sub-Surface Buoy

Depth Below Surface = 100 m

Diameter = 14.0 m

Figure 7.20

Sub-Surface Buoy: Height and External Volume

Riser Submerged Unit Weight = 100 N/m

Current Design Velocity (m/s)	Diameter = 8.0 m		Diameter = 10.0 m		Diameter = 12.0 m	
	Height (m)	Ext Volume (m3)	Height (m)	Ext Volume (m3)	Height (m)	Ext Volume (m3)
0.1	5.1	256	3.4	267	2.6	294
0.2	5.8	292	3.9	306	2.9	328
0.3	6.7	337	4.4	346	3.2	362
0.4	7.6	382	5.0	393	3.6	407
0.5						
0.6						
0.7						
0.8						
0.9						
1.0						

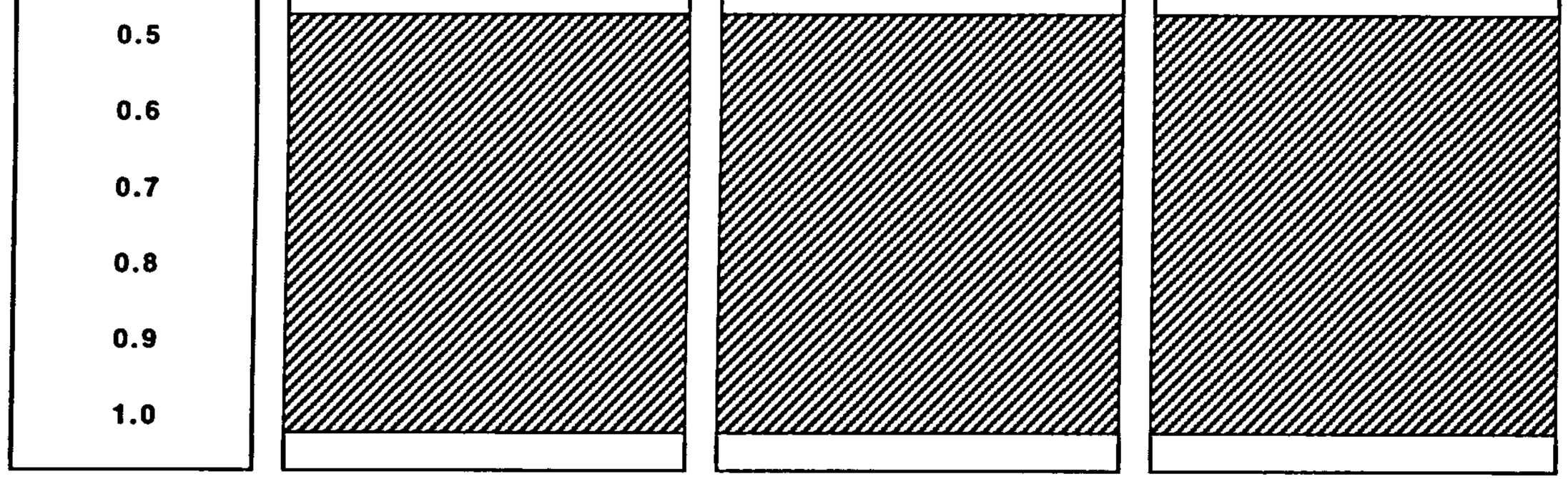

Riser

Horizontal Surface Offset = 1500 m

Vertical Offset = 1400 m

Sub-Surface Buoy

Depth Below Surface = 100 m

Table 7.4

Sub-Surface Buoy: Height and External Volume

Riser Submerged Unit Weight = 500 N/m

Current Design Velocity (m/s)	Diameter = 10.0 m		Diameter = 12.0 m		Diameter = 14.0 m	
	Height (m)	Ext Volume (m3)	Height (m)	Ext Volume (m3)	Height (m)	Ext Volume (m3)
0.1	5.7	448	4.1	464	3.2	493
0.2	6.2	487	4.5	509	3.4	523
0.3	6.7	526	4.8	543	3.7	570
0.4	7.3	573	5.2	588	3.9	600
0.5	7.9	620	5.6	633	4.2	647
0.6	8.7	683	6.1	690	4.6	708
0.7						
0.8						
0.9						
1.0						

Riser

Horizontal Surface Offset = 1500 m

Vertical Offset = 1400 m

Sub-Surface Buoy

Depth Below Surface = 100 m

Table 7.5

Sub-Surface Buoy: Height and External Volume

Riser Submerged Unit Weight = 1000 N/m

	Diameter = 10.0 m		Diameter = 12.0 m		Diameter = 14.0 m	
Current Design Velocity (m/s)	Height (m)	Ext Volume (m3)	Height (m)	Ext Volume (m3)	Height (m)	Ext Volume (m3)
0.1	8.6	675	6.1	690	4.6	708
0.2	9.1	715	6.4	724	4.8	739
0.3	9.7	762	6.8	769	5.1	785
0.4	10.3	809	7.2	814	5.4	831
0.5	11.0	864	7.7	871	5.8	893
0.6	12.0	942	8.3	939	6.2	954
0.7	13.1	1029	9.0	1018	6.7	1031
0.8	14.4	1131	9.8	1108	7.3	1124
0.9						
1.0						

Riser

Horizontal Surface Offset = 1500 m

Vertical Offset = 1400 m

Sub-Surface Buoy

Depth Below Surface = 100 m

Table 7.6

Sub-Surface Buoy: Height and External Volume

Riser Submerged Unit Weight = 1500 N/m

Current Design Velocity (m/s)	Diameter = 12.0 m		Diameter = 14.0 m		Diameter = 16.0 m	
	Height (m)	Ext Volume (m3)	Height (m)	Ext Volume (m3)	Height (m)	Ext Volume (m3)
0.1	8.2	927	6.2	954	4.9	985
0.2	8.6	973	6.4	985	5.0	1005
0.3	8.9	1007	6.7	1031	5.2	1046
0.4	9.4	1063	9.7	1493	5.5	1106
0.5	9.9	1120	7.3	1124	5.7	1146
0.6	10.5	1188	7.7	1185	6.0	1206
0.7	11.2	1267	8.2	1262	6.4	1287
0.8	12.0	1357	8.8	1355	6.8	1367
0.9						
1.0						

Riser

Horizontal Surface Offset = 1500 m

Vertical Offset = 1400 m

Sub-Surface Buoy

Depth Below Surface = 100 m

Table 7.7

Sub-Surface Buoy: Height and External Volume

Riser Submerged Unit Weight = 2000 N/m

	Diameter = 12.0 m		Diameter = 14.0 m		Diameter = 16.0 m	
Current Design Velocity (m/s)	Height (m)	Ext Volume (m3)	Height (m)	Ext Volume (m3)	Height (m)	Ext Volume (m3)
0.1	10.2	1154	7.6	1170	6.0	1206
0.2	10.5	1188	7.8	1201	6.1	1226
0.3	10.8	1221	8.0	1232	6.3	1267
0.4	11.3	1278	8.4	1293	6.5	1307
0.5	11.8	1335	8.7	1339	6.8	1367
0.6	12.4	1402	9.1	1401	7.1	1428
0.7	13.2	1493	9.7	1493	7.5	1508
0.8	14.1	1595	10.3	1586	7.9	1588
0.9	15.2	1719	11.1	1709	8.5	1709
1.0	16.6	1877	12.0	1847	9.2	1850

Riser

Horizontal Surface Offset = 1500 m

Vertical Offset = 1400 m

Sub-Surface Buoy

Depth Below Surface = 100 m

Table 7.8

Sub-Surface Buoy: Weight and Buoyancy

Riser Submerged Unit Weight = 100 N/m

Total Riser System Submerged Weight = 448 kN
45.7 tonnes

Current Design Velocity (m/s)	Sub-Surface Buoy (air) Weight (kN)	Sub-Surface Buoy (air) Mass (tonnes)	Sub-Surface Buoy Buoyancy (kN)	Sub-Surface Buoy Buoyancy (tonnes)
0.1	1571	160.1	2555	260.4
0.2	1609	164.0	2948	300.5
0.3	1658	169.0	3401	346.7
0.4	1707	174.0	3856	393.1
0.5				
0.6				
0.7				
0.8				
0.9				
1.0				

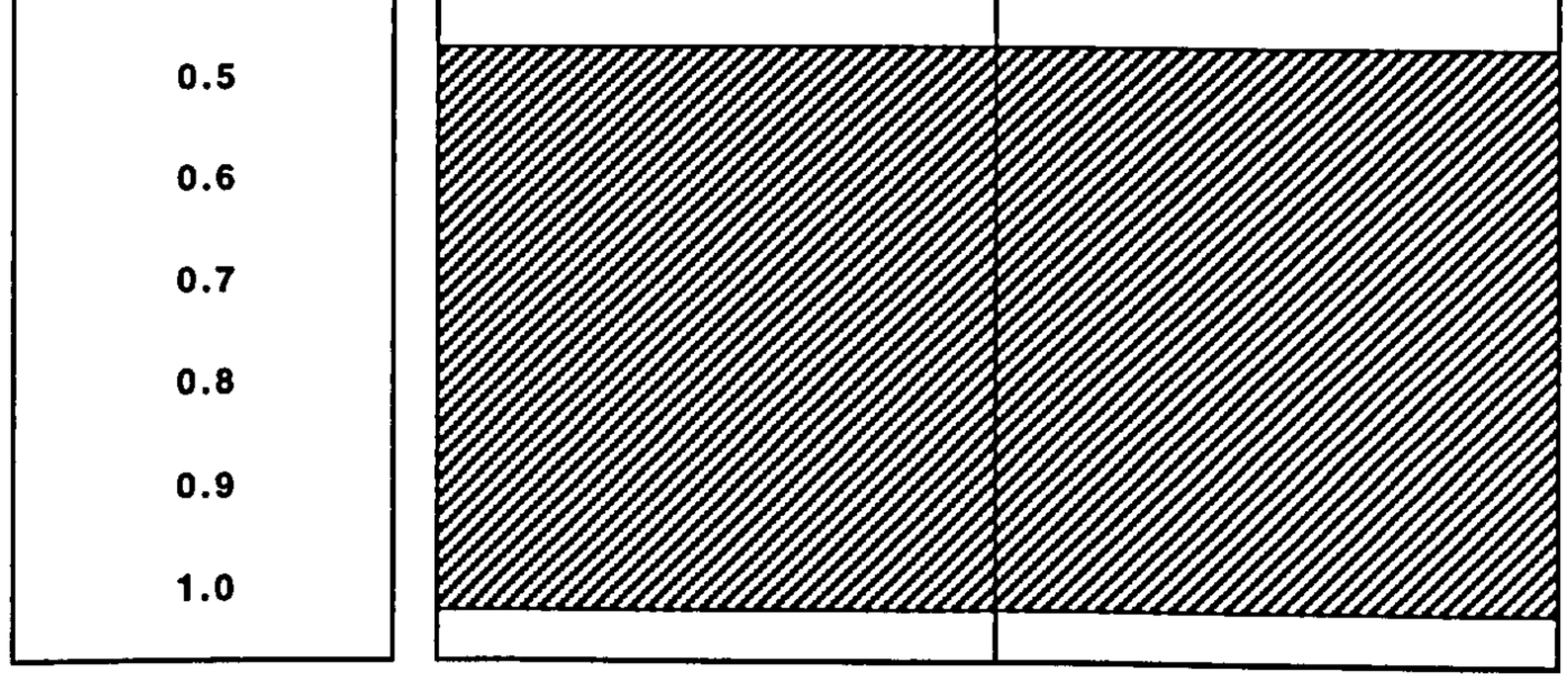

Riser

Horizontal Surface Offset = 1500 m

Vertical Offset = 1400 m

Sub-Surface Buoy

Depth Below Surface = 100 m

Diameter = 8.0 m

Table 7.9

Sub-Surface Buoy: Weight and Buoyancy

Riser Submerged Unit Weight = 500 N/m

Total Riser System Submerged Weight = 2244 kN
228.7 tonnes

Current Design Velocity (m/s)	Sub-Surface Buoy (air) Weight (kN)	Sub-Surface Buoy (air) Mass (tonnes)	Sub-Surface Buoy Buoyancy (kN)	Sub-Surface Buoy Buoyancy (tonnes)
0.1	1844	188.0	4517	460.4
0.2	1874	191.0	4909	500.4
0.3	1904	194.1	5294	539.7
0.4	1940	197.8	5737	584.8
0.5	1976	201.4	6261	638.2
0.6	2024	206.3	6838	697.0
0.7				
0.8				
0.9				
1.0				

Riser

Horizontal Surface Offset = 1500 m

Vertical Offset = 1400 m

Sub-Surface Buoy

Depth Below Surface = 100 m

Diameter = 10.0 m

Table 7.10

Sub-Surface Buoy: Weight and Buoyancy

Riser Submerged Unit Weight = 1000 N/m

Total Riser System Submerged Weight = 4488 kN
457.4 tonnes

Current Design Velocity (m/s)	Sub-Surface Buoy (air) Weight (kN)	Sub-Surface Buoy (air) Mass (tonnes)	Sub-Surface Buoy Buoyancy (kN)	Sub-Surface Buoy Buoyancy (tonnes)
0.1	2152	219.4	6920	705.4
0.2	2172	221.4	7282	742.3
0.3	2198	224.1	7730	788.0
0.4	2224	226.7	8202	836.1
0.5	2257	230.1	8766	893.6
0.6	2297	234.1	9439	962.2
0.7	2343	238.8	10253	1045.2
0.8	2396	244.2	11195	1141.2
0.9				
1.0				

Riser

Horizontal Surface Offset = 1500 m

Vertical Offset = 1400 m

Sub-Surface Buoy

Depth Below Surface = 100 m

Diameter = 12.0 m

Table 7.11

Sub-Surface Buoy: Weight and Buoyancy

Riser Submerged Unit Weight = 1500 N/m

Total Riser System Submerged Weight = 6731 kN
686.2 tonnes

Current Design Velocity (m/s)	Sub-Surface Buoy (air) Weight (kN)	Sub-Surface Buoy (air) Mass (tonnes)	Sub-Surface Buoy Buoyancy (kN)	Sub-Surface Buoy Buoyancy (tonnes)
0.1	2485	253.3	9569	975.4
0.2	2499	254.7	9924	1011.6
0.3	2520	256.9	10347	1054.7
0.4	2542	259.1	10824	1103.4
0.5	2563	261.3	11356	1157.6
0.6	2592	264.2	11994	1222.6
0.7	2628	267.9	12734	1298.1
0.8	2671	272.3	13636	1390.0
0.9				
1.0				

Riser

Horizontal Surface Offset = 1500 m

Vertical Offset = 1400 m

Sub-Surface Buoy

Depth Below Surface = 100 m

Diameter = 14.0 m

Table 7.12

Sub-Surface Buoy: Weight and Buoyancy

Riser Submerged Unit Weight = 2000 N/m

Total Riser System Submerged Weight = 8975 kN
914.9 tonnes

Current Design Velocity (m/s)	Sub-Surface Buoy (air) Weight (kN)	Sub-Surface Buoy (air) Mass (tonnes)	Sub-Surface Buoy Buoyancy (kN)	Sub-Surface Buoy Buoyancy (tonnes)
0.1	2585	263.5	11790	1201.8
0.2	2599	264.9	12063	1229.7
0.3	2614	266.5	12459	1270.0
0.4	2642	269.3	12956	1320.7
0.5	2664	271.6	13536	1379.8
0.6	2693	274.5	14131	1440.5
0.7	2736	278.9	14968	1525.8
0.8	2779	283.3	15943	1625.2
0.9	2836	289.1	17153	1748.5
1.0	2900	295.6	18596	1895.6

Riser

Horizontal Surface Offset = 1500 m

Vertical Offset = 1400 m

Sub-Surface Buoy

Depth Below Surface = 100 m

Diameter = 14.0 m

Table 7.13

CHAPTER 8

Cost Evaluation

8.1 General Description

The aim of this of short chapter is to evaluate and present an estimated cost for the catenary riser production system. This analysis will therefore provide an indication as to the economic viability of the system. At this point it is worth reiterating part of the specification set out in the introduction.

"to design a production riser system with the capability to economically exploit deep water oil and gas reserves"

The total cost and component breakdown of the total cost are presented for the sub-surface buoy concept only. Costs are evaluated and shown for both syntactic foam and nitrogen gas filled riser cases.

8.2 Costs Not Included in the Analysis

Only those costs directly associated with the materials and fabrication of the riser and sub-surface buoy are used. The following costs have not been included in the analysis:

- Offshore installation (i.e. the hire of specialist vessels ranging from tugs to dynamically positioned crane barges.
- Onshore testing.
- FPSO (could be either a new vessel or a conversion)
- FPSO moorings.
- Manifolding.
- Riser seabed connection assembly.
- Pigging system.
- Field templates, wellheads and associated seabed piping.

8.3 Cost Data

8.3.1 Syntactic Foam

A number of manufacturers, Balmoral *(UK)*, CRP *(UK)* and Emerson Cuming *(USA)*, provided quotations for the syntactic foam used in the riser. The prices varied

considerably (approximately £4000/tonne to £8000/tonne), most probably explained by the preliminary nature of the enquiries, the development status of the foams themselves and the lack of actual manufacturing experience with this quantity and type of foam. The quotation of £5,500/tonne provided by Emerson and Cuming for their Ecofloat® buoyancy module series has been used in the analysis, the reasons for this are twofold:

- Their product was used in Section 3.2 in a riser buoyancy analysis; it had the best strength to weight performance.
- The technical information they supplied was the more comprehensive.

This price includes both the cost of material and fabrication, however because this company do not have experience in producing the type (i.e. shape and size) of foam units required there is a degree of uncertainty in this quoted price.

8.3.2 Steel - Material

Steel costs are predominantly dependent upon the grade of steel used as measured by the yield strength. Catenary riser and sub-surface buoy designs are based upon a steel with a yield stress of 450 N/mm^2. This generates a unit material cost of £500/tonne as provided by British Steel. It should be noted that the same grade of steel has been used for both the carrier pipe and flowlines.

8.3.3 Steel - Fabrication

The construction of the carrier pipe would best be carried out by one of the contractors who specialise in this type of work since they will have already developed the necessary site and equipment apart from acquiring a large amount of knowledge on the critical weight/buoyancy balance and the problems associated with tow out. In the UK two such contractors are available, both on the extreme North East Coast of Scotland. A general figure of £2,500 /tonne is used in this analysis. This was an estimate also supplied by British Steel and is based upon current fabrication practices, facilities and expertise used in the manufacture of seabed pipelines.

8.3.4 Nitrogen Gas

Two companies, British Oxygen Company (BOC) and Air Products both supplied prices for Nitrogen gas for use in both the risers and sub-surface buoy. The quote from BOC was based upon a complex set of parameters, however Air products gave a price based upon unit mass of £67/tonne. This is the unit price used in the cost evaluation. Air

products also had the advantage of having Nitrogen gas storage depots at many of the major UK ports including Aberdeen. Pressure tanks situated onboard supply vessels could therefore be filled up whenever it was necessary during the installation program.

8.3.5 Flexible Surface Joints

On the basis of the flex-joints manufactured for both Shell's Auger and Mars TLP's, Oil States Industries (OSI) provided an estimated unit cost of £190,000 for a flex-joint with a capability as stated in Section 5.4. Design, tooling and other non-recurring costs would add a further £60,000.

8.3.6 Vertical Mooring Tethers

From discussions with Bridon at the 1996 OTC a unit price of £120/metre was ascertained. This figure is based upon a 132 mm diameter high performance synthetic rope with a minimum braking load capability of 5000 kN (see Section 7.5) from their *Viking 7 Deep Water Mooring Range*.

8.3.7 Flexible Risers

A unit cost of £16,000/metre is used for a bundled set of composite flexible risers hydraulically linking the sub-surface buoy to the FPSO. This figure was obtained from Coflexip.

8.3.8 A Summary of Cost Data Sources

Component	Data Source
Syntactic Foam	Emerson & Cuming
Steel (Material and Fabrication)	British Steel
Nitrogen Gas	Air Products
Flex-Joint	Oil States Industries
Vertical Mooring Tether	Bridon
Flexible Risers	Coflexip

Table 8.1

Cost Data Sources

8.4 Analysis Output

The total cost and the corresponding breakdown of this cost are given in Spreadsheet 8.1. These results are alternatively presented using a pie chart format in Figures 8.1 to 8.4. These charts show more clearly the cost influence each constituent component or assembly has on the total production system cost.

CHAPTER 8

Analysis Spreadsheets

Spreadsheet 8.1

Cost Analysis

Input Unit Cost Data

Assembly	Component	Total Cost	Costs per Unit Mass (£/tonne) Material Cost	Fabrication Cost	Total Cost	Costs per Unit Length (£/m) Total Cost
Sub-Surface Buoy	Steel		500	2,500	3,000	
	Mooring Tether					120
	Flex-Joint	250,000				
	Flexible Risers					16,000
Catenary Riser	Steel		500			
	Syntactic Foam				5,000	
	Nitrogen Gas				67	

Syntactic Foam Filled Riser

Component	Length	Mass	Cost (£m)
Steel Carrier Pipe	2166	663	1.989
Steel Flowlines	2166	1207	3.622
Syntactic Foam	2166	783	3.913
		Total:	9.524

Total Cost of Two Risers (£m): 19.049

Total Cost of System (£m): 29.700

Sub-Surface Buoy

Component	Length	Mass	Cost (£m)
Steel Structure		173	0.519
Flex-Joints		40	0.500
Nitrogen Gas		1.4	0.0001
Flexible Risers	560		8.960
Mooring Tethers	1400		0.672

Total Cost of SSB (£m): 10.65

Gas Filled Riser

Component	Length	Mass	Cost (£m)
Steel Carrier Pipe	2166	578	1.734
Steel Flowlines	2166	1207	3.622
Nitrogen Gas	2166	176	0.012
S.F Insulation	2166	36	0.179
		Total:	5.547

Total Cost of System (£m): 21.745

Total Cost Two Risers (£m): 11.094

Spreadsheet 8.1

CHAPTER 8

Results

Figures 8.1 - 8.4

Cost Breakdown of the Sub-Surface Buoy

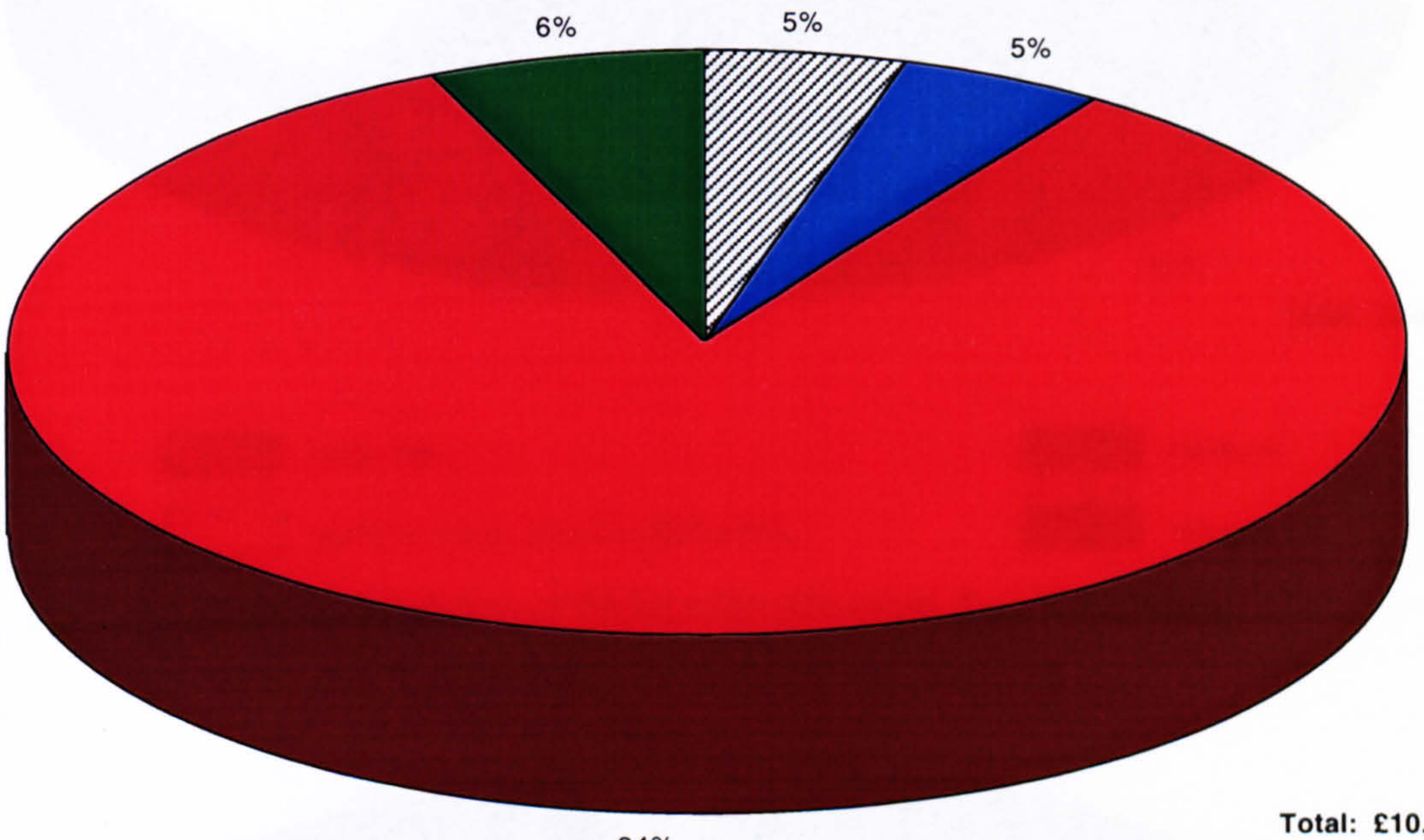

Total: £10.65 m

Diameter = 12 m

Height = 8.3 m

Depth Below Surface = 100 m

Figure 8.1

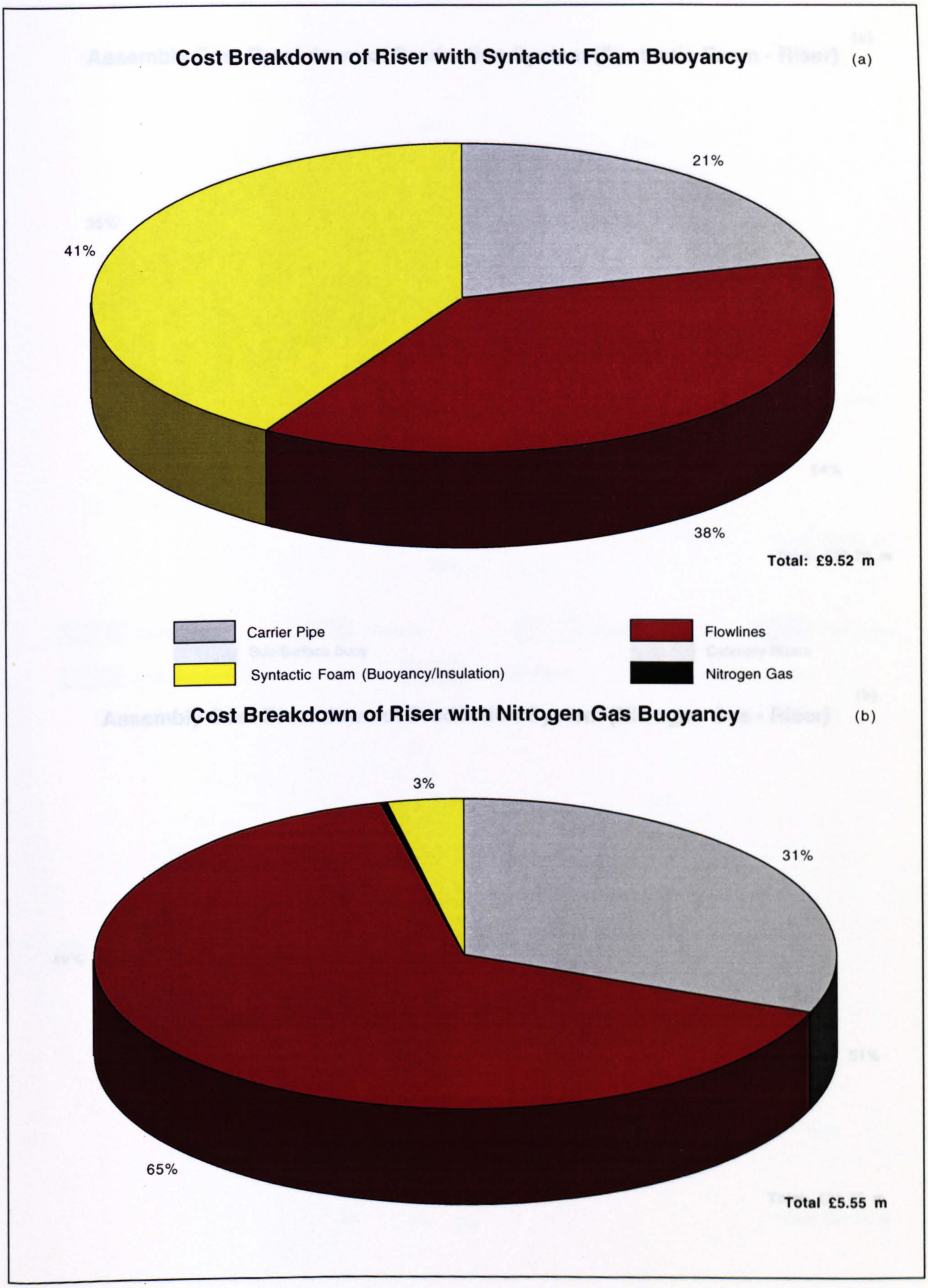

Horizontal Surface Offset = 1500 m

Vertical Offset = 1400 m

Carrier Pipe Outer Diameter = 1.25/1.1 m

Submerged Unit Weight = 733/745 N/m

(Syntactic Foam/Nitrogen Gas)

Figure 8.2

(a)

Assembly Cost Breakdown of Production System (Syntactic Foam - Riser)

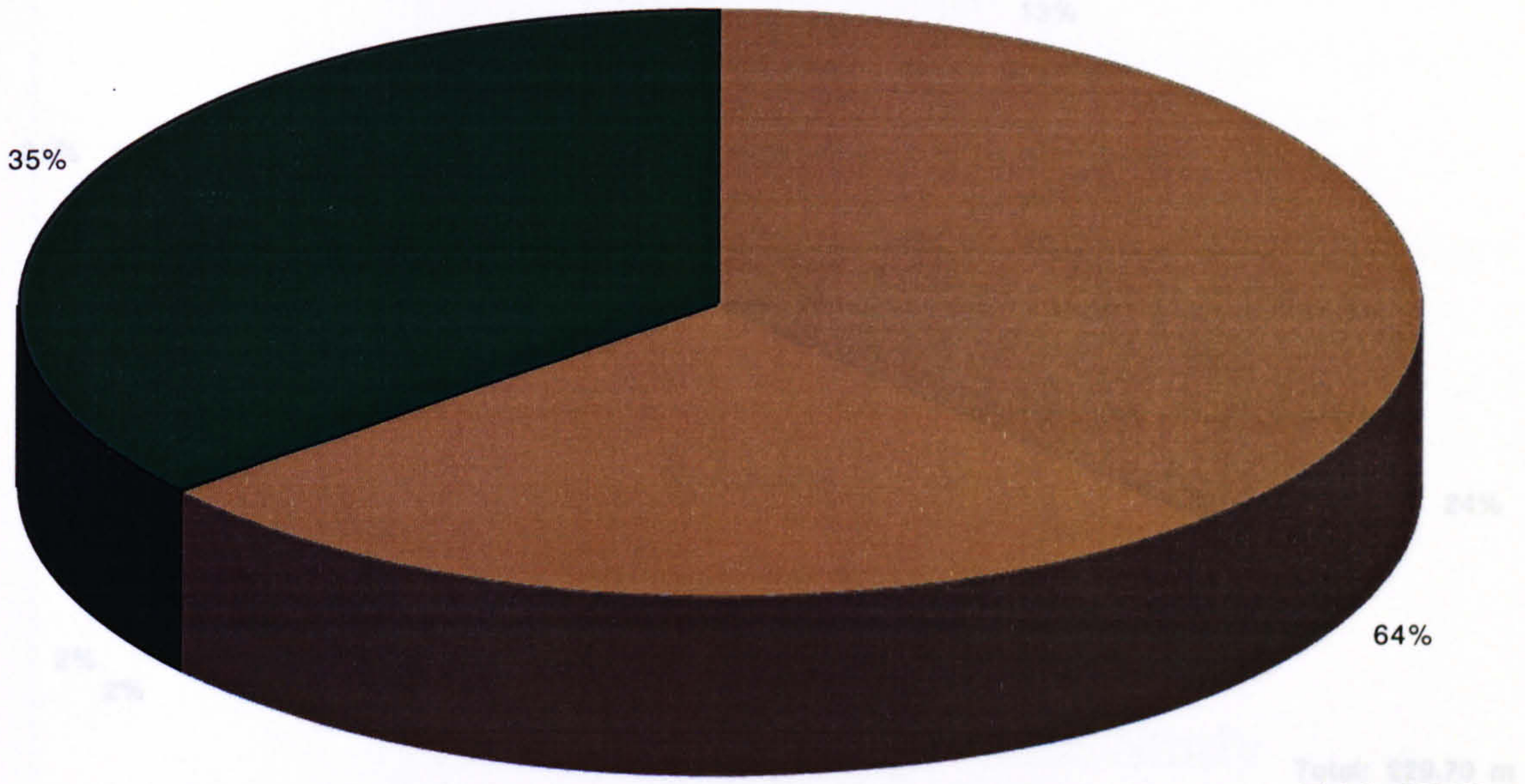

(b)

Assembly Cost Breakdown of Production System (Nitrogen Gas - Riser)

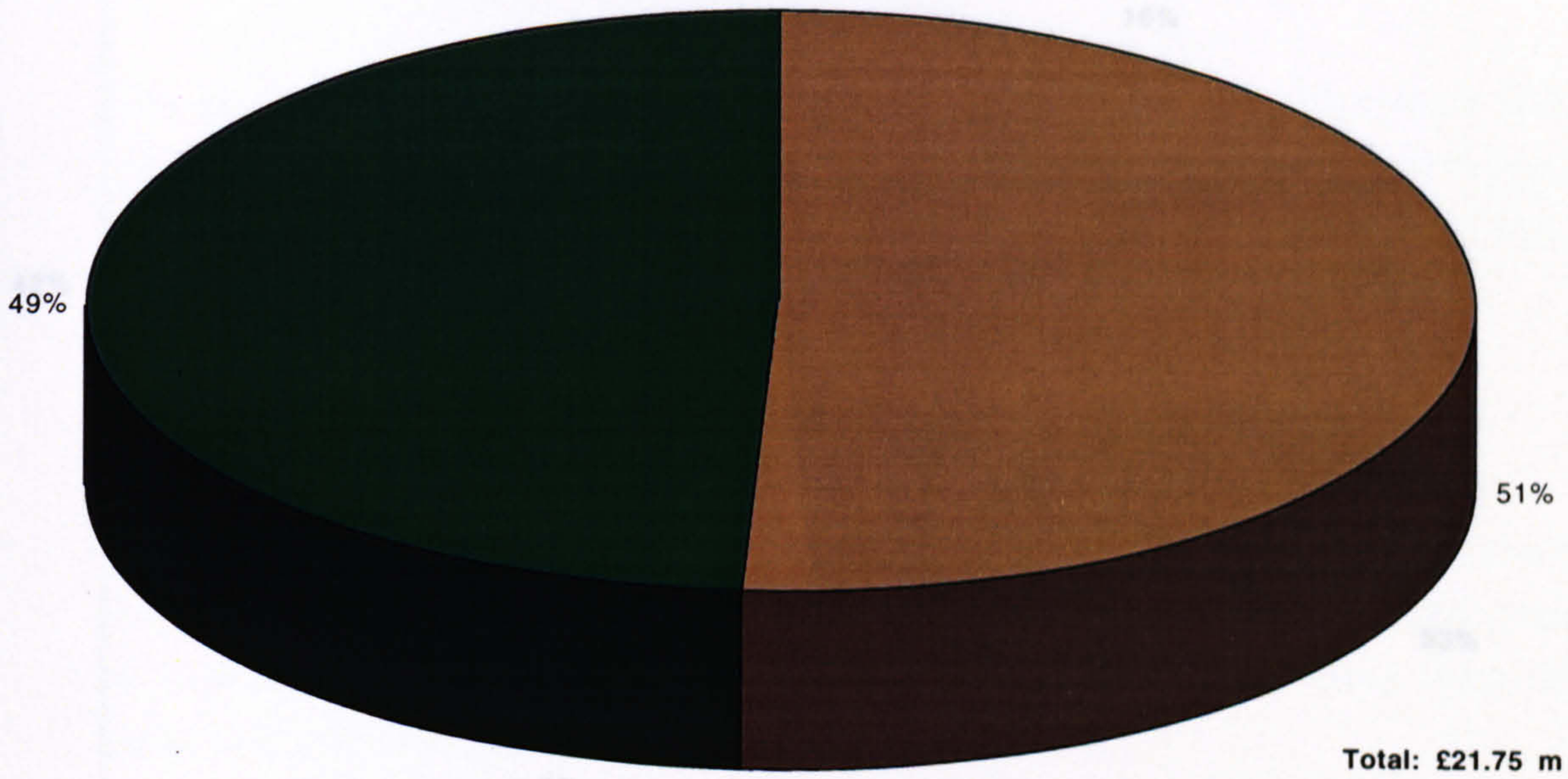

Riser

Horizontal Surface Offset = 1500 m

Carrier Pipe Diameter = 1.25/1.1 m

Sub-Surface Buoy

Diameter = 1.2 m

Height = 8.3 m

Figure 8.3

(a)

Component Cost Breakdown of Production System (Syntactic Foam - Riser)

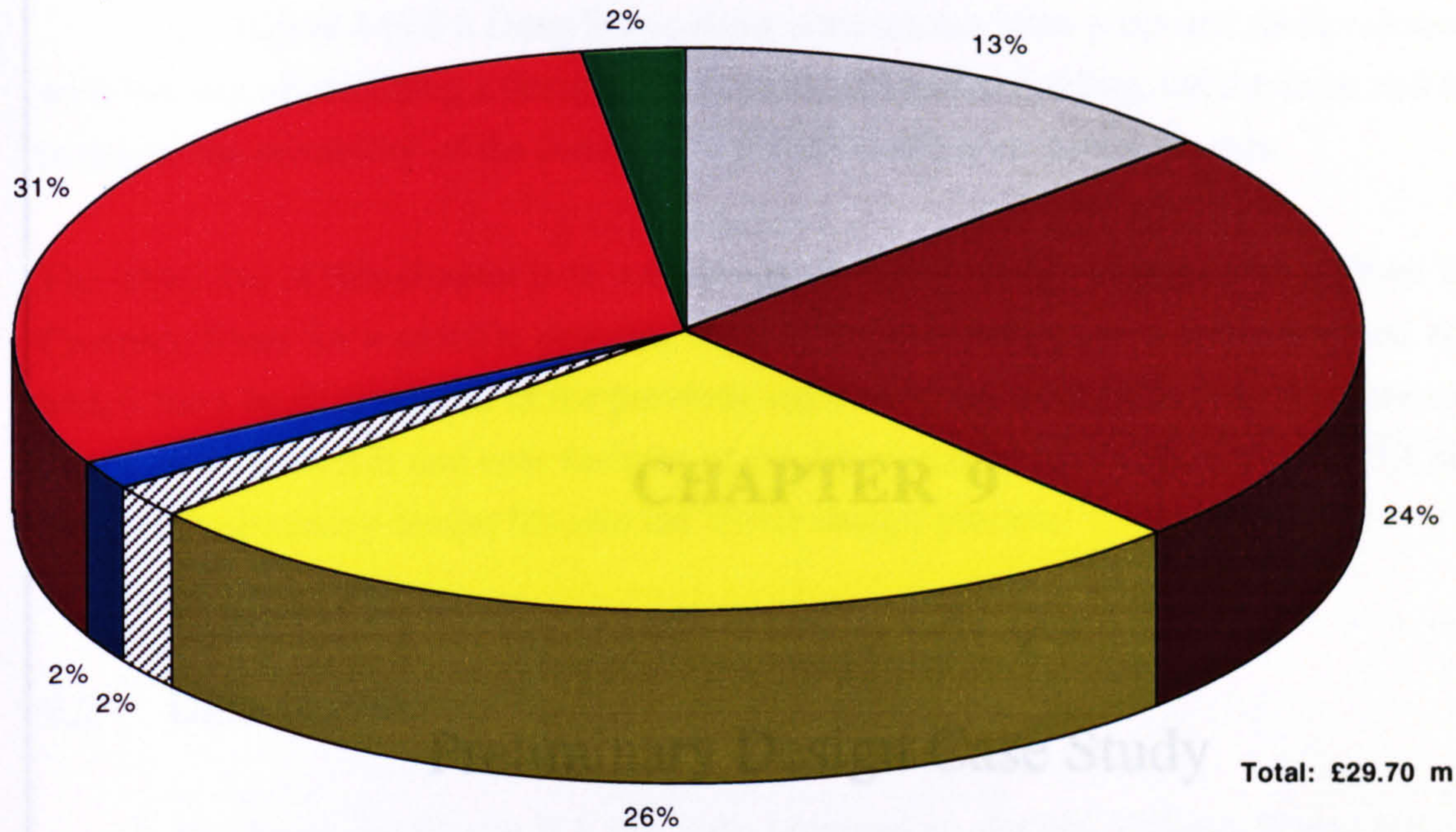

(b)

Component Cost Breakdown of Production System (Nitrogen Gas - Riser)

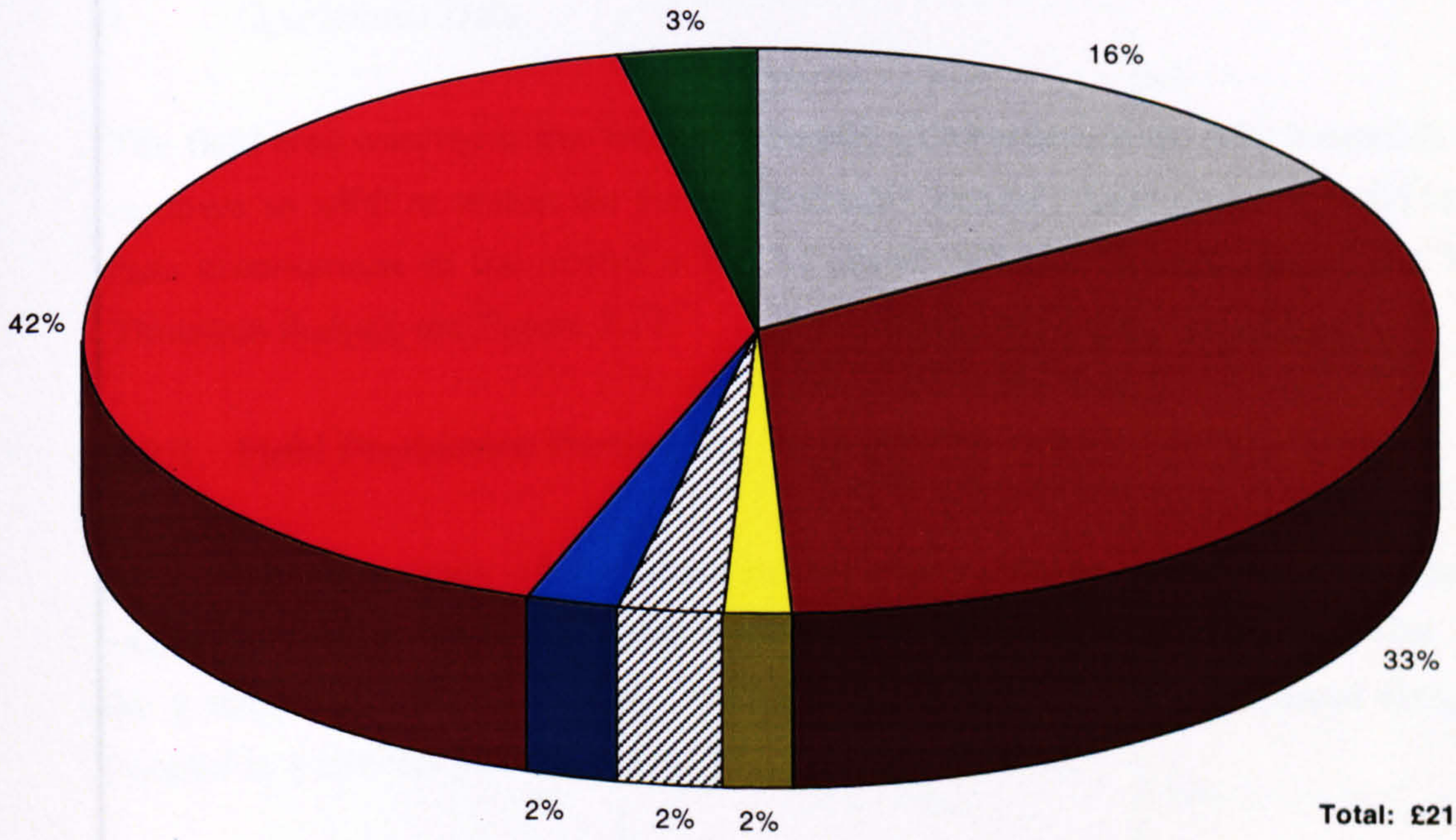

Riser

Horizontal Surface Offset = 1500 m

Carrier Pipe Diameter = 1.25/1.1 m

Sub-Surface Buoy

Diameter = 1.2 m

Height = 8.3 m

Figure 8.4

CHAPTER 9

Preliminary Design Case Study

9.1 General Description

In Chapter 1 to 8 a Deep Water Riser concept has been proposed and evaluated with the aim of providing a designer with sufficient understanding, information and tools to assess the suitability of the concept for potential offshore developments.

The objective of this chapter is to outline a preliminary design example for a Deep Water Catenary Riser for a specific potential oil field by combining the information and results which have been generated in the previous eight chapters with additional site data so that the main geometrical and cost features of the Riser can be established. Figure 9.1 shows how the preliminary design fits into the whole design process.

9.2 Data Gathering

As shown in Figure 9.1 the data required to design a Deep Water Riser are categorised as:

- Field Production Particulars
- Environmental Data
- Engineering Data
- Operational Data

The field area selected is the West of Shetland Continental Slope which extends from 200 m down to 1500 m within the Faroe-Shetland Channel. Hydrographic and Topographic data corresponds to the northern blocks above 204 (northeastwards of the Wyville - Thomson Ridge), see Figure 5.17.

9.2.2 Field Production Particulars

This case study is based upon a deep water (1500 m) wellhead arrangement which was proposed for the Rockall area (just south of Faroe-Shetland Channel) five years ago by a major oil company and is illustrated in Figure 9.2. Four wellhead templates are located in a circular pattern which has a radius of 5000 m.

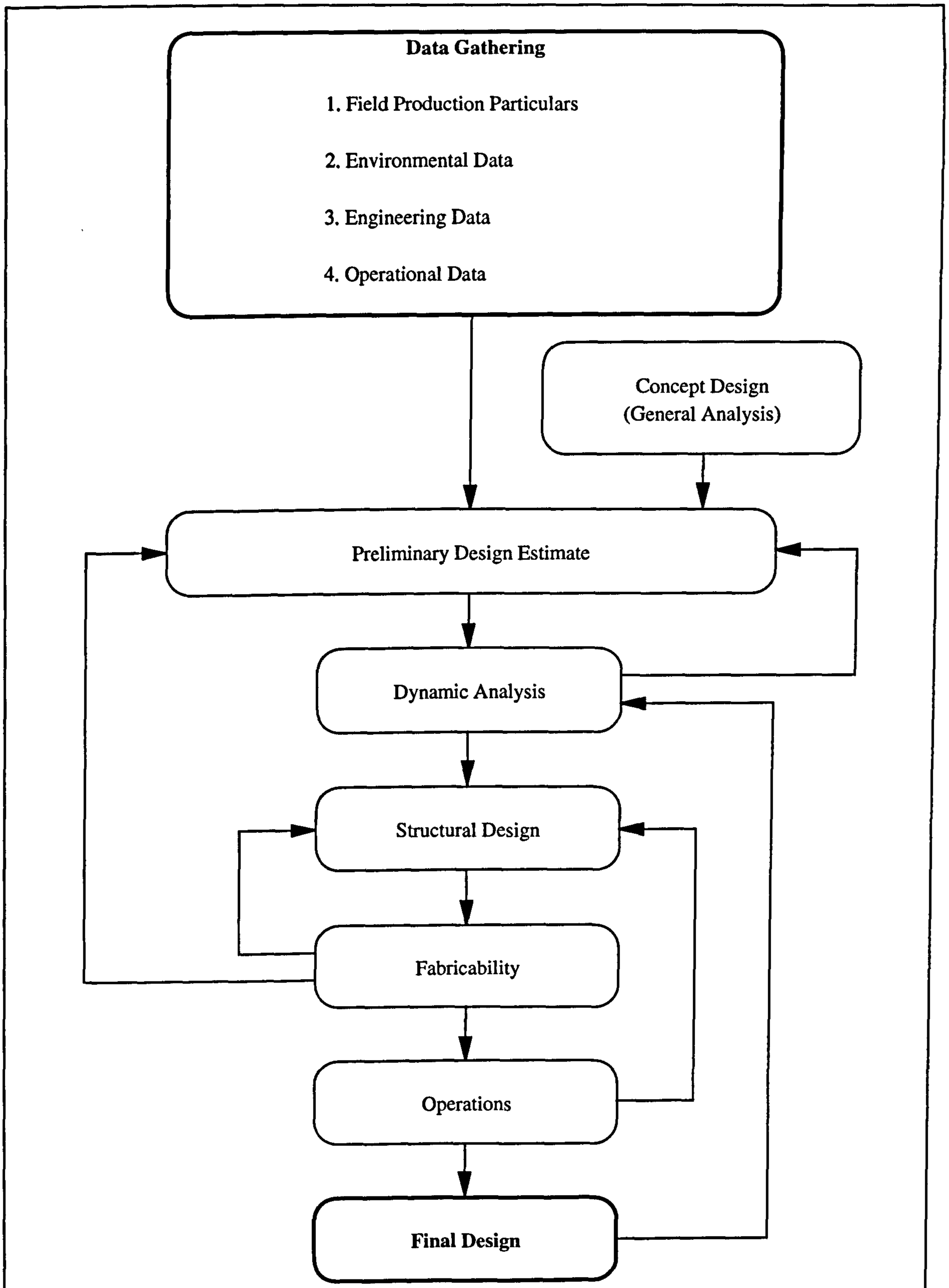

Figure 9.1
Riser Design Process

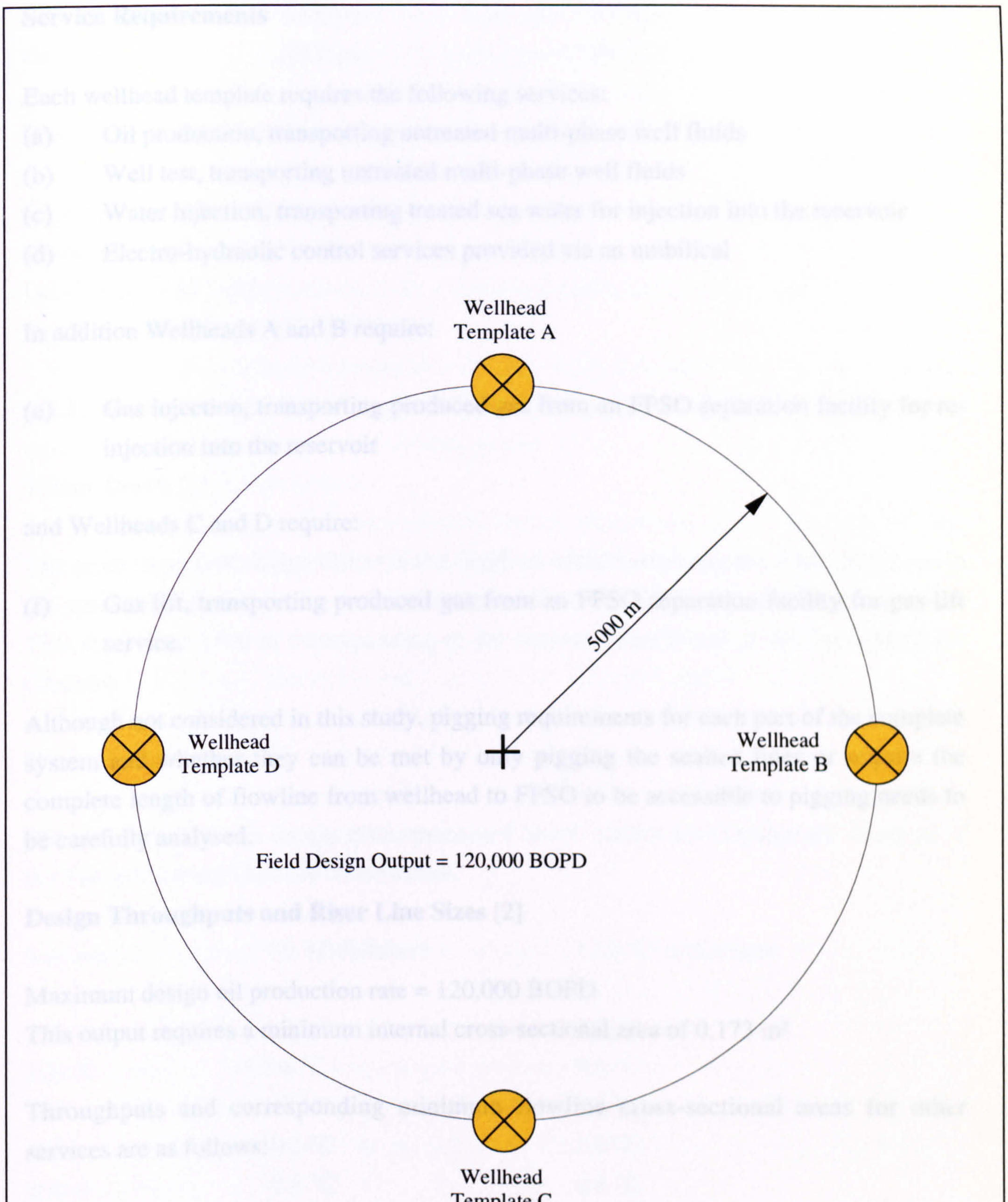

Figure 9.2

Deep Water Wellhead Arrangement

Service Requirements

Each wellhead template requires the following services:

(a) Oil production, transporting untreated multi-phase well fluids

(b) Well test, transporting untreated multi-phase well fluids

(c) Water injection, transporting treated sea water for injection into the reservoir

(d) Electro-hydraulic control services provided via an umbilical

In addition Wellheads A and B require:

(e) Gas injection, transporting produced gas from an FPSO separation facility for re-injection into the reservoir

and Wellheads C and D require:

(f) Gas lift, transporting produced gas from an FPSO separation facility for gas lift service.

Although not considered in this study, pigging requirements for each part of the complete system and whether they can be met by only pigging the seabed lines or require the complete length of flowline from wellhead to FPSO to be accessible to pigging needs to be carefully analysed.

Design Throughputs and Riser Line Sizes [2]

Maximum design oil production rate = 120,000 BOPD
This output requires a minimum internal cross-sectional area of 0.173 m^2

Throughputs and corresponding minimum flowline cross-sectional areas for other services are as follows:

Water Injection	170,000 BWPD	0.051 m^2
Gas Injection	120 MMSCFD	0.025 m^2
Gas Lift	115 MMSCFD	0.025 m^2

Design Pressures and Temperatures [2]

Oil Production	5000 psi	74 °C
Water Injection	6000 psi	10 °C

Gas Injection	6000 psi	94 °C
Gas Lift	5000 psi	94 °C

Reservoir and Product Data [3]

Reservoir pressure = 5400 psi
Reservoir temperature = 74 °C
Oil Gravity = 34 °API
Gas/Oil ratio (GOR) = 250 SCF/bbl oil

9.2.3 Environmental Data

Water Depth [1]

The most important design driver is the depth of water (assuming the Buoy is always at the same distance below the surface) since it affects the Buoy size and length of Riser. This study uses 1500 m corresponding to the deepest water found in the Faroe-Shetland Channel.

Water Temperature [1]

The sub-surface water temperatures presented below reflect the two-layered structure of the Faroe-Shetland Channel watermasses.

Surface	7.6 °C **(winter)**	12.5 °C **(summer)**
200 m	6.0 °C	9.6 °C
300 m	5.6 °C	9.5 °C
400 m	1.6 °C	9.3 °C
600 m	-0.2 °C	6.9 °C
800 m	-0.8 °C	0.6 °C
1500 m	-1.0 °C	-1.0 °C

Current Velocity, Profile and Direction

In the operational condition, the current is the major design driver of the Riser System.

In general, long term recorded data from which an accurate 50 year return period estimate can be made, may be difficult to obtain since oceanographers have only begun to record

such data in the past twenty years for a small number of sites. The designer is therefore restricted to using data recorded over a limited period (at least a full year) and be required to make some estimate for long term fluctuations in the speed.
The designer requires estimates of the following quantities in terms of velocity, profile and direction:

- 50 year return values
- A monthly estimate to identify a suitable installation weather window

Surface currents over the tow out route will not influence the Riser design. The Riser will be allowed to weather-vane in most circumstances and the currents will only have a marginal influence on the wave excitation period.

This study is based upon 50 year maximal current speeds estimated from Conslex data taken from the mooring G4 [1] whose location within the Faroe-Shetland Channel is illustrated in Figure 5.17.

Surface	**Mean** 0.5 m/s	**50 year return** 1.2 m/s
100 m	0.15 m/s	0.6 m/s
500 m	0.1 m/s	0.3 m/s
1000 m	0.1 m/s	0.4 m/s
1500 m	0.1 m/s	0.4 m/s

In the Faroe-Shetland Channel, below the crest of the Wyville-Thomson Ridge and above the sill of the Faroe-Bank Channel (see Figure 5.17) the net flow is southwestwards, directly opposite to the notheastward flow of the upper Atlantic water, although the detailed current pattern is complicated by recirculations within the Faroe-Shetland Channel. However for the purposes of this preliminary design study all the water throughout the entire water column will be assumed to flow in the same direction i.e. southwestwards.

Sea Water Density

The density of sea water is required as a function of depth. No data corresponding to the Faroe-Shetland Channel could be found and therefore this study is based upon a constant density with respect to depth of 1025 kg/m^3

9.2.4 Engineering Data

Riser Steel Characteristics

The density, yield strength, elasticity modulus and coefficient of linear expansion are required for the Riser steel to be used.

Density = 7850 kg/m^3
Yield Strength = 450 N/mm^2
Elasticity Modulus = 207000 N/mm^2
Coefficient of Linear Expansion = 1.20 E-05 °C^{-1}

Syntactic Foam Characteristics

The density, thermal conductivity and limiting temperature, as a function of water depth, of the syntactic foam are required. See Chapters 3 and 4 for this data.

Nitrogen Gas Characteristics

The density and thermal conductivity of nitrogen gas as a function of pressure are required. See Chapters 3 and 4 for this data.

Sub-Surface Buoy Mooring Tether Characteristics

The weight per metre and maximum breaking load of the fibre rope are required. See Chapter 7 for this data.

Drag Coefficient

In the operational condition, current loading should be based upon a drag coefficient of 0.7.

9.2.5 Operational Data

This section includes data on the sub-surface buoy and FPSO watch circles. In the early stages of a design it is unlikely that FPSO mooring data will be available and so estimates will have to be made based upon a 50 year return current. The possibility of a single mooring line failure will also have to be accommodated. This information is important with regard to calculating the necessary lateral separation between buoy and

FPSO. This study is based upon an FPSO watch circle diameter of 400 m (27% of water depth) with a 50 m gap between it and the buoy's watch circle

The watch circle diameter corresponding to the sub-surface buoy is set at 100 m for a given design current velocity.

9.3 Preliminary Design

9.3.1 Introduction

This section presents an outline Catenary Riser design suitable for the oil field area specified in Section 9.2

9.3.2 Hydraulics

The wellhead arrangement requirement demanded by the oil field can be met by utilising two catenary risers connected in-plane to a central sub-surface buoy. One riser will connect into wellheads A and B via a seabed pipeline with the other linking up wellheads C and D. This arrangement is illustrated in Figure 9.3.

Production and service fluid throughput requirements between FPSO and wellhead (and vice versa) would be met by using the following flowlines.

Riser (1)	Two 12" Production	Total Internal C.S.A = 0.117 m^2
	One 8" Water Injection	Total Internal C.S.A = 0.026 m^2
	One 8" Gas Injection	Total Internal C.S.A = 0.026 m^2
Riser (2)	Two 12" Production	Total Internal C.S.A = 0.117 m^2
	One 8" Water Injection	Total Internal C.S.A = 0.026 m^2
	One 8" Gas Lift	Total Internal C.S.A = 0.026 m^2

On the basis of the above sizes and assuming each wellhead requires and produces the same amount of fluid, there will be 35% of spare capacity within the production flowlines, 2% spare capacity in the water injection flowline and 4% spare capacity in both the gas injection and lift flowlines. The large amount of spare capacity in the production flowlines can be used to accommodate test production fluid as well as generally providing the operator with the flexibility to increase production output.

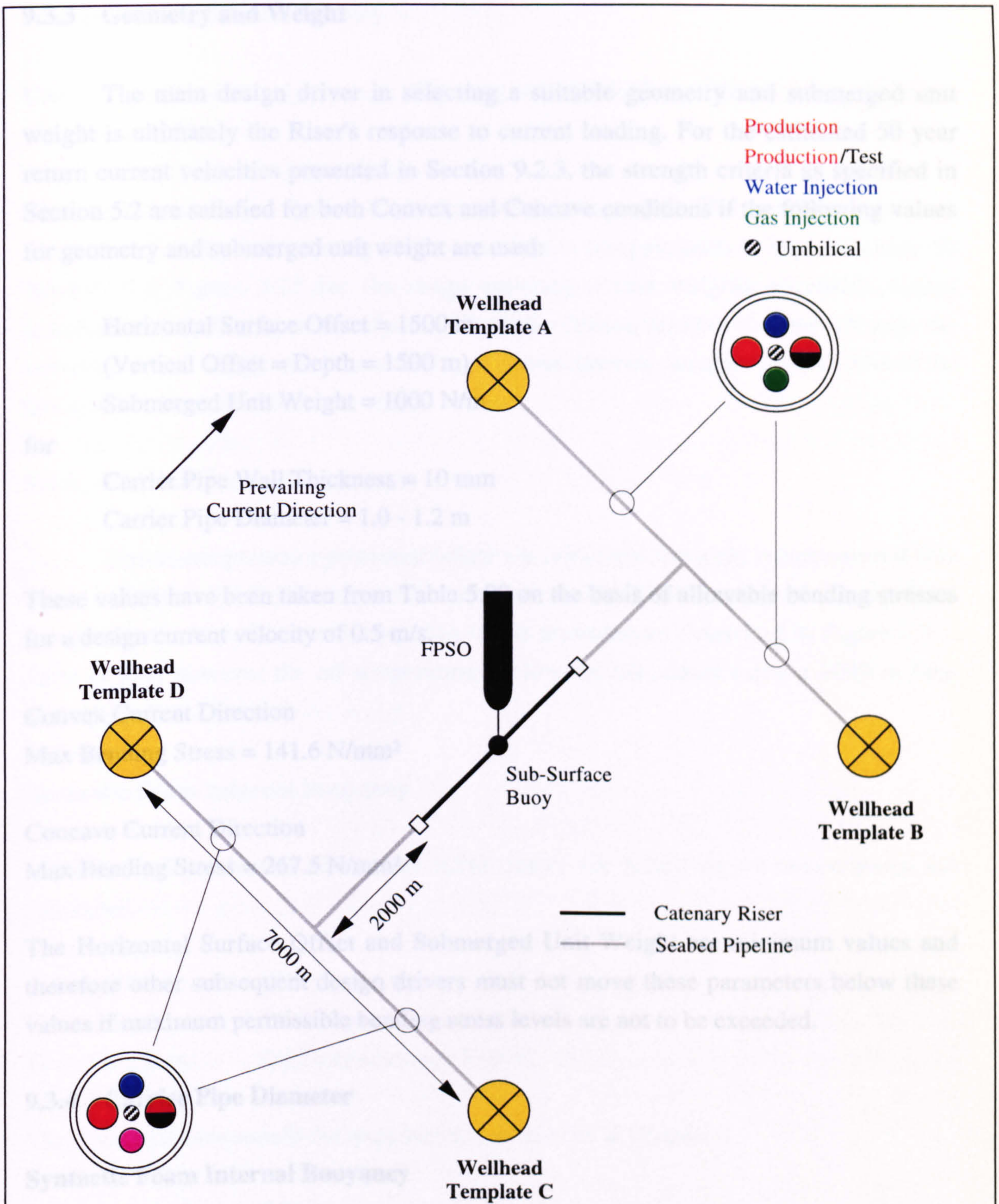

Figure 9.3

Catenary Riser and Seabed Pipeline Arrangement

9.3.3 Geometry and Weight

The main design driver in selecting a suitable geometry and submerged unit weight is ultimately the Riser's response to current loading. For the estimated 50 year return current velocities presented in Section 9.2.3, the strength criteria as specified in Section 5.2 are satisfied for both Convex and Concave conditions if the following values for geometry and submerged unit weight are used:

Horizontal Surface Offset = 1500 m
(Vertical Offset = Depth = 1500 m)
Submerged Unit Weight = 1000 N/m

for

Carrier Pipe Wall Thickness = 10 mm
Carrier Pipe Diameter = 1.0 - 1.2 m

These values have been taken from Table 5.90 on the basis of allowable bending stresses for a design current velocity of 0.5 m/s.

Convex Current Direction
Max Bending Stress = 141.6 N/mm^2

Concave Current Direction
Max Bending Stress = 267.5 N/mm^2

The Horizontal Surface Offset and Submerged Unit Weight are minimum values and therefore other subsequent design drivers must not move these parameters below these values if maximum permissible bending stress levels are not to be exceeded.

9.3.4 Carrier Pipe Diameter

Syntactic Foam Internal Buoyancy

Carrier Pipe Diameter = 1.2 m Submerged Unit Weight = 1222 N/m
(See Figure 3.10)

See Figure 3.11 for the range submerged unit weights attainable during installation by ballasting or de-ballasting flowlines. During lift the submerged unit weight can be reduced to just 100 N/m if all of the flowlines are filled with air.

Nitrogen Gas Internal Buoyancy

Carrier Pipe Diameter = 1.05 m Submerged Unit Weight = 1300 N/m
(See Figure 3.23)

These values are based upon a 10 compartment arrangement. The resulting maximum circumferential stress (occurring at the top of each compartment) is approximately 80 N/mm^2. See Figure 3.35 for the range submerged unit weights attainable during installation by ballasting or de-ballasting flowlines. During the critical initial lift stage the submerged unit weight can be reduced to a compartmental average of 1100 N/m if the internal flowlines are filled with air.

9.3.5 Flowline Insulation

The oil temperatures presented below are calculated using the environmental data given in Section 9.2.3. The ambient temperature for the Riser has been depth averaged using winter values. The seabed pipeline in the arrangement illustrated in Figure 9.3 is 5500 m long however the oil temperatures below are calculated using a 6000 m long seabed pipeline.

Syntactic Foam Internal Buoyancy

If the seabed pipeline is filled with HSM Slurry the following oil temperatures are calculated:

Wellhead Oil Temperature = 74 °C
Base of the Riser Oil Temperature = 71.2 °C
Top of the Riser Oil Temperature = 70.9 °C
(See Table 4.4)
These temperatures satisfy the requirements as laid out in Chapter 4

Nitrogen Gas Internal Buoyancy

If the seabed pipeline is again filled with HSM Slurry and the production flowlines are insulated using a 10 mm thick syntactic foam sleeve the following oil temperatures are estimated:

Wellhead Oil Temperature = 74 °C
Base of the Riser Oil Temperature = 71.2 °C

Top of the Riser Oil Temperature = 66.5 °C

(See Table 4.4)

These temperatures satisfy the requirements as laid out in Chapter 4

9.3.6 Installation - Lift Sequence

It is proposed that a semi-submersible pipe laying vessel is used to lift one end of the Riser up to the surface for connection to the sub-surface buoy. This can be achieved by attaching either steel or synthetic ropes to the end of the Riser which will then be tensioning using capstans onboard the vessel. Load will then be applied to the end of the Riser via ropes in both horizontal and vertical directions by the vessel dragging itself forward on it's anchor lines. It should be noted that in order for the both horizontal and vertical forces to be applied, the rope must be taut (see Figure 9.4).

The maximum axial load that can be applied along the rope by a typical pipe laying vessel using the technique outlined above is 330 tonnes which is equivalent to 3237 kN [4]

Syntactic Foam Internal Buoyancy

The submerged unit weight of this design in it's installation condition is approximately 100 N/m with all the flowlines full of air (see Figure 3.11). To lift this off the seabed requires a horizontal load of 2000 kN and a vertical load of 250 kN for a catenary lift profile as shown in Figure 5.34. This lift profile should ensure that bending and axial stresses during the lift sequence are within permissible limits. This loading arrangement will require an axial rope load of 2016 kN acting at an angle (from the seabed) of 7°. As a consequence approximately 12.3 km of taut line is required. This amount of rope will cause considerable storage problems and therefore a second vessel alongside will almost certainly be required. Another problem associated with using this much line are the effects of both current and self-weight.

The problem of self-weight considerably adding to the load exerted upon the pipe laying vessel can be addressed by using synthetic (usually polyester) rope which has been proposed for the sub-surface buoy tethers (see Section 7.5.4). This rope is usually either neutrally or slightly positively buoyant and so can be held taut without having to apply too much additional load. A submerged weight example can be calculated using data obtained from BRIDON (manufactures of polyester rope). A single rope with a breaking load of 5000 kN (see Table 7.2) would be sufficient since this would provide a safety

factor of 2. The diameter is 132 mm and the mass (in air) is 12.6 kg/m and so the submerged unit weight equals only -15 N/m i.e. it is slightly positively buoyant.

Vertical load exerted upon the vessel = - 184.5 kN
Horizontal load exerted upon the vessel = 700 kN (using the equations in Chapter 2 for a catenary profile)

These loads plus those applied to the riser can be accommodated within the capability of the vessel.

As a comparison a wire rope with the following parameters [5] will exert a considerable load upon the vessel:

Nominal Diameter = 119 mm
Approximate Mass = 48.8 kg/m
Minimum Breaking Load = 5905.6 kN
(Values calculated on a pro-rata basis from those given in the table in Ref [5])

Submerged Unit Weight = 366.9 N/m
Vertical load exerted upon the vessel = 4500 kN
Horizontal load exerted upon the vessel = 17500 kN (using the equations in Chapter 2 for a catenary profile)

These loads are outside the capability of pipe laying vessel.

Nitrogen Gas Internal Buoyancy

In it's installation condition this design has an average submerged unit weight of 1100 N/m along it's length with all flowlines full of air (see Figure 3.35). To lift this off the seabed requires a horizontal load of 15000 kN and a vertical load of 2000 kN for a catenary lift profile as shown in Figure 5.34. This loading arrangement will require an axial cable or rope load of 15100 kN acting at an angle (from the seabed) of approximately 7°. This load far exceeds the capability of the pipe laying vessel and so proposed to add additional buoyancy (in the form of syntactic foam modules) to the riser. The aim in doing this is to reduce the submerged unit weight down to a uniform 100 N/m i.e. the same as that for the syntactic foam internal buoyancy design. This can be achieved by adding the following buoyancy to the external surface of the following compartments:

Compartment (1) 450 N/m of buoyancy
(2) 550 N/m
(3) 650 N/m
(4) 750 N/m
(5) 900 N/m
(6) 1000 N/m
(7) 1100 N/m
(8) 1200 N/m
(9) 1300 N/m
(10) 1400 N/m

9.3.7 Sub-Surface Buoy Sizing

The sizes below are based upon a design current velocity of 0.6 m/s and a maximum buoy displacement of 50 m (as specified in Section 9.2.5).

Diameter = 14.0 m External Volume = 1185 m^3
Height = 7.7 m Mass (air) = 264.2 tonnes

These values have been taken from Tables 7.7 and 7.12 for a Riser with a submerged unit weight of 1500 N/m.

References

1. Ellet, D.J. (1992) *West of Shetlands Frontier Tranches: Physical Oceanography*, Pres Mobil EIA Seminar, February 1992.

2. Rockall Development Base Case Simulations

3. Technical Memo, Preliminary Rockall Design Criteria

4. EMD Ltd

5. Breaking Load and Weight Tables. MARINE WIRE ROPES.

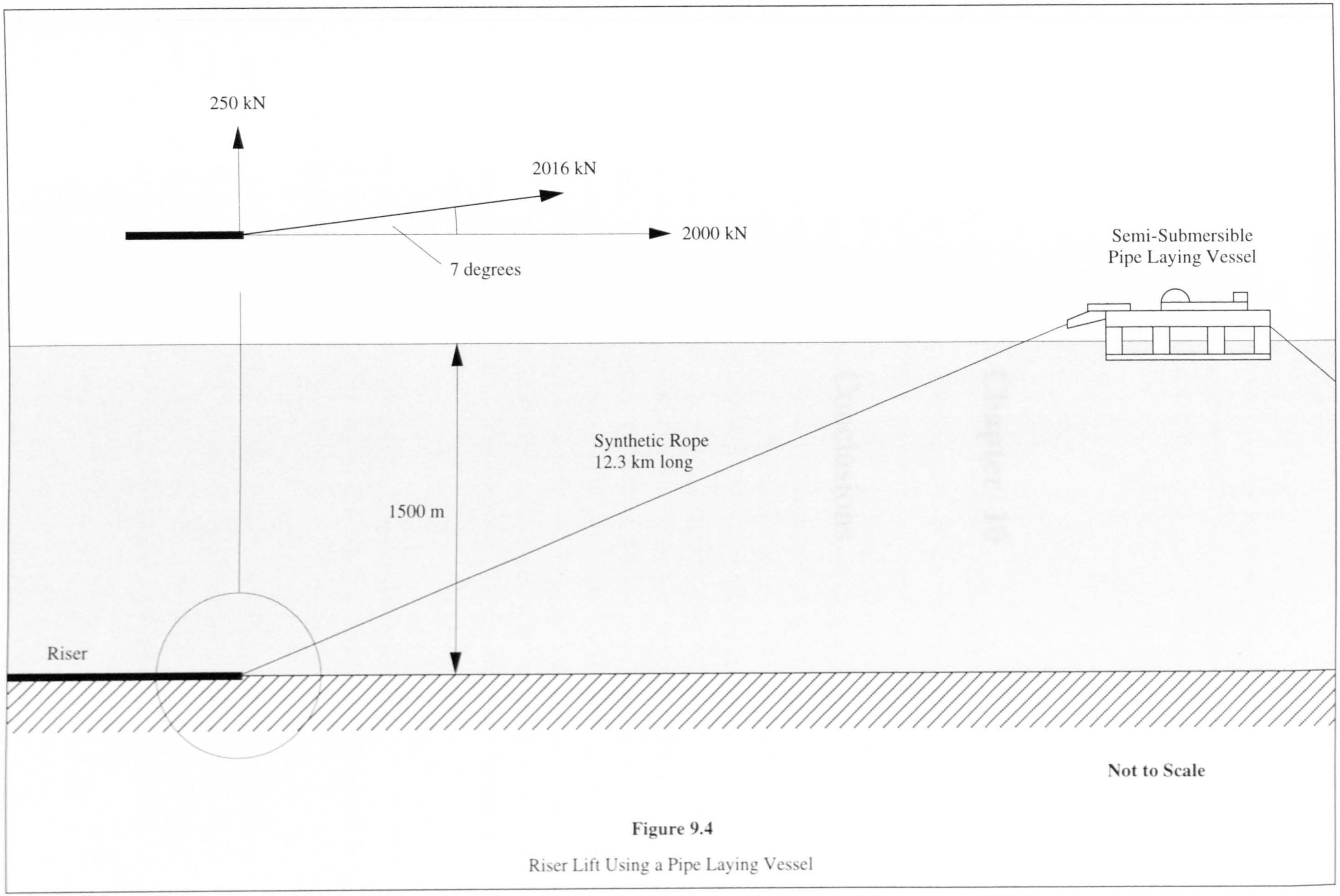

Figure 9.4

Riser Lift Using a Pipe Laying Vessel

Chapter 10

Conclusions

10.1 Specific Conclusions of Thesis

This thesis has examined and developed a deep water production riser concept by studying various aspects of the system in detail. This initial design work has provided a basis for a judgement as to whether this proposal is both technically and economically feasible. This study also helps to identify where further work is required in order for a total design evaluation to be carried out.

10.1.1 Chapter 2

The geometric analysis undertaken in Chapter 2 has established that for all three mathematical curves considered i.e. elliptic, parabolic and catenary, maximum bending moments due to self-weight occur at the seabed, except in the case of an elliptic profile when horizontal offset exceeds vertical offset. The elliptic and parabolic curves, although convenient mathematically would be very difficult to attain on a practical basis. It would require an exact buoyancy load distribution to be imposed along the riser and due to the bending flexibility of the system very little tolerance in either weight or buoyancy could be accommodated. Any benefits would be significantly out-weighed by an inevitable increase in fabrication complexity and cost. A catenary however describes the form assumed by a perfect flexible inextensible chain of uniform density suspended from two supports. Therefore a riser with a negligible bending stiffness, uniform submerged unit weight and supported at surface and seabed could accurately be assumed to take up a catenary profile. Therefore on a practical installation and production basis a catenary curve is selected as the basis of the design analysis carried out in this thesis. A catenary line analysis carried out indicates that if the horizontal surface offset is increased the effect on the stress condition is twofold:

- Increases the axial loading due to a greater suspended length of riser.
- Reduces the bending load at the seabed as a result of less curvature; the whole profile becomes much flatter.

Another important consideration is that of riser slope, as the horizontal surface offset is increased the slope at the surface (from the horizontal) decreases. This could cause connection problems at the surface vessel. Further analysis has shown that for a given horizontal offset, the bending stress at the seabed increases for a greater depth of water.

10.1.2 Chapter 3

As a result of its construction and operating depth the catenary riser is inherently heavy thereby creating high self-weight stress levels. If these stresses are to be limited the riser has to be supported which is commonly achieved through the provision of buoyancy. In Chapter 3 two different buoyancy systems suitable for a deep water catenary riser were investigated. The syntactic foam design provides the riser with a buoyancy system that is simple to use during both riser installation and operation. Its characteristics and performance are not influenced by external factors such as temperature and pressure and it doesn't impose any additional stresses on the riser structure, however it is very expensive especially when the riser is between 2000 and 3000 m in length. Nitrogen gas however is relatively cheap as shown up in a comparative cost analysis in a later chapter, although this is somewhat compromised by a considerably more complex system. A compartmental buoyancy gas system requires valves, high pressure lines as well as a large high pressure gas source. It creates an additional load on the riser structure and has a greater risk of failure.

Despite the advantages and disadvantages associated with each system the work carried out in this chapter should enable a designer to select the correct carrier pipe diameter and ballast arrangements so as to ensure an optimum riser weight during both its installation and operational lifetime whichever system is chosen.

10.1.3 Chapter 4

The work in this thesis has identified a requirement for good pipeline and flowline insulation in order for oil transportation problems such as hydration to be avoided within a deep water environment.

The results obtained from an analytical heat transfer study clearly illustrate the varied insulation effectiveness of a range of materials and arrangements. Filling the annular gap between flowlines and carrier pipe with syntactic foam offers the best barrier to oil flow heat loss with only a 1.3 °C calculated temperature drop between wellhead and production unit. However on a purely insulation basis this is a very expensive option especially as temperature reductions of up to 37 °C can be accommodated without the risk of activating production flow problems. Since nitrogen gas on its own was found to provide inadequate insulation with a calculated 44 °C drop in temperature but is however considerably cheaper and superior in providing buoyancy, it was decided to combine both the gas and the foam. As a result of this it was found that in the case of the riser a 10 mm syntactic foam layer around the oil flowlines with the rest of the available annular volume

filled with gas would yield an oil temperature at the surface of 66.5 °C. This would ensure a sizeable safety margin from any temperature dependent problems such as emulsification and hydration whilst also being cost effective and non-detrimental in terms of riser buoyancy.

In the case of the seabed pipeline, provision of buoyancy is not an important requirement which was the basis for analysing a new substance called High-Strength Silica Microsphere (HSM) Slurry. As well as having a low thermal conductivity and a high compression resistance HSM slurry offers two other advantages with regard to its potential utilisation in a seabed pipeline.

- It could be pumped into the carrier pipe after seabed installation therefore eliminating many of the problems associated with fabrication and tow-out.
- It has a relatively high density (820 kg/m^3) compared to 384 kg/m^3 for syntactic foam and will therefore provide the pipeline with weight and hence stability on the seabed.

Thermal stress is proportional to the temperature differences generated within the structure. For a wellhead temperature of 74 °C and an ambient water temperature of -1.0 °C the maximum thermally induced axial stress (would occur in the pipeline) would be 140 N/mm^2 in the carrier pipe (tensile) and 60 N/mm^2 in the flowlines (compressive).

10.1.4 Chapter 5

In Chapter 5 an installation loading analysis investigated the effects of riser geometry and submerged unit weight on bending stress, axial stress and lifting load (i.e. the vertical load exerted upon the lifting vessel). Bending and axial stresses resulting from surface and sub-surface vessel displacements were also calculated along with the corresponding riser deflection profiles.

Finally in Chapter 5 the static structural response of the riser in terms of deflections and stresses were examined for in-plane current loads. It was found that the effect of imposing a current on the *Concave* side of the catenary riser is to pull the lower end of the riser away from the seabed and in doing so increase the riser's curvature at the seabed connection point. A current acting on the*Convex* side has the opposite effect in that it pushes the lower end towards the seabed, thereby reducing the curvature at the seabed whilst increasing it slightly further up. The response of the riser system in terms of its deflection behaviour to parameters such as submerged unit weight and horizontal surface

offset is demonstrated comprehensively by the vast array of results from which the following characteristics can be identified:

- For a given current velocity the extent to which the riser deflects reduces as the submerged weight is increased.
- For a given current velocity the extent to which the riser deflects reduces as the horizontal surface offset is increased.

For the *Concave* case, the maximum bending stress is always generated at the point of contact with the seabed (as in the case of zero current) as opposed to the *Convex* condition in which the current load effectively moves the maximum bending stress from the seabed end to a location slightly further along the riser.

When a current is exerted upon the convex side of the riser the effect is to reduce the axial stress (tensile) along the entire length of the riser, the greater the current velocity the larger the reduction is. However when concave side of the riser is subjected to a current load the opposite occurs and the axial stress is increased.

Another important characteristic which becomes apparent when a catenary riser is subjected to external forces are the large angular rotations which are generated at the top end. These have to be accommodated in order to avoid creating seriously high bending moments both in the riser as well as in the surface or sub-surface connection assembly. This can be achieved through the use of flexible joints which are just becoming established within the offshore industry. A design for a surface connection system using flexible joints was proposed in this chapter.

An investigation regarding the effect of drag coefficient showed that in the coefficient range 0.3 - 1.2 the variation in structural response is very small.

10.1.5 Chapter 6

In Chapter 6 a resonant period analysis was undertaken using a numerical procedure based upon a finite difference technique and validated by an analytical method developed by Blevin for vibrating stretched strings. The results from this dynamic analysis indicated that:

- The periods of vibration rapidly converge as the mode number is increased. All the high frequencies (low periods) appear within a convergence block as opposed to the low frequencies of vibration (high periods) which are well spaced out.

- The range of natural periods increase with an increase in riser diameter. For the syntactic foam buoyancy condition the effect of increasing the riser diameter from 1.10 m to 1.30 m is to increase the natural periods by an average of 250% for all modes of vibration. This equates to a significant shift with respect to the fundamental and lower modes of vibration and a small to negligible shift in the case of the higher modes.

Overall the results suggest that the riser's high natural periods are substantially influenced by carrier pipe diameter and can therefore be positioned so as not to coincide with external excitation periods by selecting the appropriate diameter i.e. low frequency resonance can be avoided by good design. However as the mode number is increased the diameter's influence reduces and spectrum converges towards the roughly the same value irrespective of diameter. Therefore at this end of the spectrum the diameter cannot be used to move the low natural periods of vibration and hence high frequency resonance is always inevitable.

When the results obtained using the numerical method were compared with those calculated using the analytical technique for the same vibrating system, it was found that the two sets of data compared well with a discrepancy of only 5% in the fundamental period. This disparity however declines as the mode number increases, for mode 8 the difference has halved to 2.5%.

This analysis was conducted using a negliable bending stiffness assumption. Although this is true, the riser will have some bending rigidity and this will tend to effect the higher frequency modes. Further work which includes bending stiffness, however small is required to asses how big this effect is.

10.1.6 Chapter 7

As an alternative to the direct connection of the riser to the surface production vessel a study to investigate the advantages of a hybrid connection was carried out. In this study a vertically tethered sub-surface buoy onto which a catenary riser is suspended was designed and evaluated. The advantages of this system can be summarised as follows:

- Reduced displacement offsets for the riser's upper end, in both the vertical and horizontal planes. The main impact of this is to decrease the riser bending loads at the seabed.

- Decrease in wave disturbance which reduces the possibility of fatigue loading.

- Allows the surface production vessel (FPSO) to be disconnected from the riser system easily and quickly.

- Ensures that the installation of the riser system is quick and simple

10.1.7 Chapter 8

A detailed capital cost analysis for the catenary riser system was carried out and it was found that the economics compare favourably with known production systems designed for the same operational environment.

10.2 Recommended Future Work

The work in this thesis has concentrated on the riser's structural response to in-plane loading and therefore the next logical step would be to investigate out-of-plane loading. This would introduce torsion and out-of-plane bending into the stress calculations thereby increasing the complexity of the analysis. However this work would certainly be essential if either the sea currents were multi-directional or if more than two catenary risers were suspended from an FPSO turret or sub-surface buoy.

This study has not considered the loading imposed upon the riser's internal tranverse bulkheads which are especially important in the nitrogen gas buoyancy design. These bulkheads are a critical structural component with the riser and will experience a high degree of complex loading, especially at there interface with the carrier pipe. This work needs to be carried out within an overall detailed structural analysis, ultimately using FE modelling techniques.

Structural response calculations should take in to account the interaction of the seabed which could be modelled using a series of springs with a stiffness based upon the properties of the soil.

In order to demonstrate technical viability the resonant period and response analysis presented in Chapter 6 has to be extended to cover the dynamic stressing and deflection response of the riser due to external environmental excitation i.e. current. These results are important in predicting a fatigue life for the system. A dynamic load analysis should undertaken for both tow-out, lift and installed riser conditions.

One area that has been overlooked in this study but is however fundamental in the design of the riser is its fabrication and assembly. An uncomplicated and well planned assembly sequence usually results in lower construction costs as well as a reduced construction time which are two benefits fervidly sought by offshore operators. Ease of manufacture should therefore act as a main design driver for the riser. An obvious example of this is making sure the design allows adequate access for welding and inspection. It should be noted that for a riser which may have a length approaching 3 km assembly techniques will be predominantly driven by the method of launch which is currently the case for subsea pipelines.

At depths of 1500 m the temperature of ocean sea water is unaffected by conditions above the surface and can remain as low as -2 °C all year round. This can be compared to wellhead oil temperatures which can be high as 80 °C depending reservoir conditions. A heat engine that uses the hot oil as a heat source and the cold sub-surface water as a heat sink is capable of converting significant amounts of this thermal energy to mechanical and hence to electrical energy. Because the temperature difference between the heat source and heat sink is relatively small, the conversion efficiency will be low compared to the more familiar power conversion cycles. However since no fuel is required, the net cost of the energy could be made economically competitive. If a closed power conversion cycle as illustrated in Figure 9.1 could be incorporated within the catenary riser without too much disruption the electrical energy produced could be used to power electrical systems onboard an FPSO or other surface production vessel. A condensate feed pump would be located on the seabed with a small turbine and generator situated within the FPSO as shown in Figure 9.2. Hot oil within the production flowlines would act as the evaporator with the ambient sea water being used to condense the circuit fluid which would probably be ammonia.

The idea behind this was generated as a result of research into OTEC (ocean thermal energy conversion) power systems which have been designed to harness the vertical temperature gradient existing in the ocean to generate electrical power on a commercial scale. One such design is illustrated in Figure 9.3.

The challenge is to develop this idea and ultimately demonstrate that it can technically and economically provide electrical power to a surface production vessel.

References

1. Douglass, R.H., Hollett, J.S. and Karalis, A.J. (1975) *Ocean Thermal Energy: An Engineering Evaluation*, In Proc Offshore Technology Conference, OTC 2252.

2. Trimble, C.L. and Naef, F.E. (1975) *Ocean Thermal Energy Conversion*, Lockheed Aircraft Corp, In Proc Offshore Technology Conference, OTC 2258.

3. Horowitz, J.S. (1975) *OTEC - Power Systems*, Argonne National Laboratory, In Proc Offshore Technology Conference, OTC 3588.

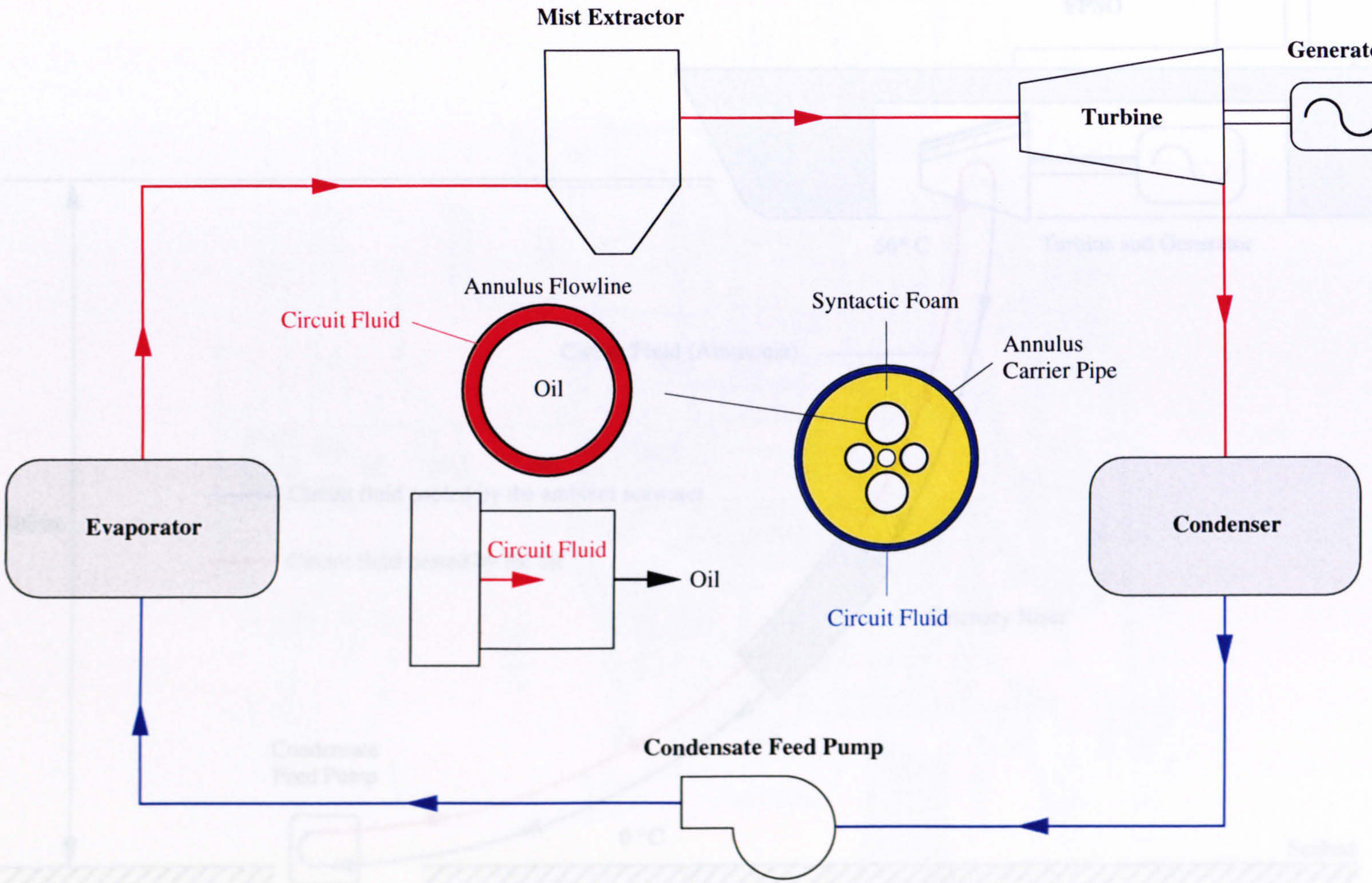

Figure 10.1

Schematic of a Closed Power System

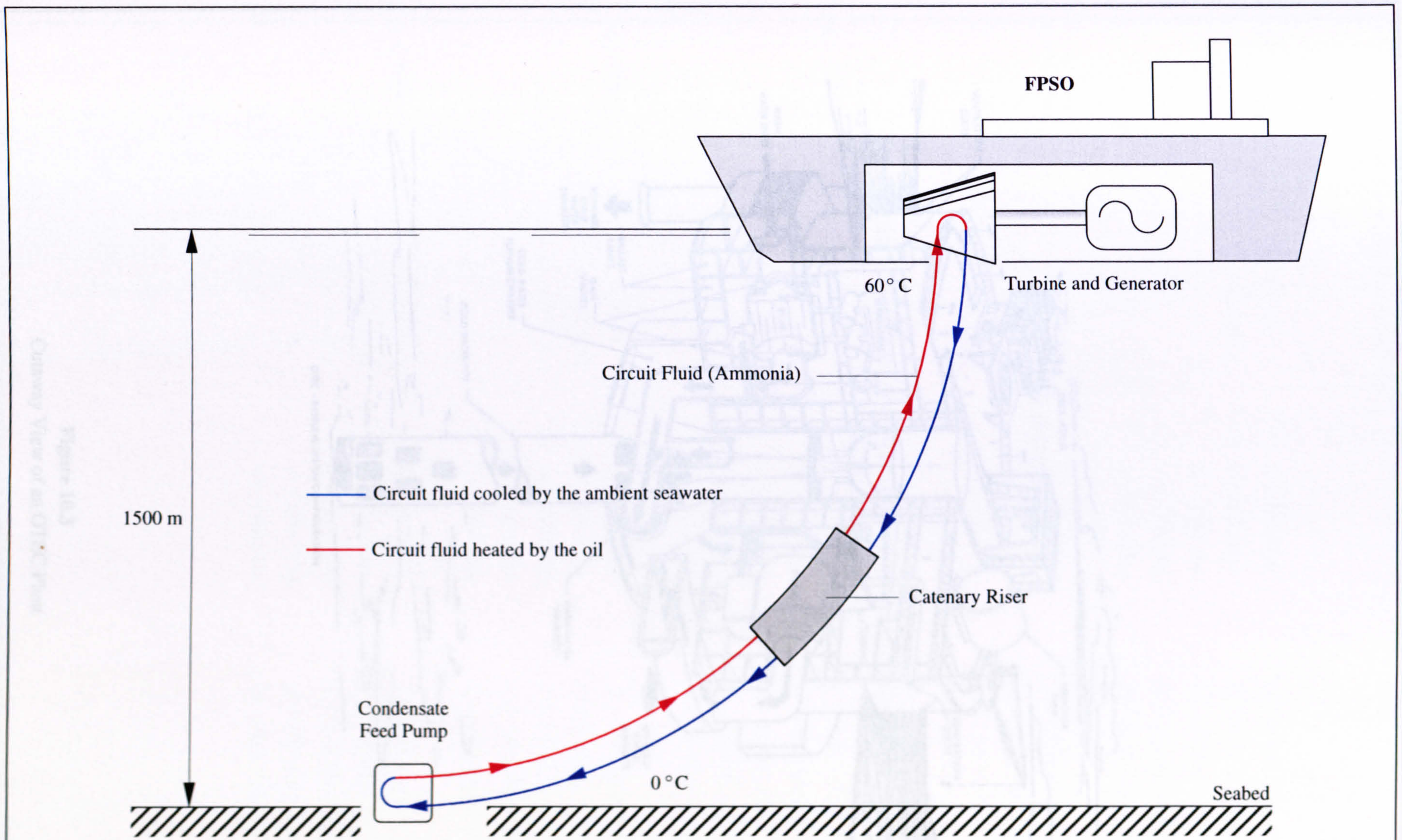

Figure 10.2

Thermal Energy Conversion

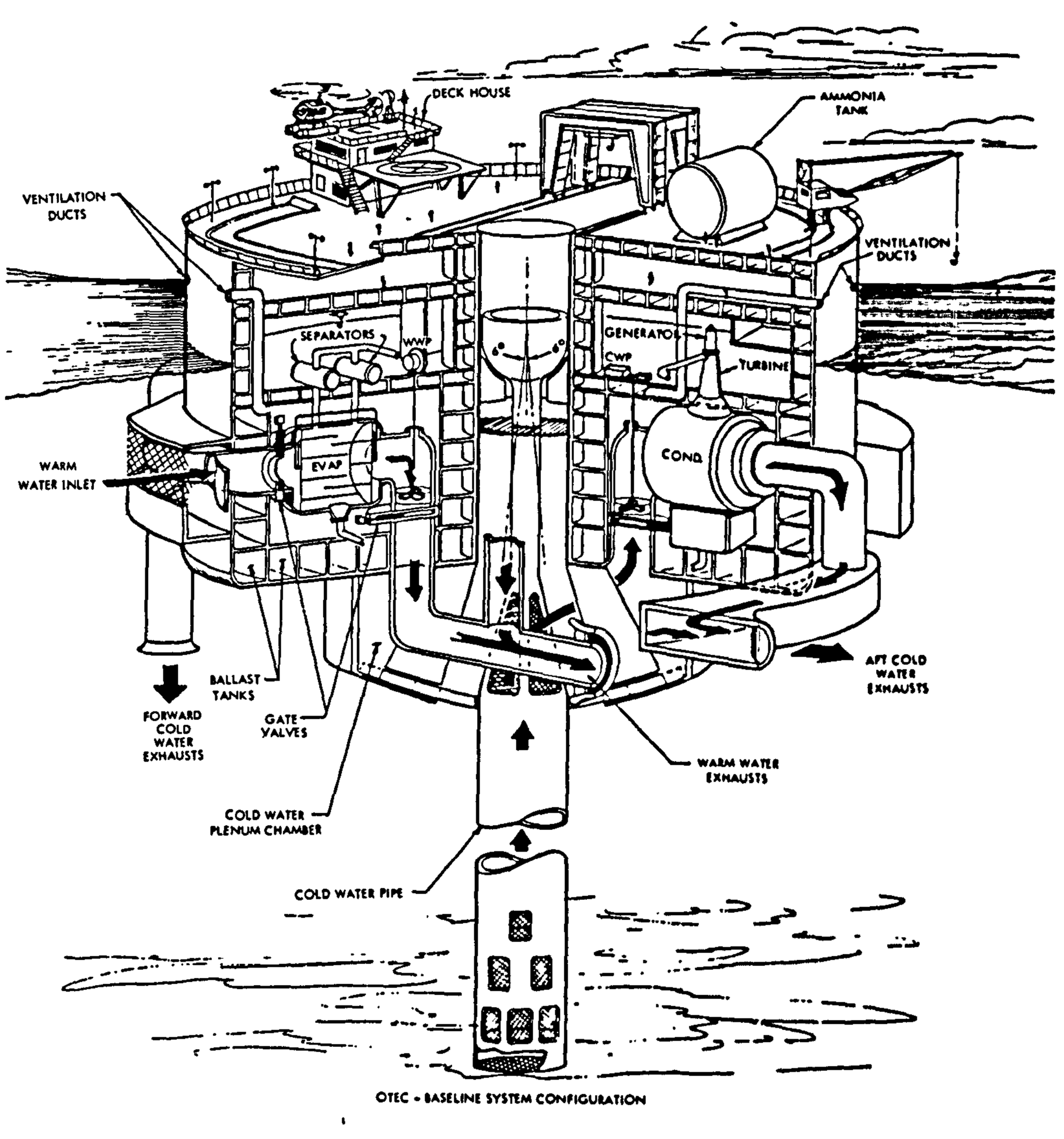

OTEC - BASELINE SYSTEM CONFIGURATION

Figure 10.3
Cutaway View of an OTEC Plant

Appendix A

Horizontal Tensions for Catenary Lines with Vertical Offsets of 1400 and 1500 m

A.1 Vertical Offset = 1400 m

a = 1000 m	c = 495.85	**w = 100 N/m**	**H = 49584.60 N**
	L = 1829.86 m	**w = 500 N/m**	**H = 247922.98 N**
		w = 1000 N/m	**H = 495845.96 N**
		w = 1500 N/m	**H = 743768.94 N**
		w = 2000 N/m	**H = 991691.90 N**
a = 1250 m	c = 715.31	**w = 100 N/m**	**H = 71530.52 N**
	L = 1990.70 m	**w = 500 N/m**	**H = 357652.60 N**
		w = 1000 N/m	**H = 715305.21 N**
		w = 1500 N/m	**H = 1072957.81 N**
		w = 2000 N/m	**H = 1430610.41 N**
a = 1500 m	c = 975.08	**w = 100 N/m**	**H = 97505.90 N**
	L = 2165.70 m	**w = 500 N/m**	**H = 487529.50 N**
		w = 1000 N/m	**H = 975058.99 N**
		w = 1500 N/m	**H = 1462588.50 N**
		w = 2000 N/m	**H = 1950117.98 N**
a = 1750 m	c = 1276.24	**w = 100 N/m**	**H = 127623.99 N**
	L = 2352.33 m	**w = 500 N/m**	**H = 638119.95 N**
		w = 1000 N/m	**H = 1276239.90 N**
		w = 1500 N/m	**H = 1914359.85 N**
		w = 2000 N/m	**H = 2552479.80 N**
a = 2000 m	c = 1619.59	**w = 100 N/m**	**H = 161960.61 N**
	L = 2548.50 m	**w = 500 N/m**	**H = 809803.06 N**
		w = 1000 N/m	**H = 1619606.12 N**
		w = 1500 N/m	**H = 2429409.18 N**
		w = 2000 N/m	**H = 3239212.24 N**

A.2 Vertical Offset = 1500 m

a = 1000 m	c = 475.68	**w = 100 N/m**	**H = 47568.33 N**
	L = 1917.56 m	**w = 500 N/m**	**H = 237841.65 N**
	Sag = 470.63 m	**w = 1000 N/m**	**H = 475683.30 N**
		w = 1500 N/m	**H = 713524.96 N**
		w = 2000 N/m	**H = 951366.61 N**
a = 1250 m	c = 683.29	**w = 100 N/m**	**H = 68325.67 N**
	L = 2073.63 m	**w = 500 N/m**	**H = 341628.35 N**
	Sag = 448.98 m	**w = 1000 N/m**	**H = 683256.70 N**
		w = 1500 N/m	**H = 1024885.05 N**
		w = 2000 N/m	**H = 1366513.40 N**
a = 1500 m	c = 928.14	**w = 100 N/m**	**H = 92814.08 N**
	L = 2243.75 m	**w = 500 N/m**	**H = 464070.40 N**
	Sag = 433.59 m	**w = 1000 N/m**	**H = 928140.81 N**
		w = 1500 N/m	**H = 1392211.21 N**
		w = 2000 N/m	**H = 1856281.62 N**
a = 1750 m	c = 1211.24	**w = 100 N/m**	**H = 121122.77 N**
	L = 2425.64 m	**w = 500 N/m**	**H = 605613.84 N**
	Sag = 422.28 m	**w = 1000 N/m**	**H = 1211227.67 N**
		w = 1500 N/m	**H = 1816841.51 N**
		w = 2000 N/m	**H = 2422455.35 N**
a = 2000 m	c = 1533.40	**w = 100 N/m**	**H = 153340.31 N**
	L = 2617.29 m	**w = 500 N/m**	**H = 766701.54 N**
	Sag = 413.80 m	**w = 1000 N/m**	**H = 1533403.08 N**
		w = 1500 N/m	**H = 2300104.63 N**
		w = 2000 N/m	**H = 3066806.17 N**
a = 2500 m	c = 2297.24	**w = 100 N/m**	**H = 229729.19 N**
	L = 3023.52 m	**w = 500 N/m**	**H = 1148645.97 N**
	Sag = 402.27 m	**w = 1000 N/m**	**H = 2297291.93 N**
		w = 1500 N/m	**H = 3445937.90 N**
		w = 2000 N/m	**H = 4594583.87 N**

a = 3000 m	c = 3222.96	**w = 100 N/m**	**H = 322301.46 N**
	L = 3452.37 m	**w = 500 N/m**	**H = 1611507.30 N**
	Sag = 395.05 m	**w = 1000 N/m**	**H = 3223014.60 N**
		w = 1500 N/m	**H = 4834521.90 N**
		w = 2000 N/m	**H = 6446029.20 N**
a = 4000 m	c = 5566.79	**w = 100 N/m**	**H = 556686.97 N**
	L = 4353.20 m	**w = 500 N/m**	**H = 2783434.85 N**
	Sag = 387.02 m	**w = 1000 N/m**	**H = 5566869.71 N**
		w = 1500 N/m	**H = 8350304.56 N**

Appendix B

FORTRAN Program Lists for Catenary Riser Lift and
and Surface Displacement Calculations

```
      PROGRAM Displacement1
C
C     This FORTRAN computer program calculates the Horizontal Tension
C     and Suspended Riser Length for a displaced catenary riser.
C     (Decrease in suspended length)
C
C     Program written by James Dingwall
C
C
C     NOMENCLATURE
C     ************************************************************
C
C     a          Horizontal Surface Offset
C     as         Suspended Horizontal Surface Offset
C     ax         Horizontal Surface Offset
C     b          Sea Depth (vertical offset)
C     by         Sea Depth (vertical offset)
C     H          Horizontal Tension Constant
C     HTension   Horizontal Tension Constant
C     Length     Total Length of Riser
C     L          Total Length of Riser
C     Ls         Suspended Length of Riser
C     L          Length of Riser
C     w          Submerged Weight
C     Ic         Integration Constant
C     dydx       Slope of Riser at x
C
C     SPECIFICATION STATEMENTS
C     ************************************************************
C
      INTEGER Final_H, Initial_H, Inc_H, No_Incs
C
      DOUBLE PRECISION a(10), b(10), L(10), w(10)
      DOUBLE PRECISION SO, VO, LR, SW, Lsi
      DOUBLE PRECISION as(100), Ls(100), Lamda(100), Ic(100), dydx(100)
      DOUBLE PRECISION Slope(0:1000), Ls_Array(0:1000), as_Array(0:1000)
      DOUBLE PRECISION HTension(100), LHS(100), RHS(100), DIFFERENCE(100)
      DOUBLE PRECISION LEFT_Ls, RIGHT_Ls, MID_Ls, MID_Slope, D
C
      PARAMETER (Initial_H=1000, Final_H=100000000, Inc_H=10000)
C
      CHARACTER*7 FILE
      CHARACTER*10 OUTFILE
      CHARACTER*6 Answer
      CHARACTER*1 Answer_sl
C
      PRINT*,'   Enter the Output Filename'
      READ (5,1) FILE
    1 FORMAT (A10)
C
      WRITE (OUTFILE,2)FILE
      OPEN (UNIT=2, FILE=OUTFILE, STATUS='NEW')
C
C     INPUT
C     ************************************************************
C
      PRINT*,'   Select the catenary parameter to be varied',
     *           ' (ax, by, Length or Weight)'
      READ*, Answer
      PRINT*,'   Enter the No of Calculations'
      READ*, No_Calcs
C
      IF (Answer.EQ.'ax    ') THEN
        DO 100, I=1, No_Calcs
          PRINT*,'   Enter the Horizontal Surface Offset (m)',I
```

```
            READ*, a(I)
  100     CONTINUE
          PRINT*,'   Enter the Vertical Offset (m)'
          READ*, VO
          PRINT*,'   Enter the Length of the Riser (m)'
          READ*,LR
          PRINT*,'   Enter the Submerged Unit Weight (N/m)'
          READ*,SW
          DO 110, I=1, No_Calcs
             b(I) = VO
             L(I) = LR
             w(I) = SW
  110     CONTINUE
C
        ELSEIF (Answer.EQ.'by    ') THEN
          DO 120, I=1, No_Calcs
             PRINT*,'   Enter the Vertical Offset (m)',I
             READ*, b(I)
  120     CONTINUE
          PRINT*,'   Enter the Horizontal Surface Offset (m)'
          READ*, SO
          PRINT*,'   Enter the Length of the Riser (m)'
          READ*,LR
          PRINT*,'   Enter the Submerged Unit Weight (m)'
          READ*,SW
          DO 130, I=1, No_Calcs
             a(I) = SO
             L(I) = LR
             w(I) = SW
  130     CONTINUE
C
        ELSEIF (Answer.EQ.'Length') THEN
          DO 140, I=1, No_Calcs
             PRINT*,'   Enter the Length of the Riser (m)',I
             READ*, L(I)
  140     CONTINUE
          PRINT*,'   Enter the Horizontal Surface Offset (m)'
          READ*, SO
          PRINT*,'   Enter the Vertical Offset (m)'
          READ*,VO
          PRINT*,'   Enter the Submerged Unit Weight (N/m)'
          READ*,SW
          DO 150, I=1, No_Calcs
             a(I) = SO
             b(I) = VO
             w(I) = SW
  150     CONTINUE
C
        ELSE
          DO 160, I=1, No_Calcs
             PRINT*,'   Enter the Submerged Unit Weight (N/m)',I
             READ*, w(I)
  160     CONTINUE
          PRINT*,'   Enter the Horizontal Surface Offset (m)'
          READ*, SO
          PRINT*,'   Enter the Vertical Offset (m)'
          READ*,VO
          PRINT*,'   Enter the Length of the Riser (m)'
          READ*,LR
          DO 170, I=1, No_Calcs
             a(I) = SO
             b(I) = VO
             L(I) = LR
  170     CONTINUE
        ENDIF
C
```

```
      PRINT*,'   Enter an initial displaced length value'
      READ*, Ls_initial
      PRINT*,'   Is the Seabed Length Zero ?'
      READ*, Answer_sl
C
C     CALCULATION
C     ************************************************************
C
      No_Incs = (Final_H - Initial_H)/Inc_H
C
      IF (Answer_sl.EQ.'N')THEN
        DO 180, I=1, No_Calcs
          DO 190, J=0, 500, 1
            Ls(I) = Ls_initial - (J*5)
            as(I) = a(I) - (L(I) - Ls(I))
C
C.....      Subroutine calculates the horizontal componenet of
C           riser tension by using an iterative technique
            CALL HORIZ_TENSION(I, as, b, Ls, w, Inc_H, No_Incs,
     *                         Initial_H, HTension, LHS, RHS,
     *                         DIFFERENCE, Lamda, Ic, dydx)
C
            Slope(J) = dydx(I)
            Ls_Array(J) = Ls(I)
            as_Array(J) = as(I)
            IF (Slope(J).GT.0.0.AND.Slope(J-1).LT.0.0) THEN
              RIGHT_Ls = Ls_Array(J)
              LEFT_Ls = Ls_Array(J-1)
              MID_Ls = (RIGHT_Ls - LEFT_Ls)/2 + LEFT_Ls
              Ls(I) = MID_Ls
              as(I) = a(I) - (L(I) - Ls(I))
C
C.....        Subroutine calculates the horizontal componenet of
C             riser tension by using an iterative technique
              CALL HORIZ_TENSION(I, as, b, Ls, w, Inc_H, No_Incs,
     *                           Initial_H, HTension, LHS, RHS,
     *                           DIFFERENCE, Lamda, Ic, dydx)
C
              MID_Slope = dydx(I)
              GO TO 200
            ENDIF
  190     CONTINUE
C
  200     D = ABS(MID_Slope)
C
  210     IF (D.GT.0.00001) THEN
            IF (MID_Slope.GT.0.0) THEN
              LEFT_Ls = MID_Ls
            ELSE
              RIGHT_Ls = MID_Ls
            ENDIF
            MID_Ls = (RIGHT_Ls - LEFT_Ls)/2 + LEFT_Ls
            Ls(I) = MID_Ls
            as(I) = a(I) - (L(I) - Ls(I))
C
C.....      Subroutine calculates the horizontal componenet of
C           riser tension by using an iterative technique
            CALL HORIZ_TENSION(I, as, b, Ls, w, Inc_H, No_Incs,
     *                         Initial_H, HTension, LHS, RHS,
     *                         DIFFERENCE, Lamda, Ic, dydx)
C
            MID_Slope = dydx(I)
            D = ABS(MID_Slope)
            GO TO 210
          ENDIF
  180   CONTINUE
```

```
      ELSE
        I=1
        Ls(I) = L(I)
        as(I) = a(I)
C
C.....   Subroutine calculates the horizontal componenet of
C        riser tension by using an iterative technique
        CALL HORIZ_TENSION(I, as, b, Ls, w, Inc_H, No_Incs,
     *                     Initial_H, HTension, LHS, RHS,
     *                     DIFFERENCE, Lamda, Ic, dydx)
C
      ENDIF
C
C     TEXT OUTPUT
C     ************************************************************
C
      DO 220, I=1, No_Calcs
        PRINT 3
        WRITE (2,3)
        PRINT 4, I
        WRITE (2,4) I
        PRINT 5, a(I)
        WRITE (2,5) a(I)
        PRINT 6, as(I)
        WRITE (2,6) as(I)
        PRINT 7, b(I)
        WRITE (2,7) b(I)
        PRINT 8, L(I)
        WRITE (2,8) L(I)
        PRINT 9, Ls(I)
        WRITE (2,9) Ls(I)
        PRINT 11, w(I)
        WRITE (2,11) w(I)
        PRINT 12, HTension(I)
        WRITE (2,12) HTension(I)
        PRINT 13, LHS(I)
        WRITE (2,13) LHS(I)
        PRINT 14, RHS(I)
        WRITE (2,14) RHS(I)
        PRINT 16, DIFFERENCE(I)
        WRITE (2,16) DIFFERENCE(I)
        PRINT 17, Lamda(I)
        WRITE (2,17) Lamda(I)
        PRINT 18, Ic(I)
        WRITE (2,18) Ic(I)
        PRINT 19, dydx(I)
        WRITE (2,19) dydx(I)
  220 CONTINUE
C
      CLOSE (2)
      STOP
C
C     FORMAT STATEMENTS
C     ************************************************************
C
    2 FORMAT (A10)
    3 FORMAT (1H0,1X,'   ---------------------------------',
     *                '---------')
    4 FORMAT (1H0,1X,'CATENARY NO. ',I2)
    5 FORMAT (1H0,1X,'   Horizontal Surface Offset = ',F6.1,' m')
    6 FORMAT (1H0,1X,'   Suspended Horiz Surface Offset = ',F6.1,' m')
    7 FORMAT (1H0,1X,'   Sea Depth = ',F6.1,' m')
    8 FORMAT (1H0,1X,'   Total Riser Length = ',F6.1,' m')
    9 FORMAT (1H0,1X,'   Suspended Riser Length = ',F6.1,' m')
   11 FORMAT (1H0,1X,'   Submerged Weight = ',F6.1,' N/m')
   12 FORMAT (1H0,1X,'   Horizontal Tension Constant = ',F12.3,' N')
```

```
   13   FORMAT (1H0,1X,'   LHS = ',F17.1,' N2')
   14   FORMAT (1H0,1X,'   RHS = ',F17.1,' N2')
   16   FORMAT (1H0,1X,'   % Difference = ',D14.7)
   17   FORMAT (1H0,1X,'   Lamda = ',F6.4)
   18   FORMAT (1H0,1X,'   Integration Constant = ',D14.7)
   19   FORMAT (1H0,1X,'   Slope at x=0 = ',D14.7)
        END
C
C       SUBROUTINES
C       ***********************************************************
C
        SUBROUTINE HORIZ_TENSION(I, as, b, Ls, w, Inc_H, No_Incs,
     *    Initial_H, HTension, LHS, RHS, DIFFERENCE, Lamda, Ic, dydx)
C
C       This subroutine calculates the Horizontal Tension for
C       a given suspended length by using an iterative technique.
C
        DOUBLE PRECISION H(0:100000), Lbi(0:100000)
        DOUBLE PRECISION as(100), b(100), Ls(100), w(100)
        DOUBLE PRECISION Lamda(100), Ic(100), dydx(100)
        DOUBLE PRECISION HTension(100), LHS(100), RHS(100)
        DOUBLE PRECISION DIFFERENCE(100)
        DOUBLE PRECISION Lb, LEFT_Lbi, RIGHT_Lbi, MID_Lbi
        DOUBLE PRECISION MID_H, LEFT_H, RIGHT_H
        DOUBLE PRECISION F
C
        Lb = ((Ls(I)**2 - b(I)**2)*(w(I)**2))/4
C       PRINT*, Lb
C
        DO 400, J=0, No_Incs
           H(J) = (J*Inc_H) + Initial_H
C          PRINT*, H(J)
           Lbi(J) = (H(J)**2)*((SINH((w(I)*as(I))/(2*H(J))))**2)
C          PRINT*, Lbi(J)
C
C          PRINT*, Lbi(J)
C
           IF((Lb - Lbi(J)).GT.0.0.AND.(Lb - Lbi(J-1)).LT.0.0)THEN
             LEFT_H = H(J-1)
             RIGHT_H = H(J)
             MID_H = (RIGHT_H - LEFT_H)/2 + LEFT_H
             MID_Lbi = (MID_H**2)*((SINH((w(I)*as(I))/(2*MID_H)))**2)
             LEFT_Lbi = Lbi(J-1)
             RIGHT_Lbi = Lbi(J)
             GO TO 410
           ENDIF
  400   CONTINUE
C
  410   DIFFERENCE(I) = (ABS(Lb - MID_Lbi)/Lb)*100
C
  420   IF(DIFFERENCE(I).GT.0.000001) THEN
          IF((Lb - MID_Lbi).GT.0.0) THEN
            RIGHT_H = MID_H
          ELSE
            LEFT_H = MID_H
          ENDIF
          MID_H = (RIGHT_H - LEFT_H)/2 + LEFT_H
          MID_Lbi = (MID_H**2)*((SINH((w(I)*as(I))/(2*MID_H)))**2)
          DIFFERENCE(I) = (ABS(Lb - MID_Lbi)/Lb)*100
          GO TO 420
          ENDIF
C
        HTension(I) = MID_H
        RHS(I) = (HTension(I)**2)*((SINH((w(I)*as(I))/
     *           (2*HTension(I))))**2)
        LHS(I) = Lb
        Lamda(I) = (w(I)*as(I))/(2*HTension(I))
        F = (w(I)*b(I))/(2*HTension(I)*SINH(Lamda(I)))
```

```
      Ic(I) = Log(F + SQRT((F**2) + 1)) - Lamda(I)
      dydx(I) = SINH(Ic(I))
C
      RETURN
      END
C
C     ****************************************************************
```

```
      PROGRAM Displacement2
C
C     This FORTRAN computer program calculates the Horizontal Tension
C     and Suspended Riser Length for a displaced catenary riser.
C     (Increase in suspended length)
C
C     Program written by James Dingwall
C
C
C     NOMENCLATURE
C     ************************************************************
C
C     a          Horizontal Surface Offset
C     as         Suspended Horizontal Surface Offset
C     ax         Horizontal Surface Offset
C     b          Sea Depth (vertical offset)
C     by         Sea Depth (vertical offset)
C     H          Horizontal Tension Constant
C     HTension   Horizontal Tension Constant
C     Length     Total Length of Riser
C     L          Total Length of Riser
C     Ls         Suspended Length of Riser
C     L          Length of Riser
C     w          Submerged Weight
C     Ic         Integration Constant
C     dydx       Slope of Riser at x
C
C     SPECIFICATION STATEMENTS
C     ************************************************************
C
      INTEGER Final_H, Initial_H, Inc_H, No_Incs
C
      DOUBLE PRECISION a(10), b(10), L(10), w(10)
      DOUBLE PRECISION SO, VO, LR, SW, Lsi
      DOUBLE PRECISION as(100), Ls(100), Lamda(100), Ic(100), dydx(100)
      DOUBLE PRECISION Slope(0:1000), Ls_Array(0:1000), as_Array(0:1000)
      DOUBLE PRECISION HTension(100), LHS(100), RHS(100), DIFFERENCE(100)
      DOUBLE PRECISION LEFT_Ls, RIGHT_Ls, MID_Ls, MID_Slope, D
C
      PARAMETER (Initial_H=10000, Final_H=100000000, Inc_H=10000)
C
      CHARACTER*7 FILE
      CHARACTER*10 OUTFILE
      CHARACTER*6 Answer
      CHARACTER*1 Answer_sl
C
      PRINT*,'   Enter the Output Filename'
      READ (5,1) FILE
    1 FORMAT (A10)
C
      WRITE (OUTFILE,2)FILE
      OPEN (UNIT=2, FILE=OUTFILE, STATUS='NEW')
C
C     INPUT
C     ************************************************************
C
      PRINT*,'   Select the catenary parameter to be varied',
     *       ' (ax, by, Length or Weight)'
      READ*, Answer
      PRINT*,'   Enter the no of Calculations'
      READ*, No_Calcs
C
      IF(Answer.EQ.'ax    ') THEN
        DO 100, I=1, No_Calcs
          PRINT*,'   Enter the Horizontal Surface Offset (m)',I
```

```
            READ*, a(I)
  100     CONTINUE
          PRINT*,'   Enter the Vertical Offset (m)'
          READ*, VO
          PRINT*,'   Enter the Length of the Riser (m)'
          READ*,LR
          PRINT*,'   Enter the Submerged Unit Weight (N/m)'
          READ*,SW
          DO 110, I=1, No_Calcs
             b(I) = VO
             L(I) = LR
             w(I) = SW
  110     CONTINUE
C
        ELSEIF(Answer.EQ.'by    ') THEN
          DO 120, I=1, No_Calcs
             PRINT*,'   Enter the Vertical Offset (m)',I
             READ*, b(I)
  120     CONTINUE
          PRINT*,'   Enter the Horizontal Surface Offset (m)'
          READ*, SO
          PRINT*,'   Enter the Length of the Riser (m)'
          READ*,LR
          PRINT*,'   Enter the Submerged Unit Weight (N/m)'
          READ*,SW
          DO 130, I=1, No_Calcs
             a(I) = SO
             L(I) = LR
             w(I) = SW
  130     CONTINUE
C
        ELSEIF(Answer.EQ.'Length') THEN
          DO 140, I=1, No_Calcs
             PRINT*,'   Enter the Length of the Riser (m)',I
             READ*, L(I)
  140     CONTINUE
          PRINT*,'   Enter the Horizontal Surface Offset (m)'
          READ*, SO
          PRINT*,'   Enter the Vertical Offset (m)'
          READ*,VO
          PRINT*,'   Enter the Submerged Unit Weight (N/m)'
          READ*,SW
          DO 150, I=1, No_Calcs
             a(I) = SO
             b(I) = VO
             w(I) = SW
  150     CONTINUE
C
        ELSE
          DO 160, I=1, No_Calcs
             PRINT*,'   Enter the Submerged Unit Weight (N/m)',I
             READ*, w(I)
  160     CONTINUE
          PRINT*,'   Enter the Horizontal Surface Offset (m)'
          READ*, SO
          PRINT*,'   Enter the Vertical Offset (m)'
          READ*,VO
          PRINT*,'   Enter the Length of the Riser (m)'
          READ*,LR
          DO 170, I=1, No_Calcs
             a(I) = SO
             b(I) = VO
             L(I) = LR
  170     CONTINUE
        ENDIF
C
```

```
      PRINT*,'   Enter an initial displaced length value'
      READ*, Lsi
      PRINT*,'   Is the Seabed Length Zero ?'
      READ*, Answer_sl
C
C     CALCULATION
C     ***********************************************************
C
      No_Incs = (Final_H - Initial_H)/Inc_H
C
      IF(Answer_sl.EQ.'N')THEN
        DO 180, I=1, No_Calcs
          DO 190, J=0, 500, 1
            Ls(I) = Lsi + (J*5)
            PRINT*,Ls(I)
            as(I) = a(I) - (L(I) - Ls(I))
C
C.....      Subroutine calculates the horizontal component of
C           riser tension by using an iterative technique
            CALL HORIZ_TENSION(I, as, b, Ls, w, Inc_H, No_Incs,
     *                         Initial_H, HTension, LHS, RHS,
     *                         DIFFERENCE, Lamda, Ic, dy/dx)
C
            Slope(J) = dydx(I)
            PRINT*, Slope(J)
            Ls_Array(J) = Ls(I)
            as_Array(J) = as(I)
            IF(Slope(J).LT.0.0.AND.Slope(J-1).GT.0.0) THEN
              RIGHT_Ls = Ls_Array(J)
              LEFT_Ls = Ls_Array(J-1)
              MID_Ls = (RIGHT_Ls - LEFT_Ls)/2 + LEFT_Ls
              Ls(I) = MID_Ls
              PRINT*,Ls(I)
              as(I) = a(I) - (L(I) - Ls(I))

C.....        Subroutine calculates the horizontal component of
C             riser tension by using an iterative technique
              CALL HORIZ_TENSION(I, as, b, Ls, w, Inc_H, No_Incs,
     *                           Initial_H, HTension, LHS, RHS,
     *                           DIFFERENCE, Lamda, Ic, dy/dx)

              MID_Slope = dydx(I)
              GO TO 200
            ENDIF
  190     CONTINUE
C
  200     D = ABS(MID_Slope)
C
  210     IF(D.GT.0.00001) THEN
            IF(MID_Slope.GT.0.0) THEN
              LEFT_Ls = MID_Ls
            ELSE
              RIGHT_Ls = MID_Ls
            ENDIF
            MID_Ls = (RIGHT_Ls - LEFT_Ls)/2 + LEFT_Ls
            Ls(I) = MID_Ls
            as(I) = a(I) - (L(I) - Ls(I))

C.....      Subroutine calculates the horizontal component of
C           riser tension by using an iterative technique
            CALL HORIZ_TENSION(I, as, b, Ls, w, Inc_H, No_Incs,
     *                         Initial_H, HTension, LHS, RHS,
     *                         DIFFERENCE, Lamda, Ic, dy/dx)

            MID_Slope = dydx(I)
            D = ABS(MID_Slope)
```

```
              GO TO 210
            ENDIF
  180     CONTINUE
        ELSE
          I=1
          Ls(I) = L(I)
          as(I) = a(I)

C.....          Subroutine calculates the horizontal component of
C               riser tension by using an iterative technique
                CALL HORIZ_TENSION(I, as, b, Ls, w, Inc_H, No_Incs,
     *                             Initial_H, HTension, LHS, RHS,
     *                             DIFFERENCE, Lamda, Ic, dy/dx)

        ENDIF
C
C       TEXT OUTPUT
C       ************************************************************
C
        DO 220, I=1, No_Calcs
           PRINT 3
           WRITE (2,3)
           PRINT 4, I
           WRITE (2,4) I
           PRINT 5, a(I)
           WRITE (2,5) a(I)
           PRINT 6, as(I)
           WRITE (2,6) as(I)
           PRINT 7, b(I)
           WRITE (2,7) b(I)
           PRINT 8, L(I)
           WRITE (2,8) L(I)
           PRINT 9, Ls(I)
           WRITE (2,9) Ls(I)
           PRINT 11, w(I)
           WRITE (2,11) w(I)
           PRINT 12, HTension(I)
           WRITE (2,12) HTension(I)
           PRINT 13, LHS(I)
           WRITE (2,13) LHS(I)
           PRINT 14, RHS(I)
           WRITE (2,14) RHS(I)
           PRINT 16, DIFFERENCE(I)
           WRITE (2,16) DIFFERENCE(I)
           PRINT 17, Lamda(I)
           WRITE (2,17) Lamda(I)
           PRINT 18, Ic(I)
           WRITE (2,18) Ic(I)
           PRINT 19, dydx(I)
           WRITE (2,19) dydx(I)
  220   CONTINUE
C
        CLOSE (2)
        STOP
C
C       FORMAT STATEMENTS
C       ************************************************************
C
    2   FORMAT (A10)
    3   FORMAT (1H0,1X,'   ---------------------------------',
     *              '---------')
    4   FORMAT (1H0,1X,'CATENARY NO. ',I2)
    5   FORMAT (1H0,1X,'   Horizontal Surface Offset = ',F6.1,' m')
    6   FORMAT (1H0,1X,'   Suspended Horiz Surface Offset = ',F6.1,' m')
    7   FORMAT (1H0,1X,'   Sea Depth = ',F6.1,' m')
    8   FORMAT (1H0,1X,'   Total Riser Length = ',F6.1,' m')
```

```
    9   FORMAT (1H0,1X,'   Suspended Riser Length = ',F6.1,' m')
   11   FORMAT (1H0,1X,'   Submerged Weight = ',F6.1,' N/m')
   12   FORMAT (1H0,1X,'   Horizontal Tension Constant = ',F12.3,' N')
   13   FORMAT (1H0,1X,'   LHS = ',F17.1,' N2')
   14   FORMAT (1H0,1X,'   RHS = ',F17.1,' N2')
   16   FORMAT (1H0,1X,'   % Difference = ',D14.7)
   17   FORMAT (1H0,1X,'   Lamda = ',F6.4)
   18   FORMAT (1H0,1X,'   Integration Constant = ',D14.7)
   19   FORMAT (1H0,1X,'   Slope at x=0 = ',D14.7)
        END
C
        SUBROUTINES
C       ************************************************************
C
        SUBROUTINE HORIZ_TENSION(I, as, b, Ls, w, Inc_H, No_Incs,
     *    Initial_H, HTension, LHS, RHS, DIFFERENCE, Lamda, Ic, dydx)
C
C       This subroutine calculates the Horizontal Tension for
C       a given suspended length by using an iterative technique.
C
        DOUBLE PRECISION H(0:100000), Lbi(0:100000)
        DOUBLE PRECISION as(100), b(100), Ls(100), w(100)
        DOUBLE PRECISION Lamda(100), Ic(100), dydx(100)
        DOUBLE PRECISION HTension(100), LHS(100), RHS(100)
        DOUBLE PRECISION DIFFERENCE(100)
        DOUBLE PRECISION Lb, LEFT_Lbi, RIGHT_Lbi, MID_Lbi
        DOUBLE PRECISION MID_H, LEFT_H, RIGHT_H
        DOUBLE PRECISION F
C
        Lb = ((Ls(I)**2 - b(I)**2)*(w(I)**2))/4
C       PRINT*, Lb
C
        DO 400, J=0, No_Incs
           H(J) = (J*Inc_H) + Initial_H
C          PRINT*, H(J)
           Lbi(J) = (H(J)**2)*((SINH((w(I)*as(I))/(2*H(J))))**2)
C          PRINT*, Lbi(J)
C
           IF((Lb - Lbi(J)).GT.0.0.AND.(Lb - Lbi(J-1)).LT.0.0)THEN
             LEFT_H = H(J-1)
             RIGHT_H = H(J)
             MID_H = (RIGHT_H - LEFT_H)/2 + LEFT_H
             MID_Lbi = (MID_H**2)*((SINH((w(I)*as(I))/(2*MID_H)))**2)
             LEFT_Lbi = Lbi(J-1)
             RIGHT_Lbi = Lbi(J)
             GO TO 410
           ENDIF
  400   CONTINUE
C
  410   DIFFERENCE(I) = (ABS(Lb - MID_Lbi)/Lb)*100
C
  420   IF(DIFFERENCE(I).GT.0.000001) THEN
          IF((Lb - MID_Lbi).GT.0.0) THEN
            RIGHT_H = MID_H
          ELSE
            LEFT_H = MID_H
          ENDIF
          MID_H = (RIGHT_H - LEFT_H)/2 + LEFT_H
          MID_Lbi = (MID_H**2)*((SINH((w(I)*as(I))/(2*MID_H)))**2)
          DIFFERENCE(I) = (ABS(Lb - MID_Lbi)/Lb)*100
          GO TO 420
          ENDIF
C
        HTension(I) = MID_H
        RHS(I) = (HTension(I)**2)*((SINH((w(I)*as(I))/
     *           (2*HTension(I))))**2)
```

```
      LHS(I) = Lb
      Lamda(I) = (w(I)*as(I))/(2*HTension(I))
      F = (w(I)*b(I))/(2*HTension(I)*SINH(Lamda(I)))
      Ic(I) = Log(F + SQRT((F**2) + 1)) - Lamda(I)
      dydx(I) = SINH(Ic(I))
C
      RETURN
      END
C
C     ***************************************************************
```

Appendix C

FORTRAN Program Lists for a Catenary Riser
Dynamic Analysis and Validation.

```
      PROGRAM Natural_Period
C
C     This FORTRAN computer program calculates a natural
C     period sprectrum for a catenary riser of specified
C     profile and weight using a FD nummerical technique.
C     It also plots the first six mode shapes
C
C     Program written by James Dingwall
C
C
C     NOMENCLATURE
C     ************************************************************
C
C     A          Matrix
C     add_mass   Unit added mass
C     ax         Horizontal surface offset
C     B          Matrix
C     buoy       Unit buoyancy
C     by         Vertical offset/sea depth
C     area       Steel area of carrier pipe
C     chord      Catenary profile chord length
C     ds         Distance between nodes
C     dydx       Slope of riser at x
C     Em         Elasticity modulus
C     H          Horizontal tension constant
C     Ht         Horizontal tension constant
C     Ic         Integration constant
C     length     Length of riser
C     od         Carrier pipe outer diameter
C     R          Eigenvalues
C     water_d    Sea Water density
C     S          Distance along the riser
C     sub_w      Submerged weight
C     t          Carrier pipe wall thickness
C     Tension    Axial tension
C     Tp         Vibration period
C     V          Eigenvectors
C     w          Vibration frequency
C     weight     Unit weight
C     Xn         Horizontal node coordinate
C     Yn         Vertical node coordinate
C
C     SPECIFICATION STATEMENTS
C     ************************************************************
C
      INTEGER Final_H, N, Nodes, Nmax, column, L, M
C
      REAL od, buoy, mass, weight, area
      REAL water_d, add_mass
C
      DOUBLE PRECISION ax, by, length, Lamda, Ic, dydx
      DOUBLE PRECISION pi, Ht, LHS, RHS, Difference
      DOUBLE PRECISION sub_w, ds, Em, AE
C
      PARAMETER (Water_d=1025)
      PARAMETER (Em=207000000000, pi=3.141592654)
      PARAMETER (Nmax=500, IA=Nmax, IV=Nmax)
      PARAMETER (Yaxis=0.8, Tmax=20.0, Tinc=1.0)
      PARAMETER (Xmax=2000.0)
      PARAMETER (Initial_H = 10000, Final_H = 6000000)
      PARAMETER (Inc_H = 1000)
C
      DOUBLE PRECISION Gn(Nmax), Sn(0:Nmax), Xn(0:Nmax), Yn(0:Nmax)
      DOUBLE PRECISION Gt(Nmax), St(Nmax), Xt(Nmax), Tension(Nmax)
      DOUBLE PRECISION ax_1(Nmax), ax_2(Nmax), ax_3(Nmax)
      DOUBLE PRECISION ax_4(Nmax), ax_5(Nmax), ax_6(Nmax)
```

```
      DOUBLE PRECISION ay_1(Nmax), ay_2(Nmax), ay_3(Nmax)
      DOUBLE PRECISION ay_4(Nmax), ay_5(Nmax), ay_6(Nmax)
      DOUBLE PRECISION A(IA,Nmax), B(Nmax,Nmax)
      DOUBLE PRECISION E(Nmax), R(Nmax), V(IV,Nmax), Vmax(Nmax)
      DOUBLE PRECISION Vx(Nmax,Nmax), Vy(Nmax,Nmax)
C
      REAL Xn_plot(Nmax), Yn_plot(Nmax)
      REAL Y_plot1(Nmax), X_plot1(Nmax)
      REAL Y_plot2(Nmax), X_plot2(Nmax)
      REAL Y_plot3(Nmax), X_plot3(Nmax)
      REAL Y_plot4(Nmax), X_plot4(Nmax)
      REAL Y_plot5(Nmax), X_plot5(Nmax)
      REAL Y_plot6(Nmax), X_plot6(Nmax)
      REAL X_surface(3), Y_surface(3)
      REAL X_vert(3), Y_vert(3)
      REAL w(Nmax), Tp(Nmax), Y(Nmax)
      REAL xT_verif1(3), xT_verif2(3)
      REAL xT_verif3(3), xT_verif4(3)
      REAL xT_verif5(3), xT_verif6(3)
      REAL xT_verif7(3), xT_verif8(3)
      REAL xT_verif9(3), xT_verif10(3)
      REAL y_verif(3)
C
      CHARACTER*7 FILE
      CHARACTER*10 OUTFILE
      CHARACTER*1 Ans_matrix
      CHARACTER*1 Ans_coef
      CHARACTER*1 Ans_tension
      CHARACTER*1 Ans_vect
      CHARACTER*1 Ans_addmass
      CHARACTER*1 Ans_sp
      CHARACTER*1 Ans_verif
      CHARACTER*36 CAP1
      CHARACTER*20 CAP2
      CHARACTER*24 CAP3
      CHARACTER*23 CAP4
      CHARACTER*29 CAP5
      CHARACTER*34 CAP6
      CHARACTER*23 CAP7
      CHARACTER*19 CAP8
      CHARACTER*10 CAP9
C
      PRINT*,'   Enter the Output Filename'
      READ (5,1) FILE
    1 FORMAT (A10)
C
      WRITE (OUTFILE,2)FILE
      OPEN (UNIT=2, FILE=OUTFILE, STATUS='NEW')
C
C     INPUT
C     ************************************************************
C
  100 PRINT*,'   Enter the Horizontal Surface Offset (m)'
      READ*,ax
      PRINT*,'   Enter the Sea Depth (m)'
      READ*,by
      PRINT*,'   Enter the Length of the Riser (m)'
      READ*,length
      PRINT*,'   Enter the Outer Diameter of the Carrier Pipe (m)'
      READ*,od
      PRINT*,'   Enter the Risers Unit Mass (kg/m)'
      READ*,mass
      PRINT*,'   Enter the Risers Submerged Unit Weight (N/m)'
      READ*,sub_w
      PRINT*,'   Enter the Risers Total Cross-Sectional Area (m2)'
      READ*,area
```

```
      PRINT*,'   Enter the No of Nodes required'
      READ*,Nodes
C
      IF (Nodes.GT.Nmax) THEN
        PRINT*,'   Too many nodes ! try again'
        GOTO 100
      ENDIF
C
      PRINT*,'  Would you like the risers coordinates and ',
     *          'tensions to be printed out (y/n)'
      READ*, Ans_tension
      PRINT*,'  Would you like the coefficients to be printed out ',
     *          '(y/n)'
      READ*, Ans_coef
      PRINT*,'  Would you like the matrix to be printed out ',
     *          '(y/n)'
      READ*, Ans_matrix
      IF (Ans_matrix.EQ.'y') THEN
        PRINT*,'   Enter the matrix column to be printed out'
        READ*, column
      ENDIF
      PRINT*,'  Would you like the eigenvectors to be printed out ',
     *          '(y/n)'
      READ*, Ans_vect
      PRINT*,'  Would you like to include added mass (y/n) '
      READ*, Ans_addmass
      PRINT*,'  Would you like a graphical output (y/n)'
      READ*, Ans_sp
      PRINT*,'  Would you like to add the verification data (y/n)'
      READ*, Ans_verif
      IF (Ans_verif.EQ.'y') THEN
        PRINT*,'   Enter the fundamental frequency period '
        READ*, T_verif1
        PRINT*,'   Enter frequency period 2'
        READ*, T_verif2
        PRINT*,'   Enter frequency period 3'
        READ*, T_verif3
        PRINT*,'   Enter frequency period 4'
        READ*, T_verif4
        PRINT*,'   Enter frequency period 5'
        READ*, T_verif5
        PRINT*,'   Enter frequency period 6'
        READ*, T_verif6
        PRINT*,'   Enter frequency period 7'
        READ*, T_verif7
        PRINT*,'   Enter frequency period 8'
        READ*, T_verif8
        PRINT*,'   Enter frequency period 9'
        READ*, T_verif9
        PRINT*,'   Enter frequency period 10'
        READ*, T_verif10
C
        CALL VERIF_PLOT(T_verif1, T_verif2, T_verif3, T_verif4,
     *                  T_verif5, T_verif6, T_verif7, T_verif8,
     *               T_verif9, T_verif10, xT_verif1, xT_verif2,
     *              xT_verif3, xT_verif4, xT_verif5, xT_verif6,
     *             xT_verif7, xT_verif8, xT_verif9, xT_verif10,
     *             yaxis, y_verif)
      ENDIF
C
C     CALCULATION
C     ***********************************************************
C
      No_Incs = (Final_H - Initial_H)/Inc_H
C
      IF (Ans_addmass.EQ.'y') THEN
```

```
          add_mass = water_d*(pi/4)*(od**2)
        ELSE
          add_mass = 0.0
        ENDIF
        AE = area*Em
        chord = SQRT((ax**2) + (by**2))
C
C..... Subroutine calculates the horizontal component of riser tension
C       by using an iterative technique
        CALL HORIZ_TENSION(ax, by, length, sub_w, Inc_H, No_Incs, Initial_H,
     *                     Ht, LHS, RHS, Difference, Lamda, Ic, dydx)
C
C..... The following calculations determine the catenary riser's nodal
C       x-y coordinates as well as the axial tension distribution on an
C       elemental basis
C
        ds = length/(Nodes + 1)
        Sn(0) = 0.0
        Xn(0) = 0.0
        Yn(0) = 0.0
        Xn_plot(1) = 0.0
        Yn_plot(1) = 0.0
        DO 110 I=2, 2*(Nodes+1), 2
           Sn(I) = Sn(I-2) + ds
           Gn(I) = ((Sub_w*Sn(I))/Ht) + SINH(Ic)
           Xn(I) = (Ht/Sub_w)*(log(Gn(I) + SQRT((Gn(I)**2) + 1)) - Ic)
           Yn(I) = (Ht/Sub_w)*(COSH(((Sub_w*Xn(I))/Ht) + Ic) - COSH(Ic))
  110   CONTINUE
        Xn_plot(2) = Xn(2)
        Yn_plot(2) = Yn(2)
        m = 1
        DO 120 I=3, (Nodes+2)
           Xn_plot(I) = Xn(I+m)
           Yn_plot(I) = Yn(I+m)
           m = m + 1
  120   CONTINUE
        St(1) = ds/2
        Gt(1) = ((Sub_w*St(1))/Ht) + SINH(Ic)
        Xt(1) = (Ht/Sub_w)*(log(Gt(1) + SQRT((Gt(1)**2) + 1)) - Ic)
        Tension(1) = Ht*COSH(((Sub_w*Xt(1))/Ht) + Ic)
        DO 130 I=3, (2*Nodes)+1, 2
           St(I) = St(I-2) + ds
           Gt(I) = ((Sub_w*St(I))/Ht) + SINH(Ic)
           Xt(I) = (Ht/Sub_w)*(log(Gt(I) + SQRT((Gt(I)**2) + 1)) - Ic)
           Tension(I) = Ht*COSH(((Sub_w*Xt(I))/Ht) + Ic)
  130   CONTINUE
C
C..... The following calculations determine the components of the
C       dynamic matrix
C
        DO 140 I=2, (2*Nodes), 2
           J = I - 1
           ax_1(I) = Tension(J) + (AE/(ds**2))*((Xn(I) - Xn(I-2))**2)
           ax_2(I) = (AE/(ds**2))*(Xn(I) - Xn(I-2))*(Yn(I) - Yn(I-2))
           ax_3(I) = -(Tension(J) + Tension(J+2)) - (AE/(ds**2))*
     *               ((Xn(I+2) - Xn(I))**2) - (AE/(ds**2))*
     *               ((Xn(I) - Xn(I-2))**2)
           ax_4(I) = - (AE/(ds**2))*(Xn(I+2) - Xn(I))*(Yn(I+2) - Yn(I))
     *               - (AE/(ds**2))*(Xn(I) - Xn(I-2))*(Yn(I) - Yn(I-2))
           ax_5(I) = Tension(J+2) + (AE/(ds**2))*((Xn(I+2) - Xn(I))**2)
           ax_6(I) = (AE/(ds**2))*(Xn(I+2) - Xn(I))*(Yn(I+2) - Yn(I))
C
           ay_1(I) = (AE/(ds**2))*(Xn(I) - Xn(I-2))*(Yn(I) - Yn(I-2))
           ay_2(I) = Tension(J) + (AE/(ds**2))*((Yn(I) - Yn(I-2))**2)
           ay_3(I) = - (AE/(ds**2))*(Xn(I+2) - Xn(I))*(Yn(I+2) - Yn(I))
     *               - (AE/(ds**2))*(Xn(I) - Xn(I-2))*(Yn(I) - Yn(I-2))
```

```
            ay_4(I) = -(Tension(J) + Tension(J+2)) - (AE/(ds**2))*
     *                ((Yn(I+2) - Yn(I))**2) - (AE/(ds**2))*
     *                ((Yn(I) - Yn(I-2))**2)
            ay_5(I) = (AE/(ds**2))*(Xn(I+2) - Xn(I))*(Yn(I+2) - Yn(I))
            ay_6(I) = Tension(J+2) + (AE/(ds**2))*((Yn(I+2) - Yn(I))**2)
  140    CONTINUE
C
         I = 2
         M = 1
         L = I - 1
         B(L,M) = ax_3(I)
         B(L+1,M) = ay_3(I)
         B(L,M+1) = ax_4(I)
         B(L+1,M+1) = ay_4(I)
         B(L,M+2) = ax_5(I)
         B(L+1,M+2) = ay_5(I)
         B(L,M+3) = ax_6(I)
         B(L+1,M+3) = ay_6(I)
C
         M = 1
         DO 150, I=4, (2*Nodes)-2, 2
            L = I - 1
            B(L,M) = ax_1(I)
            B(L+1,M) = ay_1(I)
            B(L,M+1) = ax_2(I)
            B(L+1,M+1) = ay_2(I)
            B(L,M+2) = ax_3(I)
            B(L+1,M+2) = ay_3(I)
            B(L,M+3) = ax_4(I)
            B(L+1,M+3) = ay_4(I)
            B(L,M+4) = ax_5(I)
            B(L+1,M+4) = ay_5(I)
            B(L,M+5) = ax_6(I)
            B(L+1,M+5) = ay_6(I)
            M = M + 2
  150    CONTINUE
C
         I = (2*Nodes)
         M = (2*Nodes) - 3
         L = I - 1
         B(L,M) = ax_1(I)
         B(L+1,M) = ay_1(I)
         B(L,M+1) = ax_2(I)
         B(L+1,M+1) = ay_2(I)
         B(L,M+2) = ax_3(I)
         B(L+1,M+2) = ay_3(I)
         B(L,M+3) = ax_4(I)
         B(L+1,M+3) = ay_4(I)
C
         DO 160 I=1, (2*Nodes)
            DO 170 J=1, (2*Nodes)
               A(I,J) = (-1/((mass+add_mass)*(ds**2)))*B(I,J)
  170       CONTINUE
  160    CONTINUE
         IFAIL = 1
         N = 2*Nodes
C
C..... NAG routine calculates the eigenvalues and eigenvectors
C        from the real symmetric dynamic matrix
         CALL F02ABF (A,IA,N,R,V,IV,E,IFAIL)
C
         IF (IFAIL.NE.0) THEN
           PRINT 4
           STOP
         ENDIF
C
```

```
C..... The following calculations determine the mode shapes for
C       the first six modes
C
        DO 180 K=1, N
           DO 190 J=1, N
              INa = J/2
              RNa = REAL(J)/2.0
              IF(RNa.GT.INa) THEN
                Vx(J,K) = V(J,K)
              ELSE
                Vy(J,K) = V(J,K)
              ENDIF
  190       CONTINUE
  180    CONTINUE
C
        X_plot1(1) = 0.0
        Y_plot1(1) = 0.0
        X_plot1(2) = Xn_plot(2) + 1000.0*Vx(1,1)
        Y_plot1(2) = Yn_plot(2) + 1000.0*Vy(2,1)
        m = 0
        DO 200 I=3, (Nodes+1)
           X_plot1(I) = Xn_plot(I) + 1000.0*Vx(I+m,1)
           Y_plot1(I) = Yn_plot(I) + 1000.0*Vy(I+m+1,1)
        m = m + 1
  200   CONTINUE
        X_plot1(Nodes+2) = Xn_plot(Nodes+2) + 0.0
        Y_plot1(Nodes+2) = Yn_plot(Nodes+2) + 0.0
C
        X_plot2(1) = 0.0
        Y_plot2(1) = 0.0
        X_plot2(2) = Xn_plot(2) + 1000.0*Vx(1,2)
        Y_plot2(2) = Yn_plot(2) + 1000.0*Vy(2,2)
        m = 0
        DO 210 I=3, (Nodes+1)
           X_plot2(I) = Xn_plot(I) + 1000.0*Vx(I+m,2)
           Y_plot2(I) = Yn_plot(I) + 1000.0*Vy(I+m+1,2)
        m = m + 1
  210   CONTINUE
        X_plot2(Nodes+2) = Xn_plot(Nodes+2) + 0.0
        Y_plot2(Nodes+2) = Yn_plot(Nodes+2) + 0.0
C
        X_plot3(1) = 0.0
        Y_plot3(1) = 0.0
        X_plot3(2) = Xn_plot(2) + 1000.0*Vx(1,3)
        Y_plot3(2) = Yn_plot(2) + 1000.0*Vy(2,3)
        m = 0
        DO 220 I=3, (Nodes+1)
           X_plot3(I) = Xn_plot(I) + 1000.0*Vx(I+m,3)
           Y_plot3(I) = Yn_plot(I) + 1000.0*Vy(I+m+1,3)
        m = m + 1
  220   CONTINUE
        X_plot3(Nodes+2) = Xn_plot(Nodes+2) + 0.0
        Y_plot3(Nodes+2) = Yn_plot(Nodes+2) + 0.0
C
        X_plot4(1) = 0.0
        Y_plot4(1) = 0.0
        X_plot4(2) = Xn_plot(2) + 1000.0*Vx(1,4)
        Y_plot4(2) = Yn_plot(2) + 1000.0*Vy(2,4)
        m = 0
        DO 230 I=3, (Nodes+1)
           X_plot4(I) = Xn_plot(I) + 1000.0*Vx(I+m,4)
           Y_plot4(I) = Yn_plot(I) + 1000.0*Vy(I+m+1,4)
        m = m + 1
  230   CONTINUE
        X_plot4(Nodes+2) = Xn_plot(Nodes+2) + 0.0
        Y_plot4(Nodes+2) = Yn_plot(Nodes+2) + 0.0
```

```
C
      X_plot5(1) = 0.0
      Y_plot5(1) = 0.0
      X_plot5(2) = Xn_plot(2) + 1000.0*Vx(1,5)
      Y_plot5(2) = Yn_plot(2) + 1000.0*Vy(2,5)
      m = 0
      DO 240 I=3, (Nodes+1)
         X_plot5(I) = Xn_plot(I) + 1000.0*Vx(I+m,5)
         Y_plot5(I) = Yn_plot(I) + 1000.0*Vy(I+m+1,5)
      m = m + 1
  240 CONTINUE
      X_plot5(Nodes+2) = Xn_plot(Nodes+2) + 0.0
      Y_plot5(Nodes+2) = Yn_plot(Nodes+2) + 0.0
C
      X_plot6(1) = 0.0
      Y_plot6(1) = 0.0
      X_plot6(2) = Xn_plot(2) + 1000.0*Vx(1,6)
      Y_plot6(2) = Yn_plot(2) + 1000.0*Vy(2,6)
      m = 0
      DO 250 I=3, (Nodes+1)
         X_plot6(I) = Xn_plot(I) + 1000.0*Vx(I+m,6)
         Y_plot6(I) = Yn_plot(I) + 1000.0*Vy(I+m+1,6)
      m = m + 1
  250 CONTINUE
      X_plot6(Nodes+2) = Xn_plot(Nodes+2) + 0.0
      Y_plot6(Nodes+2) = Yn_plot(Nodes+2) + 0.0
C
      DO 260 J=1, N
         w(J) = SQRT(R(J))
         Tp(J) = (2*pi)/w(J)
         Y(J) = Yaxis
  260 CONTINUE
C
C     TEXT OUTPUT
C     ************************************************************
C
      PRINT 5, ax
      WRITE (2,5) ax
      PRINT 6, by
      WRITE (2,6) by
      PRINT 7, length
      WRITE (2,7) length
      PRINT 8, od
      WRITE (2,8) od
      PRINT 9, Em
      WRITE (2,9) Em
      PRINT 10, area
      WRITE (2,10) area
      PRINT 11, AE
      WRITE (2,11) AE
      PRINT 12, mass
      WRITE (2,12) mass
      PRINT 13, add_mass
      WRITE (2,13) add_mass
      PRINT 14, sub_w
      WRITE (2,14) sub_w
      PRINT 15, Ht
      WRITE (2,15) Ht
      PRINT 16, Difference
      WRITE (2,16) Difference
      PRINT 17, Lamda
      WRITE (2,17) Lamda
      PRINT 18, Ic
      WRITE (2,18) Ic
      PRINT 19, dydx
      WRITE (2,19) dydx
```

```
      PRINT 20, Nodes
      WRITE (2,20) Nodes
      PRINT 21, ds
      WRITE (2,21) ds
      PRINT 22
      WRITE (2,22)
C
      IF (Ans_tension.EQ.'y') THEN
        PRINT 23
        WRITE (2,23)
        PRINT 24
        WRITE (2,24)
        DO 270 I=0, 2*(Nodes+1), 2
           PRINT 25, I, Sn(I), Xn(I), Yn(I)
           WRITE (2,25) I, Sn(I), Xn(I), Yn(I)
  270   CONTINUE
        PRINT 26
        WRITE (2,26)
        PRINT 27
        WRITE (2,27)
        PRINT 28
        WRITE (2,28)
        DO 280 I=1, (2*Nodes)+1, 2
           PRINT 29, I, St(I), Xt(I), Tension(I)
           WRITE (2,29) I, St(I), Xt(I), Tension(I)
  280   CONTINUE
      ENDIF
C
      IF (Ans_coef.EQ.'y') THEN
        PRINT 30
        WRITE (2,30)
        PRINT 31
        WRITE (2,31)
        PRINT 32
        WRITE (2,32)
        DO 290 I=2, N, 2
           PRINT 33, I, ax_1(I), ax_2(I), ax_3(I), ax_4(I), ax_5(I),
     *               ax_6(I)
           WRITE (2,33) I, ax_1(I), ax_2(I), ax_3(I), ax_4(I), ax_5(I),
     *                  ax_6(I)
  290   CONTINUE
        PRINT 34
        WRITE (2,34)
        PRINT 35
        WRITE (2,35)
        PRINT 36
        WRITE (2,36)
        DO 300 I=2, N, 2
           PRINT 37, I, ay_1(I), ay_2(I), ay_3(I), ay_4(I), ay_5(I),
     *               ay_6(I)
           WRITE (2,37) I, ay_1(I), ay_2(I), ay_3(I), ay_4(I),
     *                  ay_5(I), ay_6(I)
  300   CONTINUE
      ENDIF
C
      IF (Ans_matrix.EQ.'y') THEN
        PRINT 38
        WRITE (2,38)
        PRINT 39
        WRITE (2,39)
        DO 310 L=1, N
           PRINT 40, L, A(L,column), A(L,column+1), A(L,column+2),
     *               A(L,column+3), A(L,column+4)
           WRITE (2,40) L, A(L,column), A(L,column+1), A(L,column+2),
     *              A(L,column+3), A(L,column+4)
  310   CONTINUE
```

```
      ENDIF
C
      IF (Ans_vect.EQ.'y') THEN
        PRINT 41
        WRITE (2,41)
        PRINT 42
        WRITE (2,42)
        PRINT 43
        WRITE (2,43)
        DO 320 J=1, (N-1), 2
           PRINT 44, Vx(J,1), Vx(J,2), Vx(J,3), Vx(J,4),
     *                Vx(J,5), Vx(J,6)
           WRITE (2,44) Vx(J,1), Vx(J,2), Vx(J,3), Vx(J,4),
     *                  Vx(J,5), Vx(J,6)
  320     CONTINUE
        PRINT 45
        WRITE (2,45)
        PRINT 46
        WRITE (2,46)
        PRINT 47
        WRITE (2,47)
        DO 330 J=2, N, 2
           PRINT 48, Vy(J,1), Vy(J,2), Vy(J,3), Vy(J,4),
     *                Vy(J,5), Vy(J,6)
           WRITE (2,48) Vy(J,1), Vy(J,2), Vy(J,3), Vy(J,4),
     *                  Vy(J,5), Vy(J,6)
  330     CONTINUE
      ENDIF
C
      PRINT 49
      WRITE (2,49)
      PRINT 50
      WRITE (2,50)
      PRINT 51
      WRITE (2,51)
      DO 340 J=1, (N/2)
         PRINT 52, J, w(J), Tp(J)
         WRITE (2,52) J, w(J), Tp(J)
  340 CONTINUE
C
C     GRAPHICAL OUTPUT (SIMPLEPLOT)
C     *************************************************************
C
      IF (Ans_sp.EQ.'y') THEN
C
        X_surface(1) = 0.0
        Y_surface(1) = by
        X_surface(2) = 1000.0
        Y_surface(2) = by
        X_surface(3) = 2000.0
        Y_surface(3) = by
        X_vert(1) = ax
        Y_vert(1) = 0.0
        X_vert(2) = ax
        Y_vert(2) = 500.0
        X_vert(3) = ax
        Y_vert(3) = by
C
C..... Natural period spectrum
C
        CALL SCALES(0.0,Tmax,1,0.0,1.0,1)
        CALL PAGVW(2)
        CALL PAGE(29.7,21.0)
        CALL PAGMRG(1.0,1.0,1.0,4.0)
        CALL BOXPAG(.TRUE.)
        CALL PICSIZ(25.0,12.0)
```

```
          CALL BOXPIC(.TRUE.)
          CALL NEWPIC
          CALL AXSBDV('XC',0.0,Tinc)
          CALL AXIS7('XC','Natural Period (secs)')
          CALL AXCLR('YC',1)
          CALL AXSBDV('YC',0.0,0.5)
          CALL AXIS7('YC','     ')
          DO 350 J=1, (N/2)
             CALL DRAWLN(Tp(J),Y(J))
350       CONTINUE
          IF (Ans_verif.EQ.'y') THEN
            CALL BRKNCV(xT_verif1, y_verif,3,-2)
            CALL BRKNCV(xT_verif2, y_verif,3,-2)
            CALL BRKNCV(xT_verif3, y_verif,3,-2)
            CALL BRKNCV(xT_verif4, y_verif,3,-2)
            CALL BRKNCV(xT_verif5, y_verif,3,-2)
            CALL BRKNCV(xT_verif6, y_verif,3,-2)
            CALL BRKNCV(xT_verif7, y_verif,3,-2)
            CALL BRKNCV(xT_verif8, y_verif,3,-2)
            CALL BRKNCV(xT_verif9, y_verif,3,-2)
            CALL BRKNCV(xT_verif10, y_verif,3,-2)
            CALL DEFKEY(2,'T','R',2,26)
            CALL BOTHK7(0,16,' Classical Rod Theory (FD)')
            CALL BOTHK7(-2,16,' Blevin')
          ENDIF
          CALL DEFCAP(1,'O','L',9,40)
          WRITE (CAP1,90) ax
          WRITE (CAP2,91) by
          WRITE (CAP3,92) length
          WRITE (CAP4,93) mass
          WRITE (CAP5,94) add_mass
          WRITE (CAP6,95) Sub_w
          WRITE (CAP7,96) od
          WRITE (CAP8,97) Nodes
          WRITE (CAP9,98)
          CALL ADDCP7 (CAP1)
          CALL ADDCP7 (CAP2)
          CALL ADDCP7 (CAP3)
          CALL ADDCP7 (CAP4)
          CALL ADDCP7 (CAP5)
          CALL ADDCP7 (CAP6)
          CALL ADDCP7 (CAP7)
          CALL ADDCP7 (CAP8)
          CALL ADDCP7 (CAP9)
          CALL ENDPLT
C
C..... Fundamental mode
C
          CALL SCALES (0.0,Xmax,1,-200.0,1600.0,1)
          CALL PAGVW (2)
          CALL PAGE (29.7,21.0)
          CALL PAGMRG (1.0,1.0,1.0,2.0)
          CALL BOXPAG (.TRUE.)
          CALL PICSIZ (15.0,13.5)
          CALL NEWPIC
          CALL AXSBDV ('XC',0.0,200.0)
          CALL AXIS7 ('XC','X  (m)')
          CALL AXSBDV ('YC',0.0,200.0)
          CALL AXIS7 ('YC','Y  (m)')
          CALL BRKNCV (X_plot1,Y_plot1,(Nodes+2),0)
          CALL BRKNCV (Xn_plot,Yn_plot,(Nodes+2),-3)
          CALL BRKNCV (X_surface,Y_surface,3,3)
          CALL BRKNCV (X_vert,Y_vert,3,2)
          CALL DEFCAP (1,'H','C',1,20)
          CALL ADDCP7 ('Mode 1 - Fundamental')
          CALL ENDPLT
```

```
C
C..... Mode 2
C
          CALL SCALES (0.0,Xmax,1,-200.0,1600.0,1)
          CALL PAGVW (2)
          CALL PAGE (29.7,21.0)
          CALL PAGMRG (1.0,1.0,1.0,2.0)
          CALL BOXPAG (.TRUE.)
          CALL PICSIZ (15.0,13.5)
          CALL NEWPIC
          CALL AXSBDV ('XC',0.0,200.0)
          CALL AXIS7 ('XC','X  (m)')
          CALL AXSBDV ('YC',0.0,200.0)
          CALL AXIS7 ('YC','Y  (m)')
          CALL BRKNCV (X_plot2,Y_plot2,(Nodes+2),0)
          CALL BRKNCV (Xn_plot,Yn_plot,(Nodes+2),-3)
          CALL BRKNCV (X_surface,Y_surface,3,3)
          CALL BRKNCV (X_vert,Y_vert,3,2)
          CALL DEFCAP (1,'H','C',1,6)
          CALL ADDCP7 ('Mode 2')
          CALL ENDPLT
C
C..... Mode 3
C
          CALL SCALES (0.0,Xmax,1,-200.0,1600.0,1)
          CALL PAGVW (2)
          CALL PAGE (29.7,21.0)
          CALL PAGMRG (1.0,1.0,1.0,2.0)
          CALL BOXPAG (.TRUE.)
          CALL PICSIZ (15.0,13.5)
          CALL NEWPIC
          CALL AXSBDV ('XC',0.0,200.0)
          CALL AXIS7 ('XC','X  (m)')
          CALL AXSBDV ('YC',0.0,200.0)
          CALL AXIS7 ('YC','Y  (m)')
          CALL BRKNCV (X_plot3,Y_plot3,(Nodes+2),0)
          CALL BRKNCV (Xn_plot,Yn_plot,(Nodes+2),-3)
          CALL BRKNCV (X_surface,Y_surface,3,3)
          CALL BRKNCV (X_vert,Y_vert,3,2)
          CALL DEFCAP (1,'H','C',1,6)
          CALL ADDCP7 ('Mode 3')
          CALL ENDPLT
C
C..... Mode 4
C
          CALL SCALES (0.0,Xmax,1,-200.0,1600.0,1)
          CALL PAGVW (2)
          CALL PAGE (29.7,21.0)
          CALL PAGMRG (1.0,1.0,1.0,2.0)
          CALL BOXPAG (.TRUE.)
          CALL PICSIZ (15.0,13.5)
          CALL NEWPIC
          CALL AXSBDV ('XC',0.0,200.0)
          CALL AXIS7 ('XC','X  (m)')
          CALL AXSBDV ('YC',0.0,200.0)
          CALL AXIS7 ('YC','Y  (m)')
          CALL BRKNCV (X_plot4,Y_plot4,(Nodes+2),0)
          CALL BRKNCV (Xn_plot,Yn_plot,(Nodes+2),-3)
          CALL BRKNCV (X_surface,Y_surface,3,3)
          CALL BRKNCV (X_vert,Y_vert,3,2)
          CALL DEFCAP (1,'H','C',1,6)
          CALL ADDCP7 ('Mode 4')
          CALL ENDPLT
C
C..... Mode 5
C
```

```
            CALL SCALES (0.0,Xmax,1,-200.0,1600.0,1)
            CALL PAGVW (2)
            CALL PAGE (29.7,21.0)
            CALL PAGMRG (1.0,1.0,1.0,2.0)
            CALL BOXPAG (.TRUE.)
            CALL PICSIZ (15.0,13.5)
            CALL NEWPIC
            CALL AXSBDV ('XC',0.0,200.0)
            CALL AXIS7 ('XC','X  (m)')
            CALL AXSBDV ('YC',0.0,200.0)
            CALL AXIS7 ('YC','Y  (m)')
            CALL BRKNCV (X_plot5,Y_plot5,(Nodes+2),0)
            CALL BRKNCV (Xn_plot,Yn_plot,(Nodes+2),-3)
            CALL BRKNCV (X_surface,Y_surface,3,3)
            CALL BRKNCV (X_vert,Y_vert,3,2)
            CALL DEFCAP (1,'H','C',1,6)
            CALL ADDCP7 ('Mode 5')
            CALL ENDPLT
C
C..... Mode 6
C
            CALL SCALES (0.0,Xmax,1,-200.0,1600.0,1)
            CALL PAGVW (2)
            CALL PAGE (29.7,21.0)
            CALL PAGMRG (1.0,1.0,1.0,2.0)
            CALL BOXPAG (.TRUE.)
            CALL PICSIZ (15.0,13.5)
            CALL NEWPIC
            CALL AXSBDV ('XC',0.0,200.0)
            CALL AXIS7 ('XC','X  (m)')
            CALL AXSBDV ('YC',0.0,200.0)
            CALL AXIS7 ('YC','Y  (m)')
            CALL BRKNCV (X_plot6,Y_plot6,(Nodes+2),0)
            CALL BRKNCV (Xn_plot,Yn_plot,(Nodes+2),-3)
            CALL BRKNCV (X_surface,Y_surface,3,3)
            CALL BRKNCV (X_vert,Y_vert,3,2)
            CALL DEFCAP (1,'H','C',1,6)
            CALL ADDCP7 ('Mode 6')
            CALL ENDPLT
C
         ENDIF
C
         CLOSE (2)
         STOP
C
C        FORMAT STATEMENTS
C        ************************************************************
C
     2   FORMAT (A10)
     4   FORMAT (1H0,1X,'   Failure in F02ABF. IFAIL = ',I2)
     5   FORMAT (1H0,1X,'   Horizontal Surface Offset = ',F6.1,' m')
     6   FORMAT (1H0,1X,'   Sea Depth = ',F6.1,' m')
     7   FORMAT (1H0,1X,'   Total Riser Length = ',F7.2,' m')
     8   FORMAT (1H0,1X,'   Outer Diameter = ',F4.2,' m')
     9   FORMAT (1H0,1X,'   Elasticity Modulus = ',D10.4,' N/m2')
    10   FORMAT (1H0,1X,'   Cross-sectional Area = ',F6.4,' m')
    11   FORMAT (1H0,1X,'   AE = ',D12.6,' N')
    12   FORMAT (1H0,1X,'   Unit Mass = ',F6.1,' kg/m')
    13   FORMAT (1H0,1X,'   Unit Added Mass (normal) = ',F6.1,'kg/m')
    14   FORMAT (1H0,1X,'   Submerged Unit Weight = ',F6.1,' N/m')
    15   FORMAT (1H0,1X,'   Horizontal Tension Constant = ',F11.3,' N')
    16   FORMAT (1H0,1X,'   % Difference = ',D14.7)
    17   FORMAT (1H0,1X,'   Lamda = ',F6.4)
    18   FORMAT (1H0,1X,'   Integration Constant = ',D14.7)
    19   FORMAT (1H0,1X,'   Slope at x=0 = ',D14.7)
    20   FORMAT (1H0,1X,'   Number of Nodes = ',I3)
```

```
 21   FORMAT (1H0,1X,'   Distance between nodes = ',F7.2,' N')
 22   FORMAT (1H0,'           ')
 23   FORMAT (1H0,1X,'Node',2X,'Length to',4X,'Node x',6X,'Node y')
 24   FORMAT (1H ,1X,'-----------------------------------')
 25   FORMAT (1H0,1X,I3,4X,F7.2,4X,F7.2,4X,F7.2)
 26   FORMAT (1H0,'           ')
 27   FORMAT (1H0,1X,'Node',2X,'Length to',6X,'x',10X,'Tension')
 28   FORMAT (1H ,1X,'----------------------------------------')
 29   FORMAT (1H0,1X,I3,4X,F7.2,4X,F7.2,4X,F11.2)
 30   FORMAT (1H0,'           ')
 31   FORMAT (1H0,'Node',5X,'ax-1',9X,'ax-2',9X,'ax-3',9X,'ax-4',
     *         9X,'ax-5',9X,'ax-6')
 32   FORMAT (1H ,'-------------------------------------',
     *         '-----------------------------')
 33   FORMAT (1H0,I3,2X,D11.4,2X,D11.4,2X,D11.4,2X,D11.4,2X,D11.4,
     *         2X,D11.4)
 34   FORMAT (1H0,'           ')
 35   FORMAT (1H0,'Node',5X,'ay-1',9X,'ay-2',9X,'ay-3',9X,'ay-4',
     *         9X,'ay-5',9X,'ay-6')
 36   FORMAT (1H ,'-------------------------------------',
     *         '-----------------------------')
 37   FORMAT (1H0,I3,2X,D11.4,2X,D11.4,2X,D11.4,2X,D11.4,2X,D11.4,
     *         2X,D11.4)
 38   FORMAT (1H0,'           ')
 39   FORMAT (1H ,'-------------------------------------',
     *         '-----------------------------')
 40   FORMAT (1H0,I3,2X,D11.4,2X,D11.4,2X,D11.4,2X,D11.4,2X,D11.4)
 41   FORMAT (1H0,'           ')
 42   FORMAT (1H0,'Eigenvectors (x)')
 43   FORMAT (1H ,'-------------------------------------',
     *         '-----------------------------')
 44   FORMAT (1H0,D11.4,2X,D11.4,2X,D11.4,2X,D11.4,2X,D11.4,2X,D11.4)
 45   FORMAT (1H0,'           ')
 46   FORMAT (1H0,'Eigenvectors (y)')
 47   FORMAT (1H ,'-------------------------------------',
     *         '-----------------------------')
 48   FORMAT (1H0,D11.4,2X,D11.4,2X,D11.4,2X,D11.4,2X,D11.4,2X,D11.4)
 49   FORMAT (1H0,'           ')
 50   FORMAT (1H0,7X,'w(rad/s)',5X,'T(1/s)')
 51   FORMAT (1H ,1X,'--------------------------')
 52   FORMAT (1H0,1X,I3,4X,F8.3,4X,F8.4)
C
 90   FORMAT ('Horizontal Surface Offset = ',F6.1,' m')
 91   FORMAT ('Sea Depth = ',F6.1,' m')
 92   FORMAT ('Riser Length = ',F7.2,' m')
 93   FORMAT ('Unit Mass = ',F6.1,' kg/m')
 94   FORMAT ('Unit Added Mass = ',F6.1,' kg/m')
 95   FORMAT ('Unit Submerged Weight = ',F6.1,' N/m')
 96   FORMAT ('Riser Diameter = ',F4.2,' m')
 97   FORMAT ('No. of Nodes = ',I4)
 98   FORMAT ('           ')
      END
C
C     SUBROUTINES
C     ***********************************************************
C
      SUBROUTINE HORIZ_TENSION(ax, by, length, Sub_w, Inc_H, No_Incs,
     *   Initial_H, Ht, LHS, RHS, DIFFERENCE, Lamda, Ic, dydx)
C
C     This subroutine calculates the Horizontal Tension for
C     a given suspended length by using an iterative technique.
C
      DOUBLE PRECISION H(10000), Lbi(10000)
      DOUBLE PRECISION ax, by, length, Sub_w
      DOUBLE PRECISION Lamda, Ic, dydx
      DOUBLE PRECISION Ht, LHS, RHS
```

```
      DOUBLE PRECISION DIFFERENCE
      DOUBLE PRECISION Lb, LEFT_Lbi, RIGHT_Lbi, MID_Lbi
      DOUBLE PRECISION MID_H, LEFT_H, RIGHT_H
      DOUBLE PRECISION F
C
      Lb = ((length**2 - by**2)*(Sub_w**2))/4
C
      DO 800, J=1, No_Incs
         H(J) = (J*Inc_H) + Initial_H
         Lbi(J) = (H(J)**2)*((SINH((Sub_w*ax)/(2*H(J))))**2)
C
         IF((Lb - Lbi(J)).GT.0.0.AND.(Lb - Lbi(J-1)).LT.0.0) THEN
           LEFT_H = H(J-1)
           RIGHT_H = H(J)
           MID_H = (RIGHT_H - LEFT_H)/2 + LEFT_H
           MID_Lbi = (MID_H**2)*((SINH((Sub_w*ax)/(2*MID_H)))**2)
           LEFT_Lbi = Lbi(J-1)
           RIGHT_Lbi = Lbi(J)
           GO TO 810
         ENDIF
  800 CONTINUE
C
  810 DIFFERENCE = (ABS(Lb - MID_Lbi)/Lb)*100
C
  820 IF(DIFFERENCE.GT.0.000001) THEN
        IF((Lb - MID_Lbi).GT.0.0) THEN
          RIGHT_H = MID_H
        ELSE
          LEFT_H = MID_H
        ENDIF
        MID_H = (RIGHT_H - LEFT_H)/2 + LEFT_H
        MID_Lbi = (MID_H**2)*((SINH((Sub_w*ax)/(2*MID_H)))**2)
        DIFFERENCE = (ABS(Lb - MID_Lbi)/Lb)*100
        GO TO 820
        ENDIF
C
      Ht = MID_H
      RHS = (Ht**2)*((SINH((Sub_w*ax)/(2*Ht)))**2)
      LHS = Lb
      Lamda = (Sub_w*ax)/(2*Ht)
      F = (Sub_w*by)/(2*Ht*SINH(Lamda))
      Ic = Log(F + SQRT((F**2) + 1)) - Lamda
      dydx = SINH(Ic)
C
      RETURN
      END
C
C     ****************************************************************
C
      SUBROUTINE MAXIMUM(IV, Nmax, N, K, V, Vmax)
C
C     This subroutine calcluates the maximum eigenvector for a
C    *  specified eigenvalue
C
      INTEGER IV, Nmax, N, K
      DOUBLE PRECISION Max, V(IV,Nmax), Vmax(Nmax)
C
      Max = 0.0
      DO 830 J=1, N
         IF(ABS(V(J,K)).GT.ABS(Max))THEN
           Max = V(J,K)
         ENDIF
  830 CONTINUE
      Vmax(K) = Max
C
      RETURN
```

```
      END
C
C     ************************************************************
C
      SUBROUTINE VERIF_PLOT(T_verif1, T_verif2, T_verif3, T_verif4,
     *                      T_verif5, T_verif6, T_verif7, T_verif8,
     *                    T_verif9, T_verif10, xT_verif1, xT_verif2,
     *                   xT_verif3, xT_verif4, xT_verif5, xT_verif6,
     *                  xT_verif7, xT_verif8, xT_verif9, xT_verif10,
     *                  yaxis, y_verif)
C
C     This subroutine calculates the graphical coordinates for the
C     verification data.

      REAL xT_verif1(3), xT_verif2(3)
      REAL xT_verif3(3), xT_verif4(3)
      REAL xT_verif5(3), xT_verif6(3)
      REAL xT_verif7(3), xT_verif8(3)
      REAL xT_verif9(3), xT_verif10(3)
      REAL y_verif(3)
C
      DO 840 I=1, 3
         xT_verif1(I) = T_verif1
  840 CONTINUE
      DO 850 I=1, 3
         xT_verif2(I) = T_verif2
  850 CONTINUE
      DO 860 I=1, 3
         xT_verif3(I) = T_verif3
  860 CONTINUE
      DO 870 I=1, 3
         xT_verif4(I) = T_verif4
  870 CONTINUE
      DO 880 I=1, 3
         xT_verif5(I) = T_verif5
  880 CONTINUE
      DO 890 I=1, 3
         xT_verif6(I) = T_verif6
  890 CONTINUE
      DO 900 I=1, 3
         xT_verif7(I) = T_verif7
  900 CONTINUE
      DO 1010 I=1, 3
         xT_verif8(I) = T_verif8
 1010 CONTINUE
      DO 1020 I=1, 3
         xT_verif9(I) = T_verif9
 1020 CONTINUE
      DO 1030 I=1, 3
         xT_verif10(I) = T_verif10
 1030 CONTINUE
C
      y_verif(1) = 0.0
      y_verif(2) = yaxis/2
      y_verif(3) = yaxis - 0.2
C
      RETURN
      END
C
C     ************************************************************
```

```
      PROGRAM Verif
C
C     This FORTRAN computer program plots the graphical solution to an
C     equation whose roots equal the in-plane natural frequency for an
C     inclined catenary cable.
C
C     Program written by James Dingwall
C
C
C     NOMENCLATURE
C     ************************************************************
C
C     a       Horizontal offset
C     b       Vertical offset
C     H       Horizontal tension
C     mass    Unit mass
C     g       Gravity
C     L       Length of riser
C     Lc      Chord length
C     theta   Chord angle with horizontal
C
C     SPECIFICATION STATEMANTS
C     ************************************************************
C
      INTEGER J, I, Jmax
      INTEGER n, n1, n2, n3, n4, n5, n6, n7, n8, n9, n10
      INTEGER n11, n12, n13, n14
C
      DOUBLE PRECISION a, b, H, Ht, m, g, L, Lc, theta
      DOUBLE PRECISION mass, weight, pi, dw
      DOUBLE PRECISION beta(10000), eqn(10000)
      DOUBLE PRECISION start(30), end(30)
      DOUBLE PRECISION eqns(30), eqne(30), x(30)
      DOUBLE PRECISION wright(30), wleft(30), wroot(30)
      DOUBLE PRECISION eright(30), eleft(30), e(30)
      DOUBLE PRECISION Lamda(30), troot(30)
      DOUBLE PRECISION beta1(1000), beta2(1000)
      DOUBLE PRECISION beta3(1000), beta4(1000)
      DOUBLE PRECISION beta5(1000), beta6(1000)
      DOUBLE PRECISION beta7(1000), beta8(1000)
      DOUBLE PRECISION beta9(1000), beta10(1000)
      DOUBLE PRECISION beta11(1000), beta12(1000)
      DOUBLE PRECISION beta13(1000), beta14(1000)
      DOUBLE PRECISION edp(10000), wdp(10000), max
      DOUBLE PRECISION y1(2001), y2(2001), y3(2001)
      DOUBLE PRECISION y4(2001), y5(2001), y6(2001)
      DOUBLE PRECISION y7(2001), y8(2001), y9(2001)
      DOUBLE PRECISION y10(2001), y11(2001), y12(2001)
      DOUBLE PRECISION y13(2001), y14(2001)
      DOUBLE PRECISION y_as1(2001), y_as2(2001), y_as3(2001)
      DOUBLE PRECISION y_as4(2001), y_as5(2001), y_as6(2001)
      DOUBLE PRECISION y_as7(2001), y_as8(2001)
      REAL esp(10000), wsp(10000), tsp(10000)
      REAL w_as(30), Lamda_as(30), t_as(30)
      REAL w1(1000), eqn1(1000), t1(1000), normy1(2001)
      REAL w2(1000), eqn2(1000), t2(1000), normy2(2001)
      REAL w3(1000), eqn3(1000), t3(1000), normy3(2001)
      REAL w4(1000), eqn4(1000), t4(1000), normy4(2001)
      REAL w5(1000), eqn5(1000), t5(1000), normy5(2001)
      REAL w6(1000), eqn6(1000), t6(1000), normy6(2001)
      REAL w7(1000), eqn7(1000), t7(1000), normy7(2001)
      REAL w8(1000), eqn8(1000), t8(1000), normy8(2001)
      REAL w9(1000), eqn9(1000), t9(1000), normy9(2001)
      REAL w10(1000), eqn10(1000), t10(1000), normy10(2001)
      REAL w11(1000), eqn11(1000), t11(1000), normy11(2001)
      REAL w12(1000), eqn12(1000), t12(1000), normy12(2001)
```

```
      REAL w13(1000), eqn13(1000), t13(1000), normy13(2001)
      REAL w14(1000), eqn14(1000), t14(1000), normy14(2001)
      REAL normy_as1(2001), normy_as2(2001), normy_as3(2001)
      REAL normy_as4(2001), normy_as5(2001), normy_as6(2001)
      REAL normy_as7(2001), normy_as8(2001)
      REAL xl(2001)
      REAL wmax, winc, ymax, yinc, tmax, tinc
C
      PARAMETER (g=9.81, dw=0.001, pi=3.1415927)
      PARAMETER (wmax=5.0, winc=0.2)
      PARAMETER (ymax=100.0, ymin=-100.0, yinc=20.0)
      PARAMETER (tmax=60.0, tinc=5.0)
      PARAMETER (n=10000)
C
      CHARACTER*7 FILE
      CHARACTER*10 OUTFILE
      CHARACTER*36 CAP1
      CHARACTER*20 CAP2
      CHARACTER*24 CAP3
      CHARACTER*23 CAP4
      CHARACTER*24 CAP5
      CHARACTER*10 CAP6
C
      PRINT*, '   Enter the output filename'
      READ (5,1) FILE
    1 FORMAT (A10)
C
      WRITE (OUTFILE,2)FILE
      OPEN (UNIT=2, FILE=OUTFILE, STATUS='NEW')
C
C     INPUT
C     ************************************************************
C
      PRINT*,'   Enter the Horizontal Surface Offset (m)'
      READ*,a
      PRINT*,'   Enter the Sea Depth (m)'
      READ*,b
      PRINT*,'   Enter the Length of the Riser (m)'
      READ*,L
      PRINT*,'   Enter the Unit Weight (N/m)'
      READ*,weight
      PRINT*,'   Enter the Unit Mass (N/m)'
      READ*,mass
      PRINT*,'   Enter the Horizontal Tension (N)'
      READ*,H
C
C     CALCULATION
C     ************************************************************
C
      theta = ATAN(b/a)
      Lc = SQRT(a**2 + b**2)
      Ht = H/COS(theta)
C
C..... Symmetric Modes
C
      wdp(1) = dw
      wsp(1) = dw
      tsp(1) = (2*pi)/dw
      beta(1) = SQRT((mass*(wdp(1)**2))/Ht)
      eqn(1) = TAN((beta(1)*Lc)/2) - (beta(1)*Lc)/2
      J = 1
      DO 100 I=2, n
         wdp(I) = dw + wdp(I-1)
         wsp(I) = dw + wsp(I-1)
         tsp(I) = (2*pi)/wsp(I)
         beta(I) = SQRT((mass*(wdp(I)**2))/Ht)
```

```
            eqn(I) = TAN((beta(I)*Lc)/2) - (beta(I)*Lc)/2
            esp(I) = SIN((beta(I)*Lc)/2) - ((beta(I)*Lc)/2)*
     *               COS((beta(I)*Lc)/2)
            edp(I) = SIN((beta(I)*Lc)/2) - ((beta(I)*Lc)/2)*
     *               COS((beta(I)*Lc)/2)
            IF((edp(I)*edp(I-1)).LT.0.0)THEN
              wleft(J) = wdp(I-1)
              wright(J) = wdp(I)
              eleft(J) = edp(I-1)
              eright(J) = edp(I)
              J = J + 1
            ENDIF
   100    CONTINUE
C
          Jmax = J
          PRINT 10
          WRITE (2,10)
          PRINT 11
          WRITE (2,11)
          PRINT 12
          WRITE (2,12)
          PRINT 13
          WRITE (2,13)
          DO 110 J=1, (Jmax-1)
             CALL WRoots(J, mass, Ht, Lc, wleft, wright,
     *                   eleft, eright, wroot, e)
             x(J) = 0.5*SQRT((mass*(wroot(J)**2))/Ht)*Lc
             lamda(J) = (2*x(J))/pi
             troot(J) = (2*pi)/wroot(J)
             PRINT 14, J, lamda(J), wroot(J), troot(J)
             WRITE (2,14) J, lamda(J), wroot(J), troot(J)
   110    CONTINUE
C
          J =1
          start(1) = 0.0
          DO 120 I=1, n
             IF(eqn(I).GT.0.0.AND.eqn(I+1).LT.0.0)THEN
               end(J) = wdp(I)
               eqne(J) = eqn(I)
               start(J+1) = wdp(I+1)
               eqns(J+1) = eqn(I+1)
               J = J + 1
             ENDIF
   120    CONTINUE
C
          Jmax = J
          DO 130 I=1, Jmax
             IF(I.EQ.1)THEN
               w1(1) = start(I)
               beta1(1) = SQRT((mass*(w1(1)**2))/Ht)
               eqn1(1) = TAN((beta1(1)*Lc)/2) - (beta1(1)*Lc)/2
               n1 = (end(I)-start(I))/dw
               DO 140 J=2, n1
                  w1(J) = w1(J-1) + dw
                  t1(J) = (2*pi)/w1(J)
                  beta1(J) = SQRT((mass*(w1(J)**2))/Ht)
                  eqn1(J) = TAN((beta1(J)*Lc)/2) - (beta1(J)*Lc)/2
   140          CONTINUE
               max = 0.0
               DO 150 J=1, 2001
                  x1(J) = (J-1)*0.0005
                  y1(J) = 1 - ((pi*lamda(I))/2)*SIN(lamda(I)*pi*x1(J))
     *                - COS(lamda(I)*pi*x1(J))
                  IF(ABS(y1(J)).GT.max)THEN
                    max = ABS(y1(J))
                  ENDIF
```

```
  150         CONTINUE
              DO 160 J=1, 2001
                 normy1(J) = y1(J)/max
  160         CONTINUE
C
            ELSEIF(I.EQ.2)THEN
              w2(1) = start(I)
              t2(1) = (2*pi)/w2(1)
              beta2(1) = SQRT((mass*(w2(1)**2))/Ht)
              eqn2(1) = TAN((beta2(1)*Lc)/2) - (beta2(1)*Lc)/2
              n2 = (end(I)-start(I))/dw
              DO 170 J=2, n2
                 w2(J) = w2(J-1) + dw
                 t2(J) = (2*pi)/w2(J)
                 beta2(J) = SQRT((mass*(w2(J)**2))/Ht)
                 eqn2(J) = TAN((beta2(J)*Lc)/2) - (beta2(J)*Lc)/2
  170         CONTINUE
              max = 0.0
              DO 180 J=1, 2001
                 y2(J) = 1 - ((pi*lamda(I))/2)*SIN(lamda(I)*pi*xl(J))
     *                    - COS(lamda(I)*pi*xl(J))
                 IF(ABS(y2(J)).GT.max)THEN
                   max = ABS(y2(J))
                 ENDIF
  180         CONTINUE
              DO 190 J=1, 2001
                 normy2(J) = y2(J)/max
  190         CONTINUE
C
            ELSEIF(I.EQ.3)THEN
              w3(1) = start(I)
              t3(1) = (2*pi)/w3(1)
              beta3(1) = SQRT((mass*(w3(1)**2))/Ht)
              eqn3(1) = TAN((beta3(1)*Lc)/2) - (beta3(1)*Lc)/2
              n3 = (end(I)-start(I))/dw
              DO 200 J=2, n3
                 w3(J) = w3(J-1) + dw
                 t3(J) = (2*pi)/w3(J)
                 beta3(J) = SQRT((mass*(w3(J)**2))/Ht)
                 eqn3(J) = TAN((beta3(J)*Lc)/2) - (beta3(J)*Lc)/2
  200         CONTINUE
              max = 0.0
              DO 210 J=1, 2001
                 y3(J) = 1 - ((pi*lamda(I))/2)*SIN(lamda(I)*pi*xl(J))
     *                    - COS(lamda(I)*pi*xl(J))
                 IF(ABS(y3(J)).GT.max)THEN
                   max = ABS(y3(J))
                 ENDIF
  210         CONTINUE
              DO 220 J=1, 2001
                 normy3(J) = y3(J)/max
  220         CONTINUE
C
            ELSEIF(I.EQ.4)THEN
              w4(1) = start(I)
              t4(1) = (2*pi)/w4(1)
              beta4(1) = SQRT((mass*(w4(1)**2))/Ht)
              eqn4(1) = TAN((beta4(1)*Lc)/2) - (beta4(1)*Lc)/2
              n4 = (end(I)-start(I))/dw
              DO 230 J=2, n4
                 w4(J) = w4(J-1) + dw
                 t4(J) = (2*pi)/w4(J)
                 beta4(J) = SQRT((mass*(w4(J)**2))/Ht)
                 eqn4(J) = TAN((beta4(J)*Lc)/2) - (beta4(J)*Lc)/2
  230         CONTINUE
              max = 0.0
```

```
            DO 240 J=1, 2001
               y4(J) = 1 - ((pi*lamda(I))/2)*SIN(lamda(I)*pi*xl(J))
     *                   - COS(lamda(I)*pi*xl(J))
               IF(ABS(y4(J)).GT.max)THEN
                 max = ABS(y4(J))
               ENDIF
  240        CONTINUE
             DO 250 J=1, 2001
               normy4(J) = y4(J)/max
  250        CONTINUE
C
           ELSEIF(I.EQ.5)THEN
             w5(1) = start(I)
             t5(1) = (2*pi)/w5(1)
             beta5(1) = SQRT((mass*(w5(1)**2))/Ht)
             eqn5(1) = TAN((beta5(1)*Lc)/2) - (beta5(1)*Lc)/2
             n5 = (end(I)-start(I))/dw
             DO 260 J=2, n5
               w5(J) = w5(J-1) + dw
               t5(J) = (2*pi)/w5(J)
               beta5(J) = SQRT((mass*(w5(J)**2))/Ht)
               eqn5(J) = TAN((beta5(J)*Lc)/2) - (beta5(J)*Lc)/2
  260        CONTINUE
             max = 0.0
             DO 270 J=1, 2001
               y5(J) = 1 - ((pi*lamda(I))/2)*SIN(lamda(I)*pi*xl(J))
     *                   - COS(lamda(I)*pi*xl(J))
               IF(ABS(y5(J)).GT.max)THEN
                 max = ABS(y5(J))
               ENDIF
  270        CONTINUE
             DO 280 J=1, 2001
               normy5(J) = y5(J)/max
  280        CONTINUE
C
           ELSEIF(I.EQ.6)THEN
             w6(1) = start(I)
             t6(1) = (2*pi)/w6(1)
             beta6(1) = SQRT((mass*(w6(1)**2))/Ht)
             eqn6(1) = TAN((beta6(1)*Lc)/2) - (beta6(1)*Lc)/2
             n6 = (end(I)-start(I))/dw
             DO 290 J=2, n6
               w6(J) = w6(J-1) + dw
               t6(J) = (2*pi)/w6(J)
               beta6(J) = SQRT((mass*(w6(J)**2))/Ht)
               eqn6(J) = TAN((beta6(J)*Lc)/2) - (beta6(J)*Lc)/2
  290        CONTINUE
             max = 0.0
             DO 300 J=1, 2001
               y6(J) = 1 - ((pi*lamda(I))/2)*SIN(lamda(I)*pi*xl(J))
     *                   - COS(lamda(I)*pi*xl(J))
               IF(ABS(y6(J)).GT.max)THEN
                 max = ABS(y6(J))
               ENDIF
  300        CONTINUE
             DO 310 J=1, 2001
               normy6(J) = y6(J)/max
  310        CONTINUE
C
           ELSEIF(I.EQ.7)THEN
             w7(1) = start(I)
             t7(1) = (2*pi)/w7(1)
             beta7(1) = SQRT((mass*(w7(1)**2))/Ht)
             eqn7(1) = TAN((beta7(1)*Lc)/2) - (beta7(1)*Lc)/2
             n7 = (end(I)-start(I))/dw
             DO 320 J=2, n7
```

```
                w7(J) = w7(J-1) + dw
                t7(J) = (2*pi)/w7(J)
                beta7(J) = SQRT((mass*(w7(J)**2))/Ht)
                eqn7(J) = TAN((beta7(J)*Lc)/2) - (beta7(J)*Lc)/2
  320         CONTINUE
              max = 0.0
              DO 330 J=1, 2001
                y7(J) = 1 - ((pi*lamda(I))/2)*SIN(lamda(I)*pi*xl(J))
     *                - COS(lamda(I)*pi*xl(J))
                IF(ABS(y7(J)).GT.max)THEN
                  max = ABS(y7(J))
                ENDIF
  330         CONTINUE
              DO 340 J=1, 2001
                normy7(J) = y7(J)/max
  340         CONTINUE
C
            ELSEIF(I.EQ.8)THEN
              w8(1) = start(I)
              t8(1) = (2*pi)/w8(1)
              beta8(1) = SQRT((mass*(w8(1)**2))/Ht)
              eqn8(1) = TAN((beta8(1)*Lc)/2) - (beta8(1)*Lc)/2
              n8 = (end(I)-start(I))/dw
              DO 350 J=2, n8
                w8(J) = w8(J-1) + dw
                t8(J) = (2*pi)/w8(J)
                beta8(J) = SQRT((mass*(w8(J)**2))/Ht)
                eqn8(J) = TAN((beta8(J)*Lc)/2) - (beta8(J)*Lc)/2
  350         CONTINUE
              max = 0.0
              DO 360 J=1, 2001
                y8(J) = 1 - ((pi*lamda(I))/2)*SIN(lamda(I)*pi*xl(J))
     *                - COS(lamda(I)*pi*xl(J))
                IF(ABS(y8(J)).GT.max)THEN
                  max = ABS(y8(J))
                ENDIF
  360         CONTINUE
              DO 370 J=1, 2001
                normy8(J) = y8(J)/max
  370         CONTINUE
C
            ELSEIF(I.EQ.9)THEN
              w9(1) = start(I)
              t9(1) = (2*pi)/w9(1)
              beta9(1) = SQRT((mass*(w9(1)**2))/Ht)
              eqn9(1) = TAN((beta9(1)*Lc)/2) - (beta9(1)*Lc)/2
              n9 = (end(I)-start(I))/dw
              DO 380 J=2, n9
                w9(J) = w9(J-1) + dw
                t9(J) = (2*pi)/w9(J)
                beta9(J) = SQRT((mass*(w9(J)**2))/Ht)
                eqn9(J) = TAN((beta9(J)*Lc)/2) - (beta9(J)*Lc)/2
  380         CONTINUE
              max = 0.0
              DO 390 J=1, 2001
                y9(J) = 1 - ((pi*lamda(I))/2)*SIN(lamda(I)*pi*xl(J))
     *                - COS(lamda(I)*pi*xl(J))
                IF(ABS(y9(J)).GT.max)THEN
                  max = ABS(y9(J))
                ENDIF
  390         CONTINUE
              DO 400 J=1, 2001
                normy10(J) = y10(J)/max
  400         CONTINUE
C
            ELSEIF(I.EQ.10)THEN
```

```
            w10(1) = start(I)
            t10(1) = (2*pi)/w10(1)
            beta10(1) = SQRT((mass*(w10(1)**2))/Ht)
            eqn10(1) = TAN((beta10(1)*Lc)/2) - (beta10(1)*Lc)/2
            n10 = (end(I)-start(I))/dw
            DO 410 J=2, n10
               w10(J) = w10(J-1) + dw
               t10(J) = (2*pi)/w10(J)
               beta10(J) = SQRT((mass*(w10(J)**2))/Ht)
               eqn10(J) = TAN((beta10(J)*Lc)/2) - (beta10(J)*Lc)/2
  410       CONTINUE
            max = 0.0
            DO 420 J=1, 2001
               y10(J) = 1 - ((pi*lamda(I))/2)*SIN(lamda(I)*pi*xl(J))
     *                  - COS(lamda(I)*pi*xl(J))
               IF(ABS(y10(J)).GT.max)THEN
                 max = ABS(y10(J))
               ENDIF
  420       CONTINUE
            DO 430 J=1, 2001
               normy10(J) = y10(J)/max
  430       CONTINUE
C
          ELSEIF(I.EQ.11)THEN
            w11(1) = start(I)
            t11(1) = (2*pi)/w11(1)
            beta11(1) = SQRT((mass*(w11(1)**2))/Ht)
            eqn11(1) = TAN((beta11(1)*Lc)/2) - (beta11(1)*Lc)/2
            n11 = (end(I)-start(I))/dw
            DO 440 J=2, n11
               w11(J) = w11(J-1) + dw
               t11(J) = (2*pi)/w11(J)
               beta11(J) = SQRT((mass*(w11(J)**2))/Ht)
               eqn11(J) = TAN((beta11(J)*Lc)/2) - (beta11(J)*Lc)/2
  440       CONTINUE
            max = 0.0
            DO 450 J=1, 2001
               y11(J) = 1 - ((pi*lamda(I))/2)*SIN(lamda(I)*pi*xl(J))
     *                  - COS(lamda(I)*pi*xl(J))
               IF(ABS(y11(J)).GT.max)THEN
                 max = ABS(y11(J))
               ENDIF
  450       CONTINUE
            DO 460 J=1, 2001
               normy11(J) = y11(J)/max
  460       CONTINUE
C
          ELSEIF(I.EQ.12)THEN
            w12(1) = start(I)
            t12(1) = (2*pi)/w12(1)
            beta12(1) = SQRT((mass*(w12(1)**2))/Ht)
            eqn12(1) = TAN((beta12(1)*Lc)/2) - (beta12(1)*Lc)/2
            n12 = (end(I)-start(I))/dw
            DO 470 J=2, n12
               w12(J) = w12(J-1) + dw
               t12(J) = (2*pi)/w12(J)
               beta12(J) = SQRT((mass*(w12(J)**2))/Ht)
               eqn12(J) = TAN((beta12(J)*Lc)/2) - (beta12(J)*Lc)/2
  470       CONTINUE
            max = 0.0
            DO 480 J=1, 2001
               y12(J) = 1 - ((pi*lamda(I))/2)*SIN(lamda(I)*pi*xl(J))
     *                  - COS(lamda(I)*pi*xl(J))
               IF(ABS(y12(J)).GT.max)THEN
                 max = ABS(y12(J))
               ENDIF
```

```
  480         CONTINUE
              DO 490 J=1, 2001
                 normy12(J) = y12(J)/max
  490         CONTINUE
C
            ELSEIF(I.EQ.13)THEN
              w13(1) = start(I)
              t13(1) = (2*pi)/w13(1)
              beta13(1) = SQRT((mass*(w13(1)**2))/Ht)
              eqn13(1) = TAN((beta13(1)*Lc)/2) - (beta13(1)*Lc)/2
              n13 = (end(I)-start(I))/dw
              DO 500 J=2, n13
                 w13(J) = w13(J-1) + dw
                 t13(J) = (2*pi)/w13(J)
                 beta13(J) = SQRT((mass*(w13(J)**2))/Ht)
                 eqn13(J) = TAN((beta13(J)*Lc)/2) - (beta13(J)*Lc)/2
  500         CONTINUE
              max = 0.0
              DO 510 J=1, 2001
                 y13(J) = 1 - ((pi*lamda(I))/2)*SIN(lamda(I)*pi*xl(J))
     *                - COS(lamda(I)*pi*xl(J))
                 IF(ABS(y13(J)).GT.max)THEN
                   max = ABS(y13(J))
                 ENDIF
  510         CONTINUE
              DO 520 J=1, 2001
                 normy13(J) = y13(J)/max
  520         CONTINUE
C
            ELSEIF(I.EQ.14)THEN
              w14(1) = start(I)
              t14(1) = (2*pi)/w14(1)
              beta14(1) = SQRT((mass*(w14(1)**2))/Ht)
              eqn14(1) = TAN((beta14(1)*Lc)/2) - (beta14(1)*Lc)/2
              n14 = (end(I)-start(I))/dw
              DO 530 J=2, n14
                 w14(J) = w14(J-1) + dw
                 t14(J) = (2*pi)/w14(J)
                 beta14(J) = SQRT((mass*(w14(J)**2))/Ht)
                 eqn14(J) = TAN((beta14(J)*Lc)/2) - (beta14(J)*Lc)/2
  530         CONTINUE
              max = 0.0
              DO 540 J=1, 2001
                 y14(J) = 1 - ((pi*lamda(I))/2)*SIN(lamda(I)*pi*xl(J))
     *                - COS(lamda(I)*pi*xl(J))
                 IF(ABS(y14(J)).GT.max)THEN
                   max = ABS(y14(J))
                 ENDIF
  540         CONTINUE
              DO 550 J=1, 2001
                 normy14(J) = y14(J)/max
  550         CONTINUE
            ENDIF
  130     CONTINUE
C
C..... Anti-Symmetric Modes
C
          PRINT 15
          WRITE (2,15)
          PRINT 16
          WRITE (2,16)
          PRINT 17
          WRITE (2,17)
          PRINT 18
          WRITE (2,18)
          DO 560 J=1, 20
```

```
        w_as(J) = ((2*J*pi)/Lc)*SQRT(Ht/mass)
        lamda_as(J) = (Lc/pi)*SQRT(mass/Ht)*w_as(J)
        t_as(J) = (2*pi)/w_as(J)
        PRINT 19, J, Lamda_as(J), w_as(J), t_as(J)
        WRITE (2,19) J, Lamda_as(J), w_as(J), t_as(J)
560   CONTINUE
      DO 570 I=1, 8
         IF(I.EQ.1)THEN
           max = 0.0
           DO 580 J=1, 2001
              y_as1(J) = SIN((2*I*pi)*xl(J))
              IF(ABS(y_as1(J)).GT.max)THEN
                max = ABS(y_as1(J))
              ENDIF
580        CONTINUE
           DO 590 J=1, 2001
              normy_as1(J) = y_as1(J)/max
590        CONTINUE
         ELSEIF(I.EQ.2)THEN
           max = 0.0
           DO 600 J=1, 2001
              y_as2(J) = SIN((2*I*pi)*xl(J))
              IF(ABS(y_as2(J)).GT.max)THEN
                max = ABS(y_as2(J))
              ENDIF
600        CONTINUE
           DO 610 J=1, 2001
              normy_as2(J) = y_as2(J)/max
610        CONTINUE
         ELSEIF(I.EQ.3)THEN
           max = 0.0
           DO 620 J=1, 2001
              y_as3(J) = SIN((2*I*pi)*xl(J))
              IF(ABS(y_as3(J)).GT.max)THEN
                max = ABS(y_as3(J))
              ENDIF
620        CONTINUE
           DO 630 J=1, 2001
              normy_as3(J) = y_as3(J)/max
630        CONTINUE
         ELSEIF(I.EQ.4)THEN
           max = 0.0
           DO 640 J=1, 2001
              y_as4(J) = SIN((2*I*pi)*xl(J))
              IF(ABS(y_as4(J)).GT.max)THEN
                max = ABS(y_as4(J))
              ENDIF
640        CONTINUE
           DO 650 J=1, 2001
              normy_as4(J) = y_as4(J)/max
650        CONTINUE
         ELSEIF(I.EQ.5)THEN
           max = 0.0
           DO 660 J=1, 2001
              y_as5(J) = SIN((2*I*pi)*xl(J))
              IF(ABS(y_as5(J)).GT.max)THEN
                max = ABS(y_as5(J))
              ENDIF
660        CONTINUE
           DO 670 J=1, 2001
              normy_as5(J) = y_as5(J)/max
670        CONTINUE
         ELSEIF(I.EQ.6)THEN
           max = 0.0
           DO 680 J=1, 2001
              y_as6(J) = SIN((2*I*pi)*xl(J))
```

```
                IF(ABS(y_as6(J)).GT.max)THEN
                  max = ABS(y_as6(J))
                ENDIF
  680         CONTINUE
              DO 690 J=1, 2001
                 normy_as6(J) = y_as6(J)/max
  690         CONTINUE
            ELSEIF(I.EQ.7)THEN
              max = 0.0
              DO 700 J=1, 2001
                 y_as7(J) = SIN((2*I*pi)*xl(J))
                 IF(ABS(y_as7(J)).GT.max)THEN
                   max = ABS(y_as7(J))
                 ENDIF
  700         CONTINUE
              DO 710 J=1, 2001
                 normy_as7(J) = y_as7(J)/max
  710         CONTINUE
            ELSEIF(I.EQ.8)THEN
              max = 0.0
              DO 720 J=1, 2001
                 y_as8(J) = SIN((2*I*pi)*xl(J))
                 IF(ABS(y_as8(J)).GT.max)THEN
                   max = ABS(y_as8(J))
                 ENDIF
  720         CONTINUE
              DO 730 J=1, 2001
                 normy_as8(J) = y_as8(J)/max
  730         CONTINUE
            ENDIF
  570     CONTINUE
C
C       GRAPHICAL OUTPUT (SIMPLEPLOT)
C       ************************************************************
C
        CALL SCALES (0.0,wmax,1,ymin,ymax,1)
        CALL PAGVW (2)
        CALL PAGE (29.7,21.0)
        CALL PAGMRG (1.0,1.0,1.0,4.0)
        CALL BOXPAG (.TRUE.)
        CALL PICSIZ (25.0,12.0)
        CALL BOXPIC (.TRUE.)
        CALL NEWPIC
        CALL AXSBDV ('XC',0.0,winc)
        CALL AXIS7 ('XC','    ')
        CALL AXSBDV ('YC',0.0,yinc)
        CALL AXIS7 ('YC','Y')
        CALL DEFCAP (1,'O','L',6,40)
        CALL BRKNCV (w1,eqn1,n1,0)
        CALL BRKNCV (w2,eqn2,n2,0)
        CALL BRKNCV (w3,eqn3,n3,0)
        CALL BRKNCV (w4,eqn4,n4,0)
        CALL BRKNCV (w5,eqn5,n5,0)
        CALL BRKNCV (w6,eqn6,n6,0)
        CALL BRKNCV (w7,eqn7,n7,0)
        CALL BRKNCV (w8,eqn8,n8,0)
        CALL BRKNCV (w9,eqn9,n9,0)
        CALL BRKNCV (w10,eqn10,n10,0)
        CALL BRKNCV (w11,eqn11,n11,0)
        CALL BRKNCV (w12,eqn12,n12,0)
        CALL BRKNCV (w13,eqn13,n13,0)
        CALL BRKNCV (w14,eqn14,n14,0)
        CALL BRKNCV (wsp,esp,n,-2)
        WRITE (CAP1,50) a
        WRITE (CAP2,51) b
        WRITE (CAP3,52) L
```

```
      WRITE (CAP4,53) mass
      WRITE (CAP5,54) weight
      WRITE (CAP6,55)
      CALL ADDCP7 (CAP1)
      CALL ADDCP7 (CAP2)
      CALL ADDCP7 (CAP3)
      CALL ADDCP7 (CAP4)
      CALL ADDCP7 (CAP5)
      CALL ADDCP7 (CAP6)
      CALL DEFCAP (1,'U','C',1,26)
      CALL ADDCP7 ('Natural Frequency (rads/s)')
      CALL ENDPLT
C
      CALL SCALES (0.0,tmax,1,ymin,ymax,1)
      CALL PAGVW (2)
      CALL PAGE (29.7,21.0)
      CALL PAGMRG (1.0,1.0,1.0,4.0)
      CALL BOXPAG (.TRUE.)
      CALL PICSIZ (25.0,12.0)
      CALL BOXPIC (.TRUE.)
      CALL NEWPIC
      CALL AXSBDV ('XC',0.0,tinc)
      CALL AXIS7 ('XC','    ')
      CALL AXSBDV ('YC',0.0,yinc)
      CALL AXIS7 ('YC','Y')
      CALL DEFCAP (1,'O','L',6,40)
      CALL BRKNCV (t1,eqn1,n1,0)
      CALL BRKNCV (t2,eqn2,n2,0)
      CALL BRKNCV (t3,eqn3,n3,0)
      CALL BRKNCV (t4,eqn4,n4,0)
      CALL BRKNCV (t5,eqn5,n5,0)
      CALL BRKNCV (t6,eqn6,n6,0)
      CALL BRKNCV (t7,eqn7,n7,0)
      CALL BRKNCV (t8,eqn8,n8,0)
      CALL BRKNCV (t9,eqn9,n9,0)
      CALL BRKNCV (t10,eqn10,n10,0)
      CALL BRKNCV (tsp,esp,n,-2)
      CALL ADDCP7 (CAP1)
      CALL ADDCP7 (CAP2)
      CALL ADDCP7 (CAP3)
      CALL ADDCP7 (CAP4)
      CALL ADDCP7 (CAP5)
      CALL ADDCP7 (CAP6)
      CALL DEFCAP (1,'U','C',1,21)
      CALL ADDCP7 ('Natural Period (secs)')
      CALL ENDPLT
C
      M = 0
      DO 740 Lp=1, 2
         CALL GROUP (1,4)
         CALL SCALES (0.0,1.0,1,-1.5,1.5,1)
         CALL PAGVW (1)
         CALL PAGE (21.0,29.7)
         CALL PAGMRG (1.0,1.0,1.0,4.0)
         CALL BOXPAG (.TRUE.)
         CALL PICSIZ (15.0,5.0)
         DO 750 K=(Lp+M), (Lp+M+3)
            CALL NEWPIC
            CALL AXSBDV ('XC',0.0,0.1)
            CALL AXIS7 ('XC',' ')
            CALL AXSBDV ('YC',0.0,0.5)
            CALL AXIS7 ('YC','y')
            IF(K.EQ.1)THEN
              CALL BRKNCV(xl,normy1,2001,0)
              CALL DEFCAP (1,'O','C',1,6)
              CALL ADDCP7 ('Mode 2')
```

```
            ELSEIF(K.EQ.2)THEN
              CALL BRKNCV(xl,normy2,2001,0)
              CALL DEFCAP (1,'O','C',1,6)
              CALL ADDCP7 ('Mode 4')
            ELSEIF(K.EQ.3)THEN
              CALL BRKNCV(xl,normy3,2001,0)
              CALL DEFCAP (1,'O','C',1,6)
              CALL ADDCP7 ('Mode 6')
            ELSEIF(K.EQ.4)THEN
              CALL BRKNCV(xl,normy4,2001,0)
              CALL DEFCAP (1,'O','C',1,6)
              CALL ADDCP7 ('Mode 8')
            ELSEIF(K.EQ.5)THEN
              CALL BRKNCV(xl,normy5,2001,0)
              CALL DEFCAP (1,'O','C',1,7)
              CALL ADDCP7 ('Mode 10')
            ELSEIF(K.EQ.6)THEN
              CALL BRKNCV(xl,normy6,2001,0)
              CALL DEFCAP (1,'O','C',1,7)
              CALL ADDCP7 ('Mode 12')
            ELSEIF(K.EQ.7)THEN
              CALL BRKNCV(xl,normy7,2001,0)
              CALL DEFCAP (1,'O','C',1,7)
              CALL ADDCP7 ('Mode 14')
            ELSEIF(K.EQ.8)THEN
              CALL BRKNCV(xl,normy8,2001,0)
              CALL DEFCAP (1,'O','C',1,7)
              CALL ADDCP7 ('Mode 16')
            ENDIF
          CALL DEFCAP (1,'U','C',1,8)
          CALL ADDCP7 ('x/length')
  750     CONTINUE
          CALL DEFCAP (1,'N','C',1,15)
          CALL ADDCP7 ('Symmetric Modes')
          CALL ENDPLT
        M = M + 3
  740   CONTINUE
C
        M = 0
        DO 760 Lp=1, 2
          CALL GROUP (1,4)
          CALL SCALES (0.0,1.0,1,-1.5,1.5,1)
          CALL PAGVW (1)
          CALL PAGE (21.0,29.7)
          CALL PAGMRG (1.0,1.0,1.0,4.0)
          CALL BOXPAG (.TRUE.)
          CALL PICSIZ (15.0,5.0)
          DO 770 K=(Lp+M), (Lp+M+3)
            CALL NEWPIC
            CALL AXSBDV ('XC',0.0,0.1)
            CALL AXIS7 ('XC',' ')
            CALL AXSBDV ('YC',0.0,0.5)
            CALL AXIS7 ('YC','y')
            IF(K.EQ.1)THEN
              CALL BRKNCV(xl,normy_as1,2001,0)
              CALL DEFCAP (1,'O','C',1,20)
              CALL ADDCP7 ('Mode 1 - Fundamental')
            ELSEIF(K.EQ.2)THEN
              CALL BRKNCV(xl,normy_as2,2001,0)
              CALL DEFCAP (1,'O','C',1,6)
              CALL ADDCP7 ('Mode 3')
            ELSEIF(K.EQ.3)THEN
              CALL BRKNCV(xl,normy_as3,2001,0)
              CALL DEFCAP (1,'O','C',1,6)
              CALL ADDCP7 ('Mode 5')
            ELSEIF(K.EQ.4)THEN
```

```
                CALL BRKNCV(xl,normy_as4,2001,0)
                CALL DEFCAP (1,'O','C',1,6)
                CALL ADDCP7 ('Mode 7')
              ELSEIF(K.EQ.5)THEN
                CALL BRKNCV(xl,normy_as5,2001,0)
                CALL DEFCAP (1,'O','C',1,6)
                CALL ADDCP7 ('Mode 9')
              ELSEIF(K.EQ.6)THEN
                CALL BRKNCV(xl,normy_as6,2001,0)
                CALL DEFCAP (1,'O','C',1,7)
                CALL ADDCP7 ('Mode 11')
              ELSEIF(K.EQ.7)THEN
                CALL BRKNCV(xl,normy_as7,2001,0)
                CALL DEFCAP (1,'O','C',1,7)
                CALL ADDCP7 ('Mode 13')
              ELSEIF(K.EQ.8)THEN
                CALL BRKNCV(xl,normy_as8,2001,0)
                CALL DEFCAP (1,'O','C',1,7)
                CALL ADDCP7 ('Mode 15')
              ENDIF
            CALL DEFCAP (1,'U','C',1,8)
            CALL ADDCP7 ('x/length')
  770       CONTINUE
            CALL DEFCAP (1,'N','C',1,19)
            CALL ADDCP7 ('Antisymmetric Modes')
            CALL ENDPLT
          M = M + 3
  760     CONTINUE
          STOP
C
C         FORMAT STATEMENTS
C         ************************************************************
C
    2     FORMAT (A10)
   10     FORMAT (1H0,1X,'Symmetric Modes')
   11     FORMAT (1H ,'           ')
   12     FORMAT (1H0,'mode',4X,'Lamda',7X,'w',9X,'Tp')
   13     FORMAT (1H0,'--------------------------------')
   14     FORMAT (1H0,I2,3X,F8.5,3X,F8.5,3X,F8.5)
   15     FORMAT (1H0,1X,'Anti-Symmetric Modes')
   16     FORMAT (1H ,'           ')
   17     FORMAT (1H0,'mode',4X,'Lamda',7X,'w',9X,'Tp')
   18     FORMAT (1H0,'--------------------------------')
   19     FORMAT (1H0,I2,3X,F8.5,3X,F8.5,3X,F8.5)
   50     FORMAT ('Horizontal Surface Offset = ',F6.1,' m')
   51     FORMAT ('Sea Depth = ',F6.1,' m')
   52     FORMAT ('Riser Length = ',F7.2,' m')
   53     FORMAT ('Unit Mass = ' ,F6.1,' kg/m')
   54     FORMAT ('Unit Weight = ',F6.1,' N/m')
   55     FORMAT ('           ')
          END
C
C         SUBROUTINES
C         ************************************************************
C
          SUBROUTINE WRoots(J, mass, Ht, Lc, wleft, wright,
     *                      eleft, eright, wroot, e)
C
C         This subroutine calculates the roots of an equation
C
          DOUBLE PRECISION mass, Ht, Lc, wleft(20), wright(20)
          DOUBLE PRECISION eleft(20), eright(20), e(20)
          DOUBLE PRECISION right_w, right_b, right_e
          DOUBLE PRECISION left_w, left_b, left_e
          DOUBLE PRECISION mid_w, mid_b, mid_e
          DOUBLE PRECISION difference, wroot(20)
```

```
      INTEGER J
C
      left_w = wleft(J)
      right_w = wright(J)
      left_e = eleft(J)
      right_e = eright(J)
C
      mid_w = (right_w - left_w)/2 + left_w
      mid_b = SQRT((mass*(mid_w**2))/Ht)
      mid_e = SIN((mid_b*Lc)/2) - ((mid_b*Lc)/2)*
     *        COS((mid_b*Lc)/2)
      difference = ABS(mid_e)
C
      IF(right_e.GT.0.0)THEN
  800   IF(difference.GT.0.0001)THEN
          IF(mid_e.GT.0.0)THEN
            right_w = mid_w
          ELSE
            left_w = mid_w
          ENDIF
          mid_w = (right_w - left_w)/2 + left_w
          mid_b = SQRT((mass*(mid_w**2))/Ht)
          mid_e = SIN((mid_b*Lc)/2) - ((mid_b*Lc)/2)*
     *            COS((mid_b*Lc)/2)
          difference = ABS(mid_e)
          GO TO 800
        ENDIF
      ELSEIF(right_e.LT.0.0)THEN
  620   IF(difference.GT.0.0001)THEN
          IF(mid_e.GT.0.0)THEN
            left_w = mid_w
          ELSE
            right_w = mid_w
          ENDIF
          mid_w = (right_w - left_w)/2 + left_w
          mid_b = SQRT((mass*(mid_w**2))/Ht)
          mid_e = SIN((mid_b*Lc)/2) - ((mid_b*Lc)/2)*
     *            COS((mid_b*Lc)/2)
          difference = ABS(mid_e)
          GO TO 620
        ENDIF
      ENDIF
C
      wroot(J) = mid_w
      e(J) = mid_e
C
      RETURN
      END
C
C     ****************************************************************
```